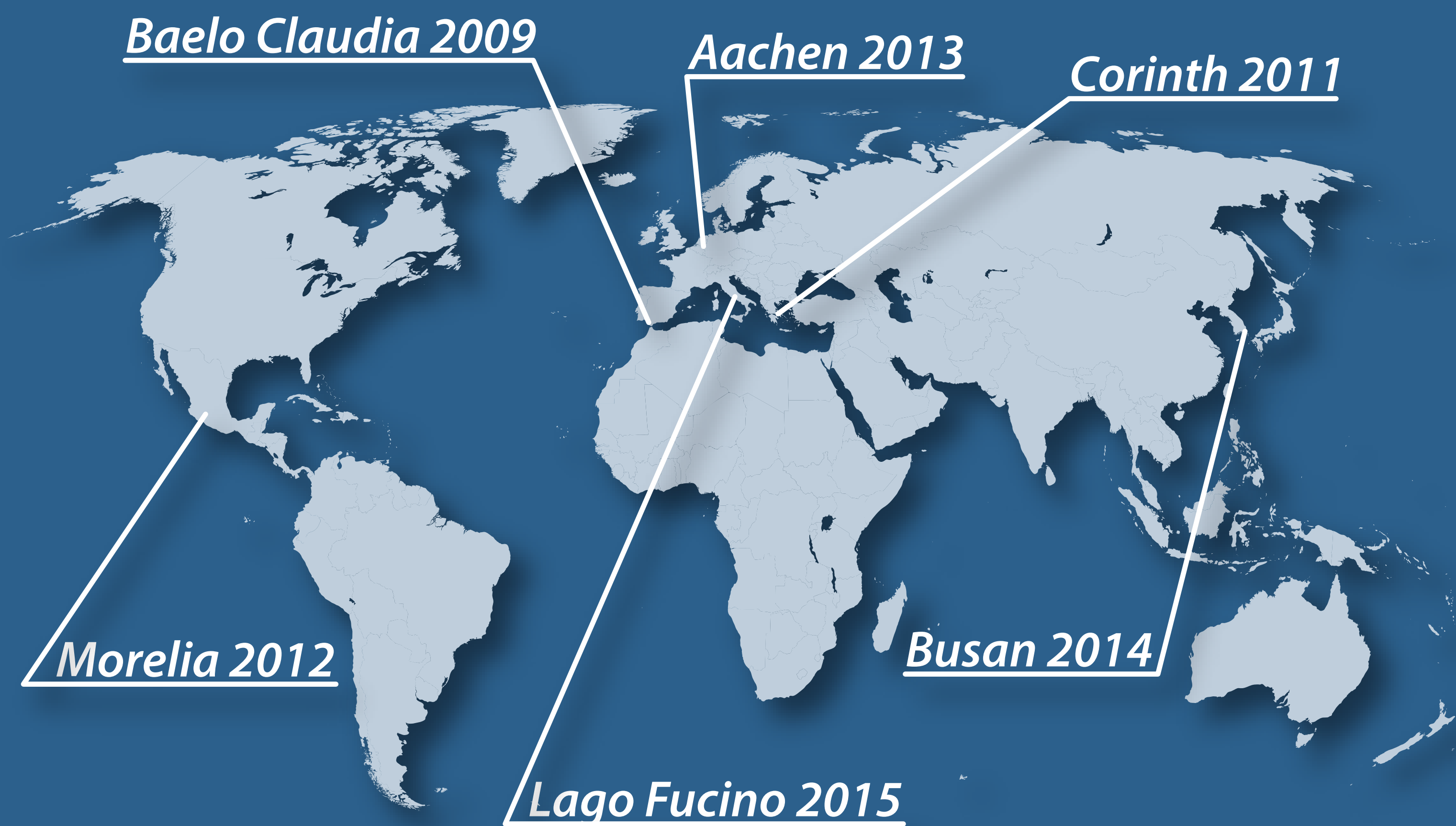


paleoseismicity.org

*Vol. 4:*
***PATA Days - Seismic Hazard, Critical Facilities and Slow Active Faults*** *(C. Grützner, A. Rudersdorf, R. Pérez-López & K. Reicherter, eds.). ISBN: 978-3-00-042796-1. Printed in Germany, 2013. 4th International INQUA Meeting on Paleoseismology, Active Tectonics and Archeoseismology, Aachen (Germany).*

*Vol. 3:*
***Earthquake Geology and Archaeology: Science, Society and Seismic Hazard*** *(R. Pérez-López, P.G. Silva, M.A. Rodríguez Pascua, V.H. Garduno Monroy, G. Suarez & K. Reicherter, eds.). Printed in Mexico, 2012. 3rd INQUA-IGCP 567 International Workshop on Earthquake Geology, Palaeoseismology and Archaeoseismology, Morelia (Mexico).*

*Vol. 2:*
***Earthquake Geology and Archaeology: Science, Society and Critical facilities*** *(C. Grützner, R. Pérez-López, T. Fernández-Steeger,, I. Papanikolaou, K. Reicherter, P.G. Silva & A. Vött, eds.). ISBN: 978-960-466-093-3. Printed in Greece, 2011. 2nd INQUA-IGCP 567 International Workshop, Corinth (Greece).*

*Vol. 1:*
***Archaeoseismology and Palaeoseismology in the Alpine-Himalayan collisional Zone*** *(R. Pérez-López, C. Grützner, J. Lario, K. Reicherter & P.G. Silva, eds.). ISBN: 978-84-7484-217-3. Printed in Spain, 2009. 1st INQUA-IGCP 567 International Workshop, Baelo Claudia, Cádiz (Spain).*

ISBN: 978-3-00-042796-1
9 783000 427961

PATA Days 2013 | Aachen, Germany

PROCEEDINGS

C. Grützner A. Rudersdorf R. Pérez-López K. Reicherter

# PATA DAYS

## Seismic Hazard, Critical Facilities and Slow Active Faults

Proceedings of the 4th International INQUA Meeting on Paleoseismology, Active Tectonics and Archeoseismology

# Seismic Hazard, Critical Facilities and Slow Active Faults

## Proceedings of the 4th International INQUA Meeting on Paleoseismology, Active Tectonics and Archeoseismology

**9-15 October 2013**

**Editors**
Christoph Grützner
Andreas Rudersdorf
Raúl Pérez-López
Klaus Reicherter

PATA
DAYS

4TH INTERNATIONAL
INQUA MEETING ON
PALEOSEISMOLOGY,
ACTIVE TECTONICS
AND ARCHEOSEISMOLOGY

Published by
Grützner & Reicherter Geosolutions UG (haftungsbeschränkt)
Schönrathstraße 68, 52066 Aachen, Germany
http://www.gr-geo.com

Edited by
Christoph Grützner, Andreas Rudersdorf, Klaus Reicherter
RWTH Aachen University
Neotektonik und Georisiken
Aachen, Germany
http://www.nug.rwth-aachen.de
&
Raúl Pérez-López
Instituto Geológico y Minero de España
Madrid, Spain
http://www.igme.es

ISBN: 978-3-00-042796-1
1st edition, 150 pcs.
Printed in Aachen, Germany.

paleoseismicity.org

Vol. 4: Seismic Hazard, Critical Facilities and Slow Active Faults (C. Grützner, A. Rudersdorf, R. Pérez-López & K. Reicherter, eds.). ISBN 978-3-00-042796-1. Printed in Germany, 2013. 4th International INQUA Meeting on Paleoseismology, Active Tectonics and Archeoseismology, Aachen (Germany).

Vol. 3: Earthquake Geology and Archaeology: Science, Society and Seismic Hazard (R. Pérez-López, P.G. Silva, M.A. Rodríguez Pascua, V.H. Garduno Monroy, G. Suarez & K. Reicherter, eds.). Printed in Mexico, 2012. 3rd INQUA-IGCP 567 International Workshop on Earthquake Geology, Palaeoseismology and Archaeoseismology, Morelia (Mexico).

Vol. 2: Earthquake Geology and Archaeology: Science, Society and Critical facilities (C. Grützner, R. Pérez-López, T. Fernández-Steeger,, I. Papanikolaou, K. Reicherter, P.G. Silva & A. Vött, eds.). ISBN 978-960-466-093-3. Printed in Greece, 2011. 2nd INQUA-IGCP 567 International Workshop, Corinth (Greece).

Vol. 1: Archaeoseismology and Palaeoseismology in the Alpine-Himalayan collisional Zone (R. Pérez-López, C. Grützner, J. Lario, K. Reicherter & P.G. Silva, eds.). ISBN 978-84-7484-217-3. Printed in Spain, 2009. 1st INQUA-IGCP 567 International Workshop, Baelo Claudia, Cádiz (Spain).

*This event was supported by:*

INQUA
International Union for Quaternary Research

AEQUA

QTECBETICA
MINECO-USAL PROYECT
CGL2012-37581-C02-01

GRÜTZNER & REICHERTER
GEOSOLUTIONS
UG (haftungsbeschränkt)


Radiocarbon Dating shouldn't take ages
BETA
Beta Analytic
Radiocarbon Dating
Since 1979
• Results in as little as 2-3 days
• ISO 17025-accredited measurements
• Outstanding customer service
Australia Brazil China India Japan Korea UK USA
Visit www.radiocarbon.com for details

# Zeitschrift für Geomorphologie

## Supplementary Issues

www.borntraeger-cramer.de/j/zfg

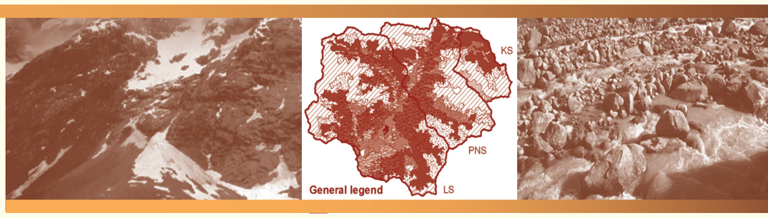


## Rainfall simulation experiments with small scale simulators

Eds.: Johannes B. Ries, Thomas Iserloh

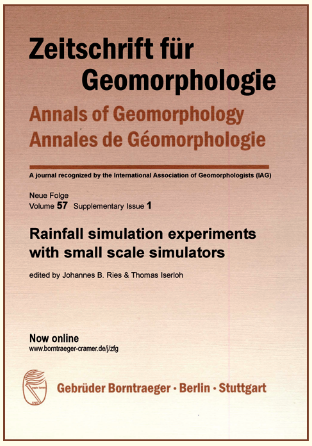


Rainfall simulation with small scale simulators is a method used worldwide to assess the generation of overland flow, soil erosion, infiltration and related processes such as soil sealing, crusting, splash and redistribution of solids and solutes by raindrop impact. Data obtained from these simulations are of great significance both for analysing simulated processes and as the source of input data for soil erosion modelling.

*This issue is of interest to all geomorphologists, soil scientists, hydrologists and practitioners interested in experimental soil erosion measurement.*

2013. 201 pages, 88 figures, 42 tables, 24 x 17 cm
(Zeitschrift für Geomorphologie, Supplementbände Volume 57 Suppl. Iss. 1)
**Order No. ES023105701 paperback € 109.–**

## Sediment Budgets in Cold Environments

### Sedimentary fluxes dynamics in the changing mountain and polar environment: Monitoring, record & consequences

Eds.: Armelle Decaulne, Grzegorz Rachlewicz, Scott F. Lamoureux, Achim A. Beylich

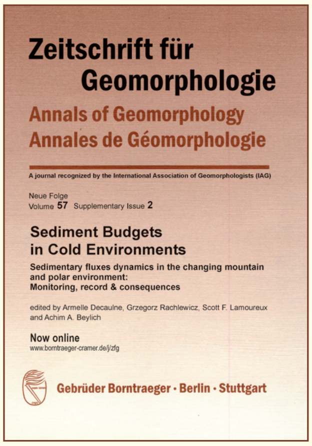


The papers in this issue highlight current topics within the SEDIBUD (SEDImentBUDgets in Cold Environments) research focus.

*This issue is of interest to all geomorphologists and Earth scientists working on sediment budgets and sediment fluxes in changing environments.*

2013. IV, 85 pages, 29 figures, 12 tables 24 x 17 cm
(Zeitschrift für Geomorphologie, Supplementbände Volume 57 Suppl. Iss. 2)
**Order No. ES023105702 paperback € 59.–**

## Quaternary Geomorphology in Tectonically Active Areas with Emphasis in Fluvio-Coastal Processes

Eds.: Niki Evelpidou, Kosmas Pavlopoulos

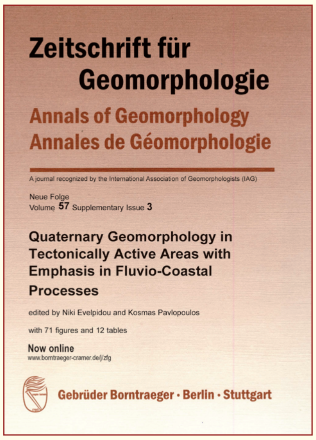


This special issue of ZfG is referred to fluvial and coastal processes mostly occurring in tectonically active regions of the Earth.

*The studies in this Supplement Issue present useful data for scientists and professionals engaged in topics related to geoarchaeology, geomorphology and tectonics and for all readers involved in engineering projects.*

2013. 137 pages, 71 figures, 12 tables, 24 x 17 cm.
(Zeitschrift für Geomorphologie, Supplementbände Volume 57 Suppl. Iss. 3)
**Order No. ES023105703 paperback ca. € 85.–**

## Reconstruction and Modeling of Palaeotsunami Events

forthcomming 2013

### Multi-proxy Approaches, Geophysical Studies, Numerical Simulations

Eds.: Andreas Vött, Klaus Reicherter, Ioannis Papanikolaou

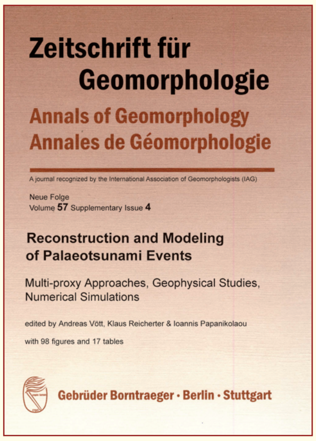


This issue comprises selected contributions from the palaeotsunami session of the 2nd INQUA-IGCP 567 International Workshop on Active Tectonics, Earthquake Geology, Archaeology and Engineering on 19-24 September 2011 in Corinth, Greece.

*The volume is of interest to all geomorphologists and geologists, tsunami experts in science and administration, for archaeologists and historians studying tsunami related effects.*

2013. 98 figures, 17 tables, 24 x 17 cm.
(Zeitschrift für Geomorphologie, Supplementbände Volume 57 Suppl. Iss. 4)
**Order No. ES023105704 paperback**


# Borntraeger Science Publishers

Johannesstr. 3a, 70176 Stuttgart, Germany. Tel. +49 (711) 351456-0 Fax. +49 (711) 351456-99
order@borntraeger-cramer.de www.borntraeger-cramer.de

# Preface

In the last 4 years, since the successful launch of our regular meetings on Earthquake Geology and Paleoseismology in Baelo Claudia (Spain) in 2009, and the following two meetings in Corinth (Greece) in 2011, and last year, the first meeting outside Europe in Morelia (Mexico) in 2012, we are very happy to welcome all of you in Aachen, Germany.

The last three meetings brought together more than 250 international scientists from earthquake geology and all neighbouring disciplines. We are expecting over 100 participants for the Aachen 2013 meeting. We have decided to rename the meeting into **PATA Days**, which stands for "Paleoseismology, Active Tectonics and Archeoseismology", and sounds a bit more youthful.

In the last years, we have seen fruitful and intense discussions, we kicked off dozens of joint projects and we started international collaborations and initiatives to extend the knowledge on past earthquakes. A large number of peer reviewed articles has been published in Special Volumes as an outcome of these conferences. It became clear that paleoseismological research is imperative to seismic hazard studies. It will gain even more importance in the emerging discussion on seismic safety of nuclear power plants and waste deposits, chemical industry and other critical facilities and infrastructure. During the Aachen 2013 meeting we are trying to deepen international collaboration, we will discuss the road map of our discipline and we will throw the points of future initiatives. A novelty is also that we do not carry out workshops in the classical sense, but provide an interdisciplinary forum for a wide range of discussions.

The INQUA Focus Group on Paleoseismology and Active Tectonics (http://tierra.rediris.es/aequa/paleoinqua.html) decided to elaborate an annual calendar to support this joint initiative. It is planned to proceed with the meetings, so we have chosen Busan, South Korea, to be the host in fall 2014. And the last meeting in the INQUA inter-congress period will be in spring 2015 in Fucino, Italy. We switched to half a year earlier than normal because of the INQUA meeting in 2015 in Nagoya/Japan, where we need to present the results in the TERPRO frame of our **INQUA Project 1299 - EEE METRICS PARAMETRIZATION OF EARTHQUAKE ENVIRONMENTAL EFFECTS (2011-2015)**: Relationships between source parameters and ESI-2007 Intensity for Modern, Historic, Ancient and Paleo Earthquakes (more: http://www.terpro.org.ar/paleoseismology.htm). And we also need to prepare new strategies for the forthcoming inter-congress period.

Examples of this variety of original research coming from this collaborative approach are publications like the Geological Society of London Special Volume 316 (2009) ***Paleoseismology: Historical and Prehistorical records of Earthquake Ground Effects for Seismic Hazard Assessment*** (K. Reicherter, A.M. Michetti & P.G. Silva, eds.), the Geological Society of America Special Papers 471, ***Ancient Earthquakes*** (2010) (M. Sintubin, I.S. Stewart, T. Niemi & E. Altunel, eds.) and the Special Volume of Quaternary International (2011) ***Earthquake Archaeology and Paleoseismology*** (P.G. Silva, M. Sintubin & K. Reicherter, eds.). In the same way, this abstract volume contains more than 80 contributions from researchers of more than 27 different countries and illustrates the upgrading shared knowledge on paleo-, ancient, historical and instrumental earthquakes and images an impressive growth of our community. ***The Geomorphology*** and ***Annals of Geophysics*** special volumes are still in progress, we had some delay.

Our workshop is co-ordinated through the website http://www.paleoseismicity.org, where earthquake information and blog posts are openly shared.

Many thanks to the Federal Office of Civil Protection and Disaster Assistance (*Bundesamt für Bevölkerungsschutz und Katastrophenhilfe*) and the Academy for Crisis Management, Emergency Planning and Civil Protection (*Akademie für Krisenmanagement, Notfallplanung und Zivilschutz*) for hosting this meeting.

A special "Dankeschön" goes to Christoph Grützner for long days preparing the meeting and Andreas Rudersdorf and Raul Pérez-López for their invaluable work with the organization and the abstract handling.

Finally, we wish all participants a fruitful conference in the northernmost vine area of Germany, where rare intra-plate earthquakes occur every now and then, where wonderful landscapes, ancient cultures, daily cool beers and wine tasting events will be paired with hot discussions.

On behalf of the organizers of the 4$^{th}$ PATA days,

*Klaus Reicherter*

We gratefully acknowledge the help and work of:

***Scientific Committee:*** Ch. Grützner (GER), T. Azuma (JPN), J. McCalpin, USA), T. Rockwell (USA), Y.-S. Kim (KOR), K. Reicherter (GER)

***Organizing Committee:*** C. Grützner (GER), T. Fernández-Steeger (GER), L. Guerrieri (ITA), H.-B. Havenith (BEL), Y.-S. Kim (KOR), A. Michetti (ITA), I. Papanikolaou (GRE), R. Pérez-López (ESP), M. Rodríguez-Pascua (ESP), P.G. Silva (ESP), M. Sintubin (BEL), T. Spies (GER), A. Vött (GER), K. Reicherter (GER)

***Excursion Committee:*** K.-G. Hinzen, M. Salamon, A. Rudersdorf, M. Mathes-Schmidt, R. Walter, T. Fernández-Steeger, K. Reicherter (all GER)

***The Organizers of the 4$^{th}$ PATA days***

*Prof. Klaus Reicherter, Dr. Christoph Grützner, Andreas Rudersdorf, M.Sc. and Prof. Pablo G. Silva*

# Program

## 9 October (WED) - Arrival in Aachen and Icebreaker Party

Arrival in Aachen
20:00 Icebreaker Party at the Kuckucksnest, Mauerstr. 92, 52064 Aachen (N50°46'22.90" E6°4'25.88"), Registration

## 10 October (THU) - Excursion to Cologne and the Lower Rhine Embayment – Archaeoseismology, Active Faults and Critical Facilities

9:30 excursion to active faults (Flerzheim, Rurrandstörung) and critical facilities (Inden open pit mine) starts at the Aachen Theatre, Theaterplatz 14, 52062 Aachen, (N50°46'19.52" E6° 5'15.38"), Registration
13:00 Arrival at Cologne, time for individual sightseeing, lunch etc.
15:00 Excursion to Roman Ruins in Cologne
17:00 Visit of Cologne Cathedral
19:00 End of excursion and arrival in Aachen
20:00 INQUA Project Business Meeting

## 11 October (FRI) - Opening Ceremony, Invited Conferences, Project Business Meeting, Ship cruise and Conference Dinner

9:00 Transfer to AKNZ Bad Neuenahr-Ahrweiler (N50°31'43.41" E7° 6'25.69"), starts at the Aachen Theatre, Theaterplatz 14, 52062 Aachen

10:30 Registration and check-In

12:00 - 13:00 Lunch

13:00 Opening ceremony:
- Organisation of the workshop: K. Reicherter
- INQUA TERPRO: A. Michetti (president)
- INQUA sub-commission on Paleoseismology: P. Silva (president)
- J. McCalpin invited talk on Paleoseismology

**14:00 - 17:00 Key notes, poster session, talks**

14:00 - 15:00 key note lectures

| 11 October Friday afternoon | Session Tsunamis and Paleotsunamis | Chaired by: N. Mörner |
|---|---|---|
| 14:00 - 14:30<br>11.1 key note | Beverly Goodman-Tchernov | Red Sea Tsunami:<br>Sedimentological Variations due to local Environmental Heterogeneity |
| 14:30 - 15:00<br>11.2 key note | Witold Szczucinksi | Limitations of tsunami deposits identification - problem of sediment sources, sedimentary environments and processes, and post-depositional changes |

15:00 - 16:00 talks

| 11 October Friday afternoon | Session Tsunamis and Paleotsunamis | Chaired by: B. Goodman-Tchernov, W. Szczucinski |
|---|---|---|
| 15:00 - 15:15<br>11.3 talk | Niklas Mörner | Tsunamis and tsunamites: origin and characteristics |
| 15:15 - 15:30<br>11.4 talk | Philipp Kempf | A new long paleo-tsunami coastal lake record from the Valdivia segment, south central Chile: A preliminary age depth model and its implications |
| 15:30 - 15:45<br>11.5 talk | Andrzej Piotrowski | Hypothetical tsunami deposits in the Rogowo area, Baltic Sea coast, North Poland |
| 15:45 - 16:00<br>11.6 talk | Shmulik Marco | Recognizing seiche and tsunami in lake sediments |

16:00 - 17:00 coffee break and poster session

17:00 - 17:45 K. Reicherter - Introduction into local geology

18:00 Departure for ship cruise and conference dinner

[18:30 Dinner at the AKNZ for those who do not participate in the ship cruise]

23:00 Return to AKNZ

## 12 October (SAT) - Scientific Talks and Poster Sessions, Keynote Lectures, wine tasting

7:00 - 8:30 Breakfast

**9:00 - 13:15 Key notes, poster session, talks**

9:00 - 11:00 Key note lectures and talks

| 12 October Saturday morning | Session Earthquake Triggered Mass Movements | Chaired by: H.-B. Havenith |
|---|---|---|
| 9:00 - 9:30<br>12.1 key note | Dave Petley | Towards an understanding of the controls on earthquake triggered landslides |
| 9:30 - 10:00<br>12.2 key note | Alexander Strom | Constraints and promises of earthquake-triggered landslides discrimination |
| 10:00 - 10:30<br>12.3 talk | Xuanmei Fan | Analysis of the distribution of landslides and landslide dams induced by the Wenchuan earthquake |
| 10:30 - 10:45<br>12.4 talk | Hans Balder Havenith | What we can learn from a blind-test for predicting earthquake-triggered landslides applied to the Wenchuan area, China – also for paleoseismological studies |
| 10:45 - 11:00<br>12.5 talk | Elisa Kagan | Seismites and mass movement events from the Dead Sea margins and depocentre |

11:00 - 11:15 break

11:15 - 13:15 key note lectures, talks

| 12 October Saturday morning | Session Society, Communication, Critical Facilities and Seismic Hazard Assessment | Chaired by: L. Guerrieri, T. Spies |
|---|---|---|
| 11:15 - 11:45<br>12.6 key note | Yoshi Fukushima | Contribution of Paleoseismology to Seismic Hazard Assessment for Nuclear Installations |
| 11:45 - 12:00<br>12.7 talk | Stéphane Baize | An outline of the geological contribution to seismic hazard assessment (SHA) for nuclear facilities |
| 12:00 - 12:15<br>12.8 key note | Rivka Amit | The use of paleoseismic data for seismic hazard evaluations of the Dead Sea Transform |
| 12:15 - 12:30<br>12.9 talk | Luigi Palumbo | Devising BDFA: a new active fault database conceived behind nuclear safety assessment in France |
| 12:30 - 12:45<br>12.10 talk | Ioannis Papanikolaou | Natural Hazards and Civil protection management framework in Greek local authorities: A questionnaire survey demonstrates why prevention fails |
| 12:45 - 13:00<br>12.11 | Luca Guerrieri | Fault Displacement Hazard in Italy: input for siting of critical facilities and land planning |

13:00 - 14:00 Lunch

**14:00 - 18:30 Key notes, poster session, talks**

14:00 - 15:00 guided poster session (Michetti)

| 12 October Saturday afternoon | Session Earthquakes, Earthquake Environmental Effects and Cascading Effects | Chaired by: F. Cinti, A. Michetti |
|---|---|---|
| 15:00 - 15:15<br>12.12 key note | Francesca Cinti | Earthquakes characteristics vs. natural, anthropic and social effects: a retrospective view from five years of M5+ in Italy |
| 15:15 - 15:30<br>12.13 talk | George Papathanassiou | Earthquake Geo Survey, an application for reporting Earthquake-Induced Environmental Effects |
| 15:30 - 15:45<br>12.14 talk | Pablo Silva | Earthquake environmental effects triggered by the 2011Lorca Event (Mw 5.2), Betic Cordillera, SE Spain): Application of the ESI-07 Scale |
| 15:45 - 16:00<br>12.15 talk | Michael Strasser | Lake sediments as natural seismographs: A compiled record of Late Quaternary earthquakes in Central Switzerland |
| 16:00 - 16:15<br>12.16 talk | Thomas Wiatr | Active bedrock fault scarps and the Terrestrial laser scanning: Insights into to active tectonics and seismic hazards |
| 16:15 - 16:30<br>12.17 talk | Alessandro Michetti | The ESI 2007 scale and the TechDoc |

16:30 - 17:00 break

17:00 - 18:30 talks

| 12 October Saturday evening | Session Paleoseismology | Chaired by: K. Reicherter, T. Rockwell |
|---|---|---|
| 17:00 - 17:15<br>12.18 key note | Young-Seog Kim | Slip distribution and compensation at fault damage zones: Its implications to fault evolution and earthquake hazard |
| 17:15 - 17:30<br>12.19 key note | Jim McCalpin | Heli Lidar mapping |
| 17:30 - 17:45<br>12.20 talk | Kris Vanneste | Paleoseismology of the Geleen fault, Lower Rhine Graben |
| 17:45 - 18:00<br>12.21 talk | Eric Salomon | Repeated folding during late Holocene earthquakes on the La Cal thrust fault near Mendoza City (Argentina) |
| 18:00 - 18:10<br>12.22 talk | Pablo Silva | Development of a numerical system and field-survey charts for earthquake environmental effects based on the Munsell Soil Color Charts |
| 18:10 - 18:20<br>12.23 advertise | Young-Seog Kim | 5$^{th}$ INQUA meeting BUSAN2014 |

18:30 dinner

**20:00 wine tasting event (bus transfer to Weingut Kriechel, or 2 km walk to the winery)**

## 13 October (SUN) - Scientific Talks and Debates, Closing Ceremony

7:00 - 8:30 Breakfast

# 8:00 check-out [important!]

**9:00 - 11:30 Key notes, poster session, talks**

| 13 October Sunday Morning | Session Paleoseismology | Chaired by I. Papanikolaou, Y.-S. Kim |
|---|---|---|
| 9:00 - 9:30<br>13.1 key note | Eldon Gath | The West Beverly Hills Lineament and Beverly Hills High School: An Unexpected Journey |
| 9:30 - 10:00<br>13.2 key note | Tom Rockwell | 4-D rupture histories of major plate boundary faults: a view into long-term fault behavior and fault interaction |
| 10:00 - 10:15<br>13.3 talk | Silke Mechernich | Rupture history and deformation cycle along the eastern Tohoku coastline (Japan) using coastal uplift, tsunami deposits and trenching at an aftershock location |

10:15 - 11:00 break and poster session

| 13 October Sunday morning | Session Paleoseismology | Chaired by: K. Vanneste, J. McCalpin |
|---|---|---|
| 11:00 - 11:15<br>13.4 talk | Jin-Hyuck Choi | Active tectonics around the Yangsan-Ulsan fault system in SE Korea (II): Fault zone analysis and fault evolution |
| 11:15 - 11:30<br>13.5 talk | Laurent Bollinger | Return period of great Himalayan earthquakes in eastern Nepal inferred from studies along the Patu and Bardibas strands of the Main Frontal Thrust. |
| 11:30 - 11:45<br>13.6 talk | Neta Wechsler | Pull-apart Basins as Fault Segment Boundaries – the case of the Sea of Galilee, Israel |

12:00 - 13:00 Lunch

**13:00 - 15:15 Key notes, poster session, talks**

| 13 October Sunday afternoon | Session Archeoseismology | Chaired by: S. Jusseret, M. Rodriguez-Pascua |
|---|---|---|
| 13:00 - 13:30<br>13.7 talk | Simon Jusseret | A new methodology for the critical assessment of earthquake related damages in archaeological context: a proof of concept for the 13th Century BC in Minoan Crete (Late Minoan IIIB) |
| 13:30 - 13:45<br>13.8 talk | Kazmer | "The rocking columns of Poreč - Archaeoseismology in the Istria Peninsula, Croatia |

13:45 - 14: 15 coffee break

| **13 October Sunday afternoon** | **Session Slow Active Faults** | **Chaired by: E. Hintersberger, P. Štěpančíková** |
|---|---|---|
| 14:15 - 14:30<br>13.9 talk | Petra Štěpančíková | Late Quaternary Activity of the Sudetic Marginal Fault in the Czech Republic: A signal of Ice Loading |
| 14:30 - 14:45<br>13.10 talk | Petr Špaček | Active tectonics in the West Carpathian Foreland: Nysa-Morava Zone and Upper Morava Basin System (Czech Republic) |
| 14:45 - 15:00<br>13.11 talk | Garcia Moreno | Seeking the source of the AD 1580 Dover-Strait/Pas-de-Calais earthquake (Western Europe). |

**15:00 - 15:30 Closing ceremony**

**15:30 bus transfer to Laacher SeeVolcanic Area, excursion natural hazards and critical facilities, then transfer to Simmerath, Hotel Paulushof (N 50°36'27.32" E6°23'3.95"), Seeufer 10, 52152 Simmerath/Rurberg**

19:00 Check-in

20:00 Dinner

## 14 October (MON) - excursion to Aachen

8:00 Breakfast

9:00 Excursion: Archeoseismology in Aachen

12:00 Time for individual sightseeing, lunch etc.

14:30 Excursion: Faults in Aachen and surroundings

18:00 bus transfer back to Hotel Paulushof

20:00 Dinner

## 15 October (TUE) - departure

8:00 Breakfast

9:00 check-out

9:15 bus transfer to Aachen Hauptbahnhof/main station

# Abstracts

INQUA Focus Group on Paleoseismology and Active Tectonics

paleoseismicity.org

# Identification of buried active structures with preliminary geophysical and morphotectonic analysis, at eastern Thessaly basin, Greece

*John Alexopoulos (1), Emmanuel Vassilakis (2), Spyridon Dilalos (1), Charilaos Pantelis (1), Taxiarchis Papadopoulos (1)*

(1) National and Kapodistrian University, Department of Geophysics & Geothermics, Athens, Greece. Email: jalexopoulos@geol.uoa.gr
(2) National and Kapodistrian University, Department of Geography & Climatology, Athens, Greece.

***Abstract:*** *Extensive ground fissures frequently occur within the eastern Thessaly basin, in central Greece and have been since 1989. This paper aims to give a preliminary explanation for their generation reasons by interpreting the results of a dense geophysical survey along the basin. This is combined with drilling data, as well as field work tectonic measurements, morphotectonic analysis and remote sensing data interpretation throughout the marginal areas of the basin. The gathering, homogenisation and organisation of different types of geo-data by using various GIS software packages led to the discovery of the alpine basement surface, which is covered by recent sediments, and possible structures that contributed to the development of the basin. The methodology of producing a 3D basement surface model and various lithology profiles across the basin, along with sediment isopach maps by combining surface with subsurface data, is described in this paper.*

***Key words****: Vertical Electric Sounding, subsurface structure, basin tectonic control, sub-surface basement map*

## INTRODUCTION

The disastrous phenomenon of aseismic ground fissure appearance is causing differential subsidence along the development axis of the eastern Thessaly basin and has been for many decades. The occurrence of several historical and contemporary earthquake events with epicentres in the broader area (Caputo, 1995) makes this area quite interesting to apply both classic and innovative research techniques.

The general orientation of the fissures (WNW-ESE) and their distribution along the basin axis (NW-SE), as well as the absence of surface structures because of the large thickness of recent sediments, led to a combined methodology including geophysical measurements and morphotectonic analysis. The results remain to be validated with gravity measurements, which are planned to be acquired during the next few months.

Vertical Electrical Soundings (VES) have been applied successfully to investigate geological-tectonic structures in other areas (Alexopoulos & Dilalos, 2010; Alexopoulos et al., 2001; Asfahani & Radwan, 2007; Caputo et al., 2003; Papadopoulos et al, 2007), and have also been combined with morphotectonic analysis (Asfahani et al., 2009). The latter is mainly used for analysing geomorphological structures by using elevation data but in any case when underground data; however, the same general techniques can be applied to underground data when subsurfaces can be identified (Vassilakis, 2006).

## STUDY AREA CHARACTERISTICS

The study area lies within the central part of mainland Greece. It is an elongated, NW-SE trending, flat basin developed to the west of a range consisting of the mountains Ossa, Mavrovouni and Pilion (from north to south). Further to the east, the North Anatolian Fault is merging with the North Aegean Trough (Papanikolaou et al., 2006), which seems to terminate at the eastern coast of the aforementioned mountain range (Fig.1) as first claimed by Caputo & Pavlides (1993).

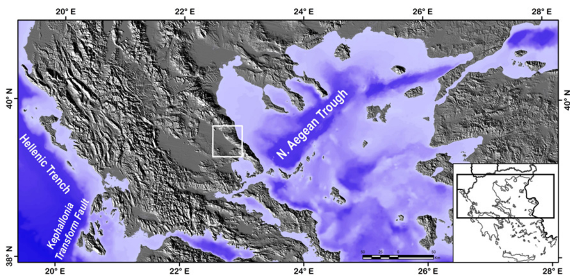


*Fig. 1: Morphological relief of the submarine (bluish) and continental (grey) central Greece. White rectangle shows the location of the area studied in this paper (magnified in Fig. 2) and the inset to the right shows the part of Greece, which is magnified in this figure.*

The alpine basement rocks, which crop out at the eastern and southeastern margins of the eastern Thessaly basin consist of metamorphic Gneiss, Marbles, Schists, Amphibolites and Ophiolitic bodies (Migiros & Vidakis, 1979). The westernmost marginal area is comprised of Neogene continental sediments, mainly conglomerates, covering alpine flysch and limestones. The tectonic contact between the metamorphic and non-metamorphic rocks lies buried under the Quaternary fluvial and lacustrine sediments of the basin (Fig.2).
For many years up until the 1960's a lake called "Karla" was present at the southeastern margin of the basin. This area has the lowest elevation and therefore all surface water collected there. During 1962 the intentional drainage of the lake was planned and undertaken, mainly because of medical (malaria) and agricultural reasons (Margaris et al., 2006). During 2000's

it was decided that a new artificial lake, more or less at the same location as the natural one, be constructed during an environmental enhancement of the area. After several years of construction a new reservoir of about 38.5 km$^2$ is now created.

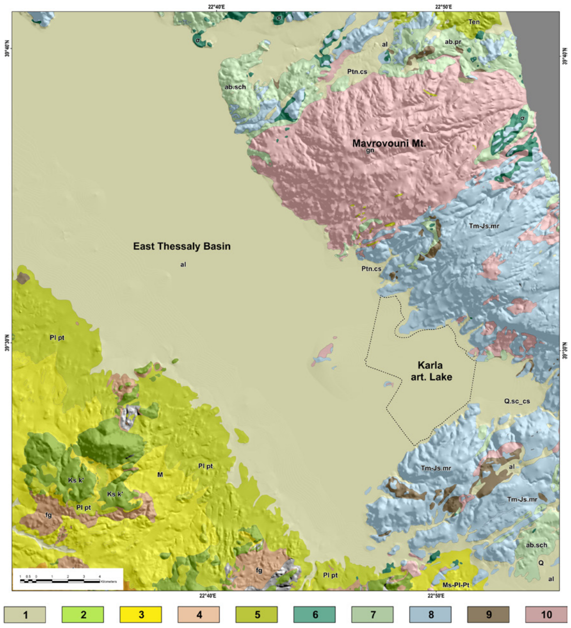


*Fig. 2: Simplified geological shaded relief map of the basin and its marginal area. Pale colours refer to Quaternary (1) Pleistocene (2) and Miocene (3) sediments, whilst intense colours refer to the alpine basement rocks, Flysch (4), Limestones (5), Ophiolites (6), Amphibolites (7), Marbles (8), Schistolites (9) and Gneiss (10). The dashed outline shows the borders of the recently filled artificial lake of Karla and west of it several basement rocks are cropping out in the middle of the basin.*

## METHODOLOGY AND RESULTS

### *Near surface geophysics*

A dense grid of 61 VES measurements (Schlumberger array) was designed and carried out covering the entire basin area. The main objective was to investigate the boundaries between the main sediment lithologies and the upper surface of the alpine basement rocks.

The geoelectrical measurement locations were distributed in the area, taking under consideration the outcrops of the basement rocks located in the marginal areas as well as at few locations inside the basin. The possible existence of a buried marginal, southwest dipping, normal fault zone at the easternmost basin area, covered by Quaternary deposits, was the most realistic case scenario for the geotectonic regime for this basin but the several basement outcrops especially in the southern central part of the basin weaken this theory a lot. Therefore the initial working hypothesis was the existence of a more complicated buried structure, comprised of several faults with various characters and trending orientations; all of them buried and impossible to be distinguished without dense subsurface investigation.

A resistivity survey was also chosen to be applied in the area, in order to investigate the stratigraphic structure of the subsurface geological formations, underlying the study area. The geoelectrical data included five (5) "in-situ" resistivity measurements on surface outcrops of the geological formations and fifty six (56) VES measurements. Additionally, data from thirty six (36) unpublished measurements, which were carried out during early 1970's were re-interpreted and re-evaluated, increasing the quantity of data for interpretation (Fig.3).

### *Geophysical-geological calibration*

In order to calibrate and better evaluate the geoelectrical results, which were collected from the VES survey, the five (5) "in-situ" resistivity measurements were carried out, on outcrops of basement rocks and more specifically on Gneiss, Marbles, Schists and Amphibolites.

These measurements contributed to a better understanding of the corresponding resistivity limits for each basement rock lithology. The interpretation of these results, revealed for marbles resistivity values of >2.000 Ohm.m and for the Gneiss 300-600 Ohm.m. Moreover, the measured resistivity for the Schists revealed values between 150-250 Ohm.m. A number of drill sections were also used for calibrating the resistivity measurements with depth, especially where the basement rock surface was encountered.

The main target of the geophysical survey was to investigate the stratigraphic structure of the subsurface geological formations, underlying the study area and determine the depth of the alpine formations (where possible). The geophysical data were processed by applying the automatic method of Zohdy (1989), composing a "multilayer" model. Beyond this, the commercial software package IX1D (v.3.5) of Interpex, was used in order to come up with the "layered" model.

In order to investigate the distribution of the geological formations in 2 dimensions, several geophysical geological sections were constructed with SE-NW and NE-SW directions, based on the measurements grid. Furthermore, based on the layered geophysical models and the preliminary geological interpretation, an effort was made to determine the depth of the alpine basement under the Quaternary deposits.

A gravity survey is planned in the near future for validating our results and combining them in an integrated study.

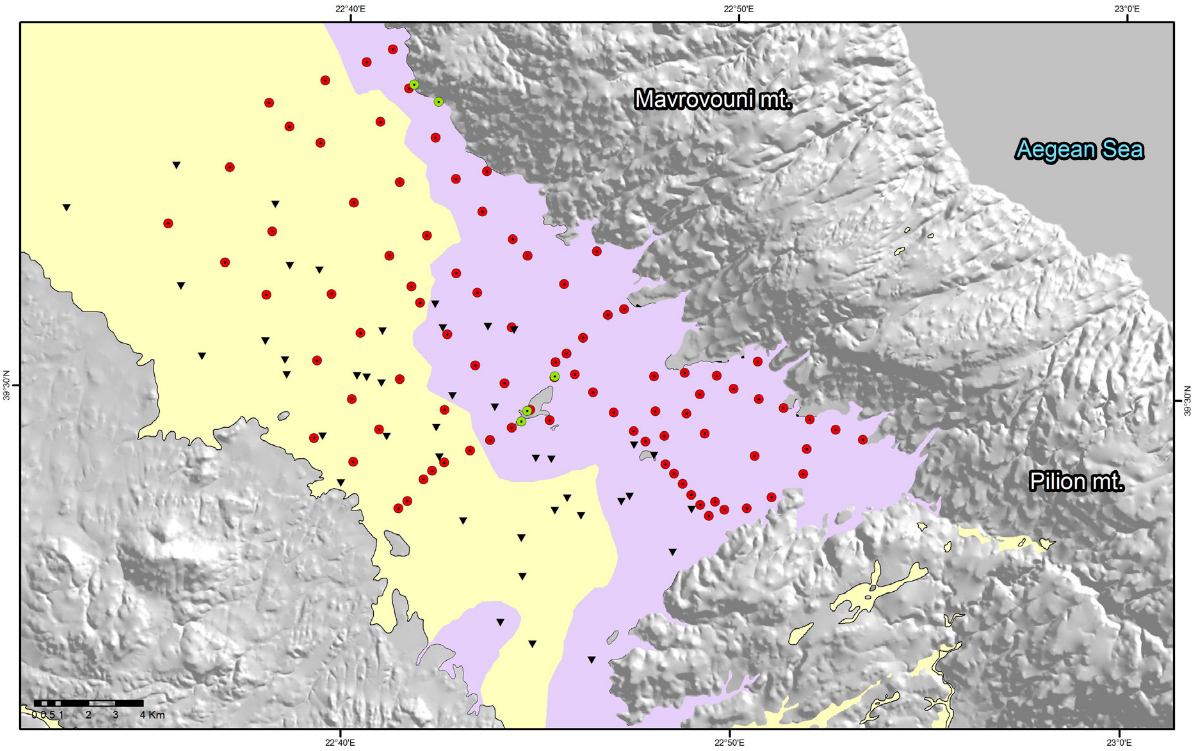


*Fig. 3: Location map of the VES measurements (red dots), In-situ resistivity measurements (green dots) and the boreholes (reverse triangles) the drill sections of which were used for the subsurface basement map. Only the Quaternary outcrops are displayed in colour as all the rest have been removed and replaced by a shaded relief. Purple color shows the areas where the alpine basement was found under the sediments at the depth of investigation.*

***Morphotectonics***

The geophysical part of the methodology revealed the basement rock surface covered by the recent basin sediments. The horizontal density and the vertical resolution of the resistivity measurements were essential in creating a lithological model for the entire study area. Additionally, the drill sections were simplified and also taken under consideration for improving the model and to extend it vertically, especially at locations where the VES signal did not penetrate specific horizons. Therefore, a subsurface map of the upper contact of the basement with the lower strata of the post-alpine sediments was created using GIS software packages such as ArcMap v.10 and ArcScene v.10.

Based on these data, a Digital Elevation Model (DEM) was created for the covered basement surface and combined with a DEM that was created from elevation data for the marginal areas, where the alpine rocks are cropping out. The single unified morphological pseudo-surface, which was synthesised, was used for further study by applying tectonic geomorphology indices and algorithms, in order to define potential blind fault zones that are buried beneath the basin material (Fig.4).

It is quite clear that the area where the alpine basement was found in relatively shallow depths (less than 250 meters), represents the gradual subsurface continuation of the eastern marginal outcrops. Two buried steep slopes, which can be attributed to southwest-dipping blind normal faults, could be identified at the shaded paleo-relief map of Fig.4. These seem to belong initially at the same fault zone, which was the main structure for the generation of eastern Thessaly basin. A third NE-SW trending structure has been probably activated at a later period and has laterally displaced the aforementioned marginal faults, separating them with a right slip movement mechanism.

**DISCUSION AND CONCLUSIONS**

The described methodology gave the opportunity to combine different techniques aiming to explain the appearance of disastrous ground fissures at residential and agricultural areas along the eastern Thessaly basin. The majority of the ground fissures are observed at areas where the thickness of the recent sediments is greater than the investigated depth (as the basement rocks were not found) and consequently this catastrophic phenomenon is highly related to the geotechnical characteristics of these lithological formations and the sudden change of underground water quantities. It would be worth to note that such characteristics as the porosity become cumulative and the greater the formation thickness is the larger amount of underground water can be stored by filling the vacuum. Consequently, over-pumping for agricultural use shrinks the aquifer and increases the vacuum mainly in between the fine grained horizons.

The systematic orientation of the ground fissures, even if the main cause seems to be the over-pumping and subsequently the compaction of several horizons due to the relatively sudden loss of the aquifer water, seems to be related to the large tectonic structures, which are buried under the quaternary formations.

Although no significant seismic activity has been observed in the intra-basin area, there are several clues implying that there are geodynamic procedures still going on. Based on the morphotectonic analysis the activity is concentrated more at the central area and not at its -more or less linear- margins. That is because it seems to be an asymmetric extensional basin, the active margin of which is dipping to the SW and the western margin is back-tilted towards the east along a major tectonic contact which is covered by the recent sediments.

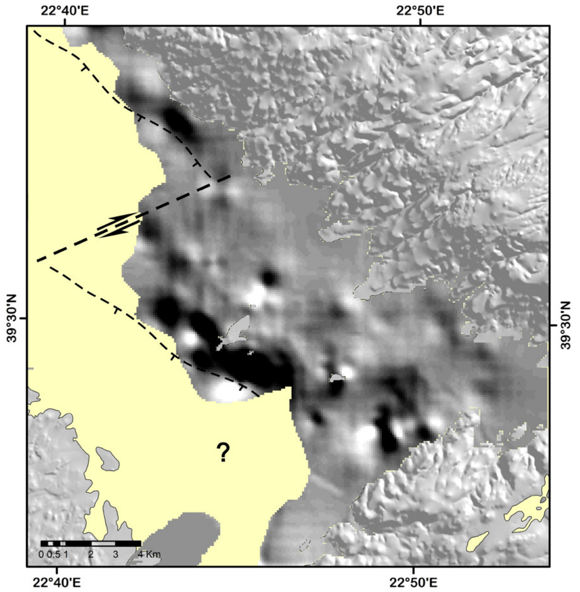


*Fig. 4: Pseudo-3D alpine basement map where the ENE-WSW trending dextral strike slip morpho-lineations seem to affect the covered alpine basement as well, by laterally displacing the extensional NW-SE trending normal faults. The question mark symbol shows lack of data at this preliminary phase of research.*

Nevertheless, several dextral strike slip tectonic structures trending WSW-ENE, possibly related to the northern branch of the active North Aegean Trough, can be identified across the marginal range by observing the shaded relief maps. This mountain range is the highest morphological relief between the basin and the trough, the tectonic influence of which seems to affect the range and fade away more westerly in the intra-basin area, as the palaeo-relief of the alpine basement extracted by geoelectrical measurements show. The dextral character of these cross cutting structures is clear either by examining the subsurface basement map or by observing the drainage network offset on each side of the morpho-lineaments that can be attributed to strike slip faulting. Nevertheless, almost horizontal striations on vertical fault surfaces were observed at marble outcrops located at the eastern marginal area, accompanied with kinematic indicators compatible with dextral movement.

**Acknowledgements:** The field work was co-funded by the Earthquake Planning and Protection Organisation (E.P.P.O.) 2009-2010 and the Special Account for Research Grants of UoA (70/4/7620, 10812). Significant improvements of this manuscript were made by taking under serious consideration the remarks of an anonymous reviewer, to whom the authors would like to express their appreciation.

## References

Alexopoulos, J.D. & S. Dilalos, (2010). Geophysical research for geological structure determination in the region of South Mesogheia (Attica). *Bulletin of the Geological Society of Greece*, XLIIII(4), 1898-1906.

Alexopoulos, J.D., J. Fountoulis, P. Kampouris, I. Mariolakos, I. & T. Papadopoulos, (2001). Geoelectrical survey for Tatoi (Athens, Greece) blind fault. *Bulletin of the Geological Society of Greece*, XXXIV(1), 121-127

Asfahani, J. & Y. Radwan, (2007). Tectonic Evolution and Hydrogeological Characteristics of the Khanaser Valley, Northern Syria, Derived from the Interpretation of Vertical Electrical Soundings. *Pure and Applied Geophysics*, 164(11), 2291-2311.

Asfahani, J., Y. Radwan, & I. Layyous, (2010). Integrated Geophysical and Morphotectonic Survey of the Impact of Ghab Extensional Tectonics on the Qastoon Dam, Northwestern Syria. *Pure and Applied Geophysics*, 167(3), 323-338.

Caputo, R., (1995). Inference of a seismic gap from geological data: Thessaly (Central Greece) as a case study. *Annals of Geophysics*, 38.

Caputo, R., & S. Pavlides, (1993). Late Cainozoic geodynamic evolution of Thessaly and surroundings (central-northern Greece). *Tectonophysics*, 223, 339-362.

Caputo, R., S. Piscitelli, A. Oliveto, E. Rizzo & V. Lapenna, (2003). The use of electrical resistivity tomographies in active tectonics: examples from the Tyrnavos Basin, Greece. *Journal of Geodynamics*, 36, 19–35.

Margaris, N., C. Galogiannis & M. Grammatikaki, (2006). Water management in Thessaly, central Greece, In: *Groundwater and Ecosystems* (Baba, A., Howard, K.F., Gunduz, O. eds.) Springer Netherlands, 237-242.

Migiros, G. & M. Vidakis, (1979). Geological Map of Greece, scale 1:50.000, sheet Agia, IGME, Greece.

Papadopoulos, T. et al., (2007). Tectonic Structure of Central-Western Attica (Greece) based on Geophysical Investigations-Preliminary Results. *Bulletin of the Geological Society of Greece*, XXXX(3), 1207-1218.

Papanikolaou, D., M. Alexandri & P. Nomikou, (2006). Active faulting in the North Aegean Basin, in: *Postcollisional tectonics and magmatism in the Mediterranean region and Asia* (Dilek, Y. & S. Pavlides, eds.). Geological Society of America Special Paper, 189– 210.

Vassilakis, E., (2006). Study of the tectonic structure of Messara basin, central Crete, with the aid of remote sensing techniques and G.I.S., PhD Thesis, National & Kapodestrian University of Athens, p. 546.

Zohdy, A.A.R., (1989). A new method for the automatic interpretation of Schlumberger and Wenner sounding curves. *Geophysics*, 54(2), 245-253.

INQUA Focus Group on Paleoseismology and Active Tectonics

paleoseismicity.org

# The 1033 A.D. earthquake: damages and kinematics from the archaeoseismic study at Hisham Palace (Jordan Valley, Dead Sea Transform Zone)

*Laura Alfonsi (1), Francesca R. Cinti (2), Guido Ventura(2)*

(1) INGV via di Vigna Murata, 605, 00143 Rome-Italy. laura.alfonsi@ingv.it
(2) INGV via di Vigna Murata, 605, 00143 Rome-Italy. francesca.cinti@ingv.it; guido.ventura@ingv.it

***Abstract:*** *A multidisciplinary approach merging archaeological information and geological data is employed at Hisham palace (724-743 A.D. – about 1400 A.D., Jordan valley sector of the Dead sea transform zone) to constrain the age of past earthquakes, identify the fault movement(s) and better define the tectonic setting of the area. Hisham palace, the main building of the Khirbet al-Mafjar archaeological site, records damages related to past seismic shaking. We analyse new coseismic data from field survey and historical pictures, critically revise the deformation pattern from literature, and review the "seismological" insights from archaeological excavations. The collected data allowed to identify the earthquake responsible for the damage at Hisham palace, recognize the possible seismogenic structure and its kinematics, contribute to reconstruct the past historical seismicity affecting the area during the palace occupation.*

***Key words***: *1033 A.D., earthquake, archaeology.*

## INTRODUCTION

The Hisham palace (724-743 A.D. – about 1400 A.D.; Baramki, 1936; Whitcomb, 1998) is the main building of the Khirbet al-Mafjar archaeological site (Jordan valley); it records damages related to past seismic shaking. The site is located within the tectonically active Dead Sea Transform zone on the western Jordan valley, and it is one of the most famous "desert castles" of the early Islamic period (Fig. 1). The 749 A.D. earthquake, whose macroseismic epicentre is unknown, is identified as the responsible for the severe damages at Hisham palace (Amiran et al., 1994). However, a relatively low (VII degree) macroseismic intensity is assigned at Hisham palace for this event, and surface faulting evidence have been found about 100 km north of Khirbet al-Mafjar (Marco et al., 2003). Reches and Hoexter (1981), found evidence for surface rupture relate to an 8th century event close to Jericho. Another earthquake occurred in the area could also have left traces on the palace architecture, i.e. the 1033 A.D. event (Table 1, Fig.1).

We bring together and analyse new data from field survey and historical pictures, critically revise the deformation pattern from literature, and review the "seismological" insights from archaeological excavations. The data and results allow us to (a) identify the earthquake responsible for the damage at Hisham palace, (b) recognize the possible seismogenic structure and its kinematics, (c) contribute to reconstruct the past historical seismicity affecting the area during the palace occupation, and (d) improve the knowledge of the seismotectonic setting of the Jordan valley.

## DAMAGE AND FAULTING AT KHIRBET AL-MAFJAR

The Dead Sea Transform zone (Fig. 1) is ca 1100 km long, N-S striking, left-lateral fault system representing the active boundary between the Arabian and African plates (Garfunkel et al., 1981). The N-S striking Jericho fault in the central sector of the Jordan valley, belongs to this system, has a prevailing strike-slip movement (Gardosh et al., 1990).

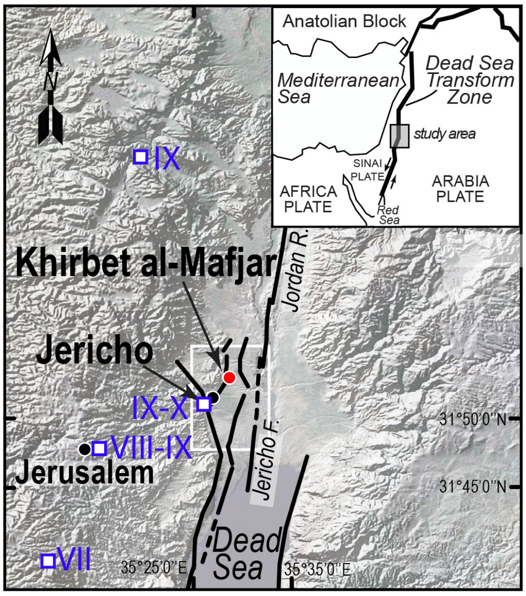


*Fig. 1: Geodynamic setting (inset) and schematic map of the Dead Sea Fault system in the Jericho valley. Macroseismic intensity of the 1033 A.D. earthquake occurred in the Khirbet area (data from Guidoboni and Comastri, 2005). Location of the archaeological site is reported.*

The ML 6.2, 1927 earthquake is the most recent event that caused damage and casualties in the Jericho settlement (Avni et al., 2002); large magnitude seismic events are documented in historical times (Guidoboni et al., 1994; Ambraseys, 2009).

Field data and available seismic lines show N-S to NNE-SSW striking sub-vertical faults bounding the eastern

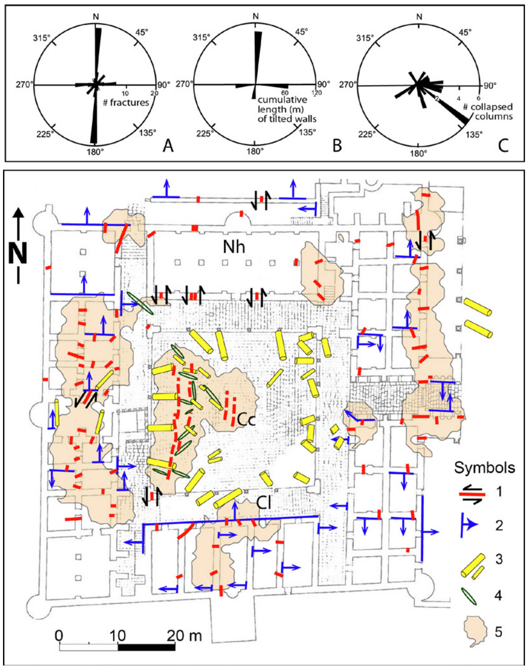

Fig. 2: Original plan of the palace modified from Hamilton (1959). Abbreviations: Nh: North hall; Cc: Central court; Cl: Cloister. Symbols: 1, crack and fault. Black arrow is the direction of movement; 2, tilting and warping of wall (arrow towards the direction of movement); 3, column of the ground floor (larger symbol) and of the first floor (smaller symbol); circle is the column top; 4, deformation of floor (sunk and popup); 5, fracture density (>1/8 m2). Insets: Rose diagram of (A) strike of fractures (B) direction of tilting vs. cumulative length of titled walls, (C) direction of column collapse.

edge of the uplifted Jericho block (Fig. 1; Lazar et al., 2006). The Khirbet al-Mafjar archaeological site is located 3 km north of Jericho.

The Palace is an Umayyad building with an almost regular squared plan and a court (Fig. 2; redrawn from Hamilton, 1959). The whole structure is built of two facing walls of calcarenite and limestone ashlar masonry with rubble filling. We executed a field survey and a new damage recognition at the palace also positioning images of the thirties (Matson and Matson, 1934-39; Baramki, 1936, 1942). Coseismic elements such as tilted structures, displaced walls and pavements, colonnade failure are summarized in Fig. 2, where about 70% of the data points are original from this study, and 30% are merged from previous analyses (Reches and Hoexter, 1981; Karcz and Kafri, 1981). The observed damage defines a severe earthquake scenario. Most of the brittle structures affects the supporting and divisor walls (Figs.

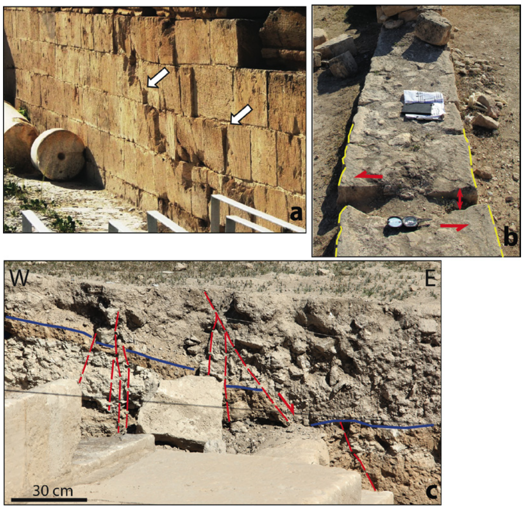

Fig. 3 a: Closely spaced faults with 10 cm left-lateral slips crossing the E-W oriented bearing wall of the North hall (view from Southeast). b: Mixed Mode I-II (open-shear) fracture of an E-W striking bearing wall (view from West). c: part of a 6-m-wide shear zone consisting of >50° dipping N-S striking fractures and faults (in red) outcropping on the north wall of an archaeological trench. Blue lines allow the eye to identify the displaced flood-related deposits. View from South.

2, 3a, b). These structures are faults and open cracks with dip generally >50° and width up to 20 cm. The faults offset archaeological structures with left-lateral slips up to 10 cm. Some structures with mixed shear (sinistral)-opening mode have been also recognized (Fig. 2-3a).

In the western portion of the pavement of the central court, roughly N-S striking cracks and vertical deformations occur (Fig. 2). The flagstones are deformed in a pop-up like array. These deformations have a linear continuity of about 30 m and align to the faults and shear-opening structures affecting the walls of the north and south cloister (Fig. 2). The fractures at Hisham palace have a preferred N-S strike and a second-order E-W strike (inset A in Fig. 2). Fracture density (shaded pale orange areas in Fig. 2) evidences two roughly N-S elongated sub-parallel areas located on the western side of Hisham palace, and one, also N-S elongated, in the eastern side. At about 50 m north of the north hall area, we observed a 6-m-wide shear zone consisting of high angle fractures and faults exposed on the northern wall of an archaeological trench (Fig. 3c).

The vertical displacement across this zone is of the order of tens of centimeters. No data are available to strictly constraint the age of faulting. The plaster and the drainage channel close to the trench wall are affected by fracturing aligned with the deformed zone.

Several walls are tilted and/or warped up to 15° (Figs. 2). Inset B in Fig. 2 shows the cumulative length of tilting, whose preferred sense is North. The occurrence of this preferred sense of tilting confirms the seismic nature of the observed damage (Paz, 1997). The overall position of the failed columns has been reconstructed from original reports and pictures and it is reported in Fig. 2. Most of colonnade collapses cluster mainly towards the south-eastern quadrant (inset C in Fig. 2). The direction of column failure is due to the traction effect of the first floor collapse.

**EARTHQUAKE TIMING**

The archaeological data testify an uninterrupted occupancy from 8th century until 1000 A.D. of the Hisham palace (Whitcomb, 1981). Therefore, if earthquakes occurred in this time period, the effects should not have implied a total destruction or remarkable occupancy contraction or abandonment. Toppled walls and columns in the central court cover debris containing 750-850 A.D. old ceramic shards (Whitcomb, 1981). Recently unearthed collapses north of the court confirm a widespread destruction after the 8th century (i.e.http://www.jerichomafjarproject.org). These elements support the action of a destructive shaking event at the site later than the 749 A.D. earthquake, even though this latter could had affected the Palace. The two well-constrained, major historical earthquakes recognized in the southern Jordan valley are the 749 and 1033 A.D. We assign a IX-X intensity degree to the here recorded Hisham palace damages, whereas a VII degree has been attributed to the 749 A.D. earthquake at the site (Marco et al., 2003). Furthermore, Whitcomb (1981) defines an increment of occupation of the palace between 900 and 1000 A.D. followed by a successive occupation in the 1200-1400 A.D. time span. On the basis of the above, and because no pottery remains are instead associated to the 1000-1200 A.D. period at Hisham palace (Whitcomb, 1981), we suggests a temporary, significant contraction or abandonment of the site as consequence of a severe destruction in the 11th century.

We propose the 1033 A.D. earthquake as the causative event for the Hisham destruction, also according with the known macroseismic pattern (Fig. 1; Guidoboni and Comastri, 2005). This event provoked heavy damage with loss of life and collapses at Jericho (Ambraseys, 2009), only 3 km apart from Hisham. The scenario related to this earthquake is fully consistent with the one we reconstructed at Hisham palace.

**SEISMOTECTONIC CONSIDERATIONS**

The preferred sense of tilting of the Hisham walls and

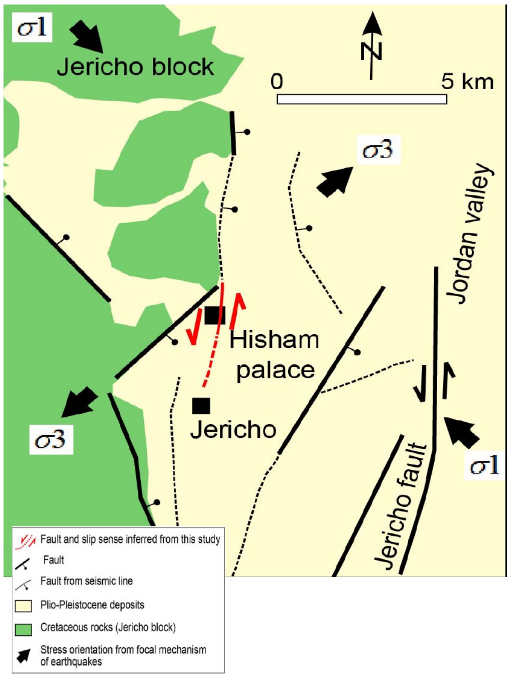


*Fig. 5: Structural sketch and stress field configuration at the Hisham palace surroundings (data from Hofstetter et al., 2007 and Lazar et al., 2006). Red line and arrows represent the co-seismic rupture and the slip related to the 1033 A.D. event inferred from this study.*

the colonnade collapse direction indicate, according to structural dynamic models by Paz (1997) and Hinzen (2009) on inelastic, inertial structures, a ground shaking by seismic waves coming from the Northern quadrant. Although the cause of most of the earthquake-induced damage at Hisham palace is ground shaking, some of the mapped features have a clear tectonic origin.

These features include (a) left-lateral faults, (b) N-S to NNE-SSW striking fractures and cracks, (c) alignments of fractures, up to 30 m long, crossing the whole palace, formed during the 1033 A.D earthquake, and (d) a 6 m wide N-S to NNE-SSW striking shear zone affecting the ground in the northern area of the palace. All these data define a syn- and post-1033 A.D. brittle deformation zone. This zone may represent the southern prolongation of the N-S striking, sub-vertical fault recognized by field and seismic data (Fig. 5). This fault accomplishes the deepening of the Jericho syn-tectonic sedimentary basin. The prevailing left-lateral slips recognized at Hisham palace along N-S to NNE-SSW striking structures are fully consistent with the strike-slip stress regime of the Jordan area of the Dead Sea fault system, which is characterized by a NW-SE sub-horizontal $\sigma 1$ (Fig. 5; Hofstetter et al., 2007). We conclude that the 1033 A.D. earthquake originates within this stress field.

## CONCLUSIONS

Khirbet al-Mafjar provides the rare opportunity to study the combined effects of seismic shaking and tectonics on an archaeological site, and to interpret these effects within a coherent seismotectonic setting. The damage scenario at Hisham palace is mostly produced by a single, strong earthquake as derived from the archaeological and field datum. The damage at Hisham indicates a minimum IX-X intensity degree for the destructive event. This latter datum when combined with the archaeological stratigraphy converge to the 1033 A.D. event as the cause of the severe and widespread damage at the site. The event occurred in an area located north of Jericho and Khirbet al-Mafjar and the probable causative fault is N-S to NNE-SSW striking, with a left-lateral strike-slip kinematic, extending North of Hisham. The fault kinematics at Hisham is fully consistent with the strike-slip stress regime acting at regional scale in the southern Jordan valley.

**Acknowledgments:** We are grateful to the Italian archaeological mission to Jericho (University La Sapienza, Rome) for on-site logistics and discussions.

## References

Ambraseys, N.N. (2005). The seismic activity in Syria and Palestine during the middle of the 8th century; an amalgamation of historical earthquakes. *Journal of Seismology* 9, 115-125.

Ambraseys, N.N. (2009). *Earthquake in the Mediterranean and in the Middle East. A Multidisciplinary Study of Seismicity up to 1900*. Cambridge University Press. 968 p.

Amiran, D.H.K., E. Arieh, & T. Turcotte (1994). Earthquakes in Israel and adjacent areas: Macroseismic observations since 100 B.C.E. *Israel Exploration Journal* 44, 260–305.

Avni, R., D. Bowman, A. Shapira, & A. Nur (2002). Erroneous interpretation of historical documents related to the epicenter of the 1927 Jericho earthquake in the Holy Land. *Journal of Seismology* 64, 469-476.

Baramki, C. C. (1936). Excavation at Khirbet el Mefjer. *Quarterly of the Department of Archaeology of Palestine* 5, 132-138.

Baramki, C. C. (1942). Excavation at Khirbet el Mefjer. *Quarterly of the Department of Archaeology of Palestine* 8, 153-159.

Gardosh, M., Z. Reches, & Z. Garfunkel (1990). Holocene tectonic deformation along the western margin of the Dead Sea. *Tectonophysics* 180, 123–137.

Garfunkel, Z., I. Zak, & R. Freund (1981). Active faulting in the Dead Sea rift. *Tectonophysics* 80, 1-26.

Guidoboni, E., A. Comastri, & G. Traina (1994). *Catalogue of ancient Earthquakes in the Mediterranean area up to the 10th Century*. SGA editorial Production.

Guidoboni, E., & A. Comastri (2005). *Catalogue of Earthquakes and Tsunamis in the Mediterranean Area from the 11th to the 15th Century*. INGV-SGA, Bologna. 1037 p.

Hamilton, R.W. (1959) Khirbat al-Mafjar: An Arabian Mansion in the Jordan Valley. *Oxford Clarendon*. 352 p.

Hinzen, K.G. (2009). Sensitivity of earthquake-toppled columns to small changes in ground motion and geometry. *Israel Journal of Earth Sciences* 58, 309-326.

Jericho Mafjar Project (2013). The Oriental Institute at the University of Chicago, http://www.jerichomafjarproject.org (January 2013).

Karcz I. & U. Kafri (1981). Studies in Archeoseismicity of Israel: Hisham's Palace, Jericho. *Israel Journal of Earth Science* 30, 12-23.

Lazar, M., Z. Ben-Avraham, & U. Schattner (2006). Formation of sequential basins along a strike–slip fault. Geophysical observations from the Dead Sea basin. *Tectonophysics* 421, 53-69.

Marco, S., M. Harta, N. Hazan, L. Lev, & M. Stein (2003). Archaeology, history, and geology of the A.D. 749 earthquake, Dead Sea transform. *Geology* 31, 665-668.

Matson, G.E., & E. Matson (1934-39). Photograph Collection, Library of Congress, Prints and Photograph Division. http://www.loc.gov/pictures/collection/matpc/ (December 2012).

Paz, M. (1997). *Structural Dynamics-Theory and Computation*. Chapman & Hall.

Reches, Z., & D.F. Hoexter (1981). Holocene seismic and tectonic activity in the Dead Sea. *Tectonophysics* 80, 235-254.

Russell, K.E. (1985). The earthquake chronology of Palestine and northwest Arabia from the 2nd through the mid-8th century A.D. *American School of Oriental Research Bulletin* 260, 37-60.

Wdowinski S., Y. Bock, G. Baer, L. Prawirodirdjo, N. Bechor, S. Naaman, R. Knafo, Y. Forrai & Y. Melzer (2004). GPS measurements of current crustal movement along the Dead Sea Fault. *Journal of Geophysical Research* 109 (B5), 1-16.

Whitcomb, D. (1998). Khirbet al-Mafjar Reconsidered: the Ceramic Evidence. *Bulletin of the American Schools of Oriental Research* 271, 51-67.

# The use of paleoseismic data for seismic hazard evaluations of the Dead Sea Transform

*Rivka Amit, Yariv Hamiel, Oded Katz, Ezra Zilberman, Benjamin Z. Begin*

Geological Survey of Israel, 30 Malkhei Israel St., Jerusalem, 95501, Israel. E-mail: rivka@gsi.gov.il

***Abstract:*** *Synthesis of paleoseismic data of several segments along the Dead Sea Transform (DST) show that each has a specific pattern of large earthquake distribution. During the last 20 ky the segments of the Arava and the Jordan valley have recurrence intervals of large events of about 1 ky while in the Hula valley the recurrence interval is 0.35 ky and 3-5 ky in the Dead Sea segment. However, beside the differences between the segments some similarities can be shown, especially in the large time frame. At least two segments, the Arava and the Dead Sea, show a similar change in earthquake pattern over time. In both segments the probability of a large earthquake (M≥6) occurring decreased gradually with time over the last 100 ky. In the southern Arava the magnitude range of earthquakes that occurred between 80 ka and 20 ka is M6.7 - M7 with average recurrence intervals of 2.8±0.7 ky, whereas the magnitude range during the last 20 ky is M5.9 - M6.7 with average recurrence intervals of 1.2±0.3 ky. In addition, over the last 100 ka the magnitude of the large events along the Dead Sea Transform ranges mainly between M5.9 and M7.5. It appears that there is an upper limit to the magnitude of the events that can be produced by the DST. It is suggested that this magnitude limit is an inherent characteristic of the DST which is controlled by the structure and the dimension of its segments. Integration of paleoseismic and historical records of strong earthquakes of the DST segments show that they all lie on the linear extrapolation of the frequency–magnitude relation of the instrumental record. The calculated b-values for the segments are between 0.85 and 1, similar to other major strike-slip faults in the world. It is concluded that the Gutenberg–Richter distribution is a stable mode in the tectonic setting of the Dead Sea fault during the past 60,000 yr. These results can be used as a basis for seismic hazard evaluations for this region.*

# An outline of the geological contribution to seismic hazard assessment (SHA) for nuclear facilities

*Stéphane Baize (1), Oona Scotti (1)*

(1) Institut de Radioprotection et de Sûreté Nucléaire, BP 6, 92262 Fontenay-aux-Roses, France. Stephane.baize@irsn.fr

***Abstract:*** *Herein, we present an outline of the contribution of geology and paleoseismology to seismic hazard assessment (SHA). The recent catastrophe at the Fukushima Nuclear Power Plants (NPPs) caused by the combination of an earthquake (EQ) and the resulting tsunami drastically reminds that "unexpected and extreme" seismic scenarios could occur and induce dramatic effects on insufficiently protected nuclear facilities. With several other examples, we emphasize that such strong scenarios sometimes could have been anticipated by accounting for available geological data. Many existing NPPs were licensed early on in the "earthquake geology" history. Detailed geological investigations should be performed around each site, to ensure that the safety of these existing reactors is not at stake concerning the potential presence of active/capable faults. During the siting process, field studies of faults play thus a primary and crucial role. The paleoseismological community faces big challenges to contribute to nuclear siting in providing to decision-makers the best constrained and reliable data and interpretations.*

***Key words***: *geology, paleoseismology, seismic hazard assessment, nuclear facilities*

## GENERAL CONSIDERATIONS ON GEOLOGICAL DATA IN SHA FOR NUCLEAR SAFETY

Geological data are used in seismic hazard assessment to define and describe the earthquake sources, both zones of diffuse seismicity and active faults. Seismic hazard assessment (SHA) implicitly covers 2 issues related to seismotectonics and earthquake (EQ) geology, which require distinct engineering strategies of mitigation: seismic ground shaking and surface faulting. In nuclear industry, geological data are basically of crucial significance for seismic hazard assessment (e.g. NRC, 2007; IAEA, 2010). They range from regional structural and large-scale data to local paleoseismological evidences. The very high level of safety required for critical facilities entails the exploration of low probabilities of exceedance of a certain natural hazard level (corresponding to a very low probability of damage). Exploring several thousands to tens of thousands years backwards in time can only be performed through geology, especially in intraplate regions where the time scale spanned by recorded and historical seismicity is too short and far from representing the earthquake cycle.

Two complementary approaches are used in SHA for nuclear safety (IAEA, 2010). The deterministic approach is based on the selection of a specific scenario. For example, in France, the scenario is inspired by the strongest earthquake known in the seismotectonic zone. The probabilistic approach considers all possible scenarios (up to some "maximum magnitude" to be defined) weighted by both their probability of occurrence and the surface of each seismotectonic zone. This approach is today widely applied in the world. Depending on the target probability of interest and the level of knowledge of the site, one method or the other will lead to higher seismic levels. However, despite their different hypotheses, procedures and objectives, these 2 methods are based on the same and crucial geological data such as large-scale geophysics, structural geology, neotectonic and seismotectonic catalogues.

## SURPRISE EQs AND RESPONSE TO THE FUKUSHIMA CATASTROPHE

In recent times, the Northridge (1994) and Darfield/Christchurch (2010-2011) earthquakes were "surprising" events for most scientists, in the sense that geological evidences of source faults were unknown (USGS, 1996; GNS, 2012). Conversely, other earthquakes occurred on well-known faults but society and part of the scientific community seemed also unaware of the hazard and the surprise came either from the high magnitudes of the events (e.g. Sumatra 2004, Sichuan 2008, Tohoku, 2011), or from the level of damages and the "old" age (several hundred years) of past damaging earthquakes associated with the source faults (e.g. L'Aquila 2009, Haiti 2010, Lorca 2011).

Nonetheless, considering existing geological datasets and calling for realistic models, such scenarios could have been anticipated (see for instance discussion by Stein et al., 2012). Previous data or subsequent discussions about the above examples can be found in McCaffrey (2007) for Sumatra 2004, Kirby et al. (2008) for Sichuan 2008, Manaker et al. (2008) for Haiti (2010), Pace et al. (2006) for L'Aquila 2009, Masana et al. (2004) for Lorca 2011. If the strength of the Tohoku EQ (2011) was unexpected for some (see for example ERC, 2005), for others (e.g. Stein et al., 2012) some existing data could have supported the occurrence of past larger earthquakes. This Tohoku EQ severely showed that extreme seismic scenarios could occur and induce dramatic effects on insufficiently protected nuclear facilities. Following this severe accident, a continental-scale effort was asked by the European Council to the national nuclear agencies and operators, in order "*to assess how nuclear installations can withstand the consequences of various extreme external events*" and test the robustness of facilities beyond their design. In the first phase of these "stress tests", national authorities concluded that NPPs could withstand with sufficient margins seismic events beyond their design (ENSREG, 2012). However, due to the tight time-schedule, these stress tests were performed without new geological investigations (e.g. in Spain and France) to assess the potentiality of faults near the NPPs. In the framework of further improvements, IRSN (scientific support of the French Authority ASN) carries out new investigations on active faults and explores both deterministic scenarios and probabilistic calculations, which involve geological data (e.g. active fault size). In Spain, the safety authority (CSN) plans to include active faults in further SHA. In the USA, the Fukushima accident led the authority (Nuclear Regulatory Commission, NRC) ordering operators to perform significant analyses (e.g. mitigation strategies to enhance the capability to maintain plant safety during a prolonged loss of electrical power) (NRC, 2013). In addition, the NRC expects in the next years (2014 in Central Eastern US; 2015 in Western US) new evaluations of seismic hazard on the basis of present-day data, "*to determine if plant structures, systems, and/or components need to be updated to protect against the new hazard*".

## SEVERAL EXAMPLES OF ACTIVE FAULTS CLOSE TO NPPs

For future siting of nuclear facilities, we claim that advances in earthquake geology (albeit a relatively new and growing discipline of Earth sciences) are sufficient in terms of concepts, tools and methods to provide the basis for a reliable characterization of earthquake sources to be used in SHA (ground shaking and surface faulting). The US (NRC, 2007) and international (IAEA, 2010) guidelines both recommend to search for an alternative site when a fault capable to generate surface displacement is identified in the vicinity (less than 5 km) of a new reactor project. For existing nuclear reactors, the strategy is to evaluate the surface displacement hazard, either through probabilistic methods (NRC, 2007; IAEA, 2010) or numerical simulations (Japan; see Okumura, 2010).

Examples of active/capable faults discovered after the licensing of reactors in both "intraplate" and "interplate" parts of the USA are discussed in McMullen (1991). More recently, several paleoseismological investigations were carried out on faults bordering the Los Alamos site (New Mexico) (e. g. McCalpin, 2005). In California, the Shoreline fault has been discovered at a few hundred meters offshore from the Diablo Canyon NPP, late in the site history (P&GE, 2011). Other cases are reported in Europe, like in Slovenia (Krsko NPP: see URSJV, 2013) or in Asia, like in Korea (Weolsung NPP: see Kim et al., 2011). These findings generally lead to the need for a reassessment of both seismic motion and surface faulting issues (e.g. NRC, 2012 for Diablo Canyon NPP). For the latter issue, these findings are treated thanks to the so-called Probabilistic Fault Displacement Hazard Analysis (PFDHA). This method requires a significant set of data concerning all the potential capable faults that could affect the reactor site, as well as robust empirical attenuation relations of displacement vs distance to fault adapted to the site (e.g. Petersen et al., 2011). Examples of these evaluations were performed in the USA for the Los Alamos site (USDE, 1999) and the Diablo Canyon NPP (NRC, 2012). In Japan, after the Chuetsu-Oki (2007) and Tohoku (2011) earthquakes, the reassessment of Japanese NPPs was fed by new and in-depth geological studies, including geophysical and paleoseismological investigations (e.g. Sato et al., 2010; Okumura, 2010; NRA, 2012; Asahi Shimbun, 2013). Japanese nuclear operators and safety authority are currently debating on the "surface faulting issue" today which affects five sites (NRA, 2012; Cyranoski, 2012). We present in figure 1 the Ohi NPP case where potentially secondary structures are suspected to be active beneath the site.

## CHALLENGES AHEAD

Because of the economic and safety challenges, the presence of an active/capable fault near a nuclear site (existing or planned) leads to rough and delicate discussions between scientists (and also between scientists and decision-makers in some cases). This is especially the case when dealing with surface faulting (or capable fault) issue because it may constitute an avoidance criterion or even an exclusion criterion. As illustrated by recent examples (e. g. Tsuruga NPP in Japan, Krsko NPP in Slovenia), the fundamental source of debate lies in the geological interpretations and criteria used to define the capability of a fault. More often than not, there is room for interpretation because the available geological data is sparse. Interpretations can thus vary between experts when it comes to deciding:

- What is the nature of observed deformations, are they tectonic/non-tectonic in origin? Are they coseismic or aseismic in origin? Are they primary, secondary or triggered features?
- Which are the dates of the most recent deformed and oldest non-deformed deposits? What does the age of deformation represent with respect to the seismotectonic context?

Furthermore, based on engineering considerations, the final decision about site suitability lies in the hands of the safety authority, who needs to decide which is the acceptable distance-to-site/surface-displacement threshold that guarantees safety.

In siting assessment, field studies of faults have therefore a primary and crucial role. The scientific community faces big challenges to contribute to nuclear siting in providing to decision-makers the best constrained and reliable data and interpretations. One can emphasize that paleoseismological experts involved in capable fault studies must use suitable techniques, adequately design the investigations, provide the best informed judgment and hopefully reduce the uncertainties in the final results and conclusions. At the end, uncertainties are sometimes considered in a conservative way. For instance, the NRC have concluded that the GETR site (California) had to be designed to withstand surface faulting as large as 3 m, even if a definitive interpretation could not be given about the observed deformations, either due to a gravitational landslide or to a tectonic fault (McMullen, 1991). The on-going debate in Japan for the Tsuruga site case (see Asahi Shimbun, 2013 and Yomiuri Shimbun, 2013) illustrates the significance of the "age" criterion. Actually, the conclusion regarding the capability of the fault running beneath the reactors depends on the precise age of the non-deformed layer overlying the fault. The licensee concludes that the fault is not capable because it is sealed by a 120/130 ka-old layer, which is the yardstick age in the Japanese regulation. In the USA, this yardstick age for defining capability is set at 50 ka (for a single event) or 500 ka (for recurring events) (NRC, 2007). Because of the worldwide variability of seismotectonic context, the international guidelines (IAEA, 2010) extend the time span reference to longer geological periods (e.g. Quaternary) which may be more representative of the seismic cycle in intraplate and cratonic areas. This crucial point needs to be thoroughly assessed by geologists in each specific case study.

## CONCLUSIONS

We emphasize that increasing the geological dataset can improve the SHA, especially for nuclear safety, and provide a more comprehensive estimate of uncertainties. Future nuclear sites, for instance in "newcomer" countries, should be investigated in detail before building, because finding out a capable/active fault after licensing at a short distance (less than 25 km) can lead to significant and expensive investigations, analyses, discussions and delays of operation. In nuclearized countries, many NPPs were licensed early in the "earthquake geology" history and a serious updating can be expected in the near future.
From the regulatory point of view, an international panel of experts is writing on behalf of the International Agency (IAEA) a technical document on the use of paleoseismology for nuclear siting purposes. This document will provide methodological tools to licensees for their paleoseismological investigations, specify the necessary investigations to successfully achieve such fieldworks, describing case studies and mentioning uncertainties associated with paleoseismological methods for their inclusion in SHA.

## References

AIST (2013). *Active fault database of Japan*. Available at http://riodb02.ibase.aist.go.jp/
Asahi, S., (2013). NRA: *Tsuruga nuclear plant sits on top of fault*. 22 May 2013. Available at http://ajw.asahi.com/.
Cyranoski D. (2012). Quake fears rise at Japan's reactors. *Nature* 494, 14-15.
ENSREG (2012). *Country Specific Reports*. Available at http://www.ensreg.eu/EU-Stress-Tests/
ERC (2005). Report from the Earthquake Research Committee, Headquarters for Earthquake Research Promotion: *National Seismic Hazard Maps for Japan*. Available at http://www.jishin.go.jp/.
GNS (2012). *2010 Darfield (Canterbury) Earthquake*. Available at http://www.gns.cri.nz/.
IAEA (2010). Seismic Hazards in Site Evaluation for Nuclear Installations. *Specific Safety Guide, SSG-9*. Available at http://www-pub.iaea.org/.
Kim S., J.H. Kihm & K. Jin, (2011). Interpretation of the rupture history of a low slip-rate active fault by analysis of progressive displacement accumulation: an example from the Quaternary Eupcheon Fault, SE Korea. *Journal of the Geological Society of London* 168, 273-288.
McCaffrey, R., (2007). The next great earthquake. *Science* 315, 1675-1676.
McCalpin, J., (2005). Late Quaternary activity of the Pajarito fault, Rio Grande rift of northern New Mexico, USA. *Tectonophysics* 408, 213–236.
McMullen, R., (1991). Selected case histories of the application of the nuclear regulatory commissions; geologic and seismic siting criteria. *NUREG*. Available at http://pbadupws.nrc.gov/ .
NRA (2013). *Technical reports about Ohi and Tsuruga NPP*. Available at http://www.nsr.go.jp/ (in Japanese).
NRC (2007). *A Performance-based approach to define the site-specific earthquake ground motion. REGULATORY GUIDE 1.208*. Available at http://www.nrc.gov/.
NRC (2012). Confirmatory Analysis of Seismic Hazard at the Diablo Canyon Power Plant from the Shoreline Fault Zone. *Research Information Letter* 12-01. Available at http://pbadupws.nrc.gov/.
NRC (2013). *Japan Lessons Learned*. Available at http://www.nrc.gov/reactors/operating/ops-experience/japan-dashboard.html.
Okumura, K., (2010). Evaluation of near-site active faults and effects on the site based on geological structures. *First Kashiwazaki International Symposium on Seismic Safety of Nuclear Installations*, November 25, 2010. Available at http://www.jnes.go.jp/seismic-symposium10/
Petersen, M.D., T.E. Dawson, R. Chen, T. Cao, C.J. Wills, D.P. Schwartz & A.D. Frankel, (2011). Fault Displacement Hazard for Strike-Slip Faults. *Bulletin of the Seismological Society of America* 101, 805-825.
PG&E (2011). *REPORT ON THE ANALYSIS OF THE SHORELINE FAULT ZONE, CENTRAL COASTAL CALIFORNIA*. Report to the U.S. Nuclear Regulatory Commission. Available at http://www.pge.com
Sato H., S. Abe & N. Kato, (2010). Deep seismic profiling for imaging earthquake source faults in the Niigata basin, central Japan. *First Kashiwazaki International Symposium on Seismic Safety of Nuclear Installations*, November 25, 2010. Available at http://www.jnes.go.jp/seismic-symposium10/
URSJV (2013). O POTRESNI VARNOSTI NEK (*The seismic safety of NEK NPP*). Available at http://www.ursjv.gov.si/si/info/posamezne_zadeve/o_potresni_varnosti_nek/
USDE (1999). *FINAL SUPPLEMENT ANALYSIS for Pit Manufacturing Facilities at Los Alamos National Laboratory, Stockpile Stewardship and Management Programmatic Environmental Impact Statement*. DOE/EIS-0236/SA-6. Available at http://energy.gov/sites/
USGS (1996). USGS Response to an Urban Earthquake: Northridge '94. *Open-File Report 96-263*. Available at http://pubs.usgs.gov/of/1996/ofr-96-0263/.
Yomiuri, S., (2013). NRA must reexamine active fault assessment at Tsuruga N-plant. 13 July 2013. Available at http://the-japan-news.com/.

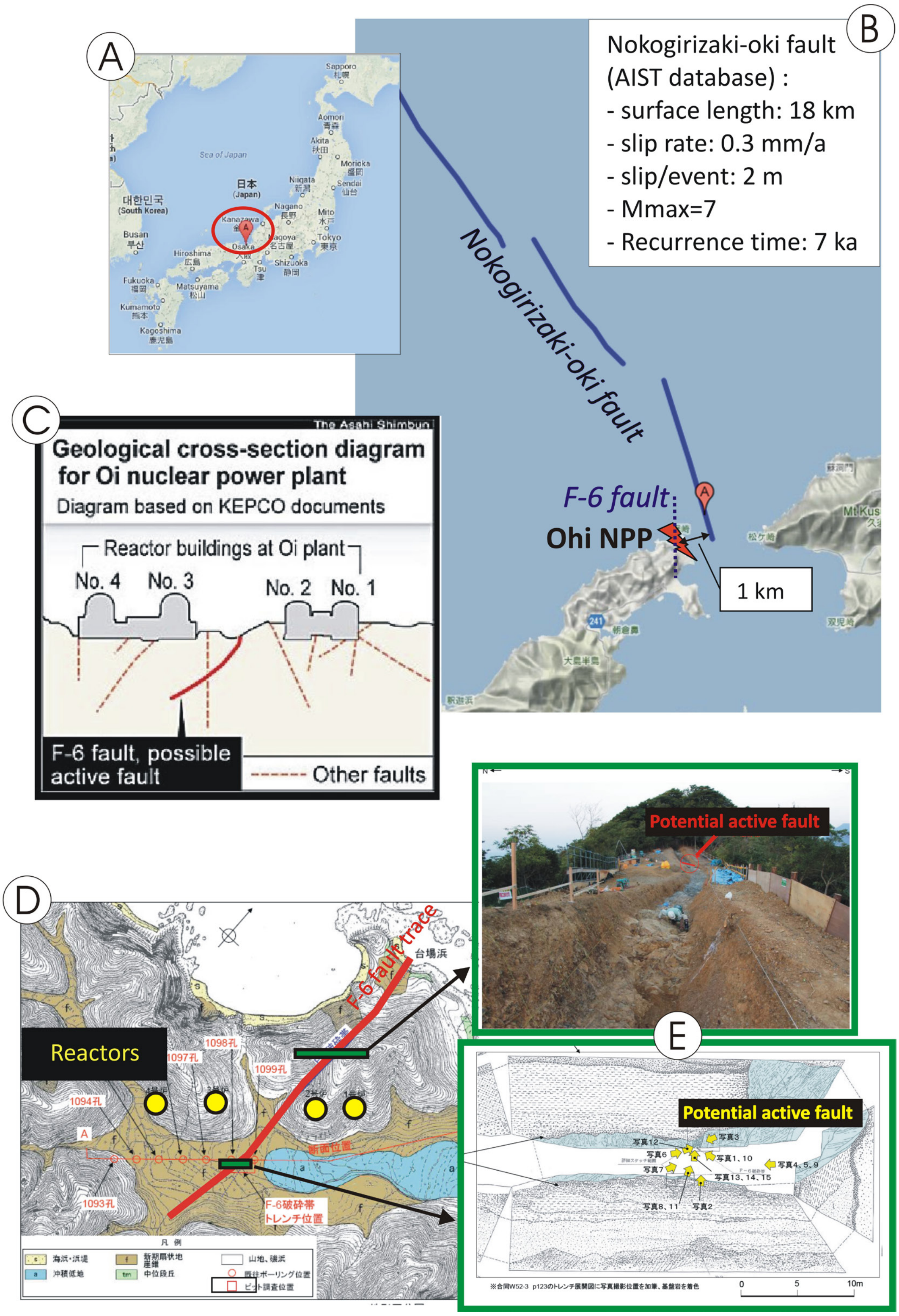


Fig. 1A: The Ohi NPP is located along the northwestern coast of central Japan. 1B: The Nokogirizaki-oki fault is mapped at only 1 km offshore from the NPP (modified from AIST, 2013). This fault is suspected to be capable generating M7 EQs. 1C: Several secondary structures are associated with this main fault, like the F-6 fault mapped in the Ohi site area (picture from Asahi Shimbun online newspaper, 2012, based on operator documents). 1D: Two trenches were excavated across this F-6 fault trace north and south to the reactors of the Ohi site (modified from documents available at NRA, 2013). 1E: These 2 trenches show evidences of possible recent displacements and the fault would then be considered as active (modified from documents available at NRA, 2013).

INQUA Focus Group on Paleoseismology and Active Tectonics

paleoseismicity.org

# Paleoseismic evidences in Last Interglacial deposits from Cope Basin (Murcia, SE Spain)

*Bardají, T. (1); Cabero, A. (2); Silva, P.G. (3); Goy, J.L. (4); Zazo, C. (5); Dabrio, C.J. (6); Lario, J. (2).*

(1) U.D. Geología. Universidad de Alcalá. 28871-Alcalá de Henares (Madrid), España. Email: teresa.bardaji@uah.es
(2) Facultad de Ciencias, UNED. 28040-Madrid, España. Email: acabero@ccia.uned.es; Javier.lario@ccia.uned.es
(3) Dpto. Geología, Universidad de Salamanca, EPTS de Avila. 05003-Ávila, España. pgsilva@usal.es
(4) Dpto. Geología, Facultad de Ciencias; Universidad de Salamanca. 37008-Salamanca, España. joselgoy@usal.es
(5) Dpto. Geología, Museo Nacional CC. Naturales, CSIC. 28006-Madrid, España. mcnzc65@mncn.csic.es
(6) Dpto. Estratigrafía, Facultad de CC. Geológicas, UCM. 28040-Madrid, España. dabrio@geo.ucm.es

***Abstract:*** *Cope basin is a small littoral plio-pleistocene sedimentary basin located in the inner part of the Aguilas Arc tectonic structure (Betic Cordillera, SE Iberian Peninsula). Tectonic activity has driven the recent evolution of the basin promoting a piano like movement of blocks that has conditioned the differential development of morphosedimentary units, however, seismic activity in this basin has not been reported, neither in the historical nor in the geological record. Complex distribution of sedimentary units within the MIS7 – MIS5 sequence is interpreted in this work as the consequence of the joint action of sea-level changes and seismic activity. Evidences of sudden uplift of coastal deposits, as well as the occurrence of liquefaction processes associated to Last Interglacial deposits cannot be interpreted without the action of strong earthquakes in the area. Seismic intensity (ESI-2007) suggest values as high as VIII-IX, what is strikingly higher than expected values in the area.*

***Key words****: Active tectonics, earthquake environmental effects, coastal deposits, Betic Cordillera, SE Spain.*

## INTRODUCTION

The Cope Basin (Fig. 1) is a relatively small littoral Pliocene - Pleistocene basin developed within the Aguilas Arch. This arched structure has been reported to be the result of a rigid-plastic indentation process driven by the collision between European and African Plates (Coppier et al., 1989).

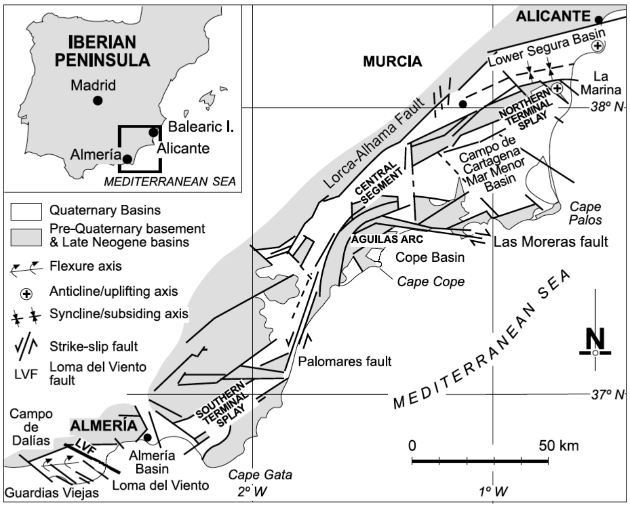


*Fig. 1: Location of Cope Basin (centre of figure) within the tectonic framework of the Áquilas Arc (Simplified after Silva et al., 1993)*

The Águilas Arc can be defined as a differentially up-thrusted cortical structure characterized by a large-scale bending of the upper crust. The sedimentary basins developed within this tectonic structure evolved differentially due to their variable orientation with respect to the northwards indentation of the Águilas Arc (Silva et al., 1993; Bardají. 1999; Bardají et al., 1999). In this sense, four different types of basins have been identified (Fig.1): Frontal Basin (Mazarrón); Inner Basin (Ramonete); Littoral Detachment Basins (Cope and Aguilas) and Lateral Strike-Slip Basin (Los Arejos). The peripheral frontal Arc absorbed the compressive tectonics caused by the indentation process, triggering the creation of E-W trending reversal faults (El Saladillo Fault, Las Moreras Fault, Fig.1) during upper Miocene. At the beginning of Pliocene, the definitive elevation of the main ranges (Las Moreras, Lomo del Bas) had as a main consequence the large-scale gravitational collapses along the previous thrust planes, and the development of the Littoral Detachment Basins of Águilas and Cope, which have evolved under N-S extensional regime within the general compressive framework.

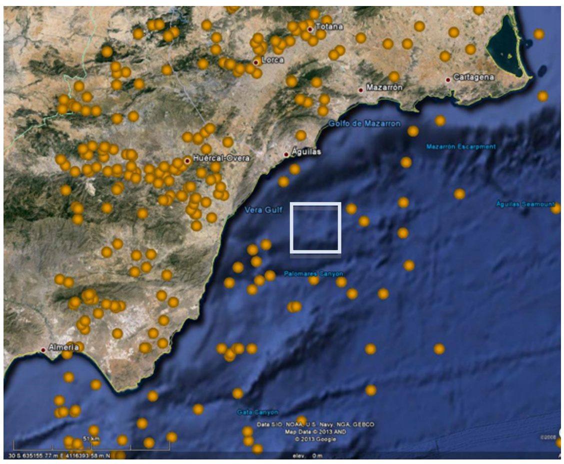


*Fig. 2.: Spatial distribution of instrumental earthquakes (M>3) in SE Iberian Peninsula (1926-2013). (IGN database browser). Location of Cope basin in the square box*

Seismicity in the area concentrates in the periphery of the Arc, Lorca-Alhama and Huercal Overa (Fig. 2), with few instrumental earthquakes with Magnitude ≥ 3 recorded, and only one stronger than 4 (M=4.5, Intensity=V; N-Águilas, 1996). Historic records evidence two more earthquakes, with intensities VI (Águilas-1596) and III-IV (Águilas, 1882), (IGN database browser).

## SEDIMENTARY SEQUENCE

Cope basin holds one of the most complete sequences of Quaternary marine terraces in SE Spain (Dabrio et al., 1991; Bardají, 1999; Zazo et al., 2003), which outcrop on top of monocline reliefs differentially uplifted along the basin. Marine deposits attributed to MIS 7 and MIS 5e develop in the seaward border of these reliefs, being separated from the older terraces by a marked scarp.

The chronology of the sequence has been fixed by different means: palaeomagnetic measurements carried out in the whole sedimentary sequence give a Pleistocene age for the whole sequence (Bardají et al., 1995); presence of Senegalese fauna, specially *Strombus bubonius*, in the most recent units, which points to a MIS 7 – MIS 5 age (Bardají et al., 2009; Zazo et al., 2003; 2013) and the existence of oolitic facies associated to these units, which are characteristic of MIS 5e in Mediterranean peninsular coasts of Spain (Bardají et al., 2009).

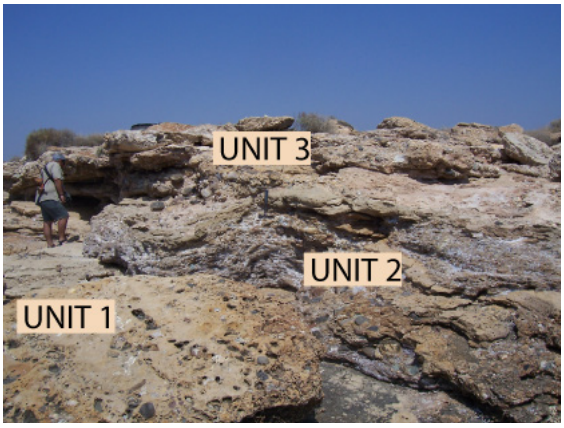


*Fig. 3: Sedimentary sequence. Units 1 to 3 explained in main text. Location of Cope basin in figs. 1 and 2*

The MIS 7 – MIS 5e sequence (Fig. 3) is composed by the following units:

Unit 1: Thinly layered littoral unit, composed by an alternation of strongly cemented foreshore calcarenites and gravels with some intercalation of terrestrial reddish gravels. This littoral-terrestrial alternation has been interpreted as induced by small-scale sea-level changes.

Unit 2: Canalised reddish-purple gravels, sands and silts, mainly composed by phyllite and schist fragments, with no carbonate cement. On top of this reddish unit a thin sandy yellowish level has been locally identified, indicating closeness to the sea-shore.

Unit 3: Gravel beach deposits, composed by quartz and betic pebbles; grain size generally diminishing from North to South of the basin. Laterally this unit seems to correspond to the oolitic beach-dune system developed in the southernmost boundary if the basin.

Present altitude of described units varies laterally due to the differential uplift of blocks. However, in each individual block Unit 3 always overlaps Units 1 and 2, indicating a higher sea level. Different sections have been analysed along the coast showing always the same geomorphologic relationships amongst the different units.

## RECONSTRUCTION OF SEA-LEVEL HISTORY

Unit 1 represent a sea level highstand tentatively attributed to MIS7. Differential uplift along the basin does not allow giving a precise height since its transgressive maximum varies from +8 to +3m depending on its location.
The subsequent sea level fall (MIS6) caused a strong erosion of Unit 1, and the deposition of Unit 2 (terrestrial). Subsequent sea level rise (MIS 5e) promoted the deposition of Unit 3, which represent a higher sea level than Unit 1 (1-2m higher).
Soon after the deposition of this gravel Unit 3, a rapid relative sea-level drop, and a subsequent long-lasting sea level still stand, gave place to the creation of a cliff and wave cut platform, excavated in the whole described sequence. This paleo-cliff and wave cut platform can be followed along the coast, at different heights depending on its location.

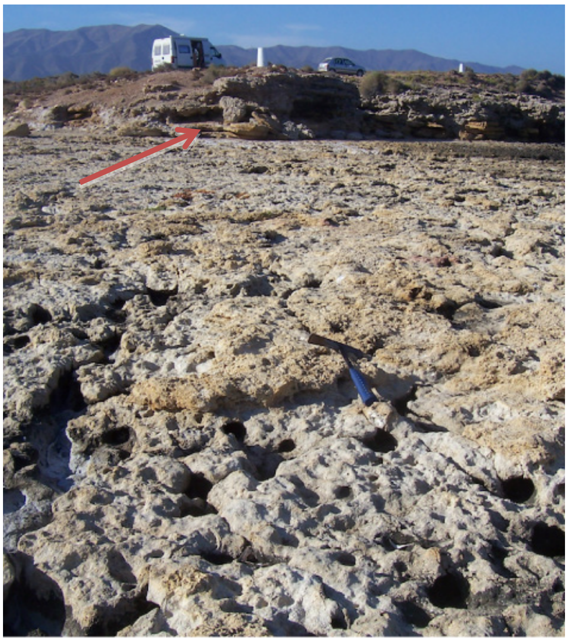

*Fig. 4: Palaeo-cliff (marked by the arrow at the background) and wave-cut platform locates above present sea level either by co-seismic uplift or by rapid sea-level drop after MIS 5e.*

## PALAEOSESIMIC EVIDENCES

Two possible geological effects of earthquakes have been identified in the basin:

Tectonic uplift: Sudden uplift is evidenced by the development of palaeo-cliff and wave cut platform (Fig. 4) affecting Units 1 to 3, before the lithification or cementation of the two most recent units. However, it is not clear whether or not this uplift was caused by an earthquake (co-seismic effect) or by sea level fall (climatic implications) or by a combination of both. A detailed altitudinal analysis comparing the height of the transgressive maximum of Unit 3 and the inner edge of wave cut platform, must be done in order to discern between co-seismic uplift or rapid sea-level drop. If only a co-seismic effect, one would expect to have different values depending on the movement of each block.

Accepting a co-seismic origin for the relative coastal uplift, with all the aforementioned reservations, the application of the ESI-2007 Scale (Michetti et al., 2007), would imply a seismic intensity VIII-IX.

Liquefaction: Different sections along the coastline show the effects of liquefaction suffered by the terrestrial Unit 2 (Figs. 3, 5) that in some cases flowed over the wave cut platform. This flow can be considered as an evidence of the instability of an un-cemented deposit once the wave cut platform was created. Although no other causes for this instability can be discarded, such as differential lay down or loading, the co-seismic origin seems to be the most probable driven factor.

Thus, accepting a co-seismic origin for this structures the application of ESI-2007 (Michetti et al., 2007) could give maximum values of VIII-IX.

*Fig. 5: Liquefaction of Unit 2.*

## CONCLUSIONS

Identification of palaeoseismic features in late Pleistocene coastal deposits from Cope Basin, allow filling the seismic record in an area with scarce historic or instrumental record. Application of ESI-2007 could help in hazard analyses in these areas. Besides that, this identification can also help in the comprehension of sea-level history in this particular basin during the most recent interglacials, especially for the identification of small-scale sea-level oscillations.

Sedimentologic and geomorphological analyses of the coastal sedimentary sequence leaded to the identification of anomalous features that can be related to seismic activity in the area during MIS5. Two different events could be identified: a first one that caused the sudden coastal uplift (1-2m), and the second one related to the liquefaction features. However, detailed topographic and chronologic analyses are required to fully understand the causes of these features and to discard other causes , as well as trying to fix the chronologic model for these events.

**Acknowledgements:** This work has been supported by Spanish Projects CGL2012-33430 y CGL2012-3781. This is a contribution to IGCP588, INQUA CMP WG on Long Term Sea Level Changes, INQUA TERPRO Project 1299 (EEE Metrics), and Research Group UCM 910198 (Paleoclimatology and Global Change). Thanks to Raúl Pérez for his earthquake support.

## References

Bardají, T., Goy, J.L., Mörner, N.A., Zazo, C., Silva, P.G., Somoza, L., Dabrio, C.J., Baena, J. (1995). Towards a Plio-Pleistocene chronostratigraphy in Eastern Betic Basins. *Geodin Acta* 8 (2), 112-126.

Bardají, T. (1999). *Evolución Geomorfológica durante el Cuaternario de las Cuencas Neógenas litorales del Sur de Murcia y Norte de Almería*. PhD Thesis, Universidad Complutense de Madrid, 492pp.

Bardaj|., M.T., Silva, P.G., Goy, J.L., Zazo, C., Dabrio, C.J., Civis, J., (1999). Recent evolution of the Águilas Arc Basins (SE Spain): Sea-level record and neotectonics. *INQUA Mediterr. Black Sea Shorelines Subc. Newsl.* 21, 21-26.

Bardají, T., Goy, J.L., Zazo, C., Hillaire-Marcel, C., Dabrio, C.J., Cabero, A., Ghaleb, B., Silva, P.G., Lario, J., (2009). Sea level and climate changes during OIS 5e in the Western Mediterranean. *Geomorphology* 104, 22–37.

Coppier, G., Griveaud, P., Larouziere, F.D., Montenat, Ch.,Ott d'Estevou, Ph., (1989). Example of Neogene tectonic indentation in the Eastern Betic Cordilleras: the Arc of Aguilas (Southeastern Spain). *Geodin. Acta* 3, 37-51.

Dabrio, C.J., Zazo, C., Goy, J.L., Santiesteban, C., Bardaj|.,T., Somoza, L., Baena, J., Silva, P.G., (1991). Neogene and Quaternary fan-delta deposits in southeastern Spain. *Cuad. Geol. Iber.* 15, 327-400.

IGN (2013) *Catálogo de terremotos* [Online]. Available from http://www.ign.es/ign/layoutIn/sismoFormularioCatalogo.do [Accesed: 12th July 2013]

Michetti, A.M., Esposito, E., Guerreri, L., Porfido, S., Serva, L., Tatevosian, R., Vittori, E., Audemard, F., Azuma, T., Clague, J., Comerci, V., Gürpinar, A., McCalpin, J., Mohammadioun, B., Mörner, N.A., Ota, Y., Roghozin, E. (2007). Intensity Scale ESI 2007. (IN: Guerreri & Vitori Eds.) Memorie Descrittive della Carta Geologica d'Italia, vol. LXXIV, Servizio Geologico d'Italia, APAR, Rome.

Silva, P.G., Goy, J.L., Somoza, L., Zazo, C., Bardaj|., T., (1993). Landscape response to strike-slip faulting linked to collisional settings: Quaternary tectonics and basin formation in the Eastern Betics, southeastern Spain. *Tectonophysics* 224, 289-303.

Zazo, C., Goy, J.L., Dabrio, C.J., Bardají, T., Hillaire-Marcel, C., Ghaleb, B., González-Delgado, A., Soler, V., (2003). Pleistocene raised marine terraces of the Spanish Mediterranean and Atlantic coasts: records of coastal uplift, sea-level highstands and climate changes. Marine Geology 194, 103–133.

Zazo, C., Goy, J.L., Dabrio, C.J., Lario, J., González-Delgado, A., Bardají, T., Hillaire-Marcel, C., Cabero, A., Ghaleb, B., Borja, F., Silva, P.G., Roquero, E., Soler, V. (2013). Retracing the Quaternary history of sea-level changes in the Spanish Mediterranean-Atlantic coasts: Geomorphological and sedimentological approach. *Geomorphology* 196, 36-49

# An Earthquake Impact Assessment Methodology for the Philippines

*Bautista, Bartolome C., Maria Leonila P. Bautista, Ishmael C. Narag, Winchelle Ian G. Sevilla, Rhommel N. Grutas and Renato U. Solidum, Jr.(1)*

(1) Philippine Institute of Volcanology and Seismology (PHIVOLCS), C.P. Garcia Ave., UP Campus, Diliman, Quezon City, Philippines. Email: bart_bautista@yahoo.com

***Abstract:*** *PHIVOLCS, together with various scientific organizations like Geoscience Australia and academic partners, improved its methodology for conducting earthquake impact assessment that incorporates ground motion simulation, exposure database building and Philippine vulnerability and fragility curves. The whole procedure is packaged in a freely-distributable software called REDAS. The fragility and vulnerability curves were developed by the local engineering community and are used to compute for physical damage (slight, moderate, extensive to total collapse), casualties (slight injuries to fatalities) and economic loss. For the exposure database, the area-based approach was used. This was done by mapping land use types and determining the building statistic in each typical land use using field surveys. To fine tune the exposure data statistics, PHIVOLCS is tapping local communities and academic institutions to continue conducting detailed building surveys. The enhanced impact assessment method has been tested in Metro Manila and results will be presented in the report.*

***Key words****: earthquake, impact, exposure, landuse, vulnerability*

# The REDAS Software: A tool for hazard and risk estimation for Philippine communities

*Bautista, Maria Leonila P., Bartolome C. Bautista, Ishmael C. Narag, Angelito G. Lanuza and Renato U. Solidum, Jr.(1)*

(1) Philippine Institute of Volcanology and Seismology (PHIVOLCS), C.P. Garcia Ave., UP Campus, Diliman, Quezon City, Philippines. Email: leyobautista@yahoo.com

***Abstract:*** *PHIVOLCS have developed a seismic hazard and risk assessment software called REDAS that can simulate ground shaking hazard, liquefaction and landslide potential and estimates tsunami wave heights, inundation extent and arrival times. The software contains database on Philippine active faults and trenches as well as historical and instrumental seismicity. Since 2006, the software is being shared with Philippine local government units as a tool for mainstreaming disaster risk reduction into the local development planning process. To date, the software has been taught to more than 50 Philippines provinces, 230 towns/cities, 10 government institutions and 17 state universities and colleges. The software distribution comes with a week-long training and post training support. Two new modules such as the Exposure Database and the Earthquake Impact Assessment had been recently been developed within REDAS. These modules allow the collection of exposure data and risks estimation covering physical damage, fatalities and economic loss.*

***Key words****: REDAS, risk, faults, seismicity, exposure*

# Evidence of Idrija fault seismogenic activity during the Late Holocene including the 1511 $M_m$ 6.8 earthquake

*Miloš Bavec (1), Jure Atanackov (1), Bogomir Celarc (1), Irka Hajdas (2), Petra Jamšek Rupnik (1), Jernej Jež (1), Vanja Kastelic (3), Blaž Milanič (1), Matevž Novak (1), Dragomir Skaberne (1), Gorazd Žibret (1)*

(1) Geological Survey of Slovenia, Dimičeva 14, 1000 Ljubljana, Slovenia. milos.bavec@geo-zs.si
(2) Ion Beam Physics, ETH Zurich, Schafmattstr. 20, 8093 Zurich, Switzerland
(3) Istituto Nazionale di Geofisica e Vulcanologia - INGV, Via Arcivescovado 8, 67100 L'Aquila, Italy

***Abstract:*** *Geological and geomorphological mapping combined with multimethod geophysical site surveying evidenced recent activity of the Idrija fault. Coseismic deformation is observed in a paleoseismological trench that is distributed along a series of fault branches. Based on the results of radiocarbon dating, combined with the historic record, we attribute the deformation to one or possibly two individual earthquakes, with a large part of it caused by the 1511 Idrija earthquake, the strongest historic seismic event registered in the region.*

***Key words****: Idrija fault, 1511 Idrija earthquake, paleoseismology, geophysics.*

## INTRODUCTION

The transition between the structural domains of the Southern Alps and the External Dinarides in the W-NW Slovenia and E Italian region of Friuli is a seismically active area with records of both historic and instrumental earthquakes. The strongest recorded historical earthquake is the 26 March 1511 $M_m$ 6.8, $I_{max}$ X EMS (Ribarič, 1979; Cecić, 2011) event. The earthquake has been known under several names such as the Idrija earthquake, the great Friuli earthquake, the W Slovenia earthquake and the Eastern Alps earthquake. Its source is still a matter of debate and different solutions have been proposed over the years (e.g. Fitzko et al., 2005; Burrato et al., 2008; Camassi et al., 2011; Košir & Cecić, 2011; Stucchi et al., 2012). Our study is a first attempt in combining several geological, geophysical and numerical techniques in identifying geological evidence of coseismic deformation along the Idrija fault.

## THE IDRIJA FAULT

The Idrija fault is geomorphologically the best expressed NW-SE oriented ("Dinaric-trending") structural feature in W Slovenia. This dextral strike-slip fault continues with the generally same trend towards SE across the NW part of the Croatian Dinarides, while towards the NW it continues in Friuli as the Ampezzo Fault system (Zanferrari et al., 2011). Its geomorphic trace can be well followed for at least 120 km. In the surroundings of Idrija town, the fault plane dips at 65 to 75 degrees toward the NE (Čar, 2010), while the estimated average dip along the full length of the fault is 77.5 degrees and its maximum depth is estimated at 14 km (Kastelic & Carafa, 2012). Its (sub)recent activity has been evaluated by several methods. From the cumulative displacement of the mercury ore body in the Idrija mine, amounting to 480 m in vertical direction and 2414 m in horizontal direction since the Miocene/Pliocene transition (Placer, 1982), a long-term slip-rate at around 0.5 mm/year was postulated.

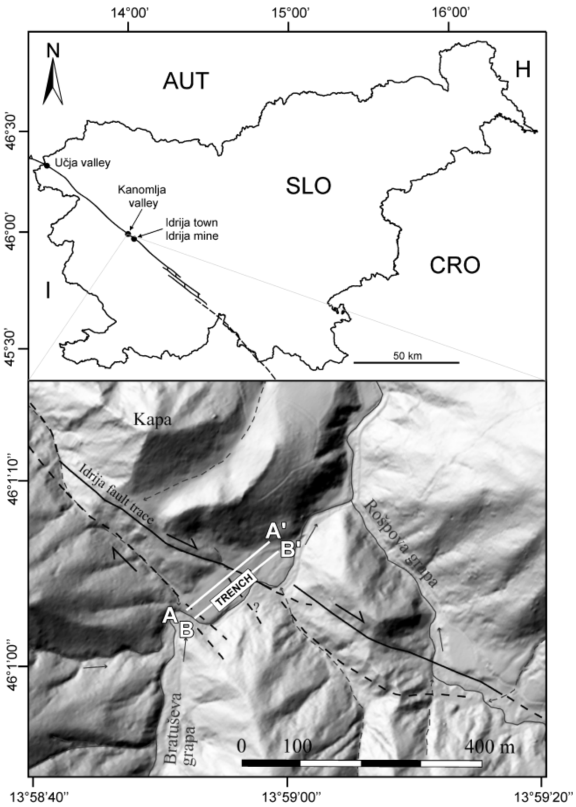


*Fig. 1: Above: general map of the Idrija fault location taken from (Placer, 2008). Below: a 2 m grid Digital Elevation Model of bare ground from the LiDAR survey of the study area. Locations of geophysical sections A-A' and B-B' and the trench site are indicated.*

8-year continuous measurements of recent displacements with a TM-71 extensimeter in the Učja valley in NW Slovenia yielded an average slip-rate of 0.26

mm/year with extreme values of up to 0.54 mm/year (Gosar et al., 2011; Čar & Gosar, 2011).

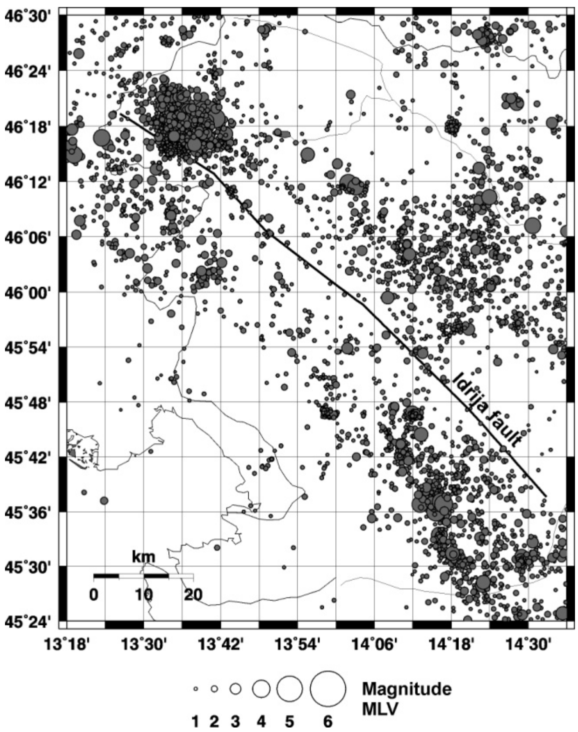


*Fig.2: Map of routinely located earthquakes in the vicinity of the Idrija fault for the period 1977 – 2010 (from Živčić et al., 2011). Note that the cluster around 46°18′N, 13°36′E belongs to two consecutive earhquakes: 1998 $M_s$ 5.7 (Bajc et al., 2001) and 2004 $M_w$ 5.2 (Kastelic et al., 2008) that were attributed to the Ravne fault that runs parrallel to the Idrija fault.*

By modeling active fault displacements in the eastern Adriatic region using a thin-shell finite element method, Kastelic & Carafa (2012) calculated long-term slip-rates between 0.06 and 0.22 mm/year with an average 0.10 mm/year displacement for the Idrija fault. Instrumental record show very little earthquake activity on the Idrija fault (Figure 2).

## GEOMORPHOLOGY AND GEOPHYSICS

Near Kanomlja valley, 5 km NW of the town of Idrija, an airborne LiDAR survey revealed several geomorphic indicators of the recent activity of the Idrija fault, such as displaced streams, truncated fluvial terraces, dry valleys, bent ridges, etc. (Cunningham et al., 2006). Detailed geomorphic field surveying confirmed the suggestion of Cunningham et al. (2006) to focus a paleoseismological study in the area of the Bratuševa grapa creek south of the Kapa hill (Figure 1). To select the most suitable site for the paleoseismological trench, we conducted electrical resistivity tomography (ERT) and seismic refraction tomography (SRT) studies along two parallel sections, each 190 m long (Figure 1) (Bavec et al., 2012). Vertical electrical sounding (VES) was also carried out in order to support the ERT interpretation.

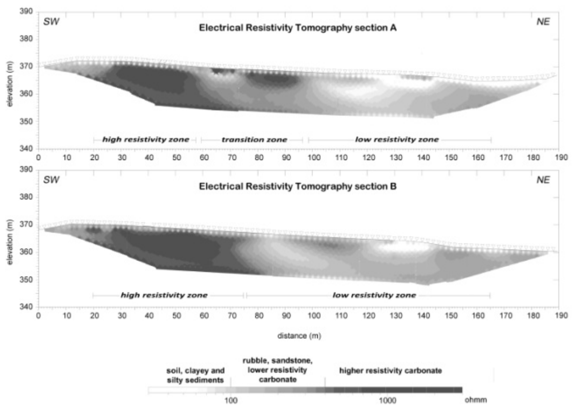


*Fig.3: Electrical resistivity tomography sections A and B. The main trace of the Idrija fault is inferred at between 60 m and 95 m in section A and between 70 m and 80 m in section B.*

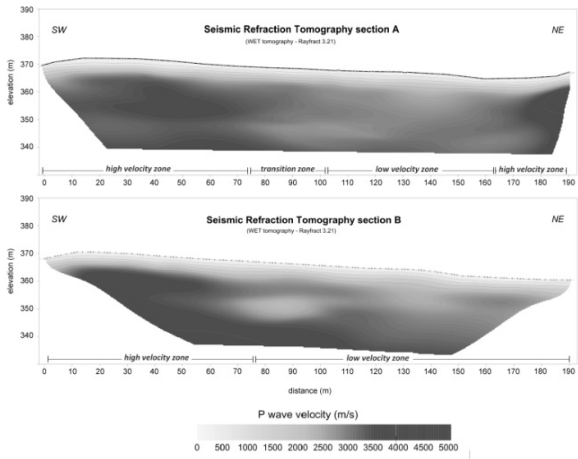


*Fig.4: Seismic refraction tomography sections A and B. The main trace of the Idrija fault is inferred at between 80 and 100 m in section A and between 70 and 80 m in section B.*

By the means of geophysical survey we estimated the sedimentary cover thickness over the Mesozoic/Paleozoic bedrock to be between 1.5 m and 2.6 m thick and we estimated the width of the fault zone at the selected site at between 80 m and 100 m. By ERT we located a sharp resistivity contrast that corresponds to the transect of maximum deformation within the bedrock at between stations 60 m and 95 m in section A and between stations 70 m and 80 m in section B (Figure 3). SRT showed a contrast in P-wave velocity that corresponds to the main deformation at between 60 m and 95 m in section A, and between 70 m and 80 m in section B respectively (Figure 4). The area of maximum bedrock deformation, identified by geophysical methods, was selected as the location where we opened the paleoseismological trench.

## PALEOSEISMOLOGICAL TRENCH

A 55 m long, 3-4 m deep paleoseismological trench, excavated in late 2012, allowed for a detailed litho-stratigraphic log (Figure 5). Hard rock basement (Unit 0) is composed of the clastic Val Gardena Formation, dolomitic tectonic breccia, and fine grained dolomite (Permian) and Hauptdolomite (Triassic). Holocene sedimentary cover overlays the hard rock basement and includes five lithologic units: 1 – erosional remnants of "older" alluvial sediments, 2 – gravelly diamict, 3 – alluvial infill of the lowest/deepest parts of depressions, 4 – alluvial and colluvial cover, 5 – soil. Unit 2 is interpreted as a single sedimentary mass flow event deposit. The Unit 3 sediments consist of various sediment types, including sandy silty polymictic gravel (Subunit 3a), sandy and silty monomictic gravel of flysch sandstone clasts (Subunit 3b) and silt, sandy silt and sandy/gravelly silt (Subunit 3c). Alluvial and colluvial sediments of Unit 4 overlay the sedimentary infill of channels and depressions.

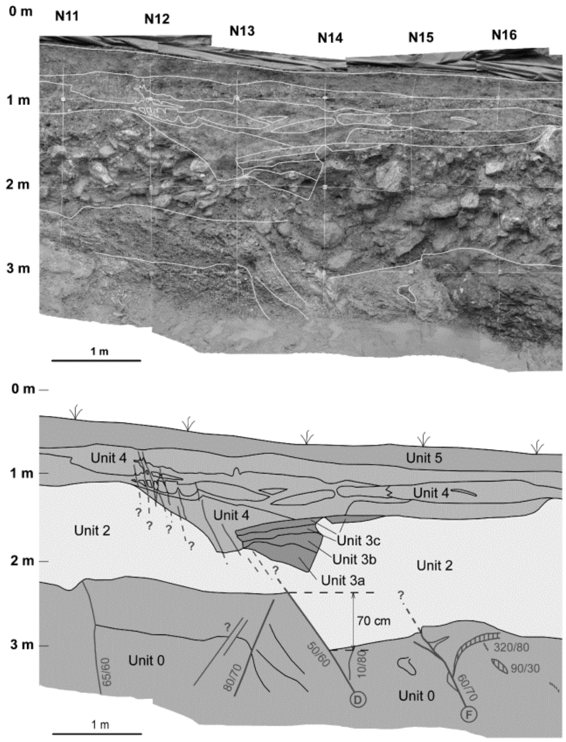


*Fig.5: Geological situation along the northern wall of the trench in section of the highest deformation concentration. Lower panel shows its lithological and structural interpretation.*

Currently available radiocarbon dates from Unit 2 (that resemble roughly the time of its deposition) are 924±64 BP (calibrated 1010 AD to 1220 AD for 2σ confidence level) and 863±74 BP (1020 AD to 1270 AD for 2σ). In Unit 4 (that postdates the deformation) the dates are 364±29 BP (1440 AD to 1640 AD for 2σ) and 364±75 BP (1420 AD to 1670 AD for 2σ). The ages correspond well with the 1511 Idrija earthquake.

With the trench location within the inner fault zone, the bedrock is expectedly dissected by anastomosing fault branches (Figure 6) that in general resemble the general structural signature of the Idrija fault.

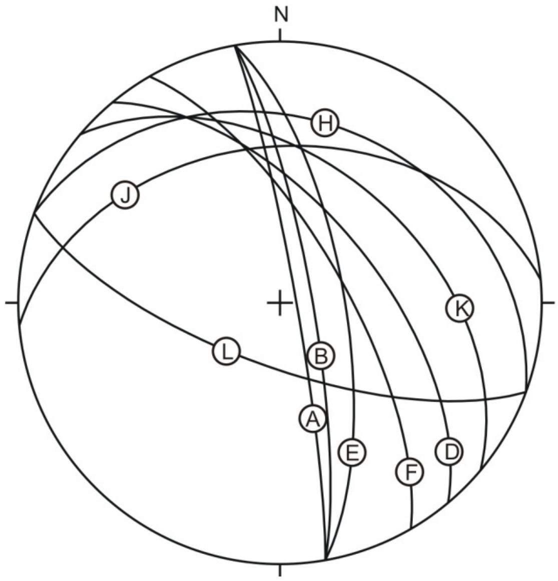


*Fig.6: The main faults in the trench (stereographic projection, lower hemisphere). The fault A exhibits vertical slickenside lineation, fault D shows apparent normal displacement that could be attributed to a normal fault or to a synthetic Riedel fault. Fault H exhibits reverse displacements. Faults D and H correspond to the theoretical model of structures in the transpressive strike-slip regime with the principal stress direction roughly in the N-S direction. The fault A would be in this case normal.*

Out of numerous fault planes identified within the trench, nine displace also the interface between the bedrock and the Holocene sedimentary cover and they can be traced also within the Holocene units. The section N11 to N15 (Figure 5) hosts the main fault in the trench. Beside the 70 cm throw of bedrock/sediment interface at station N14 the following observations lead us to interpret the observed deformation in this section as coseismic:

- above D and F fault planes we observed broken-up clasts with fracture orientation agreeing with the strike of observed fault planes,
- the gravelly diamict of Unit 2 between markers N12 and N15 is sheared and thinned to less than 25% of its original thickness,
- the infill of Units 3 and 4 into Unit 2 aligns well with the most prominent bedrock-sediment displacement along the fault D.

Indicative results were obtained by a numerical analysis of clast long axes orientation in the diamict of Unit 2 (Figure 7). Clast orientation was measured from a photo mosaic of the trench walls. In general clast long axes are in depositional position of a debris flow. However, clast fabric deviates from average the most in the vicinity of fault planes or above the zones where the fault planes remain constrained in the bedrock. In our opinion the observed clast fabric anomalies, clustered around fault planes, determined from such independent analysis strengthen our identification of the principal deformation zone and its activity.

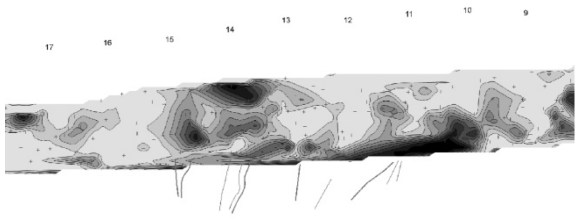


*Fig.7: Orientations of clasts measured in a part of the southern trench wall. Shades of gray darken from horizontal (white) to vertical (black). Faults are pictured within the bedrock.*

## DISCUSSION

Coseismic deformation of the Late Holocene sedimentary succession on the Idrija fault was confirmed by our investigation. At the Bratuševa grapa creek paleoseismological trench the deformation is distributed along the fault zone along at least nine fault splays. Along the main fault zone one or two consecutive seismic events can be speculated. We interpret that an important part of the deformation had occurred between the time of deposition of gravely diamict (Unit 2) and the time of deposition of the overlying alluvial-colluvial sedimentary unit (Unit 4). Given the radiocarbon dates and the historic record, we attribute this deformation to the 1511 Idrija earthquake. Here presented study is still underway and further investigations and analysis on the amount of particular event displacement as well as the total number of events is being carried out. Furthermore, attempts at identifying other suitable locations for further morphological and paleoseismological investigation are also in course.

**Acknowledgements:** This work was financially supported by the Slovenian Research Agency (P1-0011 - Program Regional Geology and L1-2383 – Project Seismotectonic Model of the Ljubljana Basin) and by the Slovenian Environment Agency (project Elaboration of Geologic Maps). The paleoseismological study was supported also by the Municipality of Idrija.

## References

Bajc, J., A. Aoudia, A. Saraò & P. Suhadolc (2001). The 1998 Bovec-Krn mountain (Slovenia) earthquake. *Geophysical Research Letters* 29 (9), 1839-1842.

Bavec, M., M. Car, R. Stopar, P. Jamšek Rupnik, & A. Gosar, (2012). Geophysical evidence of recent activity of the Idrija fault, Kanomlja, NW Slovenia. *RMZ-mater. Geoenviron* 59 (2/3), 247-256.

Burrato, P., M.E. Poli, P. Vannoli, A. Zanferrari, R. Basili, & F. Galadini, (2008). Sources of Mw 5+ earthquakes in northeastern Italy and western Slovenia: An updated view based on geological and seismological evidence. *Tectonophysics* 453, 157-176.

Camassi, R., C.H.¸Caracciolo, V. Castelli & D. Slejko, (2011). The 1511 Eastern Alps earthquakes: a critical update and comparison of existing macroseismic datasets. *Journal of Seismology* 15, 191-213.

Čar, J., (2010). Geološka zgradba idrijsko-cerkljanskega hribovja : Tolmač h Geološki karti idrijsko-cerkljanskega hribovja med Stopnikom in Rovtami v merilu 1:25.000 = Geological structure of the Idrija - Cerkno hills: Explanatory book to the Geological map of the Idrija - Cerkljansko hills between Stopnik and Rovte 1:25.000. Geological survey of Slovenija, Ljubljana, 127 p.

Čar, J. & A. Gosar, (2011). Idrijski prelom in premiki ob njem. Anno Domini 1511. *Idrijski razgledi* 56 (1), 105-118.

Cecić, I., (2011). Idrijski potres 26. marca 1511 : kaj pravzaprav vemo o njem? *Geografski obzornik* 58 (1), 24-29.

Cunningham, D., S. Grebby, K. Tansey, A. Gosar & V. Kastelic, (2006). Application of airborne LiDAR to mapping seismogenic faults in forested mountainous terrain, southeastern Alps, Slovenia. *Geophysical Research Letters* 33 (20, L20308), 1-5.

Fitzko, F., P. Suhadolc, A. Aoudia & G.F. Panza (2005). Constraints on the location and mechanism of the 1511 Western-Slovenia earthquake from active tectonics and modeling of macroseismic data. *Tectonophysics* 404, 77-90.

Gosar, A., S. Šebela, B. Košťák & J. Stemberk, (2011). On the state of the TM 71 extensometer monitoring in Slovenia: seven years of micro-tectonic displacement measurements. *Acta geodynamica et geomaterialia* 8 (4), 389-402.

Kastelic, V. & M.M.C. Carafa, (2012). Fault slip rates for the active External Dinarides thrust-and-fold belt. *Tectonics* 31 (TC3019), 1-18.

Kastelic, V., M. Vrabec, D. Cunningham & A. Gosar (2008). Neo-Alpine structural evolution and present-day tectonic activity of the eastern Southern Alps: The case of the Ravne fault, NW Slovenia. *Journal of Structural Geology* 30, 963-975.

Košir, M. & I. Cecić, (2011). Potres 26. marca 1511 v luči novih raziskav. Anno Domini 1511. *Idrijski razgledi* 56 (1), 90-104.

Placer, L. (1982). Tektonski razvoj idrijskega rudišča = Structural history of the Idrija mercury deposit. *Geologija* 25 (1), 7-94.

Placer, L. (2008). Principles of tectonic subdivision of Slovenia. *Geologija*, 51 (2), 205-217.

Ribarič, V. (1979). The Idrija earthquake of March 26, 1511 – a reconstruction of some seismological parameters. *Tectonophysics*, 53, 315-324.

Stucchi, M., A. Rovida, A.A. Gomez Capera, P. Alexandre, T. Camelbeeck, M.B. Demircioglu, P. Gasperini, V. Kouskouna, R.M.W. Musson, M. Radulian, K. Sesetyan, S. Vilanova, D. Baumont, H. Bungum, D. Fäh, W. Lenhardt, K. Makropoulos, J. M. Martinez Solares, O. Scotti, M. Živčić, P. Albini, J. Batllo, C. Papaioannou, R. Tatevossian, M. Locati, C. Meletti, D. Viganò & D. Giardini, 2012: The SHARE European Earthquake Catalogue (SHEEC) 1000–1899. *Journal of Seismology* 17 (2), 523-544.

Zanferrari, A., D. Masetti, G. Monegato & M.E. Poli, (2011). *Note Illustrative della Carta Geologica d'Italia alla scala 1:50.000, foglio 049*, Gemona Del Friuli. 258 p.

Živčić, M., M. Čarman, A. Gosar, T. Jesenko & P. Zupančič, (2001). Potresi ob Idrijskem prelomu. Anno Domini 1511. *Idrijski razgledi* 56 (1), 119-126.

INQUA Focus Group on Paleoseismology and Active Tectonics

paleoseismicity.org

# Quaternary faulting in the central Paris basin: Evidence for coseismic rupture and liquefaction

*Pierre Benoit (1), Jean Marie Grisoni (2) and Mustapha Meghraoui (3)*

(1) Laboratoire Aquanalyse, 10380 Plancy-l'Abbaye, France. Email: pierre.benoit@wanadoo.fr
(2) Université Paris 8, Département de Géographie, Bâtiment D, 2 Rue de la Liberté, 93256 Saint-Denis Cedex, France
(3) Institut de Physique du Globe, UMR 7516, 5 Rue René Descartes, 67084 Strasbourg, France

***Abstract:*** *We describe new evidence of Quaternary faulting observable in large outcrop exposures (trenches and carries) near Romilly-sur-Seine in the centre of Paris basin. Coeval normal or reverse faults affect sand, marl and gravel units that also expose liquefaction features. Quaternary units with thicknesses ranging from decimetre to metre are sealed by non-deformed deposits. The coexistence of soft and brittle tectonics with ~1 m vertical offset in a single cross-section, affecting different stratigraphic levels, reflects their diachronic nature and attest for their coseismic origin. The faulting of young deposits visible in the paleoseismic sites belong to the major regional tectonic structures, i.e. the Omey and Vittel fault system that affects the late Quaternary units of the east Paris basin. Their activity known locally as Ypresian polyphased seismites, seems to have continued until the late Quaternary. The Quaternary ruptures and coseismic nature of the fault system call for a realistic seismic hazard assessment in this intraplate tectonic environment.*

***Key words****: active faulting, liquefaction, Quaternary, Paris Basin.*

## INTRODUCTION

Intraplate Europe experienced large to moderate earthquakes (Mw > 6.0) inducing surface ruptures and liquefaction accompanied by severe damage to buildings and significant numbers of victims (Camelbeeck and Meghraoui, 1998). The coseismic indicators of tectonic activity in intraplate continental regions may rapidly disappear when the time interval between major earthquakes is often larger than 10,000 years. Paleoseismology in regions of low-level active deformation indicates, however, that return period of large earthquakes may reach 50 à to 100 ka (Meghraoui and Crone, 2001). The existence of coeval soft and brittle tectonics in lacustrine or fluvial Quaternary deposits constitutes unequivocal paleoseismic features that document past earthquake activity.

In this work, the detailed description of the active tectonics affecting the Paris basin is presented with evidence of thrust and normal faulting systems that rules out periglacial influence or lateral spreading. The existence of active faulting in both the bedrock and Quaternary units in a single site attests for the coseismic origin of the active deformation and points out the seismic hazard re-evaluation.

## REGIONAL TECTONIC SETTING

The tectonic activity in the Paris basin during the Cenozoic period has long been documented and shown in published geological sheets. Indicators of seismites (mainly sand blows) in the Ypresian have been observed on the outskirts of Romilly-sur-Seine, in the edge of the Ile de France cuesta (Plaziat, oral communication). Although, an intense past seismic activity has been described in the Fontainebleau and Bartonian sands, no causative faults were studied and properly described with their characteristics (Plaziat, 2009). The Quaternary tectonic episodes affect mainly the alluvial and lacustrine deposits but some periglacial features may appear sporadically in outcrops (Michel, 1972; Antoine, 2005).

The regional stress distribution from Pliocene to present shows an average N160 σ1 obtained from the study of fault kinematics (striations) in the east Paris basin (Grégoire, 2003). The more pronounced active tectonic deformation has been identified in seismic profiles (obtained from commercial sections of oil research) around major faults that cross stratigraphic units deemed to be Quaternary. In parallel, both instrumental and historical seismic activity in the region is shown to

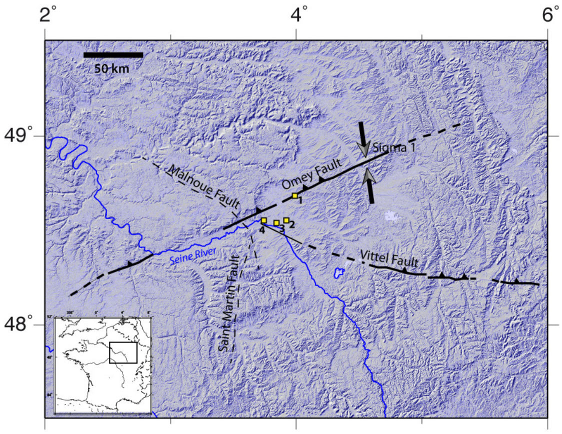


*Fig. 1: Morphotectonic map with main Quaternary Vittel and Omey faults (bold line) as mapped in the field (Institut Français du Pétrole, 2000, and" Geological map Fère champenoise 1/50000"). Yellow square with number are sites with paleoseismic features (as in text): 1 – Gourgançon, 2 – Longueville, 3 – Clesles, 4 – Sauvage. According to the regional stress distribution and N150 direction of σ1 (Grégoire, 2003), fault kinematics indicate a main reverse component. One may note the influence of the Omey and Vittel Fault and related NW block uplift on the Seine River deflection.*

be low but not negligible (Sisfrance, 2013).

**QUATERNARY SEDIMENTATION**

The studied region shows Mesozoic (chalk) outcrops unconformably covered by Quaternary deposits (geological map Paris 1/250000). During the late Quaternary and in a periglacial environment and climate, the region was subject to cryoturbation and large solifluction (mudslides). A thin loess cover occupies some depressions and a large volume of gravel and limestone sand produced by glacial alteration are visible in the great valleys of the Aube and Seine. However, the relatively large distance to the sea did not allow for a significant deepening of the valleys during glacial episodes. The Holocene units made of fine alluvial deposits cover gravel and sandy formations.

**DEFORMATIONS AFFECTING THE QUATERNARY**

The first descriptions of tectonic features and brittle deformations were carried out by Coulon (1994) and subsequently by Baize et al. (2007). The former author attributes them to seismic episodes associated with the final volcanic activity in the Massif Central. Most of outcrops are in quarries and while the latter authors refer to possible gravitational sliding on the permafrost, the possible seismic origin of the tectonic features were proposed by Benoit et al (2011). In our work, we focused our attention on sites that were poorly explored (Fig. 1): the Sauvage sand quarry, the Clesles gash, the eastern side of the Longueville sand quarry, and the base of the Gourgançon sand quarry.

**Sauvage sand quarry**

The sand quarry, which is in the region of the confluence of the Aube and the Seine, exploits the Würm and Holocene alluvial units (subsoil database). The quarry exposes faults (Figs. 2 and 3), sand blows (Fig. 4) with typical structures of find sand ejections from the bottom unit. There are also several meters thick deposits of marl showing numerous soft deformations. Brittle deformations that become soft deformations towards the top may also be observed. The shallow water table makes it impossible to access to the complete cross-section.


*Fig. 2: Exposure with faults affecting gravel and silt deposits.*

*Fig. 3: Image processing and interpretation of Fig. 2*

**Clesles gash**

This 3-m-deep gash shows a mixed alluvial filling of sand, gravel and limestone silt. The western top of the cross-section shows a significant detachment above a pervasive level of marl (photo 3). The south-eastern edge of the site shows fluidized sand ejections.


*Fig. 4: This 0.8-m-high exposure shows normal faults in the injected liquefied sand and the soil horizon.*

**Longueville sand quarry**

The North-South facing sand quarry and related cross-section at its western side in 1997 expose a significant

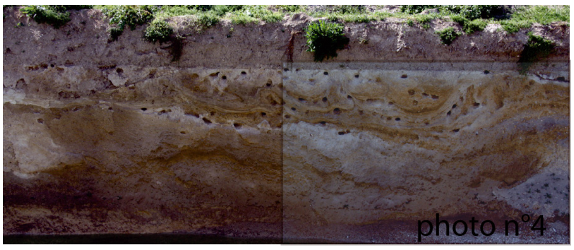


*Fig. 5: Trench exposure at Clesles with seismites (see also Fig. 6).*


*Fig. 6: ~3-m-high exposure with significant syn-sedimentary gravitational sliding next to the main fault (blue line).*

reverse fault (Baize et al., 2007). A high resolution seismic profile (Fig. 7; Piwakowski, 2000) shows the reverse fault (f) extension into the chalk. We further studied the exposure in 2009 and 2010 and made it possible to observe the eastern extension of the fault, described by Baize et al (2007) in Fig. 8. The quarry also shows a small graben and its secondary normal faults sealed towards the top (Figs. 8 and 9).

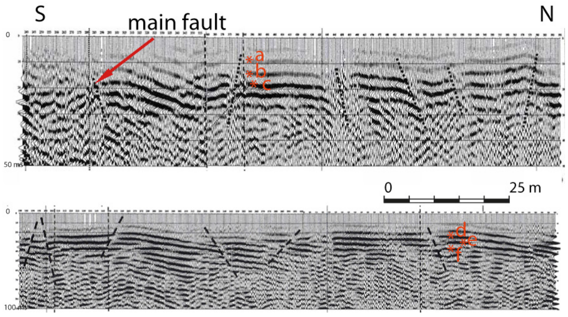


Fig. 7: High-resolution seismic profiles across the Longueville quarry site. Reflectors show the main fault (red arrow) with a reverse geometry and folding of sedimentary units reaching to 30-m-depth). a: 5, 5- b: 8,8 – c: 11 – d:14 – e: 23 – f: 33 (+ or- 7,5%). No vertical exaggeration.

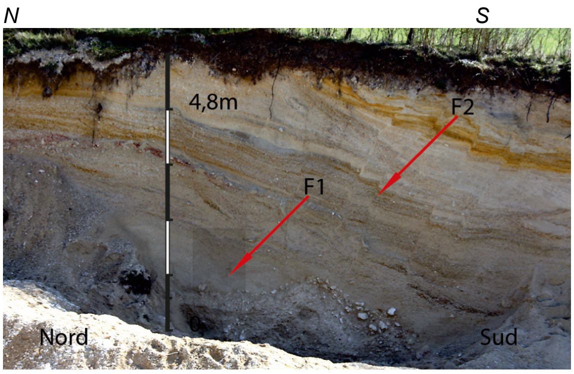


Fig. 8: 6-m- high exposure with small sealed ruptures and faulting of the entire sedimentary units.

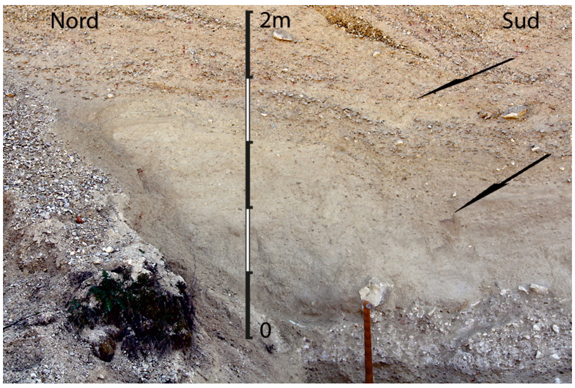


Fig. 9: The northern side of Fig. 8 shows a sealed fault (see arrows) by uppermost gravel unit

**Gourgançon sand quarry**

The NE-SW trending quarry (Fig. 10), previously investigated by Baize et al. (2007) is enlarged and deepened to obtain a large trench. In Figs. 10 and 12, the new exposure shows a set of reverse and normal faults with a decrease in the reverse fault dip towards the surface and the collapse of the overlapping lobe. The reverse fault network shows a consistent dips to the NE and exposes a total ~1 m vertical offset that attests for 2 to 3 episodes of faulting. In addition, a major liquefaction structure (sand blow) appears next to the major reverse fault (Figs. 11 and 12).

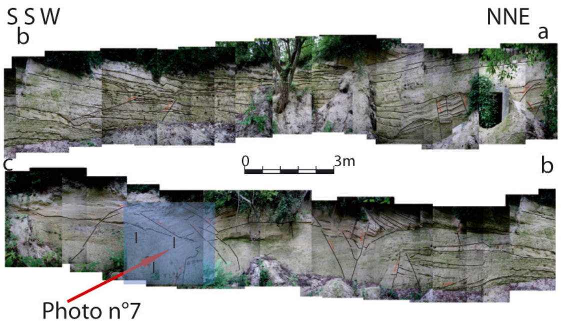


Fig. 10: Mosaic of Gourgançon quarry's showing the faults and Fig. 11 (Photo n°7) (l: liquefaction)


Fig. 11: Major reverse fault associated with liquefaction (see also Fig. 12).

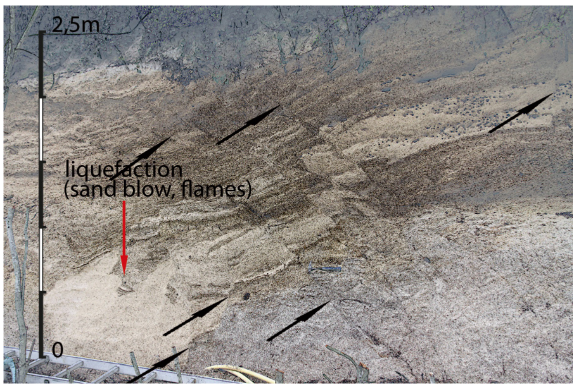


Fig.13: Reverse faulting system and folding of sedimentary units accompanied by a flame structure of liquefaction, attesting for coseismic surface deformation. Illustration with image processing (photoshop) from Fig. 11.

**DISCUSSION – CONCLUSION**

Permafrost, solifluction, gravitational sliding can be confused with tectonic features of seismic origin (Van

Vliet-Lanoë et al., 2004). In our case and in other sites in intraplate Europe, the glacial origin of some features visible in trenches is well differentiated from faulting (Demoulin, 1996; Vanneste et al., 1999). Quaternary reverse faults visible in seismic profiles (Fig. 7) and at the surface (Fig. 10) are associated with soft sediment deformations (sand blows) that contain Holocene organic materials. The major fold-related fault of Sauvage shows secondary normal faults that can be interpreted as "bending-moment fault" or "extrados" fault. As for the synsedimentary landslide and fault at Clesles, they affect only the summit of the stratigraphic units not linked to sliding on permafrost. At Longueville the extension of certain faults (normal and reverse) into the mudslide (diamicton) substratum (bed) should be noted. The absence of local karsts (Rodet, 1992) in all sites, rules out the interpretation of presumable mass sliding or lateral spreading.

Our investigations in different quarries of the Paris basin and along the the Vittel and Omey faults attest for active faulting and coseismic deformation. Main conclusions can be summarized in four points:

– The largest Quaternary tectonic features and surface deformations are near the major faults of Vittel and Omey.

– Active reverse and secondary normal structures accompanied by nearby sand blows are sealed by different stratigraphic units. The structural control of the Seine River chanel by the Omey fault and related deflection in accordance with the regional stress distribution imply a long-term activity with significant reverse slip (see also Fig. 1).

– The existence of fluid ejection, sand liquefaction and load cast at different levels of the stratigraphic section along mainly the Vittel and Omey fault zones. Prominent tectonic features represented by reverse and normal ruptures, seismites and liquefaction features are located along Omey and Vittel faults. Seismites are visible in all investigated sites and mainly in Clesles and Longueville (see Fig. 1 for location). The age of tectonic episodes is not yet characterized but sand and silt samples near fault ruptures and in sand blow units were collected during a recent field study and are currently undergoing dating by TL-OSL methods.

The active faulting and related surface deformation are very similar to those described in trenches across major surface faulting with coseismic slip. The successive vertical slip on reverse faults and size of liquefaction features such as those observed in the Gourgançon sand quarry may be associated with earthquakes of magnitude Mw ≥ 5.5. The existence of faulting episodes during the late Quaternary calls for the question on the return period of moderate to large earthquakes on, for instance, the Omey fault and its extension towards the SW, and on the Vittel - Bray fault where a late Quaternary activity is also suspected.

**References**


Antoine, P., A. Marchiol, M. Brocandel & Y. Gros, (2005). Découverte de structures périglaciaires (sand- wedges et composite-wedges) sur le site de stockage de déchets radioactifs de l'Aube (France). *C. R. Geoscience* 337, 1462–1473

Baize, S., M. Coulon, C. Hibsch, M. Cushing, F. Lemeille & E. Hamard, (2007). Non-tectonic deformations of Pleistocene sediments in the eastern Paris basin, France. *Bulletin de la Societe Geologique de France* 184 (3), 367-381.

Benoit, P., J.-M. Grisoni, B. Piwakowski & J. Argant, (2011). La craie fracturée de Charny le bachot (Aube), témoin envisageable du rejeu quaternaire des accidents de socle du bassin de Paris. *Bulletin d'information des géologues du Bassin de Paris* 48 (2), 5-16.

Camelbeeck, T. & M. Meghraoui, (1998). Geological and geophysical evidence for large paleoearthquakes with surface faulting in the Roer Graben (northwest Europe). *Geophysical Journal International* 132, 347-362.

Coulon, M., (1994). Mise en évidence et approche microtectonique des déformations quaternaires en Champagne: implications géodynamiques et consequences hydrographiques. In: *Workshop Morphogenèse cénozoïque de l'Europe de l'Ouest*. Groupe Fr. Géomorph., Rennes.

BRGM, (2013). Site sisfrance: http://www.sisfrance.net/

Demoulin,A., (1996). Clastic dykes in east Belgium: evidence of upper Pleistocene strong earthquakes west of the lower Rhine rift segment. *Journal of the Geological Society of London* 153, 803-810.

Geological map 1/50 000, (1978). Fére Champenoise, BRGM n°224.

Gregoire A. (2003). *Caractérisation des déformations mésocénozoïques et des circulations de fluides dans l'est du basin de Paris*. Doctoral Thesis, Université Henri Poincaré, Nancy 1, 294.

Institut Français du Pétrole, (2000). *Carte structurale du centre du bassin de Paris*, au toit du rhétien.

Meghraoui, M.,. Crone, A., (2001). Earthquakes and their preservation in the geological records. *Journal of Seismology* 5, 281-285.

Meghraoui, M., B. Delouis, M. Ferry, D. Giardini, P. Huggenberger, I. Spottke & M. Granet, (2001). Active normal faulting in the upper Rhine graben and paleoseismic identification of the 1356 Basel earthquake. *Science* 293, 2070-2073.

Michel, J.P, (1972). *Le quaternaire de la région parisienne.* Doctoral Thesis, Université de Paris VI.

Plaziat, J-C, (2009). Diversité et localisation chronologique des séismes dans les sables marins et éoliens du stampien, au sud de Paris. *Bulletin d'information des géologues du Bassin de Paris* 46 (4), 6-49.

Piwakowski, B., (2000). *Imagerie de la structure de subsurface par sismique réflexion très haute résolution, sur le site de Longueville sur Aube*, Société Sovep.

Philip, H., J.C. Bousquet & F. Masson, (2007). *Liquéfaction*, figure n°4.17. In: Séismes et risques sismiques, Dunod, France, 83, 87.

Rodet, J., (1992). *La craie et ses karsts*. Centre normand d'étude du karst et des cavités du sous-sol, Groupe Seine, 427- 515.

Vanneste, K., Meghraoui, M. & Camelbeeck, T., (1999). Late Quaternary earthquake-related soft-sediment deformation along the Belgian portion of the Feldbiss fault, Lower Rhine Graben. *Tectonophysics* 309, 57-79.

Van Vliet-Lanoë, B., A. Magyarib & F. Meillieza, (2004). Distinguishing between tectonic and periglacial deformations of quaternary continental deposits in Europe. *Global and Planetary Change* 43, 103–127.

# Facing Fault Displacement Hazard in Italy through paleoseismic investigations: the San Demetrio ne' Vestini (AQ) example

Blumetti Anna Maria (1), Pio Di Manna (1), Eutizio Vittori (1),Valerio Comerci (1) & Luca Guerrieri (1)

(1) ISPRA, Geological Survey of Italy, Via Brancati 48, 00144 Roma, Italy. Email: annamaria.blumetti@isprambiente.it

***Abstract:*** *After the 6 April 2009 Mw 6.3 L'Aquila Earthquake, during which coseismic surface faulting occurred causing severe damage to an aqueduct and buildings located above it, the need of a proper assessment of Fault Displacement Hazard (FDH) became evident. The Geological Survey of Italy, involved in the seismic microzonation of the San Demetrio ne' Vestini municipality (severely damaged by the 6 April event), surveyed a NW-SE trending capable fault, crossing also the historical portion of the village. In order to characterize this fault in terms of seismic and surface faulting potential, paleoseismological investigations were recently carried out through an explorative trench. These studies confirmed the fault capability: in fact, based on the stratigraphic setting exposed in the trench wall, at least 3 surface faulting events have been identified. Although radiocarbon and OSL dating is still in progress, it is possible to state that the most recent surface faulting event occurred during the Holocene, most likely in historical time.*

***Key words****: seismic microzonation, capable fault, Fault Displacement Hazard*

## INTRODUCTION

Fault Displacement Hazard (FDH) is not accounted for by the Italian national building code in seismically active areas, but only in the guidelines and criteria for seismic microzonation (Working Group MS, 2008).

The need for such regulation became evident after the 6 April 2009, Mw 6.3, L'Aquila Earthquake in Central Italy that took place on a normal fault (Paganica fault, Vittori et al., 2011) at the northern edge of the L'Aquila intermountain tectonic basin. Coseismic surface faulting occurred along this fault with surface vertical offsets up to 12 cm, causing the rupture of the water main of the Gran Sasso aqueduct feeding L'Aquila and structural damage to many houses. The notable damages, despite the modest displacement, has led FDH guidelines to become mandatory in the reconstruction plans.

The Geological Survey of Italy (Department of ISPRA) performed studies of microseismic zonation (first level) in San Demetrio ne' Vestini, one of the villages severely damaged by the 2009 event. The studies confirmed the presence of a NW-SE trending capable fault, crossing the settlement (Working Group MS–AQ, 2010). This note illustrates the first results of recent paleoseismological investigations along this fault, carried out in support of the reconstruction plan of the local municipality.

## PALEOSEISMOLOGICAL ANALYSES ALONG THE SAN DEMETRIO NE' VESTINI FAULT

In the months following the L'Aquila earthquake and in the framework of a microseismic zonation, the Geological Survey of Italy carried out a detailed geological and geomorphological survey of San Demetrio ne' Vestini village (Fig. 1). A NW-SE trending capable fault, crossing the settlement, was pointed out (Working Group MS–AQ, 2010). This fault was already identified as a Quaternary, possibly active fault by Bagnaia et al. (1992) and Bosi and Bertini (1993). It does not crop out, but is "inferred" at the base of a scarp that breaks up the flat surface of a recent fluvial terrace (Figs. 1 and 2).

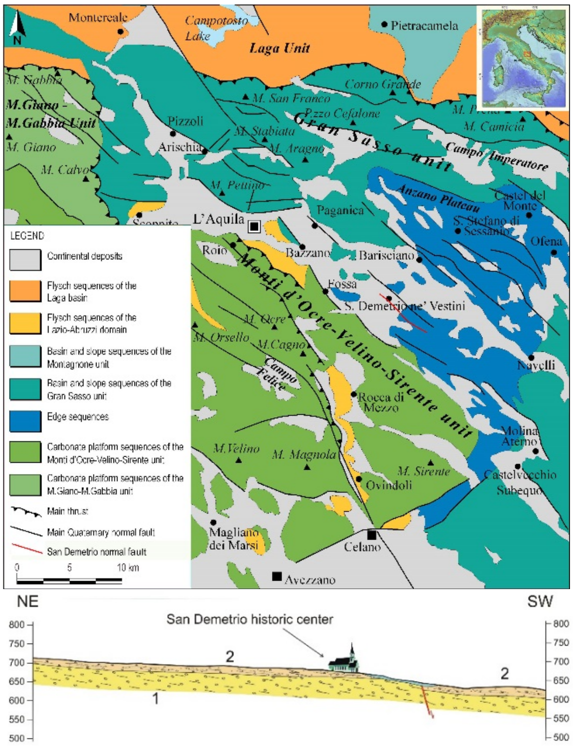


*Fig. 1: Above -Tectonic framework around the S. Demetrio fault segment. The area is part of the Apennines thrust-and-fold belt in Central Italy. Below - geological profile across the fault. Legend: 1) Fan delta conglomerates (Lower to Middle Pleistocene); 2) Gravels and sands (Middle Pleistocene). See Figure 3 for location of cross section. Modified after Working Group MS–AQ (2010).*


*Fig. 2: Panoramic (up) and close (down) view of the fault scarp related to the Demetrio fault. The orange net marks the trench site.*

In order to map an appropriate setback area in the Reconstruction Plan, and to characterize the fault capability in terms of seismic and surface faulting potential, the Mayor of the San Demetrio 'ne Vestini municipality invited ISPRA to carry out paleoseismological studies.
To contribute locating the most suitable trenching site, a geophysical survey was performed, consisting of three ERT (Electrical Resistivity Tomography) profiles and a seismic refraction tomography profile, whose results will be the subject of a following paper. One of the ERT profiles made in 2010 is reproduced in Figure 3.

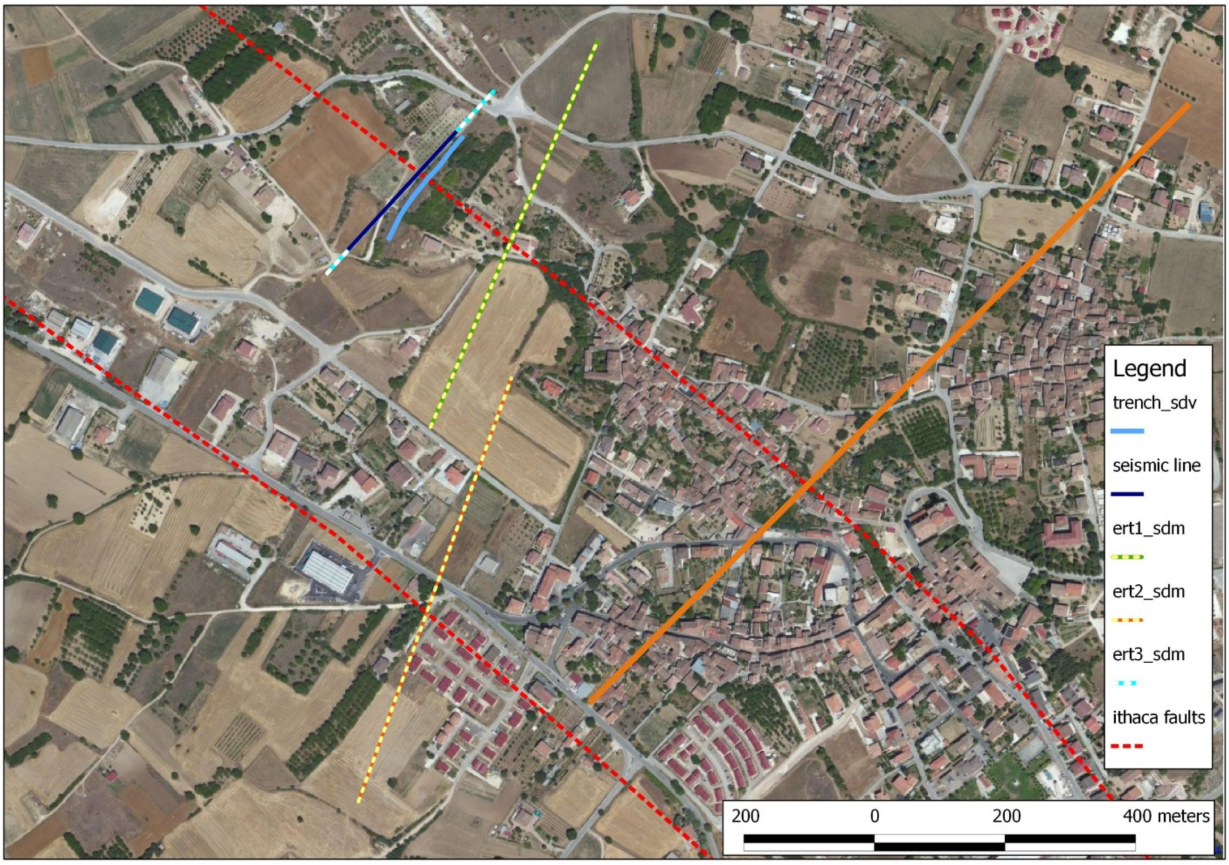


*Fig. 3: Location of the geophysical surveys performed by the Geophysical Office of ISPRA. The red dashed lines are two capable faults that cross San Demetrio village. In this study we analyse the north-eastern fault, named San Demetrio fault. The orange line locates the trace of the cross section shown in Fig 1.*

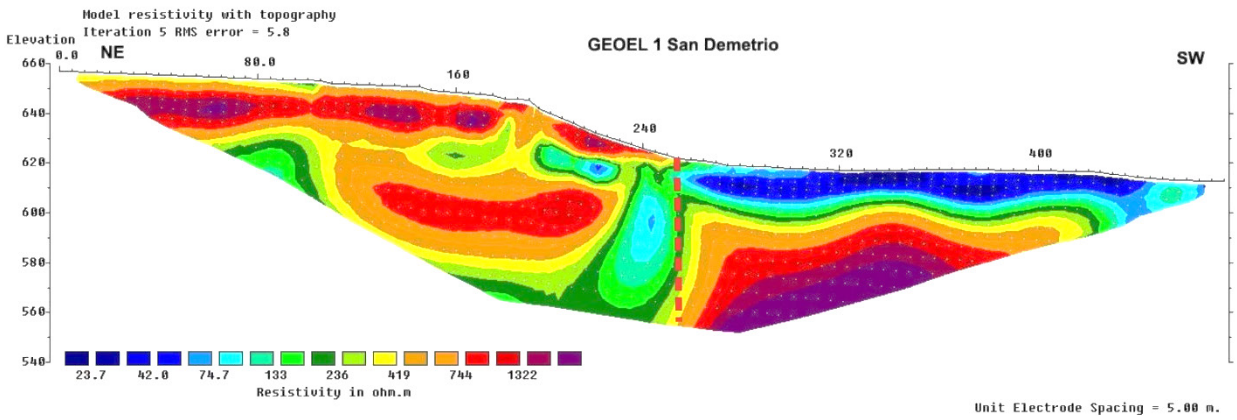


*Fig. 4: ERT profile across the San Demetrio fault (ERT1 in Fig. 3; after Working Group MS–AQ, 2010).*

It was decided to dig a trench northwest of the historical portion of the village, where morphotectonic observations and geophysical data (Fig. 4) were in good agreement indicating the occurrence of a fault cutting up close to the surface. The length of the trench (130 meters) was justified by the aim to verify the presence of other ruptures downslope, especially where the geophysical sections have pointed out some significant anomalies. Indeed, this area is being considered for future building development within the reconstruction plan after the earthquake, so the correct evaluation of the extension of the deformation zone is particularly relevant.

The detailed analysis of the stratigraphy exposed in the trench walls confirmed that the exposed fault is capable of producing surface ruptures (Figs. 5 and 6). In fact, at least two colluvial wedges were identified, the uppermost surely not older than Holocene, and probably historical, due to its likely correlation with a nearby layer containing pottery (Fig. 7). The gravel soil sealing the fault appears to be very young, surely historical because of their content of pottery shards. Other detailed stratigraphic observations indicate the occurrence of at least 3 ground rupture events in the last few thousand years. Radiocarbon and OSL datings, now in progress, will provide a more accurate temporal framework for these events.

*Fig. 5: Above: panoramic view of the trench walls that expose the San Demetrio fault. Below: the view of the fault zone exposed in the eastern wall.*

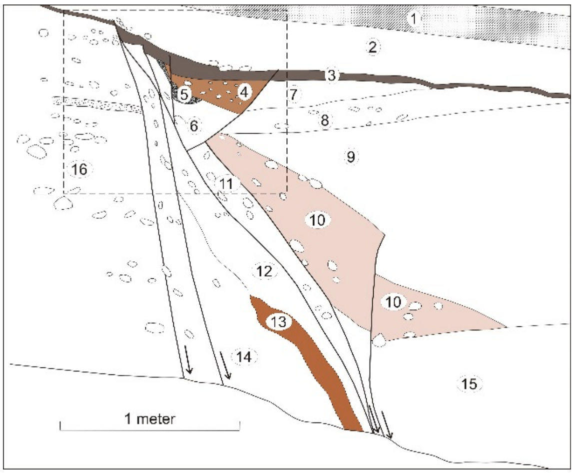


*Fig. 6: Stratigraphic sketch of the fault zone exposed in the eastern wall of the San Demetrio trench. Levels 4 and 10 are colluvial wedges. The dashed box locates Fig. 7.*

*Fig. 7: Close-up view of the upper colluvial wedges exposed in the eastern wall of the San Demetrio trench.*

**Acknowledgments:** The Authors wish to thank Valeria Eulilli, Fernando Ferri and Luca M. Puzzilli for providing the geophysical investigations, and Leonello Serva for his valuable suggestions in the paleoseismic interpretation of the stratigraphic log.

## References

Bagnaia, R., A. D'Epifanio & S. Sylos Labini, (1992). Aquila and subaequan basins: an example of Quaternary evolution in Central Apennines, Italy. *Quaternaria Nova* II, 187-209 (preprint spec. number 1, 1-23- 1989)

Bertini, T. & C. Bosi, (1993). La tettonica quaternaria nella conca di Fossa (L'Aquila). *Il Quaternario* 6, 293-314.

Vittori E., P. Di Manna, A.M. Blumetti, V. Comerci, L. Guerrieri, E. Esposito, A.M. Michetti, S. Porfido, L. Piccardi, G. Roberts, A. Berlusconi, F. Livio, G. Sileo, M. Wilkinson, K. Mccaffrey, R. Phillips & P.A. Cowie (2011). Surface faulting of the April 6, 2009, Mw 6.3 L'Aquila earthquake in Central Italy. *Bulletin of the Seismological Society of America* 101, 1507-1530.

Working Group MS (2008). *Indirizzi e criteri per la microzonazione sismica*. Conferenza delle Regioni e delle Province autonome - Dipartimento della protezione civile, Roma, 3 vols. & DVD.

Working Group MS–AQ (2010). *Microzonazione sismica per la ricostruzione dell'area aquilana*. Regione Abruzzo - Dipartimento della Protezione Civile, L'Aquila, 3 vols. & CD.

INQUA Focus Group on Paleoseismology and Active Tectonics

paleoseismicity.org

# Return period of great Himalayan earthquakes in eastern Nepal inferred from studies along the Patu and Bardibas strands of the Main Frontal Thrust

*Laurent Bollinger (1), Som Nath Sapkota (2), Paul Tapponnier (3), Yann Klinger (4), Magali Rizza (3) Jerôme Van Der Woerd (5)*

(1) CEA/DAM/DIF, Arpajon, France. Email: laurent.bollinger@cea.fr
(2) Department of Mines and Geology, National Seismic Center, Kathmandu, Nepal.
(3) Earth Observatory of Singapore, Nanyang Technological University, Singapore.
(4) Institut de Physique du Globe de Paris, CNRS, Paris, France.
(5) Institut de Physique du Globe de Strasbourg, CNRS, Strasbourg, France

***Abstract:*** *The return period of large Himalayan earthquakes (M>8.0) remains debated. Indeed, despite repeated destructions of some of the large historical cities along-strike Himalaya as attested by historical chronicles, few clear association between those records and a given segment of the Himalayan fault system are ascertained to date. Here, we describe clear evidences of modern surface deformation and ruptures attributed to the great 1255 and 1934 earthquakes in eastern Nepal. We further investigate the recent slip history of the fault system studying a long record of uplifted terraces. The first results suggest an average return period for large Himalayan earthquakes in eastern Nepal somewhere in between 774 +/- 40 and 907 +/- 150 years.*

***Key words****: Himalaya, Main Frontal Thrust, Bihar-Nepal earthquake.*

Although assessing the return period of large earthquakes along the Himalayan arc is of paramount socio-economic importance, it has remained a particularly challenging scientific issue. Indeed, large historical earthquakes, particularly the M≈7.8 1905 (Kangra) and M>8.0 1934 (Bihar-Nepal) events, were widely believed to have been blind. Furthermore to date, along most segments of the Himalayan Main Frontal Thrust (MFT), paleoseismological trenches have generally exposed much older seismic events and only one in the last 1000 years at any single site (e.g. Lavé et al., 2005; Kumar et al. , 2006, 2010).

However, detailed geomorphic mapping along the MFT in the macroseismic area of the 15/01/1934, Bihar-Nepal earthquake suggests that several of its strands ruptured recently.

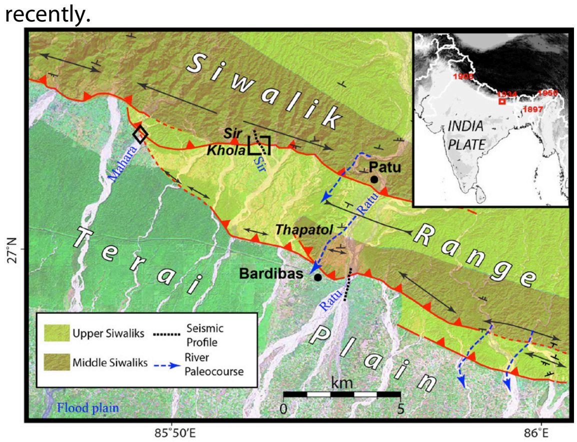


*Fig. 1: Map of the area investigated of right stepping strands between Mahara and Aurahi rivers, superimposed on a Landsat TM image. Dashed blue lines with arrows are channels abandoned by the rivers. Map in inset with the location of the site studied (red box) and the location of the largest instrumental earthquakes (7.8<M<8.6).*

We found particularly well-preserved evidences of recent faulting in the Sir river valley, where the river crosses the Patu thrust (Sapkota et al., 2013, Figure 1- black box).
We used Total-Station leveling and Terrestrial Lidar Scanning to survey the tectonic/fluvial geomorphology and log the structure of cleaned sections. Refreshing 50 m of a cliff at the base of a ≈ 30 m-high cumulative thrust escarpment along the river's eastern bank exposed four north-dipping thrusts outlined by dark gouge (Figure 2). Three of them (F1, F3, F4 from south to north) truncate ≈ 2m-thick gravel/pebble layers. The main slope-break near the base of the escarpment coincides with the emergence of F3, which emplaces sheared Siwaliks series (here Pliocene sandstones) on a wedge of soft fluvial deposits and colluvium whose proximal part contains collapsed Siwalik blocks. The emergence of F4 corresponds to local steepening of the escarpment slope, and that of F1 to an eroded scarplet, down-slope across the low-level footwall terrace T2. This F1 thrust zone emplaces a toe of folded Siwalik sandstones upon several units of conglomerates, whose fluvial origin is clear from pebbles imbricated by south-directed water-flow (Figure 3). The hanging wall strath terrace T2, which now stands 4 m above the river-bed, was uplifted by ≈ 3 m of co-seismic slip during an earthquake (E1) on the uppermost F1 splay, which is only sealed by the young fill of a still active rill channel at the foot of the eroded scarplet. Faults F1 and F3 are also exposed in a 43 m-long trench excavated at the base of the main escarpment on the river east bank. The trench confirms, and complements, the relationships of F1 and F3 with similar, and additional, fluvial and colluvial deposits. In the trench, the wedge of soft overbank and colluvial wash observed along the river-cut tops an older collapse wedge capping F3, implying the occurrence of a more ancient event (E2) on that thrust splay.

The calibrated 14C ages of 25 detrital charcoal samples collected along the river-cut and in the trench constrain the chronology of deposition, and place limits on the dates of E1 and E2 (e.g. figure 2). Six sample ages indicate that the unconsolidated T2 conglomerates offset by E1 were emplaced by the river in the period spanning the 16th to early 20th centuries, while the channel fill sealing F1 is modern. In the trench, 11 charcoal ages constrain the date of E2 on F3 to postdate fluvial conglomerates emplaced around AD 570-665 and to predate the colluvial wedge that collapsed above F3 in the 13th - 16th centuries, with a preferred age in the mid 13th century. Oxcal tests, using Bayesian models, of more refined depositional scenarios based on robust stratigraphic inferences concur to support a simple surface faulting scenario, in which E2 and E1 are the AD 1255 and 1934 earthquakes, respectively. These results bring evidences that the 15/01/1934, Mw ≈ 8.1-8,4, Bihar-Nepal earthquake was not a blind event. They also suggest it might have been a repeat of the catastrophic, AD 7/06/1255 historical event that devastated Kathmandu and mortally wounded the King.

Both ruptures are shown to affect along strike a long record of terraces uplifted along the Patu and Bardibas strands of the Main Frontal Thrust system. To investigate further the recent slip history of the fault system, we dated the sedimentary records along both structures. In addition to the presence of the two historical events aforementioned, terraces within the hangingwall of the Patu thrust recorded two additional events within the last 2800 +/-100 BP. The excavation of the footwall of a flexural fold scarp along the southern splay of the fault system reveals that those events generated transient episodes of deposition and opens the record of the past earthquakes to a minimum of 6 in the past 4500 years. All these observations suggest an average return period for large Himalayan earthquakes in eastern Nepal somewhere in between 774 +/- 40 and 907 +/- 150 years.

*Fig. 3: Photo of fault F1 : Siwaliks sandstones thrusted over drag-folded fluvial gravels and pebbles beds dated between 2460 BC to 1640AD.*

**Acknowledgements:** The research, mostly conducted in the framework of Som Nath Sapkota's PhD thesis, was funded by EOS (NTU, Singapore) and DASE (CEA, France) as well as by Project PAKSIS (ANR Cattel, France). We thank G. Cook (SUERC Radiocarbon Dating Laboratory, University of Glasgow, UK) for the charcoal samples analyses and our colleagues from National Seismic Centre from Department of Mines and Geology (Nepal) for assistance in the field.

## References

Kumar S., S.G. Wesnousky, T.K. Rockwell, R.W. Briggs, V.C. Thakur & R. Jayangondaperumal (2006). Paleoseismic evidence of great surface rupture earthquakes along the Indian Himalaya, *Journal of Geophysical Research* 111, B03304.

Kumar, S., S.G. Wesnousky, R. Jayangondaperumal, T. Nakata, Y. Kumahara & V. Singh, (2010). Paleoseismological evidence of surface faulting along the northeastern Himalayan front, India: Timing, size, and spatial extent of great earthquakes , *Journal of Geophysical Research* 115, B12422.

Lavé, J., D. Yule, S. Sapkota, K. Basant, C. Madden, M. Attal & R. Pandey, (2005). Evidence for a Great Medieval Earthquake (~1100 A.D.) in the Central Himalayas of Nepal, *Science* 307, 1302-1305.

Sapkota, S., L. Bollinger, Y. Klinger, P. Tapponnier, Y. Gaudemer & D. Tiwari, (2013). Primary surface rupture of the great Himalayan earthquakes of 1934 and 1255, *Nature Geoscience* 6, 71-76.

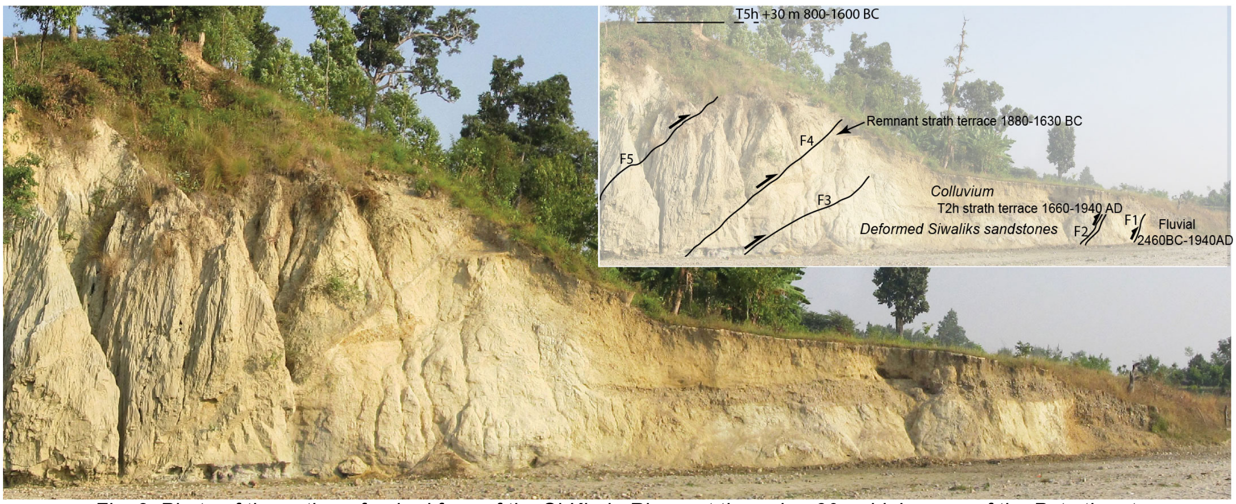


*Fig. 2: Photo of the entire refreshed face of the SirKhola River cut through a 30 m-high scarp of the Patu thrust.*

INQUA Focus Group on Paleoseismology and Active Tectonics

paleoseismicity.org

# Prediction of landslide susceptibility in a seismically active high mountain region using data mining methods – a study from Maily-Say, Kyrgyzstan

*Anika Braun (1), Tomas M. Fernandez-Steeger (1), Hans-Balder Havenith (2), Almaz Torgoev (2)*

(1) Department of Engineering Geology and Hydrogeology, RWTH Aachen University, Lochnerstraße 4-20, 52064 Aachen, Germany. Email: braun@lih.rwth-aachen.de

(2) Géorisques et Environnement, Department of Geology, University of Liège, B20 Sart Tilmann, 4000 Liège, Belgium.

***Abstract:*** *A landslide susceptibility analysis was carried out for a tectonically active high mountain region in Kyrgyzstan with data mining methods. A landslide inventory and a factor dataset based on a digital elevation model and a geological map were investigated for patterns and dependencies regarding landslide occurrence using classification algorithms. The models were evaluated for their skills and for geological plausibility in their spatial context. While algorithms like Artificial Neural Networks, Bayes Networks and Support Vector Machine produced relatively useful results regarding landslide susceptibility prediction, decision trees and Logistic Regression developed only limited skills. An ensemble model combining five models yielded no improvement. The method proofed to be useful for analysis of landslide susceptibility in remote regions where landslide occurrence is related to multiple factors. From a relatively simple dataset a maximum of information can be generated.*

***Key words****: Landslide, susceptibility, data mining.*

## INTRODUCTION

Landslides, which are here understood as mass movements of soil, rock or debris down a slope (Cruden, 1991), cause significant damage to infrastructure and fatalities worldwide. As David Petley, who started collecting data on landslide-induced fatalities in 2002, states on his weblog (Petley, 2012b), 40123 people were killed during non-seismic landslides between 2002 and 2012 (see also Petley, 2012a). If the number of fatalities due to earthquake related landslides is added the total number is 89177, which is mainly due to two large events during that period. For large earthquake events up to 30 % of the fatalities are attributed to landslides, as observed by Havenith (2011). Additionally, earthquakes often have a long-term weakening effect on slopes that may contribute to their failure some time after the seismic event.

In contrast to other natural disasters, like earthquakes or storms, the spatial occurrence and impact of landslides is more or less limited. Locations that are susceptible for landslides can be identified by the assessment of geological, geomorphological and hydrological conditions that have lead to landslides in the past and present (Varnes, 1984). The determination of landslide susceptibility is the key to an adapted land use planning which is the simplest way to prevent damage and fatalities through landslides. Landslide susceptibility is here defined as the spatial probability of landslide occurrence, set aside the temporal probability of occurrence of a triggering event.

For the determination of landslide susceptibility numerous qualitative, quantitative, direct, indirect, statistic or deterministic methods are proposed in the literature as reviewed elsewhere (e.g. Aleotti and Chowdhury, 1999). Within the last decade the use of data mining methods for the prediction of landslide susceptibility was implemented. Data mining methods originate in times when computers began to allow the storage of large amounts of data and methods for effective data analysis were needed. They aim at the discovery of patterns or new insights in data (Fayyad et al., 1996, Pyle, 1999). Typical data mining tasks are classification, segmentation or dependency problems. In landslide susceptibility analysis data mining methods simulate the reasoning process of the geologist in the field who can classify a certain geological and geomorphological situation as susceptible or not susceptible for landslides. The algorithms are trained on a dataset with known classification result in order to develop the skill to classify an unknown dataset according to the particular characteristics of the different variables. The advantage of data mining approaches for analysing landslide problems is their ability to handle large datasets and non-linear problems and their robustness regarding noisy or incomplete data. The growing amount of easily and freely accessible geodata due to the rapid development of geographical information systems (GIS) and the distribution of data via the internet during the last decades makes data mining an attractive approach for analysing landslide hazards especially in remotely located or not easily accessible, structural weak locations.

In this study the landslide susceptibility was analysed for a location in Kyrgyzstan where a complex interplay of different geological, geomorphological, hydrological, seismic and anthropogenic, preparing and triggering factors causes various types of landslides. Based on a large factor dataset and a digital landslide inventory different models were trained and tested with the Maily-Say dataset. The best models were combined in an ensemble model in order to combine the particular strengths of the different methods.

## SETTING

The former uranium mining town Maily-Say is located in the western foothills of the tectonically active Tien Shan mountain range. The Tien Shan is an orogenic belt from Variscan times which was reactivated during the collision of India and Eurasia 55 Ma ago and started to rise 10 Ma ago (Molnar & Tapponier, 1975; Bullen et al., 2001), see fig. 1. Peaks exceed heights of 7000 m.

The local geology of Maily-Say is due to the transitional position in the foothills of a high mountain area dominated by young, partially soft Jurassic, Cretaceous and Paleogene sedimentary rocks. A relatively weathering resistant, relief-forming formation is a Cretaceous limestone that was also mined for uranium. The landscape is characterised by a distinct relief with elevations between 700 m and 4000 m. The climate is predominantly dry-continental with snowfall in winter and high run off in spring.

Besides being geologically and geomorphologically disposed for slope failures because of relatively weak rocks and steep slopes, other factors like high rainfall and runoff in spring, land use and earthquakes contributed to Maily-Say's landslide history. While only few landslides were known before, landslide activity started to increase when the uranium mining began in 1946 which is probably because of mining related activities below and above ground (Torgoev et al., 2002) as well as an intensified land-use due to the fast growing town. In 1962 157 landslides were present. Uranium mining works were stopped in 1968. Landslide activity was accelerating in the 90s producing now large scaled landslides with volumes of up to 5 Million $m^3$ partly associated with the $M_s$ 6,2 earthquake in 1992, at 20 km south of Maily-Say (Havenith et al., 2006). In 2007 more than 200 landslides were present. Several times landslides dammed the main river of the valley during spring runoff causing flooding upstream and outburst floods downstream, threatening several uranium tailings that are located around the town.

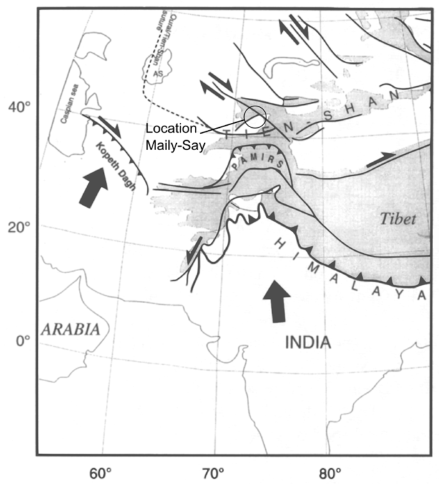


*Fig. 1: Schematic tectonic map of Southern Central Asia, from Bossu et al. (1996) with approximate location of the Maily-Say study area. Shaded areas are above 2000 m.*

## METHODOLOGY

The prediction of landslide susceptibility was based on a dataset including a landslide inventory and a set of parameters related to landslide occurrence. Landslide inventories for the years 1962, 1984, 1996, 2002 and 2007 were mapped in the course of research projects of Liège University using maps, old landslide inventories, aerial photographs, satellite images and field observations. The results presented here are only based on the 2007 inventory. The dataset of parameters related to landslide occurrence includes geology and quaternary deposits, local faults and a set of hydrological and geomorphological parameters which were extracted from a digital elevation model (DEM) with a cell size of 20 meters using a geographic information system (GIS). Among others, parameters like aspect, slope angle, curvature, distance to rivers, topographic roughness index, wetness index or flow accumulation, 23 parameters in total, were investigated.

The dataset was prepared in an extensive pre-processing procedure, as described for example in Pyle (1999), including elimination of missing values, transformation and encoding of the data, the identification of unimportant variables, balancing of the dataset, factor analysis and partitioning of the data into a training and a test dataset. In total the database contains 115600 datasets. The factor analysis revealed 5 factors, which were also used as input variables for the modelling. Different classification algorithms – an Artificial Neural Network (ANN), Bayesian Network, Discriminant Analysis, a C5.0 Decision Tree and a CHAID Decision Tree, Logistic Regression and a Support Vector Machine (SVM) - were developed with the training dataset to build the models, which were then evaluated with the test dataset. The classification result was transferred back into the GIS in order to evaluate the geological plausibility of the prediction in a spatial context.

## RESULTS AND DISCUSSION

How can the performance of a landslide prediction model be evaluated? Basically, for the result of a binary classification problem four cases can be distinguished (table 1): the occurrence of an event was predicted correctly (hit), the not-occurrence of an event was predicted correctly (correct rejection), the event was observed but not predicted (miss) or the event was predicted but not observed (false alarm). Of course one could consider the overall number of cases that were classified right by the model (hit + correct rejection = proportion correct, PC). For unfrequent events, like landslides, which are often underrepresented in datasets, this number is hardly useful for performance

*Tab. 1: Scheme with the possible cases of a binary categorical prediction result.*

| Event forecast | Event observed | |
|---|---|---|
| | no | yes |
| no | d (correct rejection) | c (miss) |
| yes | b (false alarm) | a (hit) |

validation. The dataset presented here contains around 10 % of data points where a landslide occurs. If one assumed, that all cases are "no landslide" one would still achieve a right classification of 90 % of the dataset, which is actually better than any of the model results presented here. A valuable model should develop the skill to predict landslide occurrence and not only landslide not-occurrence. A measure of this ability is the hit rate H, the ratio of hits and the sum of hits and misses (H = hits / (hits + misses)). The false alarm rate, which is the ratio of false alarms and the sum of false alarms and correct rejection (F = false alarms / (false alarms + correct rejections)), is another measure for the skill of the model. However, a false alarm is not as unfavourable as a miss, because the consequences of not predicting an event that then occurs are much more fatal than those of a false alarm (Stephenson, 2000). In contrary, in landslide prediction a model, which is good in detecting landslides but has a high false alarm rate, can be useful for giving an idea of further endangered areas. F subtracted from H gives the Pierce skill score (PSS) that is recommended by Stephenson (2000) for being the only equitable measure.

Another important issue regarding model performance is the ability to generalise. This means that the model performs not only well in the training where the classification result is known but also on a new dataset, which is usually checked with the test dataset. If the model performance is significantly poorer on the test dataset this may indicate an over-fitting of the model. The C5.0 Decision Tree e.g. shows an incredibly perfect classification, but as can be seen in table 2 and in the gain chart (fig. 2) it yields a poorer performance with the test data. The gain chart visualises how the model improves the classification result compared to a random classification with a fifty-fifty chance. In principle it shows how much data is needed (x-axis) to achieve a particular percentage of right classifications (y-axis). The steeper the curve, the better is the performance. As can be seen from table 2, table 3 and fig. 2, the results of the ANN, the Bayes Network and the SVM have a lower hit rate and a higher false alarm rate. However, especially the false alarms seem geologically logical, as can be seen from the spatial visualisation of the result in fig. 3, and provide a good idea of where future landslides are likely to occur which makes them more valuable for landslide susceptibility analysis than the perfectly fitted C5.0 Decision Tree. The CHAID Decision Tree and the Logistic Regression have a relatively high PC score, but a poor hit rate, hence they are not very useful for landslide prediction. The Discriminant analysis has the highest hit rate of all models but also the highest false alarm rate with 30 % false alarms.

As already indicated, it is important to evaluate the result also in a spatial context. A model may seem good in the numbers but eventually it makes geologically no sense. Fig. 3 shows a detail view of the classification results of different models in a spatial context. The CHAID Decision Tree e.g. (f) produces a spatial distribution of landslide bodies that is completely different from the observed landslides. The Logistic Regression seems to recognise only one type of landslides, those that are located at steep slopes. Shallow landslides, like the one in the NW corner of the map, are not recognised. Also too many scattered cells as in the NW corner of the SVM map are rather unfavourable.

In order to improve modelling results by combining the different skills of the models, an ensemble of multiple models can be generated where a decision is made using a voting rule. Ensembles are however only useful if more than five models are available and if there is no model that is significantly better than the others. In this study an ensemble of the ANN, Bayes Network, Logistic Regression, CHAID Decision Tree and SVM was generated. The C5.0 was left out as it was already too perfectly fitted. As can be seen from the gain chart the ensemble yielded no further gain in this case, the graph follows the graph of the ANN, which was obviously the most optimal model.

*Tab. 2: Classification results in %.*

| *Landslide prediction* | | Training *Landslide observed* no | Training *Landslide observed* yes | Test *Landslide observed* no | Test *Landslide observed* yes |
|---|---|---|---|---|---|
| ANN | no | 82.44 | 5.21 | 82.60 | 5.10 |
| | yes | 7.01 | 5.33 | 6.88 | 5.42 |
| Bayes Network | no | 76.77 | 5.65 | 76.96 | 5.66 |
| | yes | 12.69 | 4.90 | 12.50 | 4.86 |
| C5.0 Decision Tree | no | 89.41 | 0.50 | 88.12 | 2.77 |
| | yes | 0.05 | 10.04 | 1.36 | 7.75 |
| CHAID Decision Tree | no | 83.15 | 7.66 | 83.23 | 7.60 |
| | yes | 6.31 | 2.88 | 6.25 | 2.92 |
| Discriminant Analysis | no | 59.37 | 3.79 | 59.70 | 3.89 |
| | yes | 30.08 | 6.75 | 29.78 | 6.63 |
| Logistic Regression | no | 84.43 | 8.19 | 84.51 | 8.19 |
| | yes | 5.02 | 2.35 | 4.97 | 2.33 |
| SVM | no | 83.81 | 5.61 | 83.74 | 5.92 |
| | yes | 5.65 | 4.93 | 5.74 | 4.60 |

**CONCLUSIONS**

The intention of this study was to show how a landslide susceptibility prediction based on a relatively simple dataset can be done with data mining methods and how such a prediction may be validated. Some of the models developed relatively good skills as proofed on the unknown test dataset. While the C5.0 Decision tree was too perfectly fitted to the data, the ANN, Bayesian Network and SVM developed the skill to identify future possible landslide locations with false alarms.

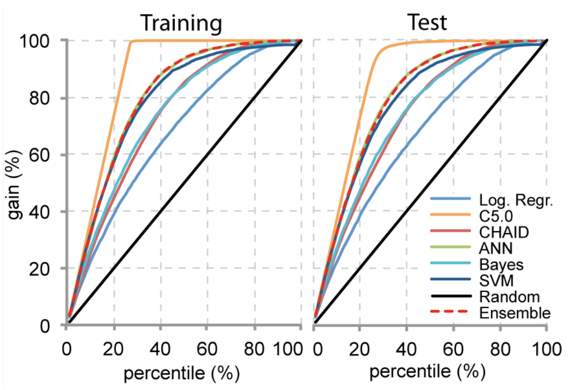


*Fig. 2: Gain charts for test and training.*

*Tab. 3: Key numbers for the evaluation of landslide prediction results based on test results.*

| | H | F | PC | PSS |
|---|---|---|---|---|
| ANN | 0.52 | 0.08 | 0.88 | 0.44 |
| Bayes Network | 0.46 | 0.14 | 0.82 | 0.32 |
| C5 Decision Tree | 0.74 | 0.02 | 0.96 | 0.72 |
| CHAID Decision Tree | 0.28 | 0.07 | 0.86 | 0.21 |
| Discriminant Analysis | 0.63 | 0.33 | 0.66 | 0.30 |
| Logistic Regression | 0.22 | 0.06 | 0.87 | 0.17 |
| SVM | 0.44 | 0.06 | 0.88 | 0.37 |
| Ensemble | 0.39 | 0.04 | 0.89 | 0.35 |

## References

Aleotti, P. & R. Chowdhury, (1999). Landslide hazard assessment: summary review and new perspectives. *Bulletin of Engineering Geology and the Environment* 58, 21-44.

Bossu, R., J.R. Grasso, L.M. Plotnikova, B. Nurtaev, J. Fréchet & M. Moisy, (1996). Complexity of Intracontinental Seismic Faultings: The Gazli, Uzbekistan, Sequence. *Bulletin of the Seismological Society of America* 86, 959-971.

Bullen, M.E., D.W. Burbank, J.I. Garver & K.Y. Abdrakhmatov, (2001). Late Cenozoic tectonic evolution of the northwestern Tien Shan: New age estimates for the initiation of mountain building. *Geological Society of America Bulletin* 113, 1544-1559.

Cruden, D. M. (1991). A simple definition of a landslide, Bulletin of the International Society of Engineering. *Geology* 43, 27–29.

Fayyad, U., G. Piatetsky-Shapiro & P. Smyth, (1996). From Data Mining to Knowledge Discovery in Databases. *AI Magazine* 17, 37–54.

Havenith, H.B., I. Torgoev, A. Meleshko, Y. Alioshin, A. Torgoev & G. Danneels, (2006). Landslides in the Mailuu-Suu Valley, Kyrgyzstan-Hazards and Impacts. *Landslides* 3, 137–147.

Havenith, H.B. (2011). Where landslides represent the most important earthquake-related hazards: the mountain areas of Central Asia. In: *Earthquake Geology and Archaeology: Science, Society and Critical Facilities* (Grützner, C., Fernández Steeger, T., Papanikolaou, I., Reicherter, K., Silva, P.G., Pérez-López, R., Vött, A. eds.), Corinth, Greece, 77-80.

Petley, D. (2012a). Global patterns of loss of life from landslides. *Geology* 40, 927-930.

Petley, D. (2012b). Ten years of collecting landslide fatality data, blog entry from 13 September 2012, the landslide blog (http://blogs.agu.org/landslideblog/2012/09/13/ten-years-of-landslide-fatality-data/).

Pyle, D. (1999). *Data preparation for data mining*. Morgan Kaufmann Publishers, 540p.

Molnar, P. & P. Tapponier, (1975). Cenozoic Tectonics of Asia: Effects of a continental collision. *Science* 189, 419-426.

Stephenson, D.B. (2000). Use of the "Odds Ratio" for Diagnosing Forecast Skill. *Weather and Forecasting* 15, 221-232.

Torgoev, I. A., Y.G. Alioshin & H.B. Havenith, (2002). Impact of uranium mining and processing on the environment of mountainous areas of Kyrgyzstan. In: *Uranium in the aquatic environment* (Merkel, Planer-Friedrich & Wolkersdorfer eds.), Springer, Berlin Heidelberg New York, 93-98.

Varnes, D. J. (1984). *Landslide hazard zonation: a review of principles and practise*. UNESCO, Paris, 63 p.

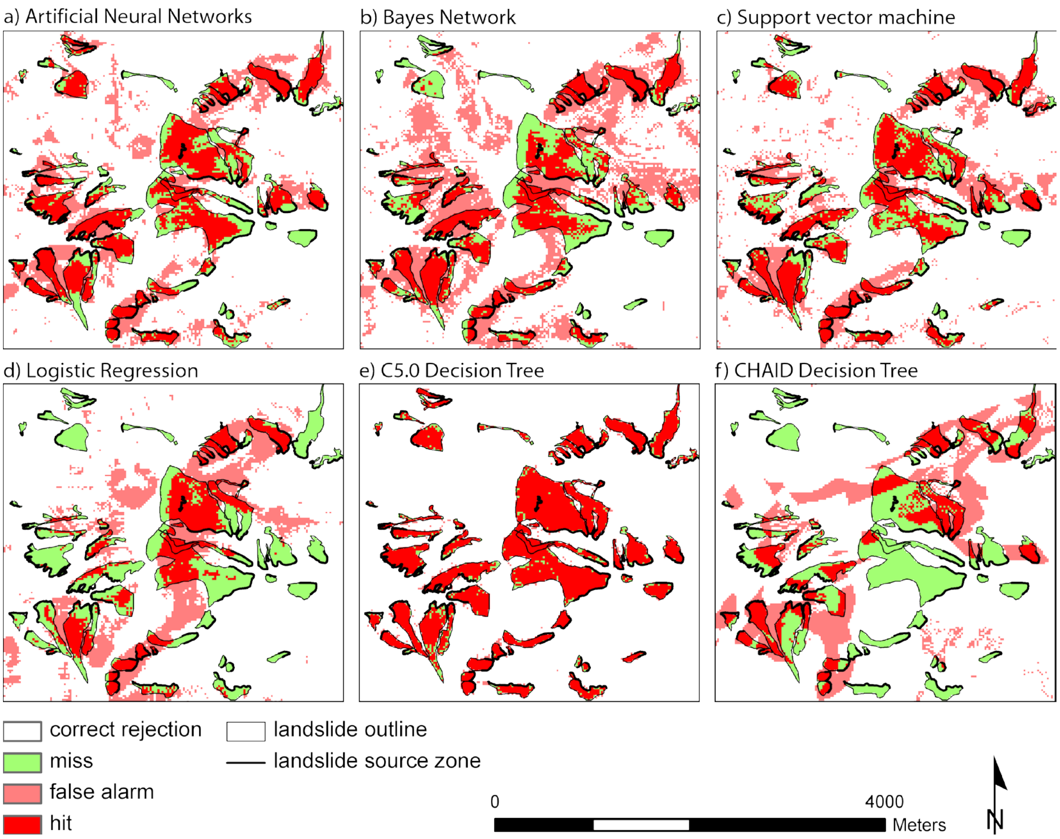


*Fig. 3: Detail view of the spatial classification result of a) ANN, b) Bayes Network, c) SVM, d) Logistic Regression, e) C5.0 Decision Tree, f) CHAID Decision Tree.*

INQUA Focus Group on Paleoseismology and Active Tectonics

paleoseismicity.org

# Active tectonics around the Yangsan-Ulsan fault system in SE Korea (I): Quaternary faults and paleoseismological studies

*Choi, Jin-Hyuck (1), Young-Seog Kim (1)*

(1) Department of Earth & Environmental Sciences, Pukyong National University, Busan 608-737, South Korea. Email: cjh0421@pknu.ac.kr

***Abstract:*** *In recorded history, since about 2 A.D. about one hundred large earthquake (M>5) have occurred in SE Korea. Recently, a number of Quaternary faults have been identified around the Yangsan and Ulsan faults. In this study, we introduce the distribution of historical earthquakes and Quaternary faults, and review previous paleoseismological studies. The results of paleoseismological studies indicate that N-S to NNE-SSW trending reverse faulting multiply occurred under E-W to ENE-WSW compression during the Quaternary. The distribution of the Quaternary faults can be subdivided into three domains; 1) The northern part of the Yangsan fault, 2) The southern part of the Yangsan fault, and 3) The eastern block of the Ulsan fault, based on fault movement and slip rate. A Coulomb 3 modelling, based on the Λ-fault model for fault geometry of the Yangsan-Ulsan fault system, indicates that the stress has become more concentrated on some specific regions during the Quaternary, and they are well matched with the distributions of Quaternary faults. However, there are still a lot of questions to be solved. Some of them are due to relatively low slip rate. More detailed paleoseismological studies around the Yangsan-Ulsan fault system will be of great benefit to gain a better understanding of active tectonics and related earthquake hazard assessments in SE Korea.*

***Key words***: *Yangsan-Ulsan fault, historical earthquake, Quaternary fault, Paleoseismology, Active tectonics.*

## INTRODUCTION

The Korean peninsula, located within the Eurasian intra-continental region, is commonly considered to be tectonically stable compared with neighbouring countries such as Japan and Taiwan. However, relatively many and big earthquakes (up to estimated magnitude 6.7) were reported in the historical records around the Yangsan and Ulsan faults, the major structural features in SE Korea. Also, more than 40 Quaternary faults have been recently discovered around the Yangsan-Ulsan fault system (e.g. Kee et al., 2009). In this study, we introduce the distribution of historical earthquakes and Quaternary faults, and review some previous paleoseismological studies to understand the characteristics of active tectonics around SE Korea.

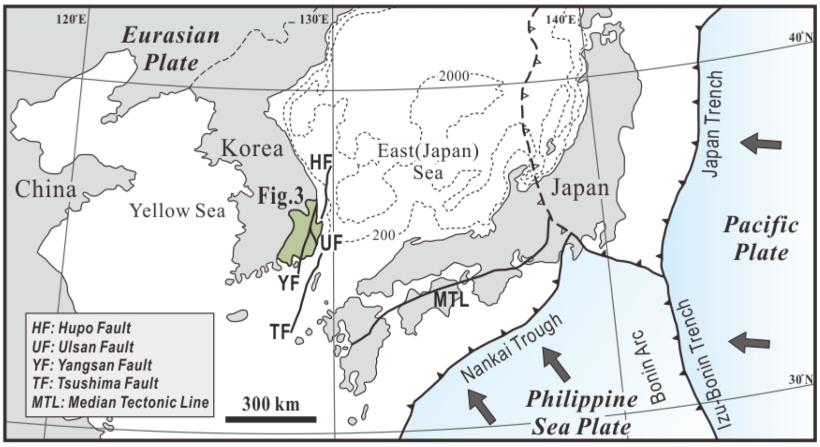


*Fig. 1: Simplified tectonic map around the East (Japan) Sea (modified from Kim and Park, 2006).*

## TECTONIC SETTING

The intraplate region around the Yangsan-Ulsan fault system shows multiphase deformation induced by the interaction of the Eurasian Plate, the adjacent Pacific Plate, the Philippine Sea Plate, and the Indian Plate (Fig. 1) (e.g., Yoon and Chough, 1995; Son et al., 2002; Choi et al., 2002; Kim and Park, 2006). Cenozoic tectonic deformation of this region has been mainly affected by the opening and closing of the East Sea (Sea of Japan). The intraplate deformation initiated back-arc rifting and the spreading of the East Sea in the late Oligocene to early Miocene (e.g., Kimura and Tamaki, 1986; Kaneoka et al., 1992; Yoon and Chough, 1995; Son et al., 2005; Choi, 2006), and this may have induced the opening of Tertiary basins and slip along many normal faults (Son et al., 2000, 2005). During the Middle Miocene, the tectonic conditions changed due to collision of the Bonin Arc with central Honshu that resulted in back-arc closing and crustal shortening (Chough and Barg, 1987; Yoon and Chough, 1995; Lee et al., 2001). The stress configuration later changed again, to E-W or ENE-WSW trending compression during the Pliocene and it continues to present day (Kang and Baag, 2004; Jun and Jeon, 2010).

## HISTORICAL EARTHQUAKES AND QUATERNARY FAULTS

Gyeongju (see the location in Fig. 3) is a seismologically active region of SE Korea. Extensive historical records of large earthquakes stretches back

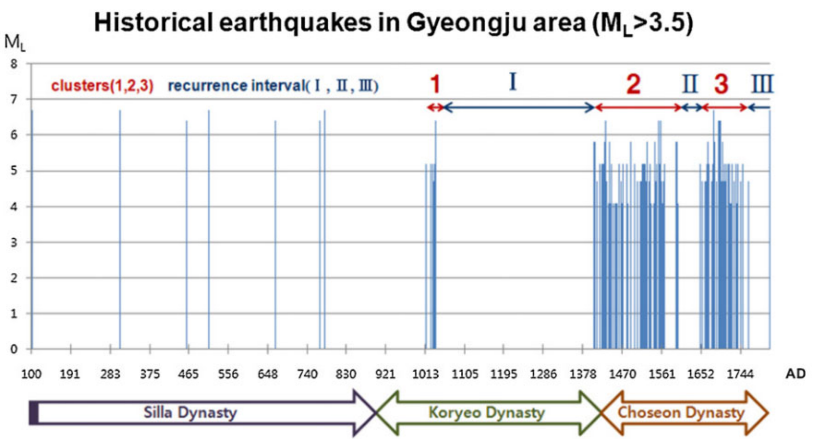


*Fig. 2: Histogram of historic earthquake catalogue from 2 A.D. to 1810 A.D. for >$M_L$ = 3.5 in Gyeongju area. It shows three earthquake clusters from 1013 A.D. and various recurrence intervals (from Jin et al., 2011).*

Large earthquake recurrence intervals often stretch over thousands of years in stable continents, thus historical records of seismicity and paleoseismic records are extremely important resources for the study of neotectonics. Furthermore, based on historical records, SE Korea experienced several large earthquakes that resulted in extensive damage to buildings and monuments at heritage sites (Jin et al., 2011). The most damaging earthquake (over 100 casualties) occurred in 779 A.D. (M=6.7) during the Silla Dynasty (Lee, 1998).

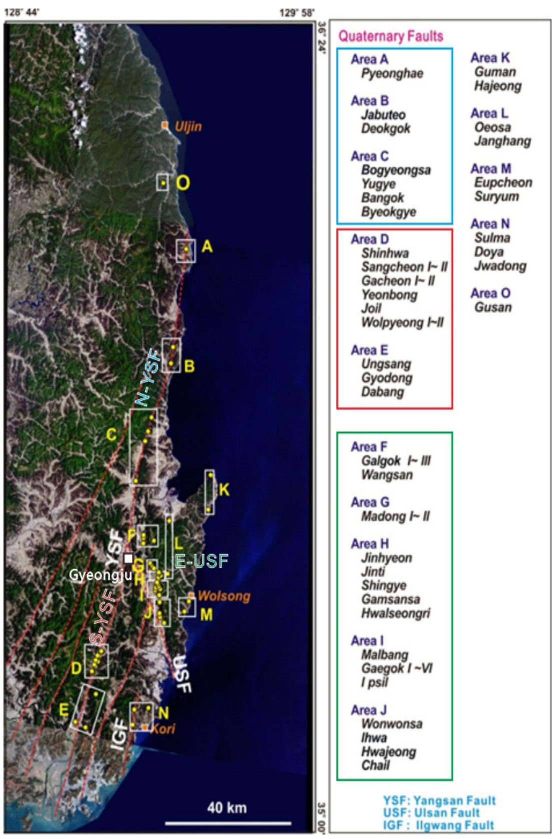


*Fig. 3: Distribution maps of Quaternary faults around SE Korea (from Kee et al., 2009).*

over 2,000 years due to its long history of civilization. About one hundred earthquakes (magnitude of 5), have been recorded in historical records in this region between 2 A.D. and 1904 A.D. (Fig. 2a) (Lee and Yang, 2006). Since 1905, instrumental earthquake records began in South Korea and about one thousand earthquakes have been recorded, less than 5 (Fig. 2b) (Baag and Kang, 2007).

Gyeongju city is located at the junction of the NNE-SSW trending Yangsan and NNW-SSE trending Ulsan faults. The distribution of Quaternary faults around the fault system shows domainal features subdivided into: 1) the northern part of the Yangsan fault, 2) the southern part of the Yangsan fault, and 3) the eastern part of the Ulsan fault (Fig. 3). Although each Quaternary faults show different characteristics, N-S to NNE-SSW trending reverse faults are dominant. Some results of fault zone analysis indicate that the present Quaternary faults experienced repeated movements including early normal or strike-slip faulting and were later reactivated as reverse faulting under almost ENE-WSW compression (e.g. Kim et al., 2004).

## PALEOSEISMOLOGICAL STUDY

Four Quaternary faults (Bogyengsa, Yugye, Bangok, and Byeikgye; Area C in Fig. 3) were discovered around the northern Yangsan fault. Yugye fault cuts young colluvial fan deposits and shows a slip rate of 0.04~0.05 mm/yr of vertical movement (Kyung and Chang, 2001). Kim and Jin (2006) suggested the estimated moment magnitude associated with the last earthquake slip is in the range of 6.5~7.5 based on 4.2 m of maximum earthquake slip (Fig. 4). The most recent earthquake event is estimated as ~2000 yr B.P. based on the radiocarbon ages of humic silt layers that have been vertically offset by about 0.5 m by recent faulting (Kyung and Chang, 2001).

The region of the southern Yangsan fault system consists of at least three strands of Quaternary faults. Fault scarps of different height on Quaternary river terraces of different ages indicate repeated late Quaternary movements (Kyung and Lee, 2006). Most Quaternary thrust or strike-slip faults indicate that the eastern block thrusted over along previous strike-slip faults (Kyung, 2003; Choi et al., 2009). Average vertical slip rate is estimated by 0.02~0.07 mm/yr and lateral slip is assumed to be several times higher than that of the vertical slip rate (Kyung, 2003).

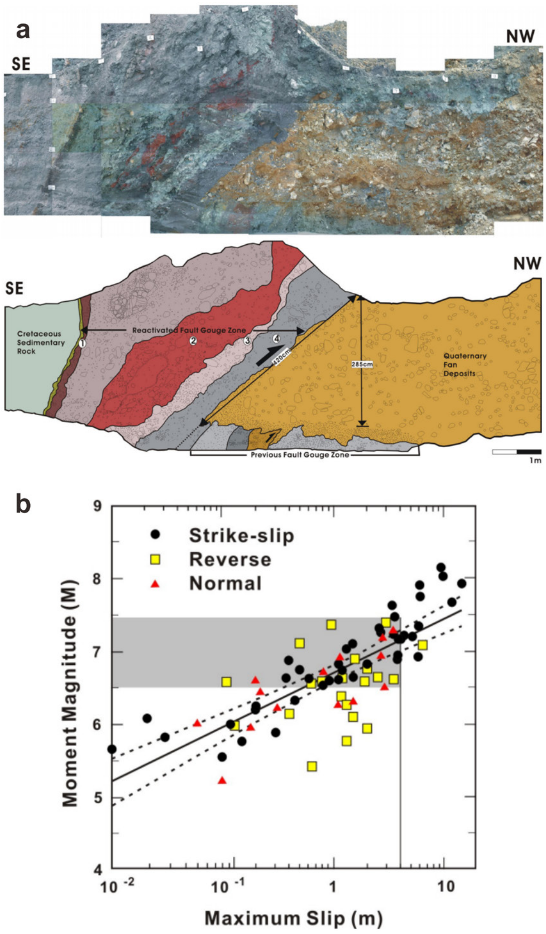


*Fig. 4: (a) Photo mosaic and sketch of the southern section of the Yugye-ri trench. (b) Estimated moment magnitude of the last Yugye Fault movement from the maximum slip of the trench (from Kim and Jin, 2006).*

An area with relatively high density of Quaternary faults has been discovered around the eastern part of the Ulsan fault (e.g. Chang, 2001; Choi, 2003). These faults are commonly characterized by repetitive reverse slips with 0.08-0.13 mm/yr of average vertical slip rate (Kyung and Lee, 2006). At least three events of reverse faulting are detected with a total offset of 2.5 m, based on geomorphic and trench analysis at the Kalgok site (Okada et al., 1999). The Wangsan fault shows a total Quaternary vertical offset of 18 m and a slip rate of 0.31~0.62 mm/yr, which is the largest offset and slip rate recorded in SE Korea (Choi, 2003). One of the most intensively studied Quaternary faults in Korea is the Eupcheon fault, which is interpreted to have four or five earthquake rupture events. Kim et al. (2004, 2011) estimated the amount of slip to be in the range of 0.7~1.8 m for each of the five identified faulting events and the earthquake magnitude in the range of $M_W$ 5.4~7.4.

## EVOLUTION OF THE YANGSAN-ULSAN FAULT SYSTEM

It is commonly accepted that E-W or ENE-WSW compression is dominant during the Quaternary up to now around the southeastern part of the Korean peninsula (Son et al., 2002; Choi et al., 2002). Han et al. (2009) explored the evolution of Yangsan-Ulsan fault system under changes of the stress regime and their internal angle from the Early Miocene to the Quaternary based on Coulomb 3 modelling. The result indicates that the consistency of high stress changes is observed in the northern & the southern parts of the Yangsan fault and especially in the eastern region of the Ulsan fault (Fig. 5a). Also, it is well correlated with the distribution of Quaternary faults and the epicenters of earthquakes around Yangsan-Ulsan fault system (Figs. 5b-c). Furthermore, uplift rate of marine terraces in the eastern block of the Ulsan fault is relatively higher than other regions (Chwae and Choi, 2007).

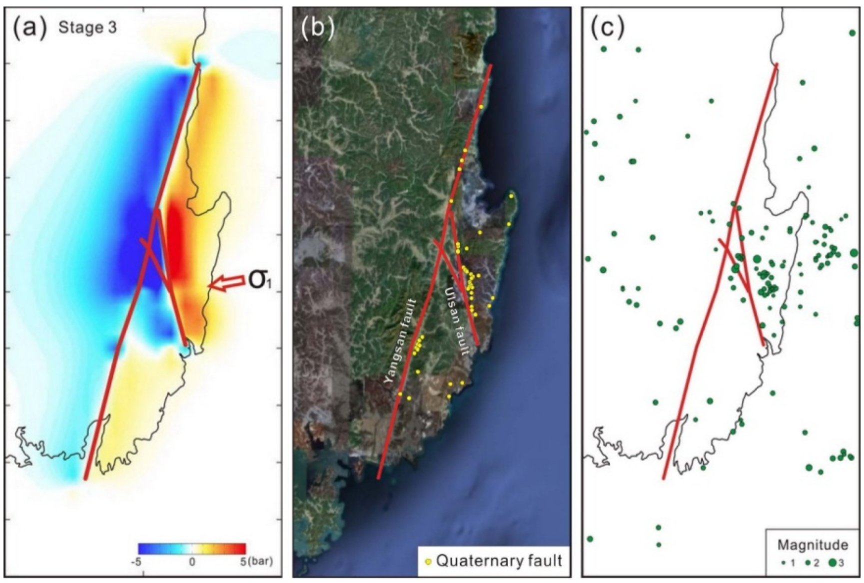


*Fig. 5: Comparison between Coulomb stress changes (a), distribution of Quaternary faults (b) and epicenters of earthquakes (c) around the Yangsan-Ulsan fault system (from Han et al., 2009).*

## DISCUSSION AND SUMMARY

In this study, we introduce the distribution of historical earthquakes and Quaternary faults. As a result, they are closely related to the fault activity of the Yangsan-Ulsan fault system under the compressional tectonic regime. The compressional tectonic regime may result from the closing of the East Sea due to subduction of the Pacific plate and/or extrusion of the Indian plate collision. Historical and paleoseismic earthquake data indicate that the Korean Peninsula is not stable continent, although slip rates are low and recurrence intervals of large earthquakes are relatively long.

Furthermore, more detailed paleoseismological studies based on the characteristics of the evolution of the fault system will be helpful in understanding earthquake hazards and active tectonics around SE Korea.

**Acknowledgements:** We thank Kwangmin Jin, Seong-Rok Han, and Minjung Lee for their positive cooperation in field-works. We also thank an anonymous reviewer for his or her constructive comments.

## References

Baag, C.-E. & T.-S., Kang, (2007). Earthquake-induced hazard and earthquake-resistant design criteria in Korea, *Proceedings of Innovative Technology of Hazard Preparedness for Super Tall Buildings*. Korea Conference on Innovative Science and Technology.

Chang, T.W., (2001). Quaternary tectonic activity at the eastern block of the Ulsan fault. *Journal of the Geological Society of Korea* 37, 431-444.

Choi. J.-H., S.-J., Yang & Y.-S., Kim, (2009). Fault zone classification and structural characteristics of the southern Yangsan fault in the Sangcheon-ri area, SE Korea. *Journal of the Geological Society of Korea* 45 (1), 9-28.

Choi, P.Y., S.K., Kwon, S.R., Lee, J.H., Hwang, J., Angelier & G.O., An, (2002). Late Mesozoic-Cenozoic tectonic sequence of Southeast Korea. *The 1st and 2nd Symposiums of the Geology of Korea Special Publications* 1, 52-88.

Choi, P.-Y. (2006). 'Singwang strike-slip duplex' around Pohang basin, SE Korea: its structural evolution and role in opening and fill of the Miocene basin, *Geoscience Journal* 10, 145-157.

Choi, W.H., 2003. Neotectonics of the Gyeongju-Ulsan area in the southeastern part of Korean peninsula. *Thesis for PhD*, Seoul National University.

Chough, S.K. & E., Barg, (1987). Tectonic history of Ulleung basin margin, East Sea (Sea of Japan), *Geology* 15, 45-48.

Chwae, U.-C. & S.-J., Choi, (2007). Active Fault Study of Korea: the past, present and future. *Quaternary Tectonics of Southeastern Korea*, 1-31.

Han, S.-R., J.Y., Park & Y.-S., Kim, (2009). Evolution modeling of the Yangsan-Ulsan fault system with stress changes. *Journal of the Geological Society of Korea* 45 (4), 361-377.

Jin, K., M., Lee, Y.-S., Kim & J.-H., Choi, (2011). Archaeo-seismological studies on historical heritage sites in the Gyeongju area, SE Korea. *Quaternary International* 242, 158-170.

Jun, M.-S. & J.S., Jeon, (2010). Focal Mechanism in and around the Korean Peninsula, *Jigu-Mulli-wa-Mulli-Tamsa* 13, 198-202.

Kee, W.-S., Y.H., Kihm, H., Lee, D.L., Cho, B.C., Kim, K.-Y., Song, H.J., Koh, S.R., Lee, Y.-K., Yeon, S., Hwang, K.G., Park & N.-H., Seong, (2009). Evaluation and Database Construction of Quaternary Faults in SE Korea. *Korea Institute of Geoscience and Mineral Resources*, IP2006-047-2009(1), 327 pp.

Kaneoka, I., Y., Takigami., N., Takaoka, S., Yamashita & K., Tamaki, (1992), $^{40}$Ar-$^{39}$Ar analysis of volcanic rocks recovered from the Japan Seafloor: Constraints on the age of formation of the Japan Sea, *Proceedings, Ocean Drilling Program, Scientific Results* 127/128, pp. 819-836.

Kim, Y.-S., J.Y., Park, J.H., Kim, H.C., Shin & D.J., Sanderson, (2004). Thrust geometries in unconsolidated Quaternary sediments and evolution of the Eupcheon Fault, southeast Korea. *The Island Arc* 13, 403-415.

Kim, Y.-S. & K., Jin, (2006). Eastimated earthquake magnitude from the Yugye Fault displacement on a trench section in Pohang, SE Korea. *Journal of the Geological Society of Korea* 42 (1), 79-94.

Kim, Y.-S. & J.Y., Park, (2006). Cenozoic deformation history of the area around Yangnam-Yangbuk, SE Korea and its tectonic significance. *Journal of Asian Earth Sciences* 26, 1-20.

Kim, Y.-S., J.-H., Kihm, & K., Jin, (2011). Interpretation of the rupture history of a low slip-rate active fault by analysis of progressive displacement accumulation: an example from the Quaternary Eupcheon Fault, SE Korea. *Journal of the Geological Society*, London 168, 273-288.

Kimura, G. & K., Tamaki, (1986). Collision, rotation, and back-arc spreading in the region of the Okhotsk and Japan Seas. *Tectonics* 5, 389-401.

Kyung, J.B. & T. W., Chang, (2001). The Latest Fault Movement on the Northern Yangsan Fault Zone around the Yugye-Ri Area, Southeast Korea. *Journal of the Geological Society of Korea* 37 (4), 563-577.

Kyung, J.B., (2003). Paleoseismology of the Yangsan fault, southeastern part of the Korean peninsula, *Annals of Geophysics* 46, 983-996.

Kyung, J.B. & K., Lee, (2006). Active Fault Study of the Yangsan Fault System and Ulsan Fault System, Southeastern Part of the Korea peninsula. *Journal of Korean Geophysical Society* 9 (3), 219-230.

Lee, G.H., H.J., Kim, S.J., Han & D.C., Kim, (2001). Seismic stratigraphy of the deep Ulleung Basin in the East Sea (Japan Sea) back-arc basin, *Marine and Petroleum Geology* 8, 615-634.

Lee, K., (1998). Historical earthquake data of Korea. *Journal of the Korean Geophysical Society* 1, 3-22.

Okada, A., K., Takemura, M., Watanabe, Y., Suzuki., J.B., Kyung, Y.H., Chae, K., Taniguchi, T., Ishiyama, D., Kawabata, H., Kaneda & T., Naruse, (1999). Trench excavation survey across the Ulsan (active) fault at Kalgok-ri, Kyongju City, Southeast of Krore. *Journal of Geography* 108, 276-288.

Son, M., H.J., SEO & I.-S., Kim, (2000). Geological structures and evolution of the Miocene Eoil basin, southeastern Korea, *Geoscience Journal* 4, 73-88.

Son, M., H.-Y., Chong & I.-S., Kim, (2002). Geology and Geological Structures in the Vicinities of the Southern Part of the Yonil Tectonic Line, SE Korea. *Journal of the Geological Society of Korea* 38 (2), 175-197.

Son, M., I.-S., Kim & Y.K., Shon, (2005). Evolution of the Miocene Waup basin, SE Korea, in response to dextral shear along the southwestern margin of the East Sea (Sea of Japan), *Journal of Asian Earth Sciences* 25, 529-544.

Yoon, S.H. & S.K., Chough, (1995). Regional strike-slip in the eastern continental margin of Korea and its tectonic implications for the evolution of Uleung Basin East Sea (Sea of Japan). *Geological Society of America Bulletin* 107, 83-97.

# Active tectonics around the Yangsan-Ulsan fault system in SE Korea (II): Fault zone analysis and fault evolution

*Jin-Hyuck Choi* and Young-Seog Kim*

Dept. of Earth & Environmental Sciences, Pukyong National University, Busan 608-737, South Korea. Email: cjh0421@pknu.ac.kr

***Abstract:*** *The Quaternary Eupcheon fault and its northern extent are exposed in the eastern block of the Yangsan-Ulsan fault system, which is characterized by a considerable concentration of Quaternary faults. We carried out detailed geometric and kinematic analyses along exposed fault zones and trench sections with the aim of understanding movement history and fault evolution of the Eupcheon fault. The geometry of the fault zone is characterized by splayed and merged patterns as well as local duplexes, and these are all typical characteristic features indicating multiple faulting events. Kinematic analysis shows that the fault zone experienced extension which produced normal faults, which were later reactivated by shortening with reverse slip. Multiple Quaternary reverse faulting events along the Eupcheon fault were identified based on the interpretation of trench logs including colluvial wedges, and measurements of displacement–distance (d–x) relationships along the fault. These kinds of approaches can be very useful tools for the study of earthquake hazards, active tectonics, and fault zone evolution.*

**Key words**: *Eupcheon fault, Fault zone analysis, Fault evolution, Reverse reactivation, Active tectonics.*

## INTRODUCTION

The NNE-SSW trending Yangsan Fault and NNW-SSE trending Ulsan Fault are major structural features in the Gyeongsang basin, southeast part of Korea (Fig. 1). Recently, more than 40 Quaternary faults have been reported along these faults (e.g., Kyoung, 2003; Kim et al., 2011). One of the main geometric features is the intersection between the two faults, which is similar to λ-fault (Du and Aydin, 1995; Kim et al., 2000; Han et al., 2009), and the eastern block of the Yangsan-Ulsan fault system is characterized by a relatively higher tectonic activity based on distribution and slip rate of Quaternary faults and uplift rate of Quaternary marine terraces (Choi et al., 2004).

The Eupcheon fault is a Quaternary fault in the eastern part of the Yangsan-Ulsan fault system, and its fault zones are well exposed in the northern extent. In this study, we analyze three-dimensional fault geometry and kinematic indicators to understand spatial and temporal fault growth and evolution. Moreover, the slip data in trench sections of the Eupcheon fault are examined to understand the movement history of the fault during the Cenozoic.

## GEOLOGIC AND TECTONIC SETTING

The Gyeongsang Basin comprises a series of Cretaceous sedimentary rocks, which are mainly composed of lacustrine siliciclastic and volcanogenic rocks (Fig. 1). These basement rocks have been intruded by Cretaceous and Tertiary igneous bodies, which are mainly batholiths and dykes of various compositions (Fig. 1). Several Tertiary basins are locally developed within the eastern block of the Ulsan fault, and Quaternary marine terraces have been reported along the coastline (Choi, 2004; Choi et al., 2004).

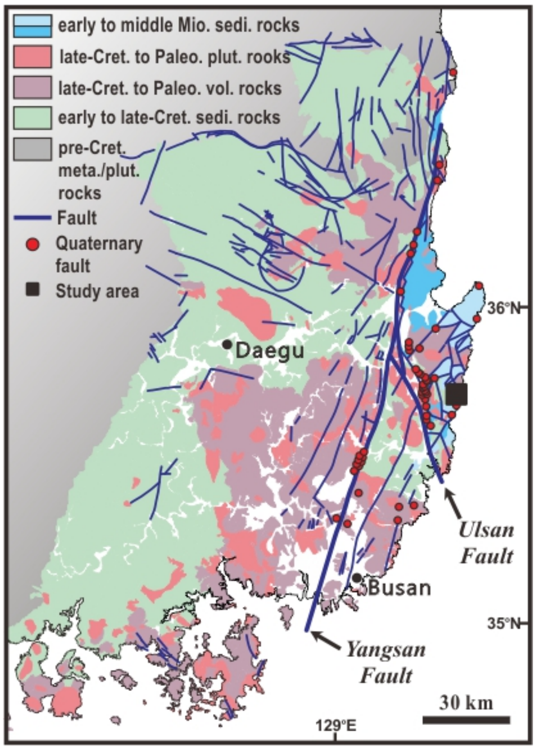


*Fig. 1: Regional geologic map of Gyeongsang Basin, SE Korea (Chough and Shon, 2010; Son et al., 2013).*

It is interpreted that the compression tectonic regime is dominant in this area from Pliocene to the present resulting from the influence of subduction of the Pacific plate and/or extrusion due to the Indian Plate collision with the Eurasian Plate (Jun and Jeon, 2010). The compressional tectonics, probably associated with the closure of the East Sea, may induce reverse faults. Note that a number of Quaternary faults with a reverse slip component have been reported in this region (Okada et al., 1994; Kyoung, 2003; Ree et al., 2003; Kim et al., 2011).

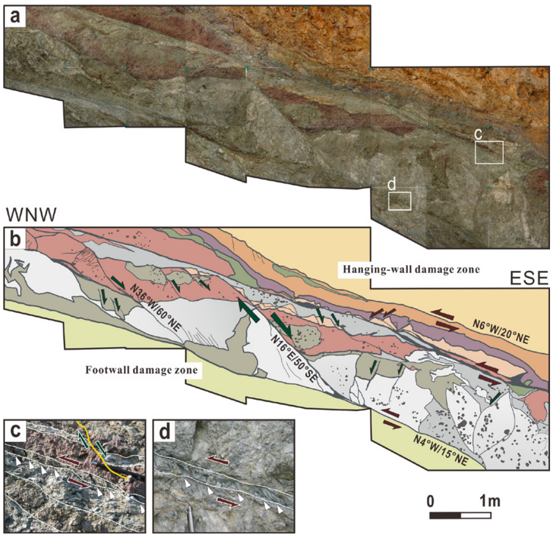


*Fig. 2: (a) Photo mosaic and (b) sketch of the detailed grid map for nearly fault-perpendicular fault zone exposure. (c, d) Cleavages within gouge zones indicate reverse slip sense (Choi et al., in preparation).*

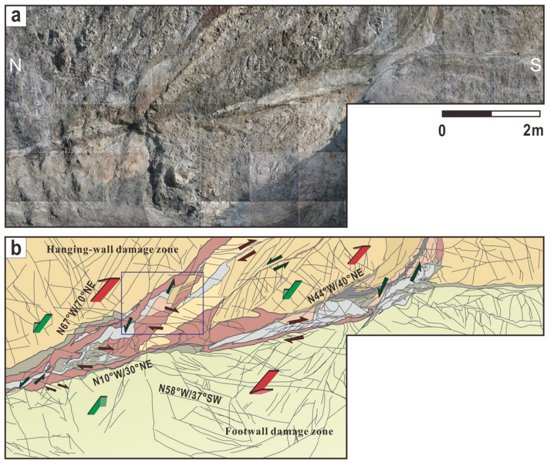


*Fig. 3: (a) Photo mosaic and (b) sketch of the detailed grid map for nearly fault-parallel fault zone exposure (Choi et al., in preparation). Duplex geometry is formed by several minor fault cores splayed out from the main fault core. Shear fabrics and secondary fractures indicate multiple slip events with opposite slip senses.*

## FAULT ZONE ANALYSIS

Fault zones are generally composed of a central fault core and its enveloping damage zones. They can be distinguished from the surrounding wall-rock which contains no deformation directly associated with the faulting (e.g., Chester and Logan, 1986; Caine et al., 1996; Kim et al., 2004a). Fault zones evolve spatially and temporally through three-dimensional volume increase, as slip accumulates. Fault zones, therefore, can show more complex architecture consisting of multiple fault cores and various damage structures (e.g., Faulkner et al., 2003). Fault zone architectures and their structural elements can reflect fault evolution, therefore many recent studies concentrate on describing three-dimensional geometries and kinematics of fault zones (e.g., Cowie and Shipton, 1998; Kim et al., 2003; Childs et al., 2009).

The N-S trending and eastward dipping main fault zone is composed of several gouge zones, showing different colours and shear senses, as well as cataclastic and fractured rocks (Fig. 2). The most geometrical feature is the splaying and merging of several gouge zones, surrounding lens-shaped duplex structures and fractured rocks (Fig. 3). These geometric features indicate that the fault zone underwent multiple slip events.

Slip indicators, such as shear fabric, cleavage and slickenline, can be mainly classified into two groups; normal and reverse slip related ones (Figs. 4a, 4b). Cross-cutting or overprinting relationships between two groups indicate that reverse slips occurred along the previous normal faults. Furthermore, we examined transport directions using the trend of slickenlines, the orientations of maximum principal stress based on cleavages, and the intersection lineations between the slip surfaces and cleavages (Fig. 4). The results indicate that the fault zone experienced repeated movements including normal slip during WNW-ESE extensional deformation stage and reverse slip during NW-SE compressional deformation stage (Fig. 4c).

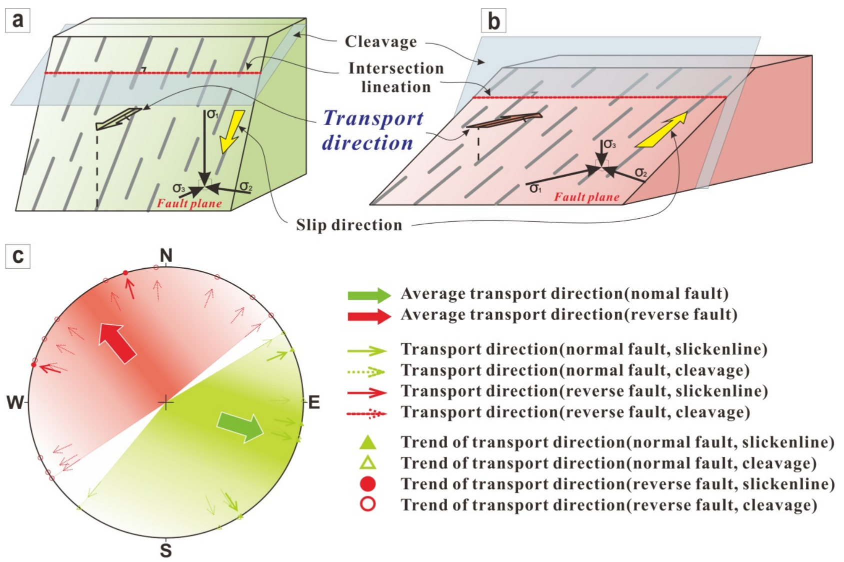


*Fig. 4: (a, b) Two conceptual schematic block diagrams for kinematic indicators associated with transport direction during normal and reverse slips, respectively. (c) Distribution of transport direction inferred from slip elements (Choi et al., in preparation).*

**TRENCH ANALYSIS**

In the trench analysis, the Eupcheon fault indicates reverse slip (strike/dip: N20E/40SE) that records 6-7 m of displacement (3-4 m vertical separation). This fault cuts the marine terrace sediments and older colluvial wedges (Fig. 5a). The hanging-wall mainly consists of well-preserved marine terrace sediments whereas the footwall contains three non-marine wedge-shaped layers of sediments, thinning and fining away from the fault plane. The upper two wedges are interpreted as colluvial wedges that formed during earthquake events (Kim et al., 2004b). The basal colluvium may be also related to the stabilization of the fault scarp during a faulting event, as the amount of disrupted pebbles, which were probably transported from the hanging-wall, increases toward the fault plane and decreases upward (Kim et al., 2011). The displacement accommodated by fault-related folding is about 1 m. The base of the middle colluvium wedge is relatively clear indicating 1.7 m of displacement.

The total displacement (overlapping faults, branch faults, and fault-related folding) represents the final accumulated displacement that accrued consecutive faulting events; the cumulative displacement profile may provide insight into the slip history of the fault, especially the gradient and stepping characteristics of the profile. Kim et al. (2011) suggest that at least three faulting events (step-like features) can be inferred from the profile as follows (Fig. 5b): 1) Units O-M, the first event with displacement of at least 0.7 m after or during the deposition of the marine terraces. 2) In units L-F, the total slip was about 1.6 m. However, the relatively flat section over units J-G indicates the possibility of two sub-events. 3) Units E-C, the estimated slip was about 1.0 m, possibly associated with the formation of the basal colluvial wedges.

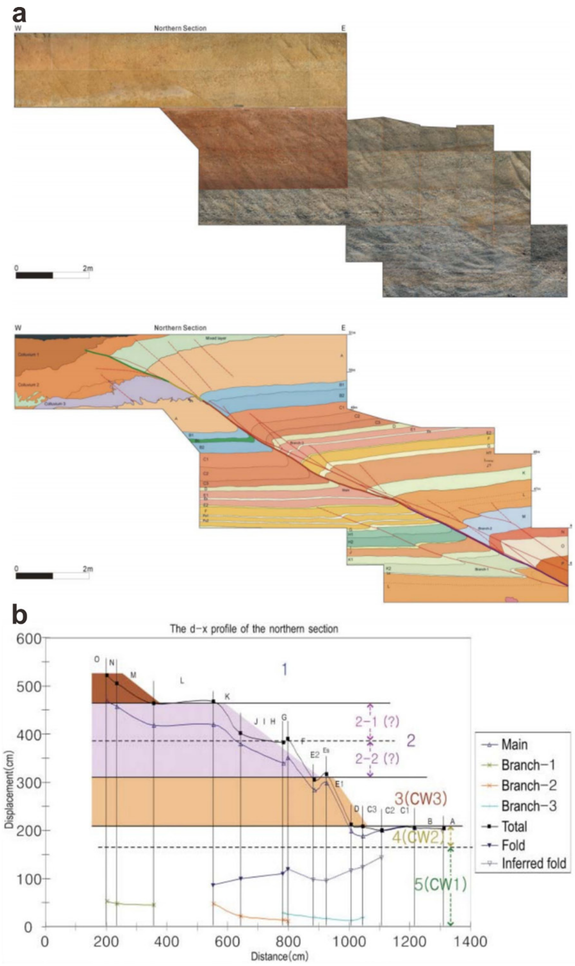


*Fig. 5: (a) Photo mosaic and sketch of the northern section of the Eupcheon trench. (b) Displacement-distance data and their step-like trends indicate cumulative displacement by multiple faulting events (from Kim et al., 2011).*

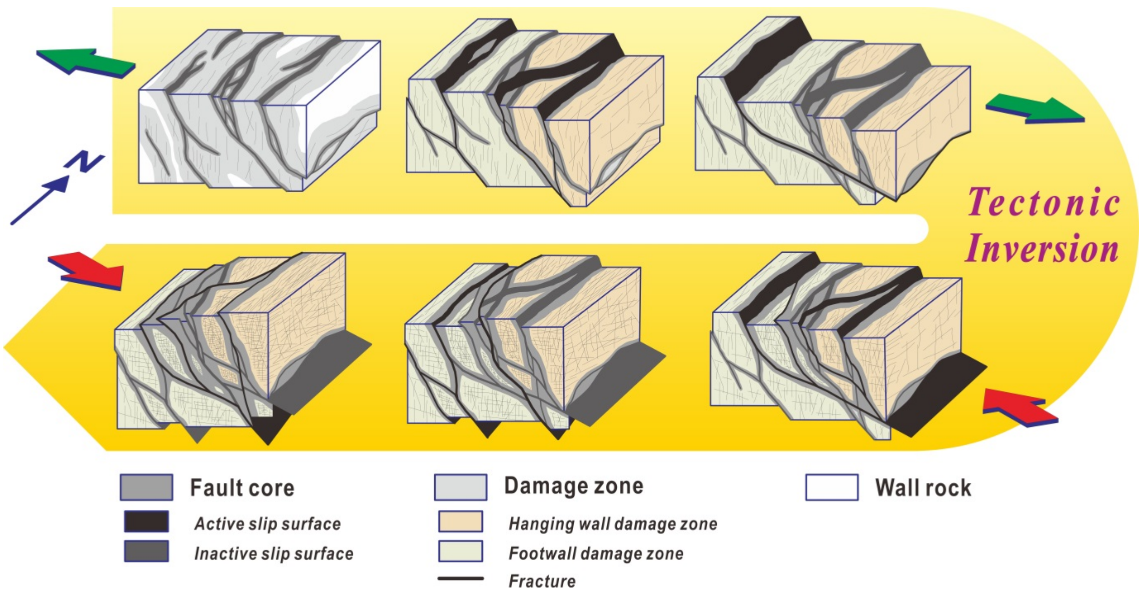


*Fig. 6: Schematic diagrams for the evolution of the Eupcheon fault in an inversion tectonic setting (Choi et al., preparation). The fault zone is interpreted as originated from normal faults inversed by reverse slips, and is much more complicate as the fault evolves.*

## DISCUSSION AND CONCLUSIONS

Fault zone architectures, based on combination of geometric and kinematic analyses, suggest that the Eupcheon fault underwent multiple slip and deformation events with opposite slip senses (Fig. 6). The later reverse slip occurred along the pre-existing normal faults and thus the final architecture of the fault zone is characterized by a reversely reactivated mature fault system

We identified multiple Quaternary faulting events upon the fault based on the analysis of colluvial wedges, and measurements of displacement–distance (d–x) relationship along the fault. The estimated amount of slip is in the range of 0.7–1.8 m for each of the identified faulting event (Kim et al., 2011), and hence the estimated moment magnitude of the earthquakes recorded upon the Eupcheon fault is in the range from M 5.4 to 7.4 (Wells and Coppersmith, 1994).

Careful analysis of fault zone architectures and slip data for the Quaternary fault would allow a helpful interpretation of the faulting history as well as the sequence of Quaternary faulting events. More detailed studies based on fault zone evolution will be helpful in understanding earthquake hazards and active tectonics around the SE Korea.

**Acknowledgements:** We thank Seok-Jun Yang, Seong-Rok Han, and Minjoo Lee for their positive cooperation in field-works.

## References

Caine, J.S., J.P., Evans & C.B., Forster, (1996). Fault zone architecture and permeability structure, Geology 24, 1025-1028.

Chester, F.M. & J.M., Logan, (1986). Composite planar fabric of gouge from the Punchbowl fault zone, California, Journal of Structural Geology 9, 621-634.

Childs, C., T., Manzocchi, J.J., Walsh, C.G., Bonson, A., Nicol & M.P.J., Schopfer, (2009). A geometric model of fault zone and fault rock thickness variations, Journal of Structural Geology 31, 117-127.

Choi, S.J., (2004). Marine terrace of Daebo–Guryongpo–Gampo, SE Korea (II). Korean Journal of Economic and Environmental Geology 37, 245-253.

Choi, S.J., U., Chwae, Y.G., Song, D., Mettitts & Y., Ota, (2004). Isosceles triangular uplift of the SE Korea. In: Abstract book of Korea Society of Economic and Environmental Geology, Spring 2004, pp. 170-173.

Chough, S.K. & Y.K., Shon, (2010). Tectonic and sedimentary evolution of a Cretaceous continental arc–backarc system in the Korean peninsula: New view, Earth-Science Reviews 101, 225-249.

Cowie, P.A. & Z.K., Shipton, (1998). Fault tip displacement gradients and process zone dimensions, Journal of Structural Geology 20, 983-997.

Du, Y. & A., Aydin, (1995). Shear fracture patterns and connectivity at geometric complexities along strike-slip faults. Journal of Geophysical Research 100, 18093-18102.

Faulkner, D.R., A.C., Lewis & E.H., Rutter, (2003). On the internal structure and mechanics of large strike-slip fault zones: field observations of the Carboneras fault in southeastern Spain, Tectonophysics 367, 147–156.

Han, S.-R., J.Y., Park & Y.-S., Kim, (2009). Evolution modeling of the Yangsan-Ulsan fault system with stress changes. Journal of the Geological Society of Korea 45 (4), 361-377.

Jun, M.-S. & J.S., Jeon, (2010). Focal Mechanism in and around the Korean Peninsula, Jigu-Mulli-wa-Mulli-Tamsa 13, 198-202.

Kim, Y.-S., J.R., Andrews & D.J., Sanderson, (2000). Damage zones around strike-slip fault systems and strike-slip fault evolution, Crackington Haven, southwest England. Geoscience Journal 4, 53-72.

Kim, Y.-S., D.C.P., Peacock & D.J., Sanderson, (2003). Mesoscale strike-slip faults and damage zones at Marsalforn, Gozo Island, Malta, Journal of Structural Geology 25, 793–812.

Kim, Y.-S., D.C.P., Peacock & D.J., Sanderson, (2004a). Fault damage zones, Journal of Structural Geology 26, 503-517.

Kim, Y.-S., J.Y., Park, J.H., Kim, H.C., Shin & D.J., Sanderson, (2004b). Thrust geometries in unconsolidated Quaternary sediments and evolution of the Eupcheon Fault, southeast Korea. The Island Arc 13, 403-415.

Kim, Y.-S., J.-H., Kihm, & K., Jin, (2011). Interpretation of the rupture history of a low slip-rate active fault by analysis of progressive displacement accumulation: an example from the Quaternary Eupcheon Fault, SE Korea. Journal of the Geological Society, London 168, 273-288.

Kyung, J.B., (2003). Paleoseismology of the Yangsan fault, southeastern part of the Korean peninsula, Annals of Geophysics 46, 983-996.

Ree, J.-H., Y.-J., Lee, E.J., Rhodes, Y., Park, S.-T., Kwon, U., Chwae, J.-S., Jeon & B., Lee, (2003). Quaternary reactivation of Tertiary faults in the southeastern Korean Peninsula: Age constraint by optically stimulated lumi-nescence dating. The Island Arc 12, 1-12.

Son, M., C.W., Song, M.-C., Kim, Y., Cheon, S., Jung, H., Cho, H.-G., Kim, J.S., Kim & Y.K., Sohn, (2013). Miocene Crustal Deformation, Basin Development, and Tectonic Implication in the Southeastern Korean Peninsula, J. Geol. Soc. Korea 49, 93-118.

Wells, D.L. & Coppersmith, K.J., (1994), New Empirical Relationships among Magnitude, Rupture Length, Rupture Width, Rupture Area, and Surface Displacement, Bulletin of the Seismological Society of America 84 (4), 974-1002.

INQUA Focus Group on Paleoseismology and Active Tectonics

paleoseismicity.org

# Earthquakes characteristics vs natural, anthropic and social effects: a retrospective view from five years of M5+ in Italy

*Francesca R. Cinti*

Istituto Nazionale di Geofisica e Vulcanologia, Via di Vigna Murata 605, 00143 Roma, Italy. Email: francesca.cinti@ingv.it

***Key words***: *earthquake, environmental and social coseismic effect, emergency response, Italy.*

## ABSTRACT

In the last five years, eighteen earthquakes of magnitude equal or larger than 5 shaked the Italian Peninsula (*Figure 1*; ISIDe Working Group (INGV, 2010). Among the most powerful from North to South: the M5.9 and M5.8 Emilia earthquakes in May 2012 within the Po Plain; the M5.2 Lunigiana earthquake in June 2013 close to the Tuscany coast; the M5.9, M5.4, and M5.1 L'Aquila earthquakes in April 2009 in the Abruzzi Apennines; the M 5.0 Pollino event in October 2012 in Northern Calabria. All these events have their hypocenters set between 5 and 17 km of crustal depth, and are caused by the northward convergence of Africa relative to the Eurasian plate. They reflect the kinematic behaviour occurring in Italy, as prevailing N-S to NE-SW compression dominates the northern and western regions of Italy and NE-SW to N-S extension is ongoing within the Apennines (e.g. Montone et al., 2004).

The two Emilia shocks and the L'Aquila mainshock were deadly events being the largest, and along with the other events they caused severe damaging and the consequent evacuation of villages in the epicentral areas during the seismic crisis (except for the Lunigiana case).
Despite the similarities among these earthquakes, several distinct features characterized each of these seismic crisis causing diffent effects on the natural, anthropic and social environments. I will shed light on this issue through the comparison of aspects of interest among the above mentioned events.

One of these features is the behaviour through time, because some earthquakes occurred as single mainshocks followed by aftershocks (e.g. Lunigiana case), other as multiple and close in time mainshocks (e.g. Emilia), and other as complex and prolonged seismic sequence of instrumental seismicity culminated with a mainshock (e.g. L'Aquila and Pollino cases). This feature appears to be critical, leading to differences in the felt areas, in the losses sufffered by population, and in the general perceptiveness of each seismic crisis, then particularly causing effects on the social, economic and cultural heritage.

Even for comparable magnitudes and earthquake source depths, the geological and topographical texture of the landscape where the events occurred is also an aspect that guided presence and type of the effects (surface faulting, liquefaction, landslides, rockfalls; *Figure 2*) produced on the natural environment.

Finally, I will address some issues raised during each of the seismic crisis concerning the cascade effects impacting on the system, e.g. on critical infrastructures in the struck areas, on the geological (and not only) emergency response. I will also discuss the impact of these five years of seismic experience on the scientific community itself.

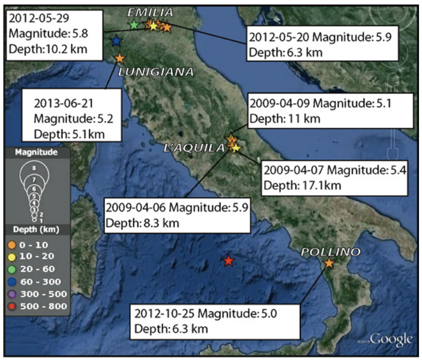


*Fig. 1: Earthquakes with magnitude equal or larger than 5 occurring in Italy since April 2009 (ISIDe Working Group INGV, 2010).*

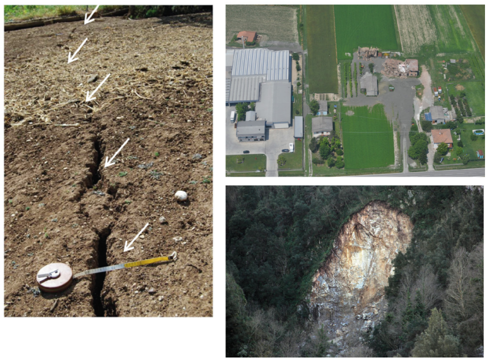

*Fig. 2: Surface faulting from 2009 L'Aquila event, pervasive liquefaction from 2012 Emilia earthquake, rock failure induced by the 2012 Pollino event.*

## References

ISIDe Working Group (INGV, 2010). Italian Seismological Instrumental and parametric database: *http://iside.rm.ingv.it*.

Montone, P., M. T. Mariucci, S. Pondrelli & A. Amato (2004). An improved stress map for Italy and surrounding regions (central Mediterranean). *Journal of Geophysical Research* 109, B10410, doi:10.1029/2003JB002703.

INQUA Focus Group on Paleoseismology and Active Tectonics

paleoseismicity.org

# Paleoseismological investigations of the eastern part of the Khlong Marui Fault Zone in Surat Thani Province, Southern Thailand

*Dürrast, Helmut (1), Prakrit Noppradit (2), Ludwig Zöller (3)*

(1) Geophysics Research Center, Prince of Songkla University, HatYai 90112, Thailand. Email: helmut.j@psu.ac.th
(2) Department of Physics, Faculty of Science, Prince of Songkla University, HatYai 90112, Thailand.
(3) Chair in Geomorphology, Universität Bayreuth, 95440 Bayreuth, Germany.

***Abstract:*** *In Southern Thailand two major strike–slip faults cross the Malay Peninsula from SW to NE, the Ranong (RFZ) and Khlong Marui Fault Zone (KMFZ). Before the 2004 Sumatra Andaman Earthquake, these faults believed to be inactive. Paleoseismological investigations of the clearly exposed western part of the KMFZ have already shown that paleoearthquakes occurred in the last few thousands of years. For the eastern part, where the fault is less exposed, this study could identify at least two events between 2.53±0.19 and 6.89±0.38 ka and between 0.59±0.13 and 2.17±0.31 ka, based on field studies and optical dating, with paleoearthquake magnitudes of maximum 7.8.*

***Key words**: Paleoseismology, OSL dating, Khlong Marui Fault Zone, active fault, Thailand*

On the 26 December 2004 the Mw 9.1 Sumatra-Andaman Earthquake occurred off the west coast of Northern Sumatra, Indonesia; resulting in a 1,600 km rupture along the fault boundary between the Indian-Australian Plate and the south-eastern part of the Eurasian Plate with fault slip of up to 15 m near Banda Aceh (Lay et al., 2004). The massive earthquake triggered a series of devastating tsunamis along the coastline of the Indian Ocean, killing a large number of people and inundating coastal communities around.

In southern Thailand, there are a series of faults, mainly the Ranong (RFZ) and Khlong Marui Fault Zones (KMFZ), as shown in Figure 1, which were identified as inactive before 2004 by the Department of Mineral Resources, Thailand (DMR), however no seismicity studies have been carried out. Watkinson et al. (2008) described the KMFZ and RFZ as major NNE-SSW trending strike-slip faults, diachronous reversal in shear sense, originated before but activated during the India–Eurasia plate collision. Seismological observations by Dürrast et al. (2007) in early 2005 have confirmed seismicity with low magnitudes (M<4.5) along the faults and in southern Thailand.

In 2006/07 the Department of Mineral Resources carried out a preliminarily study on the recurrence interval of the RFZ and the south-western and middle part of the KMFZ (DMR, 2007a). The exact location of the eastern part of the KMFZ is still unclear. Remote sensing, topographic surveys, and geophysical investigations were applied to study tectonic geomorphology and locate trenches and sampling locations. Thermoluminescence (TL), C-14, and electron spin resonance (ESR) dating were applied to determine the last fault movement. Trenching and outcrops were used to define sediment stratigraphy related to paleoearthquake.

Their study concluded that the last movement of the KMFZ was 1,200 years and that of the RFZ 2,000 years ago. Moreover, the recurrence interval of the KMFZ and RFZ is 1,000 years and 2,000 years.

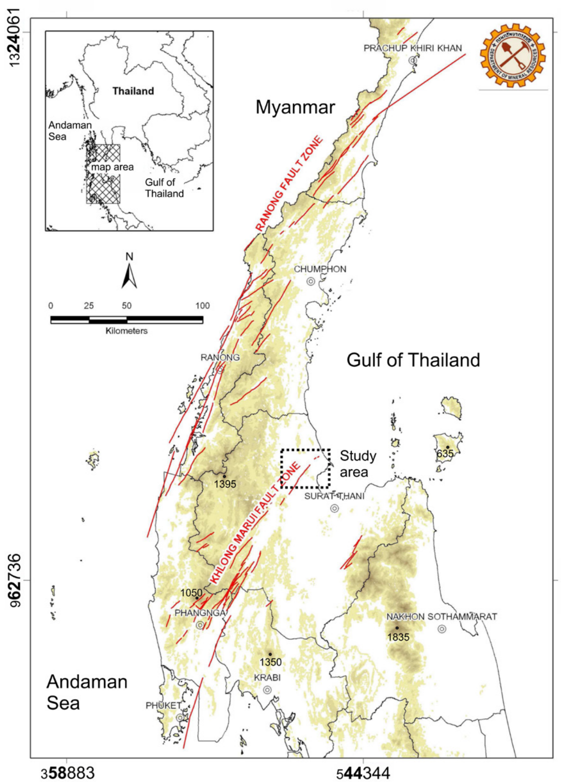


*Fig. 1: Topographic map of southern Thailand with the major fault zones (after DMR, 2007a) and study area; base map in UTM WGS-84, numbers are elevations in meters.*

In 2010/11 extensive geological and geophysical field work was carried out as part of a larger study with the objective (1) to locate the KMFZ in the western part - mainly in Surat Thani Province, north of the city of Surat Thani (see Figure 1), (2) to identify locations with

evidence for paleoearthquakes, and finally (3) dating sediments related to these events, here using optically stimulated luminescence method (OSL).
Several locations in the area showed paleoseismological events, with five sites chosen for dating (see Figure 2): V1, V2, V3 are in Vibhavadi District, TC in Tha Chang District, and CTR at the road between Chaiya and Tha Chang.

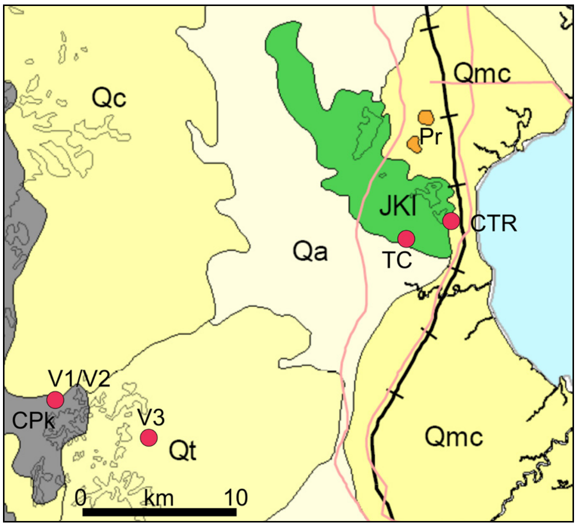


*Fig. 2: Geological map of the eastern part of Surat Thani Province, Southern Thailand, showing the locations of paleoseismological events used for dating (V1/V1, V3, TC, CTR). CPk: Carboniferous, mainly shale with sandstone and siltstone, Pr: Permian Ratburi Group, mainly limestone; Oc: Quaternary colluvial deposits; Qt: Quaternary terrace deposits, Qa: Quaternary fluvial deposits; Qms: Coastal wave–dominated deposits. Red lines – main roads, black line – railway; blue - Gulf of Thailand, to the East (after DMR, 2007b).*

Altogether ten samples were successfully collected from four sites (excluding V3) by using a cylindrical steel sample holder (10 cm in diameter and 50 cm long) during night time for protecting the sediments from light exposure. Samples were taken from different layers exposed in the outcrop mainly in horizontal direction. Both sides of the sample holders were sealed for transport until further processing in the laboratory. The OSL measurements were carried out at the University Bayreuth, Germany. Details about the sample preparation and measurement technique are described elsewhere (e.g. Fuchs et al., 2005; Lai et al. 2007).

Vibhavadi site V1 and V2 are approximately 36 m NNE of site V1 exposing the same face of the old pit. At site V1 three (see Figure 3 and 4) and at site V2 one OSL sample were taken (in Layer C, not shown here).
The OSL ages were determined using different age models described by Galbraith & Roberts (2012) with MAM3 the minimum age model and CAM the central age model, as shown in Figure 4. At Site V2 the ages are: no model: 2.48±0.09 ka, MAM3: 1.47 (1.37-159) ka, and CAM: 2.53±0.19 ka. From the ages a sedimentation and tectonic scenario can be drawn (see Figure 5).

*Fig. 3: Site Vibhavadi V1. Almost vertical face at a former sand pit. Photo to direction 160 (SSE). Scale (left side) 2 m.*

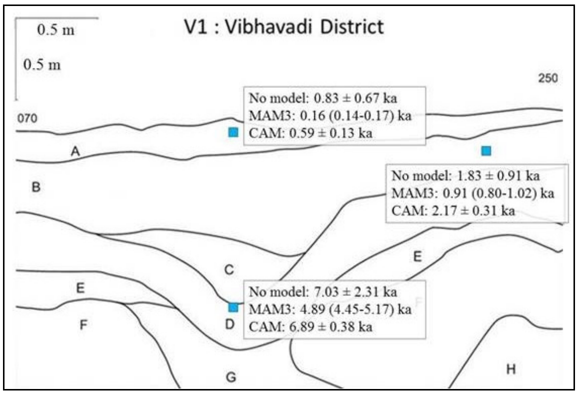


*Fig. 4: Site of Vibhavadi V1. Lithological boundaries, location of OSL samples with the ages related to different age model. A: Black top soil, B: Light brown clayey sand, C: Brown-grey coloured and medium plastic clay, with black grains and black plant material, D: Dark-grey, slightly orange gravel with a few black grains and black plant material, E: Red to ochre coloured medium plastic clay, F: Fractured white-yellow sandstone. G: Yellow-white sandy clay, H: Medium plastic white-grey-yellow silty clay. MAM3 - minimum age model, CAM - central age model.*

Before 6.89 ka a fault has already existed there indicated by the clay (G) between the sandstone layer (F). Layer (E) was deposited above (Figure 5a and b). An earthquake event, assuming a strike slip movement, but with extensional character, occurred between 2.53 and 6.89 ka (Figure 5c), with a minimum displacement in vertical direction about one meter. An estimation of the paleoearthquake magnitude gives an Mw value of 6.8 for a maximum displacement (MD) and Mw of 7.0 for an average displacement (AD). These calculations are based on regression lines from Wells & Coppersmith (1994).

Then in the sequence, layer C and later layer B was deposited (Figure 5d). After that a second event occurred, between 0.59 and 2.17 ka, assumed a strike slip movement, but with extensional character (Figure 5e). A minimum displacement took place in vertical direction of approximately 0.5 m. Also here the estimation of the paleoearthquake magnitude gives Mw of 6.6 for a maximum displacement (MD) and Mw of 6.7 for average displacement (AD). After this second event the uppermost layer A was deposited (Figure 5f).

Faults found at Vibhavadi site, with a strike of 145-325° (NNW-SSE), are likely conjugated faults of the main KMFZ. Geological and geophysical results from the study area have shown that the actual main fault is about 20 km south of the location assumed before and shown in Figure 1 (data not shown here).

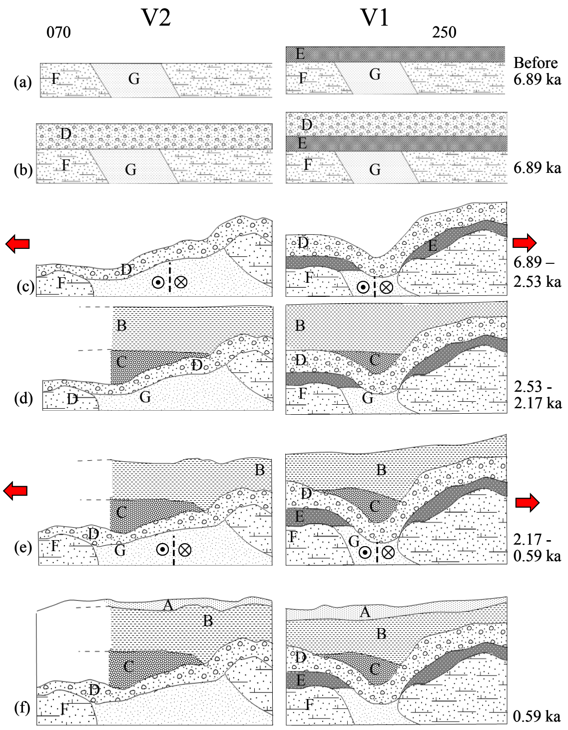


*Fig. 5: Schematic geological scenarios for Vibhavadi site V1 (left) and V2 (right) from older (a) to younger (f). Two paleo-earthquakes could be identified at (c) and (e). See also Figure 4 for the abbreviations of the layers (A-G).*

The faults in Vibhavadi clearly have an extensional character and are much older then the dating here. A river displacement in the vicinity of site V1 and V2 gives a horizontal displacement of about 18 m, likely the result of several events. However, if using MD and one event then the max. Mw is 7.8. The existence and strike direction of these faults in the subsurface have been confirmed by seismic investigations (not shown here).

The result from the paleoseismological investigations in this area have shown that conjugated faults related to the main Khlong Marui Fault Zone were active in the last 10,000 years with at least two identifiable events: between 2.53 and 6.89 ka and between 0.59 and 2.17 ka, and with a paleoearthquake magnitude of maximum 7.8.

Therefore, it can be concluded that the Khlong Marui Fault Zone was not inactive before 2004 as already shown by DMR (2007a) for the western part and that higher magnitude earthquakes can be expected along this fault. This might also the case for the Ranong Fault Zone further north (see Figure 1).

The clear categorization of the KMFZ as an active fault has further implications for the seismic hazard assessment and related mitigation efforts, e.g. engineering requirements for buildings and infrastructures.

**Acknowledgements:** The authors acknowledge support from the Electricity Generating Authority of Thailand (EGAT) and Geophysics Research Center (GRC) as well as their team members. PN was supported by Graduate School, PSU, and the Development and Promotion of Science and Technology (DPST) talent project (Thailand).

## References

DMR, (2007a). Investigation on Recurrence Interval in Areas Showing Trace of Movement along the Faults in Prachuab Khirikhan, Chumporn, Ranong, Surat Thani, Krabi, Phang Nga and Phuket Provinces (Ranong and Khlong Marui Faults). Report, Department of Mineral Recourses, Bangkok, Thailand.

DMR, (2007b). Geological map of Surat Thani Province. Department of Mineral Recourses, Bangkok, Thailand. http://www.dmr.go.th/download/pdf/South/Surat.pdf.

Dürrast, H., S. Dangmuan, & W. Lohawijarn, (2007). Khlong Marui and Ranong Fault Zones in Southern Thailand re-activated by the 26 December 2004 Mw 9.3 Sumatra-Andaman Earthquake? *Proceedings of the GEOTHAI'07 International Conference*, Dec. 21-22, 2007, Bangkok, 141–144.

Fuchs, M., J. Staub, & L. Zöller, (2005) Residual Luminescence Signals of recent river flood sediments: A Comparison between Quartz and Feldspar of fine- and coarse-grain Sediments. *Ancient TL* 23, 25-30.

Galbraith, R.F. & R.G. Roberts, (2012). Statistical aspects of equivalent dose and error calculation and display in OSL dating: An overview and some recommendations. *Quaternary Geochronology* 11, 1–27.

Lai, Z.P., H. Brückner, A. Fülling & L. Zöller, (2007) Existence of a common growth curve for silt-sized quartz OSL of loess from different continents. Radiation Measurements 42 (9), 1432-1440.

Lay, T., H. Kanamori, C.J. Ammon, M. Nettles, S.N. Ward, R.C. Aster, S.L. Beck, M.R. Brudzinski, R. Butler, H.R. Deshon, G. Ekström, K. Satake, & S. Sipkin, (2004) The great Sumatra-Andaman Earthquake of 26 December 2004. *Science* 308, 1127-1133.

Watkinson, I., C. Elders & R. Hall, (2008). The kinematic history of the Khlong Marui and Ranong Faults. *Journal of Structural Geology* 30, 1471–1554.

Wells, D.L. & K.J. Coppersmith, (1994). New Empirical Relationships among Magnitude, Rupture Length, Rupture Width, Rupture Area, and Surface Displacement. *Bulletin of the Seismological Society of America* 84, 974–1002.

INQUA Focus Group on Paleoseismology and Active Tectonics

paleoseismicity.org

# Holocene tsunamis in the southern Caribbean: Evidence from stratigraphic archives and the coarse-clast record

*Engel, Max (1), S. Matthias May (1), Peter Frenzel (2), Anja M. Scheffers (3), Dieter H. Kelletat (1), Helmut Brückner (1)*

(1) Institute of Geography, University of Cologne, Albertus-Magnus-Platz, 50923 Cologne, Germany. Email: max.engel@uni-koeln.de
(2) Institute of Earth Sciences, University of Jena, Burgweg 11, 07749 Jena, Germany
(3) Southern Cross GeoScience, Southern Cross University, PO Box 157, Lismore NSW 2480, Australia

***Abstract:*** *We present sediment cores from seven coastal geoarchives on Bonaire, southern Caribbean, containing layers of high-energy sedimentation. Tsunami deposition is inferred for some layers based on the presence of allochthonous reefal shells including articulated specimens and a high percentage of angular fragments, planktonic foraminiferal taxa and those from the deeper shelf (below storm wave base), basal unconformities and hiatuses of >1000 a, rip-up clasts, thin depositional sequences comprising basal traction carpets overlain by normally graded sand, a proximal sediment source (littoral) in the lower part of the deposit and a broad mixture (littoral, shelfal, terrestrial) in the upper part, and the lack of deposition during recent hurricane flooding. Several tsunami layers were precisely dated to 3300-3100 cal BP, whereas the record of further candidate tsunamis is more disjunct. Additional tsunami evidence is provided by the largest coastal boulders (up to 150 t; a-axis up to 10 m).*

***Key words****: Palaeotsunami, Bonaire, Tsunami vs. Storm deposit, Hazard assessment*

## INTRODUCTION

The island of Bonaire (Figure 1), Lesser Antilles, Leeward Islands, has one of the most extensively studied coarse-clast records of extreme wave events (hurricanes, tsunamis) in the Caribbean (e.g. Scheffers, 2005; Scheffers et al., 2006; Morton et al., 2008; Spiske et al., 2008; Watt et al., 2010). Strong hurricanes are known to have impacted the island in the recent past (e.g., Tecla in 1877, Lenny in 1999, Ivan in 2004; Scheffers, 2005), whereas no tsunami has been recorded in historical times. However, historical tsunamis are known from adjacent coasts (O'Loughlin & Lander, 2003). We present (i) large coastal boulders (a-axis up to 10 m, weight up to 150 t) from the N and NE coasts, and (ii) sediment cores from seven coastal geoarchives with layers of high-energy sedimentation likely associated with prehistoric tsunamis. Our approach is exemplified by a case study at Boka Bartol (Figure 1).

## METHODS

In order to test the tsunami hypothesis of Scheffers (2005), we applied a modified approach of Nott (2003) to reconstruct minimum heights of storm waves and tsunamis required to move the largest coastal boulders. Their edges were measured by DGPS. The point cloud was imported into ArcGIS and translated into 3D surfaces to calculate their volume (Figure 2). Individual densities were determined considering the different coralline lithotypes of the palaeo-reef blocks.

Holocene stratigraphic archives were sampled by percussion coring. Besides sedimentological documentation, a broad spectrum of proxy records was generated including grain size distribution, shell taphonomy, microfossils, high-resolution ITRAX XRF counts, semi-quantitative XRD, carbonate and organic contents. Chronostratigraphies are based on $^{14}$C-AMS age estimates.

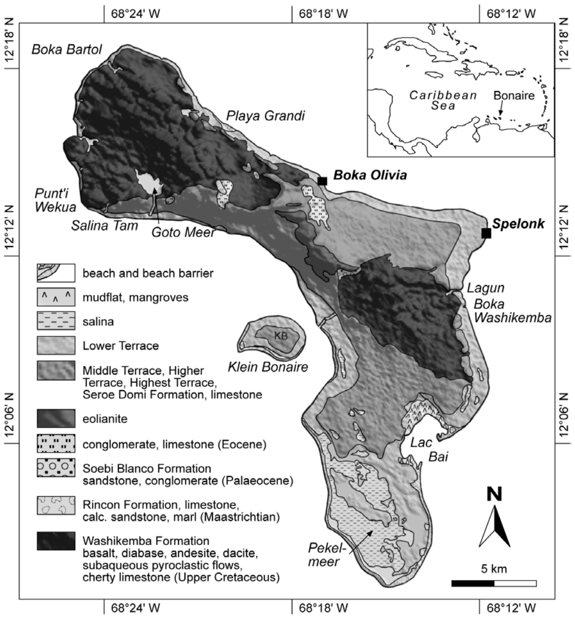


*Fig. 1: Simplified geological map of Bonaire showing the study sites (based on De Buisonjé, 1974, and other references therein; source of SRTM data: http://dds.cr.usgs.gov/srtm).*

## RESULTS AND DISCUSSION

### *Investigation of the coarse-clast record*

Boulders and blocks were investigated on top of an elevated Pleistocene reef platform at an elevation of 3.5–5 m above mean sea level and at a distance

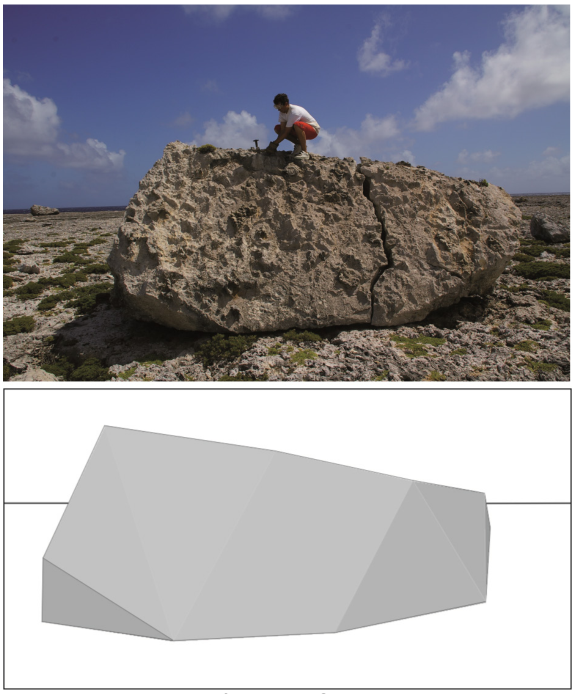

*Fig. 2: The example of boulder SPE 4 as photograph and DGPS-based 3D model for volume calculation (after Engel & May, 2012).*

*Table 1: Inferred minimum wave heights of tsunamis and storm waves required to quarry and transport each boulder, using the modified approach of Nott (2003) (after Engel & May, 2012). For comparison, values of regional extreme waves are given. SPE = Spelonk; BOL = Boka Olivia (see Figure 1).*

| Boulder | H (tsunami) in m | | H (storm wave) in m | |
|---|---|---|---|---|
| | Modified approach of Nott (2003) | | Modified approach of Nott (2003) | |
| SPE 2 | 5.3 | **Tsunami height** at Paria, Venezuela, 01 Sep 1530: c. **7.3 m** (NGDC, 2011) | 21.2 | Max. height of a **breaking wave during Hurricane Ivan** 2004, Bonaire: c. **12 m** (Scheffers & Scheffers, 2006) |
| SPE 4 | 5.4 | | 21.4 | |
| SPE 5 | 6.7 | | 26.7 | |
| SPE 6 | 6.7 | | 26.8 | |
| SPE 7 | 5.8 | **Tsunami height** at Puerto Tuy, Venezuela, 29 Oct 1900: c. **10 m** (NGDC, 2011) | 23.4 | |
| SPE 8 | 5.2 | | 20.8 | |
| SPE 9 | 1.2 | | 4.7 | |
| BOL 1 | 7.3 | | 29.3 | |
| BOL 2 | 8.9 | | 35.6 | |
| BOL 3 | 1.8 | | 7.3 | |

of 40–120 m from the coast. Entrainment and transport occurred under extreme-wave conditions during the recent sea level highstand. A higher relative sea level can be excluded for the Holocene (Milne & Peros, 2013).
Values of DGPS-based volume measurements amount only approx. 50% of the multiplication of main axes indicating that previous volume-based reconstructions of minimum wave heights and velocity required to entrain boulder deposits might be overestimated. Boulder densities considering heterogeneous lithofacies composition range between 2.07 and 2.40 g $cm^{-3}$. The largest boulders identified to have been moved during recent hurricanes weigh 1 and up to 9 t. Those remaining immobile during these events weigh up to 150 t (Engel & May, 2012).
Reconstructed minimum storm wave heights for boulders moved during recent hurricanes (4.3 and 7.3 m, respectively) are within the range of real wave heights observed, e.g., during Hurricane Ivan (Scheffers & Scheffers, 2006). Storm wave heights calculated for the largest clasts of the boulder fields (up to 35.6 m) are three times higher and far beyond any observation ever made or data ever recorded in the southern Caribbean (Table 1). In contrast, inferred tsunami heights (up to 8.9 m) are in the range of historical tsunami heights reported from Venezuela and other sites in the southern Caribbean (NGDC, 2013). Even though the approach of Nott (2003) is based on simplifying assumptions concerning the quarrying and transport processes of boulders by waves, its legitimation is underpinned by the comparison of the boulders moved during recent tsunamis and the output of Nott-type models for these boulders (e.g., Bourgeois & MacInnes, 2010). Thus, we believe that results from this study support the tsunami hypothesis on Bonaire (Engel & May, 2012).

*Investigation of the stratigraphical archives – the example of Boka Bartol*

The Holocene sediment sequence of Boka Bartol, a ria-type embayment of NW Bonaire separated from the open sea by a barrier of coral rubble, comprises at least 9 m (cores BBA 8 and 10 in Figure 3). Unit I (9.00–6.86 m below surface [b.s.] at BBA 10) represents an open embayment fringed by mangroves. Unit II (6.86–6.67 m b.s.) shows several characteristics of high-energy sedimentation (Figure 4). Unit III (6.67–2.70 m b.s.) accumulated in a poly- to hypersaline lagoon with fluctuating hydrochemistry. Unit IV (2.70–0.00 m b.s.) represents (sub-)recent sediments of the prograding alluvial fan. Tsunami deposition for Unit III is inferred based on the presence of several tsunami signature types (e.g., Goff et al., 2012), such as allochthonous reefal shells including articulated specimens, foraminiferal taxa from the deeper shelf (below storm wave base), a basal unconformity and a hiatus of >2000 a, a rip-up clast, a basal traction carpet overlain by normally graded muddy sand, a proximal sediment source (littoral) in the lower part of the deposit (traction carpet), and a broad mixture (littoral, shelfal, terrestrial) in the upper part (suspension load), and the lack of deposition during recent hurricane flooding. Boka Bartol changed from an open mangrove-fringed embayment into a poly- to hyperhaline lagoon due to the establishment or closure of the barrier of coral rubble during or subsequent to the inferred tsunami. Four coeval $^{14}C$ ages from Unit III point to a deposition around 3300–3100 cal BP. The facies change after the deposition of Unit II from mangrove peat to evaporate-rich mud indicates subaerial growth of the barrier of coral rubble separating the boka from the open sea during or subsequent to the event (Engel et al., 2013).

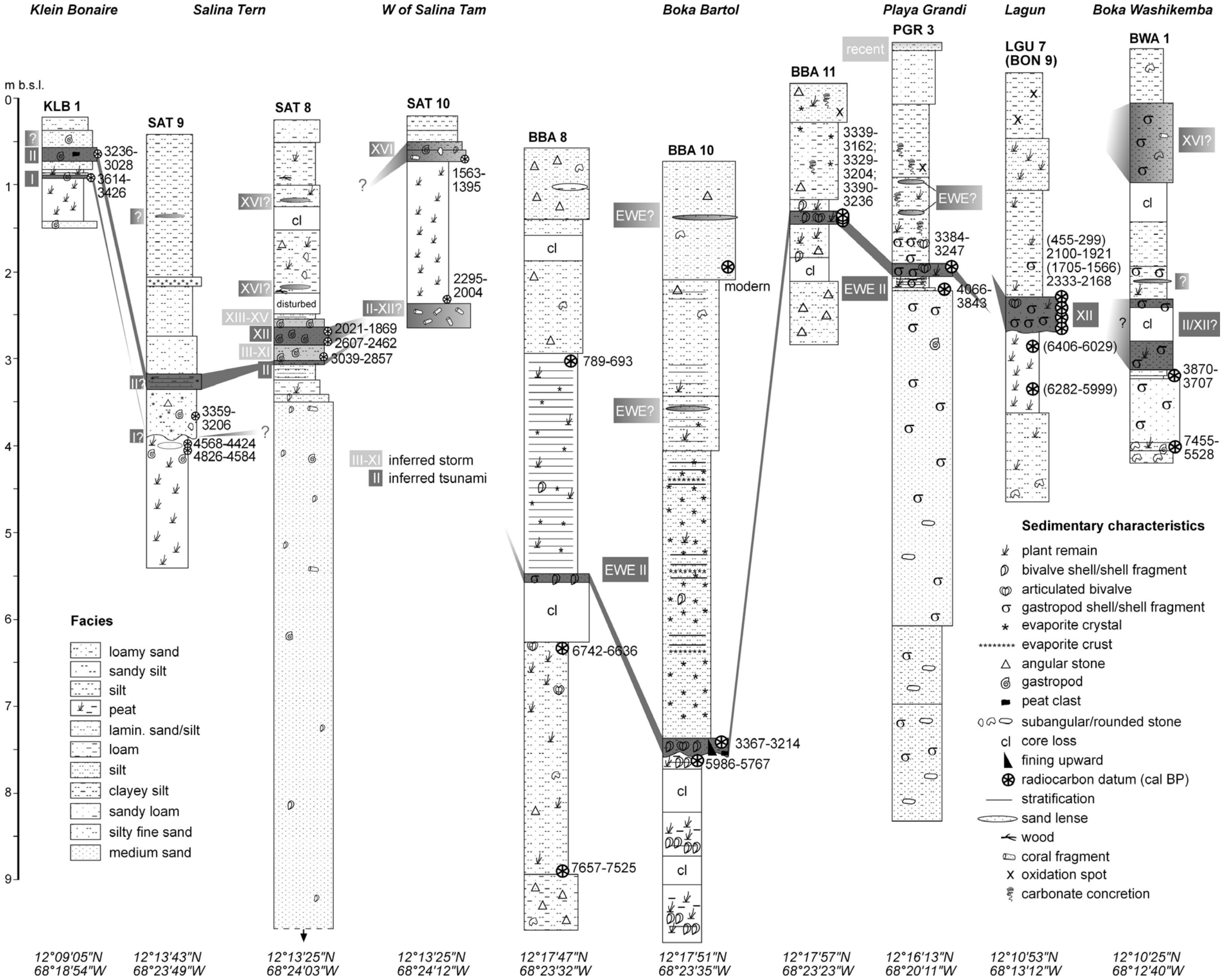


*Figure 3: Synopsis of sediment cores from coastal stratigraphical archives on Bonaire and distribution of extreme-wave events (EWE, roman numation) (Scheffers et al., 2013). The sites are shown in Figure 1. For detailed stratigraphical documentation, data and interpretation see Engel et al. (2010) for Lagun and Playa Grandi, Engel et al. (2012) for Klein Bonaire, Saliña Tern and west of Saliña Tern, and Engel et al. (2013) for Boka Bartol. $^{14}$C datings were calibrated using Calib 6.0.1 (Reimer et al., 2009).*

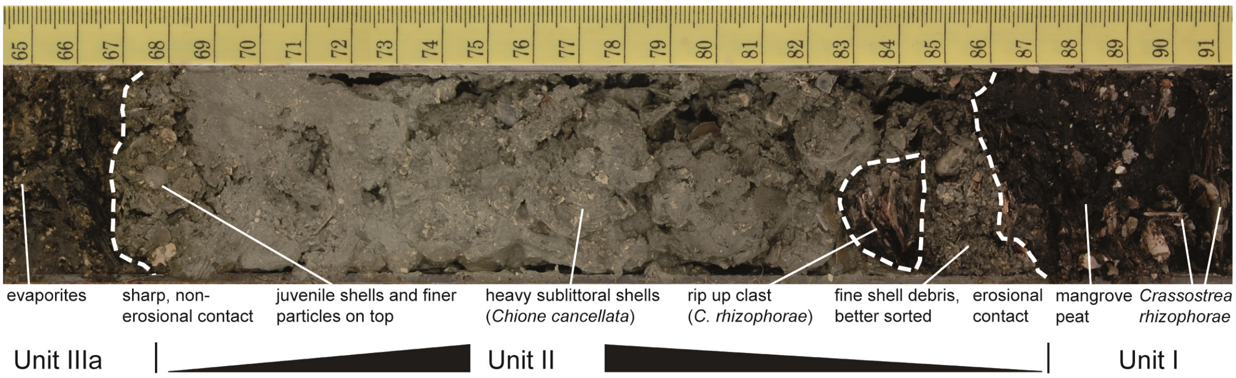


*Figure 4: Section 6.91 – 6.65 m b.s. (below surface) of sediment core BBA 10 from Boka Bartol (Figures 1, 4) showing Units I–IIIa. The photograph depicts several sedimentary features which are often – though not exclusively – related to tsunami deposits: erosional lower contact, varying degrees of sorting, rip-up clast and larger ex-situ shells. It also illustrates the significant differences in sedimentation after the event (compare Units I and IIIa) indicating strong and long-lasting changes of the geo-ecosystem due to the final closure of Boka Bartol (Engel et al., 2013).*

Unit III has counterparts on the east (Klein Bonaire, Saliña Tam, possibly between Saliña Tam and Punt'i Wekua) and west coasts (Playa Grandi, possibly Boka Washikemba). It is the best documented candidate tsunami on Bonaire (EWE II in Figure 4). Another possible tsunamite (EWE XII), dated to 2000–1700 cal BP, was detected at Lagun and Saliña Tam (Engel et al., 2012). Two further extreme-wave deposits (c. 3600 cal BP and post-1300 cal BP) show a very disjunct pattern (see KLB 1, SAT 10, BWA 1 in Figure 3).

## CONCLUSIONS

The size of boulders and sedimentary patterns of extreme-wave deposits indicate that flooding events significantly exceeding the magnitude of recent cat. 5 hurricanes occurred in prehistoric times. We conclude that these flooding events with a recurrence interval in the order of 1000 years were tsunamis, even though remaining uncertainties regarding the significance of sedimentary criteria and the boulder transport equations should not be neglected.

Trigger mechanisms for a tsunami causing hazard on Bonaire include strong earthquakes along the El Pilar fault, coastal Venezuela, as well as other earthquake sources along the southern Caribbean Plate boundary. Furthermore, explosive volcanism at the Antilles island arc (e.g., Kick 'em Jenny Volcano, Windward Islands), regional submarine landslides or teletsunamis from the open Atlantic Ocean may play a role. The Caribbean-wide tsunami exercise CARIBE WAVE/LANTEX 13 on 20 March 2013 used a tsunami scenario induced by an earthquake of $M_w = 8.5$ at the N boundary of the Bonaire microplate, 200 km NW of Bonaire, causing run-ups of >5 m along the island's coast (UNESCO/IOC, 2012).

We demonstrated that tsunamis, even if not known on Bonaire from historical accounts and recent observations, represent a hazard on the island. It is, therefore, suggested to initiate a local tsunami assessment by estimating exposure, vulnerability and preparedness in order to develop appropriate mitigation measures.

**Acknowledgements:** Funding by the Deutsche Forschungsgemeinschaft (ref. no. BR 877/26-1) is gratefully acknowledged. We appreciate the administrative and logistic support by DROB (Government of the Island Territory Bonaire/Department of Environment and Natural Resources) and STINAPA (Bonaire National Parks Foundation).

## References

Bourgeois, J. & B. MacInnes, (2010). Tsunami boulder transport and other dramatic effects of the 15 November 2006 central Kuril Islands tsunami on the island of Matua. *Zeitschrift für Geomorphologie* 54 (Suppl. 3), 175–195.

De Buisonjé, P.H. (1974*). Neogene and Quaternary geology of Aruba, Curaçao and Bonaire (Netherlands Antilles)*. Ph.D. thesis, Rijksuniversiteit Utrecht, The Netherlands.

Engel, M. & S.M. May, (2012). Bonaire's boulder fields revisited: Evidence for Holocene tsunami impact on the Leeward Antilles. *Quaternary Science Reviews* 54, 126–141.

Engel, M., H. Brückner, V. Wennrich, A. Scheffers, D. Kelletat, A. Vött, F. Schäbitz, G. Daut, T. Willershäuser & S.M. May, (2010). Coastal stratigraphies of eastern Bonaire (Netherlands Antilles): new insights into the palaeotsunami history of the southern Caribbean. *Sedimentary Geology* 231, 14–30.

Engel, M., H. Brückner, K. Messenzehl, P. Frenzel, S.M. May, A. Scheffers, S. Scheffers, V. Wennrich & D. Kelletat, (2012). Shoreline changes and high-energy wave impacts at the leeward coast of Bonaire (Netherlands Antilles). *Earth, Planets and Space* 64, 905–921.

Engel, M., H. Brückner, S. Fürstenberg, P. Frenzel, A.M. Konopczak, A. Scheffers, D. Kelletat, S.M. May, F. Schäbitz & G. Daut, (2013). A prehistoric tsunami induced long-lasting ecosystem changes on a semi-arid tropical island – the case of Boka Bartol (Bonaire, Leeward Antilles). *Naturwissenschaften* 100, 51–67.

Goff, J.,C. Chagué-Goff, S. Nichol, B. Jaffe & D. Dominey-Howes, (2012). Progress in palaeotsunami research. *Sedimentary Geology* 243–244, 70–88.

Milne, G. & M. Peros, (2013). Data-model comparison of Holocene sea-level change in the circum-Caribbean. *Global and Planetary Change* 107, 119–131.

Morton, R.A., B.M. Richmond, B.E. Jaffe & G. Gelfenbaum, (2008). Coarse-clast ridge complexes of the Caribbean: a preliminary basis for distinguishing tsunami and storm-wave origins. *Journal of Sedimentary Research* 78, 624–637.

NGDC (2013). NOAA/WDC Historical Tsunami Database at NGDC. http://www.ngdc.noaa.gov/hazard/tsu_db.shtml (last access 07.15.13.).

Nott, J. (2003). Waves, coastal boulder deposits and the importance of the pre-transport setting. *Earth and Planetary Science Letters* 210, 269–276.

O'Loughlin, K. & J.F. Lander, (2003). *Caribbean Tsunamis – A 500-Year History from 1498–1998*. Kluwer Academic Publishers, Dordrecht. 280 pp.

Reimer, P.J. (2009). IntCal09 and Marine09 radiocarbon age calibration curves, 0–50,000 years cal BP. Radiocarbon 51, 1111–1150.

Scheffers, A. (2005). Coastal response to extreme wave events – hurricanes and tsunamis on Bonaire. *Essener Geographische Arbeiten* 37.

Scheffers, A. & S. Scheffers, (2006). Documentation of Hurricane Ivan on the coastline of Bonaire. *Journal of Coastal Research* 22, 1437–1450.

Scheffers, S., A. Scheffers, U. Radtke, D. Kelletat, K. Staben & R. Bak, (2006). Tsunamis trigger long-lasting phase-shift in a coral reef ecosystem. *Zeitschrift für Geomorphologie N.F.*, Suppl. Vol. 146, 59–79.

Scheffers, A.M., M. Engel, S.M May, S.R. Scheffers, R. Joannes-Boyau, E. Hänßler, K. Kennedy, D. Kelletat, H. Brückner, A. Vött, G. Schellmann, F. Schäbitz, U. Radtke, B. Sommer, T. Willershäuser & T. Felis, (2013). Potential and limits of combining studies of coarse and fine-grained sediments for the coastal event history of a Caribbean carbonate environment. In: Sedimentary Coastal Zones from High to Low Latitudes: Similarities and Differences (Martini, I.P., Wanless, H.R. eds). *Geological Society, London, Special Publication* 388, doi:10.1144/SP388.4.

Spiske, M., Z. Böröcz, & H. Bahlburg, (2008). The role of porosity in discriminating between tsunami and hurricane emplacement of boulders e a case study from the lesser Antilles, southern Caribbean. *Earth and Planetary Science Letters* 268, 384–396.

UNESCO/IOC (2012). Exercise Caribe Wave/Lantex 13. A Caribbean Tsunami Warning Exercise, 20 March 2013. Vol. 1: Participant Handbook. *IOC Technical Series* 101.

Watt, S.G., B.E. Jaffe, R.A. Morton, B.M. Richmond & G. Gelfenbaum, (2010). Description of extreme-wave deposits on the northern coast of Bonaire, Netherlands Antilles. *USGS Open-File Report* 2010-1180.

INQUA Focus Group on Paleoseismology and Active Tectonics

paleoseismicity.org

# Analysis of the distribution of landslides and landslide dams induced by the Wenchuan earthquake

*Xuanmei Fan (1), Cees J. van Westen(2), Havenith, Hans-Balder (3), Chenxiao Tang (2)*

(1) State Key Laboratory of Geohazards Prevention and Geoenvironment Protection, Chengdu University of Technology, Erxianqiao Road, 610059 Chengdu, Sichuan. fanxuanmei@gmail.com
(2) Faculty of Geo-Information Science and Earth Observation (ITC), University of Twente, 7500 AE, Enschede, P.O. Box 217, The Netherlands.
(3) University of Liege, Department of Geology, B18, B-4000 Liege.

***Abstract:*** *The 2008 Wenchuan earthquake induced more than 60,000 coseismic landslides, among which about 800 dammed rivers. This study analyzes the relationships between landslides that lead to damming and a number of predisposing factors, and compares these relations with those of all earthquake-induced landslides. Benefiting from this large database, we analyzed the spatial variation of area density for both, the non-damming and damming landslides in order to better understand their distribution pattern and controlling factors. Nine triggering and geo-environmental factor maps were prepared and implemented on a GIS platform. The results show that distance to fault surface rupture, peak ground acceleration (PGA) and lithology play dominating roles in landslide occurrence. The fault type and hanging/foot wall effect were overlooked in previous studies, but were found important for coseismic landslides. For the damming landslides, distance-to-river factor is critical. The results are relevant for selection and weighting of predictors of landslide susceptibility models.*

***Key words****: Landslides, Landslide dams, Spatial distribution, Area density, Wenchuan earthquake*

## INTRODUCTION

Strong earthquakes are among the prime triggering factors of landslides (Keefer, 1984), which may block rivers, forming landslide dams. Some of these dams may pose serious threats to people and property due to upstream inundation and downstream dam-breach flooding. The 2008 Wenchuan earthquake triggered a vast number of landslides (about 56,000 mapped as polygons by Dai et al., 2011 and around 60,000 mapped as points by Görüm et al., 2011). Among them, more than 800 blocked rivers, forming landslide dams, see Fig. 1 (Fan et al., 2012 a, b). In terms of the amount of coseismic landslides and landslide dams, the Wenchuan earthquake ranks first among other earthquakes (Dai et al., 2011). Thus, it provides us a unique opportunity to study and compare the factors that control the spatial distribution of coseismic landslides and landslide dams. To this objective, we applied the bivariate analysis method to analyze the variation of landslide and landslide dam area density with triggering and geo-environment factors.

The devastating May 12, 2008 (Mw 7.9) Wenchuan earthquake was the largest seismic event in China in more than 50 years. It occurred on the NE-trending Longmenshan thrust fault zone (LTFZ) at a focal depth of 14-19 km (Xu et al., 2009). The LTFZ separates the Sichuan basin from the steep and heavily dissected eastern margin of the Tibetan Plateau in China. The LTFZ consists of three major sub-parallel faults: the Wenchuan-Maowen (WMF), Yingxiu-Beichuan (YBF) and Pengguan faults (PF) (Fig. 1). The coseismic rupture initiated near Yingxiu town and propagated unilaterally towards the northeast, generating a 240-km long surface rupture along the Yingxiu Beichuan fault, and a 72-km long rupture along the Pengguan fault (Shen et al., 2009).

## DATA PREPARATION

### *(1) Damming and Non-damming landslide inventory maps*

Landslide and landslide dam inventories are the direct data, which can be either point or polygon-based. In this study, we used the polygon-based landslide inventory created by Dai et al. (2011), including around 56,000 landslides which are referred to as the "non-damming landslides", and the landslide dam inventory from Fan et al., (2012a), including around 800 polygons, referred to as the "damming landslides". Notably, the landslide deposit areas should not be considered in the analysis, as only source areas are of interest in landslide occurrence. Taking the slope as an example, if the deposit areas are involved, landslides might be found occurring on very gentle slopes. Whereas the damming landslide dataset differentiated between scarp and deposit areas, the non-damming landslide dataset did not, and mapped the landslide as single polygon. To avoid such kind of bias, we took the upper 30% with the highest elevation within the undifferentiated landslide polygons and assumed that these were representing the landslide source areas. Mapping the source areas manually for 56,000 landslides was not possible. The damming and non-damming landslide initiation polygons were converted into pixel-based raster map with a grid size of 25 m for further analysis.

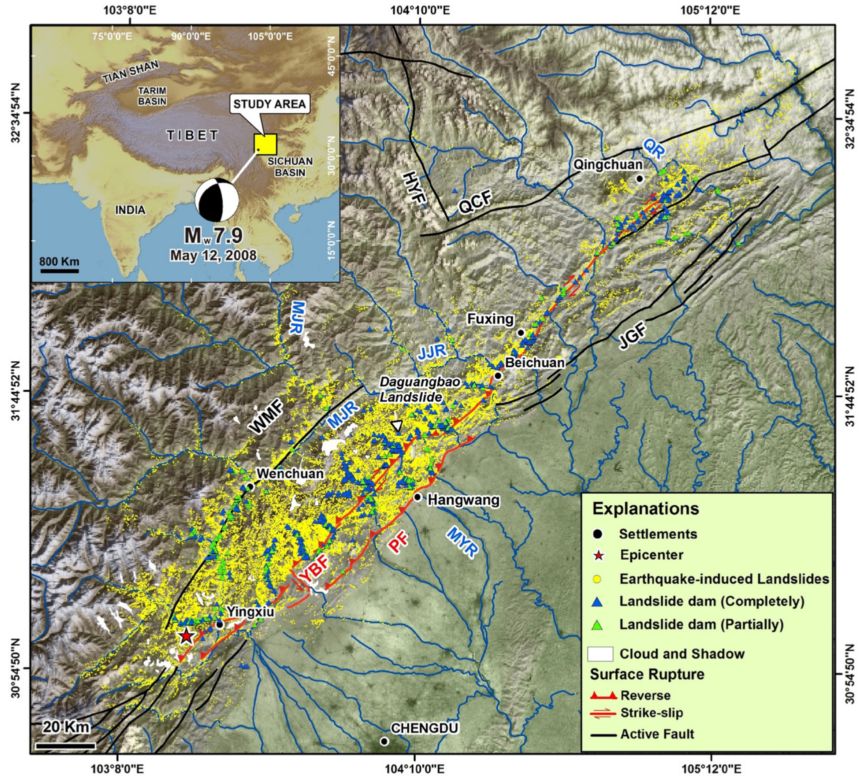


*Fig. 1: Distribution map of landslides and landslide dams triggered by the Wenchuan earthquake. The white areas are unmapped due to the presence of clouds and shadows in the post-earthquake satellite images. The following faults are indicated: WMF: Wenchuan-Maowen fault; YBF: Yingxiu-Beichuan fault; PF: Pengguan fault; JGF: Jiangyou-Guanxian fault; QCF: Qingchuan fault; HYF: Huya fault; MJF: Minjiang fault (after Xu et al., 2009). The rivers indicated in the figures are MJR: Min River; MYR: Mianyuan River; JJR: Jianjiang River; QR: Qingzhu River. The epicenter location is from USGS (2008)*

***(2) Seismic factors***

For earthquake-induced landslides, the commonly used triggering factors are: distance to fault surface rupture, peak ground acceleration (PGA) and seismic intensity. The distance-to-fault map was made by the distance calculation function in ArcGIS, and was classified in 5-km wide intervals (Fig. 2A). The PGA map was obtained from the US Geological Survey (2008), and is based on an unknown number of records of accelerometers, with interpolation of estimated amplitudes where data are lacking (Fig. 2B). It also does not include site amplification effect. However, there is no better map available. The PGA factor is highly correlated to the distance-to-fault factor. Therefore, we will focus mainly on distance-to-fault.

***(3) Geo-environmental factors***

The geo-environmental factors used in this study are: lithology, topographic factors (slope, internal relief, aspect and curvature) and distance to rivers (Fig.2C-F). The internal relief is defined as the elevation difference from a grid on slope from the closest stream. The lithology is obtained from a digital geological map that was compiled from 1:200,000 scale geological map. The data was converted to raster with a 25 m resolution. Unfortunately, the geological structure information is limited to only a few large landslides and not sufficient to be spatialized over such a large area. Thus it was not considered in this analysis.

We prepared raster maps of topographic and hydrological factors from the 25-m DEM using inbuilt algorithms in ArcGIS and SAGA (Fig.2C-F). The stream network was generated from the 25-m DEM with the upslope contributing area of 10 km2 as a threshold.

**RESULTS AND DISCUSSION**

The distribution of damming and non-damming landsides is investigated by analyzing their area-density for the above mentioned seismic and geo-environmental factors. The area density is defined as the percentage of landslide area within each class of different factors.

***(1) Seismic factors***

The speciality of the seismogenic fault of the Wenchuan earthquake is that it has both a thrust and a dextral strike-slip component. This characteristic and the hanging/foot wall effect of the fault are assumed to play an important role in controlling landslide occurrence. In order to see the effect of fault type and hanging/foot-wall difference, we combined them with the distance-to-fault factor.

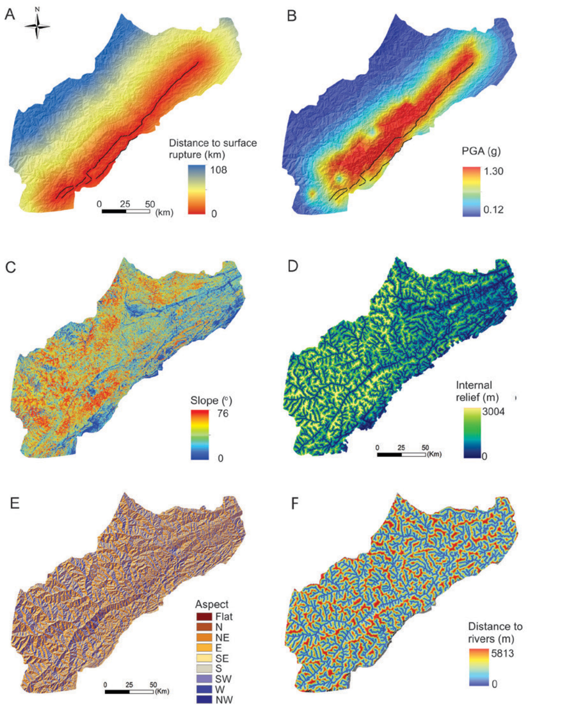


*Fig. 2: Factor maps: A and B are seismic factors (the black lines represent for the fault surface ruptures); C-F are geo-environment factors*

Fig. 3A and B show the variation of non-damming landslide-area density (NLAD) and damming landslide-area density (DLAD) with the distance to both the thrust-dominated and strike-slip-dominated fault segment. It can be seen that both NLAD and DLAD along the thrust-dominated fault segment are higher than those along the strike-slip segment. In the thrust section, the non-damming and damming landslides were distributed in a much wider region, compared to the strike-slip section; while along the strike-slip segment, the NLAD and DLAD values decrease rapidly within a 0-20 km and 0-10 km narrow band, respectively. A clear anomaly of the non-damming and damming curves is found at a distance of 25-30 km, corresponding to the Wenchuan-Maowen fault located along the Min river. This is an active fault, but it was not ruptured during the Wenchuan earthquake. However, landslides and landslide dams (mainly the partially damming ones) are densely distributed along this fault, due to the long-term tectonic activity and strong river incision. Fig. 3C and D show the hanging-wall and footwall effect on the landslide occurrence. Both the NLAD and DLAD are much higher in the hanging-wall of the fault than in the footwall. No damming landslides occurred where the distance exceeds 45 km in the hanging wall and 15 km in the footwall. The results presented in Fig. 3 demonstrate that the fault type and hanging-wall/footwall are critical in controlling landslide occurrence. Some studies (i.e. Dai et al., 2011 and Gorum et al., 2011) considered the distance to epicenter as a factor and found it has little influence on the landslide concentration. The correlations of NLAD and DLAD values with PGA are presented in Fig. 4A, showing the relative high values when the PGA is above 0.8 g.

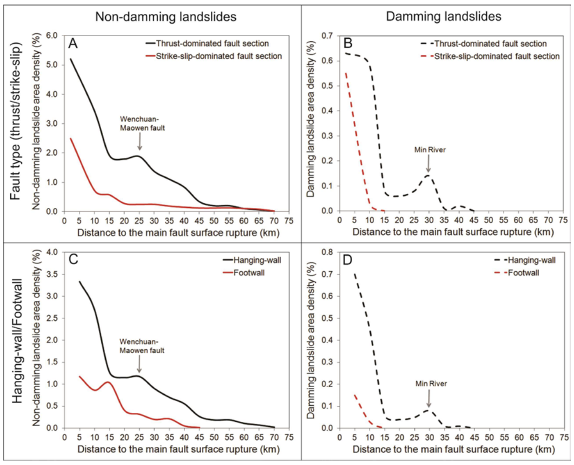


*Fig. 3: Variation of non-damming and damming landslide area density with distance to fault surface rupture: (A) along the thrust-dominated fault segment; (B) along strike-slip- dominated fault segment; (C) on the hanging-wall; and (D) on the footwall*

## *(2) Geo-environment factors*

Fig. 3 and Fig. 4 present some examples of the spatial association of topographic factors with the non-damming and damming landslide concentration. Both NLAD and DLAD values increase significantly when the slope angle exceeds 40° (Fig. 4B), most likely due to the topographic amplification of seismic waves. Regarding the internal relief, the concentration of non-damming and damming landslides has different trends (Fig. 4C). Most of the damming landslides are present on slopes relatively close to the rivers and therefore have a relatively lower internal relief than the non-damming landslides. Almost no damming landslides occurred at slopes with an internal relief above 2000 m, while non-damming landslides were most abundant in zones with internal relief between 1500 m to 2800 m. Considering the distance to rivers, it is not surprising that the damming landslides are more frequent in the vicinity of rivers, showing much lower DLAD than the NLAD values when the distance to rivers exceeds 1000 m (Fig. 4D). Both the DLAD and NLAD present very low values on the areas directly adjacent to the rivers. This is partly due to the fact that these might be floodplain areas, but also to the fact that landslides need to have a certain dimension in order to be able to block the river, and therefore start to have the highest density at some distance from the stream lines. Aspect and curvature are less effective than other factors.

Lithology is widely recognized as a controlling factor to landslide occurrence. The non-damming and damming landslides occurred in various rock types varying from Pre-Sinian rocks to Quaternary unconsolidated deposits. The slopes composed by Pre-Sinian schists and andesites have the highest NLAD and DLAD, followed by Cambrian sandstone and siltstones intercalated with slate, granitic rocks and Permian limestone and shale (Fig. 5). Field investigation also revealed that the Pre-Sinian schists are very weak and fractured, producing a large amount of landslides. The sandstone and siltstone intercalated with shale of the Cambrian age largely affects the integrity and strength of the slopes, resulting in a high density of landslides and landslide dams. The densely jointed Granitic rocks are distributed mainly in the Pengguan massif in the hanging-wall of the Yingxiu-Beichuan fault, which produced many rock avalanche. Limestone and limestone intercalated with shale are generally well stratified and densely jointed, generating both deep-seated rockslides on cataclinal slopes and shallow rockslides or rock falls on anaclinal slopes. Large rock avalanches were mostly observed in the intensely fractured granitic rock masses as well as sandstones and siltstones.

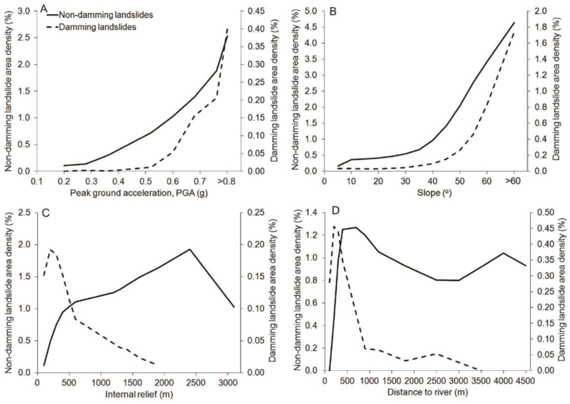


*Fig. 4: Variation of non-damming and damming landslide area density with (A) PGA (g); (B) slope (o); (C) internal relief (m); and (D) distance to rivers (m)*

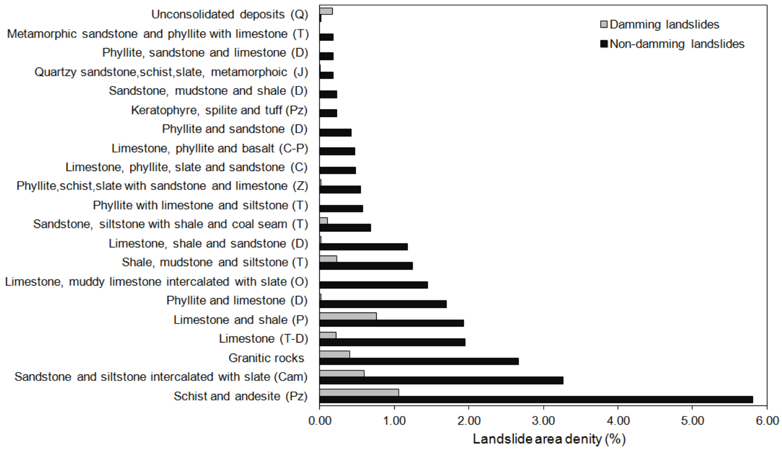


*Fig. 5: Variation of non-damming and damming landslide area density with lithology. Age: Q – Quaternary; J – Jurassic; T – Triassic; P – Permian; C-P – Carboniferous through Permian; C – Carboniferous; D – Devonian; O – Ordovician; Cam – Cambrian; Z – Sinian; Pz – Pre-Sinian*

## CONCLUSION

In this study, we analyzed the area density variation of non-damming and damming landslide-area density with commonly used factors. This contributes to a better understanding of their spatial distribution and related controlling factors. The results of this study demonstrate that distance to fault surface rupture, PGA and lithology play dominating roles in non-damming and damming landslide occurrence. Not surprisingly, the hydrological factors have stronger influence on damming landslides than the non-damming ones. The fault type and hanging/foot wall effect were ignored in previous studies, but were found important in this case for coseismic landslide occurrence.

## References

Dai, F. C., Xu, C., Yao, X., Xu, L., Tu, X. B., & Gong, Q. M., (2011). Spatial distribution of landslides triggered by the 2008 Ms 8.0 Wenchuan earthquake, China. Journal of Asian Earth Sciences, 40(4), 883-895.

Fan, X., van Westen, C. J., Xu, Q., Görüm, T., & Dai, F., (2012a), Analysis of landslide dams induced by the 2008 Wenchuan earthquake. Journal of Asian Earth Sciences, 57, 25-37.

Fan, X., van Westen, C. J., Korup, O., Görüm, T., Xu, Q., Dai, F., Huang, R., & Wang, G., (2012b), Transient water and sediment storage of the decaying landslide dams induced by the 2008 Wenchuan earthquake, China. Geomorphology, 171–172, 58-68.

Görüm, T., Fan, X., van Westen, C. J., Huang, R. Q., Xu, Q., Tang, C., & Wang, G., (2011). Distribution pattern of earthquake-induced landslides triggered by the 12 May 2008 Wenchuan earthquake. Geomorphology133 (3–4), 152-167.

Keefer, D. K., (1984). Landslides caused by earthquakes. Geological Society of America Bulletin, 95(4), 406-421.

Shen, Z.-K., Sun, J., Zhang, P., Wan, Y., Wang, M., Burgmann, R., Zeng, Y., Gan, W., Liao, H., & Wang, Q., (2009), Slip maxima at fault junctions and rupturing of barriers during the 2008 Wenchuan earthquake. Nature Geosci, 2(10), 718-724.

Xu, X., Wen, X., Yu, G., Chen, G., Klinger, Y., Hubbard, J., & Shaw, J., (2009), Coseismic reverse- and oblique-slip surface faulting generated by the 2008 Mw 7.9 Wenchuan earthquake, China. Geology 37(6), 515-518.

INQUA Focus Group on Paleoseismology and Active Tectonics

paleoseismicity.org

# Archaeoseismology in a Bronze aged settlement: La Tira del Lienzo (Totana, Spain)

*Marta Ferrater (1), Maria Ortuño (1), Eulàlia Masana (1), P.G. Silva (2), M.A. Rodríguez-Pascua (3), Guillermo Booth-Rea (4), José Miguel Azañón (4)*

(1) RISKNAT Group. GEOMODELS. Departament de Geodinàmica i Geofísica, Facultat de Geologia, Universitat de Barcelona, c/ Martí i Franquès, s/n, 08028 Barcelona, Spain. Email: marta.ferrater@ub.edu
(2) Dpto. Geología, Escuela Politécnica Superior de Ávila, Universidad de Salamanca, Ávila, Spain
(3) Instituto Geológico y Minero de España, IGME. Madrid, Spain
(4) Dpto. de Geodinámica, Universidad de Granada; Instituto Andaluz de Ciencias de la Tierra UGR-CSIC, Granada, Spain

***Abstract:*** *We present an archaeoseismological study in La Tira del Lienzo (Totana, Spain). The settlement belongs to the Argar archaeological group (2200-1550 BC, Bronze Age) and is being excavated by a team from the Departament de Prehistòria at the Universitat Autònoma de Barcelona (Spain). The site is located on the Alhama de Murcia fault zone (AMF), responsible for the 11/05/2011 Lorca earthquake, and the walls are* made up of *irregular natural blocks. We: 1) classify the existing EAEs in the site and suggest new ones according to the constructive typology; 2) carry out a structural analysis of all the identified fractures and of the AMF segment beneath the site; 3) suggest a potential earthquake occurred between the start of the second phase of occupation (1900 BC) and the present., and 4) obtain an slip rate of c. 0.03 mm/yr for the AMF based on the observed displacements in the archaeological remains.*

***Key words****: Archaeoseismology, Earthquake Archaeological Effects (EAEs), Bronze Age, Alhama de Murcia fault.*

## INTRODUCTION

The oldest worldwide archaeoseismological evidence is located in northern Iraq (Middle Palaeolithic, c. 50,000 years old), but normally archaeo-seismological studies go back as much as to the Bronze Age (c. 1700 BC; Nur & Burgess, 2008). The oldest studied archaeological site in the Iberian Peninsula is from the 1st Century AD (Tolmo de Minateda; Rodríguez-Pascua et al., 2011). The site subject of this study will record the oldest archaeoseismological record in Spain, if further evidences support it.

The type of construction used in the studied site (irregular stone blocks) is not considered in the classification of Earthquake Archaeological Effects (EAEs) proposed by Rodríguez-Pascua et al. (2011), but we have used it as a guide to describe those recorded in the site. In addition, we describe new types of EAEs. We located the EAE on a detailed microtopographic map provided by La Bastida archaeological research group (UAB).

## LA TIRA DEL LIENZO GEOLOGICAL SETTING

La Tira del Lienzo is a Bronze Age small settlement, belonging to the archaeological group of the Argar. This society was developed between 2200 and 1550 cal BC in SE Iberian Peninsula (*figure 1*; Lull 1983; Lull et al., 2011a). The first human presence in the site is dated 2050 cal BC. The final abandonment of the village took place around 1600/1550 cal BC. Two main phases of occupation are present in the site, but we focus on the second phase (1900-1550 cal BC), in which the archeoseismological evidence are preserved. The architectural features consist of rectangular rooms with walls made up of irregular stones blocks of decimetric size (Figs. 2B; 2C; Lull et al., 2011b). La Tira del Lienzo is located in the town of Totana (Murcia, Spain) just on the trace of the Alhama de Murcia fault (AMF). The fault zone in this area affects Miocene marls, gypsum (mylonitic) and hanged Quaternary alluvial fans (*figure 2D*).

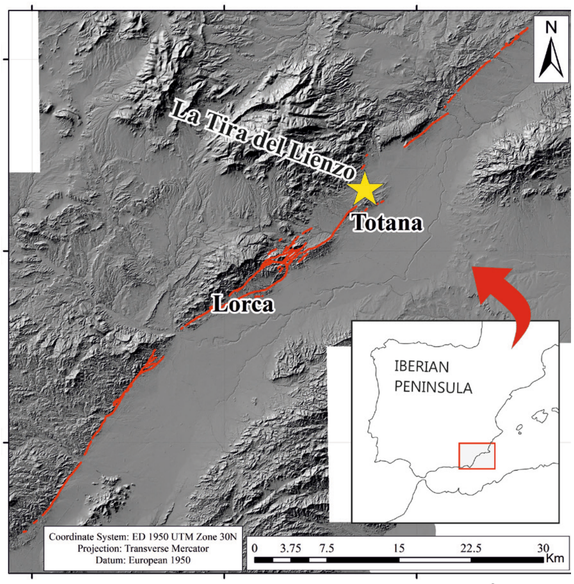


*Figure 1. La Tira del Lienzo and Alhama de Murcia fault.*

The AMF is a N45º-65ºE sinestral strike-slip fault with a reverse component, coherent with the NW-SE convergence between the Eurasian and the African plates (Silva, 1994; Martinez-Díaz, 1998). Several historical earthquakes of intensity ≥ VII occurred in the zone probably generatel by the AMF (1743 and 1746 in Alcantarilla, 1907 in Totana and in 1579, 1674, 1818 in Lorca; IGN, 2012). The stronger instrumentally recorded event occurred in Lorca on

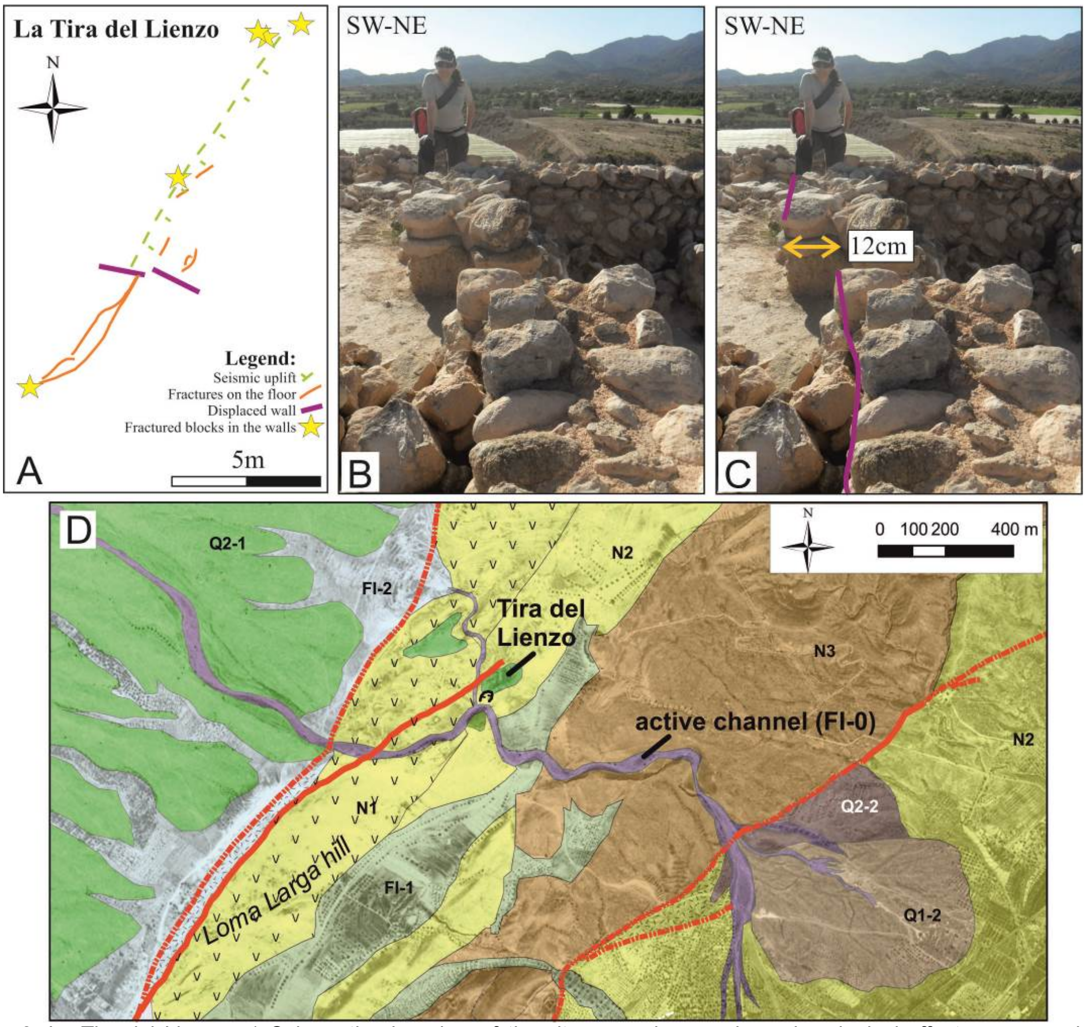


*Figure 2: La Tira del Lienzo. a) Schematic plan view of the site-area where archeoseismological effects are recorded; b) Photograph of the lateral displacement of the wall; c) interpretation of the amount of dislocation of the displaced wall; d) Geological setting of La Tira del Lienzo (legend: N1-N3, Neogene basement; Q1-Q2-2, Quaternary alluvial fans; FI0-FI-2, Quaternary fluvial infill; AMF fault traces in red, dashed (inferred traces).*

11th May 2011 has a moment magnitude of 5.2 and VII EMS intensity (López-Comino et al., 2012). Palaeoseismic studies on this fault have characterized its activity, reporting maximum magnitude values between Mw 6.1-7.0 (Silva et al. 1997; Martínez Díaz et al., 2001, Masana et al. 2004; Ortuño et al., 2012). These studies record a minimum of 6 palaeoseismic events during the last 274-174 ka. The estimated lateral slip-rates are of 0.21 mm/yr for the last 130 ka (Martinez-Díaz et al., 2003). Recent geodetic studies reveal that the slip-rate is 1.4-1.8 mm/yr (Echeverria et al., 2012).

**ARCHAEOSEISMOLOGY OF THE SITE**

The results presented here are: 1) the inventory of EAEs recorded in the site, 2) the structural analysis of both the observed fractures and the AMF fault zonet, and 3) the estimation of AMF slip-rate based on the most relevant reported EAE.

Two of the EAEs types proposed by Rodríguez-Pascua et al. (2011) are recorded in the site: a) seismic uplift and b) displaced walls (*Fig. 2B; C*). In addition, we identified two new types of deformation effects not considered by Rodríguez-Pascua et al. (2011), but mainly due to the type of building material used in the studied site is not considered by these authors. These new EAEs are: c) fractures on the rocky floor, and d) fractured blocks in the walls (*Fig. 3*; Ferrater 2013). These two new proposed EAEs have their equivalent in the classification of Rodríguez-Pascua et al. (2011), but affecting other constructional materials. Floor fractures correspond to fractures and folds in pavements, and fractured blocks in the walls would be equivalent to penetrative the fractures in masonry blocks and conjugate fractures in stucco or brick walls.

Structural analysis performed in all the fractures affecting the rocky floor of the site and the walls reveals that there are two main dominant orientations of fracturing (NE-SW and NW-SE; *fig. 3*). The main orientation (NE-SW) coincides with the direction of the AMF trace just located under the archaeological remains. In this sense, one of the floor-fractures goes through the archaeological site in NE-SE direction separating the building in two and laterally offset its walls (*Fig. 2A*). On the contrary, the fractured blocks in the walls alone cannot be considered a robust evidence of coseismic deformation, but their orientations generally match with the direction of the AMF (Fig. 3). For a true coseismic origin it will be necessary the occurrence of several fractured blocks assembled in the same vertical plane. Except for those cases where the position of the fractured blocks coincides with the occurrence of fractures on the floor and ground uplift (*Fig. 2A*), other natural causes cannot be rejected (e.g. gravitational collapse of the hill or thermic contrast).

## PALEOSEISMIC ANALYSIS

Based on the lateral displacement recorded by the offset wall (*Fig. 2A, B, C*) it is possible to estimate the slip-rate for AMF in the site. The wall, built between 1900-1550 cal BC (Lull, Mico, Rihuete, Risch, pers. comm. 2013), is 12 cm anticlockwise laterally dislocated. Considering the wall is 3912 years old (1900 plus 2012), the minimum lateral displacement is 0.031 mm/yr. The striae pitch in the fault (10°-45, *fig. 3*) make possible to estimate net slip-rates between 0.031 and 0.043 mm/yr, smaller than those reported in previous works. This could be because the fault trace affecting the site is not the main fault trace of the AMF. In fact the small hill on which is located the studied remains is a pressure ridge (Silva, 1994) and the deformation is distributed over a larger area.

In any case, at least one earthquake occurred after the construction of the second phase (< 1900 BC). This event might occur before the abandonment (causing it) or after the abandonment of the site (< 1550 BC). An event within this time gap will be consistent with two events dated by fault trenching in the central segment of the AMF: 1760-830 BC and >1650 AD (Masana et al., 2004).

## CONCLUSIONS

The Bronze Age settlement studied here is located on the AMF fault zone and affected by one of its fault branches. Four Earthquake Archaeological Effects (EAEs) have been identified suggesting the occurrence of at least one earthquake after 1900 BC. The structural analysis indicates two main directions of fracturing. The main fracture direction (NE-SW) coincides with AMF direction in the zone. The main fracture produces a left lateral displacement (c. 12 cm) on the walls remains indicating a mean slip-rate of 0.03 mm/yr for the AMF.

**Acknowledgements:** This research was founded by SHAKE CGL2011-30005-C02-02 and QTECTBETICA CGL2012-37581-C02-01 projects and supported by CSD2006-0004 "Topo-Iberia" (Consolider-Ingenio 2010). We thank the entire team of La Bastida (directors: Lull, Micó, Rihuete Herrada, Risch) for all the provided information. La Bastida is supported by: HUM2006-04610, HAR2011-25280, TSI-070100-2008-133 and 2009SGR778. We are very grateful to: Mari Hernández, Antonio Caño, Antonio Jabaloy and Fidel Martín-González.

## References

Echeverría, A., G.Khazaradze, E. Asensio, J. Gárate & E. Suriñach, (2012). Deformación cortical de las Béticas Orientales observada mediante GPS y su relación con el terremoto de Lorca. *Física de la Tierra* 24, 113-127.

Ferrater, M., (2013). Arqueosismología en La Tira del Lienzo (Totana, Murcia). In*: VI Young Researchers in Archaeology Conference. Barcelona, May 2013*.

Instituto Geográfico Nacional, IGN (2012). Servicio de información sísmica, catálogo de terremotos [online]. Instituto Geográfico Nacional. Available in: *http://www.01.ign.es/ign/layoutIn/sismoFormularioCatalogo* (accessed on January 2012).

Lull, V. (1983). *La cultura de El Argar. Un modelo para el estudio de las formaciones económico-sociales prehistóricas*. Akal, Madrid.

Lull, V., R. Micó, C. Rihuete Herrada & R. Risch, (2011a). El Argar and the Beginning of Class Society in the Western Mediterranean, In: *Sozialarchäologische Perspektiven: Gesellschaftlicher Wandel 5000-1500 v.Chr. zwischen Atlantik und Kaukasus* (S. Hansen, J. Müller eds). Deutsches Archäologisches Institut, Berlin, 381-414.

Lull, V., R. Micó, C. Rihuete Herrada, & R. Risc, (2011b). Proyecto La Bastida: economia, urbanismo y territorio de una capital argàrica. *Verdolay* 13, 57-70. ISSN: 1130-9776

López-Comino, J.A., F. Mancilla, J. Morales & D. Stich, (2012). Rupture directivity of the 2011, Mw 5.2 Lorca earthquake (spain). *Geophysical Research Letters* 39, L03301, DOI: 10.1029/2011GL050498.

Martínez-Díaz, J.J. (1998). *Neotectónica y Tectónica Activa del Sector Centro-Occidental de la Región de Murcia y Sur de Almería (Cordillera Bética – España).* Ph.D.l, UCM, Madrid, Spain.

Martínez-Díaz, J.J., E.Masana, J.L. Hernández-Enrile & P. Santanach, (2001). Evidence for coseismic events of recurrent prehistoric deformation along the Alhama de Murcia fault, southestern Spain. *Acta Geologica Hispanica* 36 (3-4), 315-327.

Martínez-Díaz, J.J., E. Masana, J.L. Hernández-Enrile & P. Santanach, (2003). Effects of repeated paleoearthquakes on the Alhama de Murcia Fault (Betic Cordillera, Spain) on the Quaternary evolution of an alluvial fan system. *Annals of geophysics* 46 (5), 775-791.

Masana, E., J.J. Martínez-Díaz, J.L. Hernández-Enrile & P. Santanach, (2004). The Alhama de Murcia Fault (SE Spain), a seismogenic fault in a diffuse plate boundary: Seismotectonic implications for the Ibero-Magrebian región. *Journal of Geophysical research* 109, B01301.

Nur, A. & D. Burgess, (2008). *Apocalypse: Earthquakes, Archaeology and the Wrath of God*. Princeton University Press. Princeton and Oxford. 309 p.

Ortuño, M., E. Masana, E. García-Meléndez, J.J. Martínez-Díaz, P. Stepancikovà, P.P. Cunha, R. Sohbati, C. Canora, J.P. Buylaert, & A.S. Murray, (2012). An exceptionally long paleoseismic record of a slow-moving fault: the Alhama de Murcia fault (Eastern Betic Shear Zone, Spain). *The Geological Society of America Bulletin* 124 (9-10), 1474-1494.

Rodríguez-Pascua, M. A.; R. Pérez-López, J. L. Giner-Robles, P. G. Silva, V. H. Garduño-Monroy, & K. Reicherter, (2011). A comprehensive classification of earthquake archaeological effects (EAE) in archaeoseismology: application to ancient remains of roman and mesoamericon cultures. *Quaternary International* 242, 20-30.

Silva, P.G., J.L. Goy, C. Zazo & T. Bardají, (1997). Paleoseismic indications along "aseismic" fault segments in the Guadalentín Depression (SE Spain). J*ournal of Geodynamics* 24 (1-4), 105-115.

Silva P.G. (1994). *Evolución Geodinámica de la Depresión del Guadalentín desde el Mioceno Superior hasta la actualidad: Neotectónica y Geomorfología*. Ph.D. UCM, Madrid, Spain.

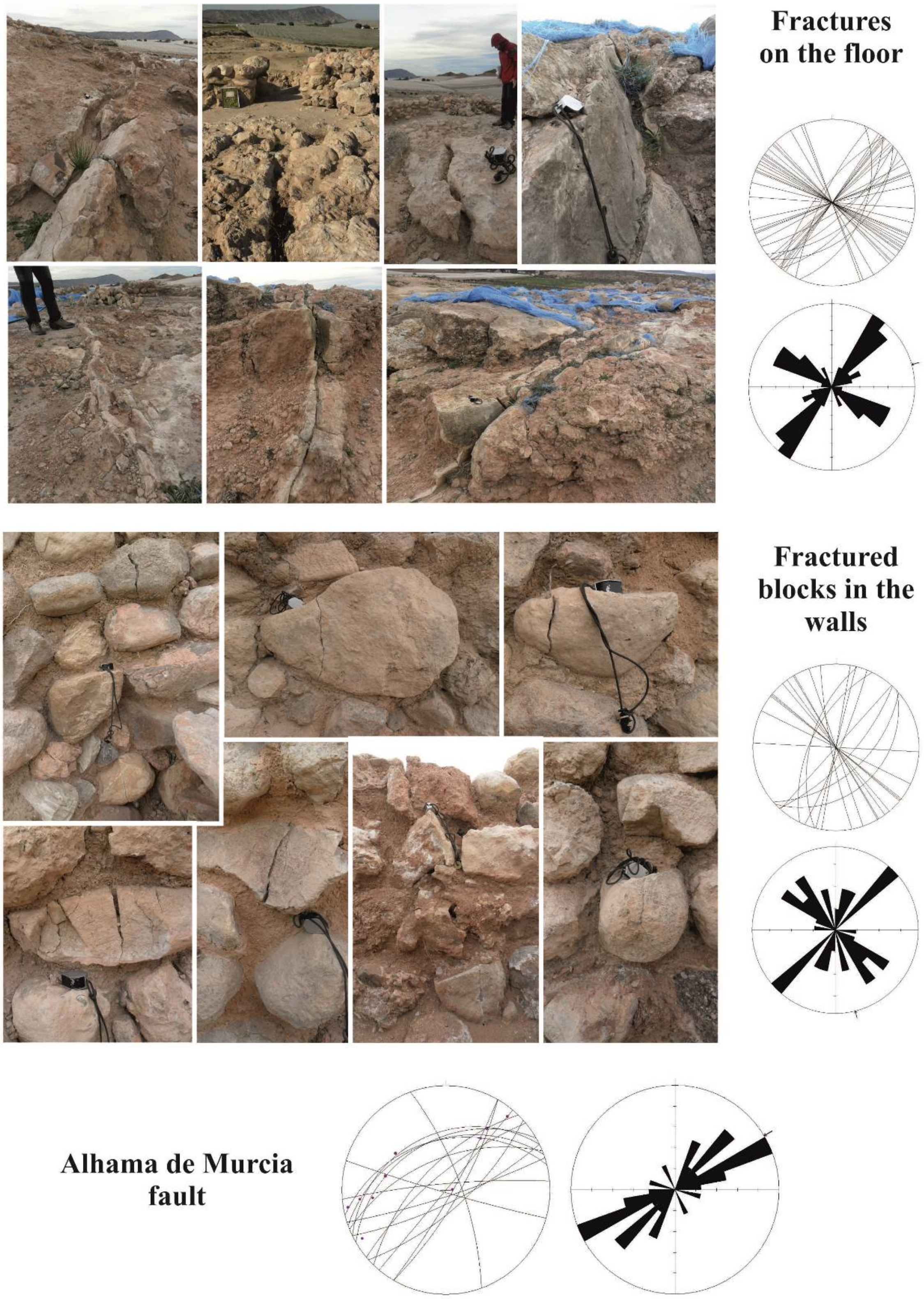


*Figure 3: Fractures on the floor and fractured blocks in the walls photographs and structural analysis. Structural analysis includes stereographic projections and rose diagrams. In the Alhama de Murcia fault structural analysis fault planes and striae are shown.*

# The contribution of paleoseismology to seismic hazard assessment for nuclear installations

*Fukushima, Yoshimitsu (1)*

(1) International Seismic Safety Centre, Division of Nuclear Installation Safety, Department of Nuclear Safety and Security, International Atomic Energy Agency, Vienna International Centre, PO Box 100, 1400 Vienna, Austria. Email: Y.Fukushima@iaea.org

***Abstract:*** *The importance of paleoseismological investigations were highlighted after the Fukushima Daiichi Nuclear Power Plant (NPP) accident in 2011, since some evidences of the Tsunami deposit were found before the accident. The International Atomic Energy Agency (IAEA) recommended using pre-historical, historical and instrumental data for seismic hazard assessment in the IAEA Safety Standard; however, coverage of the period after the historical age may be not enough for the assessment. The uncertainty of pre-historical (paleoseismological) data is very large, but the coverage period is extremely longer than the historical and instrumental data. IAEA member states, which are embarking on nuclear installations, desire a document to show them how to implement paleoseismological data for seismic hazard assessment. Before the Fukushima Daiichi NPP accident, the International Seismic Safety Centre (ISSC) was commissioned to prepare such a document in the frame of an extra budgetary project. It was an ambitious challenge to harmonize individual experts, but finally we are approaching publication.*

***Key words****: Fukushima, IAEA, seismic hazard, nuclear installation*

## BACKGROUND

In August 2005 the Onagawa Nuclear Power Plant (NPP) in Japan was automatically stopped by earthquake shaking. The NPP was not damaged but there were no guidelines regarding its restart. This was the motivation behind starting the extra budgetary project (EBP) on seismic safety. The International Atomic Energy Agency (IAEA) arranged an EBP regarding this event. A document was then prepared to evaluate the restart process. In the meantime the IAEA started to prepare a safety standard on seismic hazard (SSG-9, published in 2010).

In 2007, the Niigata-ken Chuetsu-oki earthquake shut down the Kashiwazaki-Kariha NPP. Observed earthquake ground motions exceeded the design basis earthquake ground motion by 3 to 4 times. Fundamental safety procedures stopped and cooled down the reactors and the confinement of radioactive material were fairly successful due to large design margins. This event promoted the establishment of the International Seismic Safety Centre (ISSC) in 2008.

There was also an EBP on tsunamis, such as the tsunami triggered by the 2004 Sumatra earthquake supported by Japan Nuclear Energy Safety Organization (JNES). The Nuclear and Industrial Safety Agency (NISA) of Japan supported the ISSC for establishment with another EBP.

In August 2010, all EBPs were arranged into a single large EBP which was then divided into 10 ‘work areas’. This was approved half a year before the Fukushima Daiichi NPP accident.

In January 2011, the working areas were divided again into several ‘work groups’ covering diverse issues.

In March 2011, the Fukushima Daiichi NPP accident occurred. The schedule of the EBP was pushed back, although the importance of the project was highlighted.

This extended abstract summarises the work areas, work groups and deliverables of the EBP with regard to seismic hazards. Following this, a brief outline of the technical document on how paleoseismology can contribute to the seismic hazard assessment for nuclear installations is described.

## WORK AREAS (WA) WITHIN THE EBP

The ten work areas (WA) are:

- WA1 Seismic hazards;
- WA2 Seismic design qualification and safety assessment;
- WA3 Seismic experience database;
- WA4 External events preparedness and response;
- WA5 Tsunami safety;
- WA6 Volcanic hazards;
- WA7 Engineering aspects of protection against human induced external events;
- WA8 External event safety assessment of multi-unit NPP sites;
- WA9 Information and notification systems;
- WA10 Public communication, dissemination of lessons learned and capacity buildings.

### *Goal of WA1*

The Specific Safety Guide (SSG)-9 on seismic hazards published in 2010 provided a comprehensive coverage of seismic hazard issues. We anticipate that this guide will be useful to IAEA member states in developing site specific seismic hazard assessments. However, for newcomers who are embarking on nuclear programs for the first time or expanding their nuclear energy capacity, more specific guidance will be required. WA1 of this EBP will develop guidance for the application of SSG-9.

**WORK GROUPS (WG) IN WA1**

Within WA1 Seismic hazards, different work groups were established in order to develop and provide detailed guidance for implementing SSG-9. The working groups include:

- WG 1.1 Documentation: this involves the review and completion of all documents prepared in WA1.
- WG 1.2 Identified source or diffuse seismicity: this covers the areas within seismic source modelling taking into account either identified source or diffuse seismicity as well as fault displacement hazard assessment.
- WG 1.3 Ground motion prediction equations (GMPEs) and site response: this covers the evaluation of site specific ground motion properly accounted by GMPEs with the site response.
- WG 1.4 Deep borehole observations: this involves developing deep borehole seismic observation technology and a site response database.
- WG 1.5 Slope stability and soil liquefaction: this work group is currently suspended.
- WG 1.6 Environmental seismic intensity and paleoseismology.

**OBJECTIVES OF WG 1.6**

In light of the Fukushima Daiichi NPP accident, the importance of paleoseismology was again highlighted. After the 11 March Great Tohoku earthquake, paleotsunami investigations were undertaken in the area and paleotsunami deposits were detected. These deposits were dated and it was discovered that they were caused by the AD 896 Jogan earthquake which occurred at the same location as the 11 March Great Tohoku earthquake. The objectives of this working group are, therefore, to develop and distribute an 'environmental seismic database', and to develop detailed guidelines on paleoseismology.

**DELIVERABLES**

After prioritisation by the EBP donors, two safety reports and two technical documents are being developed:

- Safety Report on fault rupture modeling for seismic hazard assessment in site evaluation for nuclear installations; undertaken by WG 1.2.
- Safety Report on diffuse seismicity on seismic hazard assessment in site evaluation for nuclear installations; undertaken by WG 1.2.
- Technical Document on ground motion prediction equations (GMPEs) and site response on seismic hazard assessment in site evaluation for nuclear installations; undertaken by WG 1.3.
- Technical Document on the contribution of paleoseismology to seismic hazard assessment in site evaluation for nuclear installations; undertaken by WG 1.6

Furthermore, a database and catalogue of Earthquake Environmental Effects (EEE) in the ISSC portal site under WG 1.6 is being carried out with the Institute for Environmental Protection and Research (ISPRA), Italy.

**TECHNICAL DOCUMENT ON THE CONTRIBUTION OF PALEOSEISMOLOGY TO SEISMIC HAZARD ASSESSMENT**

This document aims to show the great contributions that paleoseismic investigations can provide when undertaking seismic hazard assessment performed in the frame of siting procedures for nuclear installations. The objective is to assist and encourage IAEA member states, especially newcomer countries, to include paleoseismic results into the geological database.
The objectives of paleoseismic investigations in the context of nuclear installation siting include:

- Identification of seismogenic structures based on the recognition of past earthquake effects in the region;
- Improvement of the completeness of earthquake catalogues through the identification and dating of ancient, moderate to large, earthquakes, whose traces have been preserved in the stratigraphic record;
- Estimation of the maximum seismic potential associated to an identified seismogenic structure. This will typically be based on displacement per event (measureable in paleoseismic trenches), as well as from geomorphic and stratigraphic features caused by the cumulative effect of repeated large seismic events (concept of "seismic landscape");
- Calibration and validation of probabilistic seismic hazard analyses (PSHA), by using the recurrence interval of large earthquakes, and providing a "reality check" based on direct observations of earthquake environmental effects.

The document consists of:

1. Introduction
2. Paleoseismology: State of the Art
3. The Contribution of Paleoseismic Data to Improved Seismic Hazard Assessment
4. Application of Paleoseismology to NPP Seismic Hazard Assessment

**DATABASE OF EARTHQUAKE ENVIRONMENTAL EFFECTS CATALOGUE IN ISSC PORTAL**

Another substantial outcome is the database of Earthquake Environmental Effects which mirrors the EEE Catalogue, implemented by INQUA TERPRO Focus Group on Active Tectonics and Paleoseismology. This database is hosted by ISPRA and is aimed at coordinating environmental effects from modern, historical and paleo earthquakes with locations of worldwide NPP sites. By this link (https://issc.iaea.org/eee_catalogue.php), ISSC registered members can aware the presence of EEEs around the NPPs and consequently enhance the paleoseismic evaluation at the NPP site. Of course, in order to achieve this goal, it will be crucial to constantly implement the database with new data resulting from paleoseismic researches around the world.

## CONCLUSION

The need for external hazard assessments when siting nuclear installations was highlighted by the Fukushima Daiichi NPP accident. Moreover, the importance of paleoseismic investigations was emphasised in the post Fukushima Daiichi NPP accident. The ISSC was established before the accident, and the task to include paleoseismology was already identified in the EBP. More than 20 experts are currently involved in producing a technical document showing the contribution of paleoseismology to seismic hazard assessment in site evaluation for nuclear installations. It was ambitious challenge to harmonize individual experts; however, we are approaching publication with global consensus.

**Acknowledgements:** I would like to express my acknowledgement to all experts, who are involved in this project.

## References

IAEA Safety Standards Series SSG-9, Seismic Hazards in Site Evaluation for Nuclear Installations (2010).

# Late Quaternary uplift rate of Lomas de Carabajal, Lerma valley, Cordillera Oriental, NW Argentina. Insights from structural analysis and OSL dating.

*García, Víctor H. (1), Ruth A.J. Robinson (2), Fernando Hongn (3), Ernesto O. Cristallini (4), Daniel L. Yagupsky (4), Diego Winocur (4), Darío R. Vera (1)*

(1) Instituto de Investigación en Paleobiología y Geología, Universidad Nacional de Rio Negro, Isidro Lobo 516 (8332) General Roca, Rio Negro, Argentina. Email: vgarcia@unrn.edu.ar
(2) Department of Earth & Environmental Sciences, University of St Andrews. Irvine Building, St Andrews, KY16 9AL, Scotland, UK. Email: rajr@st-andrews.ac.uk
(3) Instituto de Bio y Geociencias del NOA, (UNSa-CONICET). Mendoza 2 (4400) Salta, Argentina. Email: fhongn@aol.com
(4) Laboratorio de Modelado Geológico, Instituto de Estudios Andinos (UBA-CONICET), Pabellón 2, Ciudad Universitaria C1426EHA, CABA, Argentina. Email: ecristallini@gmail.com

***Abstract:*** *Detailed structural and geological mapping was carried out in the Lomas de Carabajal region. In this area the Plio-Pleistocene Piquete Formation appears intensely folded and faulted, being unconformably overlain by the Upper Pleistocene alluvial conglomerates of the La Viña Formation. These conglomerates are folded and show growth strata geometries near their limiting faults. The N-S striking folds along the Lomas de Carabajal are en-echelon structures and have short wavelengths (<1 km). Three samples of fine-grained sediment were collected from layers that are interbedded within the conglomeratic sequence and have optically stimulated luminiscence (OSL) ages of 30.1 ka to 39.8 ka. The maximum measured vertical uplift for the dated levels is around 20 meters, giving uplift rates of 0.50-0.66 mm/yr for Upper Pleistocene-Holocene times. The master fault controlling the uplift and folding has a strike of N30W and could produce earthquakes of up M 6.5 every 450-600 years.*

***Key words****: Quaternary tectonics, Structural mapping, OSL Dating, Seismogenic source*

## INTRODUCTION

The Lomas de Carabajal are low relief hills aligned in NW sense and located at the central western Lerma valley in the Cordillera Oriental of NW Argentina. The Lerma valley is a Plio-Quaternary intermontane basin bounded by uplifted basement-cored thrust sheets (García et al., 2013). Its western boundary in this sector is oblique to the general N-S trend of the Andean chain, displaying a NW strike which is similar in orientation to the NE limit of the Metán sub-basin of the Cretaceous Salta Group rift (Monaldi et al., 2008) and the Calama-Olacapato-Toro lineament (Salfity, 1985).

The stratigraphy of the region can be divided in four sequences: 1) Early to Middle Cambrian basement composed of low grade metamorphic rocks of the Puncoviscana Formation (Turner and Mon, 1979; Escayola et al., 2011); 2) Cretaceous-Paleogene continental strata with conglomerates, sandstones, mudstones and limestones of the Salta Group rift sequence (Marquillas et al., 2005); 3) synorogenic Neogene to Pleistocene strata composed of reddish sandstones and mudstones, and brownish conglomerates interbedded with mudstones of the Guanaco and Piquete Formations respectively (Gebhard et al., 1974); and 4) Late Quaternary deposits including thick alluvial conglomerates with some sandy and muddy layers interbedded (La Viña Formation; Gallardo et al., 1996).

The actual morphostructural expression of the region is response of the inversion of the Salta Group rift from Late Miocene times and the exhumation of the basement through high angle thrusts and backthrusts (García et al., 2013). The NE border of the Metán sub-basin and, therefore the NW strike of the present-day mountain front at this area are controlled by the long-lived Calama-Olacapato-Toro lineament.

In the Lomas de Carabajal the Plio-Pleistocene Piquete Formation is intensely folded and faulted. Dips up to 60º/W and 45º/E have been measured in the northwestern and southeastern extremes of the hills, respectively, while their internal minor folds have more gently dipping limbs. The axes of these folds have N-S orientation, while the wavelength is quite short (<1 km). The en-echelon arrangement of the folds with respect to the general trend of the hills is a remarkable characteristic (Fig. 1).

The Piquete Formation is unconformably overlain by thick conglomerates and interbedded sandy and muddy layers of the Upper Pleistocene La Viña Formation. Despite the rude stratification of this sequence, dips can be measured in some key areas. The general structural trend of the sediments is the same as the underlying Piquete Formation but with folds of less amplitude. The presence of growth strata related to the bounding structures in the northwestern extreme of the Lomas de Carabajal is an outstanding feature of the La Viña Formation (Fig. 2).

Three samples of sandy silt interbeds from outcrops of the La Viña Formation exposed along the Manzano river were dated using OSL chronology. Two samples correspond to roughly the same stratigraphic level on both sides of the river at the northwestern extreme of Lomas de Carabajal (COR-322 and COR-323, Fig. 1). The third sample was collected about 1 km upstream on the left margin of the river corresponding to another growing structure (COR-325, Fig. 1). The results are summarised in the Table 1.

## DISCUSSION

The short wavelength of the Lomas de Carabajal folds and their en-echelon arrangement with respect to the general orientation of the hills reflects an interference deformation pattern and a transpressive local regime. The main deformation axis should be E-W oriented, perpendicular to the axes of the folds. The en-echelon pattern may result from the interaction of the main tectonic transport direction with a previous heterogeneity NW oriented, represented by the Calama-Olacapato-Toro lineament.

From the structural measurements and observations it is proposed that the southwestern border of the hills concentrates more deformation than the northeastern region favouring the interpretation that a backthrust is the responsible for uplifting the whole of the Lomas de Carabajal.

The minimum uplift of the dated levels with respect of the undeformed valley could be around 20 meters giving uplift rates in the order of 0.50-0.66 mm/yr. These values are in agree with those recently estimated for the last 0.1 Ma by Garcia et al. (2013) at Lomas de Medeiros and Mojotoro range in the northern extreme of the Lerma valley.

Assuming that Lomas de Carabajal is being uplifted by the reactivation of the entire NW-trending backthrust, this 16 km-long structure would be capable to produce earthquakes up M 6.5 with related average vertical displacements of 0.3 meters (Wells & Coppersmith, 1994). Recurrence intervals ranging between 450 and 600 years for such events have been obtained by dividing the average vertical displacement by the uplift rates of 0.50-0.66 mm/yr.

The M 6.2 26th February 2010 Salta earthquake was a shallow event (depth 14 km) with a compressive to transpressive focal mechanism (Garcia et al., 2011) which epicenter was located about 20 km NNE of Lomas de Carabajal. The aftershocks sequence were distributed around the mainshock and along a general NW trend. Although this quake did not produce superficial ruptures, it is proposed that it could be related to a growing structure of similar characteristics to that described for Lomas de Carabajal.

More paleoseismological work (trenches) is planned to be executed in this area in order to improve and adjust our preliminary estimations on the seismogenic potential of this morphostructure.

**Acknowledgements:** We want to thank to the projects PICTO-UNRN 2010-0175, PI UNRN 40-B-243, CiUNSa P2027, PICT 2011-1079 and PICT 2010-1441 for the funding to develop the present investigation.

## References

Arnold, L.J. & R.G. Roberts, (2009). Stochastic modelling of multi-grain equivalent dose (De) distributions: Implications for OSL dating of sediment mixtures. *Quaternary Geochronology* 4, 204-230.

Escayola, M.P., C.R. van Staal & W.J. Davis, (2011). The age and tectonic setting of the Puncoviscana Formation in northwestern Argentina: An accretionary complex related to Early Cambrian closure of the Puncoviscana Ocean and accretion of the Arequipa-Antofalla block. *Journal of South American Earth Sciences* 32, 438-459.

Gallardo, E.F., N.G. Aguilera, D.A. Davies & N.R. Alonso, (1996). Estratigrafía del Cuaternario del valle de Lerma, provincia de Salta, Argentina. XI Congreso Geológico de Bolívia, *Actas*, 483-493, Tarija.

García, V.H., F. Hongn & E.O. Cristallini, (2013). Late Miocene to recent morphotectonic evolution and potential seismic hazard of the northern Lerma valley: clues from Lomas de Medeiros, Cordillera Oriental, NW Argentina. *Tectonophysics* (in press).

Gebhard, J., A. Giudici & J. Oliver, (1974). Geología de la comarca del río Juramento y el arroyo Las Tortugas, provincias de Salta y Jujuy, República Argentina. *Revista de la Asociación Geológica Argentina* 29(3), 359-375.

Marquillas, R.A., C. del Papa & I.F. Sabino, (2005). Sedimentary aspects and paleoenvironmental evolution of a rift basin: Salta Group (Cretaceous-Paleogene), northwestern Argentina. *International Journal of Earth Sciences* 94, 94-113.

Monaldi, C. R., J. Salfity & J. Kley, (2008). Preserved extensional structures in an inverted Cretaceous rift basin, northwestern Argentina. Outcrop examples and implications for fault reactivation. *Tectonics* 27, TC1011.

Salfity, J.A., (1985). Lineamentos transversales al rumbo andino en el noroeste argentino. IV Congreso Geológico Chileno, *Actas* 2, 119-137, Antofagasta.

Turner, J.C.M. & R. Mon, (1979). Cordillera Oriental. *II Simposio de Geología Regional Argentina*, Academia Nacional de Ciencias de Córdoba 1, 57-94.

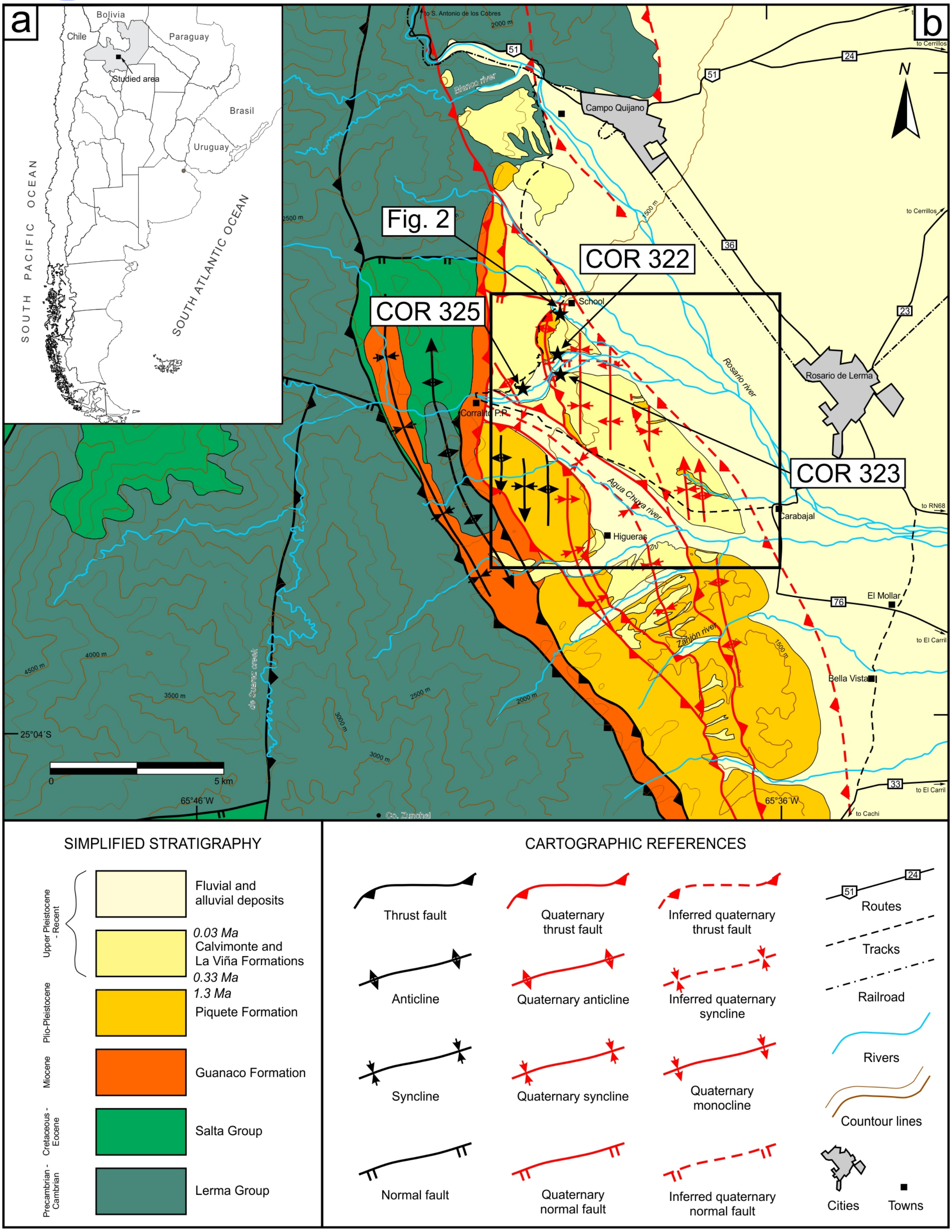


*Figure 1: a) General location of the studied area in the southern extreme of South America. b) Geological and structural map of the studied area. The black box indicates the location of the Lomas de Carabajal. The location of the picture of the Fig. 2 and the samples dated by OSL are marked with black stars.*


*Figure 2: Growth strata developed in the Plio-Plesitocene Piquete Formation (Pi) and Late Pleistocene conglomerates (Cv) related with the eastern flank of a west-vergent anticline. See location in Fig. 1.*

| SAMPLE | U (ppm) | uncert | Th (ppm) | uncert | %K | uncert | Rb (ppm) | uncert | H20 | dose rate (Gy/ka) | uncert. | N | De (Gy) | uncert (Gy) | Age (ka) | uncert (ka) |
|---|---|---|---|---|---|---|---|---|---|---|---|---|---|---|---|---|
| COR 322 | 3.17 | 0.095 | 11.29 | 0.339 | 3.19 | 0.096 | 126 | 12.6 | 3.6 | 4.526 | 0.207 | 62 | 155.4 | 10,8 | 34.3 | 2.9 |
| COR 323 | 3.36 | 0.101 | 12.89 | 0.387 | 2.81 | 0.084 | 109.3 | 10.9 | 7.4 | 4.118 | 0.179 | 54 | 164.1 | 9,8 | 39.8 | 2.9 |
| COR 325 | 2.94 | 0.088 | 12.61 | 0.378 | 2.96 | 0.089 | 117.9 | 11.8 | 4.1 | 4.306 | 0.195 | 52 | 129.7 | 6,9 | 30.1 | 2.1 |

*Table 1: Dose rate calculations, based on nuclide concentrations of sediments (using solution ICP-MS), and OSL burial ages calculated using the Minimum Age Model (e.g. Arnold and Roberts, 2009).*

# Seeking the source of the AD 1580 Dover-Strait/Pas-de-Calais earthquake (Western Europe).

*García Moreno, David (1,2), Koen Verbeeck (1), Thierry Camelbeeck (1), Marc De Batist (2), Francesca Oggioni (5), O. Zurita Hurtado (2), Willem Versteeg (2,4), Hervé Jomard (3), Jenny Collier (5), Sanjeev Gupta (5), Alain Trentesaux (6) & Kris Vanneste (1)*

(1) Royal Observatory of Belgium, Av. Circulaire 3, 1180 Uccle, Brussels (Belgium). Email: David.GarciaMoreno@oma.be
(2) Renard Centre of Marine Geology, Ghent University. Krijgslaan 281, Ghent (Belgium)
(3) Institut de Radioprotection et de Sûreté Nucléaire. Av. de la Division Leclerc 31, Fontenay-aux-Roses (France)
(4) Vlaams Instituut voor De Zee. InnovOcean site, Wandelaarkaai 7, B-8400 Oostende (Belgium)
(5) Dept. Earth Science & Engineering, Imperial College London. Prince Consort Road, London SW7 2BP (United Kingdom).
(6) Université Lille 1, Lab Geosystemes UMR 8217 Lille1/CNRS, 59 655 Villeneuve d'Ascq (France)

***Abstract:*** *On April 6th, 1580 one of the most destructive earthquakes that have occurred in north-western Europe in historical times took place in the Dover Strait (Pas de Calais). The epicentre of this seismic event, whose magnitude is estimated to be about 6.0, has been located near the offshore continuation of the North Artois Shear zone, a major Variscan tectonic structure that traverses the Dover Strait, suggesting that this structure, or some of its fault segments, may be presently active.*
*A large set of multi-beam bathymetry and high-resolution seismic-reflection data have been gathered during the last 3 years from the area between Folkestone (United Kingdom) and Sangatte (France) in order to investigate the possible Quaternary activity of the structures located in that zone. The analysis of these data has revealed a broad fault system traversing the Dover Strait consisting of several sub-parallels WNW – ESE trending faults and folds, some of them significantly offsetting middle and lower Cretaceous deposits. Possible Quaternary activity has been recognized along some of these faults; however, it has not been possible to clearly characterize this activity, for most of the features associated with possible tectonic forcing are too subtle to be separated from depositional/erosional features. The seismic reflection profiles collected for the present study have also shown that the geological map obtained from their interpretation strongly disagrees in the central part of the Dover strait with the offshore bedrock geological map presently available for this area.*

***Key words****: Submarine paleo-seismology, active tectonics, marine geology.*

INQUA Focus Group on Paleoseismology and Active Tectonics

paleoseismicity.org

# The West Beverly Hills Lineament and Beverly Hills High School: An Unexpected Journey

*Gath, Eldon (1), Tania Gonzalez (1), Joe Roe (2), Philip Buchiarelli (2), Miles Kenney (3)*

(1) Earth Consultants International, 1642 E. 4th St., Santa Ana, CA 92701, USA. Email: gath@earthconsultants.com
(2) Leighton Consulting, 17781 Cowan, Irvine, CA 92614, USA
(3) Kenney Geosciences, 1105 Vista Bonita Dr., Vista, CA 92083 USA

***Abstract:*** *Results of geotechnical studies for the Westside Subway were disclosed in a public hearing on Oct. 19, 2011, showing new "active faults" of the Santa Monica fault and the West Beverly Hills Lineament (WBHL), identified as a northern extension of the Newport-Inglewood fault. No faults had been physically observed; the faults were all interpreted from cone penetrometer probes, supplemented by core borings and geophysics. Several of the WBHL faults traversed buildings of the Beverly Hills High School (BHHS), triggering the school district to map and characterize these faults for future planning efforts, and to quantify risk to the students in the 1920's high school building. 5 exploratory trenches were excavated within the high school property, 12 cone penetrometers were pushed, and 26-cored borings were drilled. Geologic logging of the trenches and borings and interpretation of the CPT data failed to confirm the presence of the mapped WBHL faults, instead showing a 3° NE dipping sequence of mid-Pleistocene alluvial fan deposits conformably overlying an ~1 Ma marine sand. Using $^{14}C$, OSL, and soil pedology for stratigraphic dating, the BHHS site was cleared from fault rupture hazards and the WBHL was shown to be an erosional margin of Benedict Canyon, partially buttressed by 40-200 ka alluvial deposits from Benedict Wash. The consequence of the Westside Subway's active fault maps has been the unexpected expenditure of millions of dollars for emergency fault investigations at BHHS and several other private properties within a densely developed highrise urban environment. None of these studies have found any active faults where they had been interpreted, mapped, and published by the subway's consultants.*

***Key words***: *Fault investigation, hazard communication, ethics*

## INTRODUCTION

In the 1992 Association of Engineering Geologist's Annual Meeting's field trip guidebook, the West Beverly Hills Lineament (WBHL) was first identified as a geomorphic feature and placed into a structural context as a step-over between the Santa Monica and Hollywood faults (Dolan and Sieh, 1992).

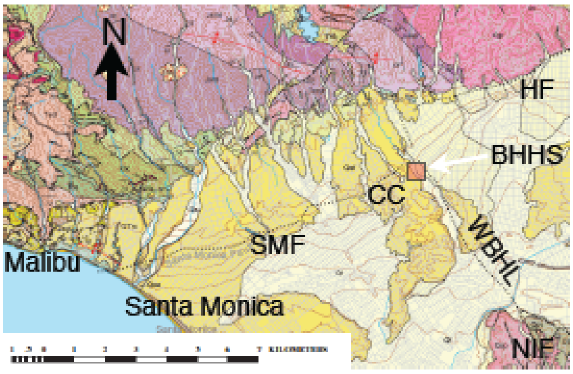


*Fig. 1: Geologic map of the Beverly Hills High School (BHHS) project site, showing the predominantly Mesozoic crystalline and metamorphic rocks of the Santa Monica Mountains to the north (top) and the Quaternary alluvial fan and fluvial deposits to the south (Yerkes and Campbell, 2005). CC – Century City; HF – Hollywood fault; NIF – Newport-Inglewood fault; SMF – Santa Monica fault; WBHL – West Beverly Hills Lineament.*

Subsequent tectonic modeling of the western LA basin assumed the presence of this N-S tectonic feature and built upon it (e.g. Hummon et al., 1994) and it became included on multiple maps (e.g. Yerkes and Campbell, 2005), despite objections from geologists of the Beverly Hills Oil Field, bisected by the lineament, who stated that no such structural feature was possible based on their 300+ well logs and operational history (Lang, 1994). Paleoseismic studies of the Santa Monica and Hollywood faults (Dolan et al., 2000a & 2000b) showed evidence for a Holocene event on each, but the two events could not be temporally correlated and the faults had average return periods of about 10 ka. Neither fault has been zoned active under the California Alquist-Priolo Earthquake Fault Zone Act despite the 13 years since the studies were published, and even less attention was given to the WBHL as a potential fault hazard because 1) it was secondary to low activity faults, 2) it had never been mapped at a scale usable for assessment, and 3) it had never been confirmed as a fault.

Preliminary geologic studies were completed for the Environmental Impact Report of the Westside Subway Extension Project from Los Angeles to Santa Monica, and the Metro Board approved the project in Sept. 2010. Additional fault-specific investigations were authorized by the Metro Board in Oct. 2010 to better understand the neotectonic structures and fault rupture hazards of the Century City / Beverly Hills area of western Los Angeles (Fig. 1), as they related to proposed subway station locations. The results of that work (PB, 2011) were simultaneously released to the public via press releases, newspapers, and an open Board meeting at Metro which posted videos of the meeting onto YouTube [http://www.youtube.com/watch?v=Omx2BTIpzAk].

The active fault map released to the media was highly alarming for the community (Fig. 2). It showed two wide zones of faults, one trending generally ENE as active strands of the Santa Monica fault zone and another generally NNW as active faults of the West Beverly Hills Lineament, now also correlated to the active Newport-Inglewood fault which was previously terminated 5 km to the south in the Baldwin Hills (Fig. 1).

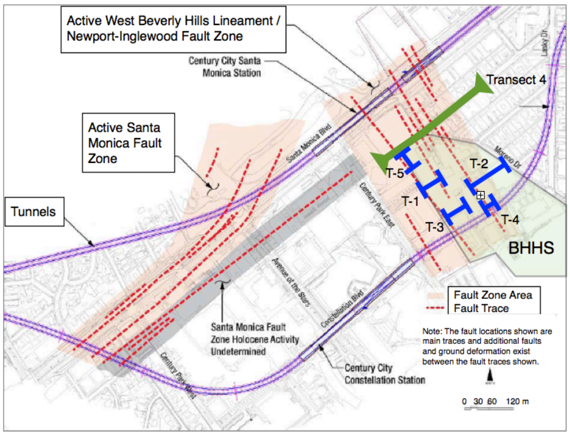


*Fig. 2: The fault map released by Metro (PB, 2011) showing the two fault zones, the proposed tunnel alignments and station locations, and their relationship to Transect 4 (Fig. 3) and Beverly Hills High School (BHHS – green shading).*

Because of the urban environment, the investigative tools used by the Metro consultants relied principally upon stratigraphic correlation of transects of cone penetrometer (CPT) probes generally spaced about 15 m apart, supplemented with occasional cored borings and seismic reflection geophysical profile lines. The CTP logs were compiled into interpreted sections showing the stratigraphy and the faults, generally drawn perpendicular to the transect. Transect 4 is of greatest relevance to BHHS (Fig. 3).

As mapped, almost the entire WBHL fault zone trended directly through the BHHS campus (Fig. 2), necessitating immediate concern for the safety of the students and employees within the iconic 1920s school building. Within the month, BHHS contracted Leighton Consulting Inc. (LCI) to undertake a detailed geologic investigation to locate and more accurately map the faults through the campus, and if possible, to better quantify the hazard that they posed. This paper summarizes the results of that study.

## INVESTIGATION

To locate and map the faults accurately enough for campus planning, the BHHS consultants relied upon a suite of investigative tools similar to Metro's consultants (borings and CPTs) but also excavated ~270 m of exploratory trenches (Fig. 4) across available portions of the BHHS campus to precisely locate, geologically log, and kinematically quantify the fault displacements that had been mapped through the school property.

In total, 5 trenches were excavated, 12 CPTs were pushed, and 26 borings were continuously cored along two transects. The initial borings were emplaced E-W across the center of the campus to correlate with the best location for the surface trenching (T-2 on Fig. 4). Early on it was realized that the borings should extend through the alluvial fan deposits, upon which the school was built, and into an underlying ~1Ma marine unit (San Pedro Fm) because this contact was easily identified and correlated from boring to boring (Fig. 5).

Metro's Transect 4 (Fig. 3) was redone using CPTs and borings in adjacent positions that were also drilled deeper to reach the San Pedro contact (Fig. 6). The alluvial fan stratigraphy was correlated using mainly the boring cores because the physical recognition of stratigraphic correlations could be observed, discussed, and agreed upon. CPT correlations suffer from cone variations, divergence from vertical, and indirect subjectivity. Within the alluvial stratigraphy, a series of buried paleosols were observed and these provided the most powerful correlations across the borings (Fig. 6).

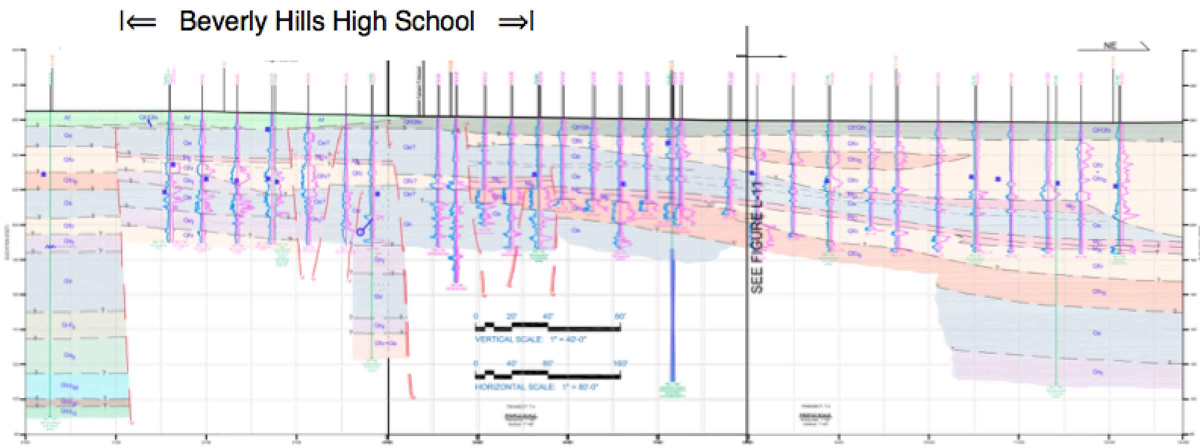


*Fig. 3: The Transect 4 cross-section lying immediately north of BHHS (Fig. 2) showing the alluvial stratigraphy and the multiple faults, as originally interpreted from the cone penetrometer test probes and borings (PB, 2011).*

*Fig. 4: One of the exploratory trenches excavated to expose and map the faults that were mapped through the BHHS, part of which is seen at the top of the photo. Each bench is about 1.3 m in height; shoring was used where space did not permit benching. No faults were found in this trench.*

*Fig. 5: Borehole correlations were made across all of the borings on the two transects to look for vertical separations of key marker units that might confirm the faults shown by Metro. Here, there is excellent correlation of the underlying San Pedro contact between borings CB-3 (left) and CB-4 (right) at ~25-30 m, despite being on opposite sides of a mapped fault.*

Pedogenic development of the geomorphic surface that forms the primary school site indicated that the soils are a minimum of 80-100 ka, and could be considerably older (ECI, 2012).

This surface soil, combined with the time required to form the multiple buried paleosols, showed that the alluvial fan deposits are of considerable age, a discovery that raised questions with respect to the degree of hazard posed by the mapped faults.

In the Metro study, no stratigraphic age estimates were made (PB, 2010); the faults were simply assumed to be Holocene in age and thus active by definition. In addition to locating and mapping the faults in this new study, there was now a necessity to determine their rupture age. If the faults could be shown to have no Holocene-age displacements, then per California criteria, the faults would be considered inactive, and the hazard to BHHS would be negligible. To achieve this, borings alone were not adequate, the faults needed to be exposed in trenches where their rupture age could be documented.

The primary trench (T-2) was excavated 100 m down the eastern lawn (Fig. 4). The slope that forms this dramatic presentation to the school is the scarp-like feature that defines the WBHL. Continuous, mid-early Pleistocene alluvial fan stratigraphy lay unbroken along the entire trench until erosionally removed by incision of Benedict Canyon wash on the eastern margin (Fig. 7). The fan deposits dip 3° NE, as were correlated in the boring transects (Fig. 6), and extend out the slope face, demonstrating that the genesis of the slope is erosional and not structural. The incision of Benedict Creek would have isolated the upper geomorphic surface, allowing the surface soil to form. Based on that pedogenic profile (ECI, 2012) this occurred 100+ ka. Subsequent alluvial fill buttressed the lower 15 m of the slope (Fig. 7). Buried paleosols within the Benedict Canyon alluvium provide a minimum pedogenic age of ~40 ka for the uppermost 5 m, and a similar OSL age of ~25 ka (ECI, 2012; LCI 2012). No fault offsets were present within the Benedict Canyon alluvium, nor within the older alluvial fan deposits. While minor strike slip faults may not be resolvable with borings alone (Fig. 6), the combination of the trenches with the boring profiles, the dip to the strata, and their multiple correlations, do make it improbable.

The only N-S fault observed was in one of the shorter trenches where two fault-like features, 3 m apart, were observed to vertically displace an alluvial layer by 10 cm, with an unknown, but minor, lateral slip component.

This fault was vertically truncated by an overlying cobble deposit and all subsequent strata. The depth of the event horizon was 2-3 m beneath the >80-100 ka surface soil, and with other intervening paleosols adding to the age, it is reliably concluded that this fault's single displacement event occurred at least 300 ka. Although unproven, it is more likely that this minor feature was not a tectonic fault, but the geologic evidence for a >300 ka seismic event (a seismite) that generated a liquefaction failure within the alluvial channel deposits.

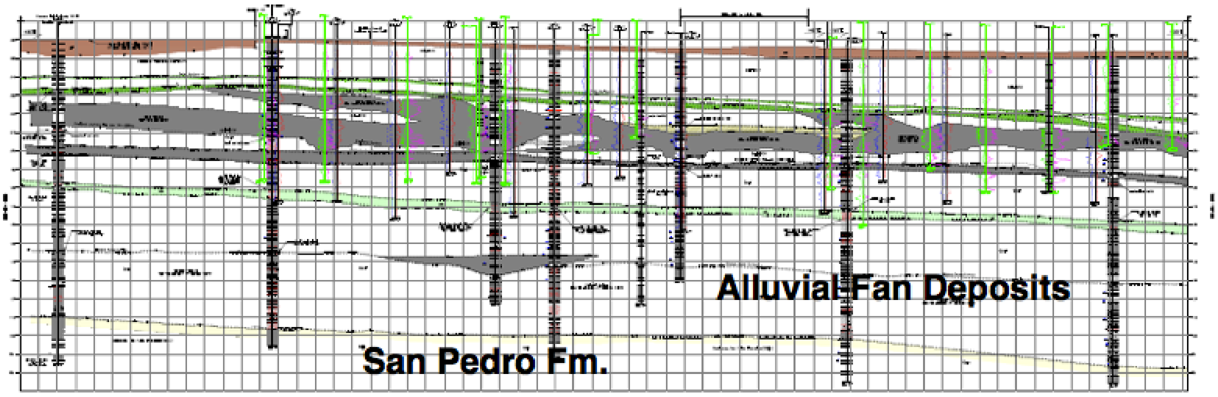


*Fig. 6: The cross-section from Fig. 3 as revised by the new cone penetrometers and borings. The green highlighted layers are paleosols that have been correlated across the section, effectively eliminating the necessity for fault offset anywhere in the section. The base of the section is the ~1 Ma San Pedro marine sand at ~50 m depth (LCI, 2012).*

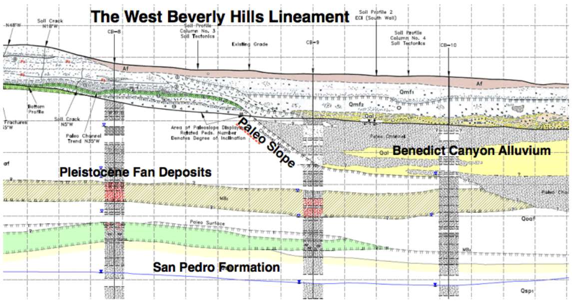


*Fig. 7: Trench log (from Fig. 4) and extended cross section showing the alluvial unconformity that explains the origin the West Beverly Hills Lineament as an erosional channel margin that has been partially backfilled by undeformed 30-200+ ka Benedict Creek sediments.*

## DISCUSSION

The lack of faults was unanticipated. While it had been hoped that the faults could be demonstrated to be inactive, there was no expectation that faults would not be present. Faults had been interpreted from considerable data, subjected to expert analysis, had been through a Metro peer review process, and yet they were not there. However, this should be a lesson to all that geologic interpretation is still an interpretation and is not, in fact, a fact. The presence of faults was anticipated, so it was easy to interpret even minor, stratigraphic irregularities as faults. When a fault was interpreted it was drawn essentially perpendicular to the transect line, despite no trend information from the 2-D transect. The faults were labelled as "active faults" because of the paradigm within which they were modelled, despite having no age control on the sediments that were interpreted as offset. In addition, they were extended long distances from the transect from which they were interpreted (Fig. 2) and as such they impacted numerous high-value properties.

The result of the Metro fault report, and the manner of its very public release, has led to the unexpected, and unwelcome, expenditure of millions of dollars by the BHHS, and millions more by other affected property owners. The City of Los Angeles cancelled previously approved development and redevelopment plans until the owners could address this new fault concern, leading to the loss of millions in cancelled contracts and business delays. Homeowners and building owners in Beverly Hills and Century City were shocked to learn their property was bisected by an active fault, and concerned that their real estate values would plummet as a result. And, Metro used the findings of their fault report to change an already approved subway alignment to avoid placing stations within the new active fault zones, and instead directed the subway directly under BHHS, a change that generated a firestorm of protest.

The finding by BHHS that the faults mapped through the school do not exist came as a pleasant surprise to the school's Board and community leaders. Similar findings by other affected property owners and developers are still coming in, but to date, none of them have found active faults through their properties as interpreted and mapped (Fig. 2). This consistent refuting of the active fault map is alarming. That such a critical map could be released to the public without any concrete evidence of a fault's existence or activity is inconsistent with good professional practice. It is the equivalent of shouting "Fire" in a crowded theatre. That is illegal. What is probable in this case is that years of litigation can be anticipated over the unexpected and apparently unnecessary expenditure of tens of millions of geologic (and legal) dollars by BHHS and the other affected owners.

**Acknowledgements:** The project summarized in this paper was made possible by Tim Buresh and the Beverly Hills Unified School District, with the participation of many other geologists and professionals. The thorough project review by J. Treiman and B. Olson of the Calif. Geological Survey is acknowledged.

## References

Dolan, J. F. & K.E. Sieh, (1992). Tectonic geomorphology of the northern Los Angeles basin: Seismic hazards and kinematics of young fault movement. In: *Engineering Geology Field Trips: Orange County, Santa Monica Mountains, and Malibu*, AEG Guidebook, p. B20-B26.

Dolan, J.F., D. Stevens, & T.K. Rockwell, (2000a). Paleoseismic evidence for an early- to mid-Holocene age of the most recent surface rupture on the Hollywood fault, Los Angeles, California. *Bulletin of the Seismological Society of America* 90, 334-344.

Dolan, J.F., K. Sieh, & T.K. Rockwell, (2000b). Late Quaternary activity and seismic potential of the Santa Monica fault system, Los Angeles, California; *Geological Society of America Bulletin* 112, 1559-1581.

Earth Consultants International, (2012). *Soil-stratigraphic studies for Beverly Hills High School, Beverly Hills, California*; ECI Project No. 3205.02, dated April 10, 2012.

Hummon, C., C.L. Schneider, R.S. Yeats, J.F. Dolan, K.E. Sieh, & G.J. Huftile, (1994). Wilshire Fault: Earthquakes in Hollywood? *Geology* 22, 291-294.

Lang, H.R., (1994). Wilshire Fault: Earthquakes in Hollywood? Comment and Reply. *Geology* 22, 959.

Leighton Consulting, Inc., (2012). *Fault hazard assessment of the West Beverly Hills Lineament, Beverly Hills High School, California*. LCI Project No. 603314-002, dated April 22, 2012.

Parsons Brinkerhoff, (2011). *Century City area fault investigation report for the Westside Subway Extension Project*, 2 volumes, PB report dated Nov. 30, 2011, available at http://www.metro.net/projects/westside/westside-reports/

Yerkes, R.F. & R.K. Campbell, (2005). *Preliminary geologic map of the Los Angeles 30'x 60' quadrangle, Southern California*. USGS, OFR 2005-1019, Digital Geologic Map, Version 1.0.

# Red Sea Tsunami: Sedimentological Variations due to local Environmental Heterogeneity

*Beverly N. Goodman-Tchernov (1,2), Yonaton Shaked (2), Timor Katz (2), N. Porat (3) Amotz Agnon(4)*

(1) Leon Charney School of Marine Sciences, Strauss Department of Marine Geosciences, University of Haifa, Israel. Email: bgoodman@univ.haifa.ac.il
(2) Interuniversity Institute of Marine Sciences, Coral Beach, Eilat, Israel
(3) Geological Survey of Israel, Jerusalem, Israel
(4) Department of Earth Sciences, Hebrew University, Jerusalem, Israel

***Abstract:*** *The recent rise in the number of studies focused on tsunamigenic sedimentological deposits, both modern and ancient, has improved our understanding of the appearance of tsunamigenic deposits and raised awareness regarding the wide range of characteristics that they present in the field, even within a single field site. Here, this phenomenon is illustrated in the results from two cores collected from the same geographical area, but from two unique microenvironments. While both were collected from the shallow uppershelf of the Northern Red Sea Gulf of Aqaba-Eilat (depths of -12 b m.s.l. and -16 b m.s.l.), offshore of dry riverbeds (wadis), one is geographically closer to the area of today's northernmost tropical coral reefs while the other is from a region nearly void of coral. The results of this study demonstrate the impact of localized environmental variations, and the need to consider a wide range of sedimentological indicators when interpreting paleotsunami deposits.*

***Key words**: tsunami, sedimentology, coral, Red Sea, technical diving*

## INTRODUCTION

Recognizing sedimentological signatures from paleotsunami events is paramount for better reconstructing the record of tsunami events, an important resource used by tsunami and earthquake modelers. Models, which depend heavily on the record of prior events, are typically limited to instrumentally recorded events (past 100 years) and textual records. In some areas this can amount to a rich database of information, while in others it may appear as if there were no events whatsoever. Developing ways to find and identify paleoevents to compare to these textual or instrumental records and/or supplement them is important as a means to create better estimates of the magnitude, timing, and regularity of these events.

There is a paucity of information regarding tsunamis in the Red sea. This may be the result of an actual absence, or this could be the result of circumstances of recording. Given the presence of neotectonic activity, some level of tsunami regularity should be expected, though the earthquake and tsunami catalogues are relatively quiet on the matter. In Ambrasey et al. 2009, in which known events from approximately 1400 AD to the 1980s are summarized, a 1068 AD event specific to the Gulf of Eilat is mentioned. Events prior to this are mostly unknown. Jordan et al. 2008 concludes, based on the lack of historical records or substantial modern examples, that the Red Sea is at low risk. Near coastal onshore trenches exposed evidence of a rapidly buried coral reef, possibly the result of a 3-4$^{th}$ century BC tsunami event (Shaked et al. 2004). As recently as 1995 following a 7.1 Mw earthquake with an epicenter about 35km south of Eilat (strike-slip, 28.826 N 34.799 E) a small tsunami was recorded at Nuweiba, Sinai, Egypt (Baer et al. 2008). Salem (2009) proposes a tsunamigenic origin for certain depositional sequences along the beachfront in the Sinai and presents a model differentiating between the sequences derived from terrestrial sources (flooding) and marine (tsunami/tempest). A systematic sampling to address the presence of tsunami deposits has not yet been carried out in the Gulf of Eilat-Aqaba.

The Gulf of Aqaba-Eilat (GOA) is flanked by granite, basalt, and conglomerate mountains to the west and east and a long valley stretching north into the flat plains of the Arava desert. The western and eastern mountain ranges have been interpreted to have an approximately 105 km offset of right normal transform fault (Freund 1970; Fig. 1). The gulf itself is uniquely characterized by an especially steep bathymetry on its eastern and western shorelines while the northern coastline exhibits a more gradual bathymetric incline, mostly likely due in part to underlying structural features, in addition to more extensive overlying sediment beds (see Makovsky et al. 2008). The Gulf is part of the Dead Sea Fault System (DSFS) wherein the most recent seismic event felt in the Eilat-Aqaba area occurred June 1, 2012 (4.9 Mw, Geophysical Institute of Israel Department of Seismology). Archaeologically, the region is along a well-known passageway connecting Egypt, Palestine, and the famous spice routes to the Far East. The Bible refers to the area in (1 Kings 9:26): "King Solomon also built ships in Ezion-Geber, which is near Eloth in Edom, on the shores of the Red Sea." In addition, the Gulf was probably an important port site linking the Nabatean cities of the region to the surrounding areas, particularly through the Roman port of Aila located near modern Aqaba.

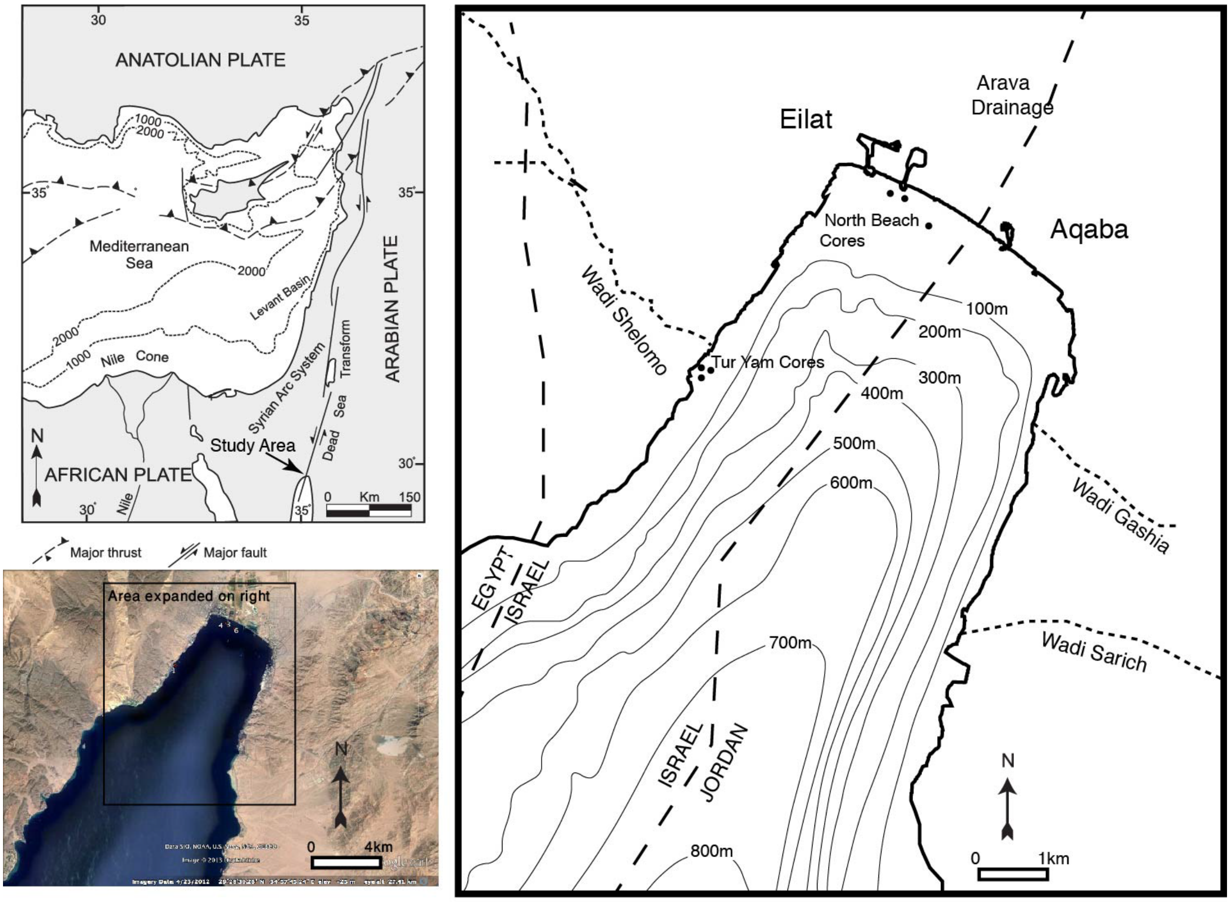


Figure 1: Upper left: Generalized tectonic map of region (adapted from Garfunkel 1998). Lower left: Satellite Image of region showing geological features (Google Earth Maps). Right: Site Map with 100m bathymetric contours, major wadis, core locations and generalized surface features (adapted from Ben-Avraham & Tibor 1993, Tibor et al. 2010, Beyth et al. 2011, ).

## METHOD

Cores were collected in two different zones of the GOA. The first area is in the northern portion, offshore from the discharge of the Wadi Arava (Arava Drainage). The second area, Tur Yam, is a small bay offshore from the discharge of Wadi Shlomo. The original aim of the study was to collect generalized sedimentological data with the purpose of better reconstructing the coastal history including coral development and sea-level change. The offshore cores were collected with divers using a pneumatic hammer (see Goodman et al. 2009). A total of 8 cores were collected (see Fig. 1). Analysis on the cores include granulometry, particle size distribution contour mapping (Beierle et al. 2002), sedimentological and mineralogical description, and micropaleontology (foraminifera in particular, methods as in Goodman et al. 2009). The cores were each split, photographed and described, then subsampled at 1 cm intervals. A portion of the cores have been fully analysed, and others only described and correlated based on similar horizons. Chronology was established based on C14 dates of marine shell, coral, and foraminifera. Optically Stimulated Luminescence (OSL) dating was also carried out, although contradictions relative to the C14 dating has led to continued assessment and discussion of those results which will appear in a future manuscript.

Four cores were split and described, and one core from each study area was studied in finer detail. The Tur Yam core ( -12.2 b m.s.l., 375cm) is characterized by medium sand with fine shell fragments with a mixed mineralogical origin similar to that found in the lithology of the nearby mountains. There are some coral fragments interspersed, with a thick horizon (~40cm) of mixed shell and broken coral fragments of varying condition from pristine to heavily worn and eroded (see Fig. 2). The general size of foraminifera within the coral horizon is greater than that of the remainder of the core, showing an absence of foraminifera below 63 micron. The core from the North Beach (-16.2 b m.s.l., 450cm) consists of silty sand interrupted by a band (~20cm) of coarser, sediments at ~160-180cm depth downcore. The anomalous band lacks foraminifera and contains higher concentrations of the terriginous sediments. The base of the core is also foram-barren, though both OSL and C14 results presented modern values, suggesting contamination by surface material after collection..

## RESULTS

Anomalous horizons from the two cores (see 'TS' horizons in Fig. 2) both present C14 ages (foraminifera in Core 4 and coral in Core 5) of approximately upper ages of 200-300 BC. This age is congruent with the anomalous horizons identified by Shaked (2004). Shaked et al. suggested a tsunamigenic origin for those horizons, and these recent cores suggest that this anomalous horizon is present in other parts of the bay. Tsunamigenic deposits are extremely diverse depending on a wide range of variables related to factors such as event size, local source material, offshore and coastal morphology. Goff et al. (2012)'s recent review of progress in tsunami research summarizes the need for the use of multiple proxies selected with attention given to the context of the site, and that not all proxies are applicable to all sites, nor do all tsunamis leave distinguishable deposits.

In the case of Eilat the preliminary results of the study suggest that the following variations of tsunamigenic indicators are present in anomalous stratigraphic horizons in the near offshore sediments. In Core 4 indicators include a radical change in grain size, sorting, mineralogical signature, and micropaleontological assemblage relative to the majority of the core, which reflects the general modern surface condition. The horizon resembles sediments typical of the terrestrial environment, but are not similar to what is seen in modern flash flood events. An explanation of this could be that the tsunami eroded, entrained, and transported beach deposits and other nearshore terrestrial sediments during the return backwash, leaving a thick enough layer that preserved despite later bioturbation, flooding, and storm events. The periodic southern storms cause insignificant disturbance to the seafloor, flood events tend to be depositional and not erosional, and bioturbation could have been stymied by the radical change in grain-size and its impact on the biological system. Core 5's horizon contains a distinctive concentration of broken coral and shell fragments, and a significant change in foraminifer size. Similar to Core 4, the surface sediments match the majority of the sediments within the core, barring the unique horizon. While there are some patchy coral areas in the nearby environment, it is mostly characterized by the medium to coarse sands transported from Wadi Shlomo during rare floods. While more hospitable to coral than the north beach site, none of the patchy corals are greater than 5-10 cm in size, and no comprehensive reefs are present. The massive coral and shell present in the horizon are indicative of transported pieces and not coral in living position. The absence of foraminifera below 63 microns is interpreted as the effect of selective transport of the smaller fraction particularly in the depositional phases (also see Qupty et al. (2013) this issue). Unlike the north beach site, the steep bathymetry both underwater and inland would have concentrated the wave height but limit the run-up distance and therefore the amount of terrestrial sediment entrained in the resulting deposit would be reduced relative to the north beach site.

## DISCUSSIONS AND CONCLUSIONS

If correct, the presence of a deposit reflecting this event in both the northernmost portion of the gulf as well as the western side, as well as the thickness of the deposit, suggests that the event may have had an impact on a much larger area than the recently witnessed Nuweiba tsunami, and may have been capable of causing damage to the coastlines of that time. The geometry of the gulf, resembling more closely a fjord than a sea, could likewise result in large but highly concentrated tsunami events. The most recent tsunami in Nuweiba was the result of strike-slip motion along the fault, which is typically viewed alone as non-tsunami generating due to the lack of horizontal displacement of water. However, secondary and tertiary effects following a strike-slip earthquake, such as underwater landslides, are more localized but equally damaging, and perhaps more common (Bardet et al. 2003). The human population at the time of the event was probably very low, or at least there was no significant centralized settlement near the collection locations, as there is a complete absence of any cultural remains in the horizons.

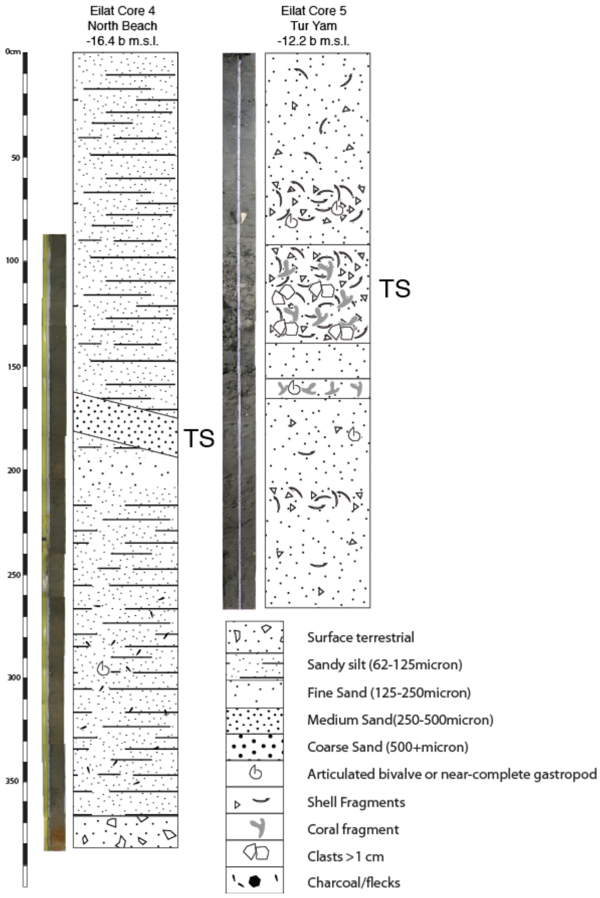


Figure 2: Cores 4 and 5. 'TS' indicates anomolous horizon which is interpreted as tsunamigenic.

This could have been, in part, due to the recently expanded harbour city of Berenike further south on the eastern coast of the Egyptian mainland south of the Suez

Canal (Sidebotham & Zitterkopf 1995), and therefore might not have merited record, or as often is the case the history was lost or destroyed later.

What is exceptional about the cores is the illustration of how the variability in the landscape results in such distinctive and unique signatures, even within the same basin, supporting the conclusions of Goff et al. 2012 and what is apparent from studies in the field (e.g. Reicherter et al. 2010, Vött et al. 2009). Also, given the rapid and immediate alteration of tsunamigenic deposits along coastlines (Szczuciński et al. 2011), this study again reinforces the usefulness and importance to pursue and study offshore deposits as a resource for discovering and describing tsunamigenic sediments (Goodman et al. 2009).

The preliminary results from these two cores suggest the present of an anomalous, possibly tsunamigenic deposit.

**Acknowledgements:** Special thanks to the Interuniversity Institute of Marine Sciences-Eilat, National Geographic, Norman Krischer, H. Dey, and O. Ben Shaprut. Important assistance was received from Y. Sharon, E. Brokovich,

## References

Ambraseys, N., (2009), Earthquakes in the Mediterranean and Middle East A Multidisciplinary Study of Seismicity up to 1900: Cambridge University Press no. 1982.

Baer, G., G. Funning, G. Shamir, & T. Wright, (2008). The 1995 November 22, M w 7.2 Gulf of Elat Earthquake Cycle Revisited, *Geophysical Journal International* 175 (3), 1040–1054.

Bardet, J.-P., C.E. Synolakis, H.L. Davies, F. Imamura, and E.A. Okal, (2003), Landslide Tsunamis: Recent Findings and Research Directions, SE - 1, Birkhäuser Basel, p. 1793–1809.

Beierle, B., S. Lamoureux, J. Cockburn, & I. Spooner. (2002). A New Method for Visualizing Sediment Particle Size Distributions, *Journal of Paleolimnology,* 27, 279–283.

Ben-Avraham, Z. & G. Tibor, (1993). The Northern Edge of the Gulf of Elat. *Tectonophysics* 226, 319–331.

Beyth, M. Y, Eyal, & Z. Garfunkel, (2011). *The Geology of the Elat Sheet Explanatory Notes*. *Geological Society of Israel*.

Freund, R., Z. Garfunkel, I. Zak, M. Goldberg, T. Weissbrod, B. Derin, F. Bender, & R. W. Girdler Wellings, (1970). The Shear Along the Dead Sea Rift [and Discussion]. *Phil Trans R Soc A* 267: 107–130.

Garfunkel, Z., (1998). Constrains on the Origin and History of the Eastern Mediterranean Basin. *Tectonophysics* 298 (1-3), 5–35.

Garfunkel, Z., I. Zak, & R. Freund, (1981), Active Faulting in the Dead Sea Rift*Tectonophysics*, 80, 1–26.

Goff, J., C. Chagué-Goff, S. Nichol, B. Jaffe, & D. Dominey-Howes. 2012. Progress in Palaeotsunami Research. *Sedimentary Geology* 243-244 70–88.

Goodman-Tchernov, B. N., H. W. Dey, E. G. Reinhardt, F. McCoy, & Y. Mart, (2009). Tsunami Waves Generated by the Santorini Eruption Reached Eastern Mediterranean Shores. *Geology* 37, 943–946.

Jordan, B.R., (2008). Tsunamis of the Arabian Peninsula A guide of Historic Events, *Science of Tsunami hazards*, 27 (1), 31–48.

Makovsky, Y, A. Wunch, R. Ariely, Y. Shaked, A. Rivlin, A. Shemesh, Z. Ben Avraham, & A. Agnon, (2008). Quaternary Transform Kinematics Constrained by Sequence Stratigraphy and Submerged Coastline Features: The Gulf of Aqaba. *Earth and Planetary Science Letters* 271 (1-4), 109–122.

Reicherter, K., D. Vonberg, T. Koster, B. Fernández-Steeger, M. Grützner, & C. Mathes-Schmidt, (2010), The Sedimentary Inventory of Tsunamis Along the Southern Gulf of Cádiz (southwestern Spain). *Zeitschrift Für Geomorphologie* 54 (Supplementary Issues): 147–173.

Salem, E. (2009). Paleo-Tsunami Deposits on the Red Sea Beach, Egypt. *Arabian Journal of Geosciences* 2,185–197.

Shaked, Y., A. Agnon, B. Lazar, S. Marco, U. Avner, & M. Stein, (2004). Large Earthquakes Kill Coral Reefs at the North-west Gulf of Aqaba. *Terra Nova* 16 (3), 133–138.

Sidebotham, & R. Zitterkopf, (1995), Routes through the Eastern Desert of Egypt, *Expedition,* 37(2), 37-50.

Szczuciński, W., (2011). The Post-depositional Changes of the Onshore 2004 Tsunami Deposits on the Andaman Sea Coast of Thailand. *Natural Hazards* 60 (1), 115–133.

Tibor, G., T. Niemi, Z. Ben-Avraham, A. Al-Zoubi, R. Sade, J. Hall, G. Hartman, E. Akawi, A. Abueladas, & R. Al-Ruzouq, (2010). Active Tectonic Morphology and Submarine Deformation of the Northern Gulf of Eilat/Aqaba from Analyses of Multibeam Data. *Geo-Marine Letters* 30 (6), 561–573.

Vött, A., H. Brückner, S. Brockmüller, M. Handl, S.M. May, K. Gaki-Papanastassiou, & R. Herd, (2009). Traces of Holocene Tsunamis Across the Sound of Lefkada, NW Greece. *Global and Planetary Change* 66 (1-2), 112–128.

# Neotectonic activity of the Milesi Fault, N Attica, Greece

*Grützner, Christoph (1), Sascha Schneiderwind (1), Ioannis Papanikolaou (2, 3), Aggelos Pallikarakis (2), Georgios Deligiannakis (2)*

(1) Neotectonics and Natural Hazards, RWTH Aachen University, Lochnerstr. 4-20, 52064 Aachen, Germany. Email: c.gruetzner@nug.rwth-aachen.de
(2) Laboratory Mineralogy - Geology, Agricultural University of Athens, Iera Odos 75, Athina 118 55, Greece
(3) AON Benfield UCL Hazard Research Centre, Department of Earth Sciences, University College London, WC 1E 6BT, London, UK

***Abstract:*** *Athens and its surroundings have repeatedly been shaken by moderate damaging earthquakes, but strong local events and severe damage are not proven by instrumental, historical, and archaeological records for the last 2,300 years. Despite this, the surroundings of Athens show clear signs of active faulting. In order to test the hypothesis of Holocene fault activity, we performed field mapping, georadar, morphological analyses and paleoseismological investigations at one of the prominent faults in N Attica, the Milesi Fault. Our data show evidence for recent seismic events and on-going tectonic activity. We can assign a minimum slip rate of 0.3 mm/yr and we are able to identify at least two post-glacial surface-rupturing earthquakes. These results make clear that strong local events in the vicinity of Greece' capital must be considered in any seismic hazard assessment.*

***Key words****: Attica, trench, wind gap, Milesi Fault, slip-rate*

## INTRODUCTION

Northern Attica in Greece is not only home to more than four million inhabitants of Athens, but is also densely populated along its coast and a major tourist destination. The Athens Metropolitan Area (AMA) has experienced several damaging, but rather moderate earthquakes in historical times. In 1999, a moderate earthquake caused 140 deaths and $3 billion of damage (Ms5.9, 15 km depth). In Oropos, an earthquake occurred in 1938, few kilometres north of Milesi. Another earthquake is reported for 1705 (Papanikolaou and Papanikolaou, 2007) somewhere between the towns of Athens and Chalkida. Strong local events in the AMA are absent or rare and the highest seismic hazard for this region is often thought to result from the very active Gulf of Corinth rift to the west. No devastating earthquakes can be found in the instrumental and historical records; archaeoseismological data evidence that no major shaking occurred during the last 2,300 years (Ambraseys and Psycharis, 2012).
However, several faults are located in the surroundings of Athens, but little is known about their contribution to the seismic hazard. Some of them show signs of Holocene activity and have a clear geomorphological expression, even fault scarps. Data on slip-rates, maximum events, and the last earthquakes is not available or ambivalent for other tectonic structures. We hypothesize that despite the lack of strong local events for the last two millennia at least some faults in northern Attica are active. For proving this hypothesis, we concentrated on one of those faults, the Milesi Fault, where promising outcrops were found and where previous studies proved the existence of post-glacial fault scarps. We did additional field work to find out whether this fault was active in recent times or not.

## GEOLOGICAL SETTING

### *Rocks*

The geology of the AMA is divided in three major units: 1 Metamorphic basement units; 2 Non-metamorphic basement units; 3 Pleistocene basins. To the NE of Athens, metamorphic rocks stretch from the city to Evia. These units formed during the Alpine orogeny and mainly consist of massive Mesozoic marbles and locally overlying Tertiary phyllites (Papanikolaou and Papanikolaou, 2007). A large-scaled NNE-SSW running detachment fault separates the metamorphic units from the non-metamorphic formations in the NW. The non-metamorphic mountain ranges also formed during the alpine orogeny and are made up of the Geotectonic Unit of Eastern Greece.
At places, ultrabasic rocks occur in pockets within the limestones as they were thrusted over the carbonates during the orogeny (Fig. 1). Further to the N, Neogene flysch and also lacustrine units are present (Papanikolaou and Papanikolaou, 2007). In between the two main basement units, Miocene sediments related to the activity of the detachment fault are preserved. Occasionally, Pleistocene and younger alluvium is present in depressions and along the coasts. The detachment fault not only separates the metamorphics from the non-metamorphics, but also runs through the Athens basin and further to the SW and as far as to the Gulf of Evia in the NE. It also appears to control neotectonic fault orientation and microseismicity. The detachment was active from Late Miocene to Early Pliocene, but still has a major influence on the neotectonics of the study region.

### *Faults*

Active faulting in the study area is controlled by the opening of the Gulfs of Evia and Corinth in the broader frame of the Aegean Subduction Zone and the westward

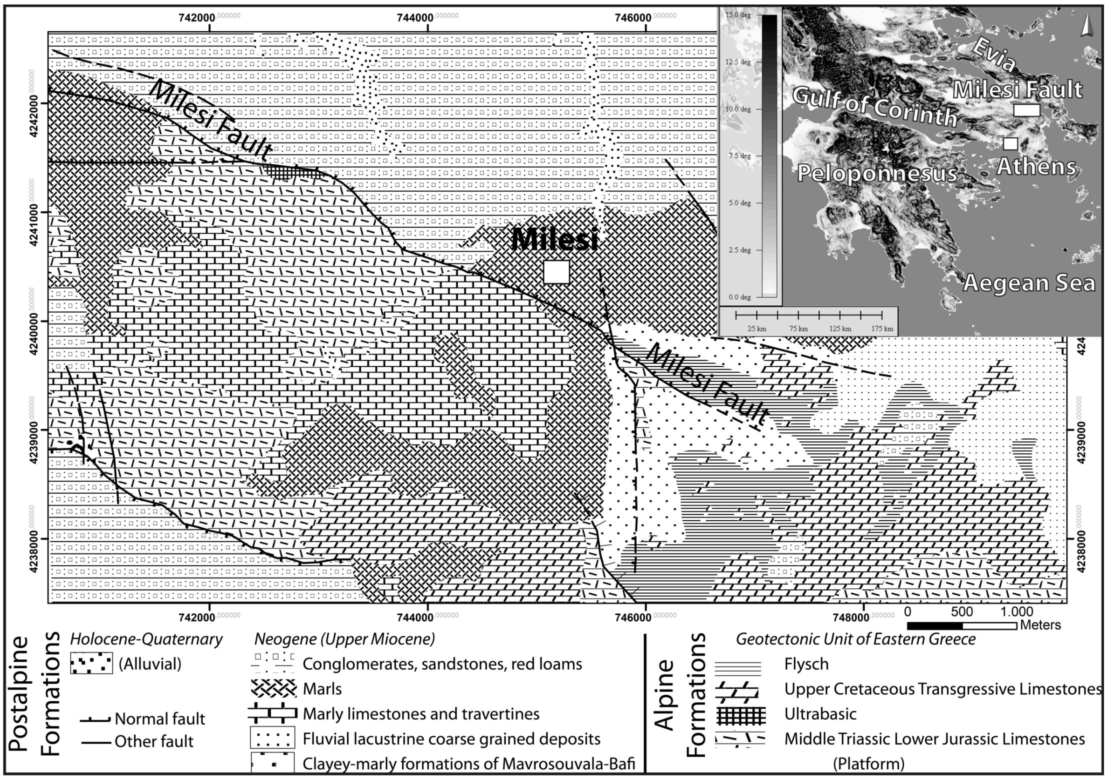


*Fig 2: Geological overview of the study area in N Attica (Katsikatsos, 2000). The garbage dump site is located at the ultrabasic rock outcrop.*

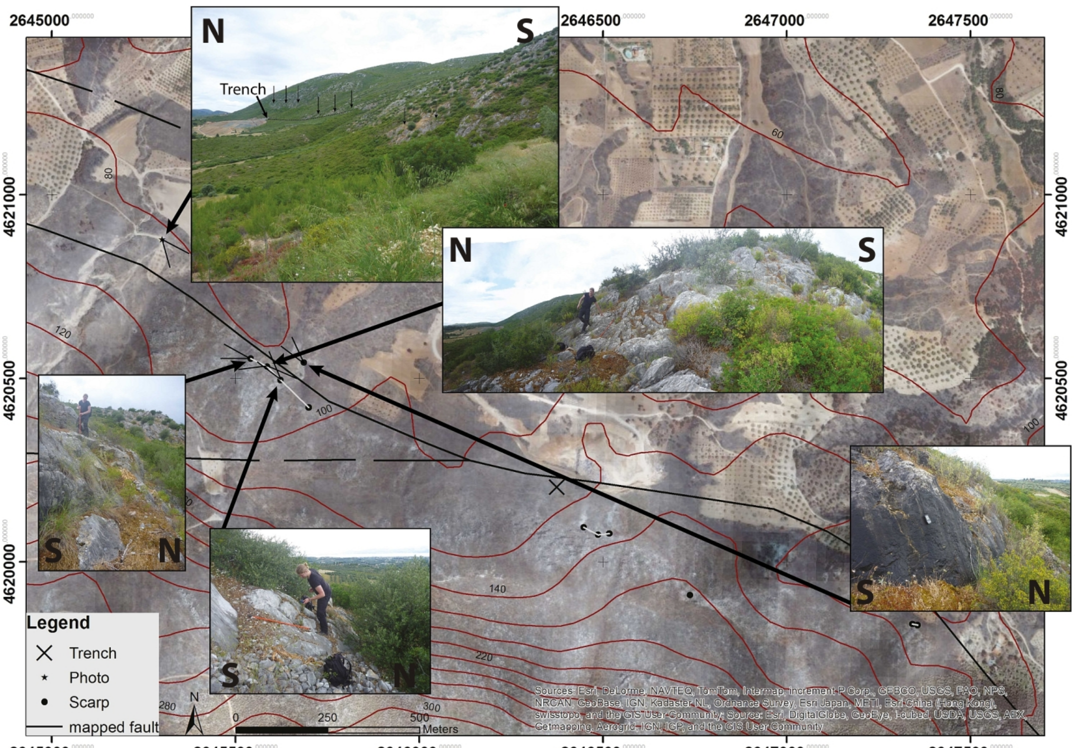


*Fig 1: Satellite image of the study area with trench location and mapped scarps. Up to three step-like arranged scarps are visible with a cummulative vertical height of more than 3 m. One of the scarps west of the trench marks the continuation of the fault found at the garbage dump site, see Fig. 4.*

pushing of the Anatolian plate. Normal faults strike E(ENE) - W(WSW) in the west of the detachment and NW-SE east of the detachment. At least seven prominent normal faults can be identified in the Sub-Pelagonian limestones W of the detachment with topographic expression (Papanikolaou et al., 2008). Their lengths vary from less than 2 km to more than 15 km (Ganas et al., 2005). The southern ones dip to the S, the northern ones (including the Milesi Fault) dip towards the N.

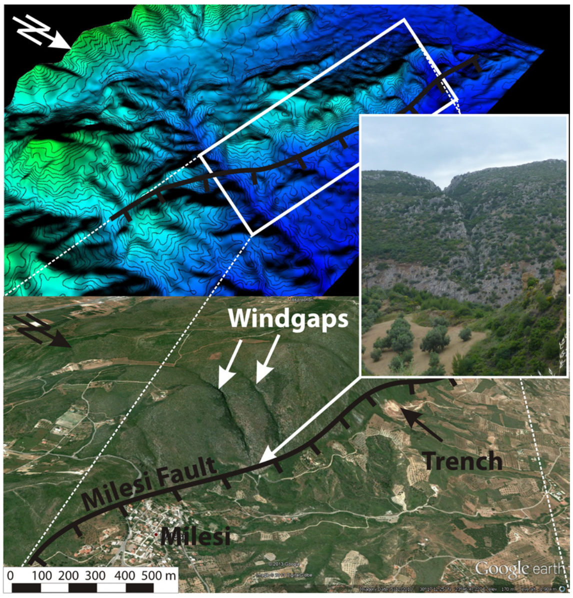


*Fig 3: ASTER digital elevation data of the study area (upper image) and the GoogleEarth satellite image prove the existence of at least two windgaps at the Milesi Fault.The deeply incised streams do not reach down to the hangingwall, but stop at the fault scarp (foto).*

## STUDY SITE

The Milesi Fault is located about 30km N of Athens. It is an E-W striking, N-dipping normal fault with a length of around 10 km. The densely populated Oropos plain is located to its north. The footwall of the fault is mainly made up of limestones (Fig. 1), but a pocket of ophiolites occurs W of Milesi village. There, a garbage dump has been built and the colluvium as well as parts of the ophiolite footwall have been removed by excavators. The hanging wall of the fault consists of colluvium, marls, conglomerates and loams. Few landslides have been identified in the soft sediments of the hanging wall. Streams and few deeply incised channels are visible in the footwall. The elevation difference between the footwall and the hanging wall is up to 300 m, the accumulated net offset is not known precisely, but more than 300 m.

## METHODS

We mapped the fault trace in order to identify post-glacial scarps in the limestones and to measure their height and orientation. A morphological analysis was made to check if the deeply incised channels are fed by a large drainage network or if they were cut off from their source by tectonic uplift. An outcrop at the Milesi garbage dump was studied in detail, since it exhibits the fault zone itself as a contact between the ophiolites and colluvium. This outcrop is comparable to a paleoseismological trench and was further excavated, cleaned, gridded, sketched, and photographed. Sampling was undertaken for C14 dating, but the results are not available yet.

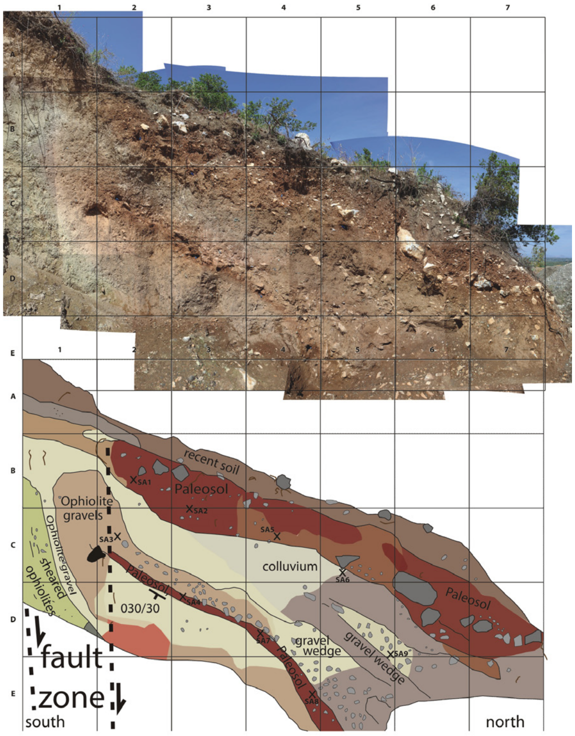


*Fig 4: Foto mosaic of the trench at the garbage dump (upper image) and sketch of the main units (lower image). Grid width is 1 m. Note the buried paleosol close to the surface and a second one at 1-2 m depth. SA: Sample location.030/30: dip direction of the second paleosol.*

## RESULTS

### *Field mapping*

We found hard rock scarps in the limestones along the entire fault (Fig. 2) and we assume a post-glacial age (older than 15 kyr; cf., Papanikolaou et al., 2005). The scarps were mainly oriented E-W and up to 5 m high in the central part of the fault. Dipping angles varied between 50° and 80° to the north. In the west, up to three different scarps are located in a staircase-like pattern with a cumulative height of 3 m. One of these scarps is the continuation of the fault observed in the trench. No mass movements were observed here. East of the trench site one major scarp was observed rather than distributed structures, with a shallower dip of around 40°-50°. The surface is very smooth and with occasional slickensides. Due to the low angle, the slope angle was the same as the dipping angle of the limestone hardrock surface close to the trench and east of this side. This made it hard to retrieve scarp heights in terms of vertical offsets. No scarps were observed in the ophiolites.
Deeply incised channels (Fig. 3) were found not to reach to the base of the slope, but being terminated by the fault scarp around 2 m above hanging wall level.

***Geomorphological analysis***

The analysis of digital elevation data, aerial imagery and field observations led to the discovery of two wind gaps a few hundred meters west of the village Milesi (Fig. 3). Papanikolaou et al. (1988) already reported on the intense incision of the stream, we found the structures being two windgaps.

***Outcrop/Trench***

The outcrop at the garbage dump site reveals the contact between the ophiolites footwall and the colluvium, separated by a fault dipping to the N with 75° (Fig. 4). The greenish-yellowish ophiolites in the footwall close to the fault clearly show shear structures and an alignment along the fault. Two paleosols can be identified in 0.5-1 m and 2-3 m depth, respectively. Both terminate at the fault zone and show a thickness of 0.15-0.30 m. They dip towards the N. Gravel layers are located on top of the paleosols and wedge-shaped structures can be identified in the outcrop.

**DISCUSSION**

The field mapping results allow us to conclude a Holocene fault activity. We can estimate a post-glacial slip rate of the Milesi Fault as evidenced by the preserved scarps. With up to 5 m unambiguous vertical offset and 15 ka since the last glacial maximum, the minimum slip rate is in the order of 0.3 mm/yr. This fits observations of the accumulated net offset. Erosion and sedimentation might obscure the real offset, but since we have found similar values in various places, the number is well-funded.

The geomorphological analysis also showed hints for relatively recent fault movement. The canyons cut at the base make clear that vertical fault movement is faster than the erosion rate. No hints for mass movements could be found at this place, so coseismic offset remains the best explanation for this observation. Furthermore, the presence of two windgaps is a sign for on-going tectonic uplift of the footwall of the Milesi Fault, thus neotectonic activity, as already pointed out by Papanikolaou et al., 1988.

The trench is situated at a place where no large-scaled mass movements were encountered. Thus, mere land sliding cannot be held responsible for the observed features. The existence of two buried paleosols points to coseismic offset along the fault at least twice, with the gravels being emplaced on top of the paleosols after the seismic event during a period of higher sedimentation because of the topographic step and maybe also by increased sediment mobilization due to the shaking. The offset between the paleosols is about 1 m, which could point to a single event of M>6. This seems to be too high for a fault with ~10 km length, where one would expect rather 0.5 m coseismic slip (Wells and Coppersmith, 1994). Thus, the possibility of creep or minor post-event sliding must be taken into. Creep and slow sliding would not explain the buried distinct paleosol, but would rather lead to a thicker soil wedge, which is why we discard this explanation. It is impossible to identify the corresponding paleosol on the footwall since there is no sedimentation on the footwall except for the present-day soil, therefore, no direct comparison can be made. Moreover, there is also one possibility that there is another one or two events in between, where no paleosol was produced. The gravel wedge in between the two paleosols could be related to such an additional event. Actually, finding paleosols in Greece is not common. C14 datings of the paleosol will allow us to date the occurrence of the seismic events and to conclude on recurrence intervals.

Georadar confirmed that the observed features are present along a larger part of the fault. We can, therefore, exclude a local effect caused by shallow sliding and we can prove that we do not look at an effect of the lithology.

Our investigations prove the hypothesis of surface-rupturing Holocene fault activity, that is, major earthquakes occur in N Attica despite the instrumental, historical, and archaeological records show no evidence. The seismic hazard assessment of this densely populated part of Greece should take into account the possibility of local M>6 events in the immediate vicinity of Greece' capital. Given that Athens is in large parts founded on thick sedimentary basins, significant peak ground accelerations must be considered.

**References**

Ambraseys, N.N. & J.A. Jackson, (1997). Seismicity and strain in the Gulf of Corinth (Greece) since 1694. *Journal of Earthquake Engineering* 1, 663-708.

Ambraseys, N.N. & Psycharis, I.N., (2012). Assessment of the long-term seismicity of Athens from two classical columns. *Bulletin of Earthquake Engineering* 10, 1635-1666.

Ganas, A., S. Pavlides & V. Karastathis, (2005). DEM-based morphometry of range-front escarpments in Attica, central Greece, and its relation to fault slip rates. *Geomorphology* 65, 301-319.

Katsikatsos, G., (2000). 1:50:000 geological map Sheet Eretria. Institute of Geology and Mineral Exploration (IGME).

Papanikolaou, D.I., E.L. Mariolakos & E.L. Lekkas, (1988). Morphotectonic observations on the Assopos basin and the coastal zone of Oropos. Contribution to the Neotectonics of Northern Attica. *Bulletin of the Geological Society of Greece* 20, 251-267.

Papanikolaou, D.I. & I.D. Papanikolaou, (2007). Geological, geomorphological and tectonic structure of NE Attica and seismic hazard implications for the northern edge of the Athens plain. *Bulletin of the Geological Society of Greece* 40, 425-438.

Papanikolaou, I.D., G.P. Roberts & A.M. Michetti, (2005). Fault scarps and deformation rates in Lazio-Abruzzo, Central Italy: Comparison between geological fault slip-rate and GPS data. *Tectonophysics* 408, 147-176.

Papanikolaou, I.D., D.I. Papanikolaou & E.L. Lekkas, (2008). Low slip-rate faults around big cities: A challenging threat. The Afindai Fault as a case study for the city of Athens. *The 14th World Conference on Earthquake Engineering October 12-17, 2008, Beijing, China*, pp.1-8.

Papazachos, B.C. & C.B. Papazachou, (1997). The earthquakes of Greece, *Ziti Editions, Thessaloniki*, p. 304.

Wells, D.L. & K.J. Coppersmith, (1994). New Empirical Relationships among Magnitude, Rupture Length, Rupture Width, Rupture Area, and Surface Displacement. *Bulletin of the Seismological Society of America* 84 (4), 974–1002.

INQUA Focus Group on Paleoseismology and Active Tectonics

paleoseismicity.org

# Fault Displacement Hazard in Italy: input for siting of critical facilities and land planning

*Guerrieri, Luca (1), Anna Maria Blumetti (1),Valerio Comerci (1), Pio Di Manna (1), Alessandro M. Michetti (2), Eutizio Vittori (1) & Leonello Serva (3)*

(1) ISPRA, Geological Survey of Italy, Via Brancati 48, 00144 Roma, Italy. Email: luca.guerrieri@isprambiente.it
(2) Dipartimento di Scienza e Alta Tecnologia, Università dell'Insubria, Via Valleggio, 11, 22100 Como, Italy.
(3) Consultant, Roma, ITALY

***Abstract:*** *The Italian territory is characterized by a great number of capable faults (i.e., faults able to produce significant ruptures/deformations at or near the surface). However, the potential of tectonic surface rupture/deformation (Fault Displacement Hazard) is not considered in seismic hazard assessment and zonation in Italy. In this paper it is proposed an assessment of FDH in Italy based on the ITHACA database, where the shape and width along capable faults as well as maximum expected surface displacements are defined in function of the seismotectonic behaviour and the severity of maximum expected earthquake. The proposed assessment indicates where FDH is expected to be relevant. In this sense, it is an helpful tool for a first selection of sites suitable to critical facilities (e.g. high-risk industrial plants). Nevertheless, the characterization of the setback around a capable fault requires a characterization of FDH at local scale, through more detailed seismotectonic and paleoseismic investigations.*

***Key words****: Fault Displacement Hazard, capable faults, critical facilities, Italy*

## INTRODUCTION

Most of Italy belongs to a complex interplate setting, characterized by a remarkable tectonic activity and shallow crustal seismicity. The Italian territory is therefore characterized by a great number of capable faults (i.e., faults able to produce significant ruptures or deformations at or near the topographic surface), that have produced several surface faulting events in historical and recent time.

The potential of tectonic surface rupture/deformation provides a specific hazard (Fault Displacement Hazard). However, this hazard is not taken into account in seismic hazard assessment and building codes in Italy.

This paper aims at providing a characterization of Fault Displacement Hazard in Italy, showing where it could be potentially relevant (zonation) and the amount of maximum expected displacements according to earthquake magnitude (ranking). Although such information is very general, it provides significant evidence for a first estimation at national level of the hazard affecting existing sites, where critical facilities/infrastructures (high-risk industrial plants up to nuclear installations) are located and for the selection of new sites suitable to host this kind of facilities.

In a larger perspective, this information should be taken into account also for ordinary land planning, towards the definition of *setback* areas (i.e. the distance from the fault trace within critical facilities and structures designed for human occupancy cannot be built, Bryant and Hart, 2007). At the moment this issue is addressed only in the guidelines and criteria for seismic microzonation (Working Group MS, 2008) but is not considered by the Italian national legislation for building in seismically active areas.

## THE ITHACA PROJECT

In order to respond to the need of a specific knowledge regarding the Fault Displacement Hazard, the Italian Agency for Environmental Protection (ANPA, later APAT, now ISPRA) in the second half of the 90' started the project ITHACA (ITaly HAzard from CApable faults). The project is aimed at building a tool for summarizing and making easily available information on capable faults, based on published sources, field checks and *ad hoc* studies (for more details, see Comerci et al., 2013).

Currently, the catalogue (Fig. 1) contains about 2000 records including faults that exhibit at least one evidence of capability among the following: a) historical coseismic surface faulting; b) creep or surficial tectonic deformation; c) Late Pleistocene-Holocene paleoseismic evidence of ground rupture; d) displacement of Quaternary deposits/landforms. Moreover, the faults are classified according to the age of the last ascertained movement.

The ITHACA database finds its application in the microzonation studies, as already acknowledged also by some regional code ( e.g. Lazio Region, D.G.R. nr. 545/2010).

## FAULT DISPLACEMENT HAZARD IN ITALY

At the moment the ITHACA database, although still incomplete and not homogeneous in terms of resolution and reliability of supporting data, is the most reliable tool for a first characterization of Fault Displacement Hazard in the entire Italian territory.

A first study focused on this topic was aimed at estimating the extent of urban areas exposed to surface faulting hazard within the ZS9 seismotectonic zonation of Italy (Guerrieri et al., 2009). The analysis was conducted for each seismotectonic zone that was

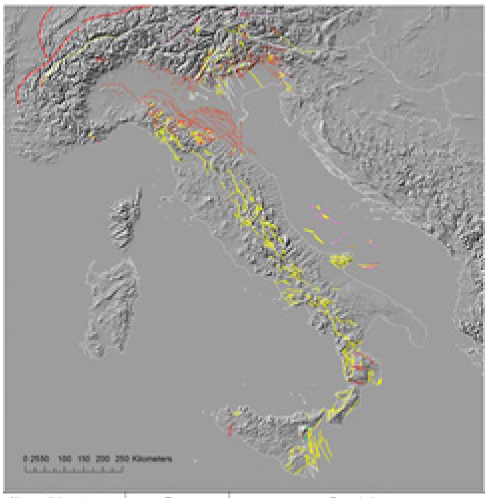


| Name of the category | Type | Description |
|---|---|---|
| FAULT CODE | text | 7 digits (first 2: country code, second 5: fault number) example: IT00003 |
| COUNTRY | text | country name |
| SYSTEM NAME | text | fault system name (e.g. Dinarides, Mid Hungarian Shear Zone, ...) |
| FAULT NAME | text | if exists... |
| KINEMATICS | text | NORMAL / REVERSE / STRIKE SLIP DEXTRAL / STRIKE SLIP SINISTRAL |
| RANK | text | PRIMARY / SECONDARY |
| GEOLOGICAL SETTING | text | brief description |
| LOCATION RELIABILITY | text | at mapping scale (1:500000): PRECISE / APPROXIMATE / INFERRED |
| MONITORING | text | description of possible monitoring networks |
| PALEOSEISMOLOGY | text | description of possible paleoseismological studies |
| CREEP | text | YES/NO |
| COSEISMIC SLIP | text | YES/NO |
| CO-SLIP NOTES | text | brief description of coseismic slip |
| ACTIVITY RELIABILITY | text | PROVEN / VERY LIKELY / POSSIBLE |
| SLIP-RATE (mm/yr) | number | if known |
| INSTR-SEISMICITY | text | YES/NO |
| HIST-SEISMICITY | text | YES/NO |
| SEISMIC EVENTS | text | list of earthquakes attributed to this fault |
| MAX-Ms | number | maximum recorded magnitude (Ms) |
| RISK LEVEL | text | vicinity of towns - hazardous facilities |
| STUDY QUALITY | text | DETAILED /TO BE IMPROVED |
| NOTES | text | if necessary |
| REFERENCES | text | author(s) and title of paper(s) |
| COMPILER | text | name of the compiler(s) |

*Fig. 1: The ITHACA database: distribution of capable faults and list of attributes (http://sgi1.isprambiente.it/geoportal/catalog/content/project/ithaca.page).*

considered homogeneous also in terms of Fault Displacement Hazard, through the intersection of ITHACA and CORINE Land Cover databases. The results of the spatial analysis have been weighted through the introduction of a Coefficient of Surface Faulting (CSF) which takes into account the expected maximum displacement for each zone (Fig. 2).

For this assessment it was considered a standard 300 m-wide buffer area around capable faults. As a result, concerning the territory within the ZS9 zonation (Meletti and Valensise, 2004), about 7% of the areas exposed to SFH (i.e. within 300 m from capable faults) is urbanized. On the other hand, a significant part of the areas exposed to SFH is located outside the ZS9 zonation, in areas characterized by low surface displacements (in the order of some centimeters) but also densely inhabited (e.g. Po Plain, cfr. Comerci et al., 2013).

In order to improve this first evaluation, we propose here a more refined zonation of the area around the mapped capable faults. The shape and width depend on the seismotectonic behaviour (i.e. type, style and amount of faulting) and the severity of maximum expected earthquake. These two factors control also the amount of maximum expected surface displacements.

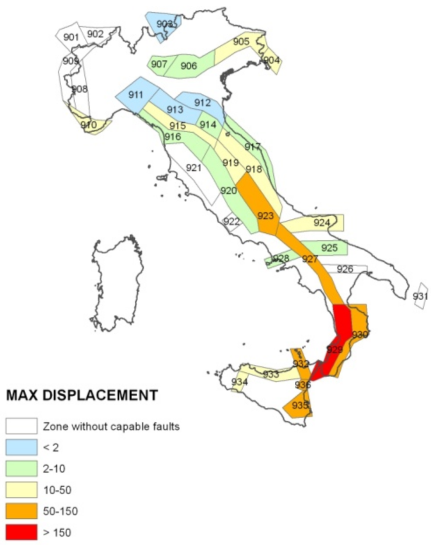


*Fig. 2: Maximum displacements (in cm) expected along mapped capable faults in each ZS9 zone (after Guerrieri et al., 2009)*

For each class, the maximum expected offsets and typical widths of the hazard zone in the footwall and in the hangingwall of the master capable fault are provided (Fig. 3 for normal faults, Fig. 4 for reverse and strike-slip faults). To this end, the capable faults recorded in ITHACA have been split into three main groups according to the prevalent fault kinematics (normal, reverse or strike-slip) and classified into different classes identified by specific maximum magnitude ranges.

In order to take into account the uncertainties affecting the location of capable faults recorded in ITHACA, a standard minimum width value equal to 30 m has been introduced on both the side of the fault trace (of course, in some cases it could be convenient to consider a larger uncertainty, if the resolution of original data sources is very scarce).

For normal faults (Fig. 3) these relationships result from a careful review of the documented normal surface faulting pattern caused by several modern and historical events occurred in the Italian territory (for more details about surface faulting pattern in extensional environment, see Boncio et al., 2012 and bibliography therein). Since in an extensional environment, surface primary ruptures (i.e. principal faulting, sensu Youngs et al., 2004) are expected to occur mainly in the hanging wall of the master fault, we have considered an asymmetric zone located mainly on the downthrown block, and width proportional to the maximum surface offset For example, for capable faults with maximum magnitude equal to 6.0 and maximum offsets lower than 5 cm, the hazard zone width is at least 50 m in the hanging wall but not more than 30 m in the footwall. Indeed, for capable faults with M max > 7.0 and maximum offsets larger than two meters (e.g. Calabria)

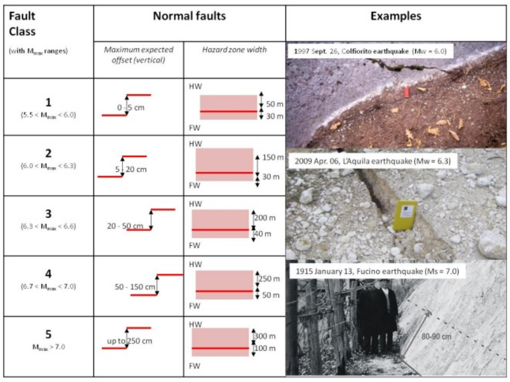


*Fig. 3: ITHACA capable faults with prevalent normal movement have been classified into five classes according to maximum magnitude range values. For each class, are provided maximum expected offsets and typical width of the hazard zone in the hanging-wall (HW) and in the foot-wall (FW) of the master capable fault. Some examples of documented surface faulting events recently occurred in normal tectonic environment are shown on the right.*

the hazard zone width is in the order of 400 m (100 m in the footwall and 300 m in the hanging wall).
Conversely, a clear documentation of surface faulting pattern occurred in compressive and strike-slip environment is quite scarce: only for the reverse 1976 event in Friuli some local surface ruptures have been interpreted by some Authors (Bosi et al., 1976; Aoudia & Suhadolc, 2000 based on Martinis and Cavallin, 1976) as surface faulting (Fig. 4, above). Moreover, a paleoseismic evidence in a compressive environment (secondary surface faulting) has been clearly documented at Monte Netto (South of Brescia, Fig. 4, below) that has allowed to identify at least three paleoearthquakes in the Late Quaternary (Livio et al., 2012).

Anyway, considering these cases but also the available cases of documented reverse surface faulting events around the world (cfr. Lettis et al., 1997) it is clear that in a compressive environment surface faulting features typically occur not only in correspondence to the main thrust but also at the hinge of the growing anticline (e.g., 1980 El Asnam earthquake), even with normal displacement, for instance due to bending-moment faults. This zone may be located at a variable distance (up to some km) in the hanging wall of the main thrust.
Thus, the width of hazard zone in the hanging wall of reverse faults has to be significantly larger than in the hanging wall of normal faults. Since the available information about reverse surface faulting is at the moment still very scarce, the proposed model introduces an asymmetric hazard zone around the reverse master fault mainly focused on the up-throwing block (hanging-wall). Although the probability of surface rupture in reverse environment is lower than in normal environment (Ross, 2011), we have conservatively considered the same maximum displacements associated to normal faults. The width of the zone is twice the corresponding width for normal faults. However, the occurrence of secondary ruptures cannot

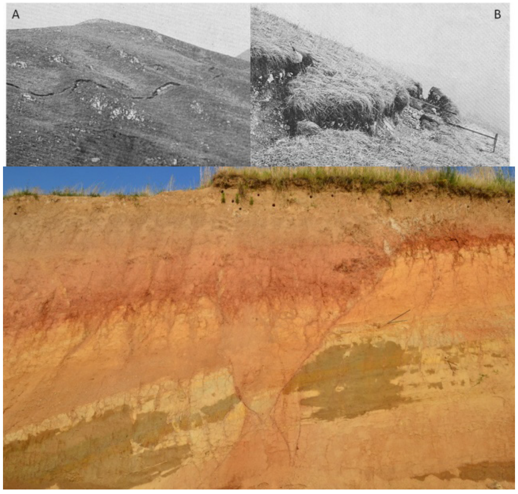


*Fig. 4: Evidence of surface faulting documented in Italy in a compressive environment.*
*Above: ground ruptures associated to the 1976 May 6th Friuli earthquake (Ms = 6.5) after Martinis and Cavallin, (1976), Bosi et al. (1976) and Aoudia & Suhadolc (2000).*
*Below: secondary surface faulting at Monte Netto, documenting at least three paleoearthquakes in the Late Quaternary associated to the reactivation of a growing fault-related fold (Livio et al., 2012).*

be excluded also at larger distance (up to some kms from the main fault) in case of growing near-surface anticlines.

For strike-slip fault systems (e.g. in the Gargano area, Puglia), a relevant role is played by surface ruptures occurring along faults located off the principal fault trace and in response to an earthquake along the principal faults (concept of distributed faulting; cfr. Petersen et al., 2011). Such faults may be linked in depth to the major structure (e.g. flower structures, pull-a-part basins, etc.), but might be also located at a distance of several hundreds of meters up to several km. Therefore, in this model, each fault segment has been managed as an independent source of Fault Displacement Hazard, locally with normal or reverse component. The hazard zone is symmetrical, 30 m wide in consistency with ITHACA resolution and expected width along principal faults (Petersen et al., 2011). Horizontal offsets are proportional to the fault class.
A peculiar situation concerns the capable faults located in the volcano-tectonic environment of Eastern Sicily (Mt. Etna and surrounding areas), for which the buffer area around each capable fault is considered symmetric and should be not more than 40 m wide (20 m on each side). This statement is confirmed by a robust field evidence of repeated surface faulting events (both coseismic surface faulting and aseismic fault creep events) in recent time, that typically affect a very narrow strip along the fault lineament.

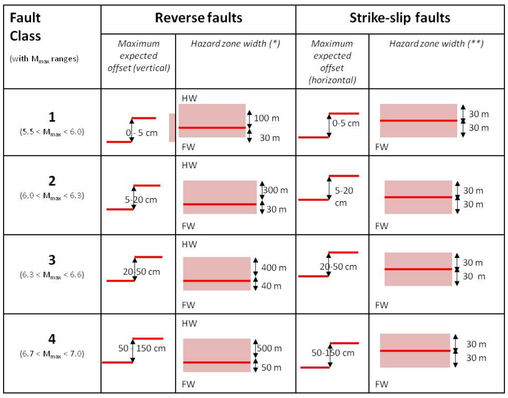


*Fig. 5: ITHACA capable faults with prevalent reverse and strike-slip movements have been classified into four classes according to maximum magnitude range values. For each class, are provided maximum expected offsets and typical width of the hazard zone in the hanging-wall (HW) and in the foot-wall (FW) of the master capable fault.*
*For reverse faults, the standard width of the hazard zone in the hangingwall is twice the corresponding width associated to the same class in normal faulting environment. For strike-slip faults the hazard zone is symmetrical (width = 30 m) along each fault linear segment of the fault zone, including also distributed faulting.*

## DISCUSSION AND CONCLUSIONS

The proposed assessment provides a first measure of the severity of the problem (capable faults ranking) since it just indicates where Fault Displacement Hazard is expected to be more critical (zonation).
Therefore, it can be considered valid only at general scale, as an helpful tool for a first selection of sites suitable to critical facilities. Of course, the characterization of *setback areas* around each capable fault needs a better characterization of Fault Displacement Hazard at local scale (e.g. Boncio et al., 2012, for FDH along normal faults). Thus, in the frame of the characterization of a selected site, this first assessment needs to be integrated by ad hoc seismotectonic and paleoseismic investigations aimed at excluding the presence of capable faults in the area around the site (up to 5 km radius, that is the standard for nuclear installations), or alternatively at estimating a Probabilistic Fault Displacement Hazard (cfr. Youngs et al., 2004 for details on this methodology).
Furthermore, concerning land management and civil building regulations near capable faults, although in Italy the national legislation for building in seismically active areas does not consider FDH, the proposed assessment will allow to address land planning towards areas where FDH is negligible or with acceptable impact (e.g. surface offsets < 2 cm) on civil buildings or critical facilities.

## References

Aoudia, A. & P. Suhadolc, (2000). Il terremoto del 6 maggio 1976 e la tettonica attiva in Friuli. In: *Le ricerche del GNDT nel campo della pericolosità sismica (1996-1999)* (Galadini, F., C. Meletti, A. Rebez, eds.). CNR-GNDT, Roma, 137-142.
Boncio, P., P. Galli, G. Naso & A. Pizzi, (2012). Zoning surface rupture hazard along normal faults: Insight from the 2009 Mw 6.3 L'Aquila, Central Italy, Earthquake and other global earthquakes. *Bulletin of the Seismological Society of America* 102 (3), 918-935.
Bosi, C., B. Camponeschi, & G. Giglio, (1976). Indizi di possibili movimenti lungo faglie in occasione del terremoto del Friuli del 6 maggio 1976. *Bollettino della Società Geologica Italiana* 94, 187-206.
Bryant, W.A. & E.W. Hart, (2007). Fault-rupture hazard zones in California: Alquist-Priolo earthwquake fault zoning act with index to earthquake fault zones maps. *California Geological Survey Special Publications* 42, 41 p.
Comerci, V., A.M. Blumetti, P. Di Manna, D. Fiorenza, L. Guerrieri, M. Lucarini, L. Serva & E. Vittori, (2013). ITHACA Project and Capable Faults in the Po Plain (Northern Italy). *Ingegneria Sismica* 1-2, 36-50.
Guerrieri, L., A.M. Blumetti, P. Di Manna, L. Serva & E. Vittori, (2009). The exposure of urban areas to surface faulting hazard in Italy: a quantitative analysis. *Italian Journal of Geosciences* 128 (1), 157-171.
Lettis, W.R., D.L. Wells & J.N. Baldwin, (1997). Empirical Observations Regarding Reverse Earthquakes, Blind Thrust Faults, and Quaternary Deformation: are blind thrust faults truly blind?. *Bulletin of the Seismological Society of America* 87 (5), 1171-1198.
Livio, F., A. Berlusconi, A.M. Michetti, G. Sileo, A. Zerboni, L. Trombino, C. Spoetl & H. Rodnight, (2012). Late Pleistocene to Holocene activity of a blind thrust deduced from surface secondary faulting: preliminary paleoseismological results on the Monte Netto site (N Italy). *Rendiconti Online della Società Geologica Italiana* 21 (2), 351-353.
Martinis, B. & A. Cavallin, (1976). The Friuli earthquake May 6, 1976: ground cracks and sand mounds. *Bollettino di Geofisica Terica ed Applicata* 19, 792-808.
Petersen, M.D., T.E. Dawson, R. Chen, T. Cao, C.J. Wills, D.P. Schwartz & A.D. Frankel, (2011). Fault Displacement Hazard for Strike-Slip Faults. *Bulletin of the Seismological Society of America* 101 (2), 805-825.
Ross, Z.E. (2011). *Probabilistic Fault Dispalcement Hazard analysis for reverse fautls and surface rupture scale invariance.* California Polytechnic State University Thesis, San Luis Obispo, 62 p.
Serva, L. & F. Fumanti, (2012). The evaluation of the reference earthquake for the siting of high risk industrial plants. *Energia Ambiente e Innovazione* 3, 72-81.
Working Group MS (2008). *Indirizzi e criteri per la Microzonazione Sismica. Conferenza delle Regioni e delle Province Autonome.* Dipartimento della Protezione Civile, Roma.
Youngs, R. R., W.J. Arabasz, R.E. Anderson, A.R. Ramelli, J.P. Ake, D.B. Slemmons, J.P. McCalpin, D.I. Doser, C.I. Fridrich, F.H. Swan, A.M. Rogers, C.J. Yount, L.W. Anderson, K.D. Smith, R.L. Bruhn, P.L.K. Knuepfer, R.B. Smith, C.M. dePolo, D.W. O'Leary, K.J. Coppersmith, S.K. Pezzopane, D.P. Schwartz, J.W. Whitney, S.S. Olig & G.R. Toro, (2003). A methodology for probabilistic fault displacement hazard analysis (PFDHA). *Earthquake Spectra* 19 (1), 191-219.

# Archaeological destruction layers – a key to high accuracy chronostratigraphy

*Hassul, Erez (1), Shmuel Marco (2), Amir Sagy (3), Israel Finkelstein (4), Katia Cytryn-Silverman (5), Eli Yannai (6) Amotz Agnon (1)*

(1) Institute of Earth Sciences, The Hebrew University, Jerusalem 91904, Israel. Email: Erez.Hassul@gmail.com
(2) Department of Geophysics and Planetary Sciences, Tel Aviv University, Tel Aviv 69978, Israel
(3) Geological Survey of Israel, 30 Malkhe Israel, Jerusalem 95501, Israel
(4) Department of Archaeology and Ancient Near Eastern Civilizations, Tel Aviv University, Tel Aviv 69978, Israel
(5) Institute of Archaeology, The Hebrew University, Jerusalem 91904, Israel
(6) Israel Antiquities Authority, Rockefeller Museum, Sultan Suleiman 27, Jerusalem 91004, Jerusalem

***Abstract:*** *The two main observables sought for in archaeoseismic studies are the extent of damage and the time of destruction. Often archaeologic chronology is insufficient or disputed between scholars. This work is an attempt to harness archaeomagnetic data acquired from destruction layers in order to constrain the timing of destruction. We expect that, in turn, archaeoseimic studies will contribute to refinement of achaeomagnetic master curves.*

***Key words****: archaeoseismology, Minoan civilization, Late Bronze Age collapse, Potential Earthquake Archaeological Effects.*

## INTRODUCTION

Astride the Dead Sea Fault and situated at the crossroads of empires, religions and cultures, the Levant features countless ancient archaeological sites dating from before the dawn of history to modern times. Numerous sites display destruction layers perhaps caused by earthquakes and conquests. These layers, if well dated, can serve as chronostratigraphic markers bearing valuable seismic and geo-magnetic data (Marco et. al.; 1997). These data can then be used for constraining dates of other sites or for testing correlations between stratigraphic layers.

## METHODOLOGY

Our work focuses on well-dated destruction layers in archaeological sites that suffered significant earthquake damage. High resolution geometrical measurements of the ruins, by a ground-based laser scanner, enable creation of 3D models of the damaged structures. These, when compared to theoretical pre-destruction models, can characterize the damage inflicted on the site and provide information about the damaging earthquakes (Hinzen at. el., 2011). A 3D model is presnted for Khirbat al-Minya (Fig 2, 3 and 4), an Umayyad palace built on the northwestern shore of the Sea of Galilee during the early 8th century CE. The palace was severely damaged by earthquakes, perhaps as the result of the mid-century seismic events which caused widespread destruction in the Galilee region (Karcz, 2004; Ambraseys, 2006). An additional, more recent, massive destruction layer associated with a conflagration contains animal remains trapped under a fallen roof. Typology suggests a 13th - 14th century dating for this event. OSL dating, correlated with known regional macroseismic data, is being conducted in an effort to constrain the dates of the destructive fires, and to establish connection to a known earthquake.

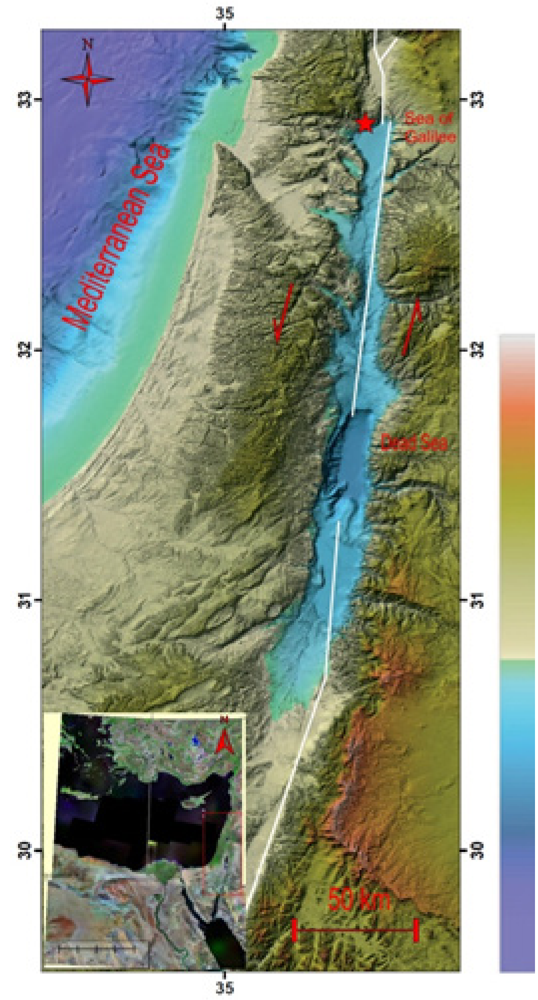


*Fig 1: Location map of the Dead Sea Transform. Khirbat al-Minya is market with a red star (After Hall & Calvo; 2005).*

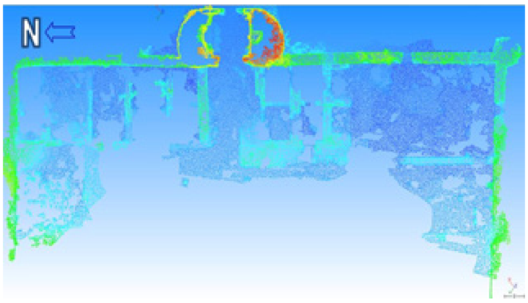


*Fig 2: plan view of a partial 3D point cloud of Khirbat al-Minya, an Umayyad palace on the northwestern shore of the Sea of Galilee. Processed in TECHNODIGIT's 3D - Reshaper®.*

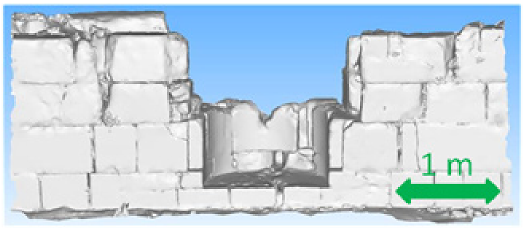


*Fig 3: A mesh of a part of the southeastern wall. Damage associated with earthquakes can by seen. Processed in TECHNODIGIT's 3D- Reshaper®.*


*Fig 4: The original part of the southeastern wall.*

Here we propose to narrow the uncertainty in the timing of the magnetic data, making the magnetic master curves useful for precise dating. An independent and valuable observable that can be extracted from destruction layers is the remnant magnetic vector containing the direction (declination/ inclination) and intensity of the geo-magnetic field prevalent on the date of the destruction.

Archaeological materials such as pottery artifacts and clay bricks, heated above the Curie temperature by fires triggered by an earthquake, or set by a conquering army, gain a magnetic vector parallel to the ambient field prevailing at that time. If the destruction layer was sealed by destruction debris or overlying layers, the artifacts can be found in situ and oriented samples studied, thus determining the direction of the magnetic vector (Fig 5) (Segal at. el., 2003; Schnepp & Lanos, 2005; McIntosh & Catanzariti, 2006; Ertepinar at. el., 2012; Hervè at. el., 2013).

**DISCUSSION AND EXPECTED CONCLUSIONS**

Recent archaeomagnetic work has narrowed the uncertainties in the determination of the magnetic

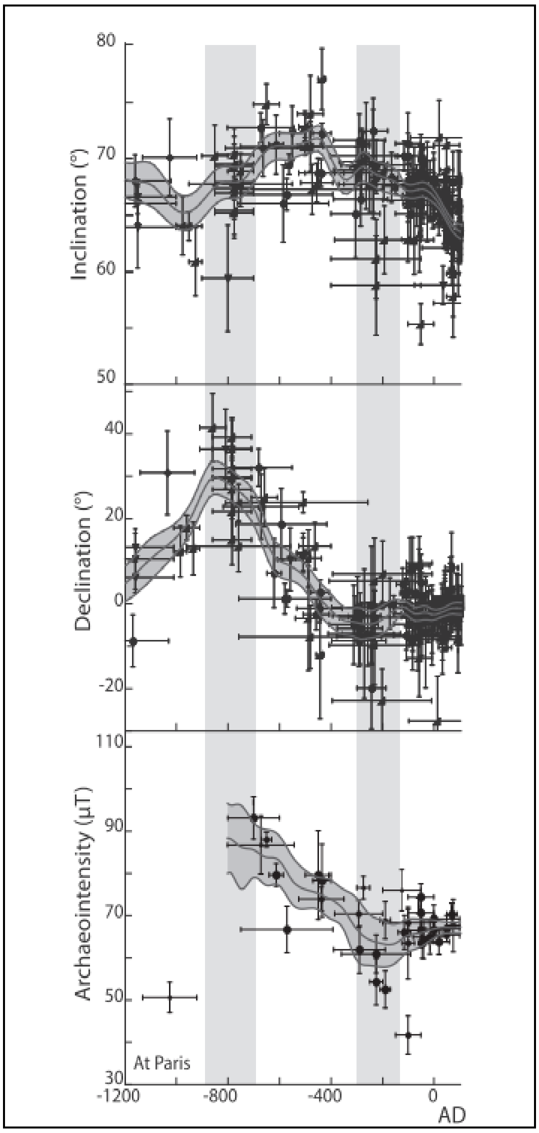


*Fig 5: A recently published example of archaeo-secular curves of variation of the direction and the intensity of the geomanetic field in Western Europe between 1200 BCE and 200 CE. All data are relocated to Paris, By Hervè at. el. (2013). Large uncertainty estimates can be seen. Our goal is to minimize these uncertainties.*

*Fig 6: Tabun MQT1 from area Q, square G4 of Tel Megiddo dated to late Iron Age I, 15 oriented specimens were sampled.*

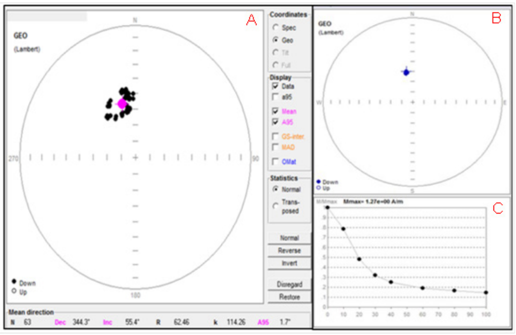


*Fig 7: Preliminary analysis on tabun NST-A frome Nabi Samwil, a 1st century CE settlment, ~7 km north of Jerusalem, Age estimate courtesy of B. Har-Even & K. Raphael. 6A - The average direction of the geo-magnetic vector that was measured on seven specimens of a tabun. 6B - The direction measures of the specimen NST-A-10. 6C - Demagnetization curve of the same specimen. All Measurements made by AGICO's JR6 spinner magnetometer.*

vector (Shaar et al., 2011; in prep.). We focus mainly on household cooking stoves (tabuns) found within destruction layers. Tabuns (Fig 6), and other heating facilities, are ideal for paleo-magnetic studies, preserving the magnetic direction prevailing the last time they were heated, and not subsequently moved. Thus they are useful even in the absence of conflagrations. Magnetic samples were collected from several layers of Tel Megiddo and at rescue excavations near the modern town of Yavne. Preliminary analysis (Fig 7) suggests that the artifacts have preserved the magnetic field in high precision. This information is crucial for research of the Earth's paleo-magnetic field. In addition, knowing the changes in the direction and intensity of the archaeo-magnetic field in adequate resolutions may enable future archaeological researchers to constrain conventional dating by an independent measurement. As a result, the magnetic vector of different destruction layers from different sites can be compared and correlated, yielding multifactorial data on the same seismic event.

**Acknowledgements:** We thank Miki Golan for pointing out the damage in Khirbat el-Minya, Dr. Ron Shaar for his guidance, Dr. Rami Weinberger and Dr. Roi Granot for the laboratory access, and Dr. John K. Hall for his significant input. This work could not have come to reality without the help and cooperation of archeologists Dr. Sharon Zuckerman, Prof. Rami Arav, Benny Har-Even, Dr. Kate Raphael, and Prof. Aren Maeir and their field assistants. Eli Ram, Eran Trabelci, Eitan Philip and Iyad Swaed assisted in the field work. Their help is greatly appreciated.

## References

Ambraseys, N. N., (2006). Earthquakes and archaeology. *Journal of Archaeological Science*, 33 (7), 1008–1016.

Ertepinar, P., C.G. Langereis, A.J. Biggin, M. Frangipane, T. Matney, T. O¨kse & A. Engin, (2012). Archaeomagnetic study of five mounds from Upper Mesopotamia between 2500 and 700 BCE: Further evidence for an extremely strong geomagnetic field ca. 3000 years ago. *Earth and Planetary Science Letters* 357–358, 84–98.

Hall, J. K., & Calvo, R., (2005). PLATE XI: Digital Shaded Relief Maps of Israel in Krasheninnikov, V. A., , Hall, J. K., Hirsch, F. and Benjamini, C. (Editors), 2005. *Geological Framework of the Levant: Volume I - Cyprus and Syria*. II - Levantine Basin and Israel. Historical Productions-Hall, Jerusalem. I, p. 498, II, p. 26, 11 A0 sized maps.

Hervȇ, G., A. Chauvin & P. Lanos, (2013). Geomagnetic field variations in Western Europe from 1500 BC to 200 AD. Part II: New intensity secular variation curve. *Physics of the Earth and Planetary Interiors*. 218, 51–65.

Hinzen, K. G., H. Kehmeier, S. Schreiber & S. K. Reamer, (2011). A Case study of earthquakes and rockfall - induced damage to a Roman mausoleum in Pinara, SW Turkey, *2nd INQUA-IGCP-567 International Workshop on Active Tectonics, Earthquake Geology, Archaeology and Engineering, Corinth, Greece*.

Karcz, I., (2004). Implications of some early Jewish sources for estimates of earthquake hazardin the Holy Land. *Annals of Geophysics* 47 (2/3).

Marco, S., A. Agnon, R. Ellenblum, A. Eeidelman, U. Basson & A. Boas, (1997). 817-year-old walls offset sinistrally 2.1 m by the Dead Sea Transform, Israel. *Journal of Geodynamics* 24 (1–4), 11–20.

McIntosh, G. & Catanzariti, G., (2006). An introduction to archaeomagnetic dating. *GEOCHRONOMETRIA* 25, 11-18.

Schnepp, E. & Lanos, P., (2005). Archaeomagnetic secular variation in Germany during the past 2500 years. *Geophysical Journal International* 163 (2), 479–490.

Segal, Y., S. Marco & R. Ellenblum, (2003). Intensity and direction of the geomagnetic field on 24 August 1179 measured at Vadum Iacob (Ateret) Crusader fortress, northern Israel. *Israel Journal of Earth Science* 52, 203-208.

Shaar, R., E. Ben-Yosef, H. Ron L. Tauxe, A. Agnon & R. Kessel, (2011). Geomagnetic field intensity: How high can it get? How fast can it change? Constraints from Iron Age copper slag. *Earth and Planetary Science Letters* 301, 297–306.

# What we can learn from a blind-test for predicting earthquake-triggered landslides applied to the Wenchuan area, China – also for paleoseismological studies

*Havenith, Hans-Balder (1), Xuanmei Fan (2), Almazbek Torgoev (1)*

(1) University of Liege, Department of Geology, B18, B-4000 Liege. Email: HB.Havenith@ulg.ac.be.
(2) State Key Laboratory of Geohazards Prevention and Geoenvironment Protection, Chengdu University of Technology, Erxianqiao Road, 610059 Chengdu, Sichuan.

***Abstract:*** *On the basis of numerical modelling results, we adapted existing empirical laws for the regional assessment of Newmark displacement and Arias Intensity. These adapted laws were used to predict landslide occurrence in the Longmen Shan mountains only on the basis of the pre-earthquake 25 m resolution Digital Elevation Model (DEM), but considering the known parameters of the 2008 Wenchuan earthquake: Mw=7.8 and the extension of the activated fault. No geological information was provided – for all sites the same average geomechanic properties of rocks and the same groundwater saturation were used. The goal was to find out how much landslide occurrence is controlled by shaking attenuation from the fault (considering hanging wall and foot wall location) and by local topographic amplification. These topographic effects were estimated on the basis of combined curvature values computed for different DEM resolutions. The comparison with the existing landslide inventory (that was not available in the beginning) is satisfactory and allows us to arrive at two general conclusions: first, if the seismic activity of a fault zone is well known, at least 80% of the locations of landslides triggered by a strong earthquake can be predicted (near the fault); second, if landslide distributions can be predicted through modelling using seismic information, the inversed process could also be completed – paleoseismic activity could be inferred from observed landslide characteristics and distributions (if the seismic origin of those can be proved).*

***Key words****: Landslides, Newmark method, Arias Intensity, topographic amplification, landslides as paleoseismic markers.*

INQUA Focus Group on Paleoseismology and Active Tectonics

paleoseismicity.org

# Holocene tsunami history of the Makran Subduction Zone (Northern Indian Ocean)

*Hoffmann, Gösta (1), Klaus Reicherter (2), Christoph Grützner (2), Magdalena Rupprechter (1), Frank Preusser (3)*

(1) German University of Technology, Department of Applied Geosciences, PO Box 1816, PC 130, Muscat, Oman
Email: goesta.hoffmann@gutech.edu.om
(2) Neotectonics and Natural Hazards, RWTH Aachen University, Lochnerstr. 4-20, 52056 Aachen, Germany
(3) Department of Physical Geography and Quaternary Geology, Stockholm University, S-10691 Stockholm, Sweden

***Abstract:*** *The Makran Subduction Zone (MSZ) is an E-W trending structure that forms the boundary between the Arabian Plate in the south and the Eurasian Plate in the north. The MSZ has the largest hazard potential in terms of tsunamis within the Northern Indian Ocean. The seismicity of the MSZ is comparatively low and the historic record is fragmentary and incomplete. Therefore, the recurrence interval of large tsunamigenic earthquakes ($M_W$>8) is unknown. The only instrumentally recorded tsunami within the MSZ occurred on 28th November 1945. We aim to reconstruct paleo-tsunami events in order to constrain recurrence intervals. We use historical, geological and archaeological data to achieve this goal. Geological evidence of paleo-tsunamis is mainly seen in block and boulder deposits along the coast. The event deposits are dated by $^{14}$C and OSL. The results suggest several tsunamigenic events in the last 5000 years. These events clearly exceeded the magnitude of the 1945-event.*

***Key words***: *Early warning system, hazard potential, Oman, extreme event deposits*

## INTRODUCTION

The Makran Subdution Zone (MSZ) is the dominating structure in the Northern Indian Ocean (NIO). Here the Arabian Plate is subducted beneath the Eurasian Plate (see Fig. 1) with a rate of about 40 mm/a (DeMets et al. 2010).

The MSZ has an along-strike extension of approximately 900 km and is divided in a western and eastern part (Kukowski et al. 2000, Smith et al. 2012). The sediment

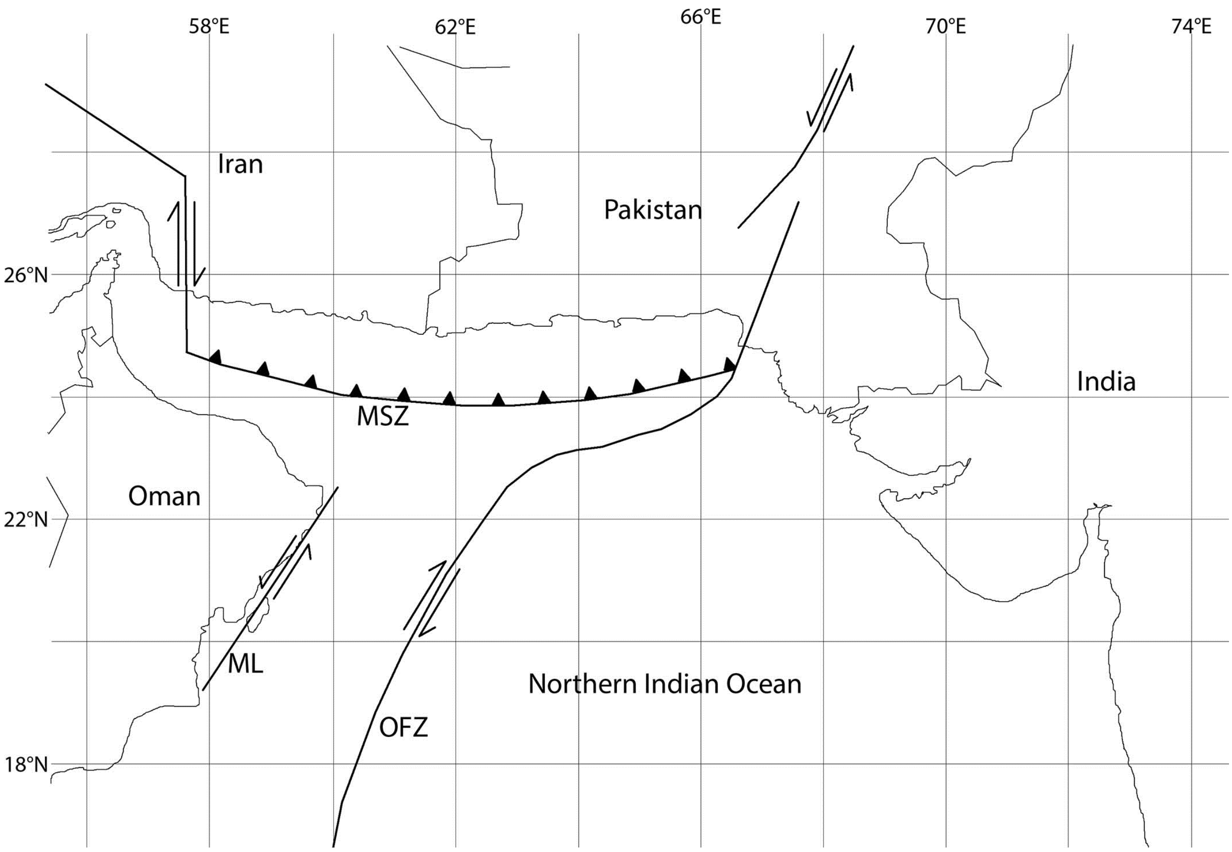


*Fig.1: Outline of the Northern Indian Ocean and bordering countries. ML: Masirah Line, MSZ: Makran Subduction Zone, OFZ: Owen Fracture Zone.*

thickness of the incoming plate is high (Kopp et al. 2000), resulting in one of the largest accretionary wedges observed at a convergent margin (Smith et al. 2013).

The seismicity of the MSZ appears to be comparatively low. Furthermore, the historic record is fragmentary and incomplete (Byrne et al. 1992) as the coastlines of the NIO are only sparsely populated. Therefore, the recurrence interval of large tsunamigenic earthquakes ($M_W$>8) is unknown.

We aim at reconstructing the Holocene tsunami history of the MSZ and use a holistic approach by utilizing a) historic records, b) archaeological evidence and c) sedimentological archives.

**RESULTS**

The only instrumentally recorded earthquake on the MSZ that triggered a tsunami occurred on 27th November 1945. A near surface shell bed in the lagoon of Sur has been interpreted as tsunamigenic and the 1945 event has tentatively been assigned (Donato et al. 2008, 2009, Pilarczyk et al. 2011, Pilarczyk and Reinhardt 2012). We interviewed old fishermen along the coastline of Oman and collected additional historic information from archives to reconstruct the 1945 event in the NIO (Hoffmann et al. 2013a). The damages reported were severe along the coastline of modern Pakistan and minor along the coastline of Oman, where wave heights of 2-3m were reconstructed. We conclude that the 1945 event is not the worst-case scenario as block and boulder deposits along Oman's coastline indicate higher energetic wave events. These block and boulder deposits are described by Hoffmann et al. (2013b). The maximum mass of these deposits is estimated as 120 ton. There is clear evidence that these blocks have been moved against gravity on top of the cliffed coastline. The blocks are colonised by marine sessile organism, indicating the former position in the intertidal area. We performed radiocarbon dating (n=55) of these organisms. Their ages reveal movement of the blocks in the Mid to Late Holocene. However, there is no statistically significant clustering within the dataset.

Additional work concentrated on the analyses of fine grained deposits which are interpreted as overwash (Fig. 2). Ground penetrating radar surveys were performed (Koster et al. in prep.) and sedimentological investigations conducted. These deposits are dated by radiocarbon (n=25). OSL dating is in progress; so far 8 samples are dated (see Fig. 2). Additional information is obtained from 2 archaeological sites; an overwash deposit on Seeb is associated with pottery that dates to the 9th and 10th century AD. An archaeological site in the easternmost part of Oman in Ras al Hadd indicates a marine inundation around 2400 BC.

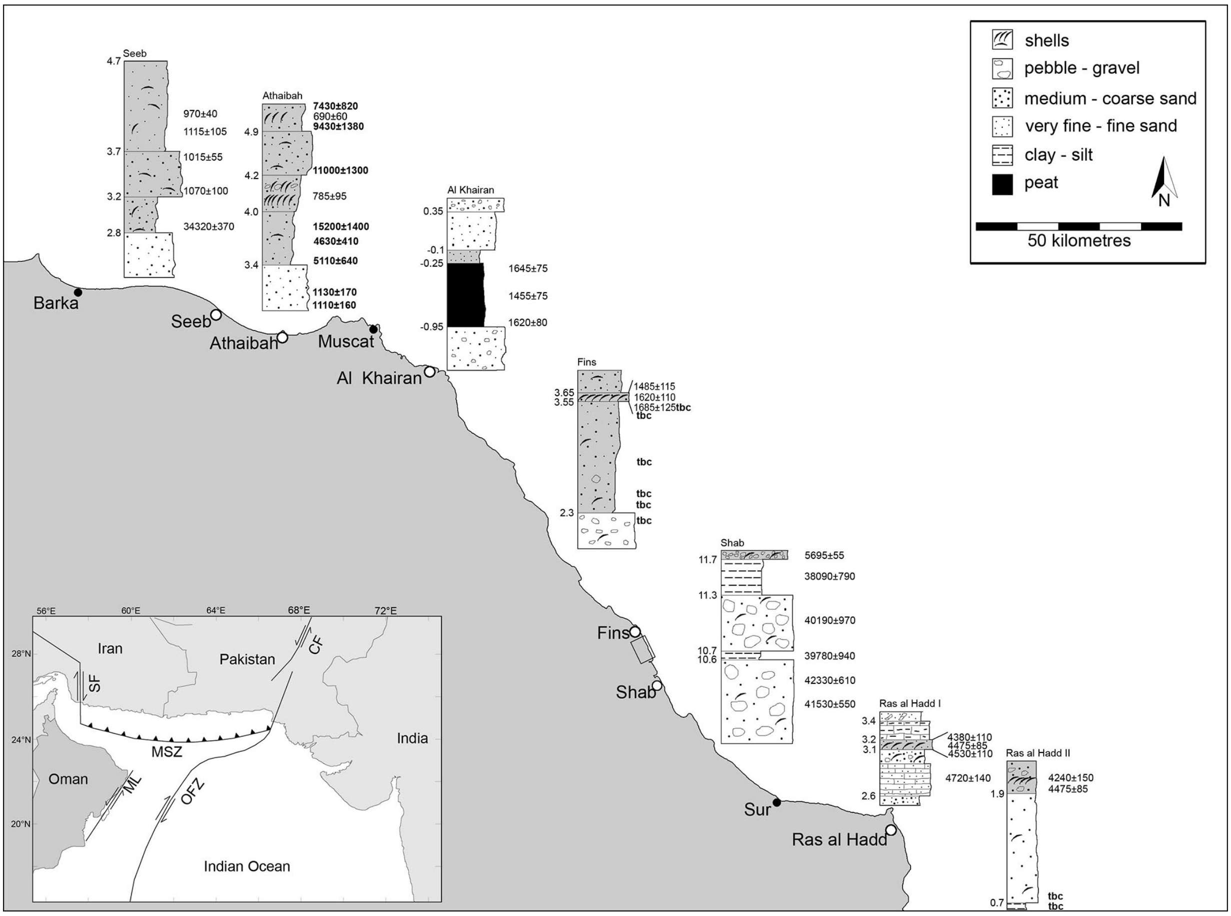


*Fig. 2: Fine grained event deposits along the coastline of Oman. Numbers indicate dating results. OSL ages are in bold (tbc: to be confirmed).*

## DISCUSSION

The detailed analyses of marine overwash deposits along the coastline of Oman are interpreted as evidence for extreme wave events within the NIO. Storm surges as well as tsunami waves may be responsible for the dislocation of the boulders and the fine grained overwash deposits. Tropical cyclones are occasionally observed along the coastline. An event in 2007 is the most intense cyclone on record in the NIO (Fritz et al. 2010). However, neither overwash deposits nor dislocation of blocks or boulders were observed, and therefore tsunamis appear to be a more likely process. Modelling results (e.g. Heidarzadeh and Kijko 2011) indicate maximum wave heights sufficient to transport the deposits.

## CONCLUSIONS

A recurrence interval of 400-450 years for the Mid to Late Holocene is calculated for tsunamis generated at the MSZ. The data are preliminary and need further investigation. The data suggest a worst-case scenario for Muscat with wave run-up in the range of 15m. The resulting inundation would affect critical infrastructure such as oil refineries and desalination plants, (Fig. 3).

**Acknowledgements:** This study is supported by a grant from the Omani Research Foundation TRC (ORG GUtech EBR 10 013) which is kindly acknowledged.

## References

Byrne, D.E., L.R. Sykes & D.M. Davis (1992). Great Thrust Earthquakes and Aseismic Slip Along the Plate Boundary of the Makran Subduction Zone. *Journal of Geophysical Research* 97, 449-478.

DeMets, C., R. G. Gordon & D. Argus, (2010). Geologically current plate motions. *Geophysical Journal International* 181 (1), 1-80.

Donato, S.V., E.G. Reinhardt, J.I. Boyce, J.E. Pilarczyk & B.P. Jupp, (2009). Particle-size distribution of inferred tsunami deposits in Sur Lagoon, Sultanate of Oman. *Marine Geology* 257, 54-64.

Fritz, H.M., C.D. Blount, F. Albusaidi & A. Alharthy, (2010). Cyclone Gonu storm surge in Oman. *Estuarine, Coastal and Shelf Science* 86 (1), 102-106.

Donato, S. V., E.G. Reinhardt, J.I. Boyce, R. Rothaus & T. Vosmer, (2008). Identifying tsunami deposits using bivalve shell taphonomy. *Geology* 36 (3), 199-202.

Heidarzadeh, M. & A. Kijko, (2011). A probabilistic tsunami hazard assessment for the Makran subduction zone at the northwestern Indian Ocean. *Natural Hazards* 56 (3), 577-593.

Hoffmann, G., M. Rupprechter, N. Al Balushi, C. Grützner & K. Reicherter, (2013a). The impact of the 1945 Makran tsunami along the coastlines of the Arabian Sea (Northern Indian Ocean) – a review. *Annals of Geomorphology Supplementary Issues*, in press, doi: 10.1127/0372-8854/2013/S-00134.

Hoffmann, G., K. Reicherter, T. Wiatr, C. Grützner & T. Rausch (2013b). Block and boulder accumulations along the coastline between Fins and Sur (Sultanate of Oman):

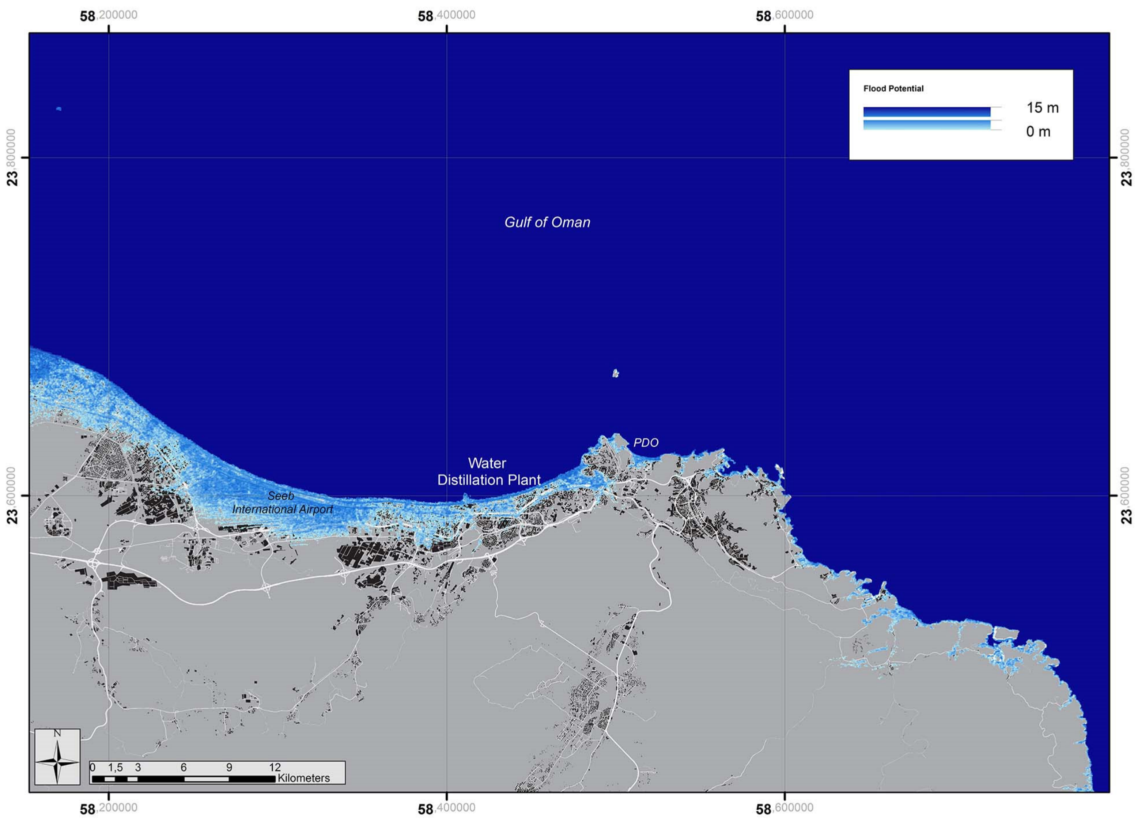


*Fig. 3: 15m inundation scenario for Muscat. Critical infrastructure is concentrated along the coastline. (Digital elevation model is SRTM based).*

tsunamigenic remains? *Natural Hazards* 65, 851-873.

Kopp, C., J. Fruehn, E.R. Flueh, C. Reichert, N. Kukowski, J. Bialas & D. Klaeschen, (2000). Structure of the Makran subduction zone from wide-angle and reflection seismic data. *Tectonophysics* 329 (1-4), 171-191.

Koster, B., C. Grützner, K. Reicherter, G. Hoffmann, (in prep.): Ground penetrating radar facies of inferred tsunami deposits on the shores of the Arabian Sea (Northern Indian Ocean).

Kukowski, N., T. Schillhorn, E.R. Flueh & K. Huhn, (2000). Newly identified strike-slip plate boundary in the northeastern Arabian Sea. *Geology* 28, 355-358.

Pilarczyk, J.E., E.G. Reinhardt, J.I. Boyce, H.P. Schwarcz & S.V. Donato, (2011). Assessing surficial foraminiferal distributions as an overwash indicator in Sur Lagoon, Sultanate of Oman. *Marine Micropaleontology* 80 (3-4), 62-73.

Pilarczyk, J.E. & E.G. Reinhardt, (2012). Testing foraminiferal taphonomy as a tsunami indicator in a shallow arid system lagoon: Sur, Sultanate of Oman. *Marine Geology* 295-298, 128-136.

Smith, G., L. McNeill, T.J. Henstock & J. Bull (2012). The structure and fault activity of the Makran accretionary prism. *Journal of Geophysical Research: Solid Earth* 117, B07407.

INQUA Focus Group on Paleoseismology and Active Tectonics

paleoseismicity.org

# Insights into the Development of a Paleoseismic Database for Germany and Adjacent Countries

*Hürtgen, Jochen (1), Klaus Reicherter (1)*

(1) Neotectonics and Natural Hazards, RWTH Aachen University, Lochnerstraße 4-20, 52056 Aachen, Germany. Email: j.huertgen@nug.rwth-aachen.de

***Abstract:*** *The area of Central Europe is an intraplate domain and is characterized by low to moderate seismicity with records of larger seismic events occurring in historical and recent times, such as the earthquakes in Basel (1356) and Roermond (1992). These records of seismicity are restricted to a few hundred years, which is geologically insignificant for a reliable seismic hazard assessment. Therefore, we are developing a paleoseismic database (PalSeisDB) that could extend the seismic record for at least one seismic cycle. Paleoseismic studies with trenching sites can provide the most reliable evidence for paleoearthquakes and are a central part of the PalSeisDB; also secondary effects such as earthquake-induced landslides or liquefaction features are documented. When finalized, the database will present an overview about the state of paleoseismic research in Central Europe and can be integrated into other projects.*

***Key words****: Paleoseismology, Paleoearthquakes, Database, Germany, Central Europe.*

## INTRODUCTION

We present the first insights into the development of a paleoseismic database (PalSeisDB) for Germany and adjacent countries. Paleoseismic evidence from published and partly unpublished studies in Central Europe has been, and is currently being, collected. This will be an extension of historical and instrumental earthquake catalogs that only date back approximately 1200 years (e.g. Leydecker, 2011; AHEAD, 2013). The events in these published catalogs do not comprise the needed temporal and spatial distribution for seismic hazard assessments as they do not cover the seismic cycle of more than thousands or ten thousands of years (Ahorner, 2001; Vanneste et al., 2013) of tectonically active structures, such as faults and folds; therefore, paleoearthquakes identified in paleoseismic investigations, which cover this extended time period, must be taken into account.

*Project Context*

Similar projects around the world, mostly on a national basis, have been undertaken or are in progress. These projects, however, do not collect paleoseismic data directly; they compile data on active faults, including their long-term behaviour. These faults are responsible for the generation of recent, ancient and paleo-earthquakes. However, for seismic hazard assessments not only does this earthquake information has to be taken into account, but also the geological relationship between source (fault) and effect (earthquake), as concluded by Basili et al. (2008). Examples of active faults and seismogenic sources databases include Italy's Database of Individual Seismic Sources (DISS version 3; Basili et al., 2008), the Quaternary Active Faults Database of Iberia (QAFI v.2.0; García-Mayordomo et al., 2012), France's Néopal project (Déformations récentes et paléoséismes, see http://www.neopal.net/, last accessed


*Fig. 1: Study area for the PalSeisDB including Germany and adjacent countries and main geological structures. BF: Black Forest, BG: Bresse Graben, EG: Eger Graben, FP: Franconian Platform, GG: Glückstadt Graben, HG: Hessian Grabens, LRG: Lower Rhine Graben, OW: Odenwald, URG: Upper Rhine Graben, VG: Vogesen, VB: Vienna Basin. Compiled from Dèzes et al. (2004), Kaiser et al. (2005), Reicherter et al. (2008), and made with Natural Earth (Free vector and raster map data @ naturalearthdata.com).*

July 2013), the U.S. Quaternary Fault and Fold Database (Haller et al., 2004), the Central and Eastern United States Seismic Source Characterization for Nuclear Facilities (CEUS, see http://www.ceus-ssc.com/, last accessed July 2013), the Active Fault Database of Japan (see http://riodb02.ibase.aist.go.jp/activefault/index_e.html, last accessed July 2013), and the Active Tectonics of the Andes database (ATA v.1.0, Veloza et al., 2012). For Europe another project has been developed known as the SHARE Database 3.2 (Seismic Hazard Harmonization in Europe, http://www.share-eu.org/, last accessed June 2013). This includes seismogenic sources (mainly active fault data) and an earthquake catalog (historical and instrumental) for the wider European area. The fault data is incorporated in our database.

To date, no such database has been developed for Germany. Therefore, we have started a project to collect paleoseismic and active fault data in a database structure similar to those in the aforementioned projects. Our project is situated in the context of an updated German Nuclear Safety Standard, called KTA 2201 (Design of Nuclear Power Plants against Seismic Events). In the revised version (latest 2011), the data from paleoseismic studies and their results should be incorporated with respect to the maximum historical or prehistorical deterministic earthquake. The new standard should include the assessment of paleoseismicity in a distance of 200 km (radius) around the specific building. The collected information is not only useful in the context of nuclear safety, but also for building regulations in a more general context (e.g. emergency facilities or infrastructure).

*Geological Framework of Central Europe*

Central Europe is an intraplate domain and is characterized by low to moderate seismicity. This is mainly caused by compressional stress from the NW-ward drifting of the African plate and ridge-push from the North Atlantic Ridge. In this setting, a large segmented rift system was formed, the European Cenozoic Rift System (ECRIS) which comprises, amongst others, the Bresse Graben (BG), the Upper Rhine Graben (URG) and the Lower Rhine Graben (LRG), and extends from west of the Alps to the North Sea (Dèzes et al., 2004; see Fig. 1). The historical and instrumental record indicates that the areas of the URG and the LRG are able to produce larger earthquakes than 5.5, such as the one in Basel (1356, M 6.0-6.5), or the 1992 Roermond earthquake (M 5.9). The neotectonic and recent activity in regions of the Alps, the Molasse Basin, the Vienna Basin (VB), and the Eger Graben (EG) are also of interest. In agreement with the requirements of the new defined Nuclear Safety Standard (KTA 2201) we, therefore, focused our study in areas prone to larger earhquakes in Germany and also in adjacent, tectonically active regions (see Fig. 1).

*Paleoseismological Evidence*

From a paleoseismic point of view, evidence for paleoearthquakes can be found in different tectonic settings and can have different appearances related to the source of the earthquake. For example, to find evidence in the geological record of a surface rupture, the magnitude of the paleoearthquake must be Mw > 5.0 (Wells and Coppersmith, 1994). Preservation in the geologic record is strongly determined by erosion and deposition rates (man-made or natural) versus the deformation rates. After McCalpin (2009), we distinguish between effects found in the vicinity of the fault (on-fault) and effects found at a distance from the fault (off-fault). A very important tool in paleoseismological studies is the excavation of trenches on capable and active faults. Within the trench walls, all on-fault effects, such as offset of strata and colluvial wedges, can be found. These are relevant to determine the age of seismic rupturing on the fault. At a distance from the fault, secondary effects can be observed, such as mass movements (e.g. Keefer, 1984, and Michetti et al., 2007) or soft-sediment deformation features (e.g. Obermeier, 1996, and Michetti et al., 2007). The extent and distribution of these effects are also strongly dependent on earthquake's parameters, the subsurface characteristics and the topograpy. These types of evidence, and others, can be used to identify paleoearthquakes and active structures and to determine their seismic hazard potential.

## STRUCTURE OF THE DATABASE (PALSEISDB)

The aforementioned types of evidence are the central part of our database. The database itself was developed in Microsoft Access 2010 and ESRI ArcGIS 10.1. Microsoft Access has been used to build the main structure of the database and to input the data from mostly published studies (e.g. peer reviewed papers, conference proceedings, etc.), but also in part from unpublished work (e.g. personal communications, and posters). In ArcGIS, the geospatial information has been collected. The locations for entries into the database were defined by georeferenced information on figures from published work or by coordinates delivered by personal communications. The records of spatial information are

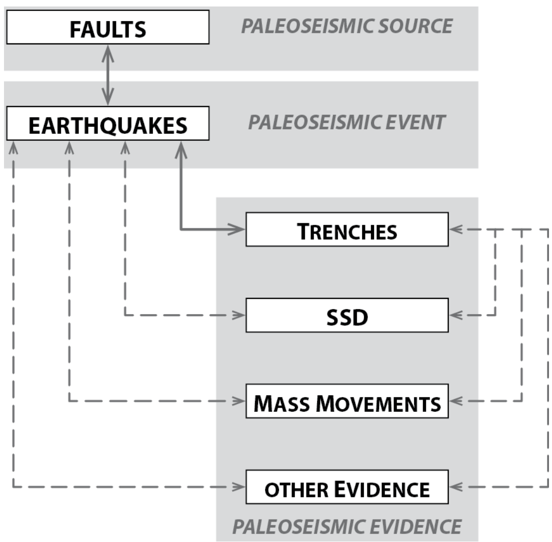


*Fig. 2: Schematic structure of the Paleoseismic Database of Germany and Adjacent Countries (PalSeisDB); SSD: soft-sediment deformations.*

saved in the geodetic datum ETRS 1989 (European Terrestrial Reference System), which is based on the Geodetic Reference System 1980 (GRS 80).

The general structure of the database is presented in Figure 2. We distinguish between the paleoseismic source, event and evidence. As previously mentioned, the data from paleoseismic trenches can give the most reliable information on the occurrence of paleoseismic events. We implemented a data table for the available trenches in the study area with some basic information on location, geometry, geologic framework, the excavated fault, the record of seismic events, and soft-sediment deformation (if documented). From the paleoseismic evidence, information on paleoearthquakes and active faults (paleoseismic source) is extracted and then input into the corresponding individual data tables with specifications on the quality of the provided data. The record for paleoearthquakes comprises the location, the date of event (mostly the determined time frame from different dating methods), the magnitude or intensity (if assignable), and some descriptions. The structure of the data table describing the active faults are mainly adopted from Italy's Database of Individual Seismic Sources (DISS version 3; Basili et al., 2008) including physical properties such as geometric (length, width, strike, dip), kinematic (rake, stress field), and seismogenic (single-event displacement, maximum magnitude, slip rate, recurrence interval, elapsed time) properties.

There are two further paleoseismic evidence types that will be documented in our database: earthquake-induced soft-sediment deformations (SSD) and mass movements. In Central Europe, only a few of these features have been documented until now, but studies in other areas (e.g. CEUS, see http://www.ceus-ssc.com/, last accessed July 2013) indicate that these are useful to evaluate the seismic potential in areas with low to moderate seismicity. For the documentation of soft-sediment deformation features, we adopted properties mainly based on the CEUS project (Paleoliquefaction Database) including the feature type (e.g. dike, sill, sand blow, sand crater), geometry (thickness, width, length), age of feature, references and some other comments. The appropriate parameters for mass movements are not yet specified in the database, but parameters like type of material involved (soil or rock), type of movement (slide, fall, etc.) and the dimensions (e.g. volume of landslide mass) are essential to assess the magnitude of the landslide triggering events (Keefer, 1984). Other, more specialized paleoseismic evidence, such as speleothem ruptures, have also been taken into account and are recorded in a separate table.

Figure 2 shows the relationship between the paleoseismic source, event and evidence (geologic record). Ideally, the earthquake event can be directly connected to a fault. With all evidence types we try to determine a paleoearthquake, which is mostly possible for paleoseismic trenches (solid line), but is limited for liquefaction, landslide and other evidence (dashed line). These last-mentioned evidence types can be found in a man-made trench, but also in natural outcrops.

## DISCUSSION

The paleoseismic record in Central Europe is relatively sparsely distributed. The area with the most available paleoseismic evidence is the Lower Rhine Graben (LRG), which has been intensively investigated by paleoseismologists over the last two decades (e.g. Camelbeeck et al., 2007; Skupin et al., 2008; Vanneste et al., 2013). Nevertheless, in this area a limited number of trenches (16) in relation to the amount of active faults have been excavated. The best investigated fault is the Feldbiss fault zone, which builds up the south-eastern border of the LRG. Distributed on its segments, it comprises nine paleoseismic trenches. The other seven trenches are distributed across other individual fault segments in the LRG (e.g. Viersen fault, Rurrand fault, Swist fault, Peelrand fault). In the Upper Rhine Graben (URG), only four paleoseismic trenches have been undertaken, e.g. at the Western Border fault in the vicinity of Osthofen (Peters et al., 2005) and at the Basel-Reinach fault south of Basel (Meghraoui et al., 2001). Outside of Germany, further trenches have been carried out in the Vienna Basin (e.g. Hintersberger et al., 2013) and in Northern Italy (e.g. Galadini et al., 2001). From these studies, paleoearthquakes can be identified. Furthermore, the secondary evidence types were also investigated and documented in a wider area, e.g. cave deposits and ruptures of speleothems in Belgium (Delaby, 2001) and landslides in Alpine lakes (e.g. Strasser et al., 2006). In conclusion, several studies have searched for paleoseismic evidence in Central Europe, mainly on a national basis. These studies can help determine paleoearthquakes, but there is definitely more research needed to understand the seismic cycle of active faults and to assess their seismic hazard.

The Paleoseismic Database for Germany and Adjacent Countries comprises all paleoseismic work that has been undertaken to date. Areas where paleoseismic data and historical and instrumental seismicity is missing suggest potential trenching or investigation sites for future paleoseismic studies. Besides that, the included collection of paleoearthquakes could be used to extend recent historical and instrumental earthquake catalogs. Until the compilation of the database, which is still in progress and will be finalized in a first version this year, we are open to extend it in some parts and integrate it with other projects. It is planned to publish the database for the general public and extend it with future studies. Detailed regularities on the published format and maintenance responsibilities are not finalized, yet.

**Acknowledgements:** We would like to thank the BGR Hannover (Federal Institute for Geosciences and Natural Resources, Germany) for its support.

## References

AHEAD, (2013). European Archive of Historical Earthquake Data, http://www.emidius.eu/AHEAD/main/, last access July 2013.

Ahorner, L., (2001). Abschätzung der statistischen Wiederkehrperiode von starken Erdbeben im Gebiet von Köln auf Grund von geologisch-tektonischen Beobachtungen an aktiven Störungen. *Mitteilungen der Deutschen Geophysikalische Gesellschaft e.V.*, 2001-2.

Basili, R., G. Valensise, P. Vannoli, P. Burrato, U. Fracassi, S. Mariano, M.M. Tiberti & E. Boschi, (2008). The Database of Individual Seismogenic Sources (DISS), version 3: Summarizing 20 years of research on Italy's earthquake geology. *Tectonophysics* 453 (1-4), 20-43.

Camelbeeck, T., K. Vanneste, P. Alexandre, P., K. Verbeeck, T. Petermans, P. Rosset, M. Everaerts, R. Warnant & M. Van Camp, (2007). Relevance of active faulting and seismicity studies to assessments of long-term earthquake activity and maximum magnitude in intraplate northwest Europe, between the Lower Rhine Embayment and the North Sea. *Geological Society of America Special Paper* 425, 193–224.

Delaby, S., (2001). Palaeoseismic investigations in Belgian caves. *Netherlands Journal of Geosciences* 80, 323–332.

Dèzes, P., S.M. Schmid & P.A. Ziegler, (2004). Evolution of the European Cenozoic Rift System: interaction of the Alpine and Pyrenean orogens with their foreland lithosphere. *Tectonophysics* 389 (1-2), 1–33.

Galadini, F., P. Galli, A. Cittadini, & B. Giaccio, (2001). Late Quaternary fault movements in the Mt. Baldo-Lessini Mts. sector of the Southalpine area (northern Italy). *Netherlands Journal of Geosciences* 80, 187–208.

García-Mayordomo, J., J.M. Insua-Arévalo, J.J. Martínez-Díaz, A. Jimenez-Díaz, R. Martín-Banda, S. Martín-Alfageme, J.A. Álvarez-Gómez, M. Rodríguez-Peces, R. Pérez-López, M.A. Rodriguez-Pascua, E. Masana, H. Perea, F. Martín-González, J. Giner-Robles, E.S. Nemser, J. Cabral & QAFI Compilers, (2012). The Quaternary Active Faults Database of Iberia (QAFI v. 2.0). *Journal of Iberian Geology* 38, 285–302.

Haller, K.M., M.N. Machette, R.L. Dart & B.S. Rhea, (2004). U.S. Quaternary Fault and Fold Database Released. *Eos Transactions* 85, 213.

Hintersberger, E., K. Decker, J. Lomax, M. Fiebig & C. Lüthgens, (2013). Fault linkage model of strike-slip and normal faults in the Vienna Basin based on paleoseismological constraints. *EGU General Assembly Conference Abstracts* 15, EGU2013–12755.

Kaiser, A., K. Reicherter, C. Hübscher & D. Gajewski, (2005). Variation of the present-day stress field within the North German Basin - insights from thin shell FE modeling based on residual GPS velocities. *Tectonophysics* 397 (1-2), 55–72.

Keefer, D.K., (1984). Landslides caused by earthquakes. *Geological Society of America Bulletin* 95, 406-421.

KTA (2011): *Kerntechnischer Ausschuss 2201.1. Auslegung von Kernkraftwerken gegen seismische Einwirkungen Teil 1: Grundsätze. Fassung 2011-11*. http://www.kta-gs.de/d/regeln/2200/2201_1_2011_11.pdf

Leydecker, G., (2011). Erdbebenkatalog für Deutschland mit Randgebieten für die Jahre 800 bis 2008. *Geologisches Jahrbuch* E (59).

McCalpin, J.P., ed., (2009). *Paleoseismology*, 2nd ed., Academic Press, San Diego.

Meghraoui, M., B. Delouis, M. Ferry, D. Giardini, P. Huggenberger, I. Spottke & M. Granet, (2001). Active normal faulting in the upper Rhine Graben and Paleoseismic Identification of the 1356 Basel earthquake. *Science* 293, 2070–2073.

Michetti, A.M., E. Esposito, et al., (2007). Environmental seismic intensity scale 2007 - ESI 2007. In: Vittori, E., Guerrieri, L. (eds.), Memorie Descrittive della Carta Geologica d'Italia, LXXIV. Servizio Geologico d'Italia, Dipartimento Difesa del Suolo, APAT, SystemCart Srl, Roma, Italy, pp. 7-54.

Obermeier, S.F., (1996). Use of liquefaction-induced features for paleoseismic analysis - An overview of how seismic liquefaction features can be distinguished from other features and how their regional distribution and properties of source sediment can be used to infer the location and strength of Holocene paleo-earthquakes. *Engineering Geology* 44, 1-76.

Peters, G., T.J. Buchmann, P. Connolly, R.T. van Balen, F. Wenzel & S.A.P.L. Cloetingh, (2005). Interplay between tectonic, fluvial and erosional processes along the Western Border Fault of the northern Upper Rhine Graben, Germany. *Tectonophysics* 406 (1-2), 39-66.

Reicherter, K., N. Froitzheim, M. Jarosiński, J. Badura, H.J. Franzke, M. Hansen, C. Hübscher, R. Müller, P. Poprowa, J. Reinecker, W. Stackebrandt, T. Voigt, H. von Eynatten & W. Zuchiewicz, (2008). Alpine tectonics II - Central Europe north of the Alps, in: McCann, T. (Ed.), *Geology of Central Europe*. Geological Society of London.

Skupin, K., K. Buschhüter, H. Hopp, K. Lehmann, R. Pelzing, J. Prüfert, M. Salamon, G. Schollmayer, A. Techmer & V. Wrede, (2008). Paläoseismische Untersuchungen im Bereich der Niederrheinischen Bucht. *Scriptum - Arbeitsergebnisse aus dem Geologischen Dienst Nordrhein-Westfalen*.

Strasser, M., F.S. Anselmetti, D. Fäh, D. Giardini & M. Schnellmann, (2006). Magnitudes and source areas of large prehistoric northern Alpine earthquakes revealed by slope failures in lakes. *Geology* 34, 1005.

Vanneste, K., T. Camelbeeck, & K. Verbeeck, (2013). A Model of Composite Seismic Sources for the Lower Rhine Graben, Northwest Europe. *Bulletin of the Seismological Society of America* 103, 984–1007.

Veloza, G., R. Styron, M. Taylor & A. Mora (2012). Open-source archive of active faults for northwest South America. *GSAT* 22, 4–10.

Wells, D.L. & K.J. Coppersmith, (1994). New empirical relationships among magnitude, rupture length, rupture width, rupture area, and surface displacement. *Bulletin of the Seismological Society of America* 84, 974–1002.

INQUA Focus Group on Paleoseismology and Active Tectonics

paleoseismicity.org

# A new methodology for the critical assessment of earthquake – related damage in archaeological contexts: a proof of concept for the 13th century BC in Minoan Crete (Late Minoan IIIB)

*Simon Jusseret (1), Charlotte Langohr (1), Manuel Sintubin (2)*

(1) F.R.S.-FNRS Postdoctoral Researcher, Université catholique de Louvain, Aegean Interdisciplinary Studies Research Group (AegIS-CEMA-INCAL), Place B. Pascal 1, L3.03.13, 1348 Louvain-la-Neuve, Belgium. Email: Simon.Jusseret@uclouvain.be

(2) KU Leuven, Geodynamics and Geofluids Research Group, Celestijnenlaan 200E, 3001 Leuven, Belgium. Email: Manuel.Sintubin@ees.kuleuven.be

***Abstract:*** *The 13th century BC (Late Minoan IIIB) represents a crucial period in the history of Crete (Greece), heralding the transition from the Bronze Age to the Iron Age through a series of destructions and abandonments. In this paper, we investigate the possibility that some of these events are related to earthquakes. For this purpose, we present a new methodology based on the recognition of Potential Earthquake Archaeological Effects (PEAEs) in archaeological sites. Reliability of PEAEs as indicators of seismic shaking is assessed based on empirical ground-motion relationships proposed for the three main types of earthquakes occurring in the area of Crete. At the sites of Malia and Sissi (north-eastern Crete), this methodology allows us to suggest that seismic shaking may represent a reasonable explanation for the observed PEAEs. A "12 October 1856 AD"-type earthquake located within the subducting African plate is suggested as a possible source for the observed damage.*

***Key words***: *archaeoseismology, Minoan civilization, Late Bronze Age collapse, Potential Earthquake Archaeological Effects.*

## INTRODUCTION

In Eastern Mediterranean archaeology, the 13th century BC is traditionally recognised as a major turning point marking the final demise of Bronze Age palatial societies and the shift towards a period of decreased social complexity conventionally called the Dark Ages (c. 1200-700 BC). Although the succession of events that led to this cultural crisis remain poorly understood, invasion of foreign populations (the so-called Sea People), internal social conflicts, climate change and earthquakes may all have played a significant role. Repeated seismic events ("seismic storm") have, in particular, been identified by Nur & Cline (2000) as responsible for site destruction and abandonment throughout the Eastern Mediterranean c. 1225-1175 BC – the so-called "Late Bronze Age paroxysm" (cf. Jusseret & Sintubin, 2013). However, Nur & Cline's (2000) hypothesis is based on a generalised model of seismic storms that may not apply to the entire Eastern Mediterranean basin. Moreover, their analysis relies on a restricted number of archaeological sites corresponding mainly to large settlements. These limitations are obvious in the context of Crete (*Fig. 1*), where three main earthquake mechanisms have been recognised (normal-faulting earthquakes, earthquakes on the subduction interface and earthquakes located within the subducting African slab, cf. Shaw & Jackson, 2010) and where numerous 13th century (Late Minoan (LM) IIIB) archaeological sites are known (cf. Langohr, 2009).

In this paper, we present a new methodology for the critical assessment of earthquake-related damage in LM IIIB archaeological contexts taking better account of the seismotectonic setting of the island (cf. Jusseret et al., accepted for publication, for an extensive discussion of our results). The study is based on a reappraisal of available archaeological data and on empirical ground-motion relationships corresponding to the three main earthquake mechanisms identified in the context of Crete. Our results indicate that most **Potential Earthquake Archaeological Effects (PEAEs)** identified in LM IIIB contexts cannot be confidently related to seismic shaking. Nevertheless, archaeological damage documented at the sites of Malia and Sissi (north-eastern Crete) may have been realistically caused by earthquake ground motions. A "12 October 1856 AD"-type earthquake located within the subducting African slab is suggested as a possible source of the earthquake-related damage at Malia and Sissi.

## SEISMOTECTONIC CONTEXT

The seismotectonic context of the Aegean is dominated by the Hellenic subduction zone resulting from the Africa-Eurasia convergence. The region is one of the most seismically active in Europe with high intermediate-magnitude seismic activity (Papazachos & Papazachou, 1997) (*Fig. 2*).

In the area of Crete, examination of focal mechanisms indicates three main types of earthquakes (*Fig. 3*).

1) Earthquakes in the subducting African lithosphere with approximately E-W P axes (here referred to as **"in-slab earthquakes"**). These earthquakes can be found in a 200 km-wide band parallel to the main bathymetric scarp of the Hellenic Trench (*Fig. 3*). Focal depths vary between 100 km in the western part of the Hellenic subduction zone and 170 km in its eastern sector. The destructive earthquake of 12 October 1856 AD (M 7.6 ± 0.3; cf. Papadopoulos, 2011) in the Aegean region most

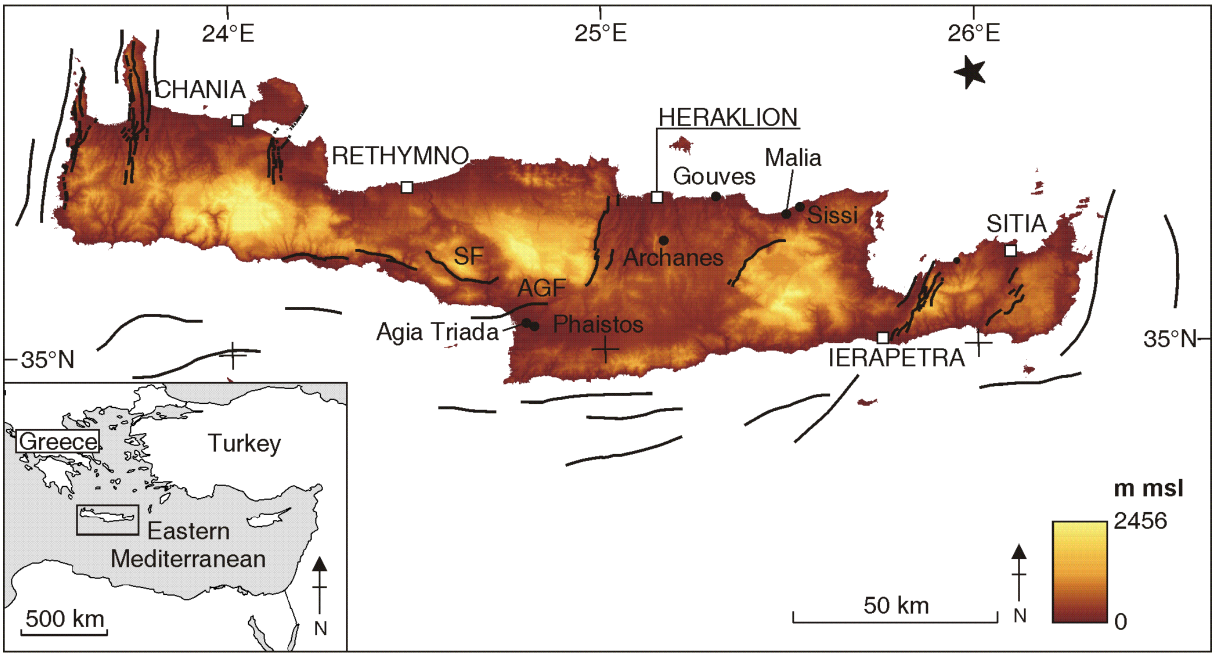


*Fig. 1: Location map showing archaeological sites (black circles) mentioned in the text and main modern towns (white squares). Black lines: active faults according to Caputo et al. (2010) and Mountrakis et al. (2012). SF: Spili Fault, AGF: Agia Galini Fault. Star: epicentral location of the 12 October 1856 AD earthquake according to Papazachos (1996). Inset: location of Crete within the Eastern Mediterranean basin. Background DEM courtesy of Laboratory of Geophysical-Satellite Remote Sensing & Archaeo-Environment (IMS-FORTH, Rethymno).*

likely corresponds to an in-slab event located between Crete and Santorini (*Fig. 1*).

2) Low-angle thrust earthquakes on the subduction interface and reverse-faulting earthquakes located on splay-faults merging with the interface at depth (here together considered as **"interface earthquakes"**). These earthquakes can be found in a 50-100 km-wide band following the Hellenic Trench (*Fig. 3*) and their focal depths generally do not exceed 45 km. Such an interface event (M 8.3, most probably located on a splay fault to the south-west of Crete) has been held responsible for the uplift of Crete by up to 10 m on 21 July 365 AD (e.g. Shaw et al., 2008).

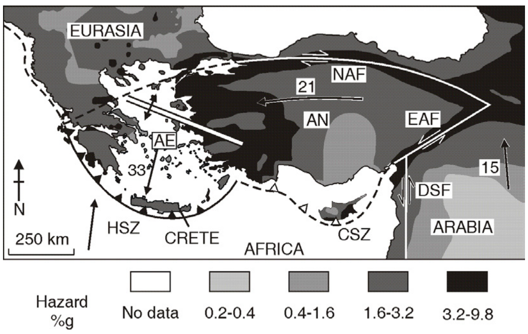


*Fig. 2: Seismotectonic setting of the Aegean region with seismic hazard (peak ground acceleration [%g] expected at 10% probability of exceedance in 50 years) after Global Seismic Hazard Assessment Program (cf. Giardini, 1999). GPS-derived plate velocities (mm/yr) relative to Eurasia according to Reilinger et al. (2006). HSZ: Hellenic subduction zone; CSZ: Cyprus subduction zone; AE: Aegean plate; AN: Anatolian plate; DSF: Dead Sea Fault; EAF: East Anatolian Fault; NAF: North Anatolian Fault.*

3) Earthquakes on predominantly N-S-oriented normal faults associated with the Aegean lithosphere (cf. Caputo et al., 2010). These **"normal-faulting earthquakes"** occur in a 150 km-wide region limited to the south by the Hellenic Trench (*Fig. 3*) and are usually shallower than 20 km. Destruction of the Minoan archaeological sites of Phaistos and Agia Triada (southern Crete) has been related to normal-faulting events, possibly located on the Spili and Agia Galini Faults (cf. Monaco & Tortorici, 2004) (*Fig. 1*).

## METHODOLOGY

*Potential Earthquake Archaeological Effects (PEAEs)*

To assess the possible role of earthquakes on LM IIIB site destructions and abandonments, we first established a comprehensive catalogue of archaeological sites occupied during LM IIIB. For each site, we then made an inventory of all earthquake archaeological effects (EAEs) based on available excavation reports and additional information provided by excavators. We define *Potential* Earthquake Archaeological Effects (PEAEs) to emphasize the uncertainty associated with the use of isolated EAEs as evidence for ancient earthquakes. PEAEs were defined according to existing classifications of EAEs (e.g. Rodríguez-Pascua et al., 2011) and adapted to the nature of Minoan archaeological relics frequently consisting of rubble architecture and associated stratigraphical evidence.

*Assessment of the ground-shaking levels and potential earthquake sources*

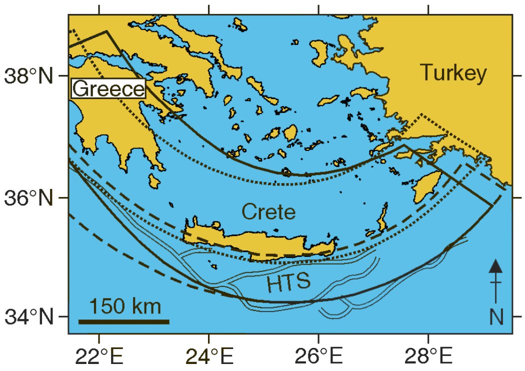


*Fig. 3: Schematic outline of areas of potential earthquake foci for the three main earthquake mechanisms identified near Crete. Thick black line: in-slab earthquakes (after Shaw & Jackson, 2010); dashed line: interface earthquakes; dotted line: N-S normal-faulting earthquakes after Benetatos et al. (2004). HTS: Hellenic Trench system after Shaw & Jackson (2010).*

The second step of our methodology was to evaluate the ground-shaking levels necessary for PEAEs to become visible in LM IIIB archaeological contexts.

Architectural characteristics of Minoan archaeological remains led us to expect that most PEAEs identifiable from excavation reports would relate to archaeological stratigraphical evidence (e.g. *in situ* broken vases, compact layers of rubble burying valuable objects and/or skeletons, localised fire damage, fallen oriented objects). In such circumstances, we estimated that PEAEs can only consistently appear in Minoan archaeological contexts if a non-negligible proportion of the building stock is subject to partial or total collapse (i.e. modified Mercalli intensities (MMI) ≥ VIII). Considering architectural characteristics of LM IIIB constructions (unreinforced rubble stone masonry), we then used Spence et al.'s (1992) fragility curves to suggest that MMI = VIII would result in partial or total collapse of c. 51% of LM IIIB constructions, against 16 % for MMI = VII. Since most LM IIIB archaeological sites consist of isolated buildings and small groups of buildings, we therefore considered MMI = VIII as a reasonable assignment for the minimum level of ground shaking necessary for PEAEs to become consistently visible on LM IIIB archaeological remains. In this study, we considered peak ground acceleration (PGA) as a measure of ground-motion intensity: for this parameter, updated empirical ground-motion relationships for the area of Greece indicate that MMI ≥ VIII correlate with PGA values ≥ 320 cm/s$^2$. Expected PGA values at LM IIIB archaeological sites were eventually assessed based on ground-motion relationships defined for the three main types of earthquakes defined in the area of Crete (Atkinson & Boore, 2003; Danciu & Tselentis, 2007), taking into account local geological conditions.

*Chronology*

Since no radiocarbon dates are available for LM IIIB archaeological contexts, we assessed the synchronicity of PEAEs between sites based on ceramic evidence. In some sites, this relative dating allowed us to obtain a chronological resolution of several decades corresponding to two ceramic sub-phases: LM IIIB1/early and LM IIIB2/late. This uncertainty led us to define the concept of the "*same earthquake*" as "*the main shock, its immediate aftershocks, as well as possibly triggered earthquakes on the same or neighboring fault segments during weeks to months after the main shock that initiated the PEAEs*".

## RESULTS AND DISCUSSION

In most LM IIIB archaeological sites, PEAEs cannot be confidently attributed to seismic shaking. The only credible evidence for earthquake-related damage can be found at LM IIIB1/early Malia and Sissi (*Fig. 1*). This evidence consists of primary (e.g. skeleton buried under rubble, localised fire damage, *in situ* broken vases) and secondary earthquake effects (e.g. stone heaps, discarded reparation material, blocked doorways sealing off collapsed structures) (*Fig. 4*).

Evaluation of possible seismic sources suggests that an in-slab earthquake of M ≥ 7.0 is capable of producing PGA values ≥ 320 cm/s$^2$ at Malia and Sissi. Such an event is comparable to the 12 October 1856 AD earthquake in the Hellenic subduction zone (*Fig. 1*). Available macroseismic intensity data for this event suggests that other LM IIIB1/early sites in central and eastern Crete may have been affected by the same earthquake. Interestingly, archaeological damage at two LM IIIB1/early sites in central Crete (Gouves, Archanes) (*Fig. 1*) has been explicitly related to seismic effects by their excavators. PEAEs recorded at Gouves and Archanes are, nevertheless, unable to ascertain this conclusion. Palaeoseismological investigations and quantitative modelling of the dynamic behaviour of Minoan constructions may, in the future, help us to assess the

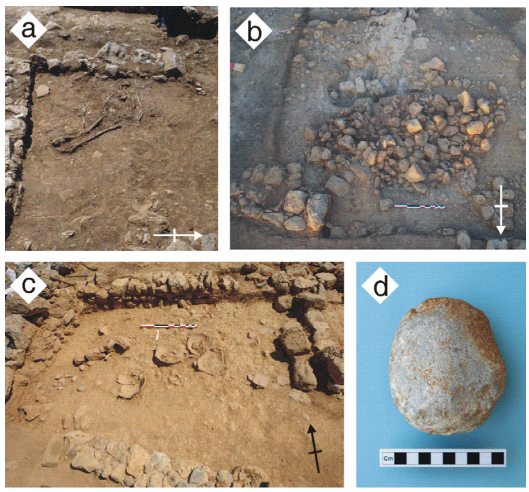


*Fig. 4: Examples of PEAEs at LM IIIB1/early Malia and Sissi. a) skeleton buried under rubble (Malia, photo courtesy of École française d'Athènes; b) pit covered by stone heap (Sissi, photo L. Manousogiannaki); c) in situ broken vessels (Sissi, photo F. Gaignerot-Driessen); d) stone tool (hammer-grinder) used for building activities and discovered in the pit illustrated in b) (Sissi, photo B. Chan).*

validity of our archaeoseismological hypothesis.

## CONCLUSION

In this research, we proposed a novel approach to ancient earthquakes in archaeological contexts dominated by rubble architecture and associated destruction layers, as exemplified in Minoan Crete. Application of this methodology to LM IIIB archaeological contexts allowed us to assess the reliability of PEAEs as indicators of earthquake ground motions. In the case of LM IIIB1/early Malia and Sissi, this proof of concept is successfully applied and suggests that a "12 October 1856 AD"-type earthquake – an in-slab earthquake – may be responsible for the observed PEAEs. On the other hand, our research does not support Nur & Cline's (2000) hypothesis according to which a seismic storm may have destroyed Minoan settlements towards the close of the LM IIIB period.

**Acknowledgements:** Part of this research benefited from the financial support of the Francqui Foundation through an Intercommunity postdoctoral fellowship granted to SJ. We are grateful to Jan Driessen and Alexandre Farnoux for allowing us to reproduce images from their respective excavations at Sissi and Malia. Apostolos Sarris kindly authorised the reproduction of the background DEM shown on Fig. 1. We are also indebted to members of AegIS (Maud Devolder, Florence Gaignerot-Driessen, Quentin Letesson, Christina Tsoraki) for sharing information regarding their work at Sissi.

## References

Atkinson, G.M., Boore, D.M. (2003). Empirical ground-motion relations for subduction-zone earthquakes and their application to Cascadia and other regions. *Bulletin of the Seismological Society of America* 93 (4), 1703-1729.

Benetatos, C., A. Kiratzi, C. Papazachos & G. Karakaisis, (2004). Focal mechanisms of shallow and intermediate depth earthquakes along the Hellenic arc. *Journal of Geodynamics* 37 (2), 253-296.

Caputo, R., S. Catalano, C. Monaco, G. Romagnoli, G. Tortorici & L. Tortorici, (2010). Active faulting on the island of Crete (Greece). *Geophysical Journal International* 183 (1), 111-126.

Danciu, L., Tselentis, G-A. (2007). Engineering ground-motion parameters attenuation relationships for Greece. *Bulletin of the Seismological Society of America* 97 (1B), 162-183.

Giardini, D. (1999). The global seismic hazard assessment program (GSHAP) – 1992/1999. *Annali di Geofisica* 42 (6), 957-974.

Jusseret, S., C. Langohr & M. Sintubin, (accepted for publication). Tracking earthquake archaeological evidence in Late Minoan IIIB (c. 1300-1200 BC) Crete (Greece): a proof of concept. *Bulletin of the Seismological Society of America*.

Jusseret, S., Sintubin, M. (2013). The origins of an old myth: Sir Arthur Evans, Claude Schaeffer and the seismic destruction of Late Bronze Age Eastern Mediterranean civilizations. *Seismological Research Letters* 84 (1), 94-100.

Langohr, C. (2009). *ΠΕΡΙΦΕΡΕΙΑ. Etude régionale de la Crète aux Minoen Récent II-IIIB (1450-1200 av. J.-C.). 1. La Crète centrale et occidentale*, Aegis 3, Presses Universitaires de Louvain, Louvain-la-Neuve, 315 pp.

Monaco, C., Tortorici, L. (2004). Faulting and effects of earthquakes on Minoan archaeological sites in Crete (Greece). *Tectonophysics* 382 (1-2), 103-116.

Mountrakis, D., A. Kilias, A. Pavlaki, C. Fassoulas, E. Thomaidou, C. Papazachos, C. Papaioannou, Z. Roumelioti, C. Benetatos & D. Vamvarakis, (2012). Neotectonic study of the western Crete. Seismic risk evaluation of the active faults. *Journal of the Virtual Explorer* 42, doi: 10.3809/jvirtex.2011.00285.

Nur, A., Cline, E.H. (2000). Poseidon's horses: plate tectonics and earthquake storms in the Late Bronze Age Aegean and Eastern Mediterranean. *Journal of Archaeological Science* 27 (1), 43-63.

Papadopoulos, G.A. (2011). *A Seismic History of Crete: The Hellenic Arc and Trench*, Ocelotos, Athens, 415 pp.

Papazachos, B. C. (1996). Large seismic faults in the Hellenic Arc. *Annali di Geofisica* 39 (5), 891-903.

Papazachos, B., Papazachou, C. (1997). *The Earthquakes of Greece*, Ziti, Thessaloniki, 304 pp.

Reilinger, R., S. McClusky, P. Vernant, S. Lawrence, S. Ergintav, R. Cakmak, H. Ozener, F. Kadirov, I. Guliev, R. Stepanyan, M. Nadariya, G. Hahubia, S. Mahmoud, K. Sakr, A. ArRajehi, D. Paradissis, A. Al-Aydrus, M. Prilepin, T. Guseva, E. Evren, A. Dmitrotsa, S.V. Filikov, F. Gomez, R. Al-Ghazzi & G. Karam, (2006). GPS constraints on continental deformation in the Africa-Arabia-Eurasia continental collision zone and implications for the dynamics of plate interactions. *Journal of Geophysical Research* 111 (B5), B05411, doi: 10.1029/2005JB004051.

Rodríguez-Pascua, M.A., R. Pérez-López, J.L. Giner-Robles, P.G. Silva, V.H. Garduño-Monroy & K. Reicherter, (2011). A comprehensive classification of Earthquake Archaeological Effects (EAE) in archaeoseismology: application to ancient remains of Roman and Mesoamerican cultures. *Quaternary International* 242 (1), 20-30.

Shaw, B., N.N. Ambraseys, P.C. England, M.A. Floyd, G.J. Gorman, T.F.G. Higham, J.A. Jackson, J.-M. Nocquet, C.C. Pain & M.D. Piggott, (2008). Eastern Mediterranean tectonics and tsunami hazard inferred from the AD 365 earthquake. *Nature Geoscience* 1, 268-276.

Shaw, B., Jackson, J. (2010). Earthquake mechanisms and active tectonics of the Hellenic subduction zone. *Geophysical Journal International* 181 (2), 966-984.

Spence, R.J.S., A.W. Coburn, A. Pomonis & S. Sakai, (1992). Correlation of ground motion with building damage: the definition of a new damage-based seismic intensity scale. In: *Proceedings of the Tenth World Conference on Earthquake Engineering, 19-24 July 1992, Madrid, Spain*, A.A. Balkema, Rotterdam, 551-556.

INQUA Focus Group on Paleoseismology and Active Tectonics

paleoseismicity.org

# Locating the on-land continuation of the submarine Avrona Fault, Gulf of Aqaba-Eilat, Israel

*Kanari, Mor (1), Tina M. Niemi (2), Shmuel Marco (1), Zvi Ben-Avraham (1),(3), Gideon Tibor (4), Abdallah Al-Zoubi (5), Abdelrahman Abueladas(5), Uri Basson (6), Neta Wechsler (1), Julie M. Bauer (2), Gal Hartman, Revital Bookman (3), Beverly N. Goodman-Chernov (3),(7)*

(1) Dept. of Geophysical, Atmospheric and Planetary Sciences, Tel-Aviv University, Tel-Aviv, Israel. Email: kanarimo@tau.ac.il
(2) Dept. of Geosciences, University of Missouri-Kansas City, MO 64110, U.S.A.
(3) Dept. of Marine Geosciences, Leon H.Charney School of Marine Sciences, Haifa University, Mt. Carmel, Haifa 31905, Israel
(4) Israel Oceanographic & Limnological Research Ltd., Tel-Shikmona, P.O.Box 8030, Haifa 31080, Israel
(5) Al Balqa Applied University, Al-Salt 19117, Jordan
(6) Geosense, Environmental and Engineering Geophysics, P.O.Box 921, Even-Yehuda 40500, Israel
(7) Interuniversity Institute for Marine Sciences, Eilat 88103, Israel

***Abstract:*** *Located at the Northern tip of the Gulf of Aqaba-Eilat, the on-land continuation of the submarine Avrona Fault underlies the Hotels District of Eilat, where seismic deformation was documented after the 1995 Nuweiba (Sinai) earthquake (7.2 Mw). This active segment of the Dead Sea Fault is the transition between the deep marine basin of the Gulf and the shallow continental basin of the Arava Valley. We try to locate the fault on-land and recover its seismic record. The trenching site was selected based on extrapolating the submarine Avrona Fault, 1945 aerial photos, and GPR survey. Trench T3 revealed liquefaction features and the fault trace: five distinct units (up to ~1.5 m depth below surface) with cumulative normal offset of ~50-60 cm. 14C dating of charcoal yield age and slip rate constraints. We suggest that the fault located at T3 is the on-land continuation of the submarine Avrona Fault.*

***Key words****: Dead Sea Fault, Avrona Fault, Paleoseismic trenching, Gulf of Aqaba-Eilat, GPR.*

## INTRODUCTION

At the north tip of The Gulf of Aqaba-Eilat (the northeast extension of the Red Sea; *Fig. 1*), reside the cities of Eilat (Israel) and Aqaba (Jordan): major economic, cultural, and recreational centers of southern Israel and Jordan, and vital aerial and naval ports. It so happens that they are both also built on active faults, which have ruptured in the past. Aqaba was completely destroyed in the 1068 AD earthquake (Ambraseys et al., 1994; Avner, 1993), and significant damage to structures in both Eilat and Aqaba was inflicted by the Nuweiba earthquake (22.11.1995; Mw 7.2) even though the epicenter was located 70 km to the south (Klinger et al., 1999). The estimation of seismic hazard to these neighboring cities is therefore vital. The peaceful hotels and beaches of Aqaba and Eilat are located on a tectonic plate boundary, which is also a transition zone between two crustal realms of the Dead Sea Fault system (DSF): the deep en-echelon submarine basins of the Red Sea (Ben-Avraham, 1985) and the shallow continental basins of the Arava (Frieslander, 2000), localizing into a single fault strand heading northward.

Previous studies of the submarine structure of the Northern Gulf of Aqaba-Eilat (NGAE) suggest slip on the east and west boundary faults is predominantly normal and recently active (Ben-Avraham, 1985; Ben-Avraham et al., 1979; Ben-Avraham and Tibor, 1993). However, recent high-resolution seismic and bathymetric data (Tibor et al., 2010; Hartman, 2012) revealed a complex fault system across the shelf of the NGAE with varying degrees of recent seismic activity, dividing the shelf into three blocks, of which the westernmost, the Eilat sub-basin, is bounded by the Eilat and Avrona faults. Hartman (2012) concludes the most active segment is the Avrona Fault (Evrona Fault in some papers), which takes most of the left-lateral slip within the basin with an average sinistral slip-rate of 0.5±0.1 mm/y through the Late Quaternary and 4±2.3 mm/y during the Holocene *(Fig. 2)*. Suggesting a Holocene normal slip-rate of ~1mm/y on the Avrona Fault, Hartman concludes that the fault is relatively young (Late Quaternary) and that its seismic activity has increased through recent time.

On-shore, several works estimated the location of the Avrona Fault at the border of the Eilat Sabkha (Garfunkel et al., 1981) and in the vicinity of the Eilat hotel district (Wachs and Zilberman, 1994). Using seismic imaging, Rotstein et al. (1994) suggested a vertical deformation band of several hundred meters wide below the eastern part of the Eilat Hotel District. Further seismic data was used by Frieslander (2000) to suggest a distinct sub-vertical discontinuity in the sediments in the same area in Eilat. Active surface faulting was observed following the Nuweiba (Sinai) earthquake in 1995 (epicenter 70 km south to Eilat), when an offset street was reported in the same hotels area (Wust, 1997). Some15 km farther north, Paleoseismic trenching in the Avrona Playa revealed late Pleistocene earthquake ruptures displaced 1-1.5m with estimated magnitudes M6.7-M7, and Holocene earthquakes displacing 0.2-1.3m with estimated magnitudes M5.9-M6.7 (Amit et al., 2002). However, the location and the paleoseismic record of the on-land continuation of the Avrona Fault, as it emerges from submarine to terrestrial domain, was not known.

## OBJECTIVE AND METHODOLOGY

We aim to locate the on-land continuation of the active submarine Avrona Fault, which underlies the Hotels District at the northern beach of Eilat (Israel) and recover its seismic record. We integrated newly suggested offshore fault location (Hartman, 2012), analysis of aerial photos from 1945, and Ground Penetrating Radar (GPR) survey to hypothesize the fault location for paleoseismic trenching site selection. Trenching revealed the fault and associated liquefaction features. Dating trench strata is in progress.

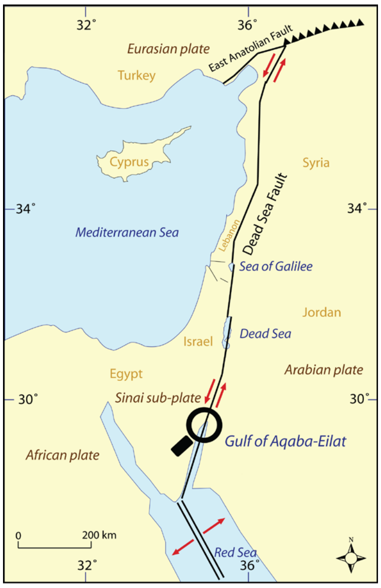


*Fig. 1 Regional tectonic overview of the Dead Sea Fault. Northern Gulf of Aqaba-Eilat (NGAE) marked in black magnifier symbol; red arrows note relative tectonic plate motion (modified after Ben-Avraham et al., 2008).*

## RESULTS AND DISCUSSION

Analysis of aerial photos from 1945 (PS 6003) lead to hypothesize two lineaments as fault traces at the eastern boundary of the Eilat sabkha (Fig. 2; red dashed lines).

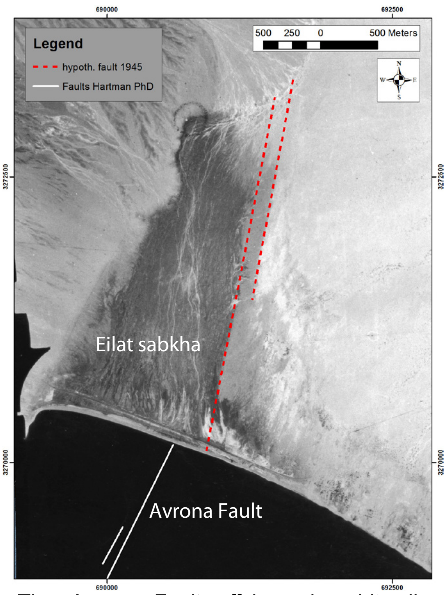


Fig 2. The Avrona Fault offshore in white line (after Hartman, 2012) and the hypothesized on-land fault trace continuation (red dashed line) based on lineaments on the eastern boundary of the Eilat sabkha in a 1945 aerial photo (PS 6003 aerial).

Constrained by the hypothesized fault trace and the offshore fault, a Ground Penetrating Radar (GPR) survey was held, in order to locate potential sites for trenching. The area is on the border between the Eilat Sabkha (west) and the fluvial environment of Wadi Arava (east), as apparent from the 1945 aerial photos *(Fig. 2)* Several potential subsurface deformations were singled out from GPR data; one of them (lines 103a and 103b) is detailed in *Fig 3*. It crosses a dirt road which has significant change in GPR data from each side, suggesting possible deformation. New palm trees were recently planted on the west side (103a), which according to the local farmers shows differences in palm tree growth rate and fertility, and ground water table depth (shallower) from the east side of the dirt road (103b). These imply possible faulting, yet the testified change in water content may impact GPR data and mask it on the west side (103a). We could not trench that site due to farming constraints. All GPR profile locations (light-blue lines) and interpreted GPR anomalies (blue circles) are presented in *Fig. 4*. A zone of several adjacent GPR anomalies was interpreted as 'anomaly zone' (blue thick line in *Fig. 4*). Most anomalies detected were at estimated depths of 3.5-4 m and deeper. The top 2.5 m in the palm plants are disturbed by planting, irrigation and palm tree roots.

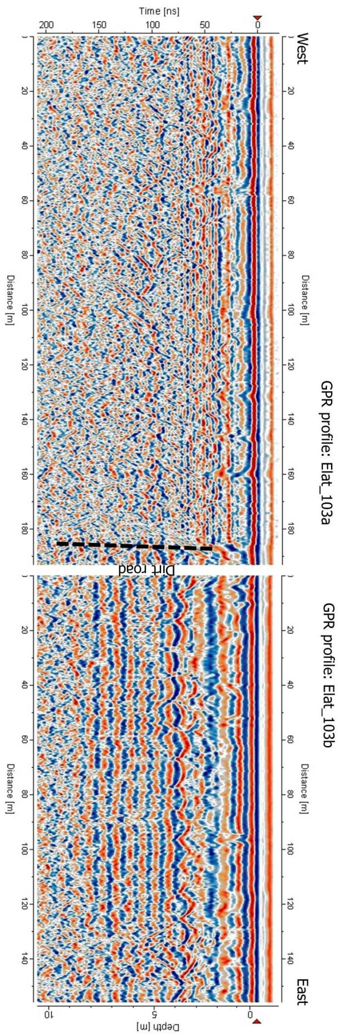


*Fig. 3. GPR lines 103a and 103b (a dirt road separates between the two segments). Distinct change in subsurface observed near the eastern end of line 103a, interpreted as possible fault (black dashed line). Data acquired using 100 MHz antenna. See Fig.4 for profile location. Data collected using RAMAC GPR system, 100 MHz antenna, trx-rx offset 1m, station interval 0.25m; GPR pulses sampled at 1340 MHz and stacked 16–32 times; average 0.1 m/ns used for depth conversion.*

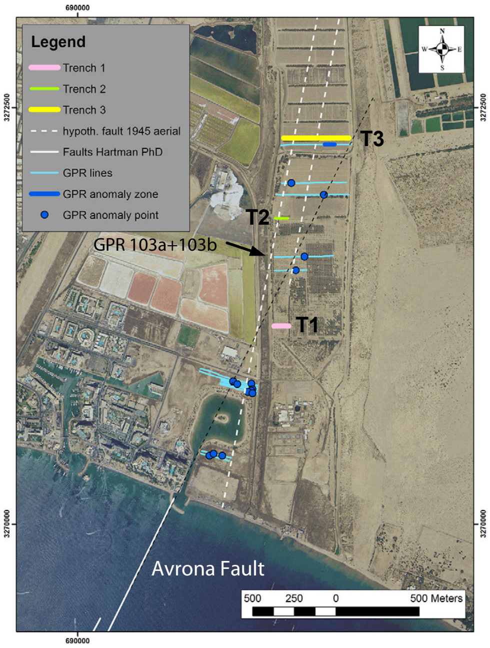


*Fig. 4. Trenching sites: Trench T1 (pink) and later T2 (green; ground water at 50cm) and T3 (yellow) were excavated following analysis of the extrapolation (black dashed line) of the offshore Avrona Fault (white solid line; after Hartman, 2012), GPR data and 1945 aerial photos. The GPR profile for lines 103a+103b is presented in Fig 3.*

Integration of all the above data *(Fig. 4)*, including the extrapolated projection of the offshore fault, and excavation permit limitations, lead to selection of a trenching site at the agricultural zone at the NE part of the study area. The first trench (T1, pink line in *Fig 4*) revealed liquefaction deformation features, but no fault trace was evident. The second trench (T2) hit ground water at 50 cm depth.

Trench T3 (~400 m long; yellow line in *Fig. 4*, photo in *Fig. 6*) hit ground water table at ~1.5 m depth. However, it revealed both liquefaction features and the fault trace itself. Five distinct units (at depths up to ~1.5 m below surface) with cumulative normal offset of ~50-60 cm were observed at the fault *(Fig 5)*. Charcoal samples were located and sampled for 14C dating. No faulting was evident at the eastern part of T3, where the GPR interpreted 'anomaly zone' was located. However, trench depth there did not reach more than 1.5 m. Two interpretations are suggested: either there's no faulting there, or it ruptured in earlier times, before the deposition of the current top 1-2 m (in agreement with GPR data there, implying deformation at depths >4 m).

Faulted trench strata are from the top 1.5 m, suggesting the fault is recently active. 14C Age determination yield age and slip rate constraints of the faulting. Dating of the liquefaction sandblows (in progress) may correlate to liquefaction features documented after the 1995 Nuweiba earthquake, or to earlier surface rupture.

*Fig. 5. (opposite) Trench T3 (north wall) log at the fault zone (E-W section). Five distinct units demonstrate a normal offset of ~50-60 cm; yellow hexagons mark 14C dating samples. Fault marked by a red star in Fig. 7.*

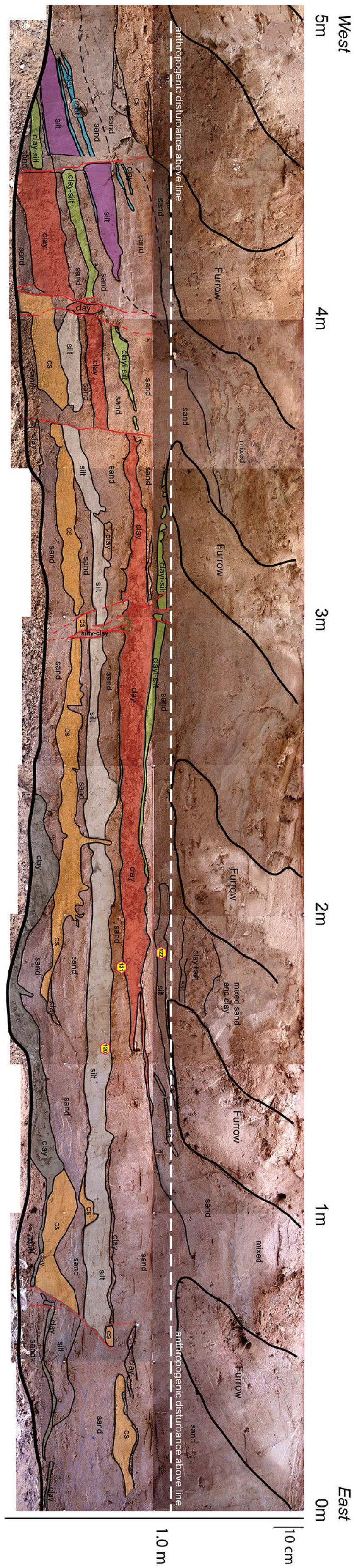

*Fig. 6. Overview of trench T3 looking west towards Eilat.*

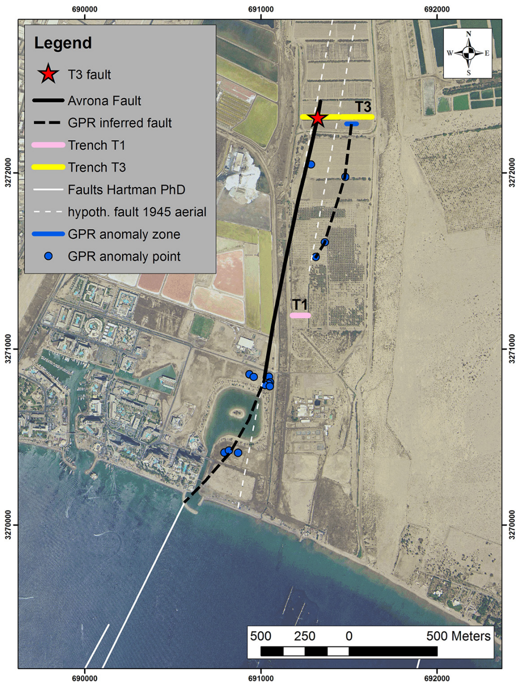


*Fig. 7. Suggested trace of the on-land continuation of the Avrona Fault in black solid line, following offshore seismic data, trench T3 fault location (red star), inferred GPR data and aerial photo morphologic analysis (white dashed line); GPR inferred fault segments in black dashed line; offshore Avrona Fault trace (white solid line) after Hartman (2012).*

Integrating offshore and on-land evidence for faulting, while considering other data that imply subsurface deformation, we suggest that the fault located at T3, as we trace it in *Fig 7*, is the on-land continuation of the submarine Avrona Fault, an active segment of the Dead Sea Fault, at its transition zone from marine to continental structural framework. It is possible that such a transition may be associated with some lateral segmenting of the deformation along time which could explain the geophysical evidence for subsurface deformation (GPR anomalies) with no evidence for current shallow surface rupture – thus yielding a deformation zone of some thickness (fault zone). Perhaps deeper trenching (using pumping due to the shallow ground water level) can reveal evidence to support that. Age determination of trench offset strata may correlate it to past earthquakes (e.g. the 1068 AD destruction of Aqaba) and shed light on the fault slip rate, thus augmenting our understanding of the dominance of this segment among the total slip on the Dead Sea Fault plate boundary in this region. This work is in progress.

**Acknowledgements:** The project was funded by USAID-MERC project TA-MOU-08-M29-036. We wish to thank the people of the farming and plants staff of Kibbutz Eilot (Israel), and especially Rafi Saar, for their good will and kind assistance during trenching excavations in their lands. We thank Tomer Ketter, Lisa Coianiz and Lana Ashqar for aiding in field work.

## References

Ambraseys, N.N., C.P. Melville and R.D.Adams , (1994). *The Seismicity of Egypt, Arabia and the Red Sea*. Cambridge University Press. 181 p.

Amit, R., E. Zilberman, Y. Enzel and N. Porat,(2002). Paleoseismic evidence for time dependency of seismic response on a fault system in the southern Arava Valley, Dead Sea rift, Israel. *Geological Society of America Bulletin*, v. 114, 192-206.

Avner, U., (1993). The history of the southern Negev and Elat in the light of new studies. In: *Elat—Man, Sea and Desert* (Cohen, M., and Shiler, E. eds). Ariel Press, Israel,113–184.

Ben-Avraham, Z., (1985). Structural Framework of the Gulf of Elat (AQABA), Northern Red Sea. *J. Geophys. Res.*, v. 90, 703-726.

Ben-Avraham, Z., G. Almagor, and Z. Garfunkel, (1979). Sediments and structure of the Gulf of Elat (Aqaba)-Northern Red Sea. *Sedimentary Geology*, v. 23, 239-267.

Ben-Avraham, Z., and G. Tibor, (1993). The northern edge of the Gulf of Elat. *Tectonophysics*, v. 226, 319-331.

Ben-Avraham Z., Z. Garfunkel and M. Lazar, (2008). Geology and Evolution of the Southern Dead Sea Fault with Emphasis on Subsurface Structure. *Annual Review of Earth and Planetary Sciences*, 36, 357-387.

Frieslander, U., (2000). The structure of the Dead Sea transform emphasizing the Arava, using new geophysical data [Ph.D. thesis], Hebrew University, Jerusalem.

Garfunkel, Z., I. Zak, and R. Freund, (1981). Active faulting in the Dead Sea Rift. *Tectonophysics*, v. 80, 1-26.

Hartman, G., (2012). Quaternary Evolution of a Transform Basin: The northern Gulf of Elat/Aqaba [Ph.D. thesis], Tel Aviv University, Tel Aviv.

Klinger, Y., L. Rivera, H. Haessler and J.C. Maurin, (1999). Active faulting in the Gulf of Aqaba: New knowledge from the MW 7.3 earthquake of 22 November 1995. *Bulletin of the Seismological Society of America*, v. 89, 1025-1036.

Rotstein, Y., U. Frieslander and Y. Bartov, (1994). Detailed seismic imaging of the Dead Sea Transform. In: *Elat: Inst. Pet. Geophys.* 11.

Tibor, G., T.M. Niemi, Z. Ben-Avraham, A. Al-Zoubi, R. Sade, J.K. Hall, G. Hartman, E. Akawi, A. Abueladas and R. Al-Ruzouq, (2010). Active tectonic morphology and submarine deformation of the northern Gulf of Eilat/Aqaba from analyses of multibeam data. *Geo-Marine Letters, 30 (6), 561-573*.

Wachs, D., and E. Zilberman, (1994). Preliminary evaluation of the seismic hazard in the Elat area. *Geol. Surv. Israel Report 13/94*. 53 p. (Hebrew, English abstract).

Wust, H., (1997). The November 22, 1995 Nuweiba earthquake, Gulf of Elat (Aqaba): postseismic analysis of failure features and seismic hazard implications: *Geol. Surv. Israel. Report GSI/3/1997.*

INQUA Focus Group on Paleoseismology and Active Tectonics

paleoseismicity.org

# The rocking columns of Poreč – archaeoseismology in the Istria Peninsula, Croatia

*Miklos Kazmer (1)*

(1) Department of Palaeontology, Eötvös University, Pázmány sétány 1/c, H-1016 Budapest, Hungary. Email: mkazmer@gmail.com.

***Abstract:*** *The Istria Peninsula in Croatia has a number of monuments from Antiquity, which bear evidence of major earthquakes. The Eufrasius Cathedral of Poreč, built in the 6th century, collapsed in parts dut to the 1440 earthquake. Nave and aisles are screened by 18 monolithic marmor columns. Azimuths of dip directions of chipping planes on tops and bottoms indicate N-S shaking. Wall of the apse and the nave, together with supporting columns, has been twisted. Floor of the 6th century cathedral is 1.9 m above the mosaic floor of a pre-existing 4th century cathedral. The latter one, being 0.3 m above high tide leve, only a few metres away from the sea, suggests that there was major coastal subsidence. This event dates the submergence of marine notches of the Adriatic coast between Trieste and Zadar (200 x 80 km area) between 4th and 6th century. Earthquake-damaged Arch of the Sergi in Pula (29-27 BC) testifies to site effects nearby the intact Roman amphitheatre. These findings indicate that Istria's ranking among regions of low seismic hazard in Croatia is to be re-considered.*

***Key words***: *archaeoseismology, Croatia, Roman age, antiquity, Middle Ages, Porec, Pula*

## INTRODUCTION

The Istria Peninsula in the northern Adriatic Sea is considered as low-seismicity area, being external to the active faults of the Dinaric frontal range (Fig. 1). Here we report a preliminary survey of buildings surviving from Antiquity, which bear evidence for major earthquakes.

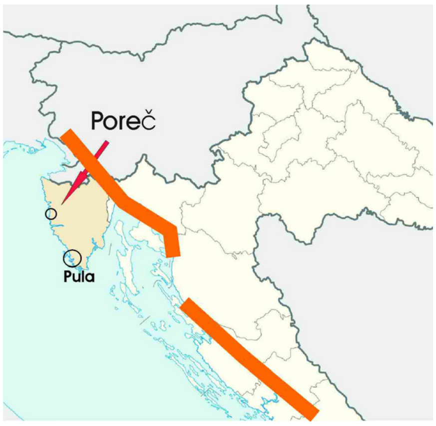


*Fig. 1. Istria with studied localities in Croatia. High-seismicity zone of the Dinaric front marked by red (after Markušić & Herak, 1999).*

## POREČ

Roman Parentium (Italian Parenzo, Croatian Poreč) has been a small coastal city in Late Antiquity. Its episcopal complex, built in 4-6th century, however, is one of a handful of Justinianic monuments to survive essentially intact (Molajoli, 1943). It holds a unique position in the art and architecture of the Early Christian era. The surviving entire cathedral complex – built by bishop Eufrasius in the 6th century – is virtually unparalleled The complex encompasses a basilica, an atrium, an episcopal palace, and a triconch chapel. The surviving decorative program includes architectural sculpture and furnishings and stucco, along with the superbly preserved wall and floor mosaics (Terry & Maguire, 2007).

In accord with Christian practice, the basilica is oriented east-west. The ground plan forms a slightly irregular rectangle, measuring approx. 19.5 m in width and 38 m in length. Two colonnades, each composed of nine marmor columns, screen the wide central nave from its two narrower, flanking side aisles. At the east, nave and aisles terminate in apses. The main apse projects externally, enclosed by a hexagonal wall; the side apses are inscribed in the masonry of the eastern wall. In elevation the central nave projects above the side aisles. The nave stands ca 18 m tall. The side aisles rise to a height of ca. 11 m (Fig. 2).

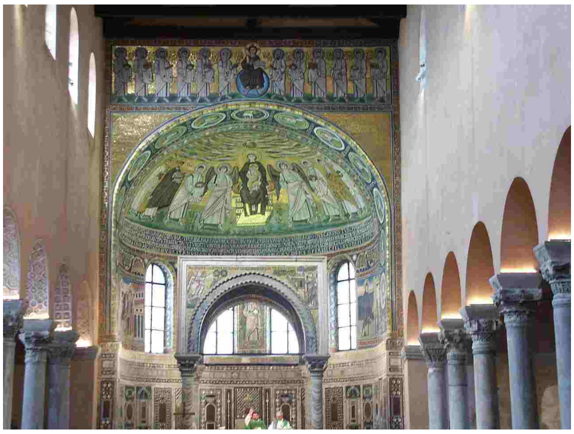

*Fig. 2. The Byzantine cathedral of Eufrasius in Poreč, 6th century. Inside view. Note that the left, northern side of the triumphal arch deviates from the vertical. Photo: Loris Romito. http://it.wikipedia.org/wiki/ File:BasilicaMosaici_1.jpg. Accessed 16 June 2013.*

In 1440, the basilica was seriously damaged by an earthquake which toppled the upper wall of the nave and most of the south aisle (Babudri, 1913). The columns of the south aisle sustained some damage, while the stucco relief work on the intrads of the south colonnade was completely destroyed.

Columns supporting the nave are of Proconnesian marble imported from the island of Marmara in the Marmara Sea (Terry, 1988: 27). The columns are of approximately uniform height: they range from 3.39 m to 3.58 m. The circumferences at the base of the shafts vary from 1.52 m to 1.77 m. A number of columns are damaged (Figs 3-4) (Terry, 1984; Terry, 1988: 27-28).

*Fig. 3. Adjacent chipping both in pillar and capital. Pillar F. #0080*

*Fig. 4. Chipping in pillar. The adjacent fracture to the right outlines a second chip. Pillar A, plinth. #0076*

**EARTHQUAKE DAMAGES**

Various damages have been observed on the columns: chipped tops and bottoms are common. These were formed when seismic excitation and torsion made the columns rock on the plinth (see Stiros, 1996, fig. 6a).

Chipped parts are either lost, replaced, or repaired with concrete. There are fractures in various dimensions (closed fractures are from geological ages, open fractures are from the site). Part of them are filled. Major fractures are reinforced with old-looking metal rings, now joined with new screws. A detailed list of damages is available in Terry (1988, footnote 71).

The walls of the southern aisle were rebuilt with Gothic windows, while the remainders are in Roman style. It is clear that the south arcade has sustained serious damage, probably from the 1440 earthquake (Terry, 1988, footnote 71).

In addition we measured the azimuth of the chipped and fractured damages by compass and plotted them on Fig. 5.

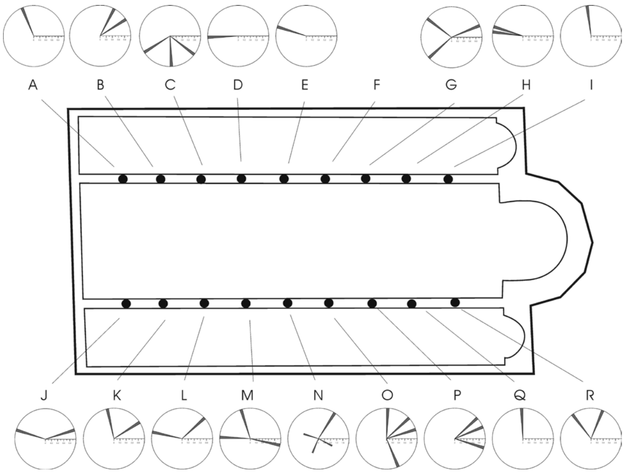


*Fig. 5. Floor plan with azimuths of dip directions of the chipping planes as observed on pillars. Most of them are of no special direction, supporting the conviction that columns are not suitable to determine the direction of earthquake epicentres (Hinzen, 2009). We should note, however, that the Eufrasius columns are fixed both at the base and at the top, therefore bound to move with the rest of the building as long as collapse does not occur. We noted that many directions are towards the north, rather than to the south. Another, prominent direction is more or less parallel with the church axis. Were thesef free-standing columns, one would account them to N-S strong motion, while it is not necessarily the case here. N-S is the easiest way of significant free vibration of the building, perpendicular to the main axis of the cathedral. Northern row F: it is the sole column without chipping.*

We noted that walls and columns of the cathedral deviate from the vertical. Northern part of the triumphal arch is clearly tilted outwards (Fig. 2), and top of the adjacent column has shifted about 10 cm to the north as well. Northern wall of the nave is mildly twisted, tilted outwards together with the triumphal arch. An earthquake origin is suggested for similar features, among others, by Kamh et al. (2008). It is noted that the cathedral is not rectangular! Whether it is due to fault dislocation (for an example see Karakhanian et al., 2008) or not, we cannot tell at the moment.

*Earthquake parameters*

An earthquake occurred in 1440 (Babudri, 1913), which can be responsible for most of the damages visible in the cathedral. We suggest the earthquake intensity is IX on the Rapp scale (Rapp, 1986): IX – good masonry damaged seriously. It yields a M 6.6-7.1 event on the Richter scale.

## SEA LEVEL

The 6th century Eufrasius cathedral has been built on top of at least three previous churches, each marked by a buried mosaic floor (Molajoli, 1940; Terry, 1995; Matejčić & Chevalier, 1998). The mosaic floor of the lowermost one, constructed in the 4th century, is 1.9 m below the 6th century Eufrasius cathedral. The lower one, being a mere 30 cm above high tide level, standing no more than 10 m from the sea, is subject to inundations several times a year. It is an improbable elevation for a church as important as this one.

The Istria coastline is known to have been subsided significantly since Roman times, marked by submerged marine notches and submerged Roman ports and other buildings along the coastlines (e.g. Faivre et al., 2010). Suggested dates for submergence range from 361 AD (Benac et al., 2004) to 1500 AD (Faivre et al., 2011). The anomalously low position of the lowermost mosaic level indicate that subsidence occurred between the construction dates of the first and the last cathedrals, i.e. between the 4th and 6th century. Whether the intercalated two mosaic-covered floor levels are related to one or more subsidence events, can be a matter of discussion. We suggest that the subsidence, which lowered all Istria by about 0.5 to 1 m, occurred between 4th and 6th century. Flat top of most submerged marine notches is evidence for single, rapid, seismic subsidence event (Pirazzoli & Evelpidou, 2012).

## PULA

Good preservation of the Pula amphitheatre, better preserved than the Colosseum in Rome, suggested to most that that there was no major earthquake in the region during the last two millennium. The amphitheatre's foundation is lying on solid Cretaceous limestone, therefore site effects were probably minimal.

The triumphal Arch of the Sergi at the former city gate of Pola (Porta Aurea) was built between 29 and 27 BC (Dzin, 2009). Apart from minor modern restoration it did not change any during the last two millennia (Fig. 6). Close observation of the masonry revealed various damages attributable to seismic activity. Shifted stones of the arch (Fig. 7) are clearly of the dropped keystone type, described by various authors (e.g. Marco, 2008) as foolproof evidence of earthquake shaking. Broken corners of blocks are further evidences of seismic shaking (Caputo & Helly, 2005; Rodriguez-Pascua et al., 2011).

As the Porta Aurea stands on soft soil, certainly site effects yielded a much higher level of damage than in the virtually undamaged amphitheatre.

## IMPLICATIONS FOR SEISMIC HAZARD

Druing the last two milennia Porec and the rest of the Istria peninsula were a seismically quiet area – this is the general understanding, expressed by the seismic zonation scheme of Croatia (Markušić & Herak, 1999). An M 5.1-6.0 seismic event offshore Porec is indicated in the earthquake map of Croatia. However, there are frequent earthquakes above M 6.0 along the various faults of the Dinaric front, 60-70 km to the NE both from Poreč and Pula (Markušić & Herak, 1999)

*Fig. 6. Western facade of the Porta Aurea in Pula.*

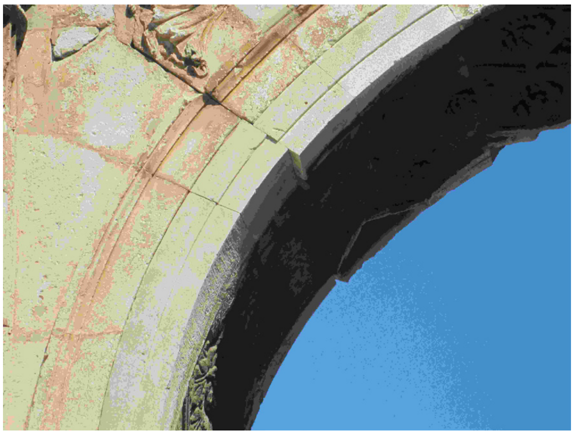

*Fig. 7. Porta Aurea, western façade, dropped ashlar in the arch.*

The AD 1440 earthquake, which damaged the Poreč cathedral, is not listed in historical catalogues (Herak et al., 1998; Ambraseys, 2009). It was certainly larger than the M 5.1-6 offshore event nearby, which is listed. Whether active faults of the the Dinaric front, those of the Čičarija-Učka range (Prelogovic in Markušić & Herak, 1999), or a suspected fault offshore Istria is responsible, is a matter of further considerations.

The even larger earthquake, which made the old cathedral of Porec and all of Istria submerge by about 0.5-1 m, is a mystery at the moment. All we know is that the area from Trieste in the north to Zadar in the south (about 200 km long and 80 km wide) has been submerged (Faivre et al., 2010). As the mechanism is unknown as yet, we cannot offer any clues for magnitude. It was a big shock anyway, bigger than any other during the last 2000 years.

**Acknowledgements:** Support of Hungarian Science Foundation grant OTKA K67.583 is sincerely acknowledged.

## References

Ambraseys, N. (2009). *Earthquakes in the Mediterranean and the Middle East. A Multidisciplinary Study of Seismicity up to 1900*. Cambridge University Press, 947 p.

Babudri, F. (1913). Le antiche chiese di Parenzo. Parenzo nella storia ecclesiastica. – *Atti e Memoria della Società Istriana di Archeologia e Storia Patria* 29, 83-207.

Benac, C., M. Juracic & T. Bakran-Petricioli, (2004). Submerged tidal notches in the Rijeka Bay NE Adriatic Sea: indicators of relative sea-level change and of recent tectonic movements. *Marine Geology* 212, 21-33.

Caputo, R. & B. Helly, (2005). Archaeological evidences of past earthquakes: A contribution to the Sha of Thessaly. *Journal of Earthquake Engineering* 9 (2), 199-222.

Dzin, K. (2009). Figural and floreal reliefs on the Sergii Arch in Colonia Pola. *Jurišićev zbornik* 2009, 143-150.

Faivre, S., E. Fouache, V. Kovacic & S. Gluscevic, (2010). Some geomorphological and archeological indicators of Croatian shoreline evolution over the last 2000 years, *Geology of the Adriatic area. GeoActa Special Publication* 3, 125-133.

Faivre, S., E. Fouache, M. Ghilardi, F. Antonioli, S. Furlani & V. Kovacic, (2011). Relative sea level change in western Istria (Croatia) during the last millennium. *Quaternary International* 232 (1-2), 132-143.

Herak, M., D. Herak & A. Markušić, (1998). Revision of the earthquake catalogue and seismicity of Croatia, 1908-1992. *Terra Nova* 8, 86-94.

Hinzen, K.-G. (2009). Simulation of toppling columns in archaeoseismology. *Bulletin of the Seismological Society of America* 99 (5), 2855-2875.

Kamh, G.M.E, A. Kallash, R. Azzam, (2008). Factors controlling building susceptibility to earthquakes: 14-year recordings of Islamic archaeological sites in Old Cairo, Egypt: a case study. *Environmental Geology* 56, 269-279.

Karakhanian, A.S., V.G. Trifonov, T.P. Ivanova, A. Avagyan, M. Rukieh, H. Minini, A.E. Dodonov & D.M. Bachmanov, (2008). Seismic deformation in the St. Simeon monasteries (Qal'at Sim'an), northwestern Syria. *Tectonophysics* 453, 122-147.

Marco, S. (2008). Recognition of earthquake-related damage in archaeological sites: Examples from the Dead Sea fault zone, *Tectonophysics* 453, 048-156.

Markušić, A. & M. Herak, (1999). Seismic zoning of Croatia. *Natural Hazards* 18, 269-285.

Matejčić, I. & P. Chevalier, (1998). Nouvelle interprétation du complexe épiscopal „pré-euphrasien" de Poreč. *Antiquité tardive* 6, 355-365.

Molajoli, B. (1940). Le costruzioni preeufrasiane di Parenzo. *Le Arti II* 1936-1940, 93-95.

Molajoli, B. (1943). *La basilica eufrasiana di Parenzo.* 2nd ed. Padua.

Pirazzoli, P.A. & N. Evelpidou, (2012): Comment on „Relative sea-level change in western Istria (Croatia) during the last millennium" by Sanja Faivre, Eric Fouache, Matthieu Ghilardi, Fabrizio Antonioli, Stefano Furlani and Vladimir Kovacic. Quaternary International, 232 (2012). *Quaternary International* 271, 130-131.

Rapp, G. jr. (1986). Assessing archaeological evidence for seismic catastrophes. *Geoarchaeology* 1 (4), 365-379.

Rodríguez-Pascua, M.A., R. Pérez-López, J.L. Giner-Robles, P.G. Silva, V.H. Garduño-Monroy & K. Reicherter, (2011). A comprehensive classification of Earthquake Archaeological Effects (EAE) in archeoseismology: Application to ancient remains of Roman and Mesoamerican cultures. *Quaternary International* 242, 20-30.

Stiros, S.C. (1996): Identification of earthquakes from archaeological data: methodology, criteria and limitations. In: Stiros, S.C., Jones, R.E. (eds): *Archaeoseismology*. Fitch Laboratory Occasional Paper 7, 129-152, The British School at Athens.

Terry, A. (1984). *The Architecture and Architectural Sculpture of the Sixth-Century Eufrasius Cathedral Complex at Poreč.* PhD thesis. University of Illinois at Urbana-Champaign, 549 p.

Terry, A. (1988). The sculpture at the cathedral of Eufrasius in Poreč. *Dumbarton Oaks Papers* 42, 13-64.

Terry, A. (1995). The conservation history of mosaic pavements at the cathedral site in Poreč: 1862-1990. *Hortus Artium Medievalium* 1, 176-186.

Terry, A. & H. Maguire, (2007). *Dynamic Splendor. The Wall Mosaics in the Cathedral of Eufrasius at Porec* (Pennsylvania State University Press, University Park, Pa, vols I-II.

INQUA Focus Group on Paleoseismology and Active Tectonics

paleoseismicity.org

# A new long paleotsunami coastal lake record from the Valdivia segment, south central Chile: A preliminary age-depth model and its implications

*Kempf, Philipp (1), Moernaut, Jasper (2,1), Vandoorne, Willem (1), Van Daele, Maarten (1), De Batist, Marc (1), Piño, Mario (3), Urrutia, Roberto (4)*

(1) Renard Centre of Marine Geology, Ghent University, Krijgslaan 281 S8, 9000 Ghent, Belgium, e-mail: philipp.kempf@ugent.be
(2) Geologisches Institut, ETH Zürich, Switzerland
(3) Instituto de Geociencias, Universidad Austral de Valdivia, Chile
(4) Centro EULA, Universidad de Concepción, Chile

***Abstract:*** *Long records of tsunami deposits can be recovered by coring coastal lakes, e.g. Bradley Lake,Cascadia (Kelsey et al., 2005). The necessity of long records arises due to the long recurrence time of the largest tsunamigenic megathrust earthquakes. The highly destructive character of earthquakes and their associated tsunami was repeatedly demonstrated in the last decade with the 2004 Sumatra earthquake ($M_W$: 9.0), the 2010 Maule earthquake ($M_W$: 8.8) and the 2011 Tōhoku earthquake ($M_W$: 9.0). Lago Huelde on Chiloé (42.5°S), Chile, is a coastal lake located in the middle of the Valdivia segment, which is known for producing the strongest ever instrumentally recorded earthquake in 1960 AD ($M_W$: 9.5). Large earthquakes are historically recorded for 1575 AD, 1737 AD and 1837 AD on this segment. We provide data to extend the known paleotsunami record to around 4000 cal. a BP with 20 event deposits (EDs) and 12 radiocarbon dates.*

***Key words***: *Lago Huelde, paleo-tsunami, age-depth model, recurrence time, earthquake*

## INTRODUCTION

Risk assessment for the largest scale of seismic hazards is often not reliable, because of insufficient data and the meaning of the hazard is skewed when the recurrence time is significantly larger than a human life span (Kossobokov, 2013). The large events in Sumatra and Japan made this, in the context of tsunami hazards, painfully clear.

Reports of the 1960 Valdivia earthquake tsunami and three of its local predecessors were previously identified in the historic record for 1575 AD, 1737 AD and 1837 AD (Lomnitz, 1970, 2004). A sedimentary record at the estuary of Rio Maullín (41°S) south-central Chile reaches back to around 0 AD with event deposits (EDs) for the 1960 AD and 1575 AD tsunami (none for 1737 AD and 1837 AD). The Rio Maullín record describes another four deposits at c.1350 AD, 1100 AD, 800 AD and 500 AD. The same record contains evidence in the diatom assemblages for co-seismic subsidence at c. 650 AD and 100 AD (these dates are very tentative and should be handled accordingly; Cisternas et al., 2005).

In this contribution we will present a composite core from Lago Huelde, a small coastal lake on la Isla Grande de Chiloé (42.6°S; Fig. 1). It contains 20 EDs which we ascribe to tsunami inundations into the lake.

## METHODS

The field work to this study was conducted in 2012. A UWITEC platform was the research vessel from which 6.3 cm diameter gravity cores and 6.3 cm diameter piston cores were recovered. Pinger sub-bottom profiles and sidescan sonar data were collected to determine the most sensible coring sites. The cores were analyzed with a GEOTEK multi sensor core logger (MSCL) for gamma attenuation density and magnetic susceptibility at an increment of 2 mm. Pictures were taken with a line scan camera and the cores were sedimentologically described.

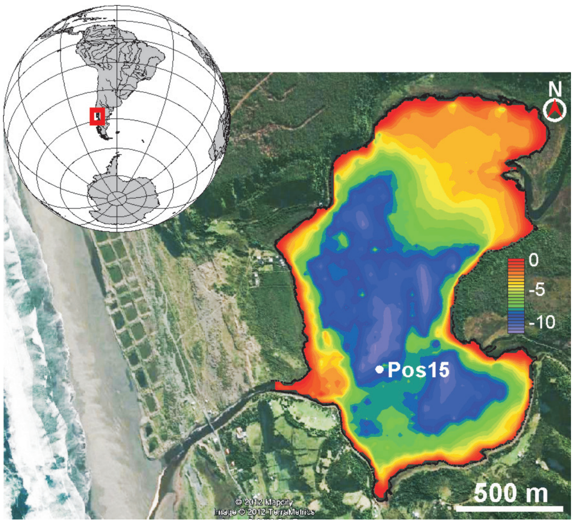


*Figure 1: Overview map of the study area, with a crude bathymetry map of Lago Huelde. The satellite image is taken from Google Earth.*

Twelve samples of radiocarbon datable material were sieved, picked, cleaned and sent to the [14]Chrono Centre for Climate, the Environment, and Chronology of Queen's University in Belfast, UK, for accelerator mass spectrometry (AMS) analysis (Tab. 1). The calibration of these dates and the age-depth model were performed using the SHCal04 calibration curve (McCormac et al., 2004) in the R based function Clam v.2.1 (Blaauw, 2010).

*Table 1: List of radiocarbon dates from this study. *) treated as an outlier.*

| lab ID | composite core depth [cm] | sample type | 14C age [14C a] | 14C error | 2σ min [cal. a BP] | 2σ max | relative area [%] | calibrated age [cal. a BP] | error |
|---|---|---|---|---|---|---|---|---|---|
| UBA-23325* | 80-81 | plant fragments | - | - | | | | postbomb | |
| UBA-23326 | 118-121 | plant fragments | 396 | 36 | 324 | 414 | 51.1 | 369 | 45 |
| | | | | | 417 | 423 | 2.2 | 420 | 3 |
| | | | | | 426 | 494 | 41.6 | 460 | 34 |
| UBA-21474* | 142.5 | wood | 1214 | 34 | 978 | 1039 | 30.2 | 1008.5 | 30.5 |
| | | | | | 1042 | 1172 | 64.8 | 1107 | 65 |
| UBA-23327 | 146-149 | plant fragments | 848 | 31 | 675 | 765 | 95 | 720 | 45 |
| UBA-23328 | 304-305 | plant fragments | 1298 | 29 | 1078 | 1265 | 95 | 1171.5 | 93.5 |
| UBA-23329 | 399.5-402.5 | leaf/plant | 2032 | 32 | 1829 | 1847 | 2.9 | 1838 | 9 |
| | | | | | 1862 | 1999 | 92.1 | 1930.5 | 68.5 |
| UBA-23330 | 449.5-450.5 | mostly one culm | 2015 | 27 | 1828 | 1848 | 5.8 | 1838 | 10 |
| | | | | | 1862 | 1954 | 77.4 | 1908 | 46 |
| | | | | | 1956 | 1988 | 11.6 | 1972 | 16 |
| UBA-21475 | 500.4 | leaf/plant | 2292 | 43 | 2148 | 2342 | 95 | 2245 | 97 |
| UBA-23331 | 561.5-564.5 | mostly one leaf | 2266 | 34 | 2135 | 2138 | 0.7 | 2136.5 | 1.5 |
| | | | | | 2141 | 2333 | 94.3 | 2237 | 96 |
| UBA-23332 | 620.5-621.5 | twiglet | 3029 | 39 | 3000 | 3266 | 91 | 3133 | 133 |
| | | | | | 3291 | 3321 | 4 | 3306 | 15 |
| UBA-23333 | 700.5-701.5 | plant fragments | 3155 | 31 | 3217 | 3233 | 2.9 | 3225 | 8 |
| | | | | | 3237 | 3389 | 92.1 | 3313 | 76 |
| UBA-23334 | 811.5-814.5 | plant fragments | 3718 | 38 | 3869 | 4093 | 92.7 | 3981 | 112 |
| | | | | | 4126 | 4142 | 2.2 | 4134 | 8 |
| UBA-21477 | 834 | culm/plant | 3692 | 35 | 3844 | 4012 | 77 | 3928 | 84 |
| | | | | | 4020 | 4020 | 0.1 | 4020 | 0 |
| | | | | | 4027 | 4083 | 17.8 | 4055 | 28 |

## RESULTS

### *Geo-acoustics and lithology*

In most cases heavy acoustic blanking due to gas in the sediment prevented deep penetration of the sub-bottom profiles. In the few seismic windows multiple strong reflections disrupt the otherwise semi-chaotic acoustic signature of the lake's sediment.

The background sediment in the lake is clayey silt with a very high content of organic matter (loss on ignition values of 20 up to 40 weight%). Rarely this background sedimentation is disrupted by thin (1 to 8 mm) grey layers with significantly less organic matter.The physical properties of the background sediment are low magnetic susceptibility and a low density. Sporadically the background sediment is faintly laminated on a 1 to 2 mm scale. The intervals of lamination are usually 5 cm to a few 10s cm long and always occur above sandy layers.

These sandy layers mark the most notable changes in the sedimentation. They range in thickness from 1 to 30 cm. The sands can be massive or can contain multiple fining upwards cycles, which in turn can incorporate multiple cycles of good to bad sorting. Mud rip-up clasts are also a common feature. These clasts can be as big as the core liner diameter and possibly bigger. They occur isolated or organized in layers. On top of the sand layers there is usually a fine grained cap of mineralogenic material rarely exceeding 1 cm in thickness.The physical properties of the sandy layers are a very high magnetic susceptibility, sometimes exceeding 1000 $10^{-5}$ SI and a comparatively high density (Fig. 2).

### *Radiocarbon Dating*

Material for radiocarbon dating is very abundant due to the high organic content. However, large intact macrofossils are uncommon, most radiocarbon samples were collected by sieving. Usually 3 cm thick intervals of background sediment and picking small macro remains of terrestrial plants, e.g. culms, leaf fragments etc. (Tab.1). Two radiocarbon dates were neglected in the age-depth model. One, because of a significantly older age in comparison to the neighboring samples, the other, because of postbomb radiocarbon values. These are probably due to reworking and contamination.

## DISCUSSION

We interpret the sandy layers as tsunami deposits due to the extremely abrupt change in flow regime during deposition, the fining upwards tendency with often multiple cycles and the mud cap at the top of the last fining upwards cycle.

### *Tsunami vs. storm surge*

The differentiation between tsunami deposits and storm surge deposits based solely on sedimentological characteristics is typically difficult (e.g. Nanayama et al., 2000; Kortekaas & Dawson, 2007; Bridge, 2008; Komatsubara et al., 2008; Goto et al., 2010; Lario et al., 2010; Buckley et al., 2012; Phantuwongraj & Choowong, 2012). However, in this study area many arguments can be made for tsunami- and against storm surge deposits, three of which are presented here:

1. The run-up distance of large tsunami exceeds the affected area of storm surge deposits (e.g. Phantuwongraj & Choowong, 2012). With 1.3 to 1.9 km distance between the core sites and the Pacific coast this points towards tsunami deposits.
2. Across the entire Humboldt current system in front of the west South American coast sea surface temperatures are too low to produce tropical cyclones (Brooks, 2008).
3. While the reports of tropical cyclones hitting the coast of Chile are non-existent in the historic records, large tsunamigenic earthquakes are reported multiple times since the 16th century (Lomnitz, 1970, 2004).

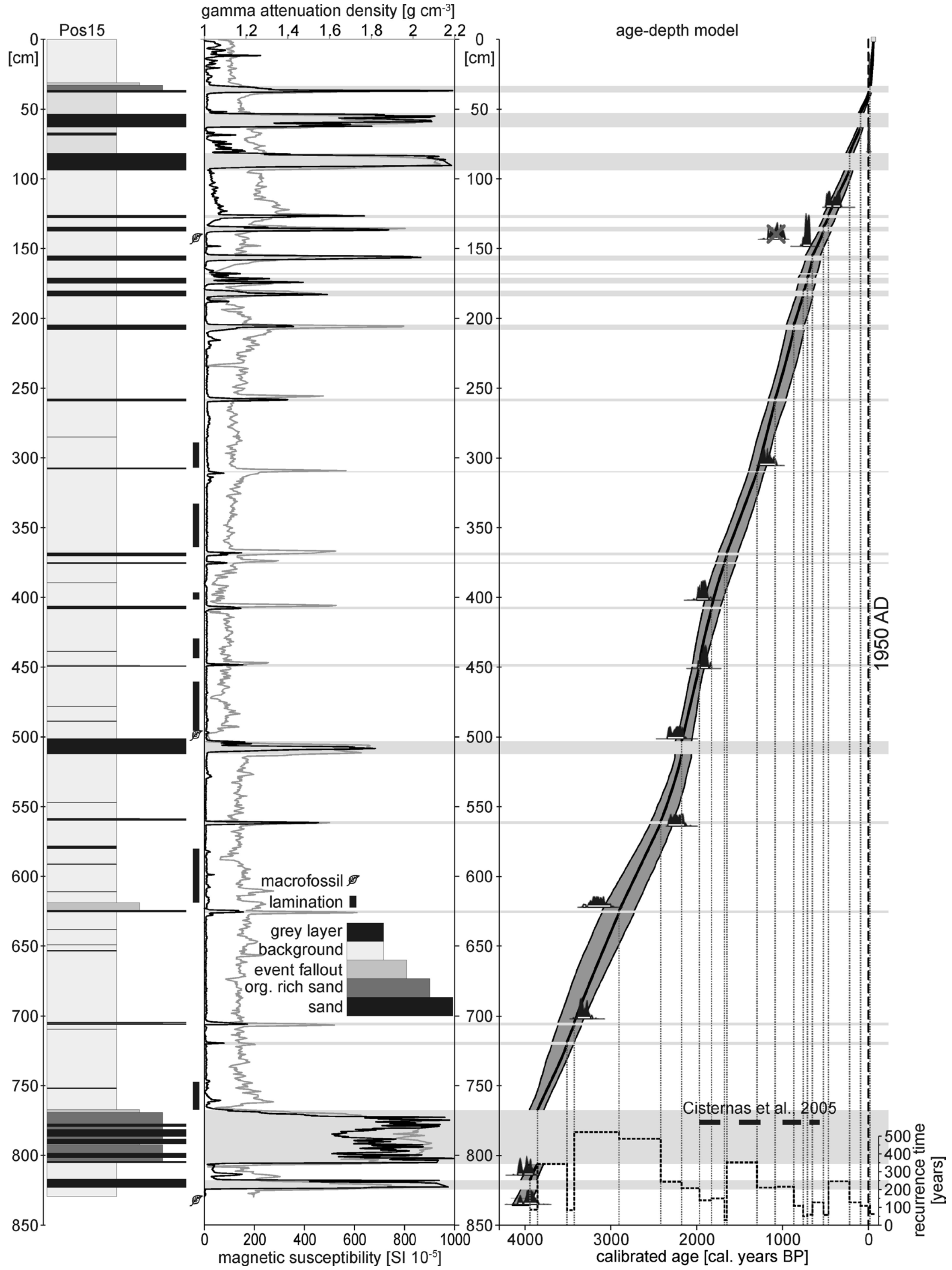


*Figure 2: Left: sedimentological log mainly dividing the core into background sediment and EDs; middle: physical property logs for gamma attenuation density (grey) and magnetic susceptibility (black); right: age-depth model with a calibrated probability distribution for each radiocarbon date (black) with the 2σ range highlighted (white bar). EDs are considered to be deposited instantaneously in this age-depth model (light grey bars) and the modeled age for each ED is projected onto the calibrated age axis (vertical grey dotted lines). The statistically best age is indicated with a black line with a 2σ confidence range as a grey area around it. At the bottom is a recurrence time graph (dashed line). The black bars under "Cisternas et al. (2005)" indicate the age ranges of already known pre-historic tsunami deposits or subsidence events at the Rio Maullín estuary in Chile, which is also on the Valdivia segment.*

*Implications of the event-chronologic record*

When making use of an age-depth model uncertainties remain (Telford et al., 2004). However, in most cases it is the age-depth model that gives the only tool to add the crucial timeframe to a geological story.

Considering accumulation rates and the local geological history the uppermost ED is likely to be from the 1960 tsunami.

Following the age-depth model down core the next ED around 60 cm depth corresponds to the 1837 AD tsunami with an modeled best statistical age of 1853 AD (2σ max: 1820 AD; 2σ min: 1874 AD). Tsunami deposits from the 1837 tsunami are not common among other paleotsunami records which demonstrates the high sensibility and preservation potential of the sedimentary basin that is Lago Huelde. One radiocarbon date from below this ED was measured to have postbomb $^{14}C$ levels and was neglected (tab. 1).

The 15 cm thick ED at around 90 cm depth is modeled to an age of 1725 AD (2σ max: 1688 AD; 2σ min: 1770 AD). The 1737 AD earthquake is the only strong known event that falls into this age range, which is why we ascribe this deposit to the 1737 AD tsunami.

The next ED, at around 127 cm depth is interpreted to correspond to the oldest historically known earthquake and tsunami in Chile from 1575 AD. The modeled age is 1479 AD (2σ max: 1569 AD; 2σ min: 1425 AD). What is surprising is the comparatively small size of the deposit, because from historic records the 1575 earthquake is comparable to the 1960 earthquake.

All EDs below that are dated to be older than the historic record. The only published paleotsunami record for the Valdivia segment that contains pre-historic EDs comes from the Rio Maullín estuary (Cisternas et al., 2005). The age ranges from that publication are plotted onto figure 2 and there is a good overlap with dated events from this study for all four pre-historic events, however, both the paleotsunami records from Rio Maullín and from Lago Huelde are not dated well enough to draw conclusions. Further dating will be carried out on the Lago Huelde record later this year.

Modelled recurrence times range from 28 to 522 years. It appears to be that tsunamis hit the west coast of Chiloé more frequently during the last 2500 years than between 4000 and 2500 cal. a BP. However, not knowing the shoreline displacement history of Chiloé for the entire period this could be an effect of lower sensitivity for tsunami deposits of the Lago Huelde system, e.g. through an overall subsidence trend the lake can have been made easier accessible for tsunami inundations.

**Acknowledgements:** PK thanks Koen De Rycker, Gauvain Wiemer and Alejandro Peña for invaluable help during fieldwork. PK is funded by the BOF (Bijzonder Onderzoeksfonds) of Ghent University.

**References**

Blaauw, M. (2010). Methods and code for `classical' age-modelling of radiocarbon sequences. *Quaternary Geochronology* 5 (5), 512-518.

Bridge, J.S. (2008). Discussion of articles in "Sedimentary features of tsunami deposits" Discussion. *Sedimentary Geology* 211 (3-4), 94-94.

Brooks, H. (2008). Extreme Weather: Understanding the Science of Hurricanes, Tornadoes, Floods, Heat Waves, Snow Storms, Global Warming and Other Atmospheric Disturbances. *Eos, Transactions American Geophysical Union* 89 (28), 258-258.

Buckley, M.L., Y. Wei, B.E. Jaffe & S.G. Watt (2012). Inverse modeling of velocities and inferred cause of overwash that emplaced inland fields of boulders at Anegada, British Virgin Islands. *Natural Hazards* 63 (1), 133-149.

Cisternas, M., B.F. Atwater, F. Torrejon, Y. Sawai, G. Machuca, M. Lagos, A. Eipert, C. Youlton, I. Salgado, T. Kamataki, M. Shishikura, C.P. Rajendran, J.K. Malik, Y. Rizal & M. Husni (2005). Predecessors of the giant 1960 Chile earthquake. *Nature* 437 (7057), 404-407.

Goto, K., T. Shinozaki, K. Minoura, K. Okada, D. Sugawara & F. Imamura (2010). Distribution of boulders at Miyara Bay of Ishigaki Island, Japan: A flow characteristic indicator of tsunami and storm waves. *Island Arc* 19 (3), 412-426.

Kelsey, H.M., A.R. Nelson, E. Hemphill-Haley & R.C. Witter (2005). Tsunami history of an Oregon coastal lake reveals a 4600 yr record of great earthquakes on the Cascadia subduction zone. *Geological Society of America Bulletin* 117 (7-8), 1009-1032.

Komatsubara, J., O. Fujiwara, K. Takada, Y. Sawai, T.T. Aung & T. Kamataki (2008). Historical tsunamis and storms recorded in a coastal lowland, Shizuoka Prefecture, along the Pacific Coast of Japan. *Sedimentology* 55 (6), 1703-1716.

Kortekaas, S. & A.G. Dawson (2007). Distinguishing tsunami and storm deposits: An example from martinhal, SW Portugal. *Sedimentary Geology* 200 (3-4), 208-221.

Kossobokov, V.G. (2013). Are seismic hazard assessment errors and earthquake surprises unavoidable? *EGU General Assembly 2013*.

Lario, J., L. Luque, C. Zazo, J. Luis Goy, C. Spencer, A. Cabero, T. Bardaji, F. Borja, C.J. Dabrio, J. Civis, J. Angel Gonzalez-Delgado, C. Borja & J. Alonso-Azcarate (2010). Tsunami vs. storm surge deposits: a review of the sedimentological and geomorphological records of extreme wave events (EWE) during the Holocene in the Gulf of Cadiz, Spain. *Zeitschrift Fur Geomorphologie* 54 301-316.

Lomnitz, C. (1970). Major Earthquakes and Tsunamis in Chile during the period 1535 to 1955. *International Journal of Earth Science f.k.a. Geologische Rundschau* 59 (3), 938-960.

Lomnitz, C. (2004). Major earthquakes of Chile: a historical survey, 1535-1960. *Seismological Research Letters* 75 368-378.

McCormac, F.G., A.G. Hogg, P.G. Blackwell, C.E. Buck, T.F.G. Higham & P.J. Reimer (2004). SHCal04 Southern Hemisphere calibration, 0-11.0 cal kyr BP. *Radiocarbon* 46 (3), 1087-1092.

Nanayama, F., K. Shigeno, K. Satake, K. Shimokawa, S. Koitabashi, S. Miyasaka & M. Ishii (2000). Sedimentary differences between the 1993 Hokkaido-nansei-oki tsunami and the 1959 Miyakojima typhoon at Taisei, southwestern Hokkaido, northern Japan. *Sedimentary Geology* 135 (1-4), 255-264.

Phantuwongraj, S. & M. Choowong (2012). Tsunamis versus storm deposits from Thailand. *Natural Hazards* 63 (1), 31-50.

Telford, R.J., E. Heegaard & H.J.B. Birks (2004). All age-depth models are wrong: but how badly? *Quaternary Science Reviews* 23 (1-2), 1-5.

INQUA Focus Group on Paleoseismology and Active Tectonics

paleoseismicity.org

# Slip distribution and compensation at fault damage zones: its implications to fault evolution and earthquake hazards

*Young-Seog Kim* and Jin-Hyuck Choi*

Dept. of Earth & Environmental Sciences, Pukyong National University, Busan 608-737, South Korea. Email: ysk7909@pknu.ac.kr

***Abstract:*** *Slip distribution along natural faults and earthquake surface ruptures, especially where they are discontinuous, provide insights into fault evolution and, hence, earthquake hazard. Thus, we here analysed detailed slip changes at fault damage zones to understand the kinematics of a fault system and the behaviour of earthquake rupture propagation, and to apply it for estimation of earthquake-induced hazards. Slip distribution at fault discontinuities along natural faults can be various depending on the evolution stage and, hence, are closely related to the segment interaction and linkage during fault growth. Slip analysis at fault damage zones along several earthquake ruptures shows slip deficit, compensation, and neutral between two slip components (vertical & horizontal) depending on the maturity of linkage zones and/or the rupture propagation direction. Therefore, the consideration of slip compensation along surface ruptures as well as damage zone structures must be very useful to understand fault evolution and, hence, to assess seismic hazards around active fault systems.*

***Key words****: Fault damage zones, Slip compensation, Fault evolution, Earthquake hazards.*

## INTRODUCTION

Faults are described as volumetric zones consisting of discrete slip surfaces, fault rocks, and associated subsidiary structures (e.g., Chester and Logan, 1986; Chain et al., 1996), and are also considered as systems that are composed of several geometric and/or kinematic fault segments (e.g., Segall and Pollard, 1983; Walsh et al., 2003). Faults commonly evolve through repeated earthquake events. Hence, the study of earthquake hazards is closely related with understanding how faults grow or evolve, and predicting the most vulnerable areas around active faults. Thus, it is necessary to understand the characteristics of the evolutional stages of active faults and, how the co-seismic surface ruptures propagate and terminate (e.g., Klinger et al., 2006; Wesnousky, 2006).

Some useful information for the kinematic features of fault and earthquake rupture could be obtained from fault damage zones around a fault system (e.g. Kim and Sanderson, 2008; Wibberley et al., 2008; Mitchell and Faulkner, 2009; Faulkner et al., 2010; Choi et al., 2012). Particularly, slip distribution at fault damage zones is one of the most important elements to understand the interaction between neighbouring faults or earthquake ruptures. Also, where faults and earthquake ruptures are discontinuous on the surface, the slip profiles reflect the behaviour of fault segments linked at depth (e.g., Kim and Sanderson, 2005). This is very important in terms of earthquake hazard analysis because it reflects whether fault and earthquake rupture propagates to the next segment or terminates (e.g., Wesnousky, 2006). We introduce here some detailed slip analyses along natural faults as well as surface ruptures associated with a few large earthaukes.

## FAULT DAMAGE ZONES & EARTHQUAKE

Fault damage zones are defined as rock volumes deformed by secondary structures around faults to accommodate displacement along the faults (e.g., Shipton and Cowie, 2003; Kim et al., 2004; Fig.1). They can be mainly classified as wall-, linking- and tip-damage zones depending on their location around segmented faults (Fig. 1a).

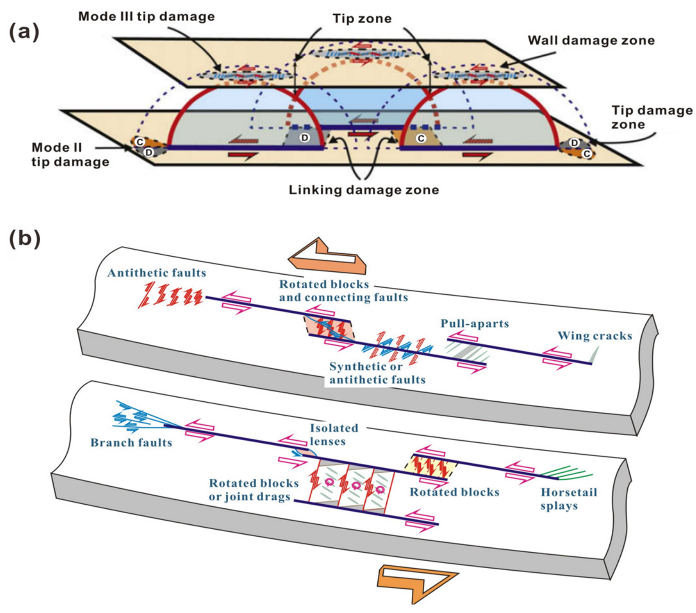


*Fig. 1: Schematic diagrams for the fault damage zones. Note that various damage patterns depending on slip mode at fault tips and locations around faults (from Kim et al., 2004).*

Linking damage zone can be defined as the area with a high intensity of secondary structures between two fault segments. Tip damage zone develops as a result of stress concentration at fault tips where slip terminates (Pollard and Segall, 1987; Cowie and Shipton, 1998). Note that the linking and tip damage zones can be applied to rupture step-overs and ends of major surface ruptures, respectively.

In earthquake ruptures, the location of the epicenter is commonly biased to one end of the rupture propagating toward the other end. Displacement profile and the density of aftershocks are developed asymmetrically, with maxima at the opposite end of the epicenter of the main shock (Sibson, 1989; Das and Henry, 2003; Kim and Sanderson, 2008). Figure 2b is a model based on the observations from geological faults and earthquake ruptures that can be used to infer the direction of propagation from the distribution of damage (aftershocks) and asymmetry of the displacement (slip) profile (Kim and Sanderson, 2008). Note that the both rupture end zones can be classified into *front* and *back* tip damage zones based on the main propagation direction of earthquake rupture.

## SLIP DISTRIBUTION & FAULT EVOLUTION

As faults evolved by linkages and connections of several fault segments, fault displacement profiles at linking damage zones have been used to provide insight into interaction between two fault segments (e.g., Peacock and Sanderson, 1991). There are mainly three stages of segment linkages during fault growth and evolution (Kim and Sanderson, 2005; Fig. 3).

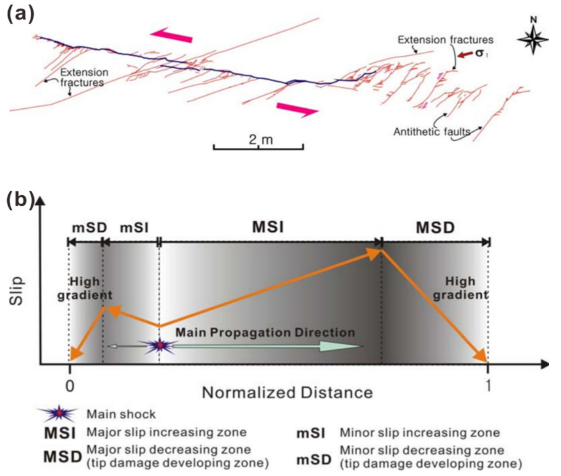


*Fig. 2: (a) Asymmetric tip damage zones around a strike-slip fault. (b) An earthquake propagation model showing that an earthquakes originate near one end of a fault segment and propagate towards the other. All these figures are from Kim and Sanderson (2008).*

Firstly, in an initial stage, there is no interaction between two segments, and these are called isolated faults or kinematic fault discontinuities. Secondly, if two segments are not physically linked but interact in slip profiles, they are called soft-linked or kinematically linked faults. These slip interactions may reflect that two segments possibly linked in depth. Finally, if two segments are physically linked by physical connecting faults, it is considered to be a hard-linked or geometrically linked fault, which can act as a single fault. In the last case, the maximum displacement is commonly observed at linking damage zones.

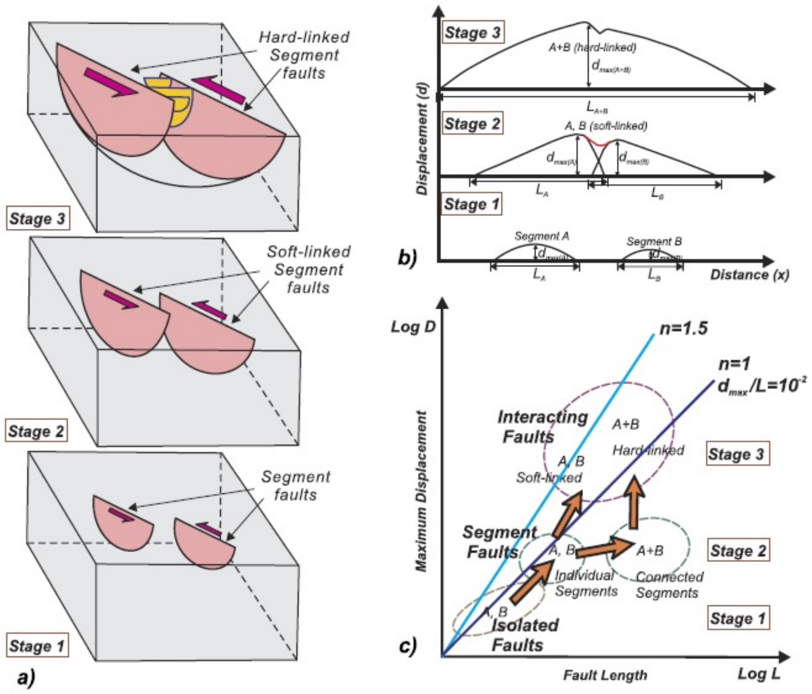


*Fig. 3: Fault segmentation and linkage (from Kim and Sanderson, 2005). Faults evolve from isolated faults to interacting faults through segment linkage. The ratio of $d_{max}/L$ increases showing step-like evolution path. Fault lengths abruptly jump at the stage of segment linkage.*

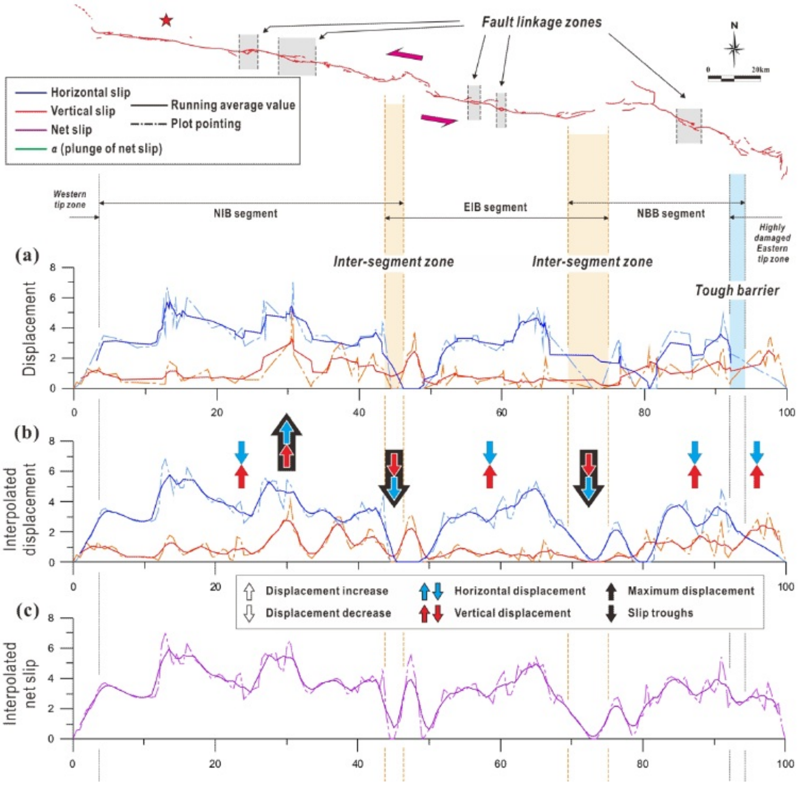


*Fig. 4: Normalized slip distributions along the 1957 Bogd surface rupture. (a) Horizontal and vertical slip data acquired by running average value. (b) Interpolated slip distributions. (c) Net slip data calculated by using horizontal and vertical slip amounts. Only two fault linkage zones show slip troughs acting as a barrier, whereas slip compensation is common at other fault linkage zones (Choi et al., 2012).*

Fig. 3c shows schematic $d_{max}$/L plots for the growth of a strike-slip fault during segment interaction and linkage. The maximum displacement ($d_{max}$) - fault length (L) relationship evolves from isolated faults through segmented faults to interacting faults with a step-like route in one of two ways. Note that the lowest $d_{max}$/L ratios occur at stage 2, where segments have just connected, while higher ratios occur for isolated faults and at the mature stage of linked faults.

## SLIP COMPENSATION & RUPTURE PROPAGATION

Stress transferring or releasing, when seismic waves pass through fault discontinuities, could determine different features such as rupture propagation and termination. In previous studies (Peacock and Sanderson, 1991; Kim and Sanderson, 2005), slip distribution along faults or surface ruptures to understand the connectivity or maturity of segmented faults system have commonly been analysed based on only the main slip components (e.g. strike-slip component along strike-slip faults). Secondary slip components (e.g. dip-slip component along strike-slip faults), however, are sometimes dominant at fault damage zones, such as linkage and tip zones. Choi et al. (2012), recently, examined slip changes between two slip components (horizontal & vertical) at step-overs and end zones along the surface rupture associated with the 1957 Gobi-Altay earthquake in Mongolia (Fig. 4).

In the tip damage zones, both slips are generally much smaller than those of other zones, and the slip patterns at the front and back tip zones are obviously different. The vertical slip at the frontal tip zones increases as the horizontal slip decreases. Choi et al. (2012) termed this as slip compensation, i.e. as one component of slip decreases the other component increases. The increase of the vertical slip component reflects higher stress releasing through intense minor dip-slip faults at front tip ends, and this may result from the higher stress releasing associated with the main propagation direction of earthquake rupture (Fig. 2).

Along the surface ruptures, there are many segment boundaries represented by local linkage zones. At some linkage zones, there is little variation in slip, while others show a remarkable reduction (Fig. 4). However, the horizontal slip component is often compensated by increased vertical slip component at several geometric linkages (Fig. 4).

Therefore, slip patterns at linking damage zones can be classified into *slip deficit*, *slip compensation*, and *slip neutral*, and they may be controlled by the structural maturities of the segmented fault systems (Fig. 3). Thus, we argue that the earthquake rupture kinematics at fault segment boundaries may be related with the properties of fault linkage. Figure 5 displays a conceptual model for the slip and damage patterns along an idealized co-seismic rupture.

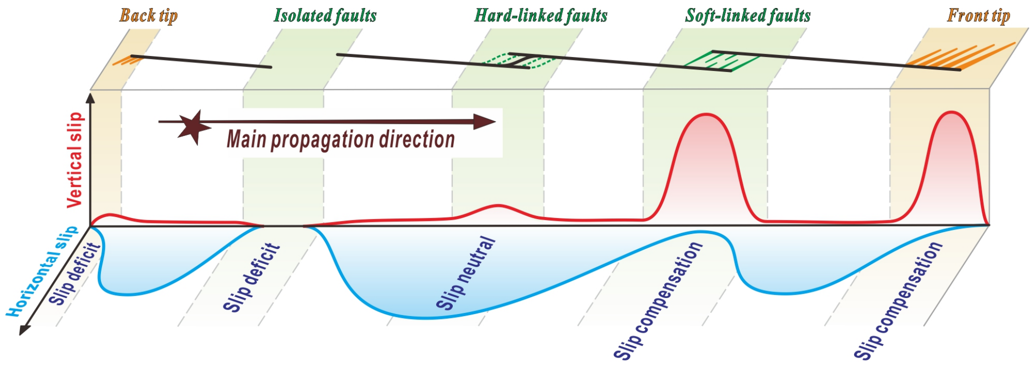


*Fig. 5: Conceptual model for the relationships between slip patterns and rupture kinematics at fault damage zones. Slip patterns at damage zones can reflect rupture propagation direction or structural maturity of faults during rupture propagation. Slip compensation are dominant at front tip zones as well as through soft-linked faults, and this means that damage structure is closely related to either releasing or transferring of coseismic stress or slip (from Choi et al., in preparation).*

## CONCLUSIONS

This study examines slip distribution and compensation at fault damage zones to understand the characteristics of fault evolution and their application to earthquake hazards. As a result, slip patterns at fault damage zones are closely related to evolutional stages of faults, and whether earthquake rupture propagate or terminate at fault discontinuities. The latter, especially, shows the importance of detailed slip analysis along active fault systems to analyze earthquake-induced hazards.

A variety of compensational patterns between main and secondary slip components are shown depending on the nature of fault linkage zones as well as main direction of fault or earthquake rupture propagation. In short, the systematic but asymmetric distribution of slip and damage zone around faults (e.g. Kim and Sanderson, 2008) can be one of the important issues to be considered for fault evolution and seismic hazard studies.

**Acknowledgements:** We thank Amagalan Bayasgalan, Dandar Enkhbayar and Battogtokh Davvasambuu for their positive cooperation in Gobi-Altay, Mongolia. We also thank an anonymous reviewer for his or her constructive comments.

## References

Caine, J.S., J.P., Evans & C.B., Forster, (1996). Fault zone architecture and permeability structure. *Geology* 24, 1025–1028.

Chester, F.M. & J.M., Logan, (1986). Composite planar fabric of gouge from the Punchbowl fault zone, California. *Journal of Structural Geology* 9, 621-634.

Choi, J.-H., K., Jin, D., Enkhbayar, B., Davvasambuu, A. Bayasgalan & Y.-S., Kim, (2012). Rupture propagation inferred from damage patterns, slip distribution, and segmentation of the 1957 MW8.1 Gobi-Altay earthquake rupture along the Bogd fault, Mongolia. *Journal of Geophysical Research* 117, B12401 (2012).

Cowie, P.A. & Z.K., Shipton, (1998). Fault tip displacement gradients and process zone dimensions. *Journal of Structural Geology* 20, 983-997.

Das, S. & C., Henry, (2003). Spatical relation between main earthquake slip and its aftershock distribution. *Reviews of Geophysics* 41, 3.

Faulkner, D.R., Jackson, C.A.L., Lunn, R.J., Schlische, R.W., Shipton, Z.K., Wibberley, C.A.J., Withjack, M.O., (2010). A review of recent developments concerning the structure, mechanics and fluid flow properties of fault zones, Journal of Structural Geology 32, 1557–1575.Kim, Y.-S., D.C.P., Peacock & D.J., Sanderson, (2004). Fault damage zones. *Journal of Structural Geology* 26, 503–517.

Kim, Y.-S., D.C.P., Peacock & D.J., Sanderson, (2004). Fault damage zones, *Journal of Structural Geology* 26, 503-517.

Kim, Y.-S. & D.J., Sanderson, (2005). The relationship between displacement and length of faults: a review. *Earth-Science Reviews* 68, 317–334.

Kim, Y.-S. & D.J., Sanderson, (2008). Earthquake and fault propagation, displacement and damage zones. In: *Structural Geology: New Research* (Landowe, S. J. & Hammler, G. M. eds.) *Nova Sci.*, Hauppauge, N. Y., 99–117.

Klinger, Y., R., Michel & G.C.P., King, (2006). Evidence for an earth-quake barrier model from Mw ~7.8 Kokoxili (Tibet) earthquake slip-distribution. *Earth and Planetary Science Letters* 242, 354-364.

Mitchell, T.M. & D.R., Faulkner, (2009). The nature and origin of off-fault damage surrounding strike-slip fault zones with a wide range of displacements: a field study from the Atacama fault system, northern Chile. *Journal of Structural Geology* 31, 802-816.

Peacock, D.C.P. & D.J., Sanderson, (1991). Displacement, segment linkage and relay ramps in normal fault zones. *Journal of Structural Geology* 13, 721-733.

Pollard, D.D. & P., Segall, (1987). Theoretical displacements and stresses near fractures in rock: With applications to faults, joints, veins, dikes, and solution surfaces. In: *Fracture Mechanics of Rock* (Atkinson, B. K. ed.) Academic, London, pp. 277-349.

Segall, P. & D. D., Pollard, (1983). Nucleation and growth of strike slip faults in granite. *Journal of Geophysical Research* 88, 555-568.

Shipton, Z.K. & P.A., Cowie, (2003). A conceptual model for the origin of fault damage zone structures in high-porosity sandstone. *Journal of Structural Geology* 25, 333-344.

Sibson, R. H., (1989). Earthquake faulting as a structural process. *Journal of Structural Geology* 11, 1–14.

Walsh, J.J., W.R., Bailey, C., Childs, A., Nicol & C.G., Bonson, (2003). Formation of segmented normal faults: a 3-D perspective. *Journal of Structural Geology* 25, 1251-1262.

Wesnousky, S., (2006). Predicting the endpoints of earthquake ruptures. *Nature* 444, 358-360.

Wibberley, C.A.J., Yielding, G. & Di Toro, G., (2008). Recent advances in the understanding of fault zone internal structure: A review. *Geological Society Special Publication*, London: 5-33.

INQUA Focus Group on Paleoseismology and Active Tectonics

paleoseismicity.org

# Multiple evidence for tsunami inundation between Barbate and Zahara de los Atunes (Gulf of Cádiz)

*Koster, Benjamin (1), Klaus Reicherter (1)*

(1) Neotectonics and Natural Hazards, RWTH Aachen University, Lochnerstraße 4-20, 52056 Aachen, Germany.
Email: b.koster@nug.rwth-aachen.de

***Abstract:*** *The coastlines around the Gulf of Cádiz were affected by numerous tsunami events listed in several published catalogues. These remarkable events damaged infrastructure and caused countless human losses. In 2010 we published our findings of an enigmatic, inferred tsunami deposit along the Barbate-Zahara de los Atunes beach section. The tsunami deposit, located at various heights above mean sea level, shows several characteristics indicative of high energy event deposits and has been dated to approx. 4 ka BP by optically stimulated luminescence (OSL) dating. In March 2013 we carried out further fieldwork using a multi-method approach including sampling outcrops as well as geophysical and geochemical investigations. Preliminary results from studies of sedimentology, magnetic susceptibility, x-ray fluorescence analysis, ground penetrating radar (GPR) and dating reveal further characteristics and support our interpretation of a high energy deposit.*

***Key words****: tsunami deposits, sedimentology, GPR, geomorphology, OSL dating, coastal vulnerability*

## INTRODUCTION

A tsunami is a high-energy event that, under certain circumstances, may destroy coastal infrastructure and cause the accumulation of large amounts of tsunami deposits. Studying the distribution and characteristics of (pre-)historical and sub-recent tsunami deposits improves the accuracy of tsunami hazard maps and early warning systems and, therefore, can help protect humans and infrastructure along tsunami threatened coastlines all over the world.

Within the Gulf of Cádiz numerous large tsunami events have been reported which left deposits along the Spanish and Portuguese coast during the Holocene (e.g. Baptista & Miranda, 2009; Reicherter et al., 2010; Álvarez-Gómez et al., 2011; Lario et al., 2011; Cuven et al., 2013).

During our initial investigations between 2008 and 2010, we found sedimentary evidence for at least one palaeotsunami at several outcrops along a beach cliff at the Gulf of Cádiz (Reicherter et al., 2010). The results of sedimentary analyses on shallow percussion drill cores in the nearby lagoons and marshlands compliment the outcrop evidence and together prove the occurrence of an ancient tsunami in this region.

Our recent work presented here continues the original research at the beach cliff between Barbate and Zahara de los Atunes; preliminary results of this ongoing research are presented and discussed.

## STUDY AREA

Our study area is situated at a beach between the cities of Barbate and Zahara de los Atunes in the Gulf of Cádiz (Fig. 1). The beach is dominated by a rocky cliff which is between 0.7 to 5.0 m high.

The investigated tsunami deposit can be found within the cliff at various heights above mean sea level and has a variable sedimentary composition.

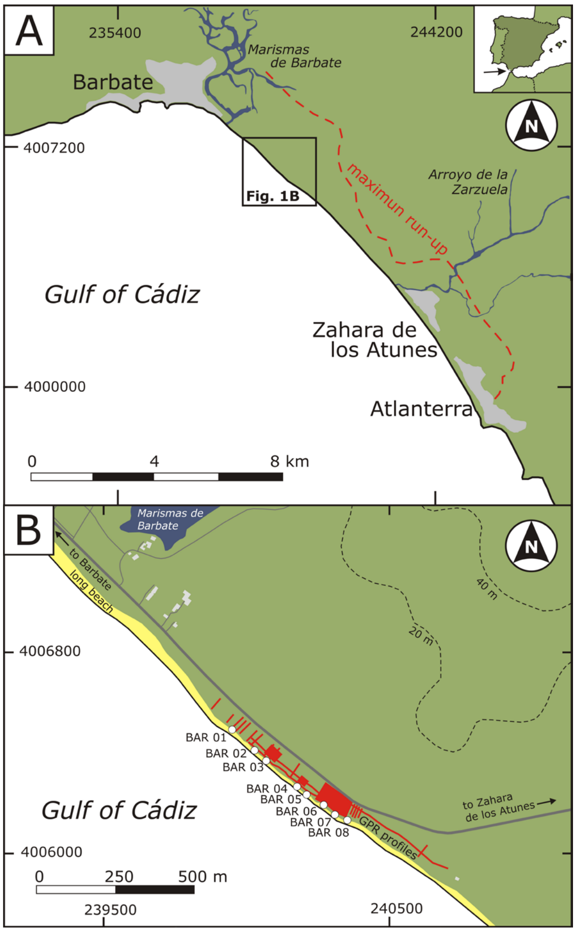


*Fig. 1: (A) Location of the study area between Barbate and Zahara de los Atunes (Gulf of Cádiz). (B) Detailed map of the investigated area; white points illustrate investigated beach profiles and red lines show the locations of GPR measurements.*

A dark brown coloured layer, showing a fining-up sequence and a palaeocurrent direction towards the sea, was found resting directly on the folded Betic substratum. The basement of the cliff mainly consists of Cretaceous to Eocene flysch deposits (Lario et al., 2011).

## METHODS

A multi-method approach was carried out to further investigate the tsunami deposit and to identify additional characteristics. Besides photo documentation and description, further sampling was undertaken on various profiles for subsequent analyses in our laboratory (e.g. grain size distribution and geochemical composition with handheld x-ray fluorescence spectrometer Niton XLt 700 series). Furthermore, magnetic susceptibility measurements were performed with a Bartington Instruments MS2 with MS2K sensor.
Ground penetrating radar (GPR) with different antenna frequencies (400 MHz and 900 MHz) was used for subsurface investigations. GPR equipment during field work consisted of a GSSI SIR-3000 data recording unit, 400 MHz and 900 MHz antennae, a survey wheel and handheld GPS. The topography on top of the cliff where the GPR measurements were carried out is mostly flat. It was, therefore, not necessary to use a dGPS unit. Data processing was performed with ReflexW V7.0 (Sandmeier Scientific Software) and included static correction, background removal, gain adjustments and velocity adaption for time-depth conversions.
In this publication we want to show preliminary results of our investigations as well as the optically stimulated luminescence (OSL) and radiocarbon dating results.

## SEDIMENTOLOGICAL & GEOCHEMICAL EVIDENCE

We found several outcrops along the 5 km long beach section between Barbate and Zahara de los Atunes as described in Reicherter et al. (2010). Since the last fieldwork periods in 2008 and 2010, the coastline has been transformed; during the last years, large winter storm events and high wave heights have eroded the beach section and exposed new outcrops. We documented all of our findings and sampled for subsequent analysis in our laboratory.
Along the cliff is a 0.1-0.4 m thick layer containing large stones, boulders and shells. Overlying this is a ~1.0 m thick dark sandy clay layer which is eye-catching (see Fig. 2). The sandy clay layer (from ~0.2-0.9 m at profile BAR 03) contains a large fining upward sequence. The layer comprises dark brown sand, and is organic- and clay-mineral rich. In some other parts of the beach section this layer also contains a slightly coarse-grained base with small conglomerates and charcoal remains. The coarse-grained layer (from ~0.9-1.2 m at profile BAR 03) below the thick sandy clay deposit is made up of stones, boulders, ripped-out beach rock pieces and subangular to rounded sandstones of the basement rock. It also contains, in some parts, large marine shells (*Acanthocardia tuberculata and A. aculeata, Glycimeris glycimeris, gastropods*). On top of this layer small accumulations of rounded gravel are visible at some locations. Both layers are described as tsunamigenic backwash deposits (Reicherter et al., 2010).

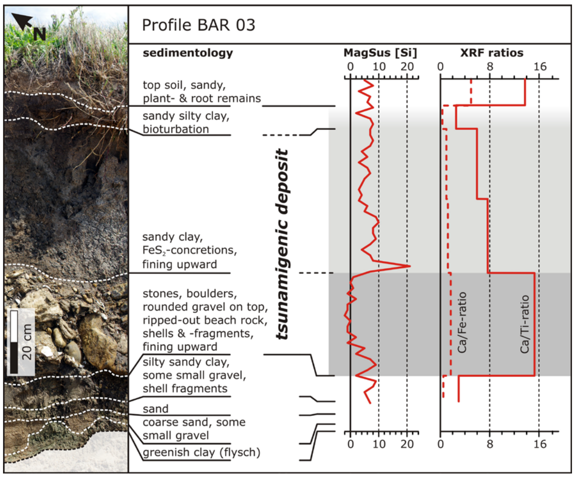


*Fig. 2: Sedimentological analysis of profile BAR 03 with interpretation of tsunamigenic deposit (left). Results of magnetic susceptibility measurements and x-ray fluorescence analysis (right) with Ca/Fe- and Ca/Ti-ratios for the same outcrop. Dark greyish colour refers to the coarse-grained layer, while light greyish colours highlight the sandy clay layer.*

We found further unspecified sedimentary features near outcrop BAR 05: an armoured mud ball or clast-coated clay clast (Fig. 3). This feature has been up to now not been described in any of the listed palaeotsunami characteristics.

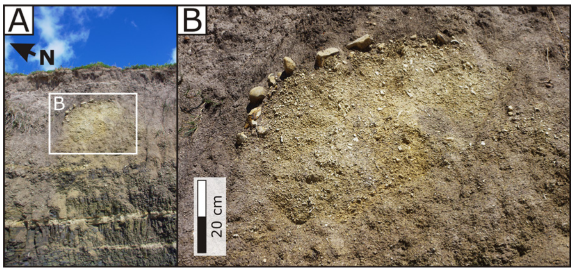


*Fig. 3: A new sedimentary feature in a palaeotsunami deposit visible as ball-like structure coated with clasts inside the sandy clay deposit (A shows the location on the cliff & B shows the feature in detail).*

As a further investigation tool we used magnetic susceptibility (MagSus) and x-ray fluorescence (XRF) measurements to support our findings. The MagSus can be used to distinguish materials from different origins (e.g., Mullins, 1977), due to their varying mineral content. Marine and terrestrial sediments show clear differences in their content of ferromagnetic, diamagnetic or paramagnetic minerals. Therefore, higher MagSus values are expected in terrigenous materials, while lower values support the idea of deposits originating from a marine environment. The MagSus value of a sample is given in dimensionless SI units. Preliminary results are shown in Fig. 2. The XRF analysis underlines the sedimentological findings and MagSus measurements. Element ratios (such as Ca/Fe and Ca/Ti) were calculated (cf. Vött et al., 2011; Chagué-Goff et al., 2012) to distinguish between marine and terrigenous components within the deposits (see Fig. 2). The handheld XRF spectrometer (Niton XLt 700 series) is limited to a specific amount of elements; therefore, we were not able to calculate element ratios such as Ba/Ti, Ca/Al, Si/Ti or Si/Al as described by Cuven et al. (2013). Further XRF measurements with a more sophisticated XRF measurement tool would improve our data.

## GPR MEASUREMENTS

We recorded 144 GPR profiles on the beach cliff to study the inner architecture of the tsunami deposits in detail. Profiles were carried out parallel as well as perpendicular to the coastline to detect as many features as possible and to have close spaced data for dense GPR grid analysis.
Our results reveal channel structures and scours in the observed stratigraphy and GPR data (cf. Koster et al., 2013) as well as a thinning of the deposit inland (Fig. 4). In GPR profiles near outcrop BAR 03 the coarse grained layer with boulders and subangular stones is characterised by some hyperbolae reflection with v = 0.10-0.12 m/ns. The backwash deposits have slight horizontal reflectors, while the layer boundaries are characterized by stronger (mostly) continuous reflectors. The basement material as well as in some parts the sandy clay layer of the backwash deposit affects the radar waves with high attenuation.

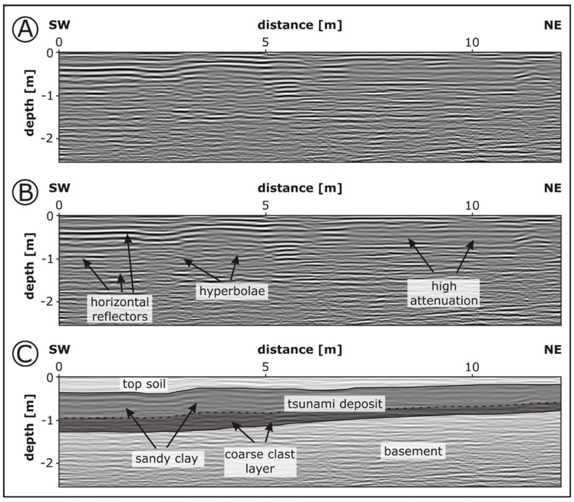


*Figure 4: GPR profile carried out perpendicular to coastline near outcrop BAR 03. (A) Processed GPR profile, (B) characteristic features, and (C) interpretation. Some characteristic hyperbolae show a lower coarse-grained layer (dark grey) inside the backwash deposit. The tsunami deposit shows clear thinning inland.*

Additionally, 3D models of the layer boundaries have been calculated to evaluate further features. These show that the lower boundary of the backwash deposit dips with a mean value of ~ 13° towards the Gulf of Cádiz; having a standard deviation value of 9° the calculated dipping angle varies between 4°-23° and the harmonic mean is ~ 7°. The mean thickness of the deposit near outcrop BAR 03 is 0.9 m. In this area we detect a minimum extent of the tsunamite ~17 m inland. Since 2008 the coastline has been transformed due to large winter storm events and high wave heights have eroded the beach section and the cliff. Due to the erosional processes along the coastline, it remains unclear how far the original extent was in a seaward direction.

## OSL DATING

Reicherter et al. (2010) suggested that the inferred tsunami deposit is related to the AD 1755 Lisbon event, but could not prove this by e.g. radiocarbon age dating. Now two optically stimulated luminescence (OSL) samples from the backwash deposit have been analysed in the Institute of Geography laboratory at Cologne University. The OSL dating confirms an age of around 4000 years BP for the deposits (4320 ± 900 years and 3880 ± 560 years; Tab. 1). Both samples have been taken ~2 m apart from each other at the base of the sandy clay backwash layer near outcrop BAR 07. According to the large error in the dating method of ~1000 years we suggest that the events E6 or E5/6 (cf. Holocene tsunami catalogue of Lario et al., 2011) could be traceable events.

*Tab. 1: OSL dates provided by Institute of Geography at University of Cologne.*

| Sample | n | % Aliquots | De (Gy) | OSL Alter (ka) |
|---|---|---|---|---|
| TB1 | 52 | 4 | 1.90 ± 0.33 | 1.55 ± 0.30 |
| | | 47 | 4.83 ± 0.33 | **3.92 ± 0.42** |
| | | 43 | 7.82 ± 0.55 | 6.35 ± 0.68 |
| | | 6 | 15.2 ± 1.7 | 12.3 ± 1.7 |
| **TB1 selected** | 15 | 100 | 5.32 ± 1.02 | **4.32 ± 0.90** |
| TB2 | 51 | 2 | 2.39 ± 0.39 | 1.78 ± 0.33 |
| | | 14 | 5.56 ± 0.51 | **4.16 ± 0.51** |
| | | 23 | 8.58 ± 0.78 | 6.41 ± 0.79 |
| | | 41 | 14.6 ± 1.0 | 10.9 ± 1.2 |
| | | 20 | 24.8 ± 2.0 | 18.6 ± 2.1 |
| **TB2 selected** | 27 | 14 | 5.19 ± 0.61 | **3.88 ± 0.56** |
| | | 32 | 8.28 ± 0.84 | 6.19 ± 0.81 |
| | | 28 | 12.8 ± 1.6 | 9.60 ± 1.44 |
| | | 27 | 20.6 ± 1.8 | 15.4 ± 1.9 |

Radiocarbon age data from a drill core sample of 2.58 m depth at Zahara de los Atunes (cf. Reicherter et al., 2010), carried out in the tidal channel area which is probably occasionally flooded, resulted in 4795 ± 25 years BP. This charcoal radiocarbon sample of a clayey peat layer was taken directly below a whitish sand sheet, which is interpreted as a tsunami deposit (Reicherter et al., 2010). The tsunamite was, therefore, deposited later than 4795 ± 25 years BP; it is not known how much of the clayey organic-rich layer was eroded during deposition.

## DISCUSSION & CONCLUSIONS

Our interpretation of the sediment depositing mechanisms along the beach section between Barbate and Zahara de los Atunes is based on former and recent field observations and documentation. Geometrical and internal sedimentary characteristics corroborate our interpretation of the occurrence of a high energy event.

Erosive and irregular bases, fining upward sequences (Reicherter et al., 2010) or mixed material from different origins (terrigenous and marine) are indicative of high energy event deposits. These features are commonly observed on other tsunami deposits worldwide (e.g., Dawson & Stewart, 2007; Bahlburg & Spiske, 2012). Also new features such as ball-like clay clasts coated with smaller coarse clasts can be observed.

Further tsunami evidence includes partly imbricated clasts which indicate a palaeo-flow direction towards the Gulf of Cádiz. Furthermore, observed channel structures and scours cannot form by fluvial systems because of the mixed marine and terrigenous composition of the deposit. Geochemical analyses provide evidence for element enrichment in the tsunamigenic layer.

We observed channel structures, scours and a landward thinning of the tsunami deposit in GPR profiles. Calculated 3D models generated a mean dipping angle of ~ 13° (harmonic mean: ~ 7°) of the base of the tsunami deposit.

In contrast to the findings of Cuven et al. (2013) in the Los Lances area, our dating of the inferred tsunami deposits yielded an age of around 4000 years BP, which fits well with two possible events described between 4000-5000 years BP by Lario et al. (2011).

The outcome of our present sedimentological and geochemical analysis as well as MagSus measurements, GPR investigations and OSL dating reveal further tsunami deposit characteristics for the study area near Barbate. These results have to be discussed carefully concerning other findings along the coast of Gulf of Cádiz as they do not always complement each other. Final analyses of all data are not yet finished, but give very promising preliminary insights.

## OUTLOOK

Future work will include the detailed evaluation of all data collected during the field campaign in March 2013 as well as detailed analysis of geochemical parameters, magnetic susceptibility grids and detailed 3D GPR subsurface models for further geomorphological interpretation.

**Acknowledgements:** The first author is deeply grateful for being funded by RWTH Aachen Scholarships for Doctoral Students. We thank Tom Rockwell, Beverly Goodmann, Kurt Decker, Niklas Mörner, Pablo Silva, Christoph Grützner, Franziska Facius and Andreas Vött for discussion in the field; thanks are extended to Alexandra Hilgers for OSL dating. We would also like to thank the 2013 Barbate beach fieldwork crew (Alexander Rösner, Fabian Stamm, Johannes Aichele, Joschka Röth & Barbara Wolff).

## References

Álvarez-Gómez, J.A., Í. Aniel-Quiroga, M. González & L. Otero, (2011). Tsunami hazard at the Western Mediterranean Spanish coast from seismic sources. *Natural Hazards and Earth System Sciences* 11 (1), 227-240.

Bahlburg, H. & M. Spiske, (2012). Sedimentology of tsunami inflow and backflow deposits: key differences revealed in a modern example. *Sedimentology* 59 (3), 1063-1086.

Baptista, M.A. & J.M. Miranda, (2009). Revision of the Portuguese catalog of tsunamis. *Natural Hazards and Earth System Sciences* 9**,** 25-42.

Chagué-Goff, C., A. Andrew, W. Szczuciński, J.R. Goff & Y. Nishimura, (2012). Geochemical signatures up to the maximum inundation of the 2011 Tohoku-oki tsunami — Implications for the 869 AD Jogan and other palaeotsunamis. *Sedimentary Geology* 282, 65-77.

Cuven, S., R. Paris, S. Falvard, E. Miot-Noirault, M. Benbakkar, J.-L. Schneider & I. Billy, (2013). High-resolution analysis of a tsunami deposit: Case-study from the 1755 Lisbon tsunami in southwestern Spain. *Marine Geology* 337, 98-111.

Dawson, A.G. & I. Stewart, (2007). Tsunami deposits in the geological record. *Sedimentary Geology* 200 (3-4), 166-183.

Koster, B., H. Hadler, A. Vött & K. Reicherter, (2013). Application of GPR for visualising spatial distribution and internal structures of tsunami deposits – Case studies from Spain and Greece. *Zeitschrift für Geomorphologie*, Supplementary Issues, *in press.*

Lario, J., C. Zazo, J.L. Goy, P.G. Silva, T. Bardají, A. Cabero & C. Dabrio, (2011). Holocene palaeotsunami catalogue of SW Iberia. *Quaternary International* 242 (1), 196-200.

Mullins, C.E. (1977). Magnetic susceptibility of the soil and its significance in soil science - a review. *Journal of Soil Science* 28 (2), 223-246.

Reicherter, K., D. Vonberg, B. Koster, T. Fernández-Steeger, C. Grützner & M. Mathes-Schmidt, (2010). The sedimentary inventory of tsunamis along the southern Gulf of Cádiz (southwestern Spain). *Zeitschrift für Geomorphologie*, Supplementary Issues 54 (3), 147-173.

Vött, A., F. Lang, H. Brückner, K. Gaki-Papanastassiou, H. Maroukian, D. Papanastassiou, A. Giannikos, H. Hadler, M. Handl, K. Ntageretzis, T. Willershäuser & A. Zander, (2011). Sedimentological and geoarchaeological evidence of multiple tsunamigenic imprint on the Bay of Palairos-Pogonia (Akarnania, NW Greece). *Quaternary International* 242, 213-239.

# Upper Pleistocene to Holocene earthquakes recorded at the western termination of the Venta de Bravo Fault System, Acambay Graben (Central Mexico)

*Lacan, Pierre (1), Ortuño, María (2), Perea, Hector (3), Baize, Stephane (4), Audin, Laurence (5), Aguirre, Gerardo (1), Zúñiga, Francisco Ramón (1)*

(1) Centro de Geociencias, Universidad Nacional Autónoma de México, Blvd. Juriquilla, 3001, 76230, Juriquilla, Querétaro, México
Email: placan@geociencias.unam.mx
(2) Dept. de Geodinàmica i Geofísica, Universitat de Barcelona, C/ Martí i Franquès s/n, 08028, Barcelona, Spain.
(3) Barcelona-CSI, Institut de Ciències del Mar - CSIC, CMIMA, Psg. Martim de la Barceloneta, 37-49, 08003, Barcelona, Spain.
(4) Institute of Radiological Protection and Nuclear Safety (IRSN), Seismic Hazard Division (BERSSIN), BP 17, 92262 Fontenay-aux-Roses, France.
(5) Institut des Sciences de la Terre, ISTerre, IRD, Université Joseph Fourier, Grenoble I, OSUG, France.

***Abstract:*** The Venta de Bravo fault is one of the longest and most active structures within the intra-arc zone of the Trans-Mexican Volcanic Belt. It defines, with the Pastores Fault, the southern margin of the Acambay graben, extending E-W along nearly 80 km. In this study, we mapped the western termination of the fault, which is divided into different branches. Through a geomorphic analysis we identified two paleoseismological sites along the main fault with a well preserved upper Pleistocene to Holocene sedimentary record. Six trenches were dug showing volcanic deposits interbedded with fluvio-lacustrine and colluvial deposits. Despite the lack of historical destructive earthquakes nearby the fault, the observed deformations in the deposits suggest that the Venta de Bravo fault produced at least four earthquakes during the last 21 ka.

***Key words****:* Acambay graben, active faults, paleoearthquake chronology, Mexico.

## INTRODUCTION

The Acambay graben is located in the Transmexican Volcanic Belt (TMVB), a 900 km long and 200 km wide extensional zone that crosses Mexico from the Gulf of Mexico, in the East, to the Pacific Coast, in the West (Fig. 1). In this region, active crustal deformation is associated with the subduction of the Rivera and Cocos plates underneath the Northamerican plate (Ferrari et al., 2012). Based on 13 vertical Quaternary slip rates determined during previous studies the deformation rate of each individual fault within the TMVB does not exceed 0.3 mm/a since the last 0.3 million years (Suter et al., 2001), and thus defines these as slow faults. Among the main fault systems that comprise the TMVB are the Chapala, Morelia, Acambay and Queretaro grabens. According to the historical seismicity catalogue, these faults, affecting the most populated region of Mexico, are capable to produce Mw=7 earthquakes. Some good characteristic examples of these intraplate earthquakes are the Chapala (1568, Mw ~ 7), Jalisco, 1875 (Mw ~ 7.1), Acambay, 1912 (mb=6.9; Urbina and Camacho, 1913) and Jalapa, 1920 events (mb = 6.4; Suarez, 1992).
This study focuses on the Venta de Bravo fault (Fig. 2), one of the longest and most active faults of the TMVB (Suter et al. 1995, 2001). This fault is part of the Morelia-Acambay fault system (Martínez-Reyes and Nieto-Samaniego, 1990; Suter et al., 1992; 1995; 2001; Garduño et al., 2009) and defines, with the Pastores Fault, the southern boundary of the Acambay graben (Langridge et al. 2000). The Venta de Bravo fault dips 50-70º to the north and is characterized by a discontinuous geomorphic trace, mainly developed on lava flows of different composition. The fault trace length is approximately 50 km and the height of the scarp in its central part reaches 300 m. Based on the age of Lake deposits affected by the fault on its eastern termination, Suter et al. (1992) calculated a vertical slip rate of 2 mm/yr for the Venta de Bravo fault since 23 ka. This slip rate appears to have been overestimated (Suter et al., 2001).

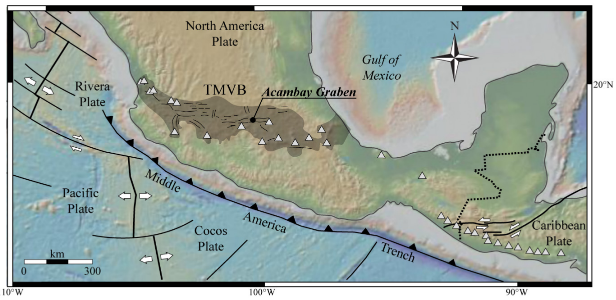


*Fig. 1: Location of the Acambay graben within the Trans-Mexican Volcanic Belt (TMVB).*

No historical destructive events were reported along the Venta de Bravo fault. However instrumental seismicity includes relatively strong earthquakes along that fault as the February 22th, 1979, mb = 5.3 Maravatio earthquake (Suter et al., 1992).
More recently, Ortuño et al. (2012) performed a paleoseismic study on the west-central part of the Venta de Bravo fault, concluding that it produced at least two earthquakes during the last 10 ka.

## PALEOSEISMOLOGICAL STUDY OF THE VENTA DE BRAVO FAULT

In order to evaluate the seismogenic activity of the Venta

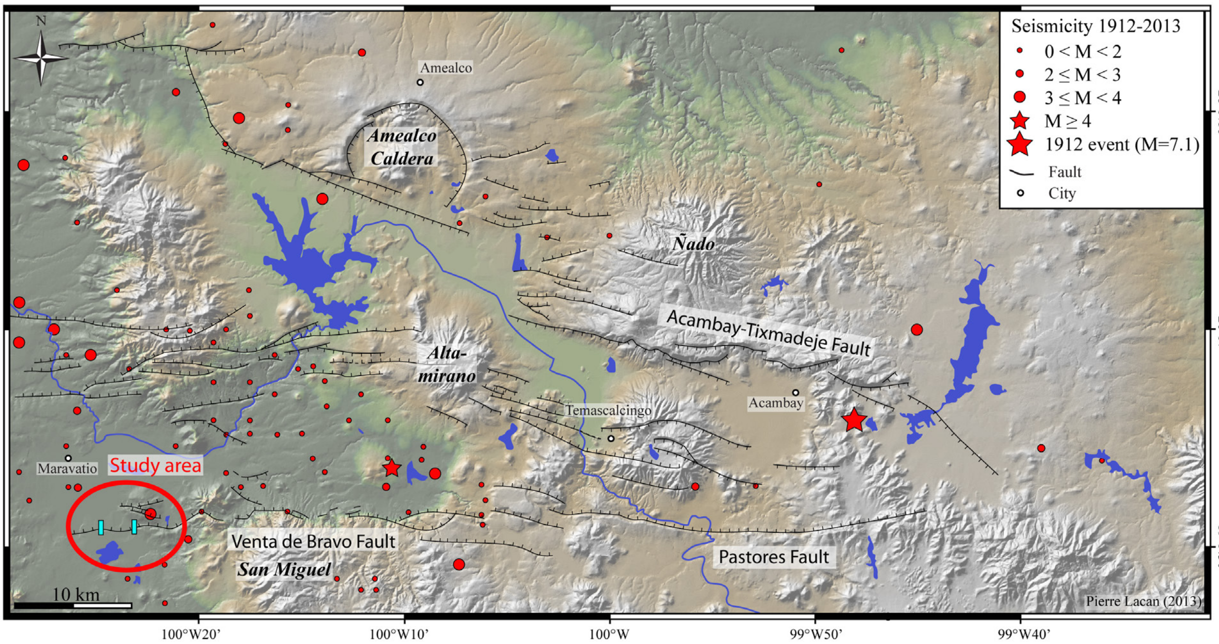


*Fig. 2: Map of the Acambay graben. Faults and historical and instrumental seismicity are reported after F.R. Zúñiga (personal communication). The red ellipse points to the trenches presented in this paper.*

de Bravo fault, we focus on its westernmost termination where a river crosses the fault trace and recent sediments are likely to be preserved. We performed an integrated study combining basic geomorphological and structural cartography to define the location of the fault trace and to identify sites suitable for paleoseismological trenching (Fig. 3). Accordingly to our observations, the western tip of the Venta de Bravo fault displays a fan-like termination array of at least 3 secondary fault segments (Fig. 3). Thus, the activity of the Venta de Bravo fault could be partially distributed along these segments. We obtained topographic profiles across the fault in order to refine the location of the fault trace across the alluvial terraces. The fault affects Upper Pleistocene to Holocene fluvio-lacustrine sequences and Pleistocene scoria cones (Suter et al., 1992). On these sites, the excavation of six trenches perpendicular to the fault trace allowed to study the last 21 ka deformation history on the western termination of the fault.

The easternmost site is the Guapamacataro site, where the fault crosses the alluvial terraces of the San Ramón River and where the Holocene seismogenic deformations are well preserved into the sedimentary record.


*Fig. 3: 3D view of the western termination of the Venta de Bravo Fault. The paleoseismological sites of Guapamacataro and Campo Hermoso are reported.*

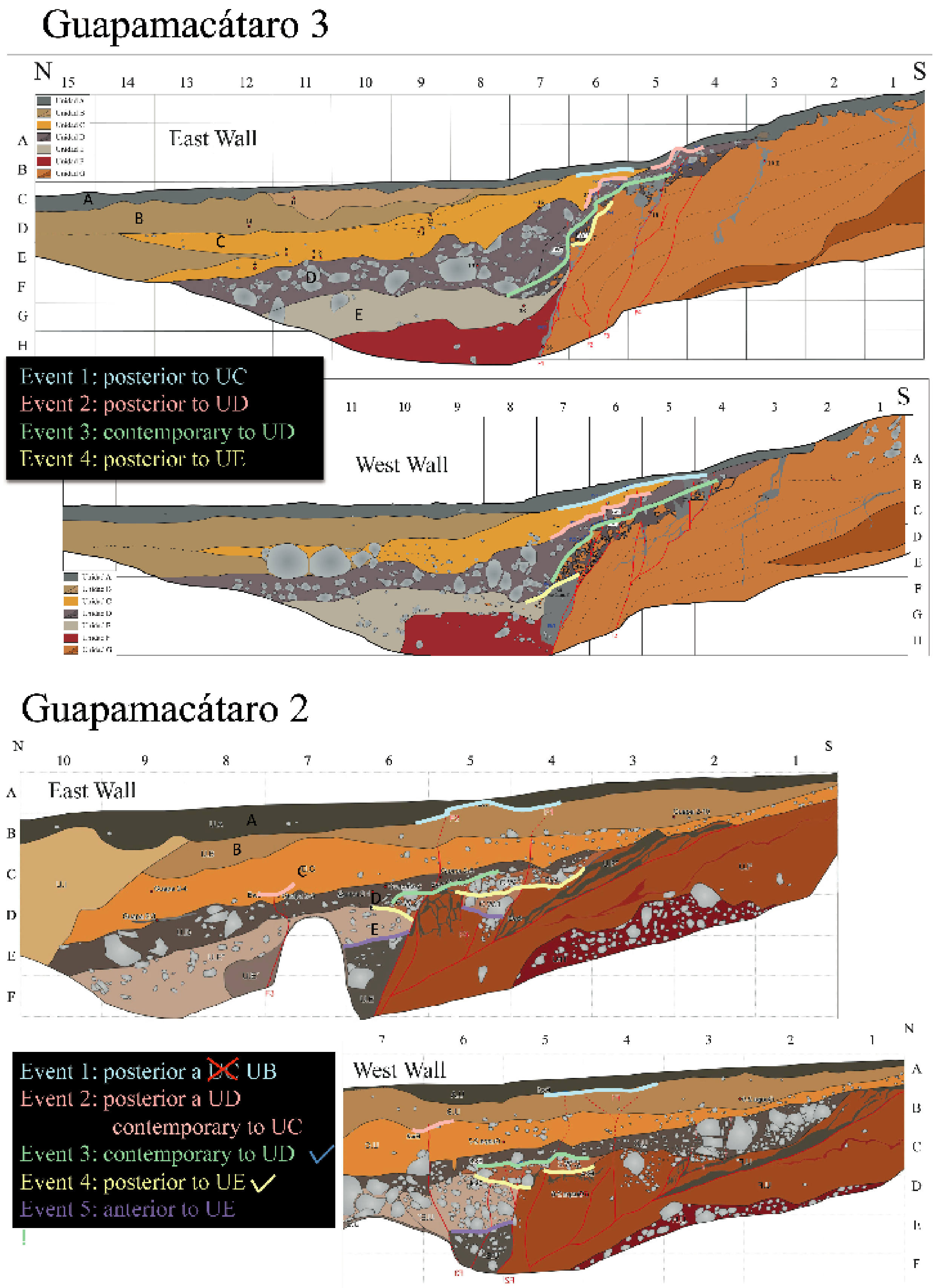


*Fig. 4: Interpretation of two of the three trenches dug on Guapamacataro site. These trenches were visited by participants of the 2012 INQUA field trip in Morelia.*

The study of three paleoseismic trenches in the Guapamacataro site leads us to identify at least four, and possibly five, paleoseismological events recorded on the alluvial terraces of the San Ramón River that are offset by the fault trace (Fig. 3 and 4). Each event corresponds to a vertical displacement between few centimeters to about 50 centimeters. Some of the events are evidenced by the presence of colluvial wedges associated to the main fault trace.

The westernmost site is the Campo-Hermoso site, which is closer to the termination of the fault system. Based on preliminary dating results, at least three seismic events were identified between 21 ka and 3.8 ka. These events correspond to a vertical displacement between 20 centimeters to 1 meter. Some of the Campo Hermoso paleoevents identified are suspected to be correlated with those identified on the Guapamacataro site.

## CONCLUSION

The study of six trenches in the Guapamacataro and Campo Hermoso sites revealed that the main segment of the western Venta de Bravo fault is active and has produced at least four earthquakes during the last 21 ka. The identified paleoearthquakes have produced moderate vertical surface displacements (< 50 cm) of the sedimentary and volcanic deposits. Samples are being processed and analysed. The result of the datings will allow us to correlate the seismic paleoevents between both sites. Furthermore, these results will lead to propose a recurrence period for that fault where no historical destructive earthquake have been reported, but, as here shown, which could produce surface rupturing events.

**Acknowledgements:** This research was founded by the Mexican Government through CONACYT (Ciencia Básica- 2009) and by the Universidad Nacional Autónoma de México- UNAM (PAPIIT-2009).

## References

Ferrari, L., Orozco-Esquivel, T., Manea, V., Manea, M., 2012. The dynamic history of the Trans-Mexican Volcanic Belt and the Mexico subduction zone. *Tectonophysics* 522-523, 122-149.

Garduño-Monroy, V. H., Pérez-Lopez, R., Israde-Alcantara, I. , Rodríguez-Pascua, M. A., Szynka-ruk, E., Hernández-Madrigal, V. M., García-Zepeda, M. L., Corona-Chávez, P., Ostroumov, M., Medina-Vega, V. H., García-Estrada, G., Carranza, O., Lopez-Granados, E., Mora Chaparro, J. C., 2009. Paleoseismology of the southwestern Morelia-Acambay fault system, central Mexico. *Geofísica Internacional* 48 (3), 319-335

Langridge, R., Weldon, R., Moya, J. and Suarez, G., 2000. Paleoseismology of the 1912 Acambay earthquake and the Acambay-Tixmadejé fault, Trans-Mexican Volcanic Belt. *J. Geophys. Res.*, 105, 3019–3037

Martínez Reyes, J., Nieto-Samaniego, A., 1990. Efectos geológicos de la tectónica reciente en la parte central de México. *Revista Instituto de Geología* 9, 33 -50.

Ortuño Candela M., Zúñiga Dávila-Madrid R., Corominas O., Perea H., Ramírez Herrera M.T., Štepancíková P., Villamor P. y Norini G., 2012. Paleoseismology of the Venta de Bravo, Tepuxtepec and Temascalcingo faults (Transmexican Volcanic Belt) . *Unión Geofísica Mexicana* 2012, Abstract SE11-8.

Suárez, G., 1992. El sismo de Jalapa del 3 de Enero de 1920. *Rev. Mex. Ing. Sism*. 42, 3–15.

Suter, M., Quintero, O., and Johnson, C.A., 1992. Active faults and state of stress in the central part of the Trans-Mexican volcanic belt, 1-The Venta de Bravo fault: *Journal of Geophysical Research*, 97, 11983–11994.

Suter, M., Quintero, O, López-Martínez, M., Aguirre-Díaz, G. and Farrar, E. 1995. 'The Acambaygraben: Active intrarc extension in the Trans-Mexican Volcanic Belt, Mexico, *Tectonics*, 14(5), 1245–1262.

Suter, M., López-Martínez, M., Quintero O, and Carrillo-Martínez, M., 2001. Quaternary intra-arc extension in the central Trans-Mexican vol- canic belt.*Geological Society of America Bulletin,* v. 113, no. 6, p. 693– 703.

Urbina, F. and Camacho, H. 1913. La zona Megaseismica Acambay–Tixmadeje, Estado de México, conmovida el 19 de noviembre de 1912, *Bol. Inst. Geol. Mex.*, 32, 125.

INQUA Focus Group on Paleoseismology and Active Tectonics

paleoseismicity.org

# Lake Issyk Kul: Neotectonic deformation of (paleo-) shorelines and their link with intermontane basin closure and lake-level fluctuations

*Angela Landgraf (1), Swenja Rosenwinkel (1), Atyr Djumabaeva (2), Kanatbek Abrakhmatov (2), Oliver Korup (1), Manfred R. Strecker (1)*

(1) Inst. Für Erd- und Umweltwissenschaften, Universität Potsdam, Potsdam, GERMANY. Email: landgraf@geo.uni-potsdam.de
(2) Kyrgyz Institute of Seismology, Bishkek, KYRGYZSTAN

***Abstract:*** *A set of paleo-shorelines and lacustrine deposits straddling Lake Issyk Kul, furnishing ample evidence for major lake-level fluctuations during the Quaternary, and helping identify transient fluvial connectivity with other basins and overflow conditions. Major historic earthquakes, tectonically deformed landforms, paleoseismological evidence, and voluminous mass movements indicate that climate alone is not the only driver for changes in lake dynamics. We aim to quantify shoreline deformation, accompanied by dating of associated marker horizons. We will focus on events and mechanisms responsible for basin closure and changes in fluvial connectivity of the lake system, recorded in the stratigraphy and geomorphology of the western lake outlet. Here, we present first results of this ongoing project from selected areas at the outlet, as well as along the northern and southern shore.*

***Key words****: Tectonic geomorphology, lake shorelines, Issyk Kul*

## ACTIVE FAULTING, SHORELINE CORRELATION, LAKE LEVEL FLUCTUATIONS, AND ENDORHEISM OF ISSYK KUL

The compressional basin-and-range topography of the Tien Shan is the result of ongoing deformation, related to the India-Asia collision (e.g., Molnar and Tapponnier, 1975; Abdrakhmatov et al., 1996; Thompson et al., 2002). Around the turn of the 19th century, a series of large earthquakes, exceeding magnitude 7, has affected the northern Tien Shan, e.g., in 1885 (Ms 6.9), 1887 (Ms 7.3), 1889 (Ms 8.3), and 1911 (Ms 8.1) (e.g., Abdrakhmatov et al., 2002). Present-day seismicity shows mostly moderate earthquake events (Kalmetieva et al., 2009). The Issyk Kul region is clearly seismically active (Fig. 1). GPS-derived velocities show that 5-6 mm/a of shortening and additionally 1-2 mm/a left shearing are accommodated between the southern and northern shores of the lake (Zubovich et al., 2010).

Lake shorelines are excellent geomorphic markers and reference horizons, because they are perfectly horizontal (that is, parallel to the local geoid) at the time of their formation. Any subsequent deformation of these markers represents the interplay of a tectonic signal with possible subsidence and rebound related to lake-level fluctuations and thus might provide information on crustal strength and differential tectonic movements (e.g., Bills et al., 1994; 2007; Adams et al., 1999).

The present-day lake Issyk Kul is located at 1607 m elevation and is surrounded by 688 km of shoreline (De Batist et al., 2002). The lake has a trapezoidal shape and is asymmetric with steeper southern than northern slopes (Fig. 2A). It reaches a maximum depth of 668 m slightly SW of the geometric basin centre. The lake is endorheic today and the present-day sill has an elevation of 1620 m. Two prominent shorelines have been recorded at elevations of about 1660 m and about 1623 m, and have been radiocarbon-dated to about 25 ka and about 500 yrs (e.g., Burgette, 2008; see Fig. 2A and B). However, some of the radiocarbon results show a clear mismatch with previous dating of lake sediments using Infrared-stimulated thermosluminescence (IRSL), with the IRSL ages being systematically younger by about 14ka (Bowman et al., 2004a; Burgette, 2008).

Historical records document additional lake-level fluctuations (Trofimov, 1978; Ricketts et al., 2001; Romanovsky, 2002 and references therein) and a network of submerged channels and terraces record a major lake-level drop of about 110 m below the present-day level (e.g., De Batist et al., 2002).

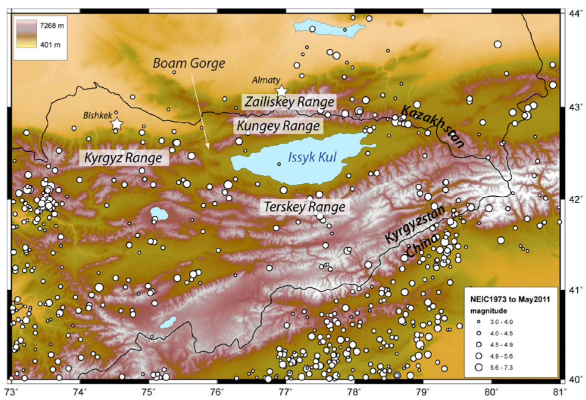


*Fig. 1: Topographic map of the Kyrgyz Tien Shan and Lake Issyk Kul and present-day seismicity of central Asia. Note the compressional basin-and- range topography which is the result of the ongoing deformation, related to the India-Asia collision. The Issyk Kul basin is located near the Kyrgyz-Kazakh border, between the Kyrgyz range in the west, the Kungey und Zailiskey ranges in the north, and the Terskey range in the south. Stars depict cities Bishkek (Kyrgyz capital) and Almaty (largest city and former capital of Kazakhstan).*

Despite previous studies, the causes and consequences of the large Issyk Kul lake-level fluctuations are not yet fully understood. It is widely assumed that the western outlet and sill plays a significant role in controlling the basin hydrology. This outlet is located in a crucial setting, sensitive to tectonic deformation or potential impoundment by mass movements. Indeed, temporal blockage of the Chu River, which formerly drained the lake, is inferred to have caused the late Pleistocene lake highstand. The course of the present-day Chu River (Fig. 2A and C) is remarkable; it bypasses the lake at its western proximity in a 90° turn, before it drains westward through the narrow Boam gorge. Importantly, a major knickpoint disturbs the longitudinal river profile at a location inside the Boam gorge that roughly coincides with the distal (western) limit of the highstand lake sediments (Fig. 2C). These lake beds have been dated to ~ 25ka, are possibly associated with the highest lake-level (Burgette, 2008), and are currently being re-incised. Again, this possible scenario emphasizes the ambiguity that lake records may provide during episodes of lake highstands.

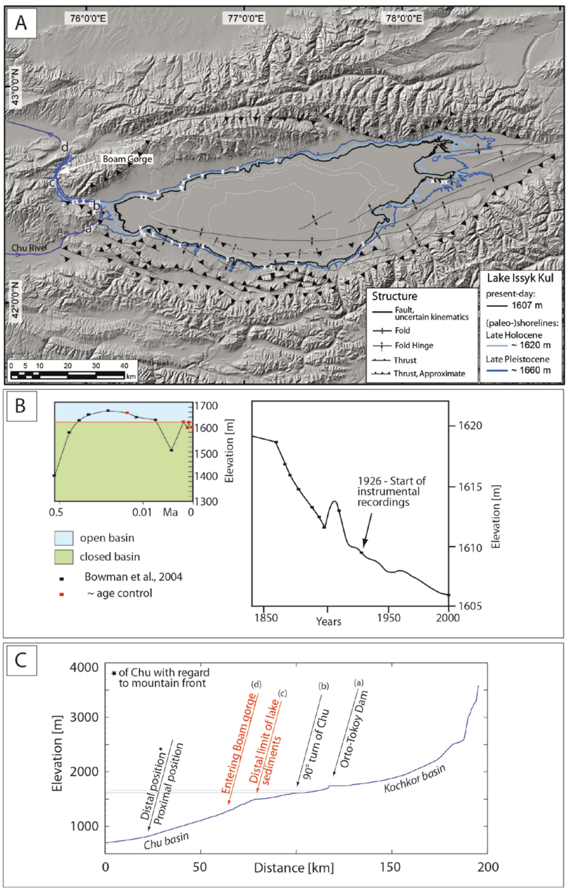


*Fig. 2: Characteristics of Issyk-Kul lake-level fluctuations and their geomorphic signature. (A) SRTM 90 m per pixel hillshade of Lake Issyk Kul with its present-day lake surface (black line) and the two prominent paleo-shorelines (blue). Bathymetry (redrawn from geological maps) is given in gray contours at 50, 100, 200, and 500 m below surface. Faults and folds are redrawn from Bowman et al. (2004) and Burgette (2008). Also highlighted is the Chu-River which presently bypasses Lake Issyk Kul, but has probably drained the lake through the Boam gorge during historical lake highstands. Small letters correspond to locations of geomorphic features shown in (C) White crosses are approximate locations of field-based measurements. (B) Summarized Issyk Kul lake-level fluctuations over time (redrawn after Trofimov, 1978 and Bowman et al., 2004). Left figure: Fluctuations from Mid-Pleistocene on, red markers indicate age control from different sources. The red line indicates the elevation of the present-day sill (1620m), thus marking the theoretical separation between open and closed basin systems, suggesting exorheic conditions during the highstands. However, tectonic deformation and/or landsliding might have temporarily elevated the sill, blocked the drainage and caused lake highstand under endorheic conditions. Right figure shows detailed historical lake-level fluctuations which is basically a steady regression to the present-day level. (C) Longitudinal river profile of the Chu River between 75° E / 42.93° N and 75.0475° E / 42.158° N. Slight disturbances in the profile can be related to geometric complexities in the river. However, the most prominent feature is a major knickpoint, located inside the Boam gorge and roughly coinciding with the distal limit of the lake sediments (marked in red). Horizontal lines correspond to the approximate elevations of the two prominent highstands.*

Clearly, understanding the dynamics of the western outlet of the lake is key to test whether the phases of lake closure and subsequent phases of re-established fluvial connectivity were associated with catastrophic events (tectonic event/landslide and outburst with/without catastrophic flooding), or, alternatively, if lake-level changes were solely driven by the longer-term effects of climate and basin hydraulics (evaporation, sediment budget, outlet erosion/retreat), as has been proposed by Garcia-Castellanos (2006). In mountainous areas, many naturally dammed lakes mainly formed by large landslides or glacier-derived debris can remain intact and trap large water bodies over timescales extending for hundreds or even several thousands of years (Hermanns and Strecker, 1999; Bookhagen et al., 2005; Strom and Korup, 2006; Korup et al., 2006; 2007; Korup and Tweed, 2007; Hewitt et al., 2008). Similar landslide dams have been documented in other parts of the Kyrgyz Tien Shan (e.g., Korup et al., 2006). Overspilling and outburst of such natural dams, however, can be accompanied by catastrophic flooding. Such large magnitude-low frequency events might be recognizable and datable in the sedimentary succession downstream of the outflow.

To better understand the Quaternary evolution of the lake and its seismically active boundaries on different time scales, we

- Generate a neotectonic map of the Issyk Kul region with an inventory of active faults, folds, and deformation-related geomorphic landforms and deposits (landslides, terraces, alluvial fans) and lake-related landforms and deposits (shorelines, wave-cut notches, lake deposits). This will be based on the synthesis of existing geologic maps, study of high-resolution satellite imagery, and exploratory field work in key locations.
- Conduct a high-resolution topographic survey of correlated shorelines and distinguish and quantify their deformation in an attempt to

separate long-wavelength warping from local seismogenic deformation and seismotectonic segmentation.

- Expand the existing shoreline chronology by further radiometric/cosmogenic dating to unambiguously correlate basin-wide deformation features and elucidate the nature of the western outlet and its role in basin closure and reopening.

Shorelines in the study area can be constructional and erosional, they are typically better developed or preserved along the southern than at the northern shore. Shoreline indicators, we have used are terraces, beach ridges, wave cut platforms, lake sediments, and delta deposits. While the appearance on satellite imagery is very pronounced in places, in the field, their exact measurements are hampered by degradational processes. For instance, cliffs, into which the shorelines are cut, are composed of easily erodible lake beds and the shorelines are typically covered by rubble. To overcome this dilemma, vertical profiles were conducted. From these profiles, intersection points between the cliff part and the wave-cut terrace part have been calculated to infer the elevation of the paleo-shoreline. In total, we have collected 78 profiles across shorelines, but also across related features as dry paleo-lagoons, and delta- or fan-related terraces using d-GPS measurements from field campaigns. Of these profiles, 22 have been measured beyond the sill and inside the Boam gorge, 12 have been measured along the northern shore, and the majority of 44 profiles come from the southern shore of Issyk Kul (see Fig. 2 for location). In only few locations, both prominent shorelines have been captured by the same profile. These data were accompanied by few terrestrial laser-scans of selected outcrops and a remote sensing survey using 2.5 m resolution SPOT imagery.

At the outlet, we have sampled the terraces for dating using terrestrial cosmogenic nuclides (depth profiles). These terraces contain and are covered with boulders measuring up to 4 m in diameter. Some of them show flute cast appearance on the ground and none has striations that would unambiguously identify them as glacial drift deposit. We measured long axes of a variety of boulders for hydraulic paleo-flow modelling and sampled the surfaces of selected examples for cosmogenic nuclide dating.

We present preliminary data from selected areas, showing the differences in shoreline-elevation and its possible relation to active tectonics. On the basis of their comparison, we will also discuss the (geomorphic) uncertainty and thus the degree to which the shoreline-elevation can be resolved in such settings.

**Acknowledgements:** We would like to thank the DFG-SPP 1006/17 for funding of this project (LA 3078/1-1).

**References**

Abdrakhmatov, K.E., Aldazhanov, S.A., Hager, B.H., Hamburger, M.W., Herring, T.A:, Kalabaev, K.B., Makarov, V.I., Molnar, P., Panasyuk, S.V., Prilepin, M.T., Reilinger, R.E., Sadybakasov, I.S., Souter, B.J., Trapeznikov, Yu.A., Tsurkov, V.Ye., and Zubovich, A.V., (1996). Relatively recent construction of the Tien Shan inferred from GPS measurements of present-day crustal deformation rates, *NATURE*, 384, 450-453.

Abdrakhmatov, K.E., Weldon, R., Thompson, S., Burbank, D., Rubin, C., Miller, M., and Molnar, P., (2001). Origin, direction, and rate of modern compression of the central Tien Shan (Kyrgyzstan), *Geologiya I Geofizika*, 42, 1585-1609.

Abdrakhmatov, K.E., Delvaux, D., and Djanuzakov, K.D., (2002). Active tectonics and seismic hazard of the Issyk-Kul Basin in the Kyrgyz Tian-Shan, in Klerx, J., and Imanackunov, B., eds., *Lake Issyk-Kul: Its natural environment*, Vol. IV. Earth and Environmental Sciences, 13, 147-160.

Adams, K. D., S. G. Wesnousky, and B. G. Bills, (1999). Isostatic rebound, active faulting, and potential geomorphic effects in the Lake Lahontan basin, Nevada and California, *Bull. Geol. Soc. Am.*, 111, 1739-1756.

Bills, B. G., S. L. de Silva, D. R. Currey, R. S. Emenger, K. D. Lillquist, A. Donnellan, and B. Worden, (1994). Hydro-isostatic deflection and tectonic tilting in the Central Andes: Initial results of a GPS survey of Lake Minchin shorelines, *Geophys. Res. Lett.*, 21, 293– 296.

Bills, B. G., K. D. Adams, and S. G. Wesnousky, (2007), Viscosity structure of the crust and upper mantle in western Nevada from isostatic rebound patterns of the late Pleistocene Lake Lahontan high shoreline, *J. Geophys. Res.*, 112, B06405.

Bookhagen, B., Thiede, R., and Strecker, M.R., (2005). Late Quaternary intensified monsoon phases control landscape evolution in the NW Himalaya. *Geology*, 33, 149-152.

Bowman, D., Korjenkov, A., & Porat, N., (2004). Late-Pleistocene seismites from Lake Issyk-Kul, the Tien Shan range, Kyrghyzstan, *Sedimentary Geology*, 163, 211-228.

Burgette, R.J., (2008). Uplift in response to tectonic convergence: The Kyrgyz Tien Shan and Cascadia subduction zone [PhD thesis]: 242 p., University of Oregon.

De Batist, M., Imbo, Y., Vermeesch, P., Klerkx, J., Giralt, S., Delvaux, D., Lignier, V., Beck, C., Kalugin, I., and Abdrakhmatov, K.E., (2002), Bathymetry and sedimentary environments of Lake Issyk-Kul, Kyrgyz Republic (Central Asia): a large, high-altitude, tectonic lake, in Klerx, J., and Imanackunov, B., eds., *Lake Issyk-Kul: Its natural environment*, Vol. IV. Earth and Environmental Sciences, 13, 101-124.

Garcia-Castellanos, D., (2006). Long-term evolution of tectonic lakes: Climatic controls on the development of internally drained basins. In: *Tectonics, Climate, and Landscape evolution*. Eds.: S.D. Willett, N. Hovius, M.T. Brandon & D.M. Fisher. GSA Special Paper 398, 283-294.

Hermanns, R. and Strecker, M. (1999), Structural and lithological controls on large Quaternary bedrock landslides in NW-Argentina. *Geological Society of America Bulletin*, 111, 934-948.

Hewitt, K., Clague, J.J., and Orwin, J.F., (2008). Legacies of catastrophic rock slope failures in mountain landscapes, *Earth Sci. Reviews*, 87, 1-38.

Kalmetieva, Z.A., Mikolaichuk, A.V., Moldobekov, B.D., Meleshko, A.V., Jantaev, M.M., Zubovich, A.V., (2009). Atlas of Earthquakes in Kyrgyzstan. ECHO, UNISDR, and CAIAG, p. 233.

Korup, O., Strom, A.L., and Weidinger, J.T., (2006). Fluvial response to large rock-slope failures - examples from the Himalayas, the Tien Shan, and the Southern Alps in New Zealand, *Geomorphology*., 78, 3-21.

Korup, O., Clague, J.J., Hermanns, R.L., Hewitt, K., Strom, A.L., and Weidinger, J.T., (2007). Giant landslides, topography, and erosion, *Earth Planet. Sci. Lett.*, 261, 578-589.

Korup, O. and Tweed, F., (2007). Ice, moraine, and landslide dams in mountainous terrain, *Quat. Sci. Rev*., 26, 3,406–3,422.

Molnar, P. and Tapponnier, P., (1975). Cenozoic Tectonics of Asia: Effects of a Continental Collision, *Science*, 189, 419-426.

Ricketts, R.D., Johnson, T.C., Brown, E.T., Rasmussen, K.A. and Romanovsky, V.V., (2001). The Holocene paleolimnology of Lake Issyk-Kul, Kyrgyzstan: trace element and stable isotope composition of ostracodes, *Palaeogeography, Palaeoclimatology, Palaeoecology*, 176, 207-227.

Romanovsky, V.V., (2002). Water level variations and water balance of Lake Issyk-Kul, in Klerx, J., and Imanackunov, B., eds., *Lake Issyk-Kul: Its natural environment*, Vol. IV. Earth and Environmental Sciences, v.13, p. 45-58.

Strom, A.L. and Korup, O., (2006). Extremely large rockslides and rock avalanches in the Tien Shan mountains, Kyrgyzstan, *Landslides*, 3, 125-136.

Thompson, S.C., Weldon, R.J., Rubin, C.M., Abdrakhmatov, K., Molnar, P., and Berger, G.W., (2002). Late Quaternary slip rates across the central Tien Shan, Kyrgyzstan, central Asia: *Journal of Geophysical Research-Solid Earth*, 107 (B9), 2203, doi:10.1029/2001JB000596.

Trofimov, A.K., (1978). Bottom relief of Issyk-Kul: Geological Basis of Seismic Division of the Issyk-Kul Hollow (in Russian). Frunze Ilim, pp. 57-66.

Zubovich, A.V., Wang, X.q., Scherba, Y.G., Schelochkov, G.G., Reilinger, R., Reigber, C., Mosienko, O.I., Molnar, P., Michajljow, W., Makarov, V.I., Li, J., Kuzikov, S.I., Herring, T.A., Hamburger, M.W., Hager, B.H., Dang, Y.m., Bragin, V.D., and Beisenbaev, R.T., (2010). GPS velocity field for the Tien Shan and surrounding regions, *Tectonics*, 29, p. 23, TC6014.

INQUA Focus Group on Paleoseismology and Active Tectonics

paleoseismicity.org

# Paleoseismicity at the Monte Netto site (Southern Alps, N Italy): blind thrust activity deduced from secondary fold-related faults

*Livio, Franz (1), Andrea Berlusconi (1), Alessandro M. Michetti (1), Andrea Zerboni (2), Luca Trombino (2), Christoph Spötl (3), Helena Rodnight (3)*

(1) Department of Chemical and Environmental Sciences, University of Insubria. Via Valleggio 11, 22100 Como (Italy). Email: franz.livio@uninsubria.it
(2) Dipartimento di Scienze della Terra "A. Desio", Università degli Studi di Milano, Via Mangiagalli 34, 20133 Milano (Italy).
(3) Institut für Geologie und Paläontologie, Universität Innsbruck. Innrain 52, 6020 Innsbruck (Austria).

***Abstract:*** *At Monte Netto site (Southern Alps, N Italy), we have found, for the first time in this area, paleoseismological evidence of recent blind thrust activity during late Pleistocene, deduced from secondary fold-related faults and liquefaction features. Extensive trench investigations conducted at this site exposed a thick loess-paleosol sequence deformed by a growing gravity-graben structure, due to secondary fold amplification; progressive displacement along the gravity graben is also associated to paleoliquefaction. Loess deposition have been dated, through $^{14}C$ and OSL, to Upper Pleistocene. We recognized 3 different normal faulting events along the gravity-graben, occurred between ca. 45 Kyr B.P and 5 Kyr B.P and due to as many paleo-earthquakes generated by the activity of the main buried seismogenic thrust. This site represents the first clear evidence in this area that strong blind thrusting earthquakes can also cause, besides broad uplift, localized medium-to-small scale deformation, thus posing some important issues on the assessment of A) surface faulting hazard, and B) even more critical, the magnitude threshold for surface faulting earthquakes in the Po Plain area.*

***Key words**: Southern Alps, Po Plain foredeep, blind thrust, fold-related faults.*

## *INTRODUCTION*

This note presents new evidence of Upper Pleistocene to Holocene blind thrust activity, preliminarily constrained through the paleoseismological analysis of second-order brittle fold-related structures in the Po Plain foredeep setting of N Italy.

The paleoseismological approach to seismic hazard assessment is particularly relevant in areas characterized by long recurrence for strong earthquakes. Anyway, in areas where surface exposures of the causative faults might actually not be available, the search for geological evidence of paleo-earthquakes seems particularly challenging. This is the case of contractional basins, where high sedimentation rates, or a very dynamic geomorphologic environment, can easily conceal the surface footprints of the local seismogenic structures.

In this line Yeats (1986) highlighted the importance of secondary structures as a tool for investigating the activity of the underlying earthquake sources. Second or third-order fault-related folds and, on the other side, fold-related faults (i.e. bending-moment or flexural slip faults), could in fact be considered as reliable proxies for the assessment of the activity of the main buried seismogenic structure (Kelson et al. 1996).

## GEOLOGIC AND SEISMOTECTONIC FRAMEWORK

The Po Plain is a wide basin characterized by the convergence of two chains, S-Alps an N Apennines, facing each other below hundreds of meters of Plio-Quaternary basin infilling (Fig.1). Neither the Southern Alps nor the Northern Apennines are characterized by high seismicity and highly active tectonic structures. Shortening rates in this sector of the Adriatic foredeep have clearly decreased from some cm/yr during the Oligo-Miocene to some mm/yr during the Pleistocene (e.g., Castellarin et al. 2006, Livio et al. 2009, Boccaletti et al. 2011).

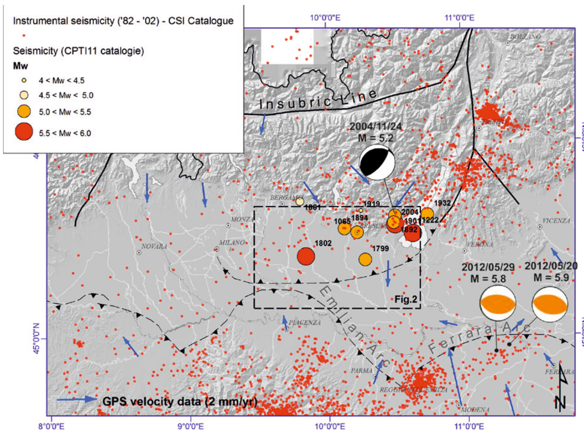


*Fig. 1: Map showing the main structural fronts buried below the Po Plain. Blue arrows indicate GPS velocity data (Michetti et al. 2012) relative to a fixed point located in the middle of the foreland sector (western Po Plain). Main historical and instrumental earthquakes and the focal mechanisms of the main recorded shocks are also reported.*

Nevertheless present-day contraction is testified by focal mechanisms, seismicity (Rovida et al. 2011), and geodetic data (Devoti et al. 2011; Fig. 1). The 2012 seismic sequence that hit Emilia Romagna and Lombardia (Fig.1 for the location and focal mechanisms of the two main events) definitely proved the seismogenic potential of a sector of the Ferrara arc, previously suspected to be aseismic. The GPS velocity field, as well, highlighted a convergence velocity spanning from ca. 1 up to 2.5 mm/yr in the central sector of Po Plain (Fig.1; Michetti et al. 2012).

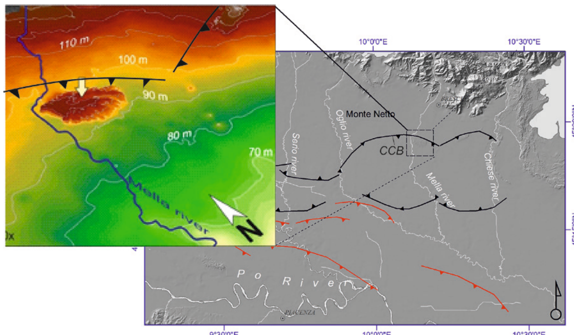


*Fig. 2: Main blind thrust of both the Alps (black) and the Apennines (red). Monte Netto hill is highlighted by a vertically exaggerated (10X) 3D perspective of a DEM. The white arrow indicates the studied site.*

## RESULTS

The studied site is located along the tip-line of the blind N-verging Capriano del Colle backthrust (CCB in Fig. 2) that is rooted in a deeper south-verging, out-of-sequence structure (Fig.2).

The hill is located above the hangingwall anticline of this backthrust. The backthrust fault tip, constrained through the interpretation of seismic reflection profiles (Courtesy of ENI E&P, Livio et al. 2009), is located ca. 1 km below the surface. Monte Netto is the surface expression of a secondary fault-related fold, partly eroded on both its sides (Fig. 3).

The Quaternary uplift history of this structure was investigated through analysis of the associated syn-growth depositional intervals (Livio et al. 2009), documenting an uplift rate of ca. 0.1 mm/yr over a 0.89 Myr-to-present time window and thus yielding a net slip rates of 0.4 mm/yr to 0.5 mm/yr.

Trench site (indicated in Fig. 2) is located in a quarry on the top of the hill, close to the trace of backthrust anticlinal hinge. Here two decametric secondary anticlines deform a sequence made of fluvial sediments overlain by strata of deeply weathered loess sediments (Fig. 4). The frontlimb of the northern anticline (Fig. 4) is characterized by presence of a gravity-graben whose collapsed sector is bounded by two normal bending-moment faults.

This secondary fold-related brittle structures offered the opportunity to date some of the last earthquakes generated by the buried seismogenic source. These events are recorded at the surface as bending-moment faulting, due to fold amplification and thus locally consistent with a quite vertical $\sigma 1$ stress orientation, accompanied by liquefaction features.

We recognized three different pedostratigraphic units (weathering horizon I to III) distinguished by sedimentological properties and degree of weathering. Their age is constrained by AMS-$^{14}$C and OSL datings, the latter performed at the Innsbruck luminescence laboratory (Fig. 5).

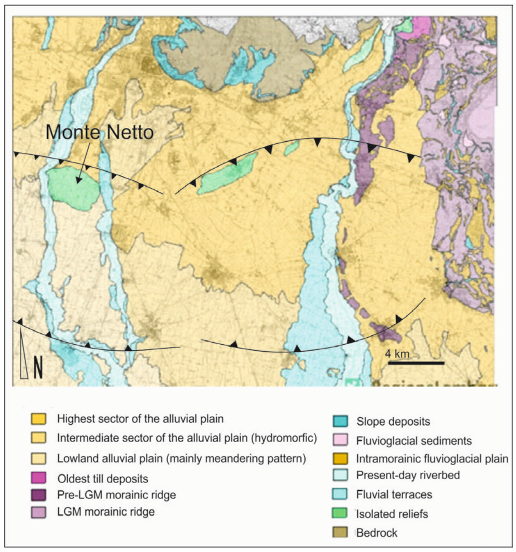


*Fig. 3: Simplified geomorphological map of the Monte Netto area. This and other similar hills (drawn in green) are surrounded by a flat alluvial area, fed on its eastern side, by a proglacial LGM sandur and subsequently eroded by the present-day drainage network during the whole Holocene. The traces of the main buried thrusts are also reported.*

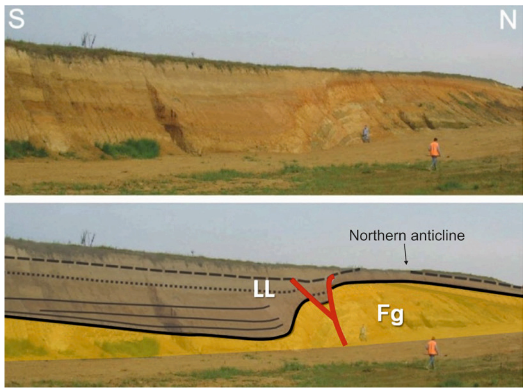


*Fig. 4: Monte Netto quarry wall: the exposed sequence is made of fluvial sediments overlain by layers of loess interlayered by deeply weathered horizons. Note the bending-moment faults affecting the external part of the anticline and deforming the whole sequence.*

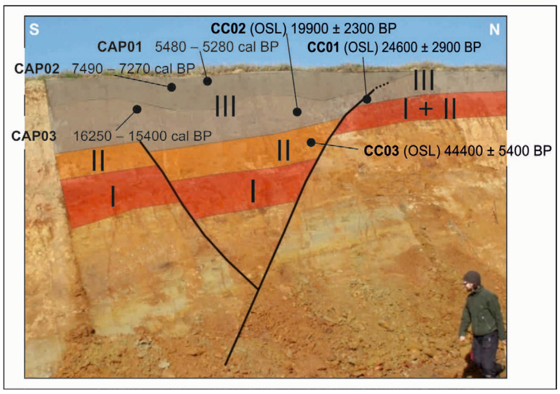


*Fig. 5: Detail on the gravity-graben. Three different pedostratigraphic units (I to III), developed on different stratigraphic units have been recognized and dated through $^{14}$C (CAP series) and OSL (CC series) methods.*

Luminescence results indicate a Late Pleistocene aggradation for the dated loess layers (Fig. 5).

Based on radiocarbon, OSL and archaeological dating, the described sequence can be summarized as follows:

- The oldest, highly rubified paleosol (I) developed on a fine-grained colluvial unit and on the overlain aeolian sediments. OSL samples from this unit cannot be dated for signal saturation due to the high dose rate of the sediments. Palaeolithic finds, which do not present a clear Levellois technology, can help dating the paleosol to the Middle Palaeolithic. This soil is clearly displaced by the bending moment faults and no colluvial wedge is present thus suggesting that the first movement of the faults occurred after paleosol I burial;
- then a long polyphasic and polycyclic cold phase followed (MIS 5d–2) and units II and III, both of them on loess/paleosols units, developed during interstadials and the Holocene.

Faulting along the observed faults occurred between the deposition of loess parent material of unit II and present. Displacement of the pedogenetic horizons recognized in unit II and III and the subsequent colluviation of the sediments into the graben, deduced from a detailed grain size analysis, allowed to recognize at least 3 different faulting events, occurred between ca. 45 kyr B.P. and ca. 5 kyr B.P. These faulting events, recognized in a secondary fold-related surface structure, are interpreted as evidence of three strong paleo-earthquakes, caused by repeated coseismic slip along the buried Capriano del Colle backthrust.

## DISCUSSION

The recognized paleo-events do not draw by far the complete Upper Pleistocene to Holocene seismic history of the main underlying thrust since not every thrusting event might have been recorded by this meter-scale secondary faults.

Nevertheless, these palaeoseismic features are a) the first ones indicating such a young activity of alpine blind thrusts in the Po Plain and b) a clear evidence that blind thrusting can also cause, besides broad uplift, localized medium-to-small scale deformation.

Michetti et al. (2012), basing on empirical relations between M and the rupturing area deduced from seismic reflection data, and, calculated, considering different rupturing scenario, a Mw range of 5.9 – 6.8. Indeed environmental effects similar to those recorded at the Monte Netto site are typically associated with macroseismic intensities >IX on the MCS scale. During the 2012 seismic sequence in Emilia, occurred only few tens of km SE of Monte Netto, the two Mw 5.9 and 5.8 ($I_o$ VIII MCS) blind thrust faulting mainshocks generated ca. 10 – 15 cm of surface cumlative uplift along the causative blind anticlines, accompanied by severe liquefaction effects, but no surface faulting. We argue that the threshold for surface faulting earthquakes in the Po Plain might be in the order of Mw 6.5 and Io IX-X, values observed perhaps only during the Jan. 13, 1117, Verona, and Dec. 25, 1222, Brescia, events.

## References

Boccaletti, M., G. Corti & L. Martelli, (2011). Recent and active tectonics of the external zone of the Northern Apennines (Italy). *International Journal of Earth Sciences* 100 (6), 1331-48.

Castellarin, A., G. Vai & L. Cantelli, (2006). The Alpine evolution of the Southern Alps around the Giudicarie faults: a Late Cretaceous to Early Eocene transfer zone. *Tectonophysics* 414, 203-223.

Devoti, R., A. Esposito, G. Pietrantonio, A. Pisani & F. Riguzzi, (2011). Evidence of large scale deformation patterns from GPS data in the Italian subduction boundary. *Earth and Planetary Science Letters* 311, 230-241.

Kelson, K., G. Simpson, R. VanArsdale, C. Haraden & W. Lettis, (1996). Miltiple late Holocene earthquakes along the Reelfoot fault, central New Madrid seismic zone. *Journal of Geophysical Reasearch* 101(B3), 6151-70.

Livio, F., A. Berlusconi, A. Michetti, G. Sileo, A. Zerboni, L. Trombino, et al. (2009). Active fault-related folding in the epicentral area of the Dec 25, 1222 (Io = IX MCS) Brescia earthquake (Northern Italy): seismotectonic implications. *Tectonophysics* 476, 320-335.

Michetti, A., F. Giardina, F. Livio, K. Mueller, L. Serva, G. Sileo, et al. (2012). Active compressional tectonics, Quaternary capable faults and the seismic landsscape of the Po Plain (northern Italy). *Annals of Geophysics* 55 (5), 969-1001.

Rovida, A., R. Camassi, P. Gasperini & M. Stucchi, (2011). *CPTI11, la versione 2011 del Catalogo Parametrico dei Terremoti Italiani*. http://emidius.mi.ingv.it/CPTI. Milano, Bologna.

Yeats, R. (1986). Active faults related to folding. In R. Wallace, *Active Tectonics*, Washington: National Academy Press, 63-79.

# Recognizing seiche and tsunami in lake sediments

*Shmuel Marco (1), Ian G Alsop (2), Oded Katz (3), Yehoshua Dray (4)*

(1) Department of Geophysics and Planetary Sciences, Tel Aviv University, Tel Aviv, Israel. Email: shmulikm@tau.ac.il
(2) Department of Geology and Petroleum Geology, School of Geosciences, University of Aberdeen, UK. Email: ian.alsop@abdn.ac.uk
(3) Geological Survey of Israel, Jerusalem, Israel. Email: odedk@gsi.gov.il
(4) Restoration of Ancient Technology, Binyamina, Israel. Email: yeshu@netvision.net.il

***Abstract***

*The lacustrine 70-15-ka Lisan Formation outcropping around the Dead Sea contains superb examples of slump folds formed in water depths of <100 m. New structural data from individual horizons demonstrate that several of these gravity-driven slumps are coaxially refolded and reworked by folds and thrusts verging both back up and then down the palaeoslope. The uppermost folds are often truncated. A progressive increase in reworking and shearing is developed up through the folded sediment, culminating in an upward-finning breccia layer that is capped by a thin, typically graded horizon of undeformed fine-grained clasts. We interpret this sequence as a seiche-related deformation. Based on the similarity of the structures in the Lisan Formation and on additional supporting observations we interpret zigzag-shaped sand injections in artificial lake deposits on the Eastern Mediterranean shore as evidence for a tsunami, possibly associated with the earthquake of 25 November 1759. If this interpretation is correct it supports the hypothesis that onshore Dead Sea Fault earthquakes can trigger tsunamis in the Mediterranean.*

***Key words**: Tsunami, Seiche, Lake Sediments, Soft Sediment Deformation, Dead Sea, Mediterranean, Archaeoseismology.*

Most studies of tsunami and seiche related deposits have focussed on coastal and near coastal zones which are readily accessible, with few investigations of deeper water settings and the potential soft-sediment deformation effects of such waves. The Late Pleistocene Lisan Formation outcropping to the west of the Dead Sea contains superb examples of sedimentary slump folds formed in water depths of <100m. Alsop and Marco (2012) have collected new structural data that demonstrate that these gravity-driven slumps may be coaxially refolded and reworked by sheared folds and thrusts verging both back up and then down the palaeoslope. This suggests that it is possible to generate up-slope flow of material in some circumstances. A progressive increase in reworking and shearing is developed up through the folded sediment, culminating in a breccia layer that is capped by a thin, typically graded horizon of undeformed silt- and sand-sized clasts (Figs. 1, 2). We suggest that these sequentially reworked deposits are consistent with seismically triggered tsunami and seiche waves that would flow back and forth across the main slump horizon triggered by the same earthquake. The folding is induced by the Kelvin-Helmhotz Instability where shear forces are formed at the sediment-water interface (Heifetz et al., 2005; Wetzler et al., 2010). The overlying fine clastics that infill local topography are considered to be deposited from turbid suspension during cessation of wave action and represent homogenite deposits (Fig. 3). Tsunami and seiche waves have previously been both numerically modelled (Ichinose and Begin, 2004) and reported in historical accounts. According to the latter, they were associated with large waves in the Dead Sea and related to earthquakes that inflicted damage in the region. Catalogues of ancient earthquakes list the CE 363, 749, 1546, 1837, and 1927 events (Ambraseys, 2009; Amiran et al., 1994). Alsop and Marco's (2012) study forms the first detailed structural analysis and interpretation of potential reworking associated with such waves in offshore settings.

This insight is applied to the Mediterranean shore, long assessed as susceptible to earthquake-related hazard such as tsunami and liquefaction. Marco et al. (2012) report the first finding of typical liquefaction features and silty sand injections observed in palaeoseismic trenches that were excavated behind a 4th century Byzantine dam on the Taninim Creek (Hebrew: Crocodile Creek). The dam rises up to 6 m above sea level. It was built some 850 m inland of the Mediterranean shore, probably for storing water that was used to flush the sand out of the Caesarea harbour. Our trenches revealed a series of flame-shape injections of silty sand that penetrate the overlying clay-rich soil (Fig. 4). Three features make the sand injections special: 1) Their lower part is commonly asymmetric with dominant southeastward vergence. 2) Zigzag shapes characterize the upper parts of many injections. 3) The size and frequency of the injections diminish gradually with distance from the dam until they completely disappear some 100 m away from it. The injections are most intense several meters from the point where the dam is badly damaged on the seaward side, which we interpret as a result of a large wave. We suggest that these observations can be explained by a tsunami wave that damaged the dam, flowed over it and filled the reservoir behind the dam. The flooding increased the pressure on the water-saturated sand layer and triggered the injection of liquefied sand. The movement of water sloshing back and forth in the lake created the zigzag shape of the injections, in the same way that seiches in

Lake Lisan did. The similarity to structures that were observed in Indonesia after the great 2004 tsunami (Matsumoto et al., 2008) and other palaeo-tsunami observations further support this interpretation. Based on the stratigraphic position, the archaeological context, and the historical accounts, we suggest that the earthquake of November 25, 1759 is the most plausible trigger for the sand injections. The observations confirm the vulnerability of the densely populated coastal plain to earthquake-triggered tsunamis and liquefaction.

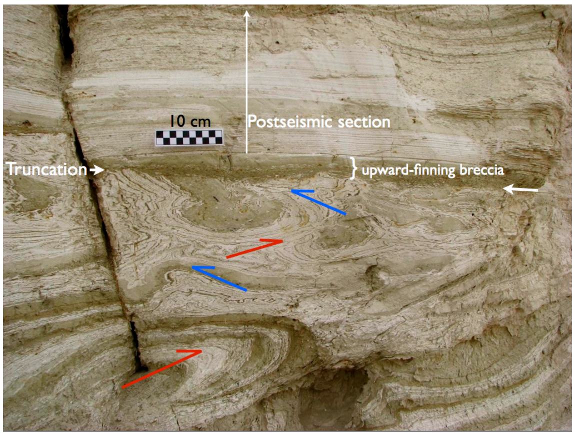


*Fig. 1: Coaxial, oppositely-verging folds (black arrows) in a slump, capped by upward fining layers with breccia at the bottom and fine-grained sand-silt at the top. The whole sequence is overlain with undeformed postseismic beds.*

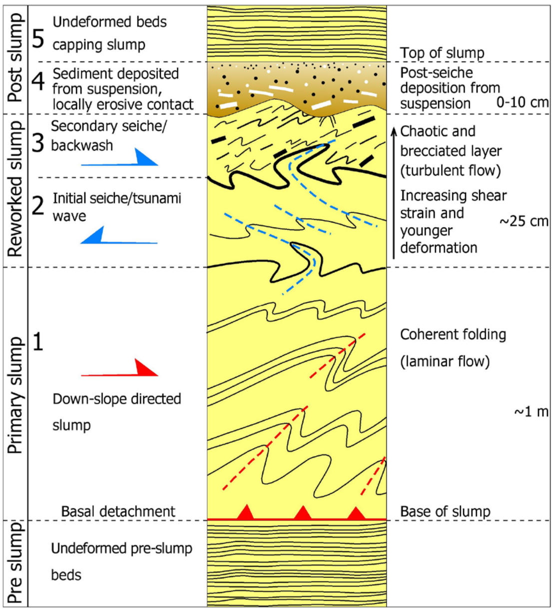


*Fig. 2: Schematic sedimentary and structural log summarizing the observed features associated with slumping (Alsop and Marco 2012).*

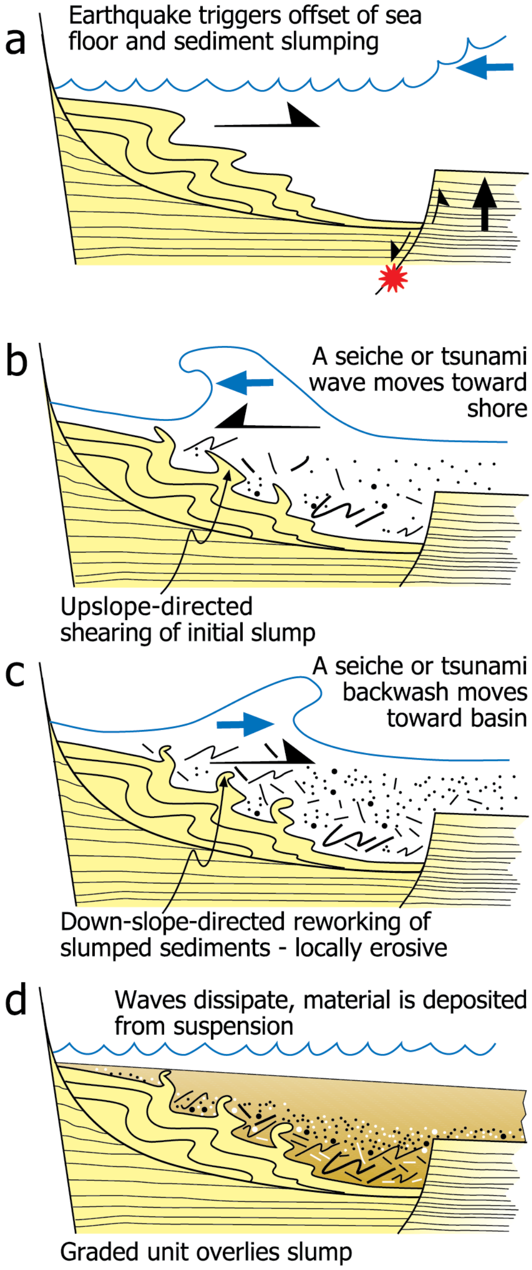


*Fig. 3: Interpretation of the sequence described in Fig. 1 (Alsop and Marco 2012).*

*Figure 4. Sand injections in the Taninim Creek, Mediterranean shore of Israel, exhibiting zigzag shapes. Scale is 10 cm.*

**Acknowledgements**

We thank Mr. John Levy, together with the Carnegie Trust and the Royal Society of Edinburgh for travel grants to IA, and the Israel Science Foundation for grant 1539/11 to SM. We are grateful to the staff of the Taninim National Park for their hospitality and assistance.

**References**

Alsop, G.I., & S. Marco, (2012). Tsunami and seiche-triggered deformation of offshore sediments. *Sedimentary Geology* 261-262, 90-107.

Ambraseys, N.N., (2009). *Earthquakes in the Mediterranean and Middle East: A Multidisciplinary Study of Seismicity up to 1900*. Cambridge University Press, Cambridge.

Amiran, D.H.K., E. Arieh & T. Turcotte, (1994). Earthquakes in Israel and adjacent areas: Macroseismic observations since 100 B.C.E. *Israel Exploration Journal* 44, 260-305.

Heifetz, E., A. Agnon & S. Marco, (2005). Soft sediment deformation by Kelvin Helmholtz Instability: A case from Dead Sea earthquakes. *Earth and Planetary Science Letters* 236, 497-504.

Ichinose, G.A. & B.Z. Begin, (2004). *Simulation of Tsunamis and Lake Seiches for the Late Pleistocene Lake Lisan and the Dead Sea*. Geological Survey of Israel, Jerusalem, p. 57.

Marco, S., O. Katz & Y. Dray, (2012). *Liquefaction on the Mediterranean shore of Israel: possible onshore evidence for past tsunami*. Israel Geological Society Annual meeting, Israel Geological Society, Ashkelon.

Matsumoto, D., H. Naruse, S. Fujino, A. Surphawajruksakul, T. Jarupongsakul, N. Sakakura & M. Murayama, (2008). Truncated flame structures within a deposit of the Indian Ocean Tsunami: evidence of syn-sedimentary deformation. *Sedimentology* 55, 1559-1570.

Wetzler, N., S. Marco & E. Heifetz, (2010). Quantitative analysis of seismogenic shear-induced turbulence in lake sediments. *Geology* 38, 303-306.

INQUA Focus Group on Paleoseismology and Active Tectonics

paleoseismicity.org

# The hanging-wall sedimentary architecture of active normal faults: planned future research on the island of Crete

*Mason, Jack (1), Wiatr, Thomas (1), Papanikolaou, Ioannis (2)*

(1) Neotectonics and Natural Hazards, RWTH Aachen University, Lochnerstraße 4-20, 52056 Aachen, Germany. Email: j.mason@nug.rwth-aachen.de

(2) Laboratory of Mineralogy & Geology, Department of Sciences, Agricultural University of Athens, 75 Iera Odos Street, 11855 Athens, Greece.

***Abstract:*** *Evidence for earthquake activity can be preserved in fault zone sedimentary architecture. For normal faults, the hanging-wall can act as a sedimentary archive, particularly when bedrock fault scarps are juxtaposed against alluvial-colluvial sediments. Sedimentary structures including colluvial wedges, disrupted and displaced strata, grabens and half-grabens, and sand blows have been successfully imaged using Ground Penetrating Radar (GPR) and Electrical Resistivity Tomography (ERT). To date, however, there has been little research carried out looking at the spatial extent of hanging-wall sedimentary structures and what parameters are required for their development, size, form, type, etc. We propose to carry out large scale geophysical reconnaissance (GPR and ERT) on the island of Crete to determine these parameters through studying various normal faults of differing lengths and orientations. Terrestrial LiDAR and trenching studies will also be undertaken at specific sites, and a combination of these techniques will be used to estimate paleomagnitudes and slip rates for various faults.*

***Key words***: *hanging-wall, sedimentary structure, geophysics, Crete*

## INTRODUCTION

When an earthquake occurs which is large enough to produce fault scarp displacement (the threshold for ground rupture and fault scarp development being around MS > 5,5; McCalpin, 2009), evidence for this activity can be preserved in fault zone sedimentary architecture. For normal faults, the hanging-wall can act as a sedimentary archive particularly when bedrock fault scarps are juxtaposed against alluvial-colluvial sediments (Fig. 1) such as those found in the southern Aegean region. On mainland Greece and Crete, active normal faults have been extensively studied (e.g. Caputo et al., 2006; Caputo et al., 2010). This is due to the area's tectonic history, high seismicity and the occurrence of regular ground rupturing earthquakes. The majority of previous studies include either the whole region or paleoseismological investigations on individual faults or fault segments.

Using geophysical reconnaissance, sedimentary structures within the hanging-walls of normal faults can be identified (e.g. Chow et al., 2001; Reiss et al., 2003). In particular Ground Penetrating Radar (GPR) and Electrical Resistivity Tomography (ERT) have been used (e.g. Grützner et al., 2012). By applying these geophysical techniques in paleoseismological studies, faulted soils can be identified prior to the excavation of expensive trenches and many surveys can be done in order to find optimum locations (e.g. Demanet et al., 2001; Anderson et al., 2003; Alasset and Meghraoui 2005; Grützner et al., 2012). Within trench walls, the sedimentary architecture of normal fault hanging-walls can be visualised very clearly, e.g. colluvial wedges, disrupted and displaced strata, grabens and half-grabens, sand blows, fissure fills, etc. The paleoseismologist is, however, spatially limited when mapping these structures as they can only be traced in two dimensions.

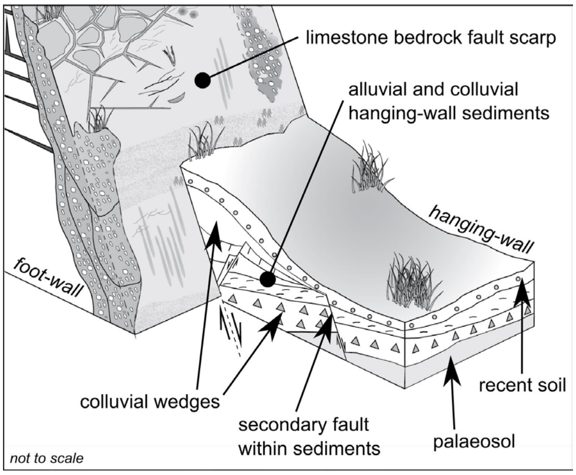


*Fig. 1: Schematic showing a bedrock fault scarp typical of Crete and some structures within hanging-wall sediments (modified after Wiatr et al. (submitted)).*

Sedimentary structures caused by co-seismic displacements can be imaged using the aforementioned geophysical techniques. To date there has been little research carried out studying the spatial extent of hanging-wall sedimentary structures and the parameters required for their development, size, form, type, etc. The most likely parameters are minimum fault length, catchment size, shaking duration, minimum intensities (ESI scale; Michetti et al. 2007) and background geology. We propose to carry out large scale geophysical reconnaissance (GPR and ERT) on the island of Crete to determine these parameters and estimate paleomagnitudes through studying various normal faults of differing lengths and orientations. The geophysical reconnaissance will be supplemented with terrestrial LiDAR surveying in order to create detailed digital elevation models of areas of particular interest. Furthermore, terrestrial LiDAR will be used to scan artificially exposed bedrock scarps in order to analyse the alluvium-colluvium's effect on scarp roughness. Trenching will subsequently be undertaken at specific sites where our studies have identified the most promising locations to view and sample recurring earthquake evidence. The main research questions which will be answered through this study are presented in this extended abstract.

## STUDY AREA

The proposed investigations will be undertaken on the island of Crete. Crete is one of the most seismically active areas in the eastern Mediterranean due to its proximity to the Hellenic subduction zone. The island displays the effects of intense Late Quaternary tectonics mainly represented by normal faulting. This normal faulting extends along two major systems which are roughly orientated WNW-ESE and NNE-SSW (Caputo et al., 2006). The footwall block of these normal faults mainly comprises carbonate and metamorphic rocks with free faces between 4 and 15 m in height, whereas the hanging-wall block comprises alluvial-colluvial Quaternary deposits (Caputo et al., 2010). The proposed research will be carried out on faults with a minimum length of 9 km which are capable of producing $M_w$ 6 earthquakes. Figure 2 shows four of the many large normal faults that will be studied.

## RESEARCH QUESTIONS

### What sedimentary structures can be seen in GPR and ERT data?

Previous work shows that a large variety of sedimentary structures can be identified in GPR and ERT data. GPR in particular is ideally suited for imaging stratigraphic features because of the high frequency of radio waves. Stratigraphic offset of sediments has been identified using GPR by many authors (e.g. Reicherter and Reiss, 2001; Anderson et al., 2003; Reiss et al., 2003; Alasset and Meghraoui 2005) and a combination of GPR and ERT was used very successfully by Demanet et al. (2001) and Grutzner et al. (2012) to image offset strata. Colluvial wedges have also been identified in GPR data by a number of authors (e.g. Chow et al., 2001; Christie et al., 2009; Denith et al., 2010); Reiss et al. (2003) identified event horizons beneath colluvial wedges indicating two co-seismic ruptures and post seismic sedimentation (Fig. 3). Other structures that have been successfully imaged include small graben structures caused by antithetic faults (Christie et al., 2009), sand blows and fault related folding (Chow et al., 2001). It is, therefore, clear that many fault related sediments can be visualised using GPR and ERT techniques. The proposed study will expand on these investigations and work will be carried out trying to identify other sedimentary structures such as secondary fault terminations at event horizons and fissure fills. We will also try to determine what happens to the sedimentary structures when there are multiple (primary and secondary) scarps. GPR and ERT will initially be carried out in areas where sedimentary structures can be seen in profile, such as areas where hanging-wall sediments have been artificially excavated, in order to calibrate the geophysical data. Typical signatures will be established for the various sedimentary structures and they will then be applied to other faults in order to confirm their characteristics. Furthermore, through quantitative and qualitative evaluation of the data, earthquake paleomagnitudes and slip rates can be estimated (e.g. Reiss et al., 2003). This information can be used to update the seismic hazard and associated risk of the region.

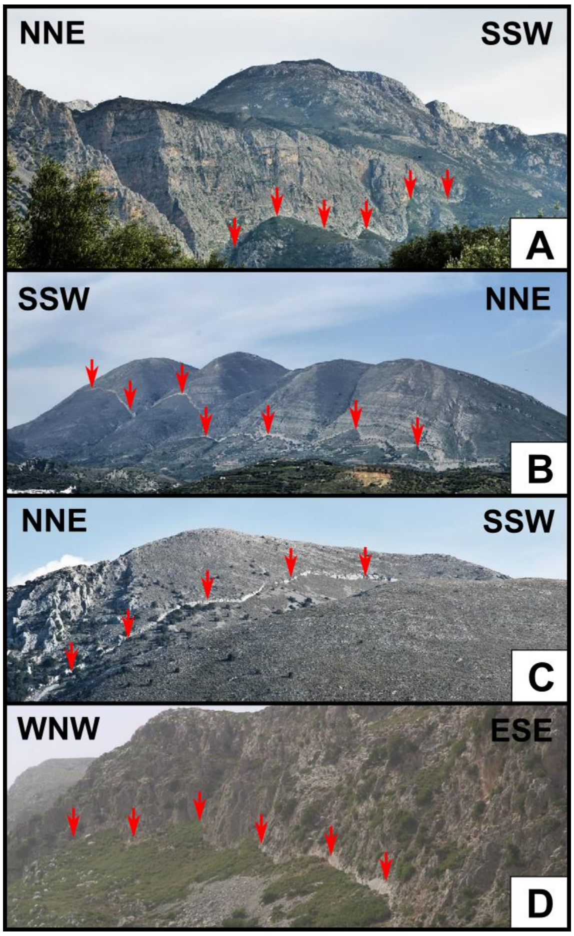


*Fig. 2: Photographs showing four large normal faults which will be studied on Crete. Arrows indicate the fault scarp location along the mountain front. A) Ierapetra fault with a length of 18 km; B) Lastros fault with a length of 11 km; C) Sfaka fault with a length of 9 km; and D) Spili fault with a length of 16 km.*

### Are sedimentary structures traceable along and perpendicular to strike?

It is not understood how the size/structure of sedimentary structures differ with distance from the fault centre and total fault length. Taking the example of colluvial wedges, how far can these be traced for different sized faults? Is there a minimum length needed to produce specific structures? These questions will be answered by carrying out parallel 2D GPR and ERT profiles both perpendicular and parallel to the fault providing pseudo- 3D profiles. This will first be carried out at the fault centre to identify the scale and form of sedimentary structures. It will then be repeated at regular distances from the fault centre and a comparison made. Fault plane measurements will also be undertaken (height, dip) so that any relationships can be analysed. After repeating this process on a variety of faults with varying lengths and orientations, along with GIS analysis of the topography, climate and sediment composition studies, it is expected that some general parameters can be identified and quantified for the production and size of various sedimentary structures in relation to fault length, dip, throw and slip rate. This information will assist in selecting optimum trench site localities; at present there are many unknowns regarding these sedimentary structures and if some features turn out to be highly variable, paleoevents could be missed, and magnitudes and recurrence intervals could be over- or underestimated.

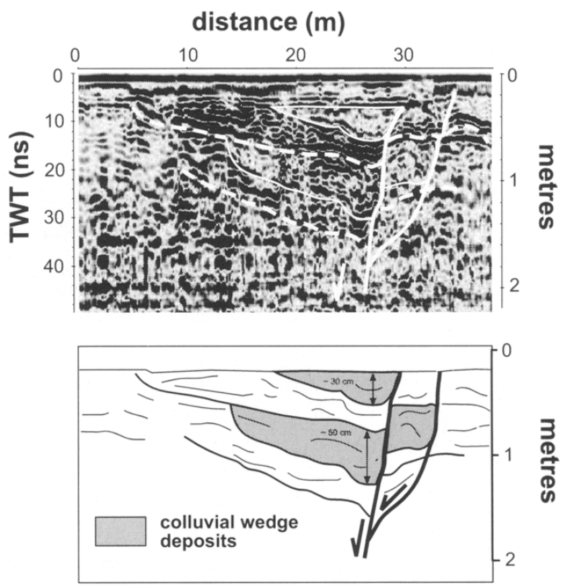


*Fig. 3: High resolution GPR image and interpretation of colluvial wedges from the Ventas de Zafarraya Fault, Spain (from Reiss et al., 2003).*

**Do the geometrical characteristics of sedimentary structures change with fault orientation / extension direction?**

As previously mentioned, there are two main tectonic domains within Crete (NNW – SSE and WNW – ESE; Fig. 2). It is widely known that hanging-walls of normal faults can rotate when extension occurs, particularly when there are parallel faults suggesting listric geometry at depth (e.g. Wernicke and Burchfiel, 1982). There are many examples of these parallel or imbricate fault blocks in Crete (e.g. the Ierapetra Fault Zone in the east, and the Rodopos Fault Zone in the northwest of the island, amongst others) which may show varying amounts of rotation. Through GPR and ERT the amount of rotation and orientation will be quantified and compared to sedimentary structure geometry.

The normal faults of Crete are predominantly dip-slip; however, many do have a slight strike-slip component (e.g. Spili fault; Wiatr et al. (in press) evidenced by kinematic indicators on fault plane surfaces such as slickenside lineations and corrugations. The palaeostress regime can, therefore, be determined for individual faults. These results will be compared to sediment structure orientation to see what relationships can be deduced.

**What is the size/orientation/offset relationship of secondary (minor) faults compared with the bedrock fault?**

As stated earlier, GPR and ERT have been used to visualise secondary or minor faults within the hanging-wall sediments (antithetic faults, grabens and half grabens). The proposed study aims to quantify the size and orientation of these secondary faults and determine what relationships there are to the geometry and kinematics of the primary bedrock fault. Moreover, many studies have shown that Aegean fault planes can migrate into the hanging-wall over time (e.g. Stewart and Hancock, 1994). The extent to which this may be happening for individual faults will also be determined.

**Do sedimentary structures caused by recent events have similar characteristics to paleoevents?**

The effect that time has had on the hanging-wall sedimentary structures caused by paleoearthquakes will be determined by comparing them to more recent earthquakes. The 1981 earthquake series in the Gulf or Corinth ruptured many normal faults in the area including the Kaparelli fault and Skinos fault which have been extensively studied (e.g. Collier et al., 1998). Hanging-wall sedimentary structure size and extent caused by this recent earthquake will be measured using GPR and ERT and compared to the older hanging-wall structures to be imaged in Crete. Furthermore, paleoseismological studies have been carried out on both the Kaparelli and Skinos faults which will provide us with good quantitative information to be used in the comparison.

**What effects do hanging-wall sediments have on the buried bedrock fault plane?**

LiDAR analysis of naturally exposed fault planes by Wiatr et al. (submitted) suggests that the roughness of exposed fault planes is predominantly affected by how long it has been exposed to the open air and, therefore, weathering effects. The authors also carried out topographic roughness analysis on anthropogenically exposed fault planes on mainland Greece. The results suggest that hanging-wall sediments are having an effect on the buried bedrock fault plane and this is dependent on the composition of the sediments. Figure 4 shows that, in general, fault plane roughness increases with height within the buried sediments, but there is a spike in increasing roughness between 2.1 and 3.1 m which is most likely due to sediment composition, i.e. a layer of sediments with a higher water content or where roots are concentrated.

The work by Wiatr et al. (submitted) will be expanded on at specific locations; there are many locations throughout Crete where hanging-wall sediments have been anthropogenically removed. Hand-held X-ray fluorescence (XRF) and magnetic susceptibility measurements will be carried out adjacent to these roughness profiles and the results calibrated to the LiDAR data. Furthermore, it is likely that soil moisture is having the largest effect on fault plane roughness; therefore, soil porosity and retention tests will be undertaken on hanging-wall sediments.

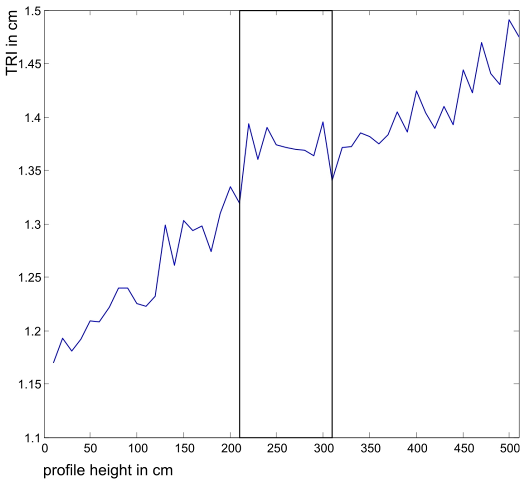


*Fig. 4: Topographic roughness index of the 5 m high Perachora fault scarp on mainland Greece. The spike in increasing roughness is highlighted (Wiatr, unpublished results).*

**Paleoearthquake magnitude estimations**

Where hanging-wall sedimentary structures have been imaged and event horizons determined, an estimation of earthquake paleomagnitudes and slip rates will be undertaken. Trenching studies will also be undertaken close to catchments where sedimentation is occurring. These will confirm paleomagnitude estimations and allow dating to be carried out. As the proposed work will cover many faults and fault segments throughout Crete, this information will be invaluable for hazard assessment in one of the most seismically active areas in the Mediterranean region.

## CONCLUSIONS

The proposed research on normal fault hanging-wall sedimentary architecture will fill the knowledge gap regarding these structures at a variety of scales. Large scale geophysical reconnaissance will be undertaken using GPR and ERT on normal faults in Crete which vary in size and orientation. Through studying the hanging-wall structures using pseudo- 3D profiles, and in combination with trenching and LiDAR studies, it is hoped that some general parameters can be identified and quantified for the production and size of various sedimentary structures in relation to fault length, dip, throw and slip rate. Paleoearthquake magnitudes will be estimated and confirmed, and this information can be used to update the seismic hazard and associated risk of the region.

**References**

Alasset, P.-J. & M. Meghraoui, (2005). Active faulting in the western Pyrenees (France): Paleoseismic evidence for late Holocene ruptures. *Tectonophysics* 409, 39-54.

Anderson, K., J. Spotila & J. Hole, (2003). Application of geomorphic analysis and ground-penetrating radar to characterization of paleoseismic sites in dynamic alluvial environments: an example from southern California. *Tectonophysics* 368, 25-32.

Caputo, R., S. Catalano, C. Monaco, G. Romagnoli, G. Tortorici & L. Tortorici, (2010). Active faulting on the island of Crete (Greece). *Geophysical Journal International* 183, 111-126.

Caputo, R., C. Monaco & L. Tortorici, (2006). Multiseismic cycle deformation rates from Holocene normal fault scarps on Crete (Greece). *Terra Nova* 18(3), 181-190.

Collier, R., D. Pantosti, G. D'Addezio, P. De Martini, E. Masana, & D. Sakellariou, (1998). Paleoseismicity of the 1981 Corinth earthquake fault: Seismic contribution to extensional strain in central Greece and implications for seismic hazard. *Journal of Geophysical Research* 103, 30001-30019.

Christie, M., G. Tsofilas, D. Stockli, & R. Black, (2009). Assessing fault displacement and off-fault deformation in an extensional tectonic setting using 3-D ground-penetrating radar imaging. *Journal of Applied Geophysics* 68(1), 9-16.

Chow, J., J. Angelier, J. Hua, J. Lee & R. Sun, (2001). Paleoseismic event and active faulting: from ground penetrating radar and high-resolution seismics reflection profiles across the Chihshang Fault, eastern Tiawan. *Tectonophysics* (333), 241-259.

Demanet, D., F. Renardy, K. Vanneste, D. Jongmans, T. Camelbeeck & M. Meghraoui, (2001). The use of geophysical prospecting for imaging active faults in the Roer Graben, Belgium. *Geophysiscs* 66, 78-89.

Denith, M., A. O'Neil & D. Clark, (2010). Ground penetrating radar as a means of studying palaeofault scarps in a deeply weathered terrain, southwestern Western Australia. *Journal of Applied Geophysics* 72, 92-101.

Grützner, C., K. Reicherter, C. Hübscher & P. Silva, (2012). Active faulting and neotectonics in the Baelo Claudia area, Campo de Gibraltar (southern Spain). *Tectonophysics* 554-557, 241-259.

McCalpin, J. (2009). *Paleoseismology*, 2nd edition. International Geophysics Series Vol. 95. Academic Press.

Michetti, A.M, E. Esposito, L. Guerrieri, S. Porfido, L. Serva, R. Tatevossain, E. Vittori, F. Audemard, T. Azuma, J. Clague, V. Comerci, A. Gürpinar, J. McCalpin, B. Mohammadioun, N.A. Mörner, Y. Ota & E. Roghozin, (2007). *Environmental Seismic Intensity scale – ESI 2007. La scala di Intensità Sismica basata sugli effetti ambientali – ESI 2007.*

Reiss, S., K. Reicherter & C.-D. Reuther, (2003). Visualization and characterization of active normal faults and associated sedimentary structures by high-resolution ground penetrating radar (GPR). *Geological Society of London Special Publications* (211), 247-255.

Stewart, I.S. & P.L. Hancock, (1994). Neotectonics. In: *Continental deformation* (Hancock, P.L., ed.), Pergamon Press, 370-409.

Wernicke, B. & B. Burchfiel, (1982). Models of extensional tectonics. *Journal of structural Geology* 4 (2), 105-115.

Wiatr, T., K. Reicherter, I. Papanikolaou, T. Fernández-Steeger & J. Mason, (in press). High resolution t-LiDAR scanning of an active bedrock fault scarp for palaeostress analysis: Spili fault (Crete, Greece). *Tectonophysics*.

Wiatr, T., K. Reicherter, I. Papanikolaou, T. Fernández-Steeger & J. Mason (submitted). t-LiDAR backscattering behaviour and analysis of structures on bedrock fault scarps.

# Devastating earthquakes of 2001-2013 and the Role of Paleoseismology

*McCalpin, James P. (1)*

(1) GEO-HAZ Consulting, Box 837, Crestone, Colorado 81131 USA. Email: mccalpin@geohaz.com

***Abstract:*** *Recent deadly earthquakes have shaken public confidence in our methods for assessing seismic hazards, and has made earthquake scientists (including paleoseismologists) wonder what we are doing wrong. As a result of the 2009 L'Aquila earthquake in Italy, six scientists were convicted of manslaughter for failing to warn the public before the earthquake. The 2011 Tohoku earthquake in Japan was a full magnitude larger (M9.0) than the design value for the Fukushima Nuclear Power Plant and the local coastal seawalls, resulting in 15,870 deaths and tens of billions of $US in damages. In both countries seismic hazard assessment is considered sophisticated and uses paleoseismic data and Probabilistic Seismic Hazard Assessments (PSHA) to ensure that low-probability earthquakes are adequately considered. Yet despite that fact, we are still experiencing deadly "surprises." The situation suggests that there is a flaw somewhere in the flow chart of seismic hazards assessment and mitigation.*

***Key words**: seismic hazards, catastrophic earthquakes, paleoseismology*

## WHO IS TO BLAME?

When modern paleoseismology was developed in the 1970s, it promised to supplement the short historic/instrumental record of earthquakes (50 yrs to a few centuries) by 2-3 orders of magnitude in time. By studying the surface ruptures of Holocene/ late Quaternary earthquakes, we could estimate Mmax for each active fault and the return time of Mmax, thus filling in the "missing" large-magnitude part of the earthquake frequency-magnitude curves (McCalpin, 1996, 2009). The seismic source parameters coming from paleoseismology are these: Mmax, return period of Mmax (recurrence interval), and slip rate.

However, Seismic Source Characterization (SSC) is only the first part of Seismic Hazard Assessment; it is followed by Ground Motion Prediction (GMP), to create the output of PSHA (a hazard curve of ground motions and their associated probabilities/return periods). Perhaps the failure can be traced to the GMP process, or to the PSHA procedure in general. The ground motions predicted then must be used in engineering design (for new buildings) and retrofits (for existing buildings). But the degree to which design is actually performed is dependent on liability and government regulations.

Based on my experience with PSHA and paleoseismic data inputs, I have the following conclusions:

## THE MAIN REASONS PSHAs HAVE UNDERESTIMATED THE HAZARD

*1. Unknown active faults are close to the site and generate unanticipated Mmax earthquakes*: 1994, M6.7, Northridge, CA, reverse/blind; 2001, M7.7, Bhuj, India, reverse/blind; 2003 M6.6, Bam, Iran, reverse/blind; 2007, M6.6, Honshu, Japan, reverse/blind (shut down K-K NPP); 2010-11, M7.1 and M6.3, Christchurch, NZ, strike-slip

*2. Active faults are known close to site, but their return time is underestimated, and/or their conditional probability of rupture was never calculated.* Most PSHAs ignore the position of a fault within its seismic cycle, and assume that the probability of Mmax is time-independent (i.e., the same within every year of the cycle). Conditional Probability says that the annual probability of Mmax is time-dependent (i.e., it increases as the fault reaches the end of its seismic cycle of strain accumulation and then release): 2005, M7.6, Kashmir, reverse; 2008, M7.9, Sichuan, reverse; 2010, M7.0, Haiti, reverse

*3. Active faults are known close to site, but their Max is underestimated*. Large underestimates occur when Mmax earthquakes break multiple segments, and the PSHA assumed only single-segment ruptures: 2010 M7.2, El Mayor-Cucapah, Mexico; 2011, M9.0, Fukushima, Japan; subduction megathrust

*4. Active faults are known close to the site, and their Mmax and recurrence times are correctly known, but the secondary damaging effects are underestimated*: Tsunami, 2004, Sumatra, M9.1; Tsunami, 2011, Japan, M9.0

## WHAT WE SHOULD DO

My observations suggest that paleoseismologists should do the following to better estimate the true hazard:
1. Use new imaging tools (e.g. LiDAR, geophysics) to discover presently-unknown blind faults and low-slip-rate faults near cities and critical sites.

2. Increase the precision of measuring the mean recurrence time of a fault and its elapsed time (time since the Most Recent Event). This would included dating long sequences of paleoearthquakes to measure the variability in recurrence and any possible clustering

in time, and the causes of clustering (random versus deterministic).

3. Use the new information above to calculate the Conditional Probability of future Mmax ruptures, and put that information into the SSC part of PSHA.

4. Rename the present process for computing probabilistic earthquake ground motions PGMA (Probabilistic Ground Motion Assessment). The use of the term PSHA (Probabilistic Seismic Hazard Assessment) should be reserved for a new comprehensive procedure that includes ALL hazards from earthquakes (surface rupture, ground motion, ground failure, and tsunami). Perhaps this could be referred to as a Comprehensive Probabilistic Seismic Hazard Assessment (CPSHA).

5. Probabilistic procedures already exist for ground motion hazards and surface rupture hazards, although the latter (Probabilistic Fault Displacement Hazard Analysis, or PFDHA) is currently subject to large uncertainties, due to lack of data on secondary coseismic faulting. There is currently no formal probabilistic method for predicting ground failure, which tends to be very site-specific (i.e., for many sites the probability of ground failure is zero, regardless of the ground motion).

6. In the CPSHA, always use independent geologic or historic evidence to perform a "reality check" on the predicted earthquake ground motions and other output parameters. An example of such a reality check is the historic "tsunami warning stones" found in Japan alter the Tohoku earthquake, and so-called "Fragile Geological Features" such as precariously balanced Rocks and speleothems.

7. Creating such a comprehensive PSHA should be the highest priority for earthquake scientists in the next decade, and should not be difficult. It will use the same SSC input for predicting the magnitude/frequency of earthquakes that cause all four hazards, and existing empirical or physical equations to model the effects of each hazard. Its comprehensive approach will help assure that no aspect of potential hazard is overlooked and "falls through the cracks."

**References**

McCalpin, J.P. (ed.), 1996, Paleoseismology: Academic Press, New York, 588 p.

McCalpin, J.P. (ed.), 2009, Paleoseismology, 2nd Edition: Academic Press, Elsevier, Amsterdam, 618 p.

INQUA Focus Group on Paleoseismology and Active Tectonics

paleoseismicity.org

# Aerial reconnaissance mapping of active faults, in the Digital Age

*McCalpin, James P. (1) & Gary A. Carver (2)*

(1) GEO-HAZ Consulting, Box 837, Crestone, Colorado 81131 USA . Email: mccalpin@geohaz.com
(2) Carver Geologic, 12201 Middle Bay Drive, Kodiak, Alaska 99615 USA. Email: cgeol@acsalaska.net

***Abstract:*** *Active faults pose a hazard of surface rupture to utilities such as pipelines and electrical transmission lines. Utility corridors in North America have been assessed for active faults beginning in the early 1970s with the Trans-Alaska [Oil] Pipeline. Over the past 10 years more utility corridors have been assessed, but their length and the short time available for fault studies has led to development of this streamlined mapping procedure that uses digital imagery, computer visualization, and real-time GPS in a GIS mapping environment.*

***Key words***: *active faults, mapping, LiDAR*

Since 2003 the authors have performed aircraft-supported, reconnaissance active fault mapping along existing and proposed utility corridors in North America. The corridors were up to 3000 km long and crossed mainly forested terrane, for which available geological maps are at regional scales of 1:250,000 or smaller. In the beginning we used paper geologic and topographic maps, but since 2010 have switched to digital mapping.

**THE OBJECTIVE**

In order to locate active faults in and near the utility corridor, we flew over every fault shown on published maps to look for evidence of Quaternary displacement. We chose this time-consuming approach because we could not, *a priori*, disprove that even an old fault might have experienced a reactivation event in the Holocene or late Pleistocene.

**THE TERRANE**

Utility corridors follow the gentlest terrane (topographic lows such as valleys) if such features lead toward its destination. But inevitably, there will be rugged terrane elements that trend perpendicular to the corridor and must be crossed, such as the mountain range shown in Fig. 1. A drawback of mountains at high latitudes is that they were recently deglaciated (15-18 ka), so evidence for postglacial faulting on low slip-rate faults may exist only as single displacement event of a meter or two.

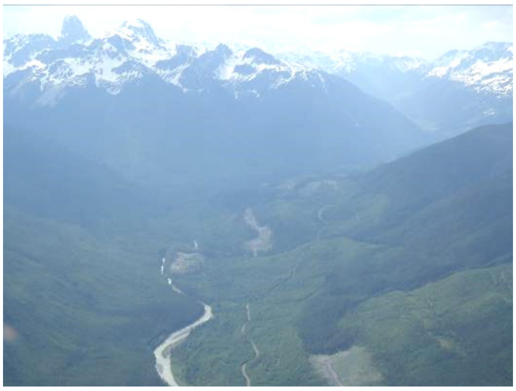

*Fig. 1. Typical terrane traversed by North American utility corridors.*

**THE PERSONNEL**

Our Mapping Team usually consists of four persons: a Lead Geologist, a 2nd Geologist, a Computer Operator, and a Bear Guard (necessary for field traverses). The Lead Geologist determines the strategy of the mapping, directs the pilot in the air, and views features ahead and on the left (port) side of the aircraft. The 2nd Geologist views features on the right (starboard) side of the aircraft. The Computer Operator manipulates the main computer while in the air, at the direction of the Lead Geologist.

**THE AIRCRAFT**

Helicopters are preferred over fixed-wing aircraft because: (1) they can fly lower and slower than fixed-wing aircraft, (2) they can hover briefly if necessary for examining exposures where it is impossible to land, and (3) they can land in small clearings.


*Fig. 2. Mid-size helicopters can land in many places for field-checking.*

Many helicopter models will seat five passengers, but we normally prefer a larger helicopter (such as the Bell 212, or "Huey") due to their better visibility out the windows, and their larger interior space needed for the computer equipment. All passengers and the pilot must be able to communicate with each other via headsets. Comfort is a secondary issue, even considering flying 8 hours per day over many days. The pilot and mechanic can be very helpful if they clearly understand the goals of our mapping, for example, in setting up a working communication system, in providing electrical power for the computer system, and arranging seating comfort.

**THE DIGITAL DATA SETS**

The computers should be loaded with all available data sets, correctly georegistered, so layers can be quickly displayed in the GIS software (we used Global Mapper v11 and v14). Data layers include:

1- The corridor centreline with numbered kilometre points along it.

2- All geologic maps showing faults; scanned versions saved as TIFFs or JPEGs. OPTION: hand-digitize the faults as a vector layer, so they can be overlaid on a raster map such as a DEM.

3- Topographic base maps (raster)

4- Published DEMS (10 m, 30 m)

5- Bare-earth LiDAR DEMs (1-2 m); normally available only in the 1 km-wide strip along the utility centerline

6- Orthophotographs (1-2 m)

**THE COMPUTER SYSTEM**

We used two computers in the air, a main one (Panasonic Toughbook 31) and a 2nd one (Lenovo X100e notebook). Both were GPS-enabled, via an internal GPS (main), and an external handheld GPS connected to the 2nd computer by a USB cable. Both computers were taken on some field traverses, but the ruggedized Toughbook performed better.

*Fig. 3. The Computer Operator (left) controls the visible layers and geographic area of the display, according to directions of the Lead Geologist (right), who sees the same display on a large monitor at his feet*

Probably the most important aspect of the airborne computer system is how fast you can display new layers on the monitors. At a speed of 200 km/hr, the helicopter travels 55 m every second. If it takes 10 seconds to change displays for the Lead Geologist, the helicopter will have travelled 550 m. If the feature of interest is now behind you, the helicopter must turn around. Each turn-around costs time and fuel, and reduces the total kilometres of faults that can be surveyed each day. We found that large raster files of geologic and topographic maps (such as uncompressed TIFF files) take too long to display at the speed of the helicopter. Although GIS professionals prefer this file format for office work, we had to shrink the files by decreasing the resolution and/or compressing them to JPEGs.

**MAPPING IN-FLIGHT**

The key feature of our system is the large (17") computer monitor at the feet of the Lead Geologist (Figs. 3, 4). This display is fed from the main computer operated by the Computer Operator behind him. The Lead Geologist views the geologic map displaying the faults, so he can direct the pilot to fly down the length of each mapped fault. The pilot can also see the monitor, which permits him to see if he is flying right above the fault trace.

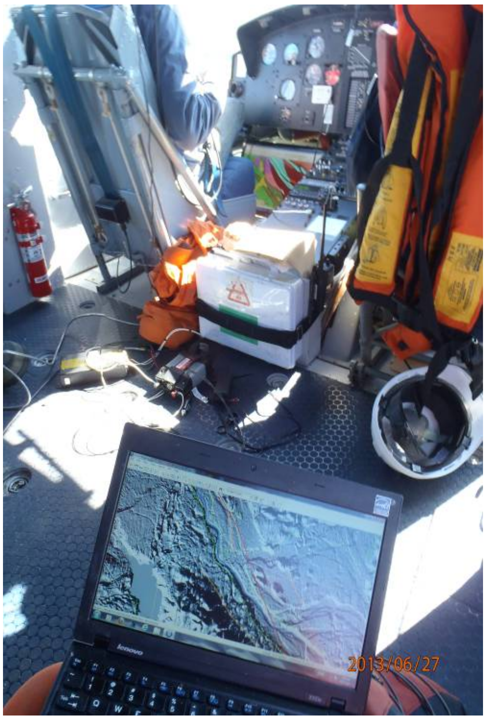

*Fig. 4: The Second Geologist maps geomorphic scarps and lineaments on-the-fly on a DEM (foreground) using a GPS-enabled computer. The monitor at the Lead Geologist's feet (top, center) shows the geologic-tectonic map of the same area.*

The Lead Geologist sits in the co-pilot seat and thus can view the fault trace ahead and to the left side (Fig. 5). The 2nd Geologist views terrane to the right and maps lineaments and all types of scarps (Fig. 6). The Computer Operator is usually too busy to look out the windows, but may have to observe left-side terrane if the Lead is busy writing notes.

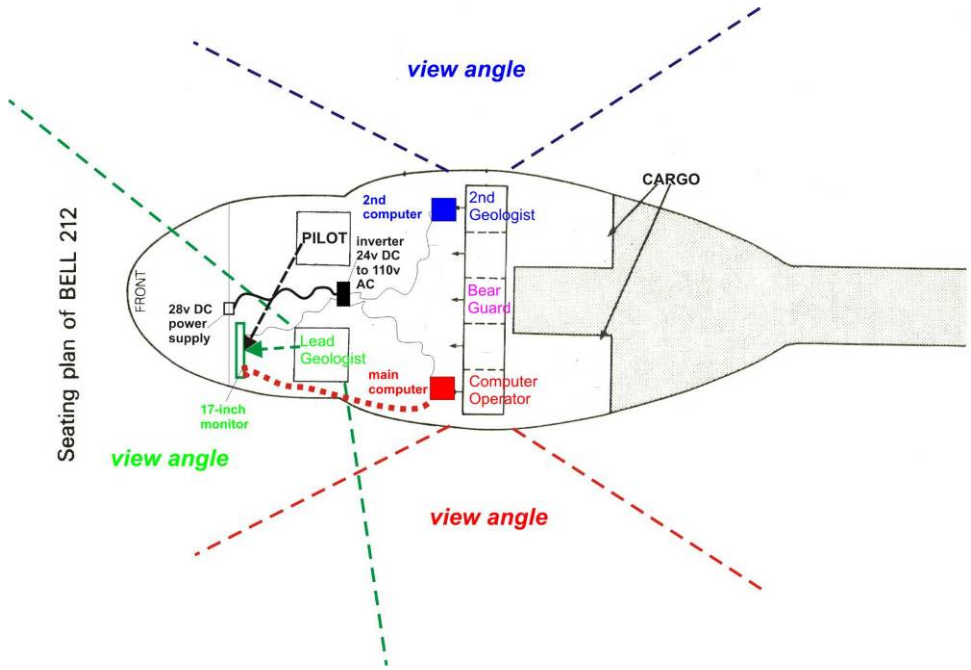


*Fig. 5. Interior arrangement of the aerial mapping team in a Bell 212 helicopter. Green, blue, and red indicate the stations and view angles of the Lead Geologist, 2nd Geologist, and Computer Operator.*

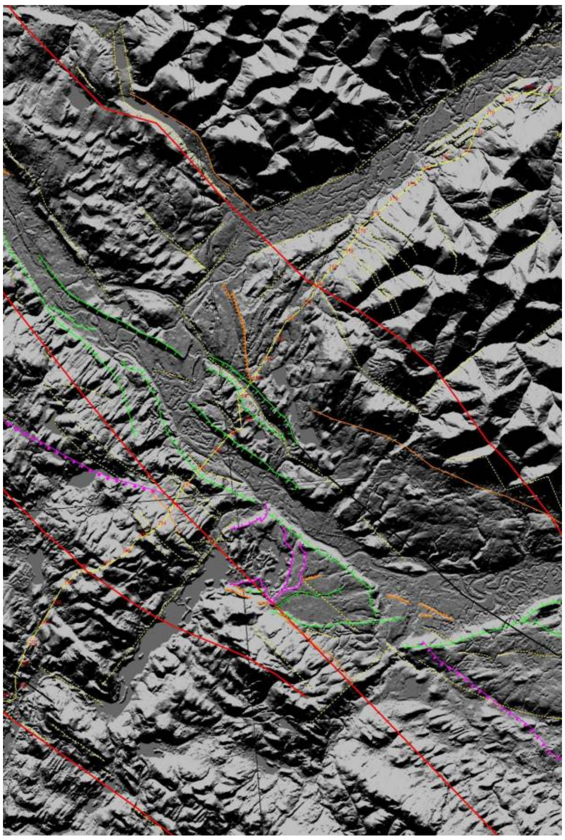

*Fig. 6. Example of aerial mapping on a 30 m DEM; width of map is 30 km. Red lines, regional strike-slip faults; purple lines with diamonds, regional thrust faults; all from published maps. Yellow line with red numbers crossing from upper right to lower left, centreline of utility corridor. Colored lines show scarps with hachures on down side; green, fluvial scarps (erosional); purple, landslide headscarps; orange, scarps of unknown origin (targets for detailed examination). Yellow dotted lines, lineaments.*

**THE PROBLEM WITH FAULTS**

Determining whether an active fault crosses a utility corridor is complicated by some basic issues described herein.

1- Faults often cannot be traced into utility corridors that occupy valleys, because valley floors are covered by young deposits (alluvium, glacial deposits). This may be true even for regional faults extending for long distances on either side of the corridor. In such cases it is reasonable to assume that the bedrock fault continues across the corridor in the subsurface, and thus future surface rupture (if it occurs) will cross the corridor.

2- The definitive evidence that a fault has (or has not) moved in the Holocene may be preserved at only one or two small locations along the fault. The probability of those locations being within the utility corridor is thus very small, especially on long faults. Conversely, in order to look for definitive evidence, one must extend the surveys along the fault trace for many km to tens of km away from the utility corridor. A rule of thumb would be to survey long regional faults at least 100 km away from the corridor in both directions.

3- Faults that trend perpendicular to the corridor are the easiest to assess from a geometric standpoint, because the area of their intersection with the corridor is minimized. Conversely, faults that intersect the corridor at a very low angle are the most problematic, because they can cross the corridor for long distances. Slight changes in the strike of the fault or in the orientation of the utility centreline can greatly change the number of fault crossings.

4- In forested areas small-scale landforms (scarps, ridges, gullies) less than about 5 m high cannot be detected from the air, unless they are accompanied by a strong difference in vegetation. Even when they are detected from a vegetation contrast, their exact size and shape cannot be observed, so their origin cannot usually be deduced (erosional vs. depositional vs. tectonic).

5- Landforms less than 5 m high can be observed in clear-cut areas, but only if the clearcuts are less than about five years old. After that, regrowth of trees again obscures the landforms. *The only way to detect small scarps and lateral offsets in forested areas is with bare-earth LiDAR DEMs of 1 m to 2 m resolution.*

6- The inability to visually detect fault scarps less than 5 m high in uncut forests poses a general constraint on the detectability of young faulting by aerial reconnaissance. What types of faults might be undetectable? One example would be a "slow" fault with a long-term slip rate of <0.33 mm/yr. Such a fault would not be expected to generate more than 5 m displacement in 15 ka, so would essentially be "invisible" to the aerial reconnaissance. Another example would be a "slow" fault with a long-term recurrence interval greater than 15 ka. A third example would be a strike-slip fault with little to no vertical displacement. The detection threshold for lateral fault offsets in a forest may be 2-3 times larger than the 5 m vertical threshold.

7- In order to design a utility crossing of an active fault, paleoseismologists must determine the displacement parameters of recent surface ruptures: strike and dip of the fault, sense of slip, and orientation and magnitude of the net slip vector (plus and minus any uncertainties). As with the age information, this type of structural information is likely to be preserved at very few places along the fault, and not likely within the corridor itself.

**RECOMMENDATIONS**

Managers of seismic hazard assessments in utility corridors need to understand the limitations of aerial reconnaissance for detecting Holocene faulting, particularly in forested regions. At present, bare-earth LiDAR DEMs offer the only way to recognize scarps smaller than 5 m high and lateral offsets several times larger. Unfortunately, most utility corridors are covered by a narrow strip of proprietary LiDAR DEMs only along the corridor centreline (typically 1000 m wide). As explained previously, the key evidence for Holocene movement and for critical fault displacement parameters are not likely to fall within such a narrow strip.

The success probability of the surface rupture assessment will be greatly increased if the LiDAR coverage is extended along the faults to some distance beyond the corridor. The exact distance depends on the length of the fault and its distance from the corridor. For short faults (<10-20 km long) in or near the corridor, the entire fault length should be covered. For longer faults (20-100 km long), the first 20-30 km outside the corridor should be covered. For regional faults, it may be necessary to extend the LiDAR out 50-60 km away from the corridor in both directions. The strip of LiDAR along the faults does not need to be very wide; 2 km should be sufficient unless the fault zone is wide and complex.

**Acknowledgements:** We thank WorleyParsons-Canada Ltd. for permitting us to publish our methodology. Several helicopter crews over the years have assisted us in the learning process about the capabilities (and limitations) of helicopters for aerial fault mapping.

# Rupture history and deformation cycle along the eastern Tohoku coastline (Japan) using coastal uplift, tsunami deposits and trenching at an aftershock location

*Silke Mechernich (1,2), Mustapha Meghraoui (1), Shinji Toda (3), Tsoyuchi Haraguchi (4), Koji Okumura (5), Matthieu Ferry (6), Hiroyuki Tsutsumi (7)*

(1) Institut de Physique du Globe, CNRS-UMR 7516, 5, rue René Descartes, 67084 Strasbourg, France. Email: mechernich.s@gmail.com
(2) Institut für Geologie und Mineralogie, Universität zu Köln, Greinstraße 4, 50939 Köln, Germany
(3) International Research Institute of Disaster Science, Tohoku University, Aoba, 6-6, Aramaki, Aoba-ku, Sendai 980-8578, Japan
(4) Department of Biology and Geosciences, Osaka City University, 3-3-138 Sugimoto, Japan
(5) Department of Geography, Hiroshima University, Kagamiyama1-2-3, Higashi-Hiroshima, 739-8522 Hiroshima, Japan
(6) Géosciences Montpellier, CNRS-UMR5243, Université Montpellier II, Place E. Bataillon, 34095 Montpellier cedex 5, France
(7) Department of Geophysics, Kyoto University, Kitashirakawa-oiwake-cho, Sakyo-ku, Kyoto 606-8502, Japan

***Abstract:*** *With the aim of better understanding the earthquake cycle in the $M_w$ 9.0 Tohoku-oki earthquake area, we assess the co-, post- and interseismic coastal deformation along eastern Tohoku coastline, compile palaeotsunami studies, and investigate the Itozawa fault that has ruptured during a $M_w$ 6.6 aftershock. Pleistocene marine terraces indicate uplift rates of 0.2–0.4 mm/a in northern Tohoku, and 0.1–0.2 mm/a along the central and southern Tohoku coastline. This variation reveals two tectonic sub-regions in which the area of lower uplift rates correlates with the 2011 coseismic subsidence. The recurrence interval of ~M>8 earthquakes is estimated to 400-750 years based on the palaeotsunami record. Trenching revealed that the penultimate earthquake on the Itozawa fault occurred 12.6-17.4 ka ago, thus it did not rupture during every M>8-class earthquake.*

***Key words****: Japan trench, vertical deformation, palaeotsunamis, palaeoseismic trenching, seismic cycle*

## INTRODUCTION

The $M_w$ 9.0 Tohoku-oki earthquake and the record of major historical seismic events on the Japan trench illustrate the active tectonic capability on the subduction zone. Recent geodetic and seismotectonic work constrains the ~500-km-long 2011 Tohoku-oki rupture area (Fig. 1a) and the related slip distribution. However, the poorly constrained seismic cycle and long-term faulting behaviour of the NE Japan subduction zone causes large uncertainties in the seismic hazard assessment and needs additional and different working approaches. Therefore our project is three fold: (i) the assessment of the coastal deformation along eastern Tohoku on different timescales (from coseismic deformation to the past 780 ka), (ii) the compilation of palaeotsunami studies, and (iii) the palaeoseismic investigation of the Itozawa fault that has ruptured during a $M_w$ 6.6 aftershock.

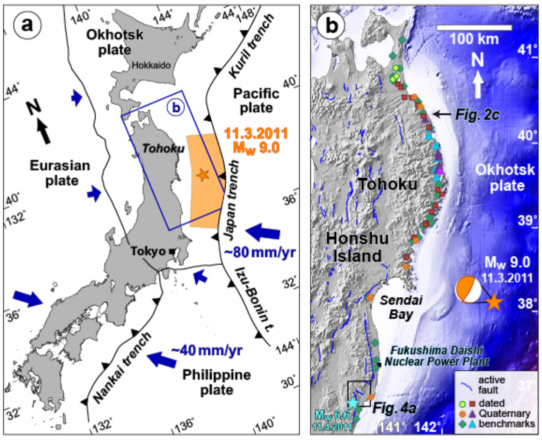


*Fig. 1: (a) Tectonic framework of the 2011 earthquake area. (b) Study sites of the dated Quaternary benchmarks along the eastern Tohoku coastline. Symbols refer to different ages (for legend see Fig. 2b).*

## METHODS, RESULTS AND DISCUSSION

*Vertical coastal deformation*

We determined the vertical deformation of the eastern Tohoku coastline (Fig. 1b) on different timescales since the correlation between short-term geodetic results and long-term geologic data is decisive for understanding of the tectonic process and the related earthquake cycle on the subducting Pacific slab. The recent coastal deformation is obtained from levelling and GPS measurements and revealed a 2011 coseismic subsidence of up to 1.2 m (Fig. 2a), and a postseismic uplift of up to 24 cm within 2 years (Ozawa et al., 2011; Geospatial Information Authority of Japan, 2013). 100 years before the earthquake, subsidence at a rate of up to ~5 mm/a was documented (e.g., Suwa et al., 2006; Nishiimura, 2012).

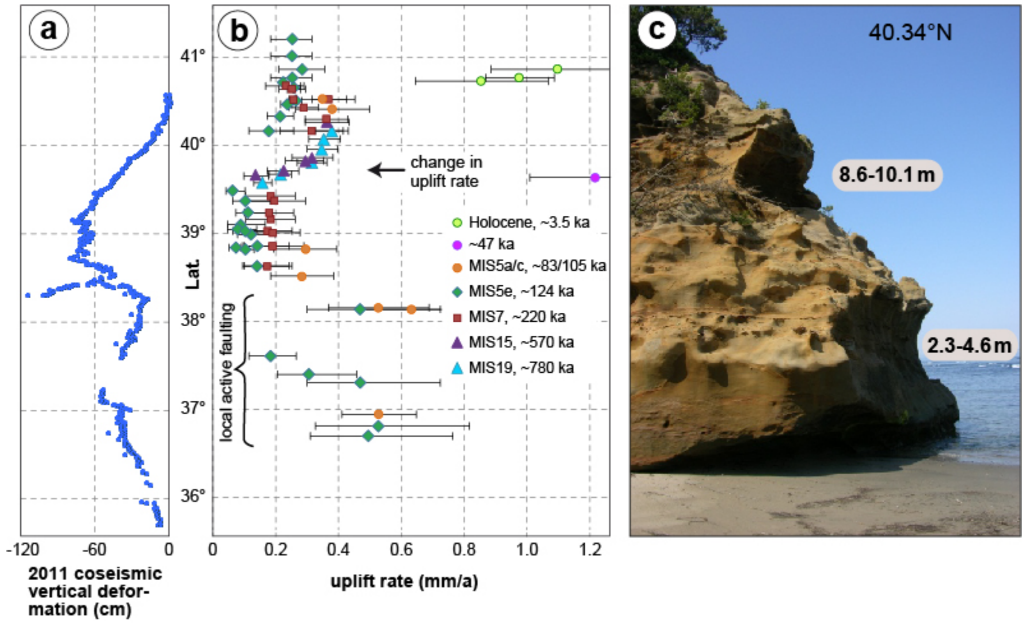


*Fig. 2: (a) Coseismic subsidence (Geospatial Information Authority of Japan, 2013) during the 2011 $M_w$ 9.0 earthquake. (b) Mid Pleistocene to Holocene uplift rates estimated from Quaternary terraces of eastern Tohoku. The data is revealed by own measurements as well as age and height information from Koike & Machida (2001), Ota & Machida (1987) and Matsu'ura et al. (2009). (c) Notches in sandstone (for location see Fig. 1b). The notches are interpreted to have formed during the rather steady state sea level since the last 6.5 ka, which would attest for the recent coastal uplift.*

The millennial vertical deformation along the coastline of eastern Tohoku is estimated from emerged marine terraces, wave-cut platforms and notches of Holocene to Mid Pleistocene age. While coastline terraces of marine isotope stages MIS5e (124 ka) to MIS19 (~780 ka) indicate uplift rates of 0.2-0.4 mm/a in the northern study area, they show only 0.1-0.2 mm/a in the central study area (Fig. 2b). Numerous lower and younger notches and wave-cut platforms are identified at several height levels between 1 and 10 m above sea level (Fig. 2c). Two radiocarbon samples of wood remnants yielded both an age of ~2.8 cal ka BP for a 3.2 m high terrace (40.7°N), and shell fragments on a notch in resistant conglomerates (39.7°N) revealed an age of 47.1 ± 2.2 cal ka BP. After correction for sea level change, both data points yield uplift rates of ~1 mm/a, which denotes clear acceleration of uplift during the Late Quaternary (Fig. 2b). Modelling of the distribution of vertical deformation *during the co-, post- and interseismic period* shows that the long-term uplift is caused by deep (>50 km) interseismic creeping on the subducting slab based on the 80 mm/a of plate convergence. This creeping conceals the successive coastal subsidence in Tohoku during M9-class earthquakes.

The distribution of lower uplift rates in the southern area coincides with the region of the strongest 2011 coseismic subsidence (Fig. 2a,b) and this implies the repetition of M~9 earthquake deformation with several cycles of coseismic subsidence on this section of the subduction zone. Furthermore, a different seismic behaviour with recent large earthquakes ($M_w$ 7.4-8.2) exists in the north, whereas a pre-2011 seismic gap of M>7.5 earthquakes prevailed in the seismically coupled southern part of the Japan trench. All factors attest for a segmentation of the subduction zone that prevailed in its actual position since at least 780 ka, and that the southern segment presumably generated several M9-class earthquakes.

*Palaeotsunami record*

We compiled the published palaeotsunami record along the coastline of the 2011 rupture area for the last 3 ka (e.g., Haraguchi & Ishibe, 2009; Sawai et al., 2012; Fig. 3). The samples were extracted in several-meter-deep sections using coring and Geoslicer techniques in lowland and shielded bays. The palaeotsunami sediments are generally marked as tens-of-centimeter medium- to coarse-grained sand often including mud clasts and shells, with texture and structure remarkably comparable to 2011 tsunami deposits. Both thin and thick (5-30 cm) tsunami sandy deposits exist in all cores and they are distinctly intercalated by peat and humic soil representing interseimic periods. A study of diatom assemblage at Odaka (Sawai et al., 2012; Fig. 3) revealed a significant amount of coseismic subsidence for the AD 869 and 1.5-ka earthquakes, emphasizing a close tectonic origin for the sand layer deposition and rules out storm surges as possible origin. The lack of tsunami sediments at some sites along the coastline might be due to lowland erosion and/or coastal morphology (e.g., cliffs). The shared $^{14}C$ time ranges of tsunami inundations reveal five well-preserved palaeotsunami horizons during the past 3 ka, which infers a recurrence interval of 400-750 years for ~M>8 earthquakes.

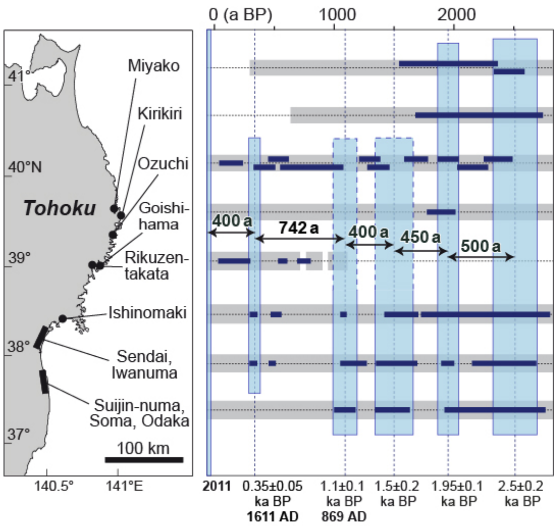


*Fig. 3: Compilation of the palaeotsunami record along the eastern coastline of Tohoku (Haraguchi & Ishibe, 2009; Sawai et al., 2012). Grey horizontal lines indicate the investigated time coverage. Radiocarbon dating brackets the tsunami deposition age. Estimated ages and their correlation to historical events suggest a recurrence interval of 400-750 years for very large seismic events (~M>8) on the Japan subduction zone.*

*Triggered earthquakes*

The Tohoku-oki earthquake significantly impacted the stress regime within the crust and resulted in reactivated onshore faulting (e.g., Toda et al., 2011). The largest onshore aftershock was the $M_w$6.6 Iwaki extensional earthquake (11th April 2011) that ruptured in a compressional area regarding the Pacific subducting plate. If the normal faults in the Iwaki region move only under the extensional stress field induced by offshore M9-class events, we may indirectly reveal the history of such megathrust earthquakes. The Iwaki earthquake ruptured the NW-trending Yunodake fault and the NNW-trending Itozawa fault both along ~15-km-long sections (Fig. 4a). These 70-80°SW-dipping faults have been reactivated simultaneously with a predominantly normal sense of shear. The maximum vertical offset on the Yunodake fault is ~0.8 m, whereas it is ~2.1 m on the Itozawa fault. Two palaeoseismic trenches were opened in September 2011 and July 2012 in the southern and northern third of the Itozawa fault, respectively (Fig 4).

At both sites, the rupture affects a rice paddy field, which provides an ideally horizontal initial state to collect detailed and accurate measurements. At the southern trench site, total station topographic profiles indicate the Iwaki earthquake generated a vertical deformation of ~1.2 m, while direct field examinations reveal that rice paddy limits have been right-laterally offset by ~0.3 m (Toda & Tsutsumi, 2013). The trench walls exposed >1.5 m thick gravels overlain by 2 m of different sand, silt, and humic soil layers deposited by the close river. Both walls revealed west-dipping, subvertical normal fault that offsets all of the stratigraphic units. The fault generated a ground-surface warping and 2011 surface breaks those fissures are filled by fine surface soil. On the southern wall, similar fissures occur ~3 m west of the 2011 rupture in the lower part of the silt unit and they are interpreted to be related to the penultimate earthquake. Units underlying this lower fissure are vertically displaced by 1.5-1.7 m, indicating that the penultimate earthquake generated a vertical offset of 30-40 cm and thus had a lower magnitude than the $M_w$6.6 Iwaki earthquake. Radiocarbon dating above and below the event horizon constrains the age of the penultimate earthquake to 12.6-17.4 cal ka BP (Toda & Tsutsumi, 2013).

At the northern trench site, the 2011 vertical deformation of ~0.6 m is accompanied with a ~0.1 m left-lateral offset. The trench exposes the 30-40-cm-thick cultivated soil overlaying a 1-m-thick red to yellow silt unit, a 2-m-thick alluvial gravel unit and a basal 0.1-1-m-thick organic-rich silt unit (Fig. 4c). Deformation associated with the 2011 rupture occurred along a subvertical fault and generated well-expressed bending at the surface. On both walls, the basal silt unit is vertically deformed by ~0.6 m, similarly to what is observed for the 2011 rupture. Furthermore, the base of the said silt unit indicates secondary faulting prior to the 2011 event with similar cracks than observed at the present-day surface (Ferry et al., 2013). Since the silt unit is dated to 30-33 cal ka BP using peat and charcoal, the penultimate event occurred between historical times and ~30 ka ago. However, the sedimentary record of the gravel might not be continuous and thus evidence for palaeoearthquakes events may be missing.

The two palaeoseismic trenches revealed that the penultimate earthquake on the Itozawa fault occurred between 12.6 and 17.4 cal ka BP at its the southern part (Toda and Tsutsumi, 2013), and at least once between historical times and ~30 ka at the northern part of the Itozawa fault (Ferry et al., 2013). Hence, the recent activity of the Itozawa fault may be entirely controlled by large to giant earthquakes along the Japan Trench. However, it is not reactivated during every M9-class earthquake, e.g. there is no evidence that it ruptured during or immediately after the A.D. 869 Jogan earthquake, which is believed to be the penultimate megathrust earthquake on the Japan trench. Thus, such onshore palaeoseismic investigations can only be a tool to discover the megathrust subduction earthquakes if they cover all faults in a specific area.

## CONCLUSIONS

The combined analysis of data from (palaeo-) geodetic, palaeotsunami, and palaeoseismic investigations enables a better understanding of the M>8-class earthquake cycle on the Japan subduction zone. According to widely distributed tsunami sediments the recurrence interval of huge earthquakes is 400-750 years. Furthermore, the palaeoseismicity and distribution of long-term uplift rates revealed a large-scale segmentation of the Japan trench with probably repeated M9-class earthquakes on the southern segment.

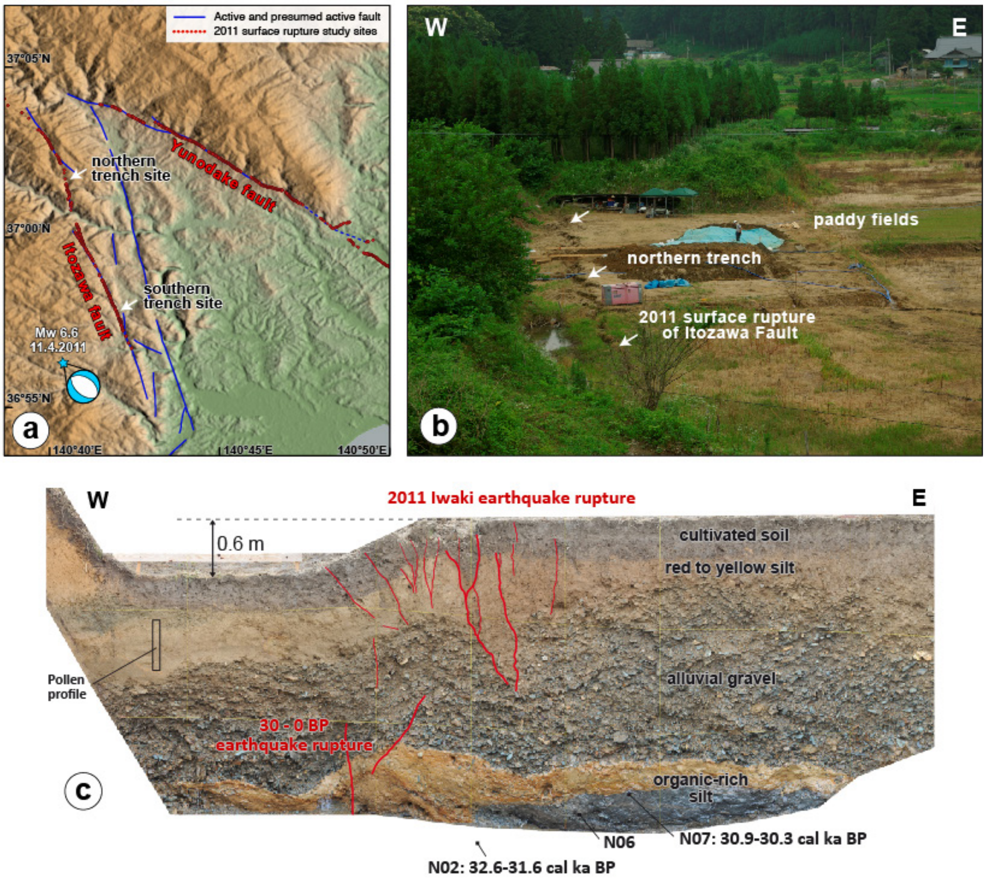


*Fig. 4: (a) Surface rupture map of the $M_w$ 6.6 aftershock on 11 April 2011 along the Yunodake and Itozawa faults (after Toda & Tsutsumi, 2013). For location see Fig. 1b. (b) The northern trench site showing the surface rupture during the Iwaki earthquake (after Ferry et al., 2013). (c) Photomosaic of the north wall of the northern trench. Cracks and fissure fill in the 30-33 ka old silt unit indicate evidence for a pre-2011 earthquake (after Ferry et al., 2013).*

**Acknowledgements:** This work is funded by the Agence National de la Recherche (ANR, France) and the Japan Science and Technology agency (JST) in the frame of the PALET Project ANR-11-JAPN-0005.

## References

Geospatial Information Authority of Japan, 2013 http://www.gsi.go.jp/ (last access May 2013).

Haraguchi, T. & T. Ishibe (2009). Large earthquake model in the central part of Off-Sanriku estimated from tsunami deposits and uplifted event layers (in Japanese), *Monthly Chikyu (Gekkan Chikyu) 31*, 223-230.

Koike, K. & H. Machida (2001). *Atlas of Quaternary Marine Terraces in the Japanese Islands (in Japanese with English abstract)*, University of Tokyo Press, Tokyo.

Matsu'ura, T., A. Furusawa & H. Saomoto (2009). Long-term and short-term vertical velocity profiles across the forearc in the NE Japan subduction zone, *Quaternary Research 71*, 227-238.

Nishimura, T (2012), Crustal deformation of northeastern Japan based on geodetic data for recent 120 years (in Japanese with English abstract), *The Journal of the Geological Society of Japan 118*, 278-293.

Ferry, M., H. Tsutsumi, M. Meghraoui & S. Toda (2013). Surface faulting along the inland Itozawa normal fault (eastern Japan) and relation to the 2011 Tohoku-oki megathrust earthquake, *Geophysical Research Abstracts 15*, EGU2013-3918, Vienna.

Ota, Y. & A. Machida (1987). Quaternary sea-level changes in Japan, in *Sea-level studies* (Tooley, M.J., Shennan, I. eds.). The Institute of British Geographers Special Publications, Blackwell Publishing, London.

Ozawa, S., T. Nishimura, H. Suito, T. Kobayashi, M. Tobita & T. Imakiire (2011). Coseismic and postseismic slip of the 2011 magnitude-9 Tohoku-Oki earthquake, *Nature 475*, 373-376.

Sawai, Y., Y. Namegaya, Y. Okamura, K. Satake & M. Shishikura (2012). Challenges of anticipating the 2011 Tohoku earthquake and tsunami using coastal geology, *Geophysical Research Letters 39*, L21309.

Suwa, Y., S. Miura, A. Hasegawa, T. Sato & K. Tachibana (2006). Interplate coupling beneath NE Japan inferred from three-dimensional displacement field, *Journal of Geophysical Research 111*, B04402.

Toda, S., R.S. Stein & J. Lin (2011). Widespread seismicity excitation throughout central Japan following the 2011 M=9.0 Tohoku earthquake and its interpretation by Coulomb stress transfer, *Geophysical Research Letters 38*, L00G03.

Toda, S. & H. Tsutsumi (2013). Reactivation of Inland Normal Faults During the Mw 6.6 11 April 2011 Iwaki Earthquake Triggered by the Mw 9.0 Tohoku-oki, Japan, Earthquake, *Bulletin of the Seismological Society of America. 103 (2B)*, 1584-1602.

# Tsunamis and tsunamites: origin and characteristics

Nils-Axel Mörner (1)

(1) Paleogeophysics & Geodynamics, Rösundavägen 17, 13336 Saltsjöbaden, Sweden. Email: morner@pog.nu

***Abstract:*** *Tsunamis hit our coasts with tremendous energy, often causing severe destruction and taking great death tolls. Generally, the driving force is a submarine earthquake. Other forces are landslides, impacts, volcanic eruptions and submarine explosion (e.g. methane venting and bomb tests). Sediments (from fine particles to big blocks), plants, animals, humans, human objects are dislocated and moved by the waves. When re-deposited in land basins, on the old land surface, at the shore or in deep water off the coast, these deposits constitute tsunami deposits or beds or layer. Geologically speaking these beds are termed "tsunamites". Tsunamites may be formed by the run-up wave, the back-swash wave-flow or by the offshore trimming of the seabed surface due to the wave rotation of large radius and rapid motion. Tsunamites often exhibit fining-upward graded bedding. Tsunami run-up deposits in lake basins are characterized by their content of planktonic species.*

***Key words****: Tsunamis, tsunamites,*

## INTRODUCTION

The word *"tsunami"* is Japanese (written *tsu-nami)* and refers to "a big harbour wave". *Tsunamites* are deposits as a function of a tsunami event. Tsunami waves are characterized by their large radius of rotation (up to a couple of kilometres) and their rapid travel-time (in the order of several 100 km/hour). The tsunami wave hits the coasts as a rapidly moving wall of water over-flowing land with disastrous effects; so for example, was the death toll at the December 26, 2004, tsunami in the Indian Ocean, about 230,000 persons, at the December 28, 1908 event in the Messina Straight in Italy, at least 100,000 persons, and at the famous Lisbon event on November 1, 1755, at least 60,000 persons.

## ORIGIN OF TSUNAMIS

Tsunami waves are generated when water masses, in the ocean or in lakes, are suddenly dislocated in the vertical dimension. This can happen by five main causes (*Fig. 1*).

- When the seabed (lake-bed) jumps up or down due to an earthquake.
- When sediments suddenly slides down the ocean bottom at submarine landslides or from the coast into the sea.
- When objects are falling down into the water at impacts, calving icebergs, and falling blocks.
- At sudden dislocations of rock masses at submarine volcanic eruptions or volcanic eruptions of islands or coastal areas.
- At submarine explosions in association with methane gas venting and nuclear bomb tests (the Bikini Atoll).

The dynamics of the tsunami waves set sediments in motions, which at their later deposition constitute tsunami deposits. These deposits may range from big blocks to fine clay particles or organic matter. Usually, those deposits exhibit graded bedding in a fining upward sequence. Tsunami deposits (beds, layers, units) are also termed *"tsunamites"* (Shiki et al., 2008; Mörner, 2013, 2014).

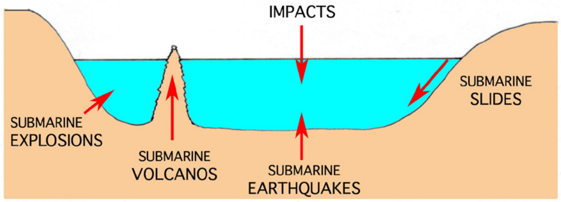


*Fig. 1. Five main factors generating tsunami waves (from Mörner, 2014).*

*1. Seismically induced tsunamis*

The majority of big tsunamis are induced by submarine earthquakes; e.g. Lisbon 1755, Messina 1908, Indonesia 2004, Japan 2011. The vertical fault dislocations (normal or reversed faulting) leads to tsunami generation because they affect the vertical water column above. Horizontal fault dislocations (strike-slip faults) usually do not generate tsunamis. Many notorious destructive tsunami events belong to this group (cf. Mörner, 2010, 2014). It should be noted that tsunamis also occur in areas, where they previously were not known to have occurred; so for example, have 18 tsunamis been recorded in Sweden after the last Ice Age (*Fig. 2*; cf. Mörner, 2003, 2011, 2012, 2013; Mörner & Dawson, 2011).

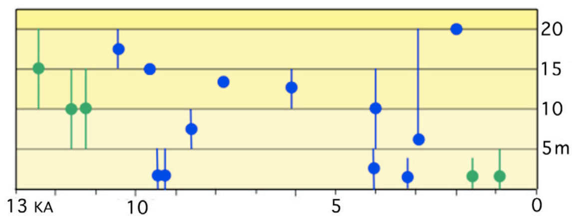


*Fig. 2. Recorded heights of tsunami events in the Baltic (blue) and Kattegatt (green) coasts of Sweden.*

*2. Landslide induced tsunamis*

Submarine landslides, or coastal earth slides into the sea or a lake, may be induced by earthquakes or gravity driven slope stability failure (avalanches). Whatever, those slide movements affect the water column and generate tsunami waves. The Storegga submarine slide had a volume of about 3,500 $km^3$, occurred about 8000 cal yrs BP and set up a major tsunami recorded along the Norwegian coast and and across the North Sea to Scotland (Dawson et al., 1988; Bondevik et al., 1997).

*3. Impact induced tsunamis*

Any celestial body falling into the sea is capable to set up a tsunami. The proposed impact at the Cretaceous/Tertiary boundary has led to much speculation on the occurrence of mega-tsunamis and tsunami derived effects and deposits (e.g. Bourgeois et al., 1988). Often the diameter of the tsunami wave, in the order of kilometres, was confused with the wave height, which is in the order of metres to a few tens of metres. When an iceberg is breaking off an ice front and falls into the sea it generates a tsunami (e.g. MacAyeal et al., 2011; Ferreira, 2011). Darwin had a breath-taking experience of this in Tierra del Fuego in 1838 (Darwin, 1839). Even stones and blocks falling down a cliff into water set up local tsunami waves.

*4. Volcanic eruption induced tsunamis*

The Krakatau eruption in Indonesia on August 27, 1883, set up a mega-tsunami of multiple waves. The wave had a maximum height of 37 m. Around 40,000 persons were killed. The 1883 Krakatau tsunami was recorded at 35 tide gauge stations scattered all over the Indian, Pacific and Atlantic oceans. The far-field records may primarily be a function of related atmospheric waves, however (point 6, below: meteotsunamis). The Island of Thera (Santorini) in the Aegean Sea exploded at a violent volcanic eruption about 1650 B.C. This event set up an extensive tsunami wave (Bruins et al., 2009), the effects of which have been very much debated and sometimes associated with the saga of Atlantis and its sudden disappearance.

*5. Explosion induced tsunamis*

The 23 nuclear bomb test explosion in the Bikini Atoll in the period 1946-1958 set up tsunami waves in the Pacific. It has recently been shown that explosive venting of methane gas as a function of a sudden phase-transition in the seabed (or lake bed) from methane ice (clathrate) to methane gas can set up tsunami waves of large height and extensive spatial impact (*Fig. 3*; Mörner, 2003, 2011, 2012, 2013; Mörner & Dawson, 2011).

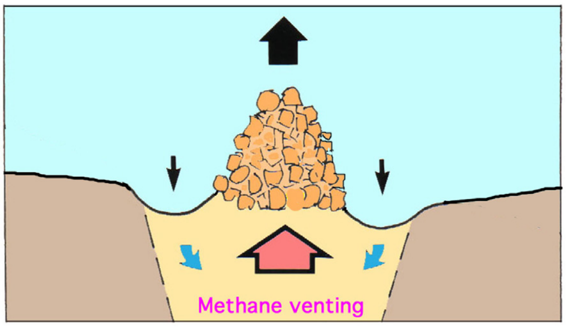


*Fig. 3. Model of explosive methane venting tectonic as recorded at several sites in Sweden (Mörner, 2003); for example at 2000 BP (Fig. 2) setting up a 20 m high tsunami wave (Mörner & Dawson, 2011).*

*6. Meteotsunamis*

As an additional process, we may include tsunami-like waves caused by atmospheric processes generating so-called *meteotsunamis* (Monserrat el al., 2006). By this process regional tsunamis may be transferred over larger distances. This seems to be the case of the very distant tsunamis in association with the Krakatau 1883 eruption (point 4 above) and the waves set up in Swedish lakes in direct timing with the Lisbon earthquake and tsunami in 1755 (e.g. Svedmark, 1904).

**ORIGIN OF TSUNAMITES**

Tsunami waves imply severe erosion and damage of cultural and natural objects in coastal areas. The re-deposition of sediments and objects set in motion by the tsunami is termed a *tsunamite* (Mörner, 2013, 2014) or tsunami deposits (beds or layers).

A tsunami wave hitting a coast usually consists of a sequence of separate waves; termed “a tsunami wave-train”. This has been recorded in the tsunami deposits (e.g. Wagner and Srisutam, 2011; Mörner, 2011, 2013).

*1. Off-shore deposits*

The tsunami wave has a large diameter of rotation. Therefore, it may generate erosion of the seafloor surface (as illustrated in Fig. 6 of Mörner & Dawson, 2011). This erosion leads to the deposition of extensive turbidites, usually in strict graded bedding. In Sweden, where the former seabed is uplifted and today constitutes dry land, these deposits can be studied in full details (Mörner, 2011, 2013). Submarine liquefaction events can occur together with tsunami events and generate the re-deposition of sandy-silty material in widespread layers of turbidite character. They are likely to be a combined effect of liquefaction and tsunami.

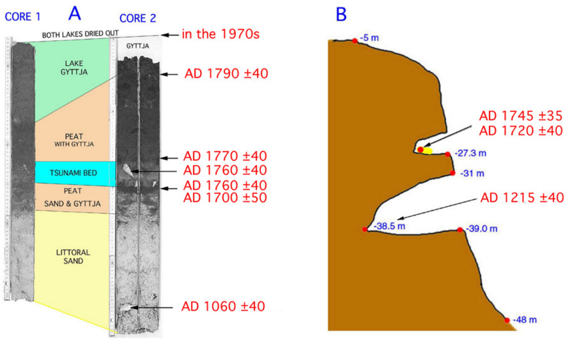


*Fig. 4. On-shore (A) and off-shore (B) records and C14-dates of a tsunami historically noted in year 1733 as a massive flooding episode in the Maldives (Mörner, 2007; Mörner et al., 2008; Mörner & Dawson, 2011).*

A tsunami wave may drag down coastal deposits to significant depths further off the coast. So, for example, "submarine sandstorms" from five tsunami events in historical time in the Maldives have generated the re-deposition of sand with shallow-water gastropods and corals in caves at depths of 27 and 38 m (Mörner & Dawson, 2011). *Fig. 4* gives the dated peat sequences on-shore (A) and submarine cave fillings off-shore (B), fitting very well with a historical documentation of a major flooding in 1733 (Mörner et al., 2008).

In near-shore areas, the tsunami may generate turbidites of angular pebbles and grits within clay beds extending far deeper than normal shore processes do (Mörner and Dawson, 2011). Submarine slides may extend as extensive turbidites out over the abyssal plane (e.g. Bouma, 1962). The AD 365 earthquake and tsunami (Stiros, 2010) generated an extensive turbidite in the Mediterranean (Polonia et al., 2013).

*2. Shore effects*

When the tsunami wave, or rather train of waves, hits a coast, it usually causes extensive erosion, destruction and relocation of objects (e.g. Keating et al., 2011). Often, the shore becomes severely remodelled (*Fig. 5*; from the fine documention of the March 11, 2011, tsunami in Japan by Tanaka et al., 2012). The material set in motion must, of course, be re-deposited either in the form of re-modelling of the shore morphology or by carrying it inlands (point 3, below) or seawards (point 1, above).

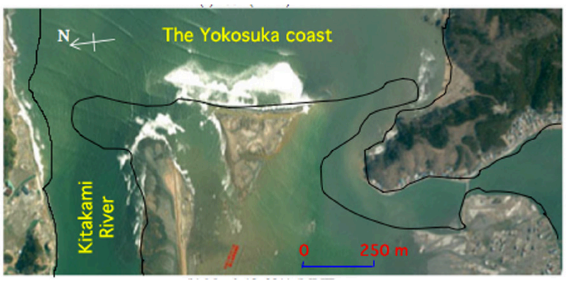


*Fig. 5. The shore of the Yokosuka coast in Japan (black line) and after (photographed land/sea configuration) at the March 11, 2011, tsunami as recorded by Tanaka et al. (2012). The coastal remodelling is extensive.*

*3. On-shore deposits*

The tsunami wave may have a height of up to some tens of metres. The breaking in over a coast generates a run-up, which may reach much higher elevations, however (e.g. Abe, 1995). The subsequent drawdown back-swash carries much material to depositional rest. This implies that the on-shore to near-shore tsunami deposits is the product of two different phases of the coastal dynamics; the on-swash beds from the run-up phase, and the back-swash beds from the drawdown phase.

*3.1. On-swash beds from the run-up phase*

The tsunami wave hits the coast with tremendous energy, capable of severe destruction and relocation even of heavy object like boulders (e.g. Keating et al., 2011). The run-up water masses become loaded with sediment particles (of all grain sizes, ranging from clay to boulders) and other objects picked up from the land surface swashed over (boats, trees, house debris, animals, humans, etc.).

Deposition usually occurs closer to the limit of the run-up where the energy decreases enough to allow for deposition. The most likely places of depositions are in depressions and lakes. The tsunami beds deposited often exhibit graded bedding (sometimes massive and chaotic).

One effective way of recording the run-up limit of past tsunamis is to core lakes at higher and higher elevation above the sea level (e.g. Mörner and Dawson, 2011). Tsunami beds recorded within normal lake deposits usually constitute of a sand layer of graded bedding containing deep-water planktonic microfossils (Mörner and Dawson, 2011).

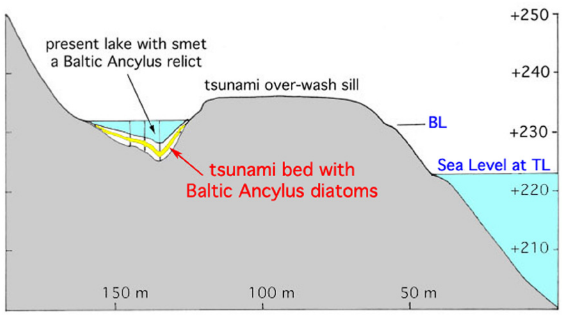


*Fig. 6. The situation at Lake Källsjön (+232 m) in Sweden, located above the highest Baltic level (BL at +131,3 m). The sill in-between had an original level of about +236 m. At the time of the 9663 BP tsunami, the Baltic level was at +223,5 m (TL). In the lakebed, there is a sandy tsunami bed (in fining-upward sequence) that contains a Baltic Lake Ancylus diatom flora. In order to enter this lake basin, the tsunami wave must have been more the 12,5 m high and to have over-wasted a sill at +236 m for about 700 m. Therefore, the tsunami wave is likely to have been, at least, 15 m high. In today's lake, a small fish( smelt) is living, which is likely to be a relict from the Lake Ancylus water, washed into the lake by the tsunami wave (Mörner, 2003, 2011; Mörner & Dawson, 2011).*

*3.2. Back-swash beds from the drawdown phase*

The back-swash phase may be responsible for the deposition of more extensive tsunami beds. Deposition primarily occurs in depressions and at the sea level.

Occasionally, material may be carried off-shores. Sometimes these deposits are full of archaeological remains like in the coastal tsunami deposits of the Santorini event (Bruins et al., 2009). Because of successively diminishing forcing at settling, even these deposits may be graded in bedding.

## CONCLUSIONS

Tsunamis are generated by five different processes; earthquakes, earth slides, impacts, volcanic eruptions and submarine explosions. Tsunami deposits or tsunamites are formed on land and in lake basins by the tsunami run-up and back-swash, at the shore by the remodelling of the coast by the tsunami wave and the re-deposition of material set in motion, and off-shore by the trimming of the tsunami wave at the seabed and the back-swash and over-wash of low islands, sometimes setting up submarine sandstorms re-depositing coastal material at great depths.

## References

Abe, K. (1995). Estimate of tsunami run-up heights from earthquake magnitudes, in Tsunami: Progress in Prediction, Disaster Prevention and Warning. *Adv. Nat. Technol. Hazards Res.*, 4, 21–35, Kluwer Acad. Press.

Blanc, P.-L. (2011). The Atlantic tsunami on November 1st, 1755: World range and amplitude according to primary documentary sources. In: Mörner, N.-A. (Ed.), *"The Tsunami Threat: Research & Technology"*, p. 423-446. Intech Publ.

Bondevik, S., J.I. Svensen & J. Mangerud (1997). Tsunami sedimentary facies deposited by the Storegga tsunami in shallow marine basins and coastal lakes, western Norway. *Sedimentology*, 44: 1115-1131.

Bourgeois, J., T.A., Hansen, P.L., Wiberg & E.G. Kauffman (1988). A tsunami deposit at the Cretaceous–Tertiary boundary in Texas. *Science*, 241, 567-570.

Bruins, H.J., J. van der Plicht & J.A. MacGillivray, (2009). The Minoan Santorini eruption and tsunami deposits in Palaikastro (Crete): dating by geology, archaeology, $^{14}$C and Egyptian chronology. *Radiocarbon*, 51, 397-411.

Bouma, A.H. (1962). *Sedimentology of some Flysch deposits: A graphic approach to facies interpretation*, 168 pp, Elsevier.

Darwin, C. 1839. *Voyage with H.M.S. Beagle* (with later editions, 1845 and 1860).

Dawson, A.G., D. Long & D.E. Smith (1988). The Storegga Slide: Evidence from eastern Scotland for a possible tsunami. Marine Geology, 82: 271-276.

Ferreira, B. (2011). When icebergs capsize, tsunamis may ensure. http://www.scilogs.com/dinner_party_science/when-icebergs-capsize/

Fonseca, J.D. (2005). *1755 o terramoto de Lisboa –the Lisbon eaerthquake*. Argumentum, 139 pp.

Keating, B.H., C.E., Helsley, M. Wanink & D. Walker (2011). Tsunami deposit research: Fidelity of the tsunami records, ephemeral nature, tsunami deposits characteristics, remobilization of sediment by later waves, and boulder movements. In: Mörner, N.-A. (Ed.), *"The Tsunami Threat: Research & Technology"*, p. 389-422. Intech Publ.

Lay, T., H. Kanamori, C. Ammon, M. Nettles, S. Ward, R. Aster, S. Beck, S. Bilek, M. Brudzinski, R. Butler, H. DeShon, H., G. Ekström, K. Satake & S. Sipkin (2005). The Great Sumatra-Andaman Earthquake of 26 December 2004, *Science*, 308, 1127– 1133.

MacAyeal, D.R., D.S. Abbott & O.V. Sergienko, (2011). Iceberg-capsize trunamigenesis. *Annals of Glaciology*, 52, 51-56.

Monserrat, S., I. Vilibic & A.B. Rabinocvich (2006). Meteo-tsunamis: atmospherically induced destructive ocean waves in the tsunami frequency band. *Nat. Hazards Earth. Syst. Sci.*, 6, 1035- 1051. www.nat-hazards-earth-syst-sci.net/6/1035/2006/

Mörner, N.-A. (2003). Paleoseismicity of Sweden - A Novel Paradigm. A Contribution to INQUA from its Sub-commission of Paleoseismology. Reno 2003, ISBN 91-631-4072-1, 320 pp.

Mörner, N.-A. (2007). Sea level changes and tsunamis. environmental stress and migration over the seas, *Internationales Asienforum*, 38, 353-374.

Mörner, N.-A. (2010). Natural, man-made and imagined disasters. *Disaster Advances*, 3 (2), 3-5.

Mörner, N.-A. (2011). Paleoseismology: The application of multiple parameters in four case studies in Sweden. *Quaternary International*, 242, 65–75.

Mörner, N.-A. (2012). Seismic hazard assessment on a nuclear waste time scale. 3rd INQUA-IGCP-567 International Workshop on Active Tectonics, Paleoseismology and Archaeoseismology, Morelia, Mexico, 19-24 Nov. 2012, *INQUA-IGCP 567 Proceedings* Vol. 3, p. 131-134.

Mörner, N.-A. (2013). Drainage varves, seismites and tsunamites. *GFF*, in press, doi: 10.1080/11035897.2013.764546.

Mörner, N.-A. (2014). Tsunami deposits. In: M.J. Kennish, Ed., *Encyclopedia of Estuaries*, in press, Springer.

Mörner, N.-A. & S. Dawson (2010). Traces of tsunami events in off- and on-shore environments. Case studies in the Maldives, Scotland and Sweden. In: Mörner, N.-A. (Ed.), *"The Tsunami Threat: Research & Technology"*, p. 371-388. Intech Publ.

Mörner, N.-A., J. Laborel & S. Dawson (2008). Submarine "sandstorms" and tsunami events in the Indian Ocean. *J. Coastal Res.*, 24, 1608-1611.

NOAA (2010). Tsunami terminology. *In:* The national tsunami hazard mittigation program. http://nthmp-history.pmel.noaa.gov/terms.html

Polonia, A., E., Bonatti, A. Camerlenghi, R.G. Lucchi, G. Panieri & L. Gasperini, (2013). Mediterranean megaturbidite triggered by the AD 365 Crete earthquake and tsunami. *Scientific Reports*, 3, doi:10.1038/srep01285.

Shiki, T., T. Tachibana, O. Fujiwara, K. Goto, F. Nanayama & T. Yamazaki (2008). Characteristic features of tsunamiites. In: *Tsunamiites – Features and Implications* (T. Shiki, Y. Tsuji, T. Yamakazi & K. Minoura, eds). Elsevier Scientific Publishing Company, 319-336.

Stiros, S.C. (2010). The 8.5+ magnitude, AD 365 earthquake in Crete: coastal uplift, topographic changes, archaeological and historical signiture. *Quaternary International*, 216, 54-63.

Svedmark, E. 1904. Jordbäfningen den 23 oktober 1904. November 3 meeting, *Geol. Fören Stockholm Förh.*, 230, 456-463.

Tanaka, H., N.X. Tihn, M. Umeda, R. Hirao, E., Pradjoko, A. Mano & K. Udo (2012). Coastal and estuarine morphology changes indiced by the 2011 great East Japan earthquake tsunami. *Coastal Engineering Journal*, 54, 1-25.

Wagner, J.-F. & C. Srisutam (2011). Grain-size and thin section characteristics of tsunami sediments from Thai-Andaman coast, Thailand. In: Mörner, N.-A. (Ed.), *"The Tsunami Threat: Research & Technology"*, p. 259-282. Intech Publ.

INQUA Focus Group on Paleoseismology and Active Tectonics

paleoseismicity.org

# New aspects of using dendrochronological analysis in paleoseismology (by the example of the SE Altai, Russia)

*Roman K. Nepop (1), Anna R. Agatova (1), Vladimir S. Myglan (2), Andrey N. Nazarov (2), Valentin V. Barinov (2)*

(1) Institute of geology and mineralogy, Koptjug av., 3, 630090 Novosibirsk, Russia. Email: agatr@mail.ru
(2) Siberian Federal University, Svobodny av., 79, 660041 Krasnojarsk, Russia

***Abstract:** Paleoseismogeology investigations of the high mountain, seismically active southeastern part of the Russian Altai reveal a previously unknown complex of earthquake induced landslides. Using dendrochronological analysis of the wood penetrating injuries of trees (both dead and living ones) caused by seismically induced rockfalls allowed establishing the date of previously unknown strong medieval earthquake. This date was also confirmed by radiocarbon dating of seismically cut fossil soil overlapped by undistorted one. The specified recurrence interval of strong (M>7) earthquakes for the SE Altai (about 400 years during the last 3 ka) argues the high regional seismicity.*

***Key words**: dendrochronology, paleoseismology, earthquake triggered landslides, Russian Altai, late Holocene*

## INTRODUCTION

Paleoearthquake age estimation is one of the key paleoseismological problems. It is a crucial point of specifying the recurrence interval of strong earthquakes and seismic hazard evaluation. The period of instrumental seismological observations is insignificant in comparison with the recurrence interval of strong earthquakes. Thus to estimate this interval the historical data are being involved as well as age evaluations of recognized paleoearthquake induced surface disturbances (both ruptures and gravitational deformations).

With this purpose the radiocarbon method is one of the most exploitable absolute dating techniques. It allows determining the age of soils, tree fragments and other organic materials which were deformed and/or buried during the earthquake. The application of the radiocarbon method is limited by ~50 ka but some problems occurred while using this technique for dating recent (2-3 ka) seismic events due to high relative methodological error and presence of several "plateaus" at the calibration curve.

In case of spreading the forest vegetation in seismically active areas dendrochronological analysis can be used as an additional and/or alternative approach. It has a great potential due to utmost precision of dating. Rings of trees - witnesses of seismic events contain both the evidence for the earthquake and its age. They give the opportunity to date different events which cause the tree injures and deaths as well as to define the time of forest recolonization on the bared surfaces.

This study presents the first experience of dating strong prehistoric earthquakes within southeastern part of the Russian Altai (SE Altai) on the basis of the dendrochronological analysis and brings new insight into this dating technique.

## STUDY SITE AND PERSPECTIVES OF APPLYING DENDROCHRONOLOGY FOR TIMING SEISMICALLY INDUCED LANDFORMS IN THE SE ALTAI

The Altai Mountains are the northern part of the Central Asia collision belt (*Fig. 1*). They stretch northwest more than 1500 km across the borders of Mongolia, China, Kazakhstan and Russia, and form a wedge shape narrowest in the southeast and widest in the northwest. The elevation increases in the opposite direction from 400 m a.s.l. to 4000 m a.s.l. The high-mountain southeastern part of the Russian Altai includes the Chuya and the Kurai intermountain depressions surrounded by

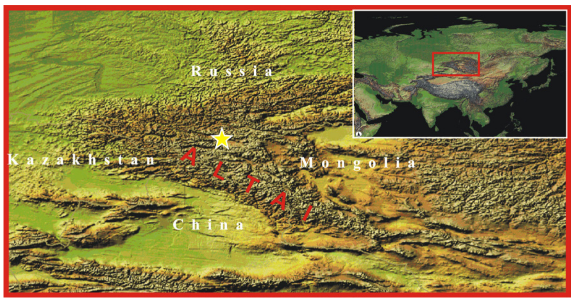


*Fig. 1: Studied area. Star shows the location of the southeastern part of the Russian Altai.*

ridges with altitudes about 3500 4200 m a.s.l.

The SE Altai is the northern extension of the Mongolian Altai, known for its high seismicity (Zhalkovskii & Muchnaya, 1975), and is the most seismically active part of the Russian Altai. Almost the whole territory of the SE Altai is characterized by seismic intensity of 8 point according to MSK scale. This is evidenced by the numerous large Holocene earthquake induced landslides and recently was supported by the 2003 Chuya earthquake ($M_S$=7.3) (Agatova & Nepop, 2011).

The dendrochronological analysis is a very promising tool and has a great potential for dating the seismically induced landforms here due to several reasons: 1) seismically induced slope processes intrude into the forest stand zone in an immediate vicinity with the modern upper timber limit (which is favorable for carrying out the dendrochronological analysis); 2) arid climate promotes good preservation of wood (up to two thousand years on stone surfaces); 3) a number of long absolute tree-ring chronologies, including the 2367-years "Mongun" one (Myglan et al., 2012) has been developed for the SE Altai and adjusted Tuva region; 4) the strong Chuya earthquake ($M_S$=7.3) that strike the SE Altai in 2003 gives the opportunity to analyze the distribution patterns of tree injuries caused by rock falls of specifically seismic origin.

## SAMPLING STRATEGY AND DATING PROCEDURE

*Initial premises*

Paleoseismological investigations revealed the repeated reactivation of the same focal zones within the SE Altai. Thus besides the estimating the germination ages of trees growing on the bare surfaces of seismically triggered landslides we have also tested the new approach of timing earthquakes which occurred already after forest regeneration. We suppose that for trees located near the scarps and talus fans (both dead and living ones) wood penetrating injures could be caused by earthquake induced rockfalls. It gives the opportunity to date such events within time limit exceeding the recurrence interval of strong earthquakes in the region. Obviously besides earthquake triggered rockfalls there are climatically driven ones. Thus as well as the number of wood penetrating injures, the simultaneity of such anomalies sustained by several trees grown on different earthquake induced landslides was taken as a criterion of their seismic origin. The accuracy of such an approach was supported by data obtained from analyzing injuries occurred on trees due to rock falls triggered by the 2003 Chuya earthquake.

*Sampling*

Detailed geomorphological investigations and process analyses were carried out using interpretation of aerial photographs, topographic maps (scale of 1:25000), and field investigations including mapping of landforms and deposits of different genesis. Paleoseismogeological investigation was applied for basing the seismic origin of studied landslides. Samples were collected from trees (both living and dead ones) located on the surfaces of the talus fans and landslides near the scarps or most active talus channels. Cores and wedge shaped samples were taken from living trees and discs – from dead ones. In order to provide reliable dating additional discs were collected from the uninjured parts of tree trunks.

*Dating procedure*

Dendrochronological analysis included tree ring width measurements with an accuracy of 0.01 mm using digital LINTAB positioning table coupled to a Zeiss stereomicroscope and TSAP system V3.5 software (Rinn, 1996). Growth curves were cross-dated using the standard correlation parameters of TSAP system V3.5 and the dendrochronological software package DPL (Holmes, 1983) with visual control of the radial growth curves. The standard procedure of building the tree ring chronologies (Shiyatov et al., 2000) on *Pinus Sibirica* Du Tour and *Larix Sibirica* Ledeb was applied for calendar dating. Anomalies (wood penetrating injuries) in the individual tree ring series were studied for identification and dating of earthquake triggered rock falls. The germination ages of trees growing on the bare surfaces of such landslides were also calculated. An age correction has been applied for the assessment of the colonization time gap and the time of surface stabilization.

## RESULTS

*Estimating the ages of strong prehistoric earthquakes*

Our paleoseismogeological investigations revealed a previously unknown complex of earthquake induced landslides in the Arydjan valley located at the northern part of the Chagan-Uzun massif (*Fig. 2*).

To provide the dendrochronological dating the local 1153-years (AD 856 till 2009) tree ring chronology on *Pinus sibirica* Du Tour was built. The year of birth of the eldest examined trees which colonized the surface of the talus fans covering landslide bodies is AD 1069 and 856 for landslides 1 and 2 respectively From 120 traumatic injuries of tree rings, three and more coincide into the

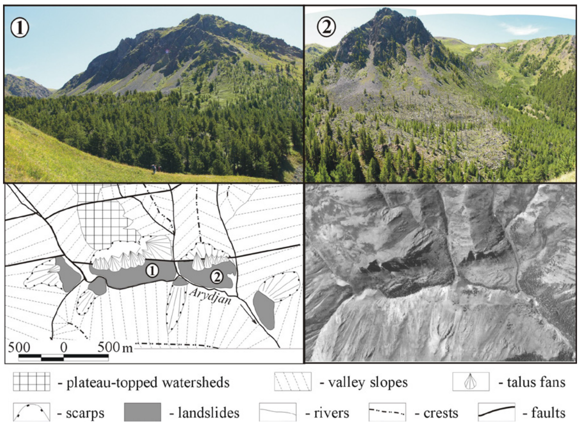


*Fig. 2: The largest earthquake triggered landslides in the Arydjan valley (location is shown by star 1 on Fig. 3)*

years 1316, 1422, 1532 and 2003 (*Fig. 3*). At the same time numerous wood penetrating injuries dated by AD 1532 for trees grown at both landslides are displayed at various heights of tree trunks. This fact implies a high magnitude of a medieval seismic event or/and its nearby epicenter. Same patterns of wood penetrating injuries caused by rockfalls, triggered by the 2003 Chuya earthquake with its epicenter located on the southern border of the Chagan-Uzun massif, allow us to assert that a strong earthquake struck SE Altai in 1532.

In order to estimate the time of creation of earthquake triggered landslides in addition to the germination ages of trees growing on their surfaces, the colonization time gap (about 100 years) and the formation time of talus fans covered landslide bodies, as well as surface stabilization period, should be taken into consideration. Due to these reasons the applied age correction can reach 2 centuries or more. Thus, it could be asserted that by AD 600-700 the studied seismically triggered

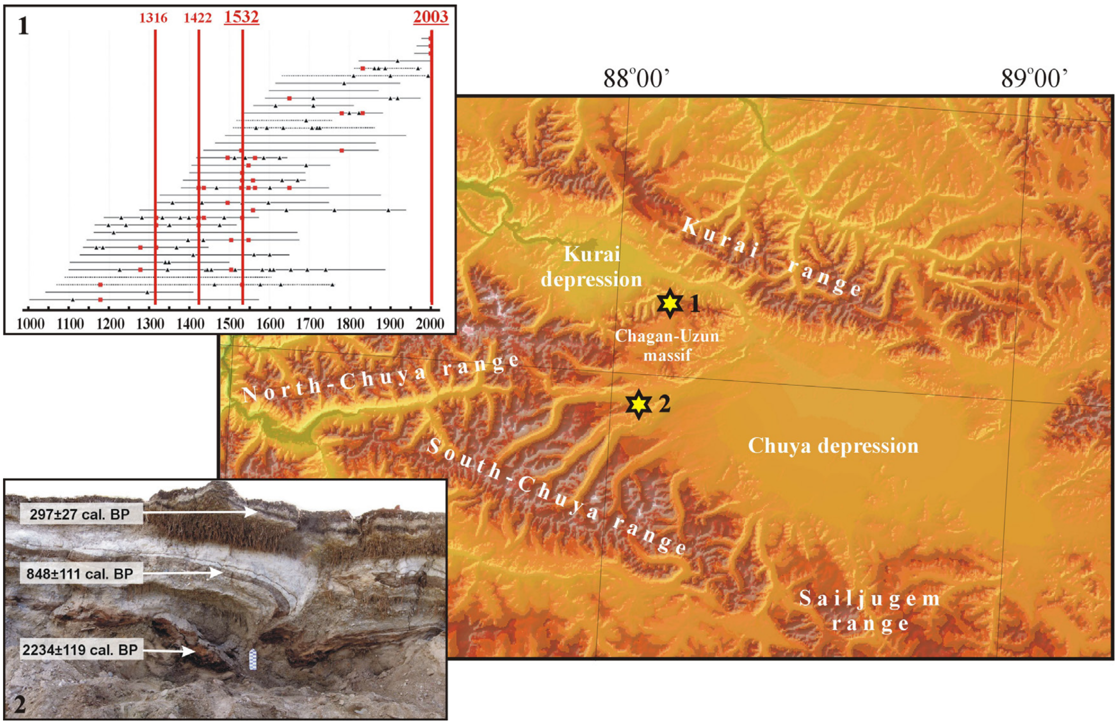


*Fig. 3: Southeastern part of the Russian Altai, sampling sites and results of 1) dendrochronological and 2) radiocarbon dating which allowed to establish the date of previously unknown strong medieval earthquake.*

landslides in the Arydjan valley already existed (available data do not allow to distinguish the time of landslides formation).

*Verifying dendrochronological data by radiocarbon dating*

The previously unknown medieval earthquake is also confirmed by radiocarbon ages of seismically cut fossil soil overlapped by undistorted fossil soil on the southern border of the Chagan-Uzun massif. A section of lacustrine and colluvial sediments with the fossil soil layers covering ancient moraines were exhumed in one of the numerous ruptures within the giant landslide triggered by the 2003 Chuya earthquake in Taldura valley. The ages of two seismically deformed fossil soil layers are 2234±119 cal. years BP (IGAN 4090) and 848±111 cal. years BP (IGAN 4105) and the age of undistorted fossil soil covering them is 297±27 cal. years BP (SOAN 8659). Thus the dendrochronologically obtained date of the 1532 seismic event lies within the time range determined by radiocarbon ages of fossil soils.

*Specifying the recurrence interval of strong earthquakes*

The obtained data allow us to specify the recurrence interval of strong ($M$>7) earthquakes for the SE Altai, which can be estimated now as about 400 years during the last 3 ka. Previously this value for the whole Holocene had been estimated as 1000-3000 years (Zhalkovskii & Muchnaya, 1975) and was later reduced to 500-900 years as a result of extensive paleoseismological research and radiocarbon dating (Rogozhin et al., 2007). New data support the high seismicity of SE Altai and allow defining the Chagan-Uzun massif as one of the major regional seismogenerating structures.

**CONCLUSION**

Dendrochronology has a great potential in paleoseismological investigations due to utmost precision of dating. Rings of trees - witnesses of seismic events contain both the evidence for the earthquake and its age. Analysis of traumas for trees grown on the surfaces of different landslides allows us to mark out tree-ring anomalies caused by specifically seismically triggered rock falls. Thus the date of strong medieval earthquake has been set up using dendrochronological analysis to a year. This date was verified by radiocarbon dating of seismically cut fossil soil overlapped by undistorted one. The ages of the oldest trees settled the bared landslides surfaces give the information about the minimal ages of these landforms. Specified recurrence interval of strong earthquakes ($M$≥7) argues for the high seismicity of the SE Altai.

Besides the obvious applied importance for local paleoseismological investigations the suggested approach can be used for timing landslides and strong paleoearthquakes for regions where instrumental seismic records or historical accounts are not available.

**Acknowledgements:** We would like to thank L.A. Orlova (IGM SB RAS, Novosibirsk) and E.P. Zazovskaya (IG RAN, Moscow) for the radiocarbon dating. The study was partly funded by Russian Foundation for Basic Researches (grants 13-05-00555 and 12-06-33040).

**References**

Agatova, A.R., Nepop, R.K., 2011. Assessing the Rate of Seismogravitational Denudation of the Relief of Southeastern Altai: The Chagan_Uzun R. Basin. Journal of Volcanology and Seismology 5(6), 53–62.

Holmes, R.L., 1983. Computer-assisted quality control in tree-ring dating and measurement. Tree-ring bulletin 44, 69-75.

Myglan, V.S., Ojdupaa, O.Ch., Vaganov, E.A., 2012. Making the 2367-year tree-ring chronology for Altai-Sayan region (mountain massif Mongun-Taiga) [Postroenie 2367-letnej drevesno-kol'cevoj hronologii dlja Altae-Sajanskogo regiona (gornyj massiv Mongun-Taiga)]. Archeology, etnography and anthropology of Eurasia [Arheologija, etnografija b antropologija Evrazii] 3, 76-83 (in Russian).

Rinn, F., 1996. TSAP V3.5. Computer program for tree-ring analysis and presentation. Frank Rinn Distribution, Heidelberg.

Rogozhin, E.A., Ovsyuchenko, A.N., Marakhanov, A.V., Ushanova, E.A., 2007.Tectonic setting and geological manifestations of the 2003 Altai earthquake. Geotectonics 41(2), 87-104.

Shiyatov, S.G., Vaganov, E.A., Kirdjanov, A.V., Kruglov, V.B., Mazepa, V.S., Naurzbaev, M.M., Khantemirov, R.M., 2000. Methods of dendrochronology. Part I. [Metody dendrohronologii. Chast' I]. Krasnojarsk University press, Krasnojarsk (in Russian).

Zhalkovskii, N.D., Muchnaya, V.I., 1975. Energy distribution of earthquakes and seismic activity in the Altai-Sayan area [Raspredelenie zemletrjasenij po energii I seismicheskaja aktivnost' Altae-Sajanskoj oblasti], in Gaiskii, V.N. (Ed.), Seismicity of the Altai-Sayan area [Seismichnost' Altae-Sajanskoj oblasti]. Nauka, Novosibirsk, pp. 5-15 (in Russian).

INQUA Focus Group on Paleoseismology and Active Tectonics

paleoseismicity.org

# Paleoseismological sites revisited on the Alhama de Murcia Fault (SE Iberia): preliminary results

*Maria Ortuño (1), Eulalia Masana (1), Héctor Perea (2), Marta Ferrater (1), José Martínez-Díaz (3), Stephane Baize (4), Ona Corominas (1)*

(1) RISKNAT Group. Departament de Geodinàmica i Geofísica, Facultat de Geologia, Universitat de Barcelona, c/ Martí i Franquès, s/n, 08028 Barcelona, Spain. Email: maria.ortuno@ub.edu
(2) Barcelona-CSI, Institut de Ciències del Mar - CSIC, CMIMA, Psg. Martim de la Barceloneta, 37-49, 08003, Barcelona, Spain
(3) Departamento de Geodinámica, Universidad Complutense de Madrid, Calle Jose A. Novais, 28040 Madrid, Spain
(4) Institute of Radiological Protection and Nuclear Safety (IRSN), Seismic Hazard Division (BERSSIN), BP 17, 92262 Fontenay-aux-Roses, France

***Abstract:*** *The El Saltador paleoseismological site, in the central part of the Alhama de Murcia fault was revisited in order 1) to find older paleo-events that help to complete the paleo-earthquake chronology; 2) to better understand the influence of the fault activity in the Quaternary sedimentary record and; 3) to constraint the net slip vector and slip rate. Eight new trenches were excavated perpendicular and parallel to the south AMF branch, exposing the sedimentary record of at least 4 paleo-earthquakes, two of them probably occurred in the last 30 ka. A changing seismic landscape could explain the sedimentary record next to the fault trace: each seismic movement resulted in an obliteration of the previous relief in the downthrown block due to the sedimentation of mud flow deposits blocked by the fault scarp. After each earthquake and during some period of calm (inter-seismic interval), head-wards erosion of the fluvial streams resulted in the restoration of the old landscape.*

***Key words****: Eastern Betics shear zone, El Saltador site, Lorca earthquake, seismic landscape, 3D trenching.*

## INTRODUCTION

The Eastern Betics Shear Zone (EBSZ) is a structural domain accommodating part of the convergence between Africa and Eurasia. Some of the active faults within this zone have been shown to be seismogenic and responsible of some of the historical damaging earthquakes occurred in SE Iberia.

In this work, we focused on the Alhama de Murcia fault (AMF, Fig. 1), the longest structure within the system (near 100 km trace length). This fault was the source of the Lorca earthquake (Mw = 5.2, 10/05/2011) and probably of many other historical earthquakes in the region. It has been studied through paleoseismological approaches in previous researches (Silva et al., 1997; Martínez et al., 2003; Masana et al., 2004; Ortuño et al., 2012) that have evidenced that the AMF has produced several morphogenic earthquakes of Mw = 6-7 during the last 300 ka. The mean recurrence period of such events ranges between 3 and 30 ka, depending on the segment (Martínez et al., 2012).

Despite the increasing number and quality of the available geologic data, the most recent slip rate and slip vector are till poorly constrained. Martinez-Díaz et al. (2003) estimated a lateral slip-rate of 0.21 mm/yr in the last 130 kyr and 0.06-0.15 mm/yr in the last 30 kyr whereas GPS data reveals Present-day slip-rates between 1.4-1.8 mm/yr (Echeverria et al., 2012). These GPS data also indicate plate shortening directions oriented 40º – 90º with respect to the AMF trace, which is consistent with reverse-left lateral movement deduced from geological and focal mechanism data (Martínez-Díaz et al., 2012)

The main goals of this research were: 1) to extend the paleoseismological data obtained 10 years ago in the El Saltador site; 2) to constraint the fault net slip, one of the kinematic parameters still known, and; 3) to understand the neotectonic control on the alluvial dynamics.

## EL SALTADOR SITE

El Saltador site is located 8 km north of Lorca, at the central part of the AMF trace (Fig. 2a). In this area, the fault zone is composed of two main fault branches: the northern AMF (NAMF) and the southern AMF (SAMF). The NAMF is oriented SSW-NNE and has controlled the uplift of the La Tercia range, located to the NW.

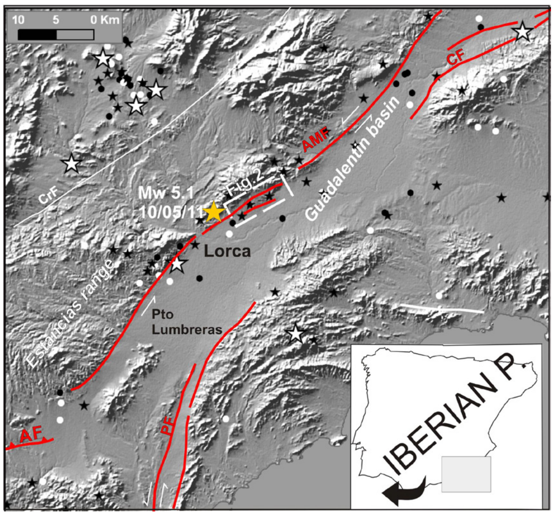


*Fig. 1: Location of the study area*

The recent activity of this branch and secondary branches is evidenced by the deformation of Late Pleistocene alluvial fans in neighbouring sites and at the El Saltador creek.
The SAMF is oriented SW-NE and its activity is assumed to be related to the NAMF. The SAMF surface expression consists of a push-up structure which is modifying the fluvial drainage and has resulted in the formation of a fault-parallel corridor between La Tercia range and the Guadalentin depression (Fig.2).

Previous researches in this area (Martínez-Díaz et al., 2003 and Masana et al., 2004) have focused on the internal branch of this push-up. This branch (N-SAMF) has offset El Saltador alluvial fan by at least 1 m (vertical). This deformation has generated the obstruction of the fluvial drainage, leading the formation of dam deposits at the toe of the fault. At least 2 paleo-earthquakes have been identified in two trenches (TR 3 and 4), with time constraints of 26.9 - 15.8 ka the older and 3.08 – 2.78 ka the younger. The minimum slip per event ranges between 0.1 and 0.9 m.

## RESULTS AND DISCUSSION

In this new campaign, we studied the most recent geological record by the study of new 8 trenches (Fig. 2b). These trenches showed up to 7 alluvial phases consisting of grain-supported conglomerates made up of a succession of layered gravels of variable grain sizes (from homometric and millimetric to highly heteromotetric and up to 0.5 m diameter). These facies reflect energetic and discontinuous proximal alluvial environment. Separating the alluvial phases, erosional surfaces are distinguished. Some of these surfaces are accompanied by incipient soil development evidenced by roots marks, edafic soil structure and calcrete nodules, which indicate time periods of non erosion/deposition. Up to 7 layers of matrix-supported conglomerate are interlayered between some of the conglomerate layers. These layers consist on predominant fine sediments (silts and clay) in which sparse clasts of variable size are floating and are interpreted as the record of mud flows.
The alluvial succession is faulted and folded by the displacement on the N-SAMF, composed of several fault branches displaying a fan distribution typical from flower structures. Furthermore, the fault activity seems to have generated repeatedly a counter slope fault scarp which has blocked the drainage, leading to the accumulation of mudflow deposits. Evidence supporting this idea is the systematic increase of the mud flow deposits towards the fault trace and the absence of them in the uplifted block. Thus, every mud flow layer was interpreted as the evidence of a paleoearthquake.

The effect of the seismic events in the local topography can be summarized as 1) uplift of the SE fault block, i.e., the downstream area. This leads to the preservation of the original channels that are progressively more incised by head-wards erosion 2) downthrown of the NW block, i.e., upstream area. This leads to the infill of the previous relief by the after seismic sediments, which obliterate the previous landscape and result in a smoother topography.

A minimum of 4 seismic events were detected in the studied trenches (Fig. 3), each of them associated with the blockage of a mud flow and with folding and faulting of the alluvial phases. Comparison with the former paleoseismic study (Martínez-Díaz et al., 2003; Masana et al., 2004) leads to correlate the 2 younger events with those previously identified, occurred in the last 30 ka. The new dating results, still unavailable, will provide age constraints to validate this correlation and to date the older events, helping to re-evaluate the recurrence time of this fault segment. Ongoing research on the paleoseismological site searches to constrain the net slip vector of the fault by the detailed cartography of paleochannel features both sides of the fault.

**Acknowledgements:** This research was founded by SHAKE CGL2011-30005-C02-02 project.

## References

Echeverría, A., Khazaradze, G., Asensio, E., Gárate, J. & Suriñach, E. (2012). Deformación cortical de las Béticas Orientales observada mediante GPS y su relación con el terremoto de Lorca. *Física de la Tierra* 24, 113-127.
Martínez-Díaz, J.J., Masana, E., Hernández-Enrile, J.L. & Santanach, P. (2003). Effects of repeated paleoearthquakes on the Alhama de Murcia Fault (Betic Cordillera, Spain) on the Quaternary evolution of an alluvial fan system. *Annals of geophysics* 46, 775-791.
Martínez-Díaz, J.J., Masana, E., Ortuño, M. (2012). Active tectonics of the Alhama de Murcia fault, Betic Cordillera, Spain. *Journal of Iberian Geology* 38 (1), 253-270.
Masana, E., Martínez-Díaz, J.J., Hernández-Enrile, J.L. & Santanach, P. (2004). The Alhama de Murcia Fault (SE Spain), a seismogenic fault in a diffuse plate boundary: Seismotectonic implications for the Ibero-Magrebian región. *Journal of Geophysical research* 109, 1-17.
Ortuño, M., Masana, E., García-Meléndez, E., Martínez-Díaz, J.J., Stepancikovà, P., Cunha, P.P., Sohbati, R., Canora, C., Buylaert, J.P., & Murray, A.S. (2012). An exceptionally long paleoseismic record of a slow-moving fault: the Alhama de Murcia fault (Eastern Betic Shear Zone, Spain). *The Geological Society of America Bulletin*, 124 (9-10), 1474-1494
Silva, P.G., Goy, J.L., Zazo, C. & Bardají, T. (1997). Paleoseismic indications along "aseismic" fault segments in the Guadalentín Depression (SE Spain). *Journal of Geodynamics* 24, 105-115.

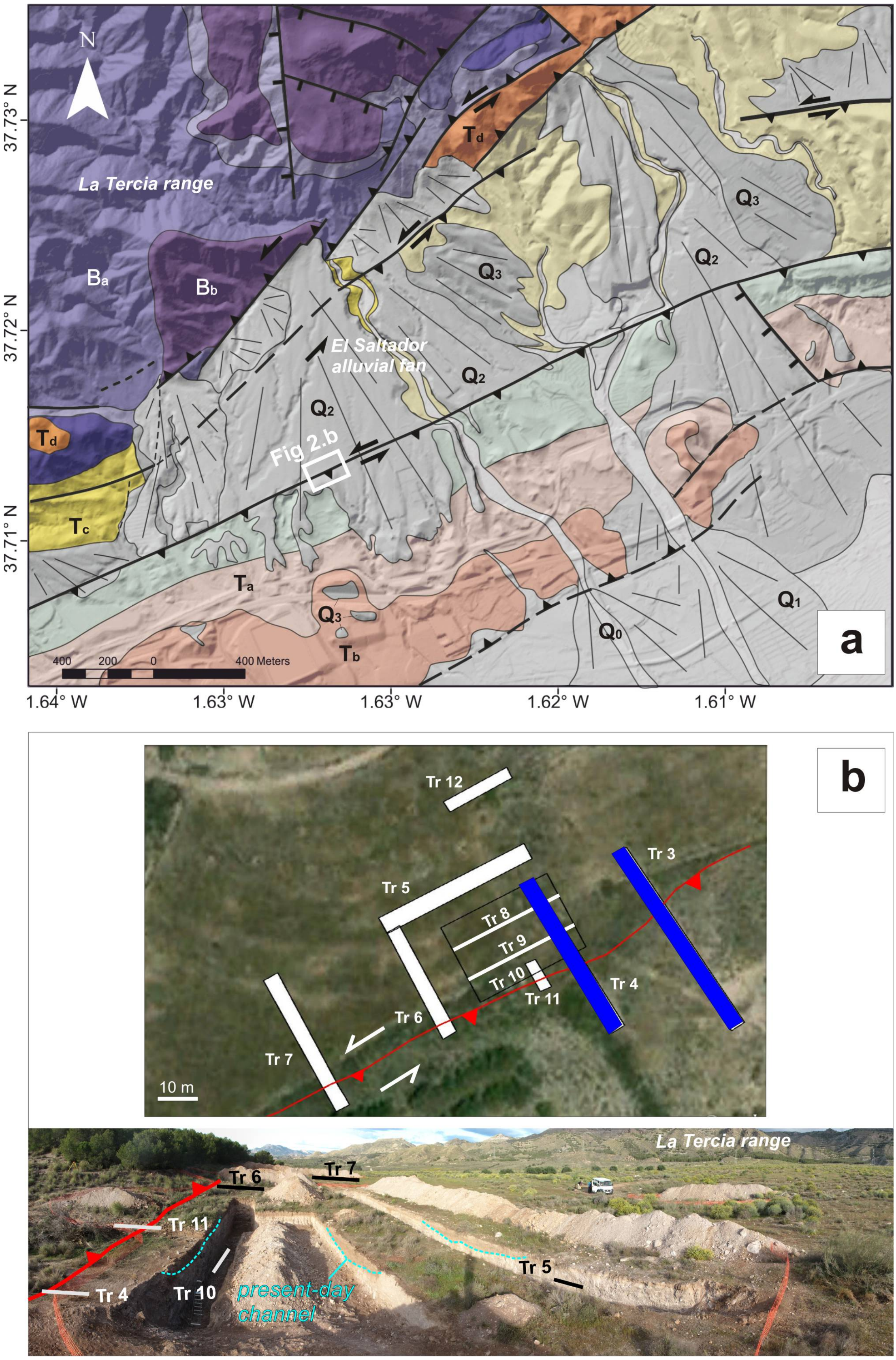


*Fig. 2: a) Geologic map of the study area in the central part of the AMF. From older to younger: Ba-b Paleozoic basement rocks, mainly filites, quartzites, schists; Ta-c; Upper-Messinian rocks (Tortonian) made up of marls, conglomerates and gypsum; Q0-4; Quaternary alluvial phases from older (4) to younger (0); b) location of the previous (3-4) and new (5-12) trenches and panoramic view of the paleoseismological site.The orientation of the trenches is indicated by a black or white bar.*

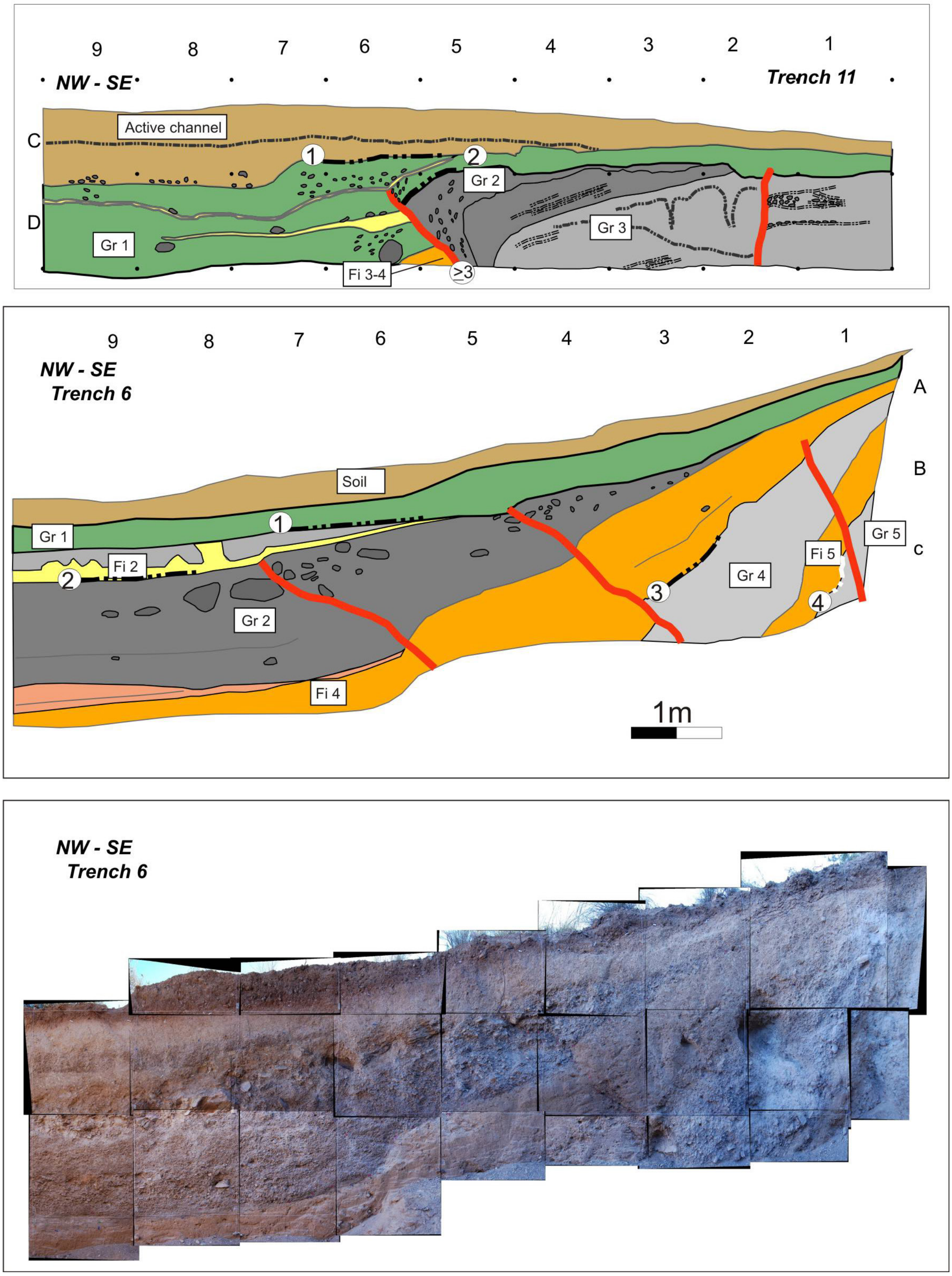


*Fig. 3: Log of El Saltador trenches 11 and 6 and fotolog of trench 6. Paleoevent horizons are marked with white dash lines. Gr; alluvial phasesmade up of gravels; Fi; mud flow faces mude up of fine sediments.*

INQUA Focus Group on Paleoseismology and Active Tectonics

paleoseismicity.org

# Paleoenvironmental analysis and active faults in the area between the Corinth and Saronikos Gulfs

*Pallikarakis, Aggelos (1), Ioannis D. Papanikolaou (1,3), Maria Triantaphyllou (2)*

(1) Mineralogy-Geology Laboratory, Department of Earth and Atmoshperic Sciences, Agricultural University of Athens, Iera Odos 75, 118-55, Athens, Greece
(2) Hist. Geology-Paleontology Department, Faculty of Geology and Geoenvironment, National and Kapodistrian University of Athens, Panepistimiopolis 15784, Athens, Greece
(3) AON Benfield UCL Hazard Research Centre, Department of Earth Sciences, University College London, WC 1E 6BT, London UK
Email: (i.papanikolaou@ucl.ac.uk)

***Abstract:*** *The aim of this paper is to study the interrelationship between paleogeography, paleoenvironment and active faults in the area between the Corinth and Saronikos Gulfs. The area is controlled by the sea level fluctuations as well as by tectonic processes involving both regional uplift and individual fault movements, resulting in highly complex paleoenvironmental patterns. Paleoenvironmental alterations were studied through borehole cores in Corinth region. Seven boreholes were drilled southwards the city of Corinth close to significant active fault traces. Samples extracted from these cores were examined in order to describe the lithology and identify paleoenvironmental modifications within them. Several lithological formations are described indicating significant lateral alterations even among neighboring boreholes. These alterations are also directly or indirectly affected by the activity of neighboring faults.*

***Key words***: *Active faults, Paleoenvironment, Foraminifera, Corinth, Boreholes*

## INTRODUCTION

The eastern part of northern Peloponnese is affected by significant onshore and offshore fault systems. The Xylokastro (offshore) and the Schinos – Pissia fault systems (onshore) are considered to be the most active (e.g., Jackson et al., 1982; Armijo et al., 1996, Roberts et al., 2009). The area though, is also affected by other less active, but significant E-W trending faults such as the Agios Vasilios and the Kechries faults located southwards the city of Corinth (Fig. 1, 2). Both of them are pure normal faults that dip towards north controlling the topography. Their length is approximately 40 km and 24 km respectively onshore and offshore (Papanikolaou et al., 1989). A secondary structure, the Kalamaki fault, has been studied as well. According to Papanikolaou et al.,(2011), this structure is the most active fault that intersects the Corinth Canal. It has a 6 km length, strikes at 075°-255° and dips towards ENE-WSW.

## STUDY AREA

Our study area is located in the easternmost tip of the Corinth Canal, till the Agios Vasilios fault towards south (Fig. 1, 2). Seven boreholes were drilled in this area. Samples were taken to characterize the lithology and any changes to the paleoenvironment within them.

The area consists of marls, sands and conglomerates (Collier & Thomson1991, Collier & Dart 1991, Leeder et al., 2002, 2003, 2008). Freyberg (1973) and Krstic & Dermitzakis (1981) through micropaleontological analysis have estimated the age of the sediments that construct the Isthmus canal at Upper Pleistocene. Anagnostopoulos et al., (1991), have described the Upper Pleistocene and Pliocene marls that structure the Corinth Canal. Collier et al. (1992) identified six marine transgressive cycles in the NW half of the Corinth Canal section up to 90 m above present-day sea level. These alterations are thought to be the product of interplay between the glacioeustatic sea level changes and the tectonic uplift of the area. The date of corals which were found in situ close to Examilia village was estimated at the Upper Pleistocene according to Collier et al., (1992) and Dia et al., (1997). Furthermore, according to Armijo et al., (1996) marine terraces mapped close to Examilia and the Kechries fault were considered to be from 125 ka till 240 ka.

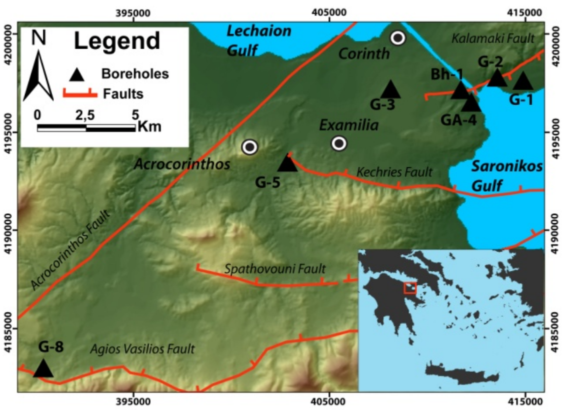


*Fig. 1 DEM of the study area with the most significant faults and the boreholes' location as was modified from Bornovas et al. 1972, Gaitanakis et al. 1985, Papanikolaou et al. 1996.*

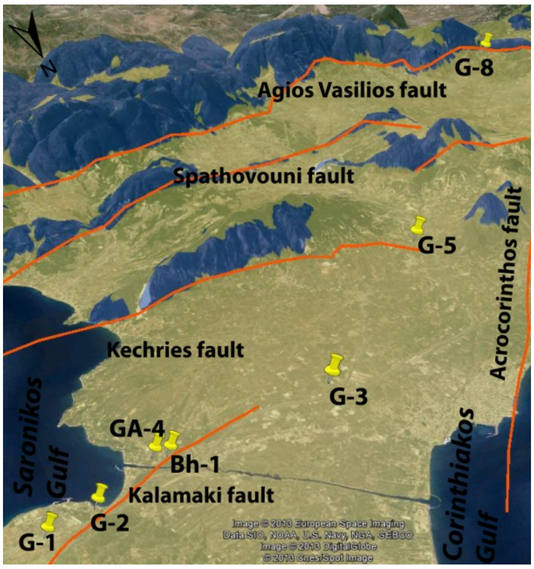


*Fig. 2 3D view of the study area based on Google Earth, showing the major fault systems and the boreholes' sites.*

**BOREHOLE DATA**

*Lithostratigraphic units*

In each borehole lithological alterations of sand, clay, gravels with ophiolite and limestone pebbles, mudstone, fragments of limestone, and soil have been recognized. It is important that among these layers no significant correlation was found even to neighboring boreholes. The latter strongly indicates that there are major lateral alterations and stratigraphic variations. Papanikolaou et al., (2011), which have examined boreholes located at the eastern tip of Corinth canal, have also encountered the same complicated lithological pattern.

In borehole Bh-1 (Fig. 3) alterations of cohesive to low cohesion sand, clay and gravels with ophiolites and limestone pebbles were found. The borehole has ended with a layer of sub angular gravels. In borehole G-1 alterations of fine to coarse and stiff to no cohesion sand, silt, and gravels with fragments of limestone was found. Till the end of the borehole gravels with very coarse sand and fragments of limestone was found. Lithology of borehole G-2 was simple and with no significant variations. The first meters was characterized as soil while the borehole ends with sandy clay. In borehole G-3 (Fig. 4) alterations of soil, clay, coarse and coherent to semi-coherent sand, reddish clay with well rounded gravels were found. Within borehole G-5 (Fig. 5) alterations of clay with sand, brown–red mudstone with gravels and fragments of limestone, reddish clay, and greenish cohesive mudstone was found. In borehole GA-4 the first 8.50 m were considered to be debris that were excavated during the construction of the Canal. Beneath them strata were characterized as reddish clay partially containing well rounded gravels with ophiolites and limestone pebbles, greenish-beige and yellowish coherent to semi-coherent coarse sand. In borehole G-8 (Fig. 6) alterations of brown to greenish clay with incoherent sand, well sorted gravels with greenish yellowish clay, boulders of fractured limestone was found. The borehole ends with weathered siltstone with no cohesion.

*Paleoenvironmental interpretations*

Approximately 140 samples were collected from these boreholes (8 from Bh-1, 56 from GA-4, 20 from G-1, 8 from G-2, 13 from G-3 and G-5, 25 from G-8). Borehole G-8 had no microfauna assemblages, therefore it was only sedimentologically examined. Each sample (10 gr dry weight) was treated with $H_2O_2$ to remove the organic matter, and subsequently was washed through a 125μm sieve and dried at 60°C. A subset of each sample was obtained using an Otto microsplitter to obtain aliquots of at least 200 benthic foraminifers. The microfauna were identified under a Leica APO S8 stereoscope. A scanning electron microscope analysis (SEM Jeol JSM 6360, Dept. of Hist. Geology-Paleontology) was used for taxonomical purposes. The studied benthic foraminiferal assemblages are relatively abundant and moderately preserved. The identified foraminiferal species were grouped in euryhaline forms mainly represented by *Ammonia* spp. large and small sized, *Elphidium* spp., *Haynesina* spp., *Aubignyna perlucida* and marine foraminiferal indicators, mostly including miliolids, and in a lesser degree full-marine species grouping *Asterigerinata, Neoconorbina*, *Rosalina* spp., *Planorbulina mediterranensis*. A series of different depositional environments were recognized through micropaleontological analysis of the benthic foraminiferal fauna (e.g. Triantaphyllou et al., 2003; Goiran et al., 2011; Papanikolaou et al., 2011).

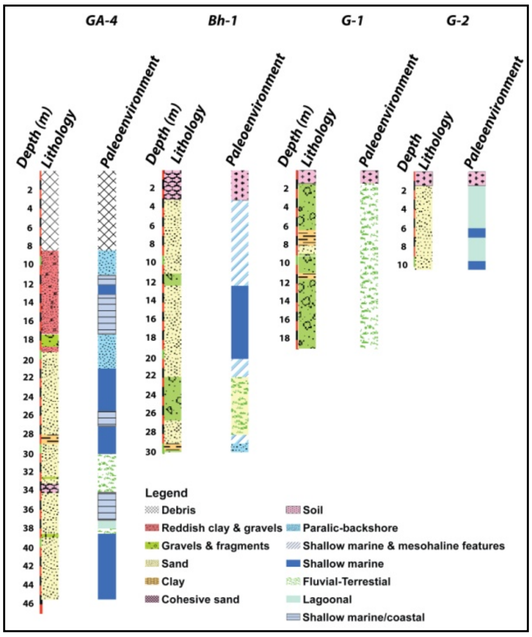


*Fig. 3 Lithological and paleoenvironmental alterations within boreholes Bh-1, GA-4, G-1, G-2 located at the immediate hangingwall of Kalamaki fault (Fig. 1).*

The first 3.00 m in Bh-1 is characterized as soil, while till 22.00 m depth there are alterations of lagoonal with shallow marine and lagoonal environment again. Till 28.00 m depth is characterized as terrestrial – fluvial environment (well rounded gravels d=4cm). From 28.00

m till 29.00 m is described as shallow marine – lagoonal paleoenvironment and till the end of the borehole at 30.00 m depth as paralic backshore. In borehole G-1 the first 1.10 m is described as soil whereas the rest of the borehole till the end at 20.00 as terrestrial – fluvial environment.

In borehole G-2 the first 1.50 m is characterized as soil. Till 6.00 m depth is described as lagoonal paleoenvironment. A thin layer till 7.00 m has been characterized as shallow marine with mesohaline features due to fresh water input. Till 9.50 m depth is characterized as lagoonal and till the end of borehole at 10.50 m shallow marine again. G-3 has no significant variations. Foraminifera are scarce and most of them broken The first 0.50 m within borehole G-3 is considered to be soil. Till 9.50 m depth few broken forams indicate a paralic or shore face environment. A thin layer beneath till 9.90 m is characterized as lagoonal. The last part of the borehole till 10.50 m contains no microfauna indicating a paralic environment.

The first 8.50 m within borehole GA-4 were not taken under consideration, since there are manmade debris from the construction of the Canal. From 8.50 till 11.00 m few broken species indicate a paralic backshore environment. Till 12.00 m depth microfauna indicate a shallow marine to coastal environment, while till 13.00 m depth a shallow marine environment. From 13.00 m to 17.40 m is characterized as shallow marine to coastal environment. Till 21.00 m depth no or few broken species indicate a terrestrial/paralic environment. The environment till 30.00 m depth is characterized as shallow marine partially coastal. Till 34.00 m is characterized as fluvial/terrestrial environment, while till 37.00 m paralic environment. Till 38.00 m depth the environment is characterized as lagoonal while till 38.50 m as terrestrial. Till the end of the borehole the environment is described as shallow marine.

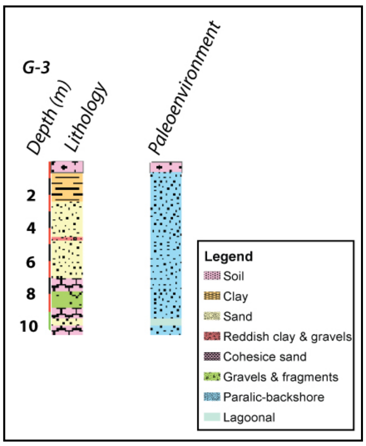


*Fig. 4 Lithological and paleoenvironmental alterations within borehole G-3 located close to the Examilia village (Fig. 1).*

Within borehole G-5 no foraminifera was found. The first 9.00 m are characterized as soil, terrestrial and fluvial-torrential environment. Beneath them till 10.00 m depth greenish mudstone indicate a lacustrine paleoenvironment. No foraminifera were found in G-8 borehole as well. The entire core is characterized as terrestrial, fluvial environment and landsliding material. Paleosoil horizons have been identified at 3.60 m till 5.00 m and from 19.00 m till 20.00 m depth.

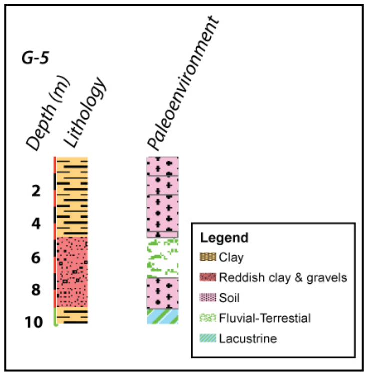


*Fig. 5 Lithological and paleoenvironmental alterations within borehole G-5 located at the immediate footwall of the Kechries fault (Fig. 1).*

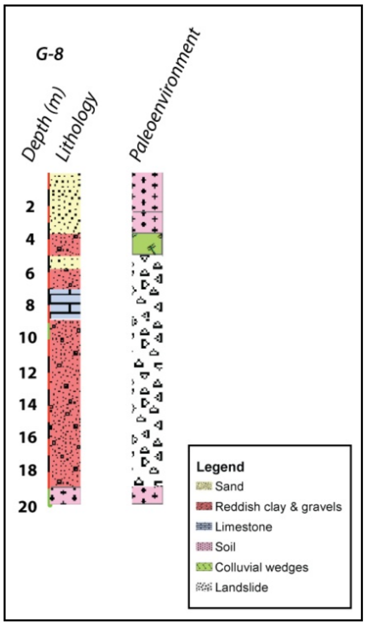


*Fig. 6 Lithological and paleoenvironmental alterations within borehole G-8 located at the immediate hangingwall of Agios Vasilios fault (Fig. 1).*

## DISCUSSION

Sedimentological procedures have been affected by active tectonics in the area of Corinth. Boreholes GA-4, Bh-1, G-1 and G-2 are located at the immediate hangingwall of the Kalamaki fault (Papanikolaou et al., 2011). If we correlate marine sediments with glacioeustatic sea level highstands and terrestrial sediments with glacioeustatic lowstands, we can suggest that within boreholes GA-4 and Bh-1 we have alterations of highstand and lowstand deposits. Within GA-4 three transgression cycles can be identified, while in Bh-1 two. Correlating the known uplift rate of the area (0.2 to 0.3 mm/yr according to Collier et al.,(1992), Turner et al.,(2010)) with global sea level change from Siddall et al., (2003), we can imply that the age of the sediments at the end of boreholes Bh-1 and G-2 are probably at 175 ka, while the age at the very bottom of core GA-2 ranges approximately between 200 ka and 225 ka. Sea transgression influence the area to a greater extend, since the fault subsides the region where the boreholes were drilled. While in boreholes Bh-1, GA-4, and G-2 marine paleoenvironment was encountered, in G-1 the environment was characterized as fluvial-terrestrial. The latter indicates that there should be a paleochannel at the site.

According to Armijo et al., (1996), the area where G-3 was drilled, is located at the Old Corinth marine terrace and estimated its age at approximately 230 ka (MIS 7). Microfauna found in the borehole indicate a paralic or shore face paleoenvironment. Therefore, we suggest that the age of the sediments might be approximately from the MIS 7. Borehole G-8 is located at the immediate hangingwall of the Agios Vasilios fault. Alterations of clay and well sorted gravels at 3.60 m to 5.00 m depth could be considered as slided material that could relate to past earthquakes. From 5.00 m to 19.00 m depth reddish clay with boulders of limestone between paleosoils at 5.00 m and 19.00 m, could represent one or more landslides that might be triggered by earthquakes. If we correlate the age of these paleosoils with previous events from Agios Vasilios fault an earthquake recurrence might be extracted.

Borehole G-5 is located at the immediate footwall of the Kechries and Acrocorinthos faults. Most of the borehole was characterized as fluvial strongly affected by a river located few meters away from the borehole. Lacustrine layers though at the end of the core, indicate the presence of an ephemeral lake. The latter could be due to the uplift caused by the Kechries and the Acrocorinthos faults.

Following the above there are interesting data extracted from each borehole. Further analysis and data constrains may lead to important outcomes regarding the interrelatioship between the paleoenvironment and the tectonic processes as well as the seismic hazard assessment.

## References


Anagnostopoulos, A.,G., Kalteziotis, N., Tsiambaos, C.,K. (1991). Geotechnical properties of the Corinth Canal marls, *Geotechnical and Geological Engineering* 9, 1-26.

Armijo, R., Meyer, B., King, G.C.P., Rigo. A., Papanastassiou, D., (1996). Quaternary evolution of the Corinth Rift and its implications for the Late Cenozoic evolution of the Aegean, *Geophys. J. Int.*, 126, 11 –53,

Bornovas, J., Lalechos, N. and Filipakis, N. (1972). 1:50.000 scale geological map, Sheet "Korinthos". Institute of Geology and Mineral Exploration

Collier, R. E. L., and C. J. Dart (1991). Neogene to Quaternary rifting, sedimentation and uplift in the Corinth Basin, Greece, *J. Geol. Soc.*, 148, 1049–1065.

Collier, R. E. L., and J. Thompson (1991). Transverse and linear dunes in an upper Pleistocene marine sequence, Corinth Basin, Greece, *Sedimentology* 38, 1021– 1040.

Collier, R.E.L., Leeder, R.M., Rowe, P. and Atkinson, T. (1992). Rates of tectonic uplift in the Corinth and Megara basins, Central Greece, *Tectonics* 1159-1167.

Dia, A. N., A. S. Cohen, R. K. O'Nions, and J. A. Jackson (1997). Rates of uplift investigated through 230Th dating in the Gulf of Corinth (Greece), *Chem. Geol*. 138, 171–184.

Freyberg, V. (1973). *Geologie des Isthmus von Korinth*, Erlangen Geologische Ablhandlungen, Heft 95, Junge und Sohn, Universitats Buchdruckerei Erlangen, 183pp.

Gaitanakis, P., Mettos, A., and Fytikas, M. (1985). 1:50.000 scale geological map, Sheet "Sofikon". Institute of Geology and Mineral Exploration.

Goiran, J.P., Pavlopoulos, K., Fouache, E., Triantaphyllou, M.V., Etienne, R., 2011. Piraeus, the ancient island of Athens: Evidence from Holocene sediments and historical archives. *Geology*.

Jackson, J.A., J. Gagnepain, G. Houseman, G.C.P. King, P.Papadimitriou, C. Soufleris, and J. Virieux (1982). Seismicity, normal faulting, and the geomorphological development of the Gulf of Corinth (Greece): The Corinth earthquakes of February and March 1981, *Earth Planetary Science Letters, 57*, 377-397.

Krstic, N., Dermitzakis, M.D., (1981). Pleistocene Fauna from a section in the channel of Corinth (Greece). *Ann. Geol. du Pays Hellen.* 30 (2): 473-499.

Leeder, M.R., Collier, R.E., Abdul Aziz, L.H., Trout, M., Ferentinos, G, Papatheodorou, G., Lyberis, E. (2002). Tectono-sedimentary processes along an active marine/lacustrine margin: alkyonides Gulf, E. Gulf of Corinth, Greece. *Basin Research* 14, 25–41.

Leeder, M. R., L. C. McNeill, R. E. L. Collier, C. Portman, P. J. Rowe, J. E. Andrews, and R. L. Gawthorpe, (2003). Corinth rift margin uplift: New evidence from Late Quaternary marine shorelines. *Geophysical Research Letters* 30, 1611.

Leeder, M.R., Mack, G.H., Brasier, A.T., Parrish, R.R., McIntosh, W.C., Andrews, J.E. & Duermeijer, C.E. (2008). Late-Pliocene timing of Corinth (Greece) rift margin fault migration. *Earth and Planetary Science Letters* 274, 132–141.

Papanikolaou, D., Chronis, G., Lykousis, V., Pavlakis, P., Roussakis, G., and Syskakis, D. (1989). 1:100.000 scale, Offshore Neotectonic Map the Saronic Gulf. Earthquake Planning and Protection Organization, National Centre for Marine Research, University of Athens.

Papanikolaou, D., Logos, E., Lozios, S. and Sideris, Ch. (1996). 1:100.000 scale Neotectonic Map of Korinthos Sheet, Earthquake Planning and Protection Organization, Athens.

Papanikolaou I.D., Triantaphyllou, M., Pallikarakis A., Migiros, G. (2011). Active faulting towards the eastern tip of the Corinth Canal: Studied through surface observations, borehole data and paleonenvironmental interpretations. Earthquake Geology and Archaeology: Science, Society and Critical facilities. 2nd INQUAIGCP 567 International Workshop, Corinth (Greece), 182-185.

Roberts, G. P., S. L. Houghton, C. Underwood, I. Papanikolaou, P. A. Cowie, P. van Calsteren, T. Wigley, F. J. Cooper, and J. M. McArthur (2009). Localization of Quaternary slip rates in an active rift in 105 years: An example from central Greece constrained by 234U-230Th coral dates from uplifted paleoshorelines, *Journal of Geophysical Research*, 114, B10406.

Triantaphyllou, M.V., Pavlopoulos, K., Tsourou, Th. & Dermitzakis M.D., 2003. Brackish marsh benthic microfauna and paleoenvironmental changes during the last 6.000 years on the coastal plain of Marathon (SE Greece). *Rivista Italiana Paleontologia et Stratigafia* 109 (3), 539-547.

Turner, J. A., Leeder, M. R., Andrews, J. E., Rowe, P. J., Van Calsteren, P., Thomas, L. (2010). Testing rival tectonic uplift models for the Lechaion Gulf in the Gulf of Corinth. *Journal of the Geological Society of London*, 167, 1237- 1250.

Siddall, M., E. J. Rohling, A. Almogi-Labin, C. Hemleben, D. Meischner, Schmelzer, and D. A. Smeed (2003), Sea-level fluctuations during the last glacial cycle. *Nature* 423, 853 – 858.

# Devising BDFA: a new active fault database conceived behind nuclear safety assessment in France

*Luigi Palumbo (1,2), Stéphane Baize (2), Marc Cushing (2), Hervé Jomard (2), Claire David (1,2)*

1) Institute for Radiological protection and Nuclear Safety, BP 17 - 92262 Fontenay-aux-Roses, FRANCE. Email: l.palumbo@neodyme.fr
(2) Pôle Géoscience, Agence R&D NEODYME, 6 rue de la Douzillère, 37300 Joué les Tours, France.

***Abstract:*** *The French Institute of Radioprotection and Nuclear Safety (IRSN) is implementing the BDFA, a new database whose task is to define and characterize active faults known in France. This database would be a first step towards the release of seismic source models and therefore serves to deterministic and probabilistic hazard analysis. Here we present the BDFA framework and a first thematic map of the Eastern France where is located the nuclear facility of Fessenheim. In this region, the data arising from literature 1) question nuclear facilities guidelines, and 2) directly emphasize the need to promote supplementary geological investigations to improve seismic hazard analysis.*

***Key words****: Fault Database, Nuclear facilities, France*

## INTRODUCTION

The practice acquired in nuclear regulation over the last decade as well as the feedback arisen from recent earthquakes consequences on Nuclear Power Plant (e.g., Kashiwazaki-Kariwa in 2007, Fukushima and North Anna in 2011), have challenged the research axes of the IRSN (French Radioprotection and Nuclear Safety Institute). Hence, the geological aspects of Seismic Hazard Analysis (SHA) have been formalized by 3 research axes : (1) updating national seismotectonic zones pattern (Baize et al., 2013); (2) performing and publishing collaborative studies on specific active faults (cf. Baize et al., 2002 ; Cushing et al. 2008); and (3) implementing the BDFA, a database concerning the potentially active fault of the European France (BDFA from the French terms of *Base de Données des Failles Actives* which means Active Faults DataBase).

These issues directly follow key aspects reported in the General Recommendations for SHA in Site Evaluation (cf. International Atomic Energy Agency, 2010); namely, the IAEA points out seismic motion and surface faulting around nuclear sites.

The above mentioned third axis started in 2009 and consists in the on-going BDFA project; it represents a first step to support SHA calculation through a collection of seismic sources information. BDFA is funded by the IRSN and the French Ministry for environment.

This paper introduces the BDFA framework and the active fault map outlook of the Eastern France. Currently, the project is dealing with faults located in 50-km-radius centred on French nuclear facilities (Fig. 1); this ratio balances the need to cover entirely the country with the willing to detail well fault segments around the NPPs. Yet this is a minimal distance and in a future BDFA could enlarge the area of investigation by including fault segments located in additional critical facilities and inhabited areas too.

## THE BDFA PRINCIPLES

Located in intraplate region, France is far away from the main tectonic active plate boundaries; it is mainly characterised by low to moderate seismotectonic activity. Yet researches prove that significant earthquakes (cf. historical catalogue, SISFRANCE) struck these regions, sometimes coupled with surface faulting (e.g. Sébrier et al., 1995).

BDFA may rely on some previous works which deal with similar issues, namely ; 1) the seismotectonic map released by Grellet et al. (1993), 2) the IRSN catalogue of faulting evidences affecting the Quaternary deposits (Baize et al., 2002), and, 3) the catalogue of neotectonic clues (www.neopal.net). The work of Grellet et al. (1993) was then the first attempt in synthetize neotectonic and active faults over France; hence it is the main cartographic reference of BDFA (cf. figure 1).

Crucial aspect of the database is discriminating whether a fault is active or not; this task represents an important challenge because proofs of activity could be not so predictable, moreover over a tectonics intraplate region. Geologically, fault activity is based on the age of the last associated deformation observed: the younger deformation, the higher probability of fault activity is. Hence, discerning which segment is active or not means establish a temporal threshold: active faults will be arbitrary bounded up with recognised deformation being younger than this limit. This point out how promoting paleoseismology needs attention because these investigations lead and scale up both quality and amount of the above-mentioned boundaries.

For intraplate region, International nuclear safety guidelines (cf. IAEA, 2010) fix as appropriate the limit of the Plio-Quaternary (5 Ma). It is significantly different than the one proposed by the US Nuclear Regulatory Commission (NRC) which lowers the limit to 0.5 Ma.

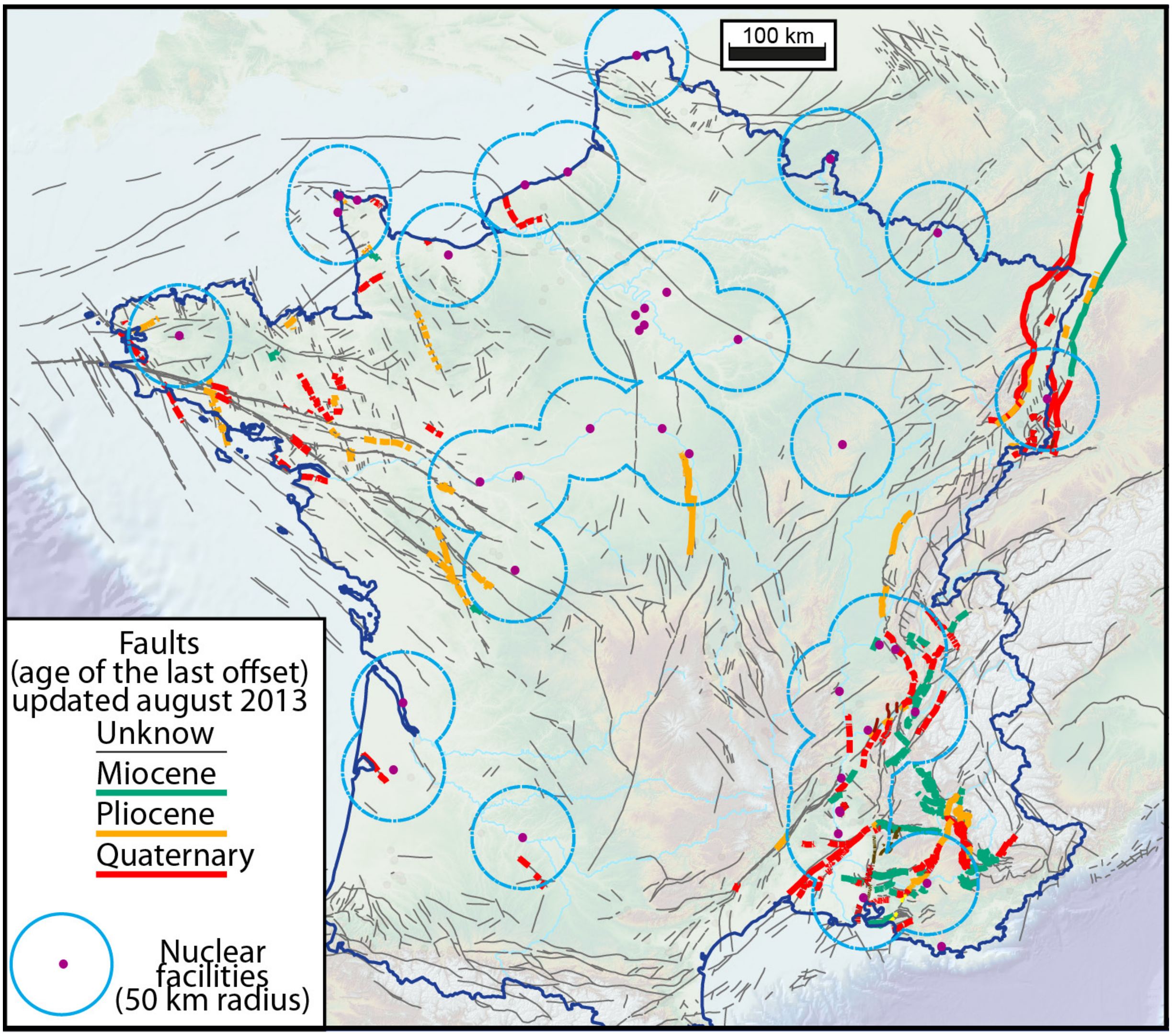


*Fig. 1: BDFA map (modified from neotectonic map from Grellet et al., 1993). The circles (50 km radius) centre nuclear facilities in France.*

The IAEA paradigm appears undoubtedly more appropriate for the French scenario because, widely, faulting reactivation of past structures is possible. Indeed tectonic stress field has not experienced changes since the end of Miocene and segment orientation is still optimally oriented to accommodate slip faulting. Complementary, Plio-Quaternary deposits are generally accessible. The above items underpin the working principles and the implement of BDFA, respectively.

Guidelines stated/adopted in other tectonic contexts are ill-suitable for France context, instead: Galadini et al. (2012) for Italy, state as inactive a fault sealed with sediments 20 ka old. However, this limit appears unsuitable because of tectonics intraplate seismic cycles; plus, nuclear safety guidelines refer to a longer timescale. In other words, both seismotectonic context and regulations reject such recommendation.

Another key factor in the BDFA is the geometry of the surficial fault trace; they are established by the analysis of a broad literature including geological and thematic maps at different scales (1/250,000 and locally at 1/50000), Digital Elevation Models, aerial photographs and specific publications. Because fault traces could be subtle to individuate, BDFA consider four degrees of uncertainty (reliable, uncertain, hidden, and suspect).

GIS structure underpins BDFA. The cartography part is paired with tables; therefore segments are coupled with several data whose original sources can be traced. Each fault system is also paired with a specific file describing the implemented parameters and the geomorphic/tectonic/seismic scenario. In these files, eventual ambiguities are discussed. Finally each file is recalled in a larger regional introduction which first contextualises the region and then reviews somewhat the needs to optimise the knowledge of the region.

All of these documents follow a strict review: they are first commented internally in the IRSN then the file is reviewed by a specialist external to IRSN.

The BDFA is arranged in tables structured in a relational model database; each fault segment is uniquely associated with an ID (it serves as key of the relation in database).

The main table encompasses several items concerning geometry, age, and kinematics. Relationships between fault segment and both historical and instrumental earthquakes are possible to establish through table's links. Coordinates of neotectonic indications (cf. NEOPAL database) and earthquakes parameters (cf. SISFRANCE and Baumont and Scotti, 2010) are also georeferenced.

A complementary table belongs to BDFA. This summarizes several values and attempts to quantify the fault activity degree of each segment fault. This aim is accomplished through the following empirical expression (cf. Baize et al., 2013);

$$\mathbf{AI = (S + 0.1) \cdot (S + Age + M + 3H + 4I + 2G)}$$

AI (Activity Index) can be esteemed for each defined segment, with:

- S: estimation of structural knowledge. It may be valued 0 or 1, according to well-known or unknown tectonic structures, respectively.
- M: morphological expression of the faulting. It may be valued 0 or 1, according to negligible or prominent surficial expression, respectively.
- Age: time of last recognized displacement. It may be valued 1, 2, or 3 for Paleogene, Neogene, and Quaternary, respectively.
- H: historical seismicity parameters. It may be valued 0 or 1, if such earthquake epicentre is located outside or inside an area widening 5 km of the fault trace, respectively.
- I: instrumental seismicity parameters. It may be valued 0 or 1, if such earthquake epicentre is located outside or inside an area widening 5 km of the fault trace, respectively.
- G: geodetical data indicating displacement along the fault. It may be valued 0 or 1, according to lack or recognised movement, respectively.

The AI could aim to compare faulting activity among segments of the same region, i.e. segment experiencing both similar tectonic stress conditions and seismic cycles. A comparison of segments among different regions is limited by instrumental and unsystematic causes: for instance, the AI could be sensitive to seismic network density as well as it could suffer local distribution of investigations and result. So far, AI > 5 seems always be associated to active faults; yet AI low values cannot be likelihood exclude faulting activity.

Seismic hazard information are not directly filled in BDFA, yet this database would serve as a provider of data for physical and mathematic models of hazard computations.

**AN EXAMPLE FOR THE EASTERN FRANCE**

In 1356 an earthquake struck and destroyed Basel in Swiss. This city is located over the Rhine Graben tectonic structure. Past investigations have supported that faulting occurred along W-trending buried faults (e.g. Meyer et al., 1994) or with a N-trending basement segment linkage This background led the identification of the *Basel Zone* (Baize et al., 2013), that is a seismotectonic area which does not include the entire Rhine Graben structure. Accordingly to other seismotectonic maps of France (e.g. Terrier et al., 2000) the NPP of Fessenheim is not located over this seismotectonic area. In other words, the *Basel Zone* considers that the epicentre of an earthquake as such of 1356 could be not located closer than ≈ 40 km from the NPP of Fessehneim.

In a recent assessment evaluation (cf. RESONANCE, 2007) this limit has been discussed. Indeed, W-trending basement segments have been located ≈ 15 km south of the NPP (Ustaszewski et al., 2005); hence the Basel zone boundary could change, and could be located closer to the NPP of Fessehneim. In addition, the hypothesis that the Basel earthquake could be associated to N-trending (so called *rhenish*) structures is also supported by Meghraoui et al. (2001) and Nivière et al. (2008). Namely, Nivière et al. indicate north-trends active faults located even 7 km far from the NPP (cf. the Rhine River Fault, in fig.2). These segments could be associated to M = 6.6-6.8 earthquakes, that is the same magnitude esteemed for the Basel earthquake (Baumont and Scotti, 2010).

After the nuclear disaster of Fukushima, worldwide Nuclear Power Plants authorities reconsidered earthquake hazard level safety. The ongoing post-Fukushima discussions have led a part of the seismic hazard community to envisage "extreme" events, albeit improbable, as scenarios against which Nuclear Power Plants need to be prepared. One possible way to foresee these "extreme" events may be evaluating the maximum size of the earthquake sources (i.e. the active faults). In that sense, the presented database may also be useful. We also point out that according international guides, the capable fault issue should be explored for some NPP sites such as Fessenheim as presented here before. The capable fault issue examination however requires a detailed and local dataset that this database does not fulfil, because this is a data compilation of mainly regional scales and of poor resolution, gathered in the literature. But it will allow prioritising the zones to investigate further.

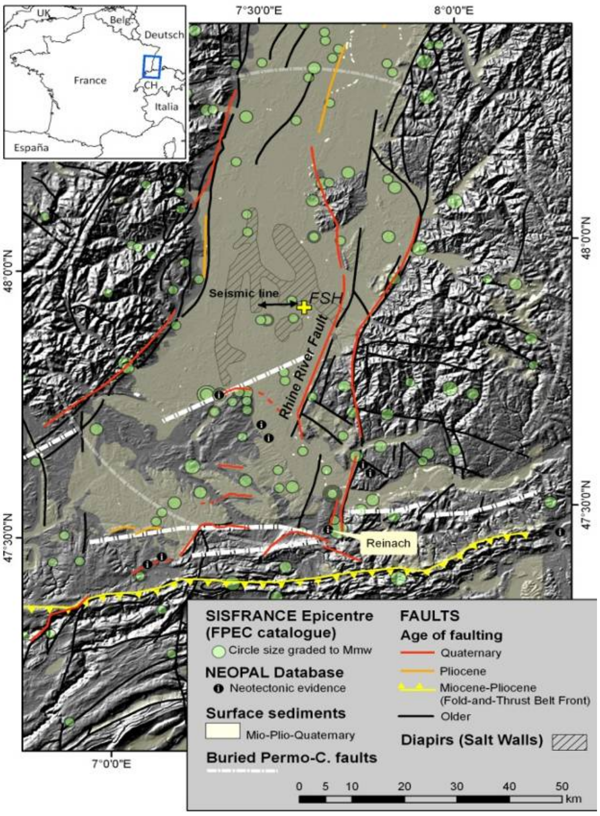


*Fig. 2: Potential active faults located in the Fessenheim region. BDFA, nearby the NPP (yellow cross), with the maximal age of faulting indicated by colour (red: Quaternary; orange: Pliocene; yellow: Miocene (or Pliocene?). Location of seismic section is the black double-arrow. FPEC is the French historical catalogue available in Baumont and Scotti (2010); Buried Permo-Carboniferous faults are from Ustaszewski et al. (2005); diapirs contours from Wannesson (1998).*

## CONCLUSION

The IRSN has a key role in the seismic hazard of French NPP; BDFA doesn't include seismic hazard information, yet it attempts to have a vital role in this issue: physical and mathematic models which serve to hazard computations could in future rely on BDFA's data. As an example, fault-based seismotectonic models for future Probabilistic Seismic Hazard Assessment (PSHA) can obtain parameters from BDFA (i.e., geometry, segmentation, slip rate, and magnitude). Namely the BDFA can be appropriate to model the above mentioned extreme events. BDFA framework is arranged to give back information over few levels of competences, so that different users can glean or examine in depth information stored according to their needs, however. First released in internet will be probably achieved in 2014.

**Acknowledgements:** This work is founded by the French Ministry of environment and IRSN. Nils-Alex. Mörner provided helpful comments.

## References

Baize S., E.M. Cushing, F. Lemeille, T. Granier, B. Grellet, D. Carbon, P. Combes & C. Hibsch, (2002). Inventaire des indices de rupture affectant le Quaternaire en relation avec les grandes structures connues, en France métropolitaine et dans les régions limitrophes. *Mémoire H. S., 175, 1 pl. H.T* 142, (2002)

Baize, S., E. M Cushing., F. Lemeille & H. Jomard, (2013). Updated seismotectonic zoning scheme of Metropolitan France, with reference to geologic and seismotectonic data / Zonage sismotectonique actualisé de la France métropolitaine, à partir des données géologiques et sismotectoniques (10 figs; 2 app.). *Bulletin de la Société Géologique de France* 184, p. 225-259.

Baumont, D., & Scotti O., (2011). The French Parametric Earthquake Catalogue (FPEC) based on the best events of the Sisfrance macroseismic database - Version 1.1 - IRSN/DEI/2011-012 in AHEAD Working Group, 2013. *AHEAD, the European, distributed Archive of Historical Earthquake Data*, doi:10.6092/INGV.IT-AHEAD

Cushing, E. M., O. Bellier, S. Nechtschein., M. Sébrier., A. Lomax., P. Volant., P. Dervin., P. Guignard & L. Bove, (2008). A multidisciplinary study of a slow-slipping fault for seismic hazard assessment: the example of the Middle Durance fault (SE France). *Geophys. J. Int*. 172, 1163-1178.

Galadini, F., E. Falcucci, P. Galli, B. Giaccio, S. Gori, P. Messina, M. Moro, M. Saroli, G. Scardia & A. Sposato, (2012). Time intervals to assess active and capable faults for engineering practices in italy. *Engineering Geology* 139-140, 50-65.

Grellet B., P. Combes, T. Granier & H. Philip, (1993). Sismotectonique de la France métropolitaine dans son cadre géologique et géophysique. *Mém. n. s. Soc. géol. Fr.*164, 2 volumes.

IAEA (2010). Seismic hazards in site evaluation for nuclear installations : safety guide. Vienna : *International Atomic Energy Agency*. *IAEA safety standards series*. ISSN 1020–525X ; no. SSG-9.

Meghraoui M., B. Delouis, M. Ferry, D. Giardini, P. Huggenberger, I. Spottke & M. Granet, (2001). Active normal faulting in the Upper Rhine graben and paleoseismic identification of the 1356 Basel earthquake. *Science* 293, 2070-2073.

Nivière, B.,A. Bruestle, G. Bertrand, S. Carretier, J. Behrmann & J.C. Gourry, (2008). Active tectonics of the southeastern Upper Rhine Graben, Freiburg area (Germany). *Quaternary Science Reviews* 27, 541-555.

RESONANCE study (2007). Centrale Nucléaire de Fessenheim : appréciation du risque sismique. Expertise RÉSONANCE Ingénieurs-Conseils SA, 277/MK/CL, septembre 2007.

Sébrier M., A. Ghafiri & J.L. Blès, (1997). Paleoseismicity in France: Fault trench studies in a region of moderate seismicity. *J. Geodyn* 24, 207-217.

SisFrance, BRGM, EDF, IRSN (2012). http://www.sisfrance.net

Terrier M., J.L. Blès, P. Godefroy, P. Dominique, M. Bour & C. Martin, (2000). Zonation of Metropolitan France for the application of earthquake-resistant building regulations to critical facilities Part 1: Seismotectonic zonation. *J. Seismol* 4, 215-230.

Ustaszewski, K., M.E. Schumacher, & S.M. Schmid (2005). Simultaneous normal faulting and extensional flexuring during rifting: An example from the southernmost upper rhine graben. *International Journal of Earth Sciences* 94(4), 680-696.

Wannesson (1998). Alsace. Rapport régional d'évaluation pétrolière. Institut Français du Pétrole.

# Growth folding and uplift of Lower and Middle Pleistocene marine terraces in Kephalonia: implications to active tectonics

*Dimitrios Papanikolaou (1), Maria Triantaphyllou (1)*

(1) Faculty of Geology and Geoenvironment, National and Kapodistrian University of Athens, Panepistimioupolis 15784, Athens, Greece.

***Abstract:*** *Lower and Middle Pleistocene marine terraces have been determined in Kephalonia Island, Ionian Sea both in Paliki Peninsula in the west and in the southern coastal zone of the Aenos mountain range. Characteristic assemblages of Gelasian, Calabrian and Middle Pleistocene age have been determined and at least two marine terraces with calcarenites have been distinguished; the older terrace dated about 0.9 Ma in Paliki but 1.6 Ma in the Airport and the younger terrace about 0.4 Ma in both areas. A remarkable difference in the orientation of the marine terraces is observed with N-S direction in Paliki Peninsula and WNW-ESE direction in southern Kephalonia. Ample folding is observed affecting even the topmost Middle Pleistocene beds with dips of 15-20º above intensively folded Miocene – Early Pliocene strata. Maximum uplift indicated by the marine terraces is located along the eastern coast of Paliki and the southern coast of central-east Kephalonia in accordance with results from DGPS and PSInSAR geodetic data.*

***Key words****: Pleistocene stratigraphy, active compression, Hellenic arc, Ionian Islands, tectono-eustatism*

## INTRODUCTION

Kephalonia Island is located on the tectonic front of the Hellenic thrust and fold belt developed only a few decades of km east of the Hellenic Trench in the Ionian Sea, representing the active plate boundary between the European and African plates, which has a complex history of oceanic and continental subduction (e.g. Royden and Papanikolaou, 2011). The geological structure of the upper crust includes the relative autochthon unit of Paxos, occurring on Paliki peninsula in the west and on the major part of the central Kephalonia, and the allochthon tectonic nappe of the Ionian unit, occurring along the eastern part (Fig. 1). The stratigraphy of Paxos unit comprises a thick shallow water carbonate platform with ages from Early Cretaceous to Early Miocene (K-Mi), followed by Middle Miocene clastic sequences of flysch type (Mm). The Ionian nappe on Kephalonia is composed of the Late Triassic to Eocene carbonates (Tr-E) without the flysch at the top of the sequence as known from mainland Greece. Overthrusting of the Ionian nappe took place during Middle – Late Miocene but compressional deformation continued also in the Late Miocene – Early Pliocene (Ms-Pli) (Mercier et al, 1972; Underhill, 1989; van Hinsbergen et al, 2006). Late Pliocene to Pleistocene marine sediments (Pl-Pt) have been reported on Kephalonia (Triantaphyllou, 1996, 2001; Triantaphyllou et al., 1999, 2010; Agiadi et al., 2011) without an established stratigraphic succession and correlation to tectono-eustatic movements.

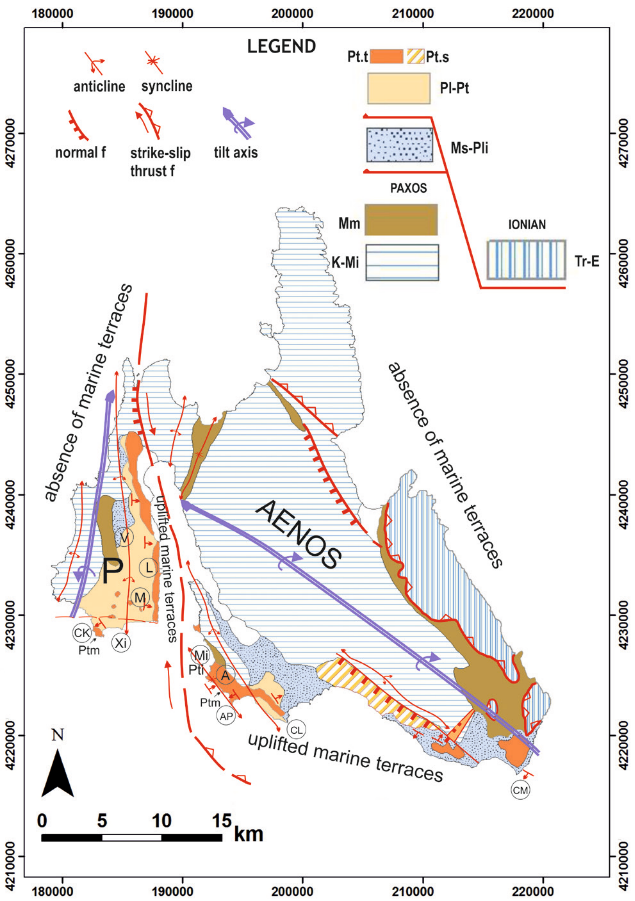


*Fig. 1. Simplified geological map of Kephalonia (modified after BP and IGME maps). Explanation for the stratigraphic symbols is given in the text. P: Paliki, CK: Cape Kounopetra, Xi: Cape Xi, L: Lixourion, V: Vlichata, M: Mantzavinata, Mi: Minies, A: Airport, AP: Ag. Pelaghia, CL: Cape Liakas, CM: Cape Mounta.*


*Fig. 2. Panoramic view of the marine Pleistocene in south Paliki peninsula, Kephalonia seen from Vlıchata village. The planar surfaces at the top of the hills correspond to the hard sandstones of the marine terraces overlying the soft Pleistocene marls. Marine terrace No 1 corresponds to Megas Lakkos whereas No 2 corresponds to the hill 101m near Manzavinata village.*

**NEW DATA ON THE MARINE PLEISTOCENE TERRACES OF KEPHALONIA**

Our investigations have concluded to a preliminary stratigraphic framework of the Quaternary formations of Kephalonia, deposited unconformably on top of the underlying Mesozoic to Late Tertiary formations. Biostratigraphy is based on calcareous nannofossil analyses and biozonal scheme and subsequent ages are according to Rio et al. (1990) and Raffi et al. (2006). The older sediments, comprising marls, have been dated at the base of Gelasian at about 2.5 Ma. Successive beds of marls have been dated to range from Gelasian to Calabrian as well as to Middle Pleistocene up to the zone MNN19f (0.61-0.47 Ma), (Pl-Pt).

*Fig. 3. The younger marine terrace of Paliki peninsula above Middle Pleistocene marls, in Kounopetra cape at the western edge of Akrotiri bay.*

Apart from marls there are some distinctive sandstone beds (Pt.t), which represent marine terraces with impressive planar landforms in the landscape corresponding to at least two discrete levels (Figs. 2-4). The relics of the older terrace can be observed in several hills at the southern parts of Paliki Peninsula in Western Kephalonia (Fig. 2). The younger terrace can be observed in the area of Cape Kounopetra (Fig. 3) and along the coastal range of Lixouri (see map on Fig. 1) where the underlying marls have been dated as Middle Pleistocene; abundant *P. lacunosa* and common *Gephyrocapsa* sp.3 support the documentation of biozone MNN19f (0.97-0.61 Ma). On the contrary, the older terrace observed in a more inland position has yielded Calabrian age for the underlying marls (Fig. 4); In particular, Triantaphyllou (1996), Triantaphyllou et al. (1999) determined the first presence of normal-sized gephyrocapsids >4μm, implicating the boundary of biozone MNN19-MNN19b, which correlates to the Gelasian-Calabrian boundary. This has also been confirmed in other localities during the present study, namely 2 km eastwards in the bifurcation towards Soulari village. The older beds of the Pleistocene sequence have been determined in the area of the village Vlichata where the base of the Gelasian was documented, based on abundant presence of *P. lacunosa*, *Calcidiscus macintyrei* and rare specimens of *Discoaster brouweri* (MNN18 biozone).

*Fig. 4. Close view of the older marine terrace of Paliki peninsula above Lower Pleistocene (Calabrian) marls forming the hill 101m south of Manzavinata village.*


*Fig. 5. Panoramic view of the Lower (1) and Middle Pleistocene (2) marine terraces of south Paliki peninsula (from Cape Xi to hill 101 m, near Manzavinata), as seen from the area of Megas Lakkos (61 m elevation) at the east.*

The relative position of the two terraces can be observed in the panoramic view of the area between Cape Xi and Manzavinata village (Fig. 5), where the younger terrace occurs at elevations 20-40 m and the older at elevations 60-80 m.

A similar occurrence of two marine terraces can be seen in the area along the southern coast of Central Kephalonia from the airport in the west to the Mounta cape in the east. In specific, the base of the older terrace was found in the area of Minies at the western edge of the airport and has been determined as Calabrian (MNN19c; 1.66-162 Ma), based on the evaluation of calcareous nannofossil assemblages (abundant *P. lacunosa* and *Gephyrocapsa* spp. 3-3.5μm, rare *Helicosphaera sellii* and *Gephyrocapsa* >4μm, absence of *C. macintyrei*). The marls right below the sandstones of the younger terrace found in the area of Aghia Pelagia are dated as Middle Pleistocene age (MNN19f; 0.97-0.61 Ma), similar to the younger terrace of Paliki. In particular, calcareous nannofossil analysis implicates the level of temporary disappearance of *Gephyrocapsa* sp.3 at 0.79 Ma (e.g., Papanikolaou et al., 2011), based on the common presence of small *Gephyrocapsa* spp. and *P. lacunosa*, whereas *Gephyrocapsa* sp.3 displays values <1%.

The Middle Pleistocene has also been determined at the southern edge of the airport (upper part of MNN19f; 0.61-0.47 Ma, above the extinction of *Gephyrocapsa* sp.3), as suggested by very abundant *Pseudoemiliania lacunosa* and total absence of *Gephyrocapsa* sp.3 specimens.

## TECTONIC OBSERVATIONS

Although the first impressionof the outcrops implies a planar horizontal attitude of the marine terraces with a simple vertical effect of tectono-eustatic nature the detailed observation of the dip of the strata reveals significant dips of 10-20° on opposite directions, which would imply either the existence of normal faults (which would tilt the strata) or bending and folding. Thus, the dips of the Pleistocene strata in the airport area at southern Kephalonia have shown the existence of an anticline and a syncline developed at the NW-SE direction subparallel to the coast (Fig.1). Characteristic outcrops occur with dips towards the north and the south along the coastal zone (Fig. 6 and Fig. 7). Especially the outcrop in the port of Aghia Pelagia shows the Middle Pleistocene beds dipping inlands with 15° to the north towards the Aenos mountain range. The anticlinal axis observed on the Pleistocene formations coincides with the underlying anticlinal axis of a close fold observed within the early Tertiary formations of Paxos unit involving also the Late Miocene – Early Pliocene formations of cape Liakas (Underhill, 1989; van Hinsbergen et al., 2006). The analysis of our sampling from the marls along the coast to the west of Avythos has yielded an Aquitanian age (MNN2, at 22.76-22.03 Ma; very abundant nannofossil assemblages with *Discoaster drugii*, *Discoaster deflandrei* and *Helicosphaera carteri*).

*Fig. 6. The Middle Pleistocene beds dipping inlands to the North, in the Aghia Pelagia area*

*Fig. 7. The Middle Pleistocene beds dipping seawards to the South, in the area west of Avythos and Aghios Antonios.*

Thus, the NW-SE anticline represents a growth folding developed at least during the time span of early Pliocene to the end of Middle Pleistocene. The same ample folding can be observed in the southern coastal area of Paliki Peninsula in the west, where the Pleistocene beds form a N-S direction anticline (Fig. 8). The direction of folding and the general co-parallel axis of uplift point out two very different tectonic directions: N-S at Paliki Peninsula in the west and NW-SE in southern central-east Kephalonia.

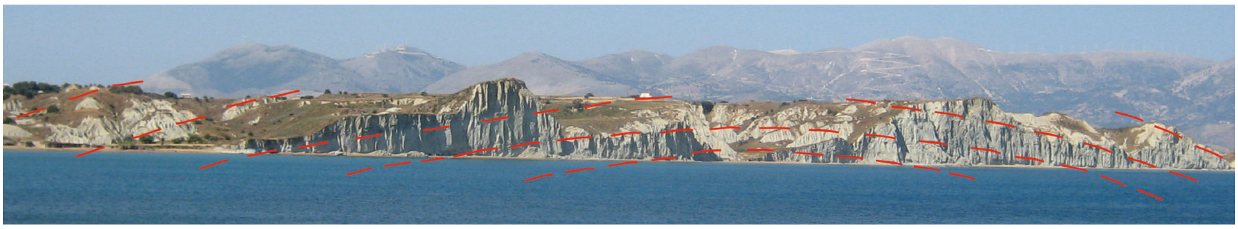

*Fig. 8. The anticlinical form observed along the Akrotiri bay at the southern coast of Paliki peninsula west of Cape Xi, within the Lower Pleistocene marine beds.*

## DISCUSSION AND CONCLUSIONS

The determination of Pleistocene marine terraces in Kephalonia has some regional implications especially in relation to Zakynthos island, where a similar geological history has been described for the «post-orogenic formations» where two unconformities/disconformities occur within the Pleistocene sequence in the form of marine terraces (Papanikolaou et al., 2010, 2011).

The younger terrace of Zakynthos (formation Q3, e.g., in Cape Aghios Nikolaos or in Cape Gaidaros) is equivalent to the younger terrace of Kephalonia observed both in Paliki (Kounopetra) and Southern Central-east Kephalonia (Aghia Pelagia) with an approximate age 0.4 Ma. On the contrary, the lower unconformity/terrace of Zakynthos (formation Q2a, e.g. in Cape Gerakas or village Gerakari) is equivalent to the older terrace of Paliki (e.g., Soulari) with an age of about 0.9 Ma, but not to the terrace in the airport of southern central-east Kephalonia (Minies coast) where the older unconformity is 1.66-1.62 Ma. This difference in the age of the marine terraces is more likely to be related to the different tectonic trend observed in Paliki and in southern central-east Kephalonia. Uplift rates cannot be estimated except for a minimum uplift of 150 m of the Middle Pleistocene terrace. The tectonic division between the two blocks of Kephalonia is probably a complex dextral strike-slip structure (Fig. 1) which has accommodated the important rotations observed in the area (e.g. van Hinsbergen et al., 2006). The axes of maximum uplift indicated by the marine terraces in Kephalonia located in the N-S direction in Paliki and in WNW-ESE in central-east Kephalonia (Fig. 1), coincide with uplift zones recently obtained from DGPS and PSInSAR geodetic data (Lagios et al., 2012).

## References

Agiadi K., Triantaphyllou M., Girone A., Karakitsios V. (2011). The early Quaternary palaeobiogeography of the eastern Ionian deep-sea Teleost fauna: A novel palaeocirculation approach. *Palaeogeography, Palaeoclimatology, Palaeoecology* 306 (3-4), 228-242.

B.P. Co. LTD., 1971. The Geological Results of Petroleum Exploration in Western Greece. *Institute for Geology and Subsurface Research (now I.G.M.E.) Special Report* 10.

IGME, 1985. *Geological sheet of Kefallonia.*

Lagios E., Papadimitriou P., Novali F., Sakkas V., Fumagalli A., Vlachou K.. & Del Conte S. (2012). Combined Seismicity Pattern Analysis, DGPS and PSInSAR Studies in the Broader Area of Cephalonia (Greece). *Tectonophysics*, 524-525, 43-58.

Mercier JL, Bousquet B, Delibassis N, et al. (1972). Deformations en compression dans le Quaternaire de rivages ioniens (Cephalonie, Grece). Donnes neotectoniques et sismiques. *Comptes Rend. Acad. Sci.,* 175, 2307–2310.

Papanikolaou, M., Papanikolaou, D., Triantaphyllou, M.V., (2010). Significance of unconformities within the Late Pliocene-Middle Pleistocene uplifted marine sequences in Zakynthos Island. *Bull.Geol.Soc.Greece,*XLIII,475-485.

Papanikolaou M.D., Triantaphyllou M., Platzman E., Gibbard P., Macniocaill C., Head M.J. (2011). A well-established Early – Middle Pleistocene marine sequence on SE Zakynthos island, Western Greece: magneto-biostratigraphic constraints and palaeoclimatic implications. *J. Quat. Sci.* 26 (5), 523-540.

Raffi I, Backman J, Fornaciari E, et al. (2006). A review of calcareous nannofossil astrobiochronology encompassing the past 25 million years. *Quat. Sci. Rev.* 25, 3113–3137.

Rio D, Raffi I, Villa G. (1990). Pliocene–Pleistocene calcareous nannofossil distribution patterns in the Western Mediterranean. *ODP, Sci. Res.* 107, 513–533.

Royden L.H., Papanikolaou D.J. (2011). Slab segmentation and late Cenozoic disruption of the Hellenic arc. *Geochem. Geophys. Geosyst.* 12, Q03010.

Triantaphyllou, M.V., (1993). Biostratigraphical and ecostratigraphical observations based on calcareous nannofossils, of the Eastern Mediterranean Plio-Pleistocene deposits. *Gaia* 1, 1996, Univ. Athens, 229pp.

Triantaphyllou, M.V., (2001). Quantitative calcareous nannofossil biostratigraphy of Bay Akrotiri section (Cefallinia island, W.Greece). *Bull. Geol. Soc. Greece*, XXXIV/2, 645-652.

Triantaphyllou, M.V., Dimiza, M.D., Papanikolaou, M.D., (2010). Early Pliocene deposits in Kephallonia (Ionian Islands): Biostratigraphy and paleoenvironmental-paleoclimatic implications. *XIX CBGA Congress. Thessaloniki, 2010, Geologica Balcanica.*

Triantaphyllou, M.V., Drinia, H. & M.D. Dermitzakis, 1999. Biostratigraphical and paleoenvironmental determination of a marine Plio/Pleistocene outcrop in Cefallinia island. *Geologie Mediterraneenne* XXVI, 1 / 2, pp.3-18.

Underhill JR. 1989. Late Cenozoic deformation of the Hellenide foreland, western Greece. *Geol. Soc. America Bulletin* 101:613–634.

van Hinsbergen, D.J.J., D.G. van der Meer, W.J. Zachariasse, and J.E. Meulenkamp (2006). Deformation of western Greece during Neogene clockwise rotation and collision with Apulia, *Int. J. Earth Sci.*, 95, 463–490.

INQUA Focus Group on Paleoseismology and Active Tectonics

paleoseismicity.org

# Natural hazards and civil protection management framework in Greek local authorities: a questionnaire survey demonstrates why prevention fails

*Papanikolaou, Ioannis D. (1,2,3), Dimitrios Papanikolaou, (2), Michalis Diakakis (2), Georgios Deligiannakis (1,2)*

(1) Mineralogy-Geology Laboratory, Department of Earth and Atmospheric Sciences, Agricultural University of Athens, Iera Odos 75, 118-55, Athens, Greece. Email: i.pap@aua.gr
(2) Laboratory of Natural Hazards, Faculty of Geology and Geoenvironment, National and Kapodistrian University of Athens, Panepistimioupolis, 15784, Athens, Greece. Email: dpapan@geol.uoa.gr
(3) Department of Earth Sciences, Birkbeck College and University College London, WC 1E 6BT, London UK. Email: i.papanikolaou@ucl.ac.uk

***Abstract:*** *Earthquakes, floods and forest fires are the main causes of natural disasters in Greece, causing human casualties and result in remarkable economic losses on a yearly basis. Since 2002 following a new legislation regarding civil protection issues, the Greek Local Authorities have a key role on mitigation and prevention practices, whereas their responsibilities have been further increased in 2010 after the administrational Kallikratis reform. In order to evaluate the existing structure and assess the effectiveness of the existing civil protection framework in this new administrative level, we conducted the largest survey in Greece, covering 41.2% of the country municipalities. Results show that inadequate prevention actions and mitigation processes are caused by structural deficiencies, poor training and problematic conditions regarding human resources and administrative bodies. More than 50% of the people responsible for civil protection have inadequate qualifications and are poorly or not trained, while shortage in equipment and funds is incriminating the poor interagency organization. Responses showed that civil protection personnel lack adequate training and expertise, many are overstretched with several duties, while several prevention actions are carried out by seasonal or voluntary staff. Existing regulations are not followed by a significant portion of municipalities since 19.3% have not established a civil protection office and 24.1% of the municipalities have not compiled an action plan yet. Finally, the vast majority of the civil protection personnel (84.5%) are not familiar with the EU emergency number 112.*

***Key words****: Civil Protection, Local Authorities, Risk Mitigation, Questionnaire Survey, Prevention Actions.*

## INTRODUCTION

Natural disasters have resulted, during the last decades, in a significant rise in numbers, costs and affected population (Swiss Re, 2013, Munich Re, 2013, EM-DAT, 2013). According to the UN Office for Disaster Risk Reduction (UNISDR) press release on 15th May 2013, economic losses linked to disasters are "out of control" (e.g. so far this century, direct losses from disasters are in the range of $2.5 trillion) and will continue to escalate unless disaster risk management becomes a core part of business investment strategies. Europe, despite the efforts both in legal and organizational level, is no exception to this regime, as international disaster statistics show positive trends regarding the impact of natural hazards in the region (EM-DAT, 2013).

In the face of a growing number of natural disasters and the increasing costs associated with them, Greece has devoted significant efforts and resources in natural hazards mitigation during the last decades. Despite the significant legislative efforts (e.g. 2001/792/EC, 2007/60/EC Directives, 3013/2002 Act) and even though a number of steps have been taken towards improving civil protection, recent catastrophic events have illustrated the weaknesses of current approaches.

In particular, events such as the 1999 Athens earthquake, as well as the 2007 and 2009 wildfires, have shown the inadequacy of prevention and mitigation practices. Given the enhanced civil protection responsibilities, assigned by the Greek national law (Acts 3013/2002, 3852/2010) to local authorities in Greece, this work analyses and evaluates the existing structure and current management framework under which local authorities function and examines their risk mitigation practices.

## METHODOLOGY

We conducted the largest questionnaire survey regarding civil protections issues, among the Greek municipalities. To this aim, we used an innovative online tool to assess current framework. Therefore, a network connecting civil protection departments of municipalities was developed, based on an Internet platform that acted also as a communication tool. After the 2010 Kallikratis administrational reform, the new structure cancelled the pre-existing 76 prefectures and replaced them with 13 larger regions of administration (the Peripheries) and downsized the 910 municipalities and 124 communities to 325 larger and stronger municipalities. This major reform has a significant impact on the natural hazard prevention policies and management framework, since a large part of the prefecture responsibilities, including civil protection, were transferred to the new fewer, but stronger municipalities. Therefore, we had at this time the opportunity to evaluate the new structure. Overall, we had feedback either online or offline from 134 municipalities across the country (out of 325) representing 41.2% of the municipalities of Greece and 41.5% of the population (Fig.1).

Through this network, municipal civil protection officials completed surveys designed to obtain and quantify information on several aspects of civil protection practices and infrastructure. In particular, the examined factors included: (i) personnel and equipment, (ii) inter-agency cooperation, (iii) training, (iv) compliance with existing regulations and (v) persistent problems encountered by civil protection departments that prevent the effectiveness of current practices.

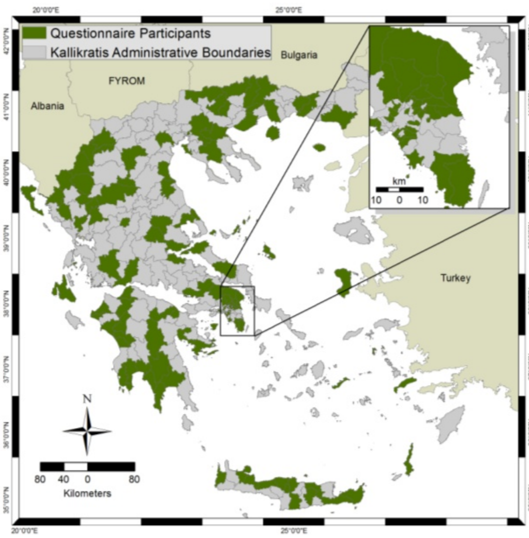


*Fig. 1: Municipalities that participated in the survey.*

## RESULTS

Responses showed that civil protection personnel lack adequate training and expertise (Tables 1 & 2). Many are overstretched with several duties (Fig. 2a), while still 12.1% of them do not use a PC in the civil protection office (Fig. 2b). Approximately half of the heads of civil protection offices do not hold a university degree (Table 1), only 27% have a relevant scientific background (13% geoscientists or 14.3% engineers) (Fig. 2c) and more than half of them are elected members and not permanent staff (Fig. 2d), implying that no continuity is secured.

*Table 1: Qualification of the person in charge of the civil protection department.*

| | |
|---|---|
| Secondary Education | 50.6% |
| University degree | 25.9% |
| Technical Educational Institute's degree | 15.3% |
| Postgraduate (Masters or PhD) | 8.2% |

*Table 2: Training of personnel regarding natural disasters and in relation with their duties.*

| | |
|---|---|
| No training | 36.6% |
| Self-trained | 18.7% |
| Trained from central Civil Protection authorities | 18% |
| Trained from the Fire Service | 17.3% |
| Trained from KEDKE (Central Union of Municipalities & Communities of Greece) special seminars | 9.3% |

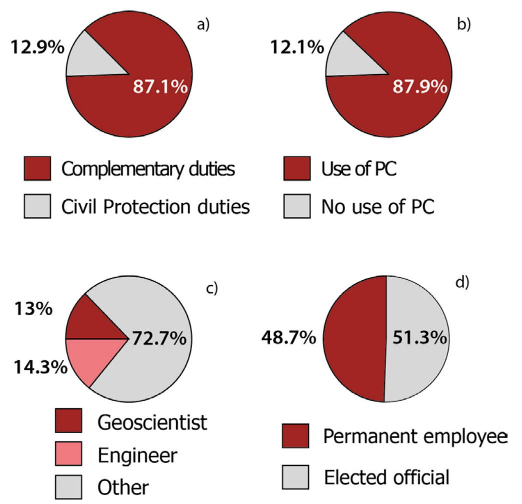


*Fig. 2: a) Duties charged to the head of civil protection dept., b) Use of PC in the civil protection office, c) Expertise of the head of civil protection department, d) Appointment of the head of the civil protection dept.*

Inter-agency cooperation is shown to be poor and organizational learning from international practices not adequate. Half of the municipalities report that the authorization processes are too slow so that prevention actions are severely delayed. Existing regulations are not followed by a significant portion of municipalities (Fig. 3a,b). More than 10 years since the 3013/2002 Act, 19.3% of the municipalities have not established a civil protection office, 13.7% of the Local Coordination Councils do not schedule annual meetings and 26.3% of these meetings are found to be simple procedural (Fig. 3c). Moreover 24.1% of the municipalities have not compiled an action plan yet (Fig. 3d). The action plan is the main handbook and primary tool of every municipality for reducing the risk of natural hazards and is the core of the prevention strategy. However, these action plans, risk analysis and maps are of decisive importance not only for prevention and operational planning purposes, but can also prove useful during the crisis and the rehabilitation processes. Existing action plans lack important information, present no spatial data (e.g. Sapountzaki et al. 2011), do not have a strategy or set priority measures. Indeed, 85% of the municipalities do not use risk maps and spatial data, which are of decisive importance for compiling the plans. As a result, existing plans are predominantly catalogues and tables of information that only present authorized personnel and equipment.

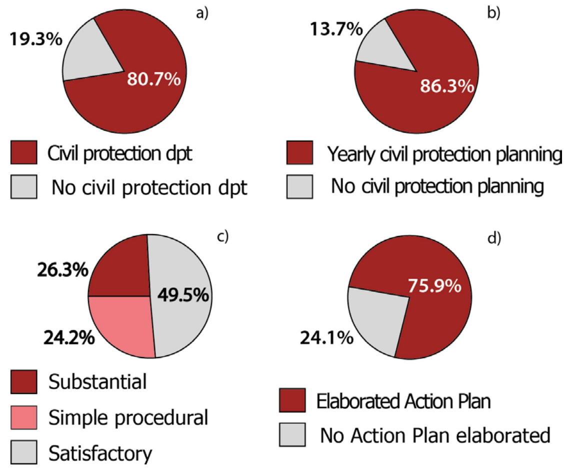


*Fig. 3: a) Municipalities that have established a civil protection department, b) Municipalities where Local Coordination Councils charged with civil protection planning meet yearly, c) Rating of the overall efficiency of the yearly civil protection planning meetings, d) Municipalities that have elaborated an action plan.*

Furthermore, emergency drills are not repeated on an annual basis for most of the civil protection departments' personnel (Table 3).

*Table 3: Repeatability of emergency drills for all personnel involved in civil protection.*

| | |
|---|---|
| Never | 68% |
| Once per year | 47% |
| Twice per year | 35.3% |
| Three or more per year | 17.7% |

Overall, underfunding, poor coordination of the different actors involved, lack of training and understaffing, lack of proper equipment and several other issues (Table 4) are held responsible by officials for preventing effectiveness of current practices. Finally, the majority of the civil protection personnel (84.5%) are not familiar with the EU emergency number 112.

*Table 4: Main factor preventing the effective compilation and implementation of action-plans (10 Most frequently reported).*

| | |
|---|---|
| 1.Poor training | 39.3% |
| 2.Equipment shortage | 37.5% |
| 3.Underfunding | 35.7% |
| 4.Understaffing | 28.6% |
| 5.Poor coordination with different bodies | 19.6% |
| 6.Poor cooperation with voluntary organizations | 10.7% |
| 7.Public awareness | 8.9% |
| 8.Not focusing on prevention | 8.9% |
| 9.Bureaucracy / Timely processes | 5.4% |
| 10. Lack of prevention actions | 5.4% |

**DISCUSSION**

Since the 3013/2002 and the recent 3852/2010 Acts of Parliament, the Local Authorities have increased their responsibilities in civil protection actions. Local Action Plans for natural disasters prevention are of high importance for the level of preparedness of the local civil protection departments. A large number of municipalities have not yet elaborated a Local Action Plan, but the majority of the existing action plans consist of catalogues and tables of information that only present authorized personnel and equipment.

Operational ineffectiveness addressed in all factors is examined in this survey. Inherent major weaknesses in Local Authorities are reflected in the availability and quality of the personnel and equipment, inter-agency cooperation, training of the staff, and compliance with existing regulations. The majority of the municipalities that took part in this survey pointed out basic structural shortcomings, demonstrating that funding is not the only reason for prevention failure.

Civil protection in many cases is underrated in the municipality planning. This is also supported by the fact that the importance of natural hazards as a presumable limitation is ignored in the vast majority of the municipalities' short term strategic planning. An illustrative example is that seismic hazard is only addressed in less than 10% of the municipalities' strategic plans, while earthquakes are the dominant natural disaster in Greece in terms of human casualties and economic losses (EM-DAT, 2013).

**CONCLUSIONS – RECOMMENDATIONS**

In general, civil protection in Greece has a short history, since it was founded in 1995, whereas the legal framework was established in 2002. Taking into account the existing regulations and the current situation in civil protection bodies across the country, it should be noted that although the Act 3013/2002 is still the main legal instrument in the field of civil protection, several provisions described in it are not yet applied 10 years after its establishment. For instance, civil protection offices have not been founded in all municipalities of the country, action plans have either not been developed or are of low quality. Funding is thought to be the dominant constraint for civil protection actions. However, the results of this survey strongly impose that prevention failure is attributable to a combination of inadequate practices. Underqualified staff and little or no training of the civil protection personnel seem to be among the most serious reasons for poor prevention results.

A significant number of municipalities have not developed a local action plan. However, the survey demonstrates why municipalities are not capable of incorporating civil protection actions. For example, the head of the Civil Protection Department is not a permanent employee in half of the cases, many of the heads of the departments are overstretched by other duties than civil protection and there is still a considerable number of Local Authorities that have not even established a civil protection department yet.

The municipalities seem to underestimate their role in civil protection. This is also supported by the fact that more than 50% of the people in charge of the civil protection departments hold only a secondary education degree. Considering that the municipalities that responded in the survey are probably more sensitive and interested in civil protection, then the overall situation along the entire country can be even worse.

Overall, this survey demonstrated the inefficiencies of the current management framework, making feasible to extract a series of recommendations towards policy makers. The recommendations concern not only the local authorities in Greece, but the central government and the EU as well. For example, the Central government should supervise local authorities and check whether they comply with legislation. In addition, the EU and central governments should provide a framework regarding the minimum competencies for selecting civil protection personnel. The personnel should be university graduates specialized in geosciences, emergency management or engineering. Moreover, they should be permanent staff to avoid incoherence in policy-implementation and prevention actions and strategies. Central governments should establish training programs in collaboration with the EU. Organizations like the European Group on Training (EGP) and the International Search and Rescue Advisory Group (INSARAG) can develop such programs, possibly also in collaboration with academics and MSc courses on Natural Hazards from European Universities. Programs supervised and coordinated by the EU will secure the quality and completeness of training and are expected to enhance international cooperation of civil protection units. Finally, the EU should consider increasing further the awareness of 112 in Greece, primarily towards the civil protection personnel and then to the general public.

**Acknowledgements:** This work was held under the LIFE+ project "Local Authorities Alliance for Forest Fire Prevention - LIFE08/ENV/GR/000553" which is implemented with the contribution of the LIFE financial instrument of the European Community. Further information on the project's objectives and deliverables are available on www.forestcities.gr

## References

Civil Protection Improvement Act 3013/2002. Athens: Official Government Gazette.

EM-DAT, (2013). *Natural Disasters Trends.* [Online]. Available at: http://www.emdat.be/natural-disasters-trends

EU Directive 2001/792/EC, OJ L 297, p. 7-11. Available at: http://eur-lex.europa.eu/LexUriServ/LexUriServ.do?uri=OJ:L:2007:288:0027:0034:en:pdf

EU Directive 2007/60/EC, OJ L 288, p. 27-34. Available at: http://eur-lex.europa.eu/LexUriServ/LexUriServ.do?uri=OJ:L:2001:297:0007:0011:EN:PDF

UNISDR (2013). UN warns that economic losses from disasters are out of control and urges private sector to reduce risk. Press release 15 May 2013 by the United Nations Office for Disaster Risk Reduction – UNISDR 2013/15.

UNISDR (2013) From Shared Risk to Shared Value –The Business Case for Disaster Risk Reduction. Global Assessment Report on Disaster Risk Reduction. Geneva, Switzerland: United Nations Office for Disaster Risk Reduction (UNISDR). ISBN 978-92-1-132038-1, United Nations 2013.

Munich Re, (2013). Natcatservice. Downloadcenter for statistics on natural catastrophes. [Online]. Available at: http://www.munichre.com/en/reinsurance/business/non-life/georisks/natcatservice/default.aspx

New Architecture of Local Government and Decentralized Administration – Kallikratis Programme Act 3852/2010. Athens: Official Government Gazette

Sapountzaki K., Wanczura S., Casertano G., Greiving S., Xanthopoulos G., Ferrara F., (2011). Disconnected policies and actors and the missing role of spatial planning throughout the risk management cycle. Natural Hazards 59, 1445–1474. 2011.

Swiss Re, (2013). *Sigma*. [Online]. Available at: http://www.swissre.com/sigma/

INQUA Focus Group on Paleoseismology and Active Tectonics

paleoseismicity.org

# Earthquake GeoSurvey, an application for reporting earthquake-induced environmental effects

*George Papathanassiou (1), Vasilis Kopsachilis (2)*

(1) Department of Geology, Aristotle University of Thessaloniki, Greece gpapatha@auth.gr
(2) Department of Geography , University of Aegean, Greece, vkopsachilis@geo.aegean.gr

***Abstract: Earthquake GeoSurvey*** *is an application that can be used by earth-scientists and engineers during field surveys in order to report the earthquake-induced environmental effects (EEE). The app has been designed based on the EEE form, proposed by the* ***INQUA TERPRO Focus Area on Paleoseismology and Active Tectonics****, for reporting earthquake-induced deformations and processing the collected data at the end of a post-earthquake reconnaissance field survey. As an outcome, the earthquake environmental effects can be documented and the macroseismic intensity will be evaluated based on the Environmental Seismic Intensity-2007 (ESI-07) scale. The post-earthquake report can be exported as kmz file and consequently uploaded to a GIS environment.*

***Key words****: earthquake, survey, environmental effects, application, android*

## INTRODUCTION

The basic goal of the project is to develop two applications for tablets and smartphones, using either android system or iOS that will be used by earth-scientists and engineers during field surveys in order to document the earthquake-induced environmental effects.

In order to achieve this, the project was mainly designed based on the Earthquake Environmental Effects form, proposed by the INQUA TERPRO SubCommission Group for reporting earthquake-induced deformations (Michetti et al. (2007), and the recommendations of GEER, Geotechnical Extreme Events Reconnaissance, (GEER, 2011) regarding data processing after a post-earthquake reconnaissance field survey.

In particular, via this application the user is able to document primary and secondary effects, collect GPS waypoints (in decimal degrees using WGS84) and thus, geo-tag the collected photos. The type of effects that can be reported and described in detail are surface faulting, slope failures, liquefaction, tsunami, ground cracks, hydrological anomalies and other effects like trees shaking (Fig. 1). For example, regarding the earthquake-induced liquefaction, the user can select a subtype of liquefaction from a list including the three most characteristic ones (ejection of sandy material, subsidence and lateral spreading), describe in detail the failure within an extra field, report the maximum diameter of sand boils, select either water or sand ejection and finally locate the site by activating the GPS and take a photo of the liquefaction manifestation. In addition, the macroseismic intensity can also be evaluated using the ESI-07 scale and the relevant chart that is provided.

Finally, the data that have been collected during the field survey are saved on the SD card of the smarthphone/tablet as KMZ file and consequently can be used by Google Earth and other GIS application for further processing. The most direct presentation of the collected data can be achieved using Google Earth, where the collected data are plotted with different symbols-icons depending on the type of failure. In this way, the collected information can be separated and maps showing the spatial distribution of one-type or combination of earthquake-induced failures can be developed including geo-tagged photo.

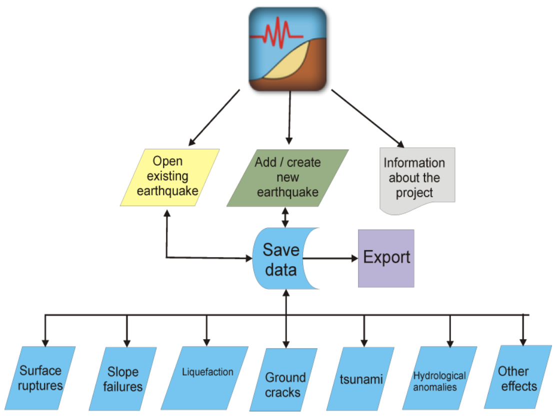


*Fig. 1: Flowchart of the Earthquake Geo Survey*

## DATA MODEL

In this chapter, we describe the data model of the Earthquake GeoSurvey application that was designed to adequately describe earthquakes and environmental effects. The main concepts of the Data model are earthquake and effect, which are represented in the application according to OOP (object-oriented Programming) principles as classes.

The *earthquake* class is used for describing the earthquake itself. An earthquake is described by the following attributes: code, date (dd/mm/yy), earthquake magnitude, magnitude type (Mw or Ms), ESI epicentral intensity, epicentral area, country, longitude and latitude (WGS84). The class representation is depicted in Fig. 2.

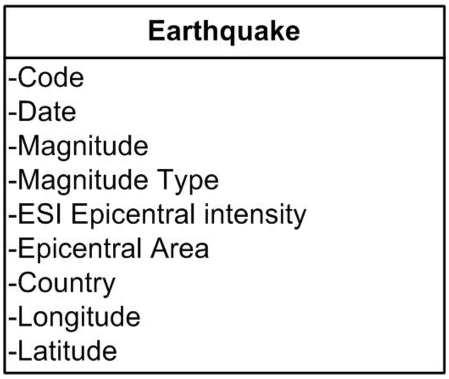


*Fig. 2: Earthquake Class*

Effect classes describe earthquake-induced environmental effects. Following the recommendations provided by the EEE form (Michetti et al., 2007), the environmental effects have been grouped into 7 types. These types of effects that can be reported and described are: surface faulting, slope failures, liquefaction, tsunami, ground cracks, hydrological anomalies and other effects. Each effect is described by different attributes depending on its effect type. For example, dip information might be meaningful for a surface faulting effect and do not apply for a slope movement effect. However, all effect types share common attributes such as ID and Longitude/Latitude. For that reason our data model was designed according to class inheritance principle. Class inheritance in programming means that a class can inherit behaviour and attributes from other classes, which called base, super or parent classes

In our model, the *Effect* class is used as a parent class and there are seven more child classes that represent each effect type (Fig. 3*)*. The common attributes (which are ID, Subtype, Date, Description, Longitude, Latitude, ESI-07 scale and Photo) are represented by the *Effect* parent class. Each child class hold attributes that are specific to the effect type and also inherits the attributes from its parent class *Effect*. For example, a slope movement effect is represented by the *Slope Movement* class and is described by the attributes ID, Subtype, Date, Description, Longitude, Latitude, ESI-07 Scale, Photo, Blocks Dimension and Total Volume.

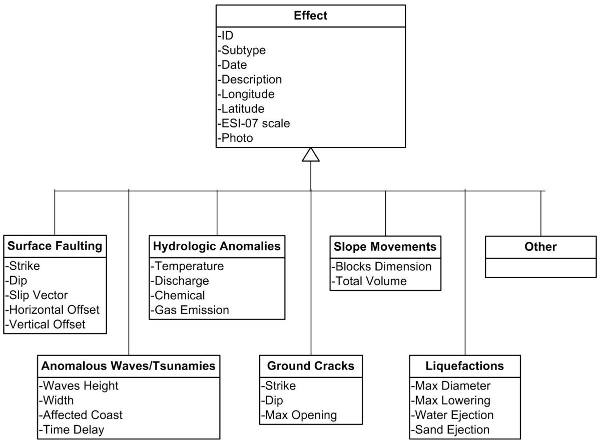


*Fig. 3: Effect Class Diagram*

**KML STRUCTURE**

In the Earthquake GeoSurvey application collected data are stored in KML (Keyhole Markup Language) files. KML is an XML notation for expressing geographic annotation and was developed for use with Google Earth, which is a software for viewing of Earth satellite imagery, maps and user defined overlays of geographic information (GEER, 2011). Each KML file holds information about an earthquake, visualization styles and earthquake's environmental effects in XML elements.

At the top of each KML document XML elements *name, Timestamp and Extended Data* holds information about the earthquake itself such as name, date, magnitude etc. (Fig.4).

```xml
<name>earth-1</name>
<Timestamp><when>24-3-2013</when></Timestamp>
<ExtendedData>
    <Data name="Magnitude"><value>12</value></Data>
    <Data name="MagnitudeType"><value>Mw</value></Data>
    <Data name="Intensity"><value>3</value></Data>
    <Data name="Country"><value>greece</value></Data>
</ExtendedData>
```

*Fig. 4: XML elements for describing earthquake*

*Style* XML elements define styles for effect visualization in Google Earth. Each effect, depending on its type, is visualized in Google Earth with its type symbol (icon) and a custom information popup. The Effect icon is similar to the icons proposed by Silva et al. (2008) in order to maintain the consistency between the ESI-07 scale and the application. Therefore, in KML document there are seven *Style* elements, one for each effect type. In these elements, the type symbol and info popup template are defined (Fig. 5).

```
<Style id="Surface Faulting">
    <IconStyle><Icon><href>http://.../rupture.png</href></Icon></IconStyle>
    <BalloonStyle>
        <text><![CDATA[<h1>$[Type]</h1><h2>$[Subtype]</h2><hr/>
                <h3> Description: $[Description]</h3>
                <h3> ESI-07 Scale: $[esi]<h3> Strike  : $[Strike]
                <img src='$[photo]'/>]]>
        </text>
    </BalloonStyle>
</Style>
```

*Fig. 5: XML style element*

Each effect is described by a *Placemark* XML element. In KML document there are as many *Placemark* XML elements as effects. *Placemark* elements contain sub-elements that fully describe an effect (Fig. 6). In particular, the *Name* sub-element holds ID, the *Style Url* sub-element associates this effect with a visualization style depending on its type, the *Point* sub-element holds longitude and latitude, the *TimeStamp* sub-element holds effect's reporting date and finally, the *ExtendedData* sub-element contains more sub-elements that hold other information that fully describe the effect such as subtype, description, ESI-07 scale and name of the photograph.

```
<Placemark>
    <name>q1</name>
    <styleUrl>#Surface Faulting</styleUrl>
    <Point><coordinates>26.55899175,39.106032150000004</coordinates></Point>
    <TimeStamp><when>24-3-2013</when></TimeStamp>
    <ExtendedData>
        <Data name="Type"><value>Surface Faulting</value></Data>
        <Data name="Subtype"><value>Oblique</value></Data>
        <Data name="Description"><value></value></Data>
        <Data name="photo"><value>q1.jpg</value></Data>
        <Data name="esi"><value>3</value></Data>
</Placemark>
```

***Fig. 6: Placemark XML element***

## APPLICATION DEVELOPMENT

At present time only the Andorid application has been developed, while the design of the iOS application structure has been already started. Earthquake GeoSurvey application for Android was developed in Eclipse IDE (Integrated Development Environment). Eclipse is anIDE for android application development as it supports the Android Development Tools (ADT) plugin, and integrates the Android SDK (Software Development Kit) which is essential for application developing for Android Devices. The programming language used for the application development is Java.

During development phase application was tested on a HUAWEI U8180 device with the following features: Android 2.2.2 OS, 2.8 in. display, capacitive touch screen, 512MB memory, 3.15 megapixel camera, 4 GB SD card, and GPS. The application runs on devices with Android 2.2 OS version or newer. It requires access to camera and GPS receiver features and permission to write to device's external storage.

Each earthquake is stored in a KMZ file that is compressed kml files containing zero or more supporting files such as images. KMZ files are stored in device SD card under Earthquake GeoSurvey folder. The application makes use of the device GPS receiver in order to capture effect's location (longitude and latitude) in WGS84 coordinate system. Camera enables application users to take pictures for an effect and thus, each photo can be tagged with location.

## USE CASE

In this chapter we present the Earthquake Geo Survey application according to the following use case scenario.

*Scenario: Creating a new earthquake file and adding an effect*

In order to add earthquake effects, first an earthquake file must be created. At the application's home screen (Fig.7), user should click on *New Earthquake* Button. At the new screen, there is an earthquake form that the user should fill with current earthquake-related data (Fig.8). To create the earthquake file the user should click at the *Save* Button at the bottom of the screen. A new KMZ file was created and stored in the SD card of the device. The name of the newly created file is the same with the value that the user entered in the *Code* field.


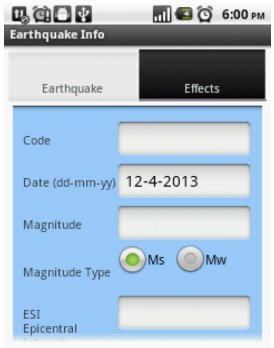


*Fig. 7: Home Screen*    *Fig. 8: Earthquake Screen*

Now the user can add an effect to current earthquake by clicking on the *Effects* Tab at the top of the screen and then by clicking at *Add New Effect* Button (Fig. 9). We should note that at this time the effect list is still empty for the selected earthquake. At the next screen (Fig. 10) user must select the effect type that he will report. Depending on the user selection the appropriate effect type screen will appear.

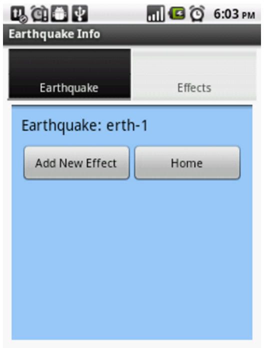


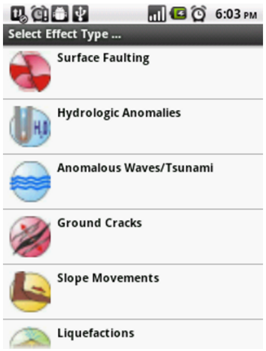


*Fig. 9: Effect List Screen* *Fig. 10: Effect Types Screen*

Effect Screen (Fig.11) contains a form with fields that the user should fill in order to describe the effect. The effect location can be captured by clicking on the *GPS Off* button. The effect's longitude and latitude will appear on the screen as soon as the user location is detected. User can add a photograph from the effect place by clicking at the *Photo* button. When the user fill the form, can add the effect to the earthquake file by clicking at the *Add Effect* button at the bottom of the screen. He can return to the effect list screen and preview the newly added effect by clicking at the *Effect List* button (Fig. 12).

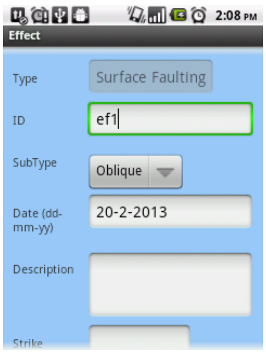


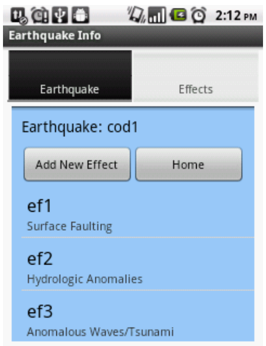


*Fig. 11: Effect Screen* *Fig. 12: Effect List Screen*

Once the earthquake file created, it can be used by Google Earth and other GIS applications. In Google Earth, the collected data are plotted with different symbols depending on the type of failure. Also, when the user clicks on an effect an information popup appears containing information about the effect and a picture (Fig. 13).

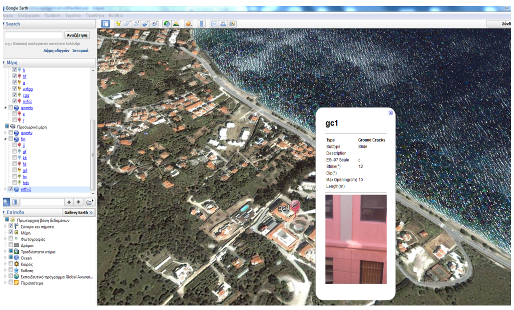


*Fig. 13: Google Earth Visualization*

## DISCUSSION

The development of this application is the first step of the INQUA TERPRO Focus Area on Paleoseismology and Active Tectonics in the new era of online information-exchange. The version presented in this article provides the adequate tools and functions that geologists and engineers are needed on the field for documenting the effects of an earthquake.In addition, new functions are planned to be developed in order to increase the usefulness of the application such as activation of the compass that can be used for reporting surface faulting and the direct linkage to the web site of Earthquake Environemntal Effects for on-line presenation of the collected data.

**Acknowledgements:** The application is the result of the activities of the INQUA TERPRO Focus Area on Paleoseismology and Active Tectonics and is developed in the frame of the INQUA Project 1299 - EEE METRICS (PARAMETRIZATION OF EARTHQUAKE ENVIRONMENTAL EFFECTS: Relationships between source parameters and ESI-2007 Intensity for Modern, Historic, Ancient and Paleo Earthquakes)

## References

GEER (2011). Manual for GEER Reconnaissance Teams, v3, pp. 13

Michetti, A. M., E. Esposito, L. Guerrieri, S. Porfido, L. Serva, R. Tatevossian, E. Vittori, F. Audemard, T. Azuma, J. Clague, V. Comerci, A. Gurpinar, J. McCalpin, B. Mohammadioun, N. A. Morner, Y. Ota, and E. Roghozin (2007). Intensity Scale ESI (2007). In Memorie Descrittive Carta Geologica d'Italia L. Guerrieri and E. Vittori (Editors), APAT, Servizio Geologico d'Italia - Dipartimento Difesa del Suolo, Roma, Italy, 74, 53 pp.

Silva P. G., Rodríguez Pascua M. A., et al. (2008). Catalogación de los efectos geológicos y ambientales de los terremotos en España en la Escala ESI-2007 y su aplicación a los estudios paleosismológicos. Geotemas 6:1063–1066.

# Towards an understanding of the controls on earthquake triggered landslides

*Petley, David (1)*

(1) Department of Geography, Durham University, South Road, Durham, DH1 3LE, UK. Email: d.n.petley@durham.ac.uk

***Abstract:*** *In recent years awareness of the potential impacts of coseismic landslides in high mountain areas has increased. In particular, the 1999 Taiwan, 2005 Pakistan/India and 2008 China earthquakes have resulted in very large numbers of landslides that inflicted substantial levels of loss. At present our understanding of coseismic landslide processes remains weak, primarily because the collection of field data for these events is very challenging, whilst their simulation in the laboratory is also difficult. There is also a mismatch between the approach often used when planning for an earthquake disaster in less developed countries, which is often based on an earthquake scenario, and the general coseismic landslide hazard maps that are often generated. This paper uses the assessment of potential landslides from a large earthquake in Nepal to illustrate key aspects of coseismic landslide processes and to indicate areas of future research.*

***Key words****: earthquake, landslide, Nepal, seismic hazard.*

## INTRODUCTION

In 1999 the Mw=7.6 Chi-Chi earthquake in Taiwan brought to the attention of the scientific community the impact of co-seismic landslides. This seismic event triggered over 20,000 landslides across the Central Mountain range (Shou et al., 2011), causing substantial levels of loss in terms of both lives and economic damage. The landslides substantially hindered the rescue and recovery effort because major communications and transportation networks were destroyed. Levels of landslide activity remained anomalously high for at least five years after the earthquake, causing substantial further damage (Shou et al., 2012 for example). Movement through the fluvial network of the sediment released by failed slopes extended the impacts of the earthquake well beyond the area of high ground motions; in places river beds aggraded by over 20 metres, causing substantial damage (Shou et al., 2012).

Subsequent large earthquakes in high mountain areas have repeated this pattern. Thus, in the 2005 Mw=7.6 Kashmir earthquake in India and Pakistan, about 25,000 people were killed in landslides triggered by the seismic event. In the 2008 Mw=7.9 Wenchuan earthquake over 20,000 people were killed in mass movements. In the latter event a total of 828 barrier lakes, formed when landslide sediments blocked the river valleys, proved to be a very major problem; over 200 barrier lakes needed to be mitigated, requiring a very substantial effort on the part of the authorities at a time when resources should have been focused on the immediate needs of the survivors of the earthquake (Fan et al., 2012). Unusually, China had the resources needed to manage such an extreme scenario.

It is reasonable to assume that future large earthquakes in high mountain areas will generate substantial numbers of earthquake-triggered landslides, and that these will inflict high levels of loss on mountain communities. Hence, there is an urgent need to improve levels of understanding of seismically-induced landslides. However, at present the knowledge of the processes occurring within slopes during seismic accelerations remains poor. The response of upland topography during seismic excitation is in itself inherently complex. In addition, steep slopes have, for example, non-linear material responses and are sensitive to the effects of pore pressure changes, which may respond both to seismic forcing and to deformation-induced effects. Measuring slope behaviour during large earthquake events is challenging, whilst laboratory apparatus generally struggle to reconstruct the complex stress states that occur in slopes during earthquakes.

## COSEISMIC LANDSLIDE HAZARD IN NEPAL – AN ILLUSTRATION OF COMPLEX SLOPE RESPONSE

Much of the Himalayan Arc is prone to large earthquake events (Bilham & Ambraseys 2005; Feldl & Bilham 2006), with historic evidence suggesting that previous events have triggered many damaging landslides due to the combination of steep topography in tectonically-deformed, weak rocks; the high uplift rates; and the intense monsoonal rainfall. Indeed, in terms of numbers of events and levels of loss the southern edge of the Himalayan Arc is the most important global hotspot for landslide activity (Petley 2012), even without a large earthquake event. An area of particular concern within the Himalayas is the Central Seismic Gap, a large seismic gap located in western Nepal, which has the potential to generate an earthquake of Mw>8 (Rejandran & Rajendran 2008), associated with a potential rupture of the Main Frontal Thrust. This paper uses this seismic gap to illustrate the challenges of understanding the likely impact, in terms of landslides, of such a major seismic event.

Some previous studies have correlated spatial patterns of landslides with the modelled or measured distribution of seismic parameters such as peak ground acceleration. Whilst in some areas, such as in Taiwan in 1999, the correlation appears to be strong, in others the relationship appears to be much less significant. Thus, for example, the patterns of landsliding in the 2005 Kashmir earthquake does not seem to be correlated with modelled ground accelerations, but instead to be controlled by proximity to the surface expression of the earthquake-generating fault, with most of the landslides occurring on the hanging wall block within a small number of kilometres of the fault trace. A similar pattern has been observed for the 2008 Wenchuan earthquake, although in this case it is apparent that the pattern of landslide activity varies along the length of the fault, apparently in response to changes in the faulting mechanism. Thus, the landslide distribution in a future earthquake in the Central Seismic Gap (CSG) will depend upon the faulting mechanism of the causative event.

Some work has also been undertaken to examine the relationship between earthquake magnitude and the area affected by landslides or the number of landslides triggered. In general there is a positive correlation between these two variables, as expected, but for any given earthquake magnitude the area affected by landslides carries over about three orders of magnitude. Part of this variation may be controlled by the land area in which landslides can be triggered; thus, some areas subject to earthquakes lie on alluvial plains in which landslides are not likely. However, even when this is factored in, there is still a very high level of variation. A key control appears to be the weather conditions both in the period prior to the earthquake and on the day of the event itself. If conditions have been dry prior to the earthquake, and indeed on the day of the event, then the level of landslides triggered by the earthquake is substantially lower than if rainfall levels have been high. Thus, in the context of Nepal an earthquake during the monsoon period (June to September) would generate higher levels of landsliding than if it were to occur in the dry winter months. The worst possible scenario from this perspective would be a large earthquake on a rainy day at the end of the monsoon period, especially if the monsoon that year had been particularly intense.

The key approach to generate landslide hazard assessment for earthquake events has been the so-called Newmark sliding block model (Jibson et al. 2000 for example), which considers the behaviour of a slope in terms of a rigid block sliding on an inclined plane. This approach calculates the critical horizontal acceleration required to induce movement of the block. Thus, for any given earthquake event the displacement of the block is determined; it is assumed that a critical threshold displacement represents the point at which collapse of the slope will occur, allowing a hazard map to be generated. However, this approach considers only horizontal accelerations, whilst recent large earthquakes have suggested that vertical accelerations may be important. Perhaps more significantly, laboratory experiments at Durham suggest that the relationship between, and phasing of, horizontal and vertical accelerations may be of fundamental importance, suggesting that the Newmark approach may need refinement in order to generate susceptibility and hazard maps of the required quality.

**A SCENARIO-BASED COSEISMIC LANDSLIDE MODEL FOR NEPAL**

In Nepal, there has been a growing awareness in recent years of the potential for a large CSG earthquake.

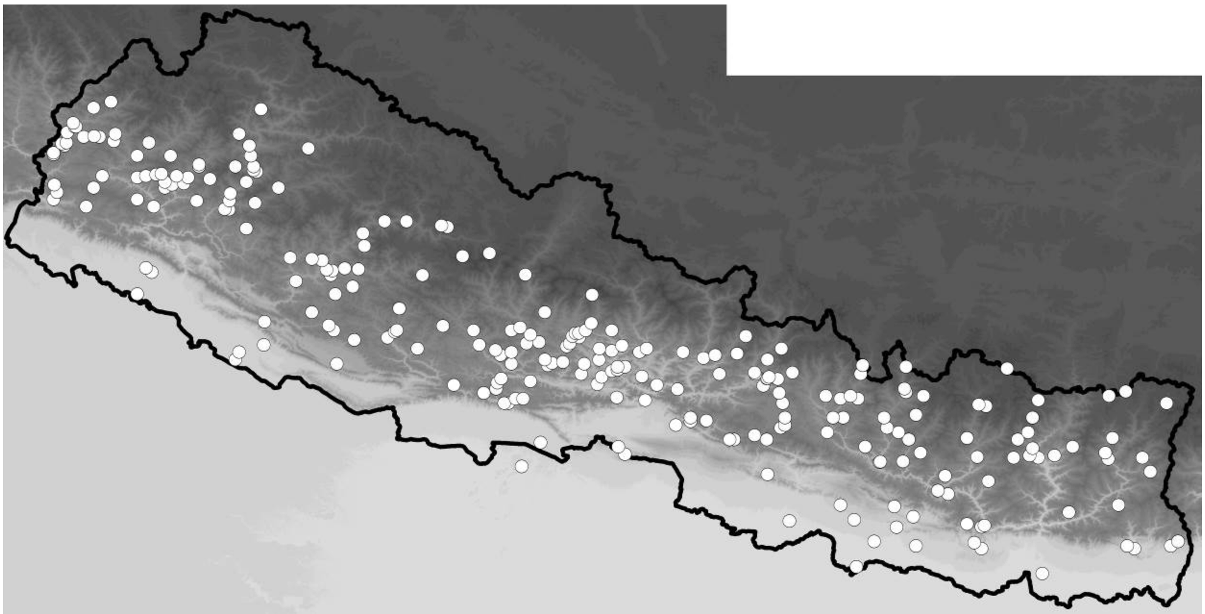

Fig. 1: The distribution of fatality-inducing landslides in Nepal overlain onto a regional Digital Elevation Model

Preparedness and awareness-raising have tended to focus on a scenario-based approach rather than in terms of general seismic hazard maps. Whilst seismically-induced landslide hazard maps have been generated, these do not usually fit with this scenario-based approach. As part of an alternative approach, in recent years, at Durham,a database has been compiled of landslides within Nepal that have caused losses of life (Fig. 1). This distribution suggests that the key physical factors in determining fatality-inducing landslide occurrence in Nepal are the relief and the magnitude of the triggering event (in the case of most landslides the annual precipitation, see Fig. 2). However, perhaps surprisingly the best factor to explain the distribution of fatality-inducing landslide events in Nepal is the density of the road network (Fig. 3). Road density may be a proxy for population density, which is a key factor in the occurrence of fatality-inducing landslides. Thus, the road density explains landslide impacts, although since poorly constructed roads can increase landslide susceptibility, this may be an additional causative factor.

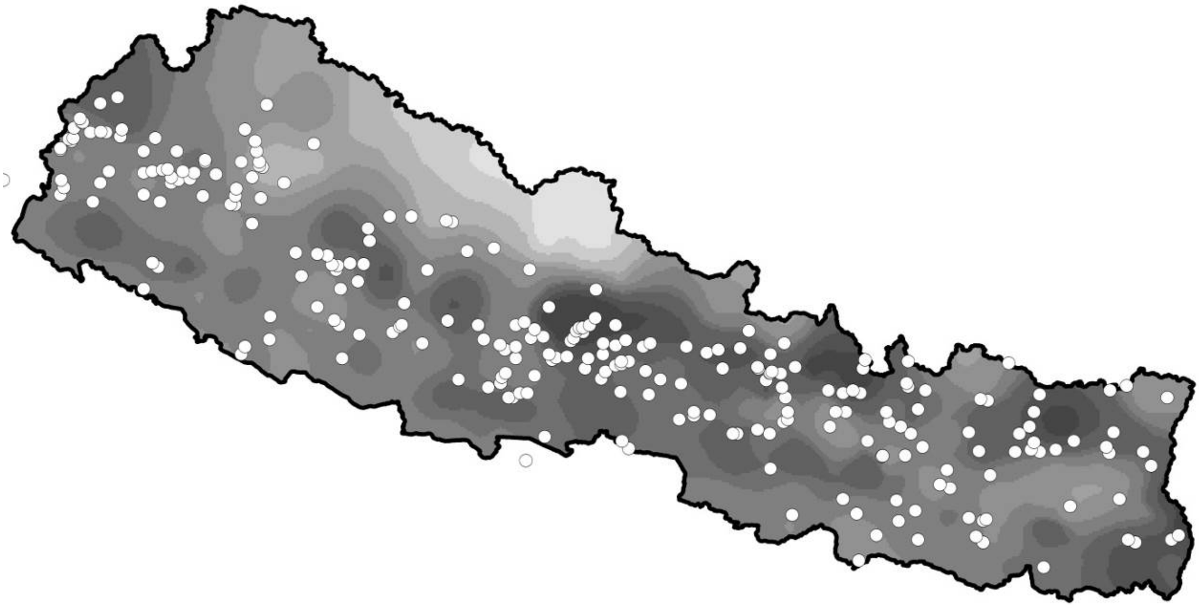

Fig. 2: The distribution of fatality-inducing landslides in Nepal overlain onto an annual precipitation map

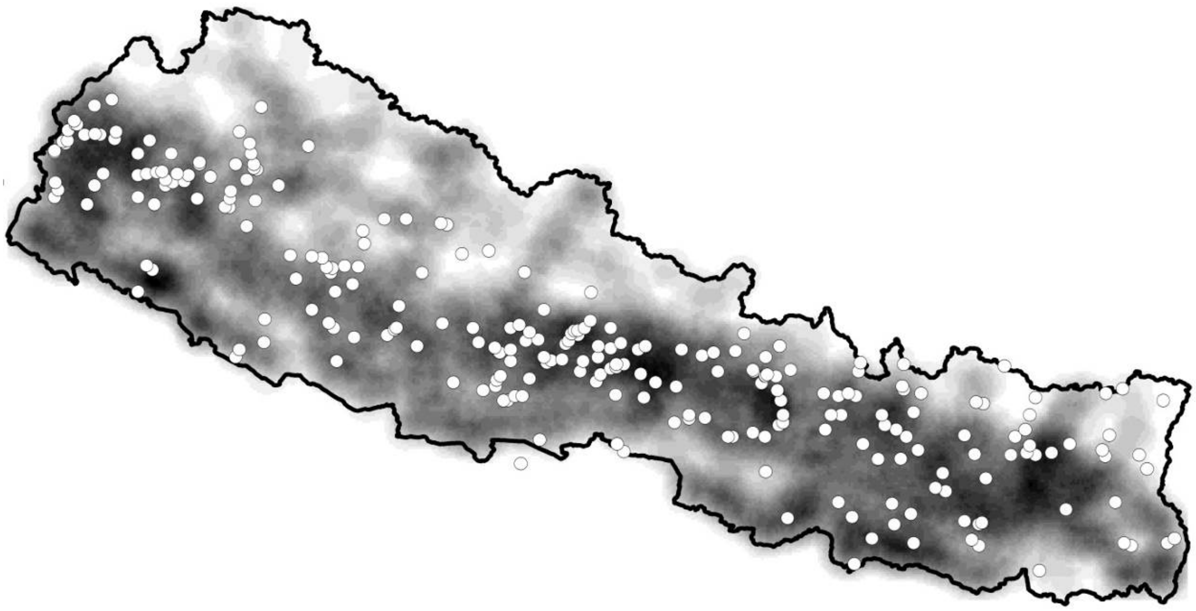

Fig. 3: The distribution of fatality-inducing landslides in Nepal overlain onto a map of road network density

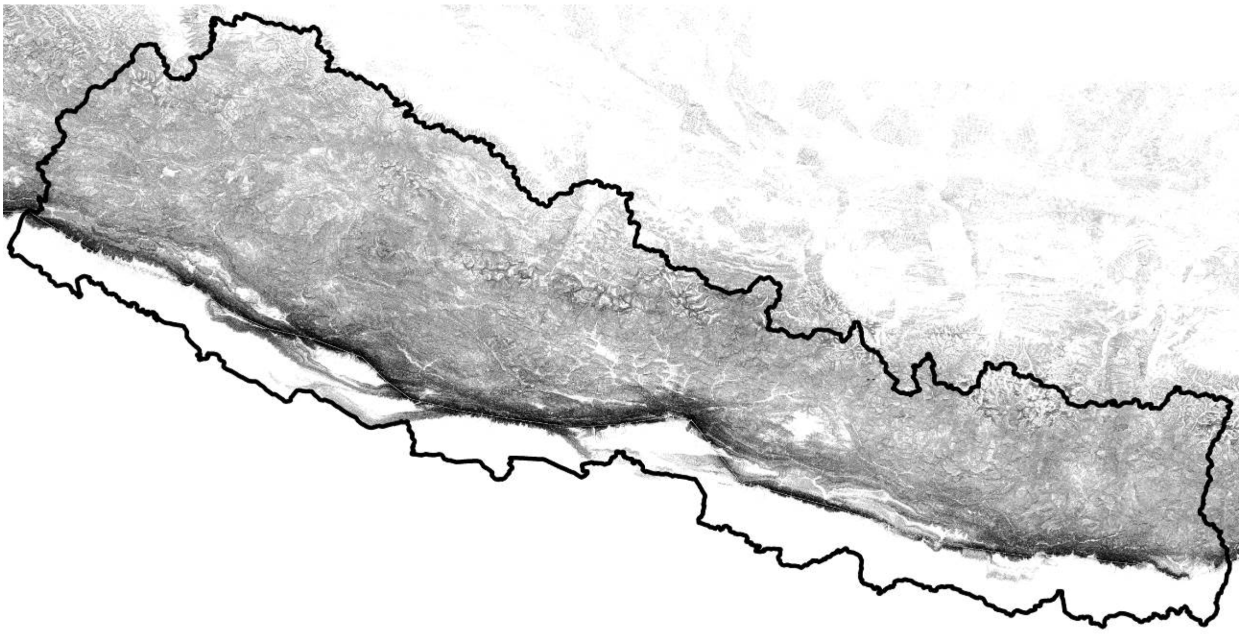

Fig. 4: A draft coseismic landslide hazard map for a Main Boundary Fault rupture event in Nepal. Such an event would likely rupture a portion of the fault, although the map covers the entirety of the fault

Thus, a potential approach to the development of a scenario-based landslide hazard map for a Central Gap earthquake might combine the topography with distance from fault, modelled here with a simple inverse distance relationship (Fig. 4). This model assumes a rupture along the entirety of the Main Frontal Thrust, although in reality it is Central and Western Nepal that are of concern here. It is unlikely that a rupture would extend along the entirety of the fault. The model suggests a very high level of landslide activity along the southern edge of the mountain chain, primarily because this is the location of the earthquake-inducing fault (the Main Frontal Thrust). However, given that all roads into the major city in Nepal, Kathmandu, have to cross the fault in mountainous terrain, this is a key finding. It is unlikely that these roads will be useable after a large earthquake, which would create severe logistical issues in terms of rescue and rehabilitation operations.

**DISCUSSION AND CONCLUSIONS**

At present the level of understanding of landslides associated with earthquakes is low, primarily because of the complexity of the mechanisms of failure. Further work is needed to understand these processes.

In Nepal, a large earthquake would probably generate large numbers of landslides, which would in turn cause substantial levels of loss and would severely disrupt the rescue and recovery operation. The level of landsliding would be likely to remain at an elevated level for many years. In this study, an a large earthquake on the Main Frontal Thrust has been described. Although this needs further refinement, it serves to illustrate the likely landslide impacts of such an event.

**Acknowledgements:** This work has been undertaken as part of the NERC/ESRC-funded Earthquakes Without Frontiers project, grant NE/J01995X/1.

**References**

Bilham, R. & N. Ambraseys, (2005). Apparent Himalayan slip deficit from the summation of seismic moments for Himalayan earthquakes, 1500-2000. *Current Science* 88 (10), 1658-1663.

Fan, X.M., C.J. van Westen, Q. Xu, T. Gorum & F.C. Dai, (2012). Analysis of landslide dams induced by the 2008 Wenchuan earthquake. *Journal of Asian Earth Sciences* 57, 25-37.

Feldl, N. & R. Bilham, (2006). Great Himalayan earthquakes and the Tibetan plateau. *Nature* 444 (7116), 165-170.

Jibson, R.W., E.L. Harp & J.A. Michael, (2000). A method for producing digital probabilistic seismic landslide hazard maps. *Engineering Geology* 58 (3-4), 271-289.

Petley, D.N., (2012). Global patterns of loss of life from landslides. *Geology* 40(10), 927-930.

Rajendran, C.P. & K. Rajendran, (2005). The status of central seismic gap: a perspective based on the spatial and temporal aspects of the large Himalayan earthquakes. *Tectonophysics* 395 (1-2), 19-39.

Shou, K.J., C.Y. Hong, C.C. Wu, H.Y. Hsu, L.Y. Fei, J.F. Lee & C.Y. Wei, (2011). Spatial and temporal analysis of landslides in Central Taiwan after 1999 Chi-Chi earthquake. *Engineering Geology* 123 (1-2), 122-128.

Shou, K.J., L.Y. Fei, J.F. Lee, C-Y. Wei, S.T. Huang & Y.C. Lin, (2012). Landslides and catchment sedimentation in the Ta-Chia River influenced by the 1999 Taiwan Chi-Chi earthquake. *International Journal of Remote Sensing* 33 (15), 4815-4840.

# Hypothetical tsunami deposits in the Rogowo area, Baltic Sea coast, North Poland

*Andrzej Piotrowski (1), Witold Szczuciński (2), Paweł Sydor (1), Jarmila Krzymińska (3), Jan Seidler (1)*

(1) Polish Geological Institute-National Research Institute Pomeranian Branch, Wieniawskiego 20, 71-130 Szczecin, Poland. Email: andrzej.piotrowski@pgi.gov.pl
(2) Institute of Geology, Adam Mickiewicz University, Maków Polnych 16, 61-606 Poznań, Poland, Email: witek@amu.edu.pl
(3) Polish Geological Institute-National Research Institute Marine Geology Branch, Kościerska 5, 80-328 Gdańsk, Poland. Email: jarmila.krzyminska@pgi.gov.pl

***Abstract:*** *Several areas along the southern coast of the Baltic Sea have been studied in order to find potential tsunami deposits. Here, we report for the first time the presence of sandy strata together with analysis of their sedimentary textures and structures, microfossil content and their absolute dating. The analysis revealed that the strata were deposited by rapidly ingressing sea water deep inland near the village of Rogowo as well as at the mouth of the Rega river near Mrzeżyno, Western Pomerania, North-western Poland.*

***Key words****: tsunami deposits, Baltic Sea coast, Rogowo, "Sea Bears", radiocarbon dating*

## INTRODUCTION

We present the preliminary results of a geological study carried out at the Polish coast of the Baltic Sea in order to verify historical and mythical information about peculiar marine waves. These waves, in the past referred to by the local people as "Sea Bears", occurred during various weather conditions, lasted for a short period and advanced inland rapidly. Such sudden ingressions of water were preceded by a loud roar and sometimes by a retreat of water. They were recorded in Darłowo and other areas in 1497, in Rogowo at the mouth of the Rega river in 1396 and 1757, in Łeba and Kołobrzeg in 1779 as well as in Kołobrzeg in 1853. It was assumed that the waves had a seismic origin related to submarine mass movements over the steep bed of the Baltic Sea near Gotland, Bornholm and Gdańsk. These landslides could have had a seismic origin; alternatively, if methane craters are found in the Baltic Sea bed, they could have been caused by gas explosions. Earlier authors related the origin of such waves to atmospheric events (Credner, 1889; Doss, 1907), meteorite impacts (Rotnicki et al., 2008) or less often to tectonic events (e.g. Bolle, 1846; Piotrowski, 2006). The possibility of tsunamis being related to the Scandinavian uplift was suggested by Mörner (2008) and Nikonow (2004).

## STUDY AREA

The initial study results presented here come from one of three analysed coastal areas, i.e. from the Rogowo area. The study site is located to the east of the Rega river mouth and covers the adjacent floodplains of the Rega river but also the spit and the bed of the Resko Przymorskie lake stretching up to Rogowo.

According to Brüeggemann (1784), at least one classic "Sea Bear" event took place in this area, on the 3rd of April 1757 at the mouth of the Rega river. The biggest town in this area, located over a dozen kilometres to the south of the coast, is Trzebiatów (Treptow), and this town is mentioned in historical records.

Brüeggemann (1784) reported that on that day, at noon, when the sea was calm, a wave, high enough to carry a ferry and cast it deep inland, entered the area. Are there any traces left by this event? This is the question which the geological investigation, which included 15 trial pits and 200 shallow boreholes, tried to answer.

## RESULTS

The result was that continuous, locally nearly continuous, layers of sand were found within peat deposits located on the coastal plain at levels insignificantly above the mean sea level.

The maximum lateral extent of the most extensive layer stretches 1400 m to the south of the current coastline. The thickness of this hypothetical tsunamite varies between 0.5 and 20 cm, but it is typically 8 cm and it is rather uniform. It is the thickest in the northern part of the area. Its lateral southern and south-eastern extent has been contoured. Currently, sedimentological analysis of its texture and structure, radiocarbon dating as well as optically stimulated luminescence (OSL) dating are being carried out.

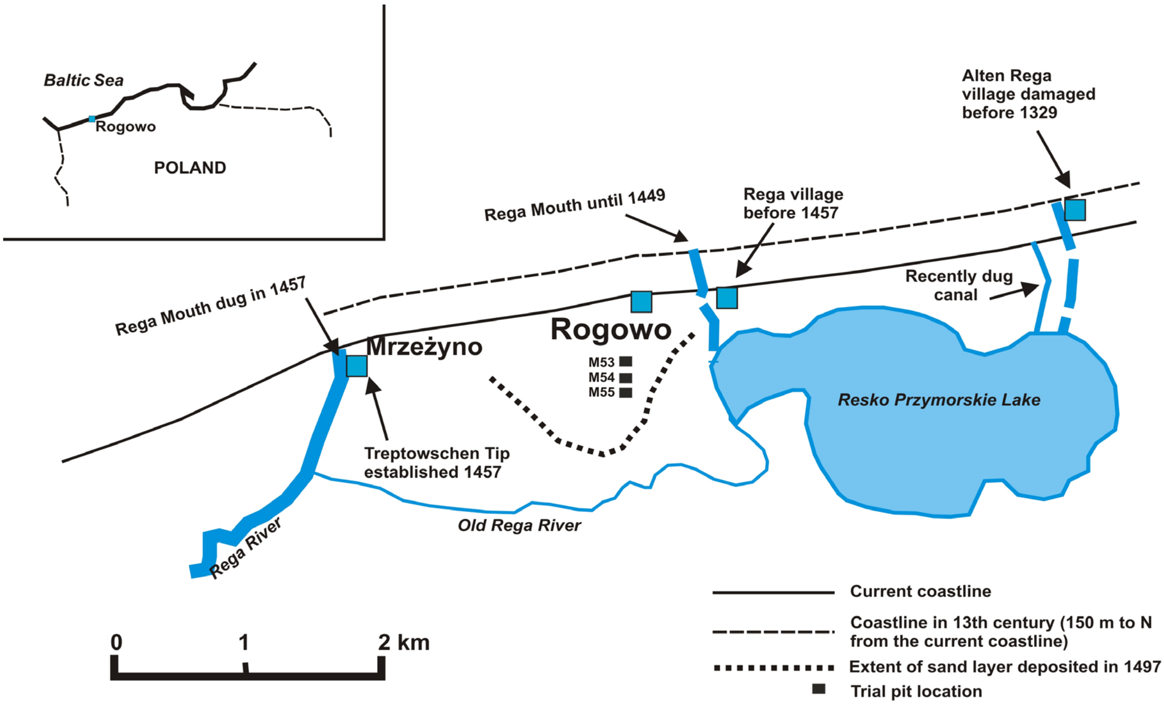


*Fig. 1. Site location map of the Rogowo area*

The boundary with the underlying peat stratum is sharp. No internal stratification was noted within the layer, and it contains root traces. The sand is medium and well sorted, but includes fragments of peat. To the south of the current Rega river mouth (Fig. 1.), there are two layers of sand, and the lower one stretches 1.4 km inland.

Samples for diatom analysis were collected from trial pits M53, M54 and M55, and they are marked on the location map included. The samples were collected from the boundary of the sand stratum and the underlying peat, and all include brackish diatom species, typical for the Southern Baltic. Samples for ostracod analysis were taken from 80 locations, but no fossils were found. The locations of boreholes, excavations and geological sections are shown on the map (Fig. 1).

Radiocarbon analysis involved accelerator mass spectrometry (AMS) and was carried out by the laboratory at Adam Mickiewicz University in Poznań.

- The chronology of studied sediments and approximate age of the event layers were based on high precision AMS $^{14}C$ dating performed on bulk organic matter from soils. 25 samples were selected and after careful removal of fresh rootlets they were measured in the Poznań Radiocarbon Laboratory (Poland) using the 1.5 SDH – Pelletron Model 'Compact Carbon AMS'.
- The dates were converted into calibrated ages using the calibration program CALIB Rev. 6.1.0 Beta and the IntCal09 calibration dataset (Remer et al. 2009). Seven samples contained modern, postbomb carbon indicating a post-1960 age. To constrain the age of the samples, they were calibrated using the CALIBomb Radiocarbon Calibration program and the northern hemisphere $^{14}C$ datasets. The modern samples are presented in percent modern carbon (pMC). The calibrated ages are reported with a two standard error age range (standard error of 2).

According to $^{14}C$ dating, the upper sand layer which has a smaller lateral extent and is described in the historical record from 1757 is associated with an event that occurred between 1720 and 1820. The lower sand layer, having a greater extent, represents an event which took place between 1410 and 1520, and was described as "Sea Bear" event in 1497. The layer found near the Rega river mouth, to the south of its current location, represents an event which happened between 1170 and 1270; no historical record about this event has been found.

## SUMMARY

The study focuses on areas in which the occurrence of peculiar waves, also referred to as "Sea Bears", has been described in historical records. Dating of the layers enables us to correlate our findings with historical descriptions. The location of the Rega mouth changed as a result of catastrophic events as did the locations of fishing and harbour villages (Alten Rega, Rega, Treptowschen Tip). The authors hope that the outcome of this geological study can be used to connect possible wave events at the Southern Baltic coast with seismic events in this region. A comparative study of investigated areas from the southern coast of the Baltic Sea may help to solve this problem (Szczuciński, 2008). The research was funded by the National Science Centre of Poland.

## References

Bolle E., 1846 – *Ausführliche Beschreibung des gegenwärtigen Zustandes des Königlisch-Preussischen Herzogthums Vor- und Hinterpommern*, Stettin.

Brüggemann L.W., 1784 – *Ausführliche Beschreibung des gegenwärtigen Zustandes des Königlisch-Preussischen Herzogthums Vor- und Hinterpommern*, Stettin.

Credner R., 1889 – Über den "Seebär" der westlichen Ostsee von 16./17. Mai 1888. *Jahresber. D.Geogr. Ges. zu Greifswald*. R.3, 1886-1889.

Doss B., 1907 – Über ostbaltische Seebären. *Beiträge zur Geophysik*, t.8., 367-399

Mörner N.A., 2008 – Tsunami events within the Baltic, *Polish Geological Special Papers* 23, 71-76.

Nikonov A.A., 2004 – Evidence of paleotsunami in the Early holocene Lake Kunda (southern coast of the Gulf of Finland), *Doklady Earth Science* 396, 477-480.

Piotrowski A., 2007 – The influence of the neotectonics on historical events. In: *Niedermayer R.O. et al. (ed.) Geo-Pomerania, Szczecin, Geology cross-bordering the Western and Eastern European Platform, Excursion Guide, Biuletyn Państwowego Instytutu Geologicznego 424, 58-60.*

Rotnicki K., Czeniawska J., Muszyński A., Michalik J., 2008 – Fossil hollows at Rowy (Gardno-Łeba Coalstal Plain, Polish Middle Coast): evidence of an extreme storm surge or a meteorite impact in the Middle Holocene? Results of a preliminary study. In: *International Conference of Evironmental Impact of Tsunami*, September 25-28, 2008, Słubice, Poznań, Poland, 79–75.

Szczuciński W., 2008 – Potencjalne skutki geologiczne i środowiskowe tsunami na wybrzeżu Bałtyku. In: *Holoceńskie przemiany wybrzeży i wód południowego Bałtyku – przyczyny uwarunkowań i skutki* (ed. Rotnicki K., Jasiewicz J., Woszczyk M.) Poznań – Bydgoszcz.

INQUA Focus Group on Paleoseismology and Active Tectonics

paleoseismicity.org

# Searching for the offshore tsunamigenic layers from the Santorini related tsunami and the 1956 tsunami at Palaikastro, Crete to better understand tsunami parameters in the shores of Israel

*Qupty, Nairooz (1), Costas Synalokis (2), Alexander MacGillvray (3), Beverly Goodman Tchernov (1, 4)*

(1) Leon Charney School of Marine Sciences, Department of Marine Geosciences, University of Haifa, Mt. Carmel Israel 31905
Email: bgoodman@univ.haifa.ac.il
(2) Hellenic Center for Marine Research, Heraklion, Greece
(3) Palaikastro Excavations, British School at Athens, Greece
(4) Interuniversity Institute for Marine Sciences, Coral Beach, Eilat, Israel 88100

***Abstract:*** *In October 2011, a small geological sample collection was carried out offshore and onland at Palaikastros, Crete. Previously, tsuamigenic deposits were recognized in shallow (less than 30 m) upper shelf offshore deposits from Caesarea Maritima, Israel. At Palaikastros, Late Minoan period tsunamigenic layers were reported on coastal cliffs. Preliminary results from coring offshore these Santorinian tsunamigenic layers reveal two distinctive anomalous horizons. The deeper and older disturbance is most probably related to the Santorini eruption and the shallower disturbance may represent the 1956 AD tsunami event. These results are then compared to the coastal tsunamigenic findings to learn more about the offshore and onland preservation of the tsunamigenic layers. Using computer modeling, we will compare the characteristics of these layers to layers from the same events at Caesarea as a far-field comparison to better understand the coastal hazards in the eastern Mediterranean.*

***Key words****: tsunami, archaeology, sedimentology, micropaleontology.*

## BACKGROUND

According to previous studies and observations, we are aware that tsunami risk associated with earthquakes, offshore slumping, and volcanoes are present in the Mediterranean Sea. Computer modeling can evaluate the arrival times and the damages that such tsunamis can cause. However, those models are far more precise and useful when the parameters are securely anchored in field observations and data from sedimentological analysis of previous tsunamis (Synolakis et al., 2008). Our research focuses on two events: The 1956 AD tsunamigenic earthquake and the Santorini eruption of ~1600 BC and their sedimentological footprint both in Israel and Crete.

Previous studies along the coast of Palaikastro, eastern Crete (Fig. 1), have revealed preserved tsunami deposits in 9 m high cliffs (Bruins et al., 2008). The deposits are dated to the volcanic eruption of Santorini (~1600 BC), which was one of the largest eruptions in human antiquity (McCoy & Heiken, 2000). Cores collected offshore from Caesarea, Israel have revealed tsunami deposits contemporaneous to that same event (Goodman-Tchernov et al., 2009). The magnitude and inland inundation of this tsunami wave in Caesarea are unknown.

The 1956 AD tsunami left on-land deposits on Astypalaea Island, close to the seismic source in the Aegean Sea, about 100 km from Crete Island (Dominey–Howes et al., 2000). Only tide gauge recordings are available for the same event along the shore of Israel, as no known damages or sedimentological signature was left behind (Beisel et al., 2009).

For each event, there are variety of different data sets regarding source magnitude and far and near field tsunamigenic impacts and sedimentological remains. However, more data sets are needed in order to fully understand the characteristics and impacts of these events. The aim of this study is to use this information matrix, and add new insights from our investigations in Crete and Israel, to increase the understanding of these events and to improve numerical tsunsmigenic models.

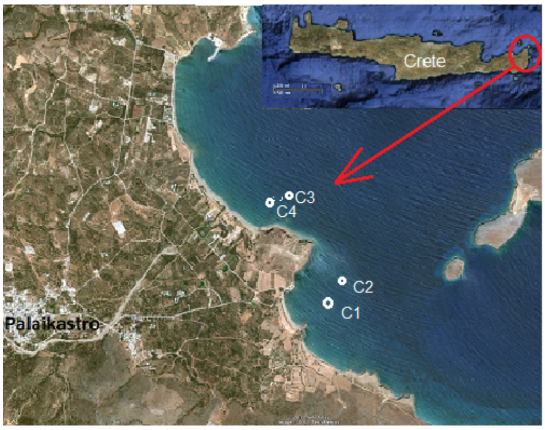


*Figure 1: Satellite view for Crete, Palaikastro, the area of study and the recently collected cores (marked with C1, C2, C3 and C4). The red rectangle indicates the general area of Palaikastros excavations.*

## RESEARCH QUESTIONS AND APPROACHES

In this research we aim to find answers to the following questions

1. Santorini event (~1600 BC):
   Can the run-up values, inundation heights, propagation area and the maximum wave height of tsunamis on the Israeli coastline be reconstructed by numerical modelling using data from offshore sediments both from near-field (Crete) and far-field (Israel) locations?

Approach: We will try to detect the tsunamigenic layers of the Santorini tsunami event in offshore Palaikastro cores. We will then compare between the characterization and structure of these layers to deposits from the same event found offshore of Caesarea by Goodman-Tchernov et al., 2009. Finally we will apply these additional parameters (in particular aspects of fluid dynamics and transport) of both places to tsunami models and compare to data from previous tsunami modelling.

2. What are the advantages of offshore paleotsunami studies compared to on-land studies? Are the tsunami deposits from the same event better preserved offshore than on-land in the same area?

Approach: To answer this, we will compare the thicknesses and the preservation conditions (character and composition of the sediment and the micro-fauna) of expected offshore tsunami deposits in Palaikastro cores from the Santorini event and the on-land preserved layer. Also, we will revisit the upper portions of previously analyzed offshore cores from Caesarea to determine if the small waves recorded from the 1956 AD event left any discernible sedimentological markers offshore.

3. What are the differences between the intensities of the tsunami waves reaching the Israeli coasts from different mechanisms? How does the magnitude of the trigger in the Aegean affect the level of damage of the Israeli coast in contrast to the effects on the Crete coasts?

Approach: We will determine if there is preservation for both of the events (the Santorini and the 1956 tsunami) in the cores from Palaikastro, and if so compare it to the terrestrial reports of the same events from previously reported Santorinian tsunamigenic deposits by Bruins et al., 2008 and newly collected onland samples. In addition, we will mine the Israeli sedimentological reports to see how these waves impacted sediments in Israel.

The results of this study will be used for numerical simulating, for the first time, of the tsunami wave inundation, run-up heights and behavior for the two events. Moreover, comparison between the coastal damages of these two events is useful as they both consist of source events in the Aegean followed by tsunamis in which the far-field impact includes the Israeli coastline, a useful far-field marker as it is at the easternmost extent of the Mediterranean. The trigger for each of the tsunami events is different but they were both considered exceptionally large events in the Mediterranean. The final aim of this study is to better understand Mediterranean related tsunami events, the deposit preservations, and possible coastal damages. This study will also help in improving tsunami models by providing field data to the numerical simulations.

## DATASETS AND METHODS

In search for the tsunamigenic layers, several indicators are expected to be found: a chaotic layer composed of different portions of grain sizes, while the other non-tsunamigenic layers made up of more typical upper-shelf sediments, in the case of this region, posidonia-bed, and sandy sediments as observed during this study.

A tsunami wave usually has two primary phases; overwash and backwash: seawater overcoming the shoreline and running into the terrestrial region and then reversing back to the sea. The specific character of the tsunami deposits depend on the circumstances of the individual areas, but the key component is the expectation of anomalous, allochtonous deposits which are chaotic and unique relative to the typical marine sediment sequence. It has also been observed in some cases that a tsunamigenic layer can have a thin top layer composed of clay size sediments. This 'mud cap' layer is the consequence of the decreased water energy after the backwash of the tsunami wave and sequential deposition of varying grain sizes in the resulting slowing of fluid flow (Dominey-Howes, 2004; Dominey-Howes et al., 2006; Scheffers & Kelletat, 2004; Goodman-Tchernov et al., 2009). Furthermore, inconformity is expected to be found between the tsunamigenic layer and the layer underneath it, since the latter is disturbed from the wave flow. This information will be obtained from the grain size analysis, and by studying the contacts between the distinctive layers (difference in the color, sharp contact, etc.). X-ray fluorescence (XRF) analysis will reveal the different elements derived from different sources (deep marine, near environment and coastal areas). This method is useful along with the grain size analysis to distinguish the chaotic layer.

In the tsunamigenic layer, the assemblage of the foraminifera is expected to be mixed and inappropriate relative to the position in which it is found. Foraminifera of different species have varying environmental preferences, dependent on particular water properties (temperature, depth, etc.). Therefore, in the tsunamigenic layer, it is anticipated that foraminifers of species which are indicative to specific range of water depths and/or environmental parameters will be found out of their typical living context, indicating transport. The most indicative foraminifera are the species that are more sensitive to the water properties and they are found in a narrow range of water depths. The indicative foraminifera are not only used for detecting the tsunamigenic layer, but also for determining the depth of influence of the tsunami wave which deposited the layer. In addition, another indicator is the preservation condition of the foraminifera; foraminifera in tsunamigenic layers are expected to be more broken, eroded, and perhaps exhibit a different size range (due to selective transport of different sizes) relative to those in non-impacted horizons, as the result of the wave power and the distance of transportation (Mamo et al., 2009).


*Figure 2: Core descriptions. The numbers on top of the cores describe the water depth where each core was collected. The green lines indicate the erosive bases of the chaotic layers. The red and black lines are respectively refer to the sampling location of the A and B cluster of foraminifera in figure 3.*

The study relies on both previously and recently collected and analyzed materials from Crete and Israel. Recognition of anomalous horizons, and their interpretation (whether storm, normal, or tsunami) is done based on a combined multi-proxy approach including micropaleontology (foraminifera primarily), granulometry, elemental analysis (XRF), and geoarchaeology (when archaeological deposits are present).

The samples are from offshore cores, coastal baulk grab samples, and excavation sample. In Caesarea, the sample sources available include previously analysed offshore cores, excavation subsamples, and newly collected coastline archaeological baulk sub-samples. In the autumn of 2011, sediment samples were collected from the coastal cliffs and cores offshore from the preserved tsunamigenic cliffs of Palaikastro, Crete (Fig. 1). Four cores of ~1 m were collected using manual hammering in the shallow continental shelf (~10 m b.s.l. at core 1, ~15 m b.s.l. at core 2, ~16 m b.s.l. at core 3 and ~8 m b.s.l. at core 4; Fig. 2).

The cores were split into two halves, one is being used for sampling and the other one is stored as archive. Half of the core that we decided to work with was photographed, logged and sub-sampled in 1 cm interval.

All the core portions, the coastal baulk samples and the excavation sample have been analyzed granulometry, mineralogically (with a binocular) and foraminifera is being picked in chosen intervals from all the cores, beach and bulk samples.

## PRELIMINARY RESULTS

According to the current results, we are able to distinguish chaotic layers from regular condition layers within the cores. The foraminifera assemblage of the chaotic layers seem to be larger, with a higher breakage and erosion percentage and more varied in comparison with foraminifera from the non-tsunamigenic layers (Fig. 3). Moreover, the grain size analysis of the cores show a clear grain size variation in the chaotic layers (course sand along with clay size sediments), more poorly sorted (higher standard deviation value) whereas the regular condition layers (which are mainly composed of silty sand sediments) are better sorted, with a much narrower grain size range (lower standard deviation).

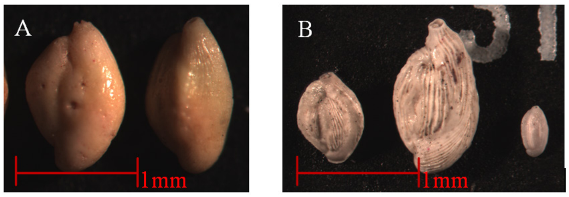


*Figure 3: A. Foraminifera photographed from core 1, from the "tsunamigenic" layer, 5 cm from the top of the core (Fig. 2). B. foraminifera from the same core but from a deeper (20 cm) "non-tsunamigenic" layer (Fig. 2). Foraminifers from the "tsunamigenic" layer are more eroded and have less distinctive ribbing.*

## DISCUSSION

Coring offshore ancient Palaikastro revealed two "chaotic deposits". The granulometry and micropaleontological analysis implemented so far support the assumption that these chaotic layers may be related to tsunami events. Storm events are eliminated since storm deposits leave numerous discrete layers and not a single chaotic homogenous layer (Morton et al., 2007). Perhaps the upper disturbance is related to the 1956 AD tsunami and the lower and deeper one is related to the Santorini eruption tsunami event (Fig. 2). Further information regarding the date of the "chaotic layers'" deposition, the complete micropaleontological information and elemental analysis will give a more clear understanding of the characteristics of these deposits.

**Acknowledgements:** Thanks are given for valuable field assistance to Y. Aluma, G. Lopez, P. Vavilis, K. Baika, & G. Dimitrios. The project is supported by Israel Science Foundation and Norman Kirscher.

## REFERENCES

Beisel, S., L. Chubarov, I. Didenkulova, E. Kit, A. Levin, E. Pelinovsky, Y. Shokin & M. Sladkevich, (2009). The 1956 Greek tsunami recorded at Yafo, Israel, and its numerical modeling. *Journal of Geophysical Research* 114(C9), 1-18.

Bruins, H., J.A. MacGillivray, C. Synolakis, C. Benjamini, J.K. Hanan, J. Kisch, A. Klügel & J. van der Plicht, (2008). Geoarchaeological tsunami deposits at Palaikastro (Crete) and the Late Minoan IA eruption of Santorini. *Journal of Archaeological Science* 35, 191-212.

Dominey-Howes, D.T.M., (2004). A re-analysis of the Late Bronze Age eruption and tsunami of Santorini, Greece, and the implications for the volcano-tsunami hazard. *Journal of Volcanology and Geothermal research* 130, 107-132.

Dominey-Howes, D.T.M., A. Cundy & I. Croudace, (2000). High energy marine flood deposits on Astypalaea Island, Greece: possible evidence for the A.D. 1956 southern Aegean tsunami. *Marine Geology* 163(1-4), 303-315.

Dominey-Howes, D.T.M., G.S. Humphreys & P.P. Hesse, (2006). Tsunami and palaeotsunami depositional signatures and their potential value in understanding the Late-Holocene tsunami record. *The Holocene* 16(8), 1095-1107.

Goodman-Tchernov, B.N., H.W. Dey, E.G. Reinhardt, F. McCoy & Y. Mart, (2009). Tsunami waves generated by the Santorini eruption reached Eastern Mediterranean shores. *Geology* 37(10), 943-946.

Mamo B., L.C. Strotz & D. Dominey-Howes, (2009). Tsunami sediments and their foraminiferal assemblages. *Eatrth-Science Reviews* 96, 263-278.

McCoy, F. & G. Heiken, (2000). Tsunami Generated by the Late Bronze Age Eruption of Thera (Santorini), Greece. *Pure and Applied Geophysics* 157, 1227-1256.

Morton, R.A., G. Gelfenbaum, B.E. Jaffe, (2007). Physical criteria for distinguishing sandy tsunami and storm deposits using modern examples. *Sedimentary Geology* 200, 184**e**207.

Scheffers, A. & D. Kelletat, (2004). Bimodal tsunami deposits – a neglected feature in paleo-tsunami research. *Coastline Reports* 1, 67-75.

Synolakis, C.E., E.N. Bernard, V.V. Trrov, U. Kanoglum & F.I. Gonzalez, (2008). Validation AND Verification of tsunami numerical models. *Pure and Applied Geophysics* 165, 2197-2228.

INQUA Focus Group on Paleoseismology and Active Tectonics

paleoseismicity.org

# Descriptive and kinematic analysis of fault damage structures around the N-S trending faults in Khajeh Morad leucogranite, southeastern Mashhad, NE Iran

*Sowreh Rezaei (1), Behnam Rahimi (2), Jin-Hyuck Choi (1), Young-Seog Kim (1)*

(1) Dept. of Earth & Environmental Sciences, Pukyong National University, Busan 608-737, South Korea. Email: Rsoureh@yahoo.com
(2) Dept. of Geology, Faculty of Sciences, Ferdowsi University of Mashhad, Mashhad-Iran.

***Abstract:*** *Descriptive and kinematic analyses of the N-S trending faults, within the batholith of Khajeh Morad Leucogranite in southeast of Mashhad city, NE Iran, were carried out based on fault damage model to understand the deformational characteristics of the study area. Various secondary structures, such as horsetail and pull-apart basin, are observed along the faults, indicating both right-lateral and left-lateral strike-slips. The fault reactivation with opposite slip senses is also supported by tree structures showing two sets of extensional fractures on both sides of a fault tip. The cross-cutting relationship between the two sets indicates that right-lateral strike-slip faults were inversely reactivated by left-lateral strike-slip movements. Also, there are some evidences of normal faulting; vertical offsets and slickenlines. This preliminary study indicates that the studied area had experienced at least three different stages of deformation. We argue that damage structures can be helpful to understand fault kinematics and deformation history, especially, in homogeneous rocks.*

***Key words****: Khajeh Morad leucogranite, fault damage zones, pull-apart structures, tree structure, reactivated faults.*

## INTRODUCTION

Fault damage zones are defined as deformed rock volumes where secondary structures have developed around faults to accommodate displacement along the faults (e.g. McGrath and Davison, 1995; Shipton and Cowie, 2003; Kim et al., 2003, 2004; Myers and Aydin, 2004). The geometries of damage structures can be good indicators to understand fault kinematics, such as slip sense. It is much useful, especially, for homogeneous rocks such as granite because there are no visible offset markers. Furthermore, multiple damage structures and their cross-cutting relationships can be used to infer deformation history and related paleo-stress regimes (Kim et al., 2001).

Structural discontinuities, such as bedding, fractures, and pre-existing faults, commonly acts as weak planes for slips by renewed stress build-up (e.g., Sibson, 1985; Morris et al., 1996). Thus fault reactivation can occur more easily along pre-existing discontinuities than making new faults (Scholz, 1998) if the principal stress conditions are well matched.

Fault damage zones can be mainly classified as wall-, linking- and tip-damage zones depending on their location along segmented faults (Kim et al., 2004).

Linking damage zone can be defined as the area with a high intensity of secondary structures between two fault segments. Linking damage zones can be sub-divided into extensional and contractional zones depending on the slip sense and stepping direction of faults. Pull-apart structures are a typical pattern of extensional linking damage zones (Kim et al., 2004).

Tip damage zone develops as a result of stress concentration at fault tips. Horsetail structure is one of the typical tip damage patterns, and they tend to form when slip dies out gradually toward the fault tip (Kim et al., 2000).

In this paper, we analyzed faults and their damage patterns in granite to understand the characteristics of faults and deformation history. Especially, we focused on geometric features of several sets of brittle deformation structures and cross-cutting relationships between them to understand kinematic characteristics of faults which had experienced multiple slip events.

## TECTONIC SETTING AND GEOLOGIC BACKGROUND

The main tectonic features in Iran result from the northward movement of Arabian plate (about 22 mm/yr) with respect to Eurasian plate. The Allah Dagh-Binalud mountain ranges, in NE Iran, partly accommodate this northward motion and, hence are a significant part of convergence tectonics involving thrust and strike-slip faults as well as folds (e.g., Shabanian et al., 2010).

The active tectonics of the NE Iran is characterized by NE dipping active reverse faults and NW trending right-lateral strike-slip to oblique-slip reverse faults (e.g., Shabanian et al., 2010). The seismicity around this area also indicates that the NE Iran is a seismically active region (Tatar et al., 2004; Fig. 1). Although the structural studies to understand deformation history and active tectonics are widely attempted, it is insufficient to characterize the tectonic of northeast Iran (Shabanian et al., 2009).

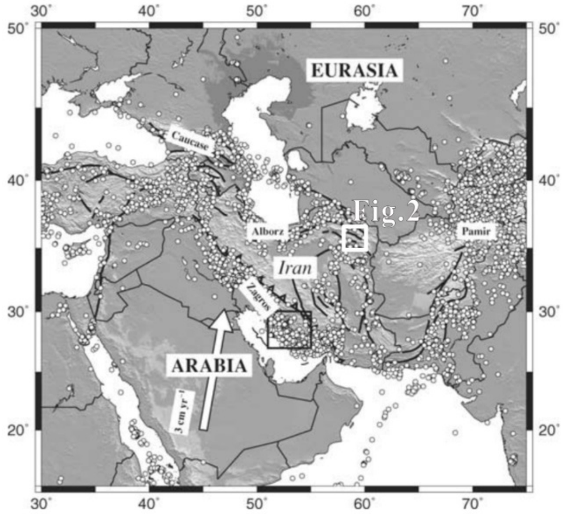


*Fig. 1: Tectonic and seismic map around Iran (Tatar et al., 2004). The arrow shows the Arabian motion relative to Eurasia, and the open circles are earthquakes (M>4.5) from the period between 1967 and 1998. See location of Fig.2 in the figure.*

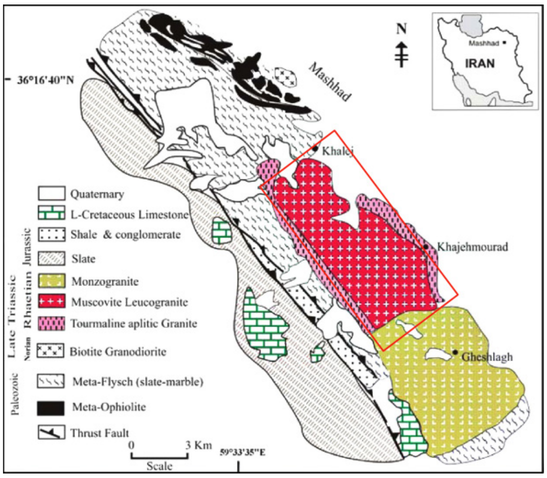


*Fig. 2: Simplified geological map around study area. The box indicates the study area (Kaimpour, 2009).*

Southeastern part of Mashhad city in northeast Iran, is composed of several Triassic to Cretaceous plutons. The study area is one of the main plutons NW-SE trending batholith, which is located between longitude of 59 ° 32 ′ E to 59 ° 41 ′ E and latitude of 36°7N to 36°13′N (Fig. 2). Karimpour et al. (2006) suggested that this granite belongs to syn-collisional S-type Granites, which intruded into the Paleo-Thetys remnants. Fig. 3b shows fracture map of the study area. Note that although several fracture sets developed within this pluton, the N-S trending fault and associated fractures are the most dominant structural features and they are clearly visible on satellite images (Fig. 3a).

## FIELD OBSERVATIONS

The trend of the major N-S faults in the study area is in the range from N10W to N20E, and dip to east. Various damage structures are observed at the tip and/or linkage zones of the N-S trending faults (Rezaei and Rahimi, 2011). The main descriptive features of the damage structures are as follows;

Firstly, horsetail fractures are very common at tips of N-S fractures, and they indicate both right-lateral (Fig. 4a) and left-lateral movements (Fig. 4b). Also, these indicate that the slips occurred under NE-SW and NW-SE trending $\sigma_1$ (maximum compressive stress). Note that the orientation of the extension fractures is commonly parallel with the maximum principal stress in the tectonic regime.

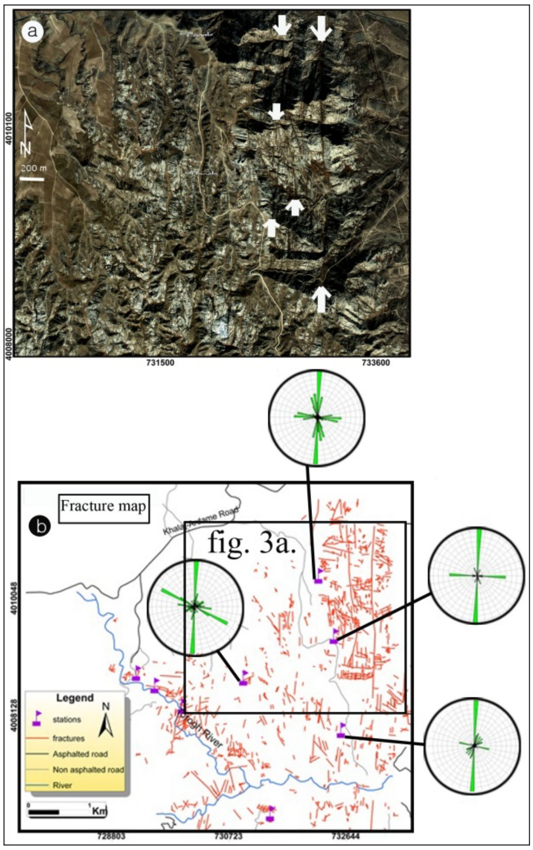


*Fig. 3: (a) Google Earth image of a part of study area. White arrows show the N-S liniments. (b) Fracture map of a part of the study area base on field data. Rose diagrams show the distribution of the fracture sets in the study area. See location of Fig.3 (a) in Fig.3 (b).*

Secondly, pull-apart structures are developed at the linking damage zones of N-S faults. In Fig. 4c, pull-apart structures including extensional fractures are observed in the right-steps between two fault segments. Also, several pull-aparts are filled with Quartz-Tourmaline minerals, and this is related with the opening of fractures. Thus, this can be interpreted as right-lateral strike-slip faults. In the contrast, as shown in Fig. 4d, extensional linking damage structures are also observed in the left-steps between two fault segments. This might indicate an evidence of left-lateral strike-slip movements, and hence, we suggest that the N-S trending faults underwent fault reactivation with opposite slip senses.

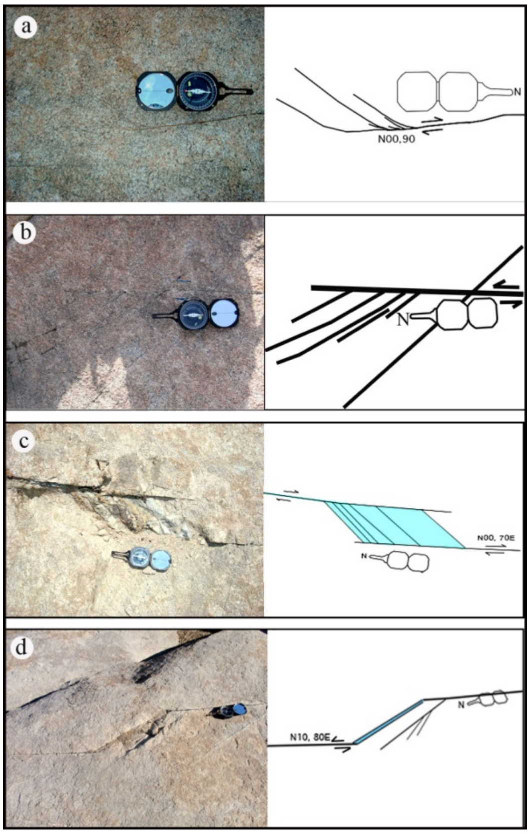


Fig. 4: Tip damage zones and linking damage zones along N-S faults. (a) Horsetail structures indicate right lateral movement along faults. (b) Horsetail structures indicate left-lateral movement. (c) Pull-apart structure indicates right-lateral movement along faults. (d) Pull-apart structure indicates left-lateral movement along faults (Quartz-Tourmaline minerals have filled pull-aparts).

Although horsetail structures are commonly developed at one side of a fault tip, sometimes two sets of horsetails with different orientations are observed at a fault tip. This is called as 'tree structure' and implies that the fault experienced reverse reactivation (Kim et al., 2001).

This is related with extensional fractures at tip damage zones which is mainly developed normal to the orientation of maximum tensile stress. Although almost damage structures indicate strong strike-slip movements along N-S faults (Fig.4), several structural elements on slip surfaces indicate that the faults also experienced normal faulting (Fig. 5). Note that vertical slip lineations and sub-horizontal slicken steps are obviously associated with normal faulting (Fig. 5a). Furthermore, geomorphic offsets show a visible throw related with normal faults (Fig. 5b). Thus, we suggest that the study area also experienced E-W trending extension.

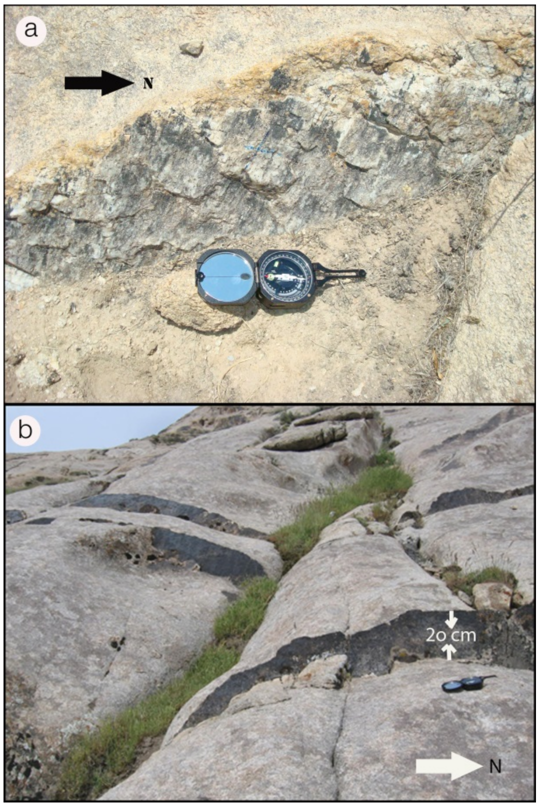


Fig. 5: (a) Slickensides of N-S faults. Slicken steps on the fault surface indicate normal faulting. (b) Clear throw along fault surfaces indicates normal movement along these faults.

## DISCUSSION

This study describes the damage patterns around the N-S trending faults in the study area, and the results indicate that there are three different slip events. In order to understand the deformation history and related paleo-stresses, we examined angular relationships between main faults and damage structures, and cross-cutting relationships between damage structures showing different orientations. Firstly, the NE-SW trending extension fractures have approximately 30° with the main faults, whereas the NW-SE trending extension fractures have about 60° (Fig. 6). Generally, secondary fractures commonly have an angular relationship of around 30 degree to main slip surfaces on non-deformed homogenous rocks (Fig. 6). However, the angle between main and secondary fractures can be various when slip occur in heterogeneous rocks or previously faulted rocks. Thus, we suggest that the NE-SW fractures may be developed at a relatively earlier deformation event. Secondly, two damage structures show cross-cutting relationship between them around the tree structures (Fig. 6).

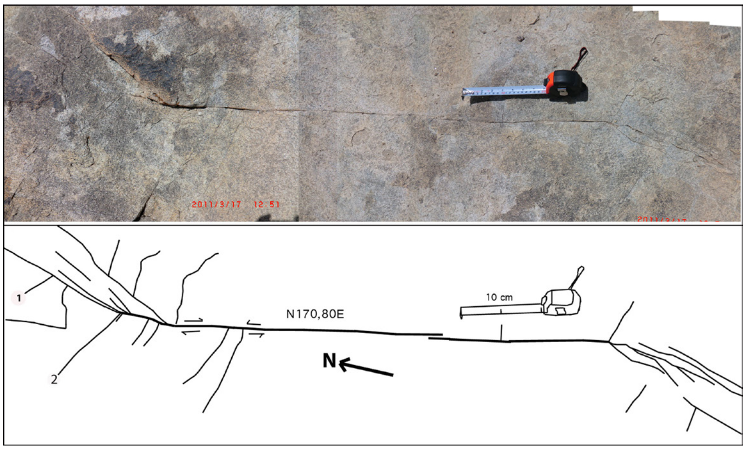


*Fig. 6. Tree structures at the tip of a N-S fault. These structures observed in this study area indicate both right-lateral and left-lateral movements along N-S faults (numbers indicate NW-SE trending fractures terminate against to the NE-SW fractures with approximately right angle).*

Some NW-SE trending fractures terminate against to the NE-SW fractures with approximately right angle. The stopping and termination of the NW-SE trending fractures against NE-SW fractures indicate their relatively ages between these two fractures. That is, the NW-SE trending fractures are developed later than the NE-SW fractures. Our results show that the tree structures are good indicators of deformation history as well as fault kinematics in this area.

## CONCLUSIONS

This study is a descriptive and kinematic analyses for preliminary study of the faults and their damage structures in homogeneous granite in southeast of Mashhad city, NE Iran. The kinematic analysis of the structural elements show that the N-S faults had experienced at least three different stages of fault movement. Particularly, tree structures, developed by reversely reactivated strike-slip faults, indicate that these faults underwent multiple slip events under different tectonic regimes.

It is not easy to interpret deformation history for multiply deformed faults on homogenous rocks because previous slip elements can be easily removed by latter slip events. This study mainly focused on descriptive and kinematic analyses of damage structures, and the results indicate that damage structures can give much information for slip history. Thus, we suggest that detailed analysis of damage zones can be very useful to understand fault kinematics as well as deformational history in any specific areas.

**Acknowledgements:** We thank all involved officials of Ferdowsi University who supported us to do this research. We also thank an anonymous reviewer for his or her constructive comments.

## References

Karimpour, M.H., (2009). Rb-Sr and Sm-Nd Isotopic Composition, U-Pb-Th (zircon) Geochronology and Petrogenesis of Mashhad Paleo-Tethys granitoids, *Ferdowsi University of Mashhad*, Iran (grant P/742-87/7/14).

Karimpour, M.H., L. Farmer, C. Ashouri, & S. Saadat., (2006). Major trace and REE geochemistry of paleo-Tethys Collision-Related Granitoids from mashhad,Iran. *Journal of Sciences of the Islamic Republic of Iran* 17 (2), 127-154.

Kim,Y.-S., J.R. Andrews & D.J. Sanderson, (2001). Reactivated strike-slip faults: example from north Cornwall, UK. *Tectonophysics* 304, 173-194.

Kim, Y.-S., D.C.P. Peacock & D.J. Sanderson, (2003). Mesoscale strike-slip faults and damage zones at Marsalforn, Gozo Island, Malta. *Journal of Structural Geology* 25, 793–812.

Kim,Y.-S., D.C. Peacock & D.J. Sanderson, (2004). Fault damage zones. *Journal of Structural Geology* 26, 503-517.

McGrath, A.G. & I. Davison, (1995). Damage zone geometry around fault tips. *Journal of Structural Geology* 17, 1011-1024.

Morris, J.S., C.D. Frith, D.I. Perrett, D. Rowland, A.W. Young, A.J. Calder & R.J. Dolan, (1996). A differential neural response in the human amygdala to fearful and happy facial expressions. *Nature* 383, 812-815.

Myers, R.D. & A. Aydin, (2004). The evolution of faults formed by shearing across joint zones in sandstone. *Journal of Structural Geology* 26 (5), 947-966.

Rezaei, S. & B. Rahimi, (2011). Preliminary analysis of fractures of Khajeh Morad leucogranite, south- east of Mashhad. *30th Conference of Earth Sciences, Geological Survey of Iran*, Tehran, Iran.

Scholz, C.H., (1998). Earthquakes and friction laws. *Nature* 391, 37-42.

Shabanian, E., O. Bellier, L. Siame, N. Arnaud, M.R. Abbassi & J.J. Cochemé, (2009). New tectonic configuration in NE Iran: Active strike-slip faulting between the Kopeh Dagh and Binalud mountains, *Tectonics* 28 (5), TC5002.

Shabanian, E., O. Bellier, M.R. Abbassi, L. Siame & Y. Farbod, (2010). Plio-Quaternary stress states in NE Iran: Kopeh Dagh and Allah Dagh Binalud mountain ranges *Tectonophysics*, 480, 280–304.

Shipton, Z.K. & P.A. Cowie, (2003). A conceptual model for the origin of fault damage zone structures in high-porosity sandstone, *Journal of Structural Geology* 25, 333-344.

Sibson, R. H., (1985). A note on fault reactivation. *Geology* 7, 751-754.

Tatar, M., Hatzfeld, D. & M. Ghafory-Ashtiany, (2004). Tectonics of the Central Zagros (Iran) deduced from microearthquake seismicity. *Geophysical Journal International* 156, 255-266.

# 4-D ruptures histories of major plate boundary faults: A view into long-term fault behavior and fault interaction

*Rockwell, Thomas (1), Neta Wechsler (2), Koji Okumura (3)*

(1) Geological Sciences, San Diego State University, San Diego, CA 92182. Email: trockwell@geology.sdsu.edu
(2) Dept. of Geophysics and Planetary Sciences, Tel-Aviv University, Tel Aviv 69978, Israel. Email: netawe@post.tau.ac.il
(3) Graduate School of Letters, Hiroshima University, 1-2-3 Kagamiyama, Higashi-Hiroshima, 739-8522, Japan. Email: kojiok@me.com

***Abstract***: *Long paleoseismic records from three major plate boundaries, the complex southern San Andreas fault system of southern California, the Dead Sea Transform in the Levant, and the North Anatolian fault in Turkey, provide insights into long-term rupture behavior of plate boundary fault systems as a function of fault zone complexity. Large earthquakes on the San Jacinto, San Andreas and Imperial faults of southern California exhibit evidence for mode-switching between earthquake clusters and more periodic behavior. Similarly, the Dead Sea Transform, where the fault transitions from a simple to a complex system in northern Israel, exhibits clusters of moderate earthquakes interspersed with large earthquakes with large displacements, followed by periods of quiescence. In contrast, the simple (single-stranded) central portion (1944 rupture segment) of the North Anatolian fault exhibits both characteristic and periodic behavior whereas the western, multi-stranded section of the NAF exhibits more variability in terms of earthquake timing. These differences in rupture behavior are attributed to fault and stress interaction in complex fault systems versus relatively simple loading and strain release in the simple example.*

***Key words***: *paleoseismology, fault behaviour, fault and stress interaction*

## INTRODUCTION

Understanding long-term behavior of earthquakes is the key to forecasting future large seismicity, as well as to understanding fundamental processes that govern large earthquake production along plate boundary faults. There are fundamental assumptions that go into the models used to forecast future seismicity, although some assumptions about the behavior of faults and fault systems are contradictory, such as that they behave in a periodic fashion (Reid, 1911; Bakun and McEvilly, 1984), that they have characteristic ruptures (Schwartz and Coppersmith, 1984; Sieh, 1996), or that their behavior is variable in time and space (Field and Page, 2011; Weldon et al., 2004). These assumptions are often made from insufficient observations, due in part to the relatively short time passed since the advent of instrumental seismology, and in part to the incomplete (in time and space) record than can be gleaned from longer-term sources such as historical texts or paleoseismic records. For example, in areas where long historical records exist, and where earthquake geology and paleoseismology are combined with archeology, it may be possible to determine earthquake production, and potentially slip and slip distribution, through many earthquake cycles. Here, we present a summary of observations from several paleoseismic sites with long records, and argue that simple faults behave differently than complex fault systems.

## OBSERVATIONS FROM THE SAN ANDREAS AND SAN JACINTO FAULTS

*The Complex Fault System of Southern California*

The San Andreas fault system in southern California is complex, with multiple parallel strands distributed across a broad plate boundary (Figure 1). The San

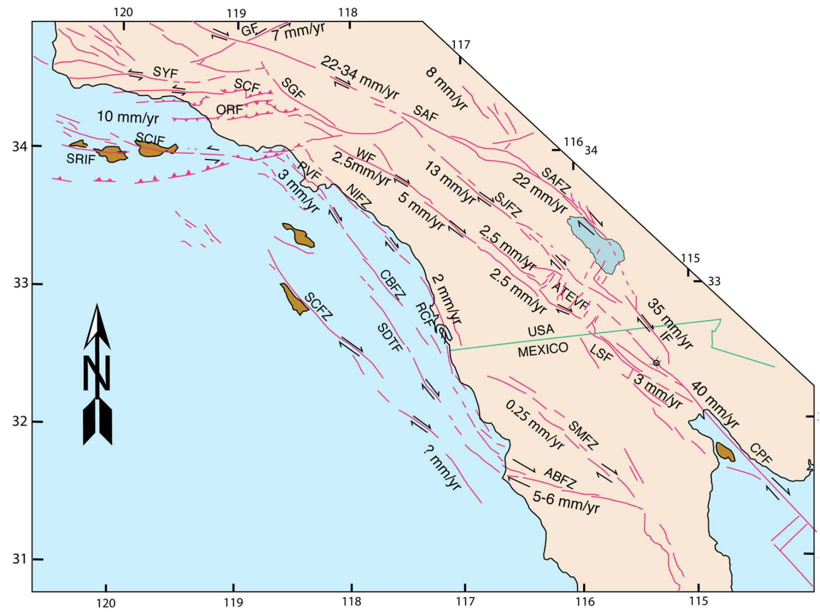


*Figure 1. Map of southern California faults associated with the southern San Andreas fault system, with slip rates. SAF = San Andreas fault, SJF = San Jacinto fault. All other abbreviations are standard for southern California.*

Andreas, San Jacinto and Imperial faults accommodate the majority of plate boundary slip (Rockwell et al., 1990; Fialko, 2006; Bennett et al., 2004), but these still only account for about 60-70% of the total relative motion between the Pacific and North American lithospheric plates, with the balance being on other nearby faults. Consequently, rupture on one fault will produce changes in the state of stress on other, nearby faults (Harris and Simpson, 1992; Stein et al., 1992; 1994; Harris and Day, 1993; King et al., 1994).

The southern San Andreas, San Jacinto and Imperial faults are three of the best-studied faults in the world in terms of their paleoseismology, with over 30 paleoseismic sites in the Salton Trough area alone. Figure 2 shows the earthquake ages and their probability distributions for sites along the central San Jacinto fault,

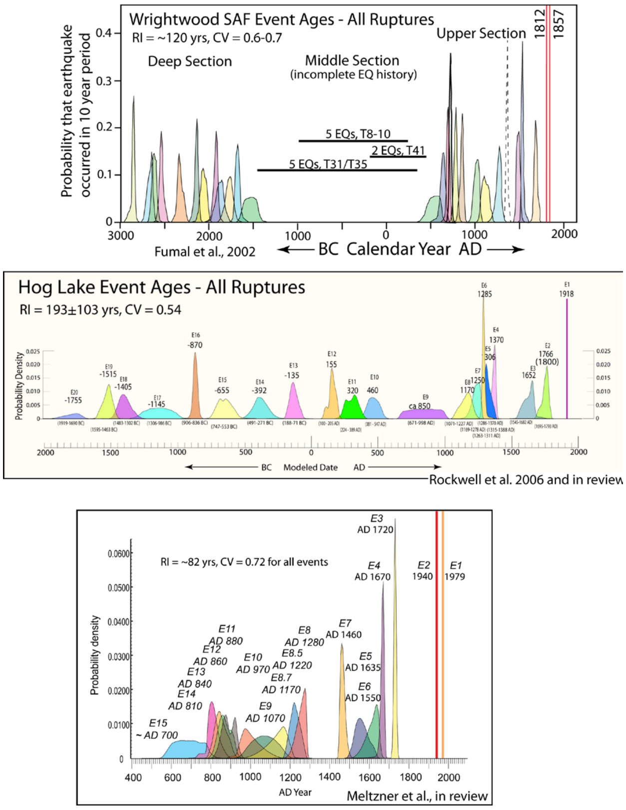


*Figure 2. Probability functions for earthquake ages from the San Andreas fault at Wrightwood (upper record; Fumal et al., 2002), the San Jacinto fault at Hog Lake (middle record; Rockwell et al., 2006 and in review), and the Imperial fault at Dogwood Road (Tsang, 2011).*

the south-central San Andreas fault and the Imperial fault. Note that the coefficient of variation (CV) is relatively high (0.4-0.6) at all sites, when averaged over at least 15 or more earthquakes, and that there are clusters or periods of enhanced earthquake activity when earthquake production appears elevated.

Similarly, the Dead Sea Transform (DST) in the Middle East (Figure 3) shows clustering and exhibits a high CV for the past two millennia (Figure 4) where the fault transitions form a simple plate boundary to the south and a complex boundary to the north in Lebanon and Syria.

In contrast, the simple portion of the North Anatolian fault in north central Turkey appears to behave in a much more characteristic and periodic fashion, whereas the complex western part has a more irregular behavior (Figure 5). The fault zone extends for over 1200 km from eastern Turkey westward to the Aegian Sea. Near Bolu at the western end of the 1944 rupture, the fault splays into multiple branches that extend westward to the Aegian Sea. Thus, the western part of the fault zone is complex, with multiple strands, similar to the San Andreas system in California. Earthquake recurrence along this western section is irregular (Rockwell et al., 2009), with a CV of 0.48 for the 1912 rupture segment near the Gulf of Saros in the Aegean Sea.

However, the central section of the North Anatolian fault is expressed as a narrow single-active trace which ruptured in 1944 as part of a sequence of large earthquakes (Kondo et al., 2005; Okumura et al., in prep.). There are no other parallel faults within two hundred kilometers with which to interact, so the only static stress changes from nearby earthquakes are from adjacent segments along strike, hence resulting in a sequence of closely timed events in the past century. The central segment has ruptured six times in the past 1600 years with remarkably similar displacement per event at regularly spaced time intervals, within uncertainty (Kondo et al., 2009; Rockwell et al. 2010; Okumura et al., in prep.). The CV for slip is around 0.1 for the past five events, whereas for timing for the past six events, it is about 0.17, much smaller than from either

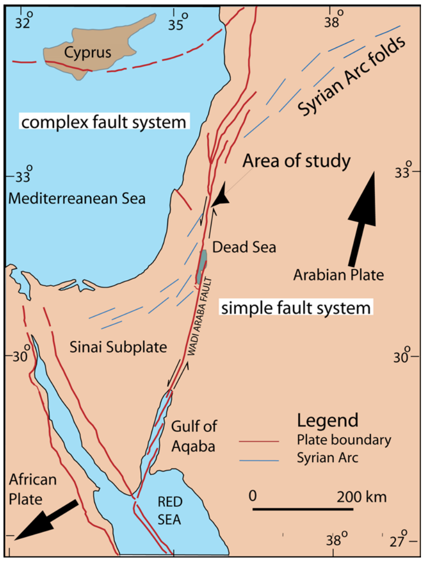


*Figure 3. Map of the Dead Sea Transform in the Middle East. Note the simple fault geometry between the Gulf of Aqaba and the Sea of Galilee (study area), versus multiple strands to the north.*

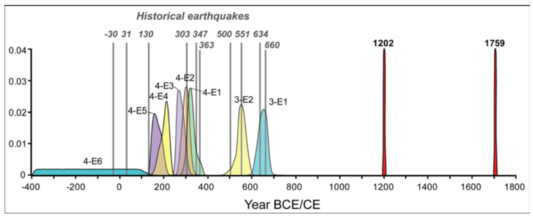


*Figure 4. Probability functions for earthquake ages at the Beteiha site in northern Israel (Wechsler et al. in prep).*

the complex part of the NAF, the southern San Andreas, San Jacinto or Imperial faults, or the Dead Sea fault, at least for the past 1500 years. These observations argue for structural control as a factor in earthquake recurrence.

## DISCUSSION AND CONCLUSIONS

Paleoseismic records were presented from complex fault systems in southern California (San Andreas fault system), Israel (Dead Sea Transform) and western Turkey (North Anatolian fault), and compared to the record from the simple central section of the North Anatolian fault in north central Turkey. By a complex system, we mean that there are multiple parallel or intersecting faults that have sufficiently high slip rates to interact at the timeframe of the earthquake cycle. In southern California, this criterion is met for the San Andreas system from the

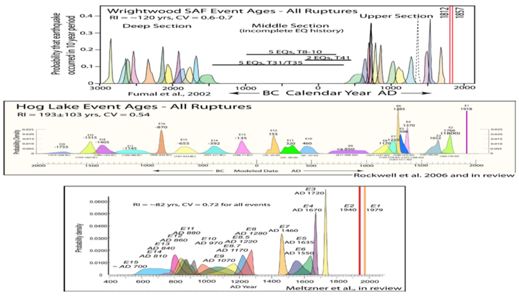


*Figure 5. Probability functions for earthquake ages from the western, more complex section of the North Anatolian fault near the Gulf of Saros along the 1912 rupture (Rockwell et al., 2009) and from along the 1944 rupture east of Gerede (Rockwell, 2010, Okumura et al., in prep.) where the fault is essentially a single strand. Note the much more periodic distribution of earthquakes along the simpler central section of the NAF.*

Transverse Ranges southward into Mexico. In fact, there are both parallel faults strands with significant slip rates and intersecting faults, making the southern California system particularly complex. Similarly, the western part of the North Anatolian fault system has parallel fault strands west of Bolu, with the majority of strain accumulation apparently on the northern trace, but with significant slip on other traces as well (McClusky et al., 2003; Reilinger et al., 2006). For these complex fault systems, earthquake recurrence is irregular, with a coefficient of variation that is close to or exceeds 0.5. The CV for the Wrightwood record is about 0.7, but this may be influenced by being in an overlap zone between 1857-type earthquakes and those that break predominantly to the south. The Hog Lake site is within the Anza seismicity gap, which is generally considered a strong section, or asperity, along the fault, and although overlap from earthquakes to the north is possible, they are more likely to be moderate events, as occurred in 1918. Here, the CV is about 0.5 for the entire 4000 year-long record. In contrast, the 1944 segment along the North Anatolian fault in north-central Turkey appears to also produce similar displacements from event to event (characteristic, CV = 0.1) but at fairly regular intervals in time (CV = 0.17). The principal difference in fault system architecture is that all of the geodetic strain accumulation is attributed to this narrow, highly localized, single-stranded fault. This leads to the hypothesis that simple faults may be much better "behaved" in terms of large earthquake recurrence, whereas complex systems interact at the time frame of the loading cycle.

The above examples can be used to argue for fairly characteristic behavior along these major plate boundary strike-slip faults. However, regularity of earthquake timing appears to be much more complicated, with complex fault systems experiencing much more variability than the simple north-central section of the North Anatolian fault. These observations suggest that fault interaction likely interferes with quasi-periodic recurrence along faults.

The most likely mechanism for fault interaction is coulomb stress loading. Rupture on one fault will change the static stress on nearby faults (Harris and Simpson, 1992; Stein et al., 1992; 1994; Harris and Day, 1993; King et al., 1994; Parsons, 2005). For end-to-end segments, there is a large increase in stress at the rupture tip, and this mechanism is believed to be responsible for the sequential ruptures along the North Anatolian fault from 1939 to 1999 (Stein et al., 1997; Parsons et al., 2000; Parsons, 2004). It is also the reason that Istanbul is now considered at elevated risk from a large earthquake, as the Marmara Sea remains the only un-ruptured portion of the fault zone for the past 250 years.

Large earthquakes also affect the state of stress along adjacent faults at certain distances and azimuths, and can either increase or decrease coulomb stress depending on the relative locations of the ruptured and un-ruptured faults, and the sense and amount of displacement in the earthquake. It is this mechanism that may affect the timing of large earthquakes on a fault.

For instance, if the central San Jacinto fault is close to failure and a large 1857-type earthquake on the San Andreas were to occur, this would have the effect of decreasing coulomb stress on the San Jacinto fault, and perhaps delaying the expected earthquake by a decade or two. Similarly, a large earthquake on the southernmost San Andreas may cause additional loading on the parallel San Jacinto fault, thereby advancing the timing and causing rupture before the "expected" event.

Another factor is the action of cross-faults that intersect a master fault at a high angle (Nicholson et al., 1986). The Superstition Hills earthquake (1987, M6.6) is believed to have been triggered by the Elmore Ranch event (1987, M6.2), which occurred about 11 hours earlier on a perpendicular cross fault (Hudnut et al., 1989). The cross-fault rupture produced a significant decrease in normal stress on the Superstition Hills fault, essentially unclamping the fault (Hudnut et al., 1989).

In conclusion, if simple fault systems behave in a more predictable manner than complex systems, both in terms of timing and displacement, then it seems reasonable that much could be learned by modeling the behavior and interaction of faults in a complex system by assuming relatively simple physics that may be common to all of the faults that comprise the system. Clearly, more examples of long, well-constrained earthquake sequences are need to test this idea, but if simple faults do behave in a predictable fashion, it may provide a pathway to more accurate earthquake forecasting in regions of complex fault systems, such as in southern California where the combination of high strain rates and dense population lead to high seismic risk.

## References


Bakun, W.H., & T.V. McEvilly, (1984). Recurrence Models and Parkfield, California, Earthquakes, *Journal of Geophysical Research* 89 (B5), 3051-3058.

Bennett, R.A., A.M. Friedrich, & K.P. Furlong, (2004). Codependent histories of the San Andreas and San Jacinto fault zones from inversion of fault displacement rates, *Geology* 32 (11), 961-964.

Fialko, Y., (2006). Interseismic strain accumulation and the earthquake potential on the southern San Andreas fault system, *Nature* 441, 968-971.

Field, E.H. & M.T. Page, (2011). Estimating earthquake-rupture rates on a fault or fault system, *Bulletin of the Seismological Society of America* 101, 79-92.

Fumal, T.E., R.J. Weldon II, G.P. Biasi, T.E. Dawson, G.G. Seitz, W.T. Frost & D.P. Schwartz, (2002). Evidence for large earthquakes on the San Andreas fault at the Wrightwood, California, paleoseismic site: A.D. 500 to present, *Bulletin of the Seismological Society of America* 92 (7), 2726-2760.

Harris, R.A. & R.W. Simpson, (1992). Changes in static stress on southern California faults after the 1992 Landers earthquake, *Nature* 360, 251-254.

Harris, R.A. & S.M. Day, (1993). Dynamics of fault interaction: Parallel strike-slip faults, *Journal of Geophysical Research* 98 (B3), 4461-4472.

Hudnut, K.W., L. Seeber, & J. Pacheco, (1989). *Geophysical Research Letters* 16, 199-202.

King, G.C., R.S. Stein, & J. Lin, (1994). Static stress changes and the triggering of earthquakes, *Bulletin of the Seismological Society of America* 84 (3), 935-953.

Kondo, H., Y. Awata, O. Emre, A. Dogan, S. Ozalp, F. Tokay, C. Yildrim, T. Yoshioka, & K. Okumura, (2005). Slip distribution, fault geometry, and fault segmentation of the 1944 Bolu-Gerede earthquake rupture, North Anatolian fault, Turkey, *Bulletin of the Seismological Society of America* 95 (4), 1234-49.

Kondo, H., V. Ozaksoy, & C. Yildrim, (2009). Slip history of the 1944 Bolu-Gerede earthquake rupture along the North Anatolian fault system—Implications for recurrence behavior of multi-segment earthquakes, *Journal of Geophysical Research*, accepted, October, 2009.

McClusky, S., R. Reilinger, S. Mahmoud, D. Ben Sari, & A. Tealeb, (2003). GPS constraints on Africa (Nubia) and Arabia plate motions, *Geophysical Journal International* 155 (1), 126-138.

Nicholson, C., L. Seeber, P. Williams, & L.R. Sykes, (1986). Seismicity and fault kinematics through the eastern Transverse Ranges, California: Block rotation, strike-slip faulting and low-angle thrusts, *Journal of Geophysical Research* 91 (B5), 4891-4908.

Okumura, K., T.K. Rockwell, N. Wechsler & S. Akciz, (2013, in prep.). Periodic and characteristic earthquakes on a simple fault: An example from the North Anatolian fault in Turkey. *For Bulletin of the Seismological Society of America*.

Parsons, T., (2004). Recalculated probability of M≥7 earthquakes beneath the Sea of Marmara, Turkey. *Journal of Geophysical Research* 109, B05304.

Parsons, T., A. Barka, S. Toda, R.S. Stein & J.H. Dieterich, (2000). Influence of the 17 August 1999 Izmit earthquake on seismic hazards in Istanbul, *in A. Barka, O. Kozaci, S. Akyuz and E. Altunel (Eds.), The 1999 Izmit and Duzce Earthquakes: Preliminary results, pp. 295-310, 2000.*

Parsons, T., (2005). Significance of stress transfer in time-dependent earthquake probability calculations. *Journal of Geophysical Research* 110, B05S02.

Reid, H.F., (1911). *The Mechanics of the Earthquake, The California Earthquake of April 18, 1906*, Report of the State Investigation Commission, Vol.2, Carnegie Institution of Washington, Washington, D.C.

Reilinger, R., S. McClusky, P. Vernant, S. Lawrence, S. Ergintav, R. Cakmak, H. Ozener, F. Kadirov, I. Guliev, R. Stepanyan, M. Nadariya, G. Hahubia, S. Mahmoud, K. Sakr, A. ArRajehi, D. Paradissis, A. Al-Aydrus, M. Prilepin, T. Guseva, E. Evren, A. Dmitrotsa, S. V. Filikov, F. Gomez, R. Al-Ghazzi, & G. Karam, (2006). GPS constraints on continental deformation in the Africa-Arabia-Eurasia continental collision zone and implications for the dynamics of plate interactions, *Journal of Geophysical Research*, *111*, 1-26.

Rockwell, T.K., C. Loughman, & P. Merifield, (1990). Late Quaternary rate of slip along the San Jacinto fault zone near Anza, southern California: *Journal of Geophysical Research* 95, 8593-8605.

Rockwell, T., G. Seitz, T. Dawson, & J. Young, (2006). The long record of San Jacinto fault paleoearthquakes at Hog Lake: Implications for regional strain release in the southern San Andreas fault system. *Seismological Research Letters* 77 (2), 270.

Rockwell, T., D. Ragona, G. Seitz, R. Langridge, A. Barka, E. Aksoy, G. Ucarkus, B. Akbalik, D. Satir, A. Meltzner, Y. Klinger, M. Meghraoui & M. Ferry, (2009). Paleoseismology of the North Anatolian Fault near the Marmara Sea: Implications for Fault Segmentation and Seismic Hazard. Reicherter, K., Michetti, A.M. and Silva, P.G. (eds) *Paleoseismology: Historical and Prehistorical Records of Earthquake Ground Effects For Seismic Hazard Assessment*. *The Geological Society of London Special Publications,* 316**,** 31-54.

Rockwell, T., (2010). The non-regularity of earthquake recurrence in California: Lessons from long paleoseismic records in simple versus complex regions. Eos, Transactions, American Geophysical Union, 91, presented at 2010 Fall Meeting, AGU, San Francisco, California.

Rockwell, T., G. Seitz, J. Young & T. Dawson, (2013, in rev.). A 4000 year record of surface ruptures along the central San Jacinto fault at Hog Lake: Mode switching between irregular recurrence and quasi-periodicity, *Bulletin of the Seismological Society of America*.

Schwartz, D.P. & K.J. Coppersmith, (1984). Fault behavior and characteristic earthquakes: Examples from the Wasatch and San Andreas fault zones, *Journal of Geophysical Research* 89, 5681-5698.

Sieh, K., (1996). The repetition of large-earthquake ruptures, Proceedings of the National Academy of Sciences 93, 3764-71.

Stein R.S., G.C.P. King & J. Lin, (1992). Change in failure stress on the southern San Andreas fault system caused by the 1992 Magnitude = 7.4 Landers earthquake. *Science* 258, 1328-1332.

Stein R.S., G.C.P. King & J. Lin, (1994). Stress triggering of the 1994 M = 6.7 Northridge, California, earthquake by its predecessors, *Science* 265, 1432-1435.

Stein R.S., A.A. Barka & J.H. Dieterich, (1997). Progressive failure on the North Anatolian fault since 1939 by earthquake stress triggering, *Geophysical Journal International* 128, 594-604.

Tsang, R., T.K. Rockwell, A.J. Meltzner & P.M. Figueiredo, (2011). Toward development of a long rupture history of the northern Imperial fault in Mesquite basin, Imperial County, southern California. Thesis paper on file in Dept. of Geological Sciences, San Diego State University, 51 p.

Wechsler, N., Rockwell, T.K., Marco, S., and Agnon, A., 2013 in prep for BSSA, Surface rupture history of the Dead Sea Transform in Beteiha Valley: irregular earthquake recurrence for the past two millennia.

Weldon, R.J., K.M. Scharer,T.E. Fumal, and G.P. Biasi, (2004), GSA Today, v. 14, 4.

INQUA Focus Group on Paleoseismology and Active Tectonics

paleoseismicity.org

# Earthquake Archaeological Effects (EAEs) triggered by the Middle Age Catalonian seismic crisis in the Romanesque heritage (NE Spain)

*M.A. Rodríguez-Pascua (1), M.A. Perucha, (1), P.G. Silva (2), R. Pérez-López (1), J.L. Giner-Robles (3), F. Martín-González (4).*

(1) Instituto Geológico y Minero de España. C/ Ríos Rosas, 23. 28003-Madrid, Spain. Email: ma.rodriguez@igme.es
(2) Dpto. Geología. Escuela Politécnica Superior de Ávila. Univ. Salamanca. 05003-Ávila, Spain
(3) Dpto. Geología. Facultad de Ciencias. Univ. Autónoma de Madrid. Cantoblanco. Tres Cantos, Madrid, Spain
(4) Área de Geología. ESCET. Univ. Rey Juan Carlos. C/ Tulipán, s/n. Móstoles, 28933 Madrid, Spain

***Abstract:*** *during the 15th century several earthquakes struck Catalonia (NE Spain) triggering important damage in the main "Romanesque Buildings" of the zone. The three main events had intensities between VIII and IX (EMS-98), and occurred during a time-interval of 2 years (1427-1428 AD). The most destructive event was the last one on February 1428 AD (Camprodón, IX). The epoch documents of monasteries and convents offer relevant information on the occurred damage affecting these religious buildings and nowadays it is possible to observe earthquake archeological effects (EAEs) in the Romanesque heritage of the zone. This work deals with the analysis of the preserved EAEs by means of the application of structural geology analysis. The performed analysis indicates a directionality of the seismic ground motion consistent with the location of the Camprdón meizoseismic epicentre. This orientation could be useful in future intervention/restoration works on the Catalonian Romanesque heritage.*

***Key words**: Earthake Archaeologica Effects (EAEs), Middle age, Romanesque heritage, NE Spain.*

## INTRODUCTION

One of the most important seismic crises during historic times in Catalonia (NE Spain) occurred during the years 1427-1428, with three main earthquakes: Amer (1427/03/19; I=VIII), Olot (1427/ 05/15; I=VIII) and Camprodón (1428/02/2; I=IX) (Fig. 1). The historical chronicles describe important destruction in the region especially that related to the Camprodón event (Olivera et al., 2006). Using this information and revisiting the

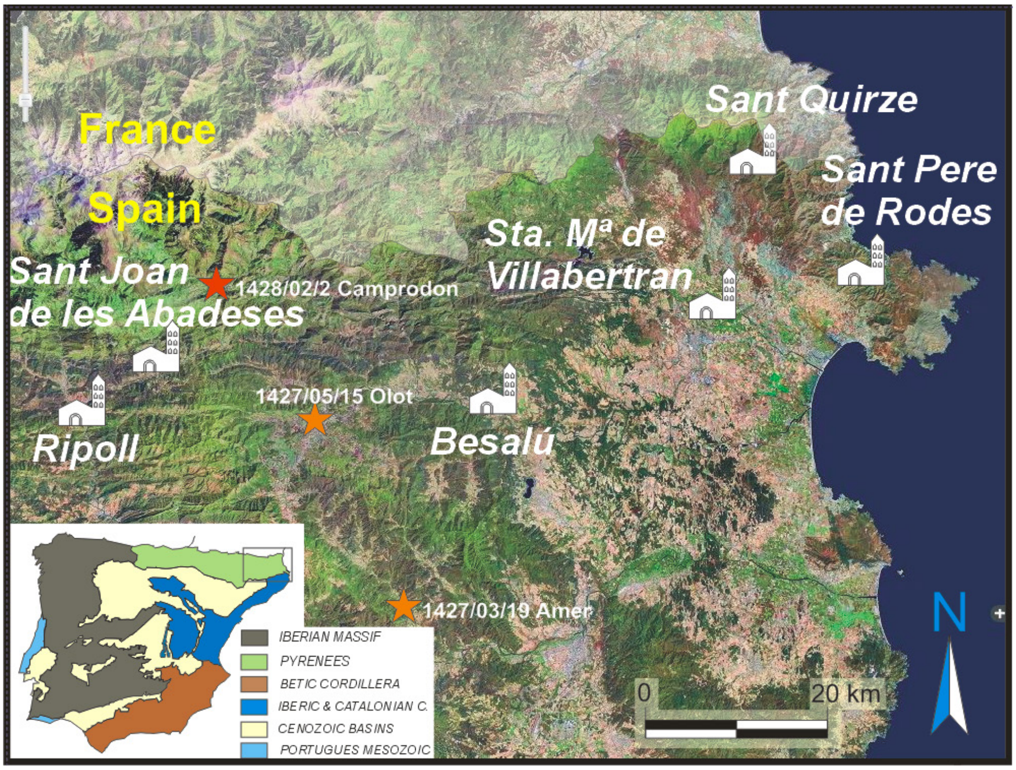


*Fig. 1: Geographic location of the meizoseismic area of the Middle Age Catalonian crisis. The stars represent the epicenters of the historic earthquakes (EMS98 intensity: VIII for the orange star and IX for the red star). The cities and Romanesque churches represent the locations of EAEs identified in this work.*

Romanesque heritage of the meizoseismic zone, we had compiled a set of Earthquake Archaeological Effects (EAEs) according to the classification of Rodríguez-Pascua et al. (2011). The seismogenic source of this seismic series has been related with the NW-SE Amer Fault by Perea et al. (2012). Following these authors the three main earthquakes are aligned on the fault trace and their timing sequence migrated from SE to NW.

## EAEs IN THE ROMANESQUE HERITAGE AND STRUCTURAL ANALYSIS

We have analyzed different EAEs preserved in the Middle Age buildings (Romanesque style) of the area. These buildings were affected by at least one of the historical earthquakes of the analyzed seismic series. The application of conventional of structural geology analyses to EAEs (e.g. Giner et al., 2009, 2011, 2012; Rodríguez-Pascua et al., 2012) result on preferred trajectories and directions of ground motion during the earthquake. In the following paragraphs we describe the different EAEs induced by the Camprodón earthquake (1428 AD) grouped by towns and/or monasteries:

*Sant Joan de les Abadeses Abbey*: Located 11 km SW of the meizoseismic epicenter (Fig. 1), the main apse and the old hostel of the monastery were destroyed by the earthquake, but rebuilt after that. Nowadays it is possible to observe several EAEs inside of the church such as, dipping broken corners, displaced masonry blocks and tilted walls. All of these EAEs are compatible with a NW-SE seismic ground motion at N175ºE.

*Ripoll Monastery*: Located 19 km SW of the epicenter (Fig. 1), was seriously damaged by the earthquake. The vault of the main nave and the western bell tower collapsed during the earthquake. The analyzed data indicate that the main ground motion direction was near-perpendicular to the N40ºE orientation of the main nave of the church, therefore NW-SE at N130ºE.


*Fig. 2: Displaced masonry blocks in Sant Vicent Church (Besalú): A) displaced and repaired masonry blocks in the rose window of the apse and B) close view of the displacement.*

*Besalú*: it is a beautiful medieval town, plenty of Romanesque monuments located at 30 km SE of the epicentre. In this town we have studied six buildings (religious and civil), but the most interesting examples of EAEs are recorded in the Sant Vicent Church, where penetrative fractures in masonry blocks, dipping broken corners and displaced masonry blocks (Fig. 2) are observed. This set of EAEs is compatible with a NE-SW seismic ground motion at N045ºE. Other interesting site is the ruins of the Pujada de Santa María Church, where restored dropped key stones in the window of the main apse are nicely preserved today (Fig. 3). This EAE is compatible with a similar ground motion direction at N164ºE. The rest of the EAEs recorded in this Medieval town are fairly bracketed between these two reported orientations.

*Fig. 3: Dropped and repaired key stones in the window of the main apse of the Pujada de Santa María Church (Besalú).*

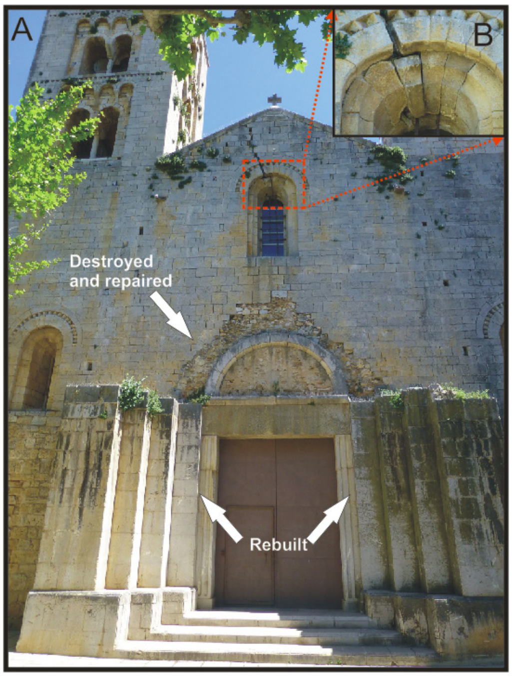


*Fig. 4: EAEs of the Canonica de Santa María de Vilabertrán: A) main facade of the monastery and B) close view of the dropped key stone of the window.*

*Canonica de Santa María de Villabertrán*: This monastery, located 50 km east of the epicentre displays an interesting collection of EAEs. The main gate of the church was destroyed and repaired after de earthquake (Fig. 4A). The window located in this same frontal facade shows displaced masonry blocks, dropped key stones (Fig. 4B) associated to a large crack running towards the roof of the building. These EAEs are large penetrative strain structures and it is possible to observe them inside of the church. In the cloister of this building are also preserved repaired arches and displaced masonry blocks. In the NW wall of the refectory the key stones of a window were horizontally displaced (Fig. 5). This set of EAEs is compatible with a NW-SE ground motion of N165ºE.

*Fig. 5: Key stones displaced horizontally in the refectory of the monastery of the Canonica of Santa María de Vilabertrán.*

*Sant Quirze de Colera Abbey:* This medieval building founded in 927 AD was rebuilt in 1123 AD and it is possible observe the original foundations with apparent anti-seismic structures formed by assembled stones with spike-like disposition. Later was seriously damaged by the 1428 AD earthquake and in 1441 the abbey was eventually abandoned by ruin. The building is located 58 km ENE of the epicentre and the main set of EAEs preserved in this building is composed by tilted walls, dropped key stones, warped arches (Fig. 6), penetrative fractures in masonry blocks and repaired arches. The orientations of all these EAEs are compatible with a NW-SE seismic ground motion of N170ºE.

*Sant Pere de Rodes Monastery*: This building, located at 69 km from the epicenter, is the farthest from those analyzed in this study and consequently only displays scare evidences of EAEs. The more relevant ones are penetrative fractures in masonry blocks, dropped and repaired key stones and fairly tilted walls. We interpreted that the main component of ground motion was NW-SE, perpendicular to the major nave of the church.

*Fig. 6: Warped arch and repaired key stones (made of bricks) in the monastery of Sant Quirze de Collera.*

**DISCUSSION AND CONCLUSIONS**

The Camprodón earthquake of February of 1428 caused important damage in the province of Girona (NE Catalonia). The EAEs reported in this study are located between c. 10 (*Sant Joan de les Abadeses) to c. 70 km (Sant Pere de Rodes) from the epicentre, but damage was strong in a radius of 50 km around the epicentre (e.g. Villabertran and Besalú)*: The extensive damage recorded in Sant Quirze de Cólera at c. 60 km from the epicenter can be explained by a possible topographic amplification (narrow mountain valley), but its early abandonment after the earthquake (1441 AD) might amplify some of the reported EAEs. In any case is evident that Intensity VI EMS assigned to this zone (Fig. 7), mainly collected from littoral sites (Oliveira et al., 2006) does not explain the observed damage.

The present study present the most relevant EAEs presently preserved in the Romanesque heritage of the area. The geological structural analysis of the different set of EAEs collected in six localities/sites indicates a mean and consistent NW-SE direction for the seismic ground motion (Fig. 7) in the southern zone of the epicentral area. Only in the case of the locality of Besalú two perpendicular orientations of ground motion are recorded in the studied buildings. Therefore, seems evident that this locality was also struck by the previous Amer earthquake in 1427 AD; VIII EMS) located about 28 km SW in an orthogonal direction to the Camprodón event (1428 AD; IX EMS), located 30 km NW from Besalú (Fig. 1). It is necessary to highlight that all the affected towns or buildings analyzed in this work was severely affected by the 1428 Camprodón event (Oliveira et al., 2006), which is the largest one recorded in the Pyrenees. The reported archaeseismological data and analysis is useful to improve the knowledge on the seismicity of the area and on a particular event. This kind of data can be also used in future restoration works of the Romanesque heritage in the zone, identifying those elements and/or orientations of the ancient buildings prone to undergone severe damage during future seismic events generated by the same seismic source.

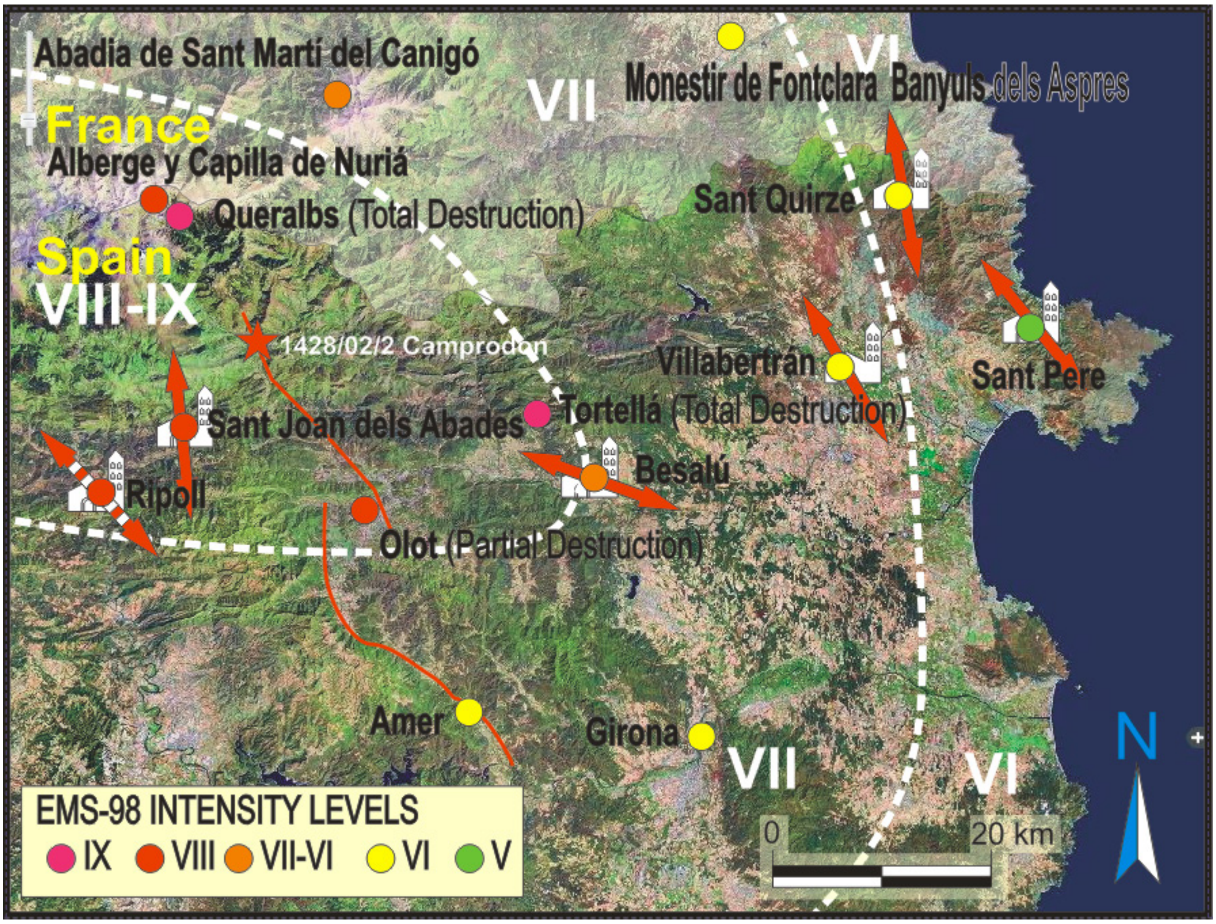


*Fig. 7: Isoseismal lines of the Camprodón earqhquake (1428; I=IX; EMS98) (modified from Olivera et al., 2006). The red lines are segments of the Amer Fault. The solid red arrows represent the mean ground movement during the earhtquake obtained by geological structural analysis of EAEs. The dashed arrows are interpreted from EAEs reported in historical documents.*

**Acknowledgements:** This work is supported by the Spanish research project CGL2012-37281-C02.01 (USAL) and the Spanish Civil Society Rodríguez & Perucha Geo-Traveling Ltd. This is a contribution of the INQUA TERPRO Project 1299 (EEE Metrics) and the Working group QTECT-AEQUA.

## References

Giner-Robles, J.L., Rodríguez-Pascua, M.A., Pérez-López, R., Silva, P.G., Bardají, T., Grützner, C. and Reicherter, K. (2009). *Structural Analysis of Earthquake Archaeological Effects (EAE): Baelo Claudia Examples (Cádiz, South Spain)*. Instituto Geológico y Minero de España, 130 pp.

Giner-Robles, J.L., Silva Barroso, P.G., Pérez-López, R., Rodríguez-Pascua, M.A., Bardají Azcárate, T., Garduño-Monroy, V.H., and Lario Gómez, J. (2011). Evaluación del daño sísmico en edificios históricos y yacimientos arqueológicos. Aplicación al estudio del riesgo sísmico. Proyecto EDASI. Serie Investigación. Fundación MAPFRE, 96 pp.

Giner-Robles, J.L., Pérez-López, R., Silva, P.G., Rodríguez-Pascua, M.A., Martín-González, F. and Cabañas, L. (2012). Aplicaciones en Arqueosismologia. *Boletín Geológico y Minero de España,* 123 (4): 503-513.

Olivera, C., Redondo, E., Lambert, J., Riera Melis, A. and Roca, A. (2006). Els terratrèmols dels segles XIV i XV a Catalunya. Monografies nº 30. Institur Cartogràfic de Catalunya, Barcelona: 407 pp.

Perea, H, Masana, E. and Santanach, P. (2012). An active zone characterized by slow normal faults, the northwestern margin of the Valencia trough (NE Iberia):a review. *Journal of Iberian Geology*, 38 (1): 31-52.

Rodríguez-Pascua, M.A., Pérez-López, R., Silva, P.G., Giner-Robles, J.L., Garduño-Monroy, V.H., and Reicherter, K. (2011). A Comprehensive Classification of Earthquake Archaeological Effects (EAE) for Archaeoseismology. *Quaternary International*, 242(1): 20-30.

Rodríguez-Pascua, M.A., Pérez-López, R., Martín-González, F., Giner-Robles, J.L. and Silva, P.G. (2012). Efectos arquitectónicos del terremoto de Lorca del 11 de mayo de 2011. Neoformación y reactivación de efectos en su Patrimonio Cultural. *Boletín Geológico y Minero de España*, 123 (4): 487-502.

# Preliminary intensity correlation between macroseismic scales (ESI07 and EMS98) and Earthquake archaeological effects (EAEs)

*M.A. Rodríguez-Pascua(1), P.G. Silva(2), R. Pérez-López(1), J.L. Giner-Robles(3), F. Martín-González(4), Perucha, M.A. (1).*

(1) Instituto Geológico y Minero de España. C/ Ríos Rosas, 23. 28003-Madrid. Spain. Email: ma.rodriguez@igme.es, r.perez@igme.es, ma.perucha@igme.es
(2) Dpto. Geología. Escuela Politécnica Superior de Ávila. Univ. Salamanca. 05003-Ávila. Spain. Email: pgsilva@usal.es
(3) Dpto. Geología. Facultad de Ciencias. Univ. Autónoma de Madrid. Cantoblanco. Tres Cantos. Madrid. Spain. Email: jorge.giner@uam.es
(4) Área de Geología. ESCET. Univ. Rey Juan Carlos. C/ Tulipán, s/n. Móstoles, 28933 Madrid. Spain. Email: fidel.martin@urjc.es

***Abstract:*** *Using the main constructive typologies used earlier than 20th Century, especially those related to the historical heritage, this paper correlates the different EAEs with the macroseismic scales EMS-98 and ESI-07. We propose minimum and maximum intensity levels for different building types, such as those related to the use of adobe, stone, brick and masonry. This work aims to establish preliminary seismic intensity intervals from the nature and styles of seismic deformations in historical buildings that can be applied to the archaeseismological analysis of heritage buildings and archaeological sites.*

***Key words****: Earthquake Archaeological Effects (EAEs), ESI07 intensity scale, EMS98 intensity scale, historical heritage.*

## INTRODUCTION

Using the classification of Earthquake Archaeological Effects (EAEs) proposed by Rodríguez-Pascua et al (2011), this study proposes a correlation between the EAEs and the EMS98 (Grünthal, 1998) and ESI07 (Michetti *et al*., 2007) macroseismic scales. The proposed correlation is based on the occurrence of different types of EAEs in the building fabric at different EMS98 intensity levels and the related earthquake environmental effects (EEE) catalogued in ESI07 macroseismic scale. The idea is to create a preliminary methodology leading to estimate the seismic intensity from archaeoseismological analyses in archaeological sites and historical heritage.

## ENVIRONMENTAL SEISMIC INTENSITY SCALE (ESI07)

According to the EAE classification proposed by Rodríguez-Pascua et al (2011), these effects can be divided into geological ones and those produced in the building fabrics. The geological effects were seriously dismissed in the early development of the EMS98 intensity scale, but largely differentiated by the ESI07 macroseismic scale (Michetti *et al*., 2007). For this reason, we use the ESI07 scale to assign the intensity intervals to the EAEs related to geological effects, as can be liquefactions, landslides, etc.

All the geological effects at their most energetic level can cause the total destruction of an archaeological site or a heritage building. Consequently, the maximum intensity level considered in this work will always be XII for all the EAEs. The minimum limit is assigned using the lowest intensity at which a geological effect can be preserved in the geological or geo-archaeological record. In the case of landslides, rock falls, anthropic compacted ground and liquefactions is possible to establish these minimum bounds by means of the combination of both macroseismic scales (ESI07 and EMS98). Some intensity mismatches in the lower bounds of these scales only occur for anthropic compacted ground and rock falls. For the rock falls the minimum EMS98 intensity is VI, but IV for the ESI07 intensity (Fig. 1).

## EUROPEAN MACROSEISMIC SCALE EMS-98

In the case of the establishment of the minimum values of intensities for the EAEs on the fabric of buildings, we only used the EMS98 scale. To establish the minimum values is taken into account those of the construction types considered in the EMS98 scale normally used in historical buildings, heritage and archaeological sites, considering the following ones: (1) Rubble stone; (2) Adobe (earth brick); (3) Simple stone; (4) Brick; and (5) Masonry.

Comparing these five constructive types with the vulnerability intervals (5 values in alphabetical code; A - F) and the building damage classes (numerical code; 1-5) considered in the EMS98 scale, enable us to establish the minimum values of intensity in which the damages (EAEs) appear (Fig. 2). The most vulnerable constructive types have intensity V (rubble stone and adobe), but the most seismic resistant constructive types (masonry) reach this minimum value at Intensity VII (Fig. 2). The total destruction of these constructive types considered in the EMS98 occur from Intensity VIII to IX (rubble stone and adobe), but reach from intensity X for the more resistant masonry buildings (Fig. 2). Between these minimum and maximum values there is a zone in which all EAEs occur, being possible establish seismic intensity intervals indicative for particular EAEs previously to the total destruction of a building.

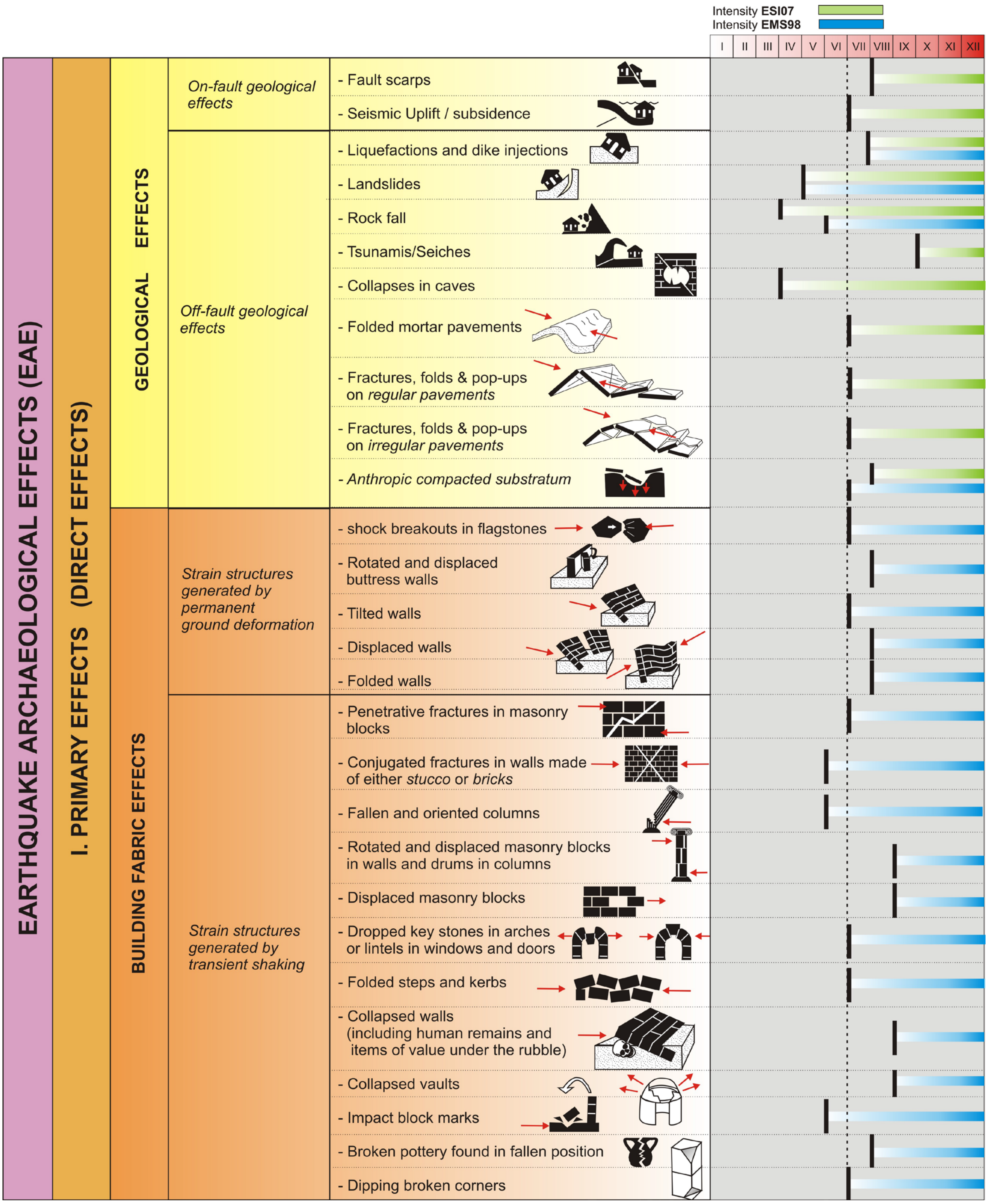


*Fig. 1: Earthquakes Archaeological Effects (EAEs) classification relative to intensity intervals in which these structures can be generated taking into account the macroseismic scales ESI07 and EMS98. The black bars indicate the minimum intensity limit from which is generated a certain EAE. Modified from Rodríguez-Pascua et al. (2011).*

Combining the intensity intervals extracted from the ESI07 scale (Fig. 1) and the EMS98 scales (Fig. 2), the EAE lower minimum value is intensity IV (rock falls) and the EAE higher minimum value intensity X (tsunamis). Above these values the scale will be saturated. If a particular archaeological site/building records different EAEs, these deformation structures may indicate the minimum and maximum values of the "bracketed seismic intensity" experienced in the site. These bracketed intensity values (minimum and maximum) will indicate the seismic intensity interval in which damage was produced (e.g. VII-X). A finer estimation is possible, depending on the frequency and size of the maximum intensity EAE indicators a double (e.g. VIII-IX) or unique (e.g. X) ESI Intensity can be proposed. In any case the use of the proposed methodology is particularly interesting "when and where" EAEs indicators will be associated with Earthquake Environmental Effects (EEEs).

**THE CASE OF THE ANCIENT ROMAN CITY OF *BAELO CLAUDIA* (CÁDIZ, SPAIN)**

The ancient Roman city of Baelo Claudia is a well known archaeoseismological site located in the Bolonia Bay (Cádiz, SW of Spain). Presently, the roman remains are protected and since the 1980s decade is within the network of Archaeological Parks of the Andalusia Regional Government.

Baelo Claudia was founded in the 2nd Century BC and was destroyed two times by earthquakes (40-60 AD and 350-395 AD). After the second earthquake the city was abandoned (Menanteau *et al*., 1983; Sillères, 1997). The destruction layers in the archaeological site were interpreted like earthquakes by these authors. Silva et al.

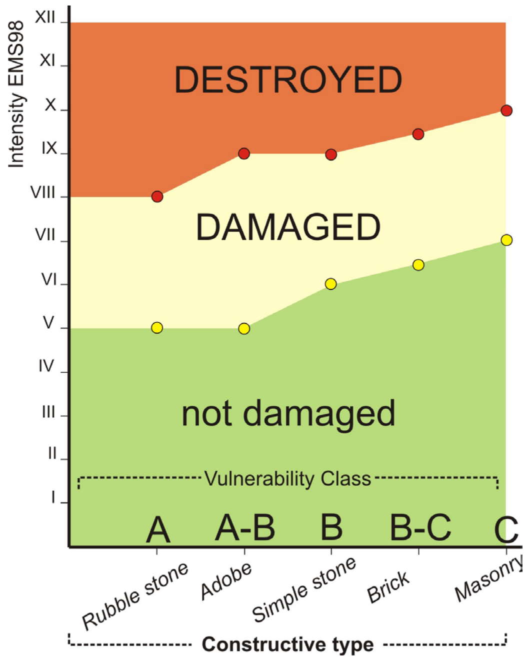


*Fig. 2: EMS98 seismic intensity intervals from the damage onset and destruction in historical buildings and archaeological sites. Also are considered the vulnerability values and damage classes for fabric buildings proposed by this macro-seismic scale.*

(2005; 2009) studied the deformation structures located inside of the archaeological site and made a geomorphological research of the zone. These works support the seismic hypothesis, provide a first catalogue of preserved earthquake effects in the archeological site, performed a first structural analysis and proposed possible seismic sources and preliminary intensity levels for the ancient earthquakes. Further geophysical research and fault trenching in the zone (Grützner et al., 2012) help to refine the seismic history associated to the Roman city.

Using the earthquake effects preserved in the roman remains of *Baelo Claudia* Giner-Robles et al. (2009) launched a new methodology using a systematic structural geology analysis of the EAEs. These authors also catalogue more than one hundred EAEs and finally produced a detailed map of the most damaged sector of the roman city during the last earthquake in 350-395 AD (Giner et al., 2013). In summary the methodological approach proposed by Giner et al. (2009) is eventually focused in the estimation of the mean direction of ground motion during the earthquake. These authors obtain a consistent NE-SW mean direction of ground motion using more than one hundred different EAEs, congruent with a near-field offshore seismic source SSW of the Bolonia Bay. Further seismic-profiling in the offshore zone identified at least a couple of NNW-SSE active faults affecting to the Plio-Quaternary filling and the submarine topography (Grürtzner et al., 2012).

Considering the complete sets of EAEs catalogued by the abovementioned authors, the most important EAEs of the classification of Rodríguez-Pascua et al. (2011) are present in the ancient city of Baelo Claudia. This is the main reason to select this, maybe unique, archeaeological site as an example case for the estimation of bracketed intensities by means of the methodology proposed in this work. The most common EAEs recorded in this site, and the estimated seismic intensity intervals obtained by the combination of the EMS98 and ESI07 scales are the following ones:

- (FOC) Fallen oriented columns: VI-XII
- (IBM) Impact block marks: VI-XII
- (DBC) Dipping broken corners: VII-XII
- (DKS) Dropped key stones: VII-XII
- (FPV) Folded pavements: VII-XII
- (FSK) Folded steps and kerbs: VII-XII
- (SBK) Shocks breakouts in flagstones: VII-XII
- (PFB) Penetrative fractures masonry blocks: VII-XII
- (TWL) Tilted walls: VII-XII
- (DWL) Displaced walls: VIII-XII
- (FWL) Folded walls: VIII-XII
- (DMB) Displaced masonry blocks: IX-XII

Analyzing this list, is clear that intensity VIII was clearly surpassed and considering the EAE marker with higher minimum intensity value (DMB; Fig. 3), a minimum intensity of IX can be firmly proposed for the 350-395 AD earthquake, but in a range that could reach intensity XII. Authors like Menanteau et al. (1983) or Sillères (1997), suggested an X MSK intensity, considered as a minimum value for Silva et al. (2005; 2009), and in the range (IX-XII) of the proposed here. However, taking into account the frequency and size (length or amplitude) of all the EAEs markers of intensity VII and VIII, and the high number an centimetric scale of the DBM recorded in the site Intensity IX-X is the minimum bracketed value to be considered from the EAEs recorded in *Baelo Claudia*.

*Fig. 3: Displaced masonry blocks in the market of the ancient roman city of Baelo Claudia. Minimum macroseismic EAE intensity: IX.*

## CONCLUSIONS

The proposed methodology for the estimation of macroseismic intensities in archaeological and / or historic buildings is based on the combination of the macroseismic scales ESI07 and EMS98, as well as in the classification of EAEs. With the intensity values proposed by both scales is possible to set the minimum intensities values that can generate several sets of EAEs. This make possible to estimate the seismic intensity intervals triggering the EAEs. In the case-example of Baelo Claudia the number of different recorded EAEs, their overall oriented disposition, their frequency and their size lead to the application of the proposed methodology. The application of this methodology is possible only with a numerous set of particular EAEs or with few sets of different EAEs. Their application to isolated cases is no recommended. From this analysis is clear that Intensity VII is the minimum value from which different sets of EAEs are frequent, but widespread from intensity VIII and IX. Taking into account that several of the buildings of *Baelo Claudia* collapsed during the event (Basilica, Market, Temples) and the severe damage caused in the pavement of the *Decumanus maximums*, *Foro* and Theater (e.g. Sillìeres, 1997; Silva et al., 2009) a minimum "archeoseismic intensity" in the range of IX-X can be firmly proposed for the 350-395 AD event.

The archeoseismic methodology proposed in this work can offer bracketed intensity values indicating the minimum intensity value recorded in the historical heritage and archaeological sites. This is a preliminary step to the systematization and further parametrization of EAEs. The case studies of recent instrumental events are necessary to calibrate the proposed archaeoseismic methodology. In this sense, the Spanish working group QTECT-AEQUA has collected and catalogued EAE data for the recent events of Lorca 2011 (SE Spain, 5.2 Mw), Pianura Padana 2012 (N Italy, 6.3 Mw) and Chistchurch (New Zealand; 6.3 Mw) in modern and historical buildings. The application of this methodology to the EAEs recorded in the historical heritage of these events will help to refine the archaeoseismic parametrization proposed here.

**Acknowledgements:** This work is supported by the Spanish research project QTECBETICA (CGL2012-37281-C02.01; USAL). This is contribution of the INQUA TERPRO Project 1299 (EEE Metrics) and the Working group QTECT-AEQUA.

## References

Giner-Robles, J.L., Rodríguez-Pascua, M.A., Pérez-López, R., Silva, P.G., Bardají, T., Grützner, C. y Reicherter, K. (2009). *Structural Analysis of Earthquake Archaeological Effects (EAE): Baelo Claudia Examples (Cádiz, South Spain)*. Instituto Geológico y Minero de España, 130 pp.

Grünthal, G. (1998). *European Macroseismic Scale 1998: EMS98*. Ed. Musée Natioal d´Historie Narurelle. Luxembourg. 99pp.

Grützner, C., Reicherter, K., Hübscher, C. and Silva, P.G. (2012). Active faulting and neotectonics in the Baelo Claudia area, Campo de Gibraltar (southern Spain). Tectonophysics. 554–557, 127-142.

Menanteau, L., Vanney, J.R., Zazo, C. (1983). *Belo II: Belo et son environment (Detroit de Gibraltar). Etude physique d´un site antique*. Casa de Velázquez. Serie Arqcheologie, 4, Broccard, París.

Michetti A.M., Esposito E., Guerrieri L., Porfido S., Serva L., Tatevossian R., Vittori E., Audemard F., Azuma T., Clague J., Comerci V., Gurpinar A., Mc Calpin J., Mohammadioun B., Morner N.A., Ota Y. and Roghozin E. 2007. Intensity Scale ESI 2007. En: Guerrieri L. & Vittori E. (Eds.): Memorie Descrittive Carta Geologica d'Italia., 74, Servizio Geologico d'Italia – Dipartimento Difesa del Suolo, APAT, Roma, 53 pp.

Rodríguez-Pascua, M.A., Pérez-López, R., Silva, P.G., Giner-Robles, J.L., Garduño-Monroy, V.H., y Reicherter, K. (2011). A Comprehensive Classification of Earthquake Archaeological Effects (EAE) for Archaeoseismology. *Quaternary International*, 242: 20-30.

Sillières (1997). *Baelo Claudia: Una ciudad Romana de la Bética*. Junta de Andalucía- Casa de Velázquez, Madrid.

Silva, P.G., Borja, F., Zazo, C., Goy, J.L., Bardají, T., De Luque, L., Lario J., Dabrio, C.J. (2005). Archaeoseismic record at the ancient Roman City of Baelo Claudia (Cádiz, south Spain). Tectonophysics, 408 (1-4): 129-146.

Silva, P.G., Reicherter, K., Grützner, Ch., Bardají, T., Lario, J., Goy, J.L., Zazo, C. and Becker-Heidmann, P. (2009). Surface and subsurface palaeoseismic records at the ancient Roman city of Baelo Claudia and the Bolonia Bay area, Cádiz (south Spain). *Geological Society of London, Special Publication*, 316: 93-121.

INQUA Focus Group on Paleoseismology and Active Tectonics

paleoseismicity.org

# Buried faults in desert environments: the application of the H/V spectral ratio technique for subsurface mapping, a case study from the Ejina Basin, Inner Mongolia, China

*Rudersdorf, Andreas (1), Hans-Balder Havenith (2), Klaus Reicherter (1)*

(1) Neotectonics and Natural Hazards, RWTH Aachen University, Lochnerstraße 4-20, 52056 Aachen, Germany. Email: a.rudersdorf@nug.rwth-aachen.de

(2) Géorisques et Environnement, Université de Liège, 4000 Sart Tilman, Liège, Belgium. Email: hb.havenith@ulg.ac.be

***Abstract:*** *The "Gobi corridor of left-lateral transpression" between the northern Tibetan Plateau and the Gobi-Altai ranges has extensively been investigated by earth scientists. Since many sub-basins are remote, research publications often lack ground truthing. The Ejina Basin in the lower reaches of the Hei River provides large sedimentary successions for climate reconstruction but also yields evidence for large faults. In this study we show the applicability of the H/V spectral ratio technique (HVSR) as a fast and easy to use method to derive information on thicknesses of sedimentary successions, basement topography or faulting. Dependent on basic assumptions of subsurface properties, the H/V method remains subject of thorough processing and/or cross-validation with other geological or geophysical data.*

***Key words****: Buried faults, H/V spectral ratio technique (HVSR), subsurface mapping, Central Asia, Gobi Desert.*

## INTRODUCTION

The endorheic Ejina Basin (also Gaxun Nur Basin, Hei River Basin, Ruoshui Basin) in the eastern Gobi desert is a valuable archive for Quaternary climate reconstruction north of the Tibetan Plateau. Situated in the stress field between the actively indenting Tibetan Plateau and the Central Asian Orogenic Belt in a complex, yet extensively studied basement setting, evidence for active intraplate deformation open a space for detailed research.

## GEOLOGICAL AND TECTONIC SETTING OF THE EJINA BASIN WITHIN CENTRAL ASIA

Continental breakup, ocean subduction and continental collision in Central Asia have produced complex geological basement domains of various ages dating back to the growth of the Central Asian Orogenic Belt (Badarch et al., 2002), which was formed mainly during the Neoproterozoic and Early Paleozoic. The continental accretion was terminated by the collision with the North China and Tarim cratonic blocks (Stampfli et al., 2002).
Mesozoic breakup of the Gondwana supercontinent and Tethys subduction lead to major crustal shortening and the collision of the Indian and Eurasian continents during the Cenozoic, forming high-relief mountain ranges: the Tibetan Plateau (Royden et al., 2008). The ongoing northward motion of the Indian plate at velocities of up to over 40 mm/a (Meade, 2007; Vergnolle et al. 2007; Zhang et al., 2004) and the eastward movement of the Tibetan Plateau leads to collision-related displacements even far in the interior of the Eurasian continent (Cunningham, 2013).
Present day-tectonics between the Tibetan Plateau and the Gobi Altai as part of the Central Asian Orogenic Belt (Fig. 1) concentrates on the sinistral Altyn Tagh strike-slip fault, its eastern continuations and the Qilian Shan thrust front (Chinese *shan* = mountain), its northern extensions as the northern and northeastern termination of the Tibetan Plateau (Hetzel, 2013) as well as the sinistral faults in the Gobi Altai Ranges with the major Gobi-Tien Shan Fault System (Cunningham, 2013; Hartmann, 2003); an area called the "Gobi corridor of left-lateral transpression" (Cunningham et al., 1996).
The Ejina Basin (Fig. 1) is a huge inland delta in the arid to hyperarid Gobi Desert and is bounded by the Gobi Altai ranges in the north, the Bei Shan in the west and the Badain Jaran Shamo (Chinese *shamo* = sand sea) in the east and southeast. The basin is controlled by the interplay between active fluvial and alluvial sedimentation from the Hei He (Chinese *he* = river) from the south and eolian erosion by northwesterly winds. The Hei He system has a catchment area of 130.000 km² and drains the Qilian Shan to the north. Several distributaries have dried out in the 20th century due to irrigation, water overusage and associated lowering of

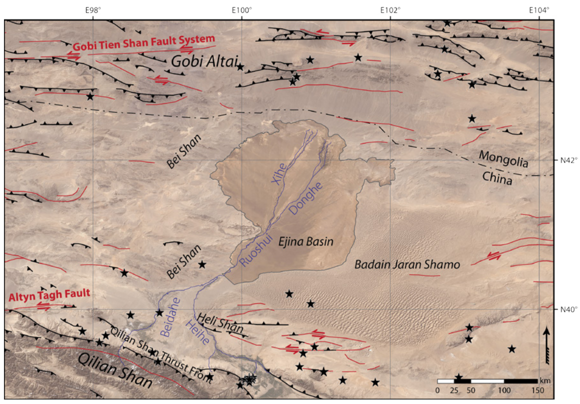


*Fig. 1: The Ejina Basin between the Qilian Shan (Tibetan Plateau, south) and Gobi Altai ranges (north). Black stars: instrumental seismicity with M>3, red lines: sinistral strike-slip faults, black lines: thrust faults, fault lines after Cunningham (2013) and Hetzel et al. (2004).*

the ground-water table (Qi & Luo, 2005) leading to the desiccation of the Gaxun Nur terminal lake.

The Late Mesozoic basin formation is described by Meng et al. (2003) as part of a wider extensional basin system in the present-day China-Mongolia border region with numerous sub-basins, bounded by both high- and low-angle normal faults as well as low-angle detachments offsetting pre-Cretaceous strata. Triassic sequences are missing. Cretaceous fluvial, alluvial and lacustrine sediments fill the basins during and after the inactivation of the Mesozoic NE-SW striking fault systems.

The Quaternary sedimentary succession comprises intercalations of alluvial fan deposits, eolian sands, lacustrine sediments and evaporates of up to 300 m total thickness (Wünnemann et al., 2007; Zhang et al., 2006). The tops of the successions are mostly covered by a thin layer of coated gravel ("Gobi gravel", e.g. Hartmann et al., 2011; Lü et al., 2010; Wünnemann et al., 2007). Lithologies also change laterally over short distances (Fig. 2) due to the (inland) deltaic environment.

The basin boundaries are gradually defined and represent the rugged and partly strongly eroded Bei Shan (W and NW) and Gobi Altai ranges (N and NE). They comprise significantly older units (Fig. 2) of Precambrian to Mesozoic ages with mostly granitic intrusions of Triassic ages. Possible intra-basin and basin-bounding faults are, if mapped, only generally studied (Fig. 2; Lü et al., 2010 and references therein; Becken et al., 2007; Hölz et al., 2007) and basin-wide conclusions on tectonic activity are sparse (Hartmann et al., 2011) due to the meager desert environment, bad accessibility and military sensitivity of the study area.

Recent regional instrumental seismicity is diffuse (Fig. 1) and often not associable to certain faults and is completely absent within the Ejina Basin. However, fault activity is assumed in Neotectonic times (Hartmann et al. 2011) and dating irregularities of a drilling project (time inversion at depth, see Zhang et al., 2006) yield further evidence for more recent fault activity.

The Ejina Basin is morphologically very flat, but gently inclined northwards at elevations between 1200 m a.s.l. in the southwesternernmost basin and 900 m a.s.l. in the Gaxun Nur area with a mean slope of circa 0.2 %. The convex delta shape also spreads over a large distance with mean slopes of ±0.3 %.

## H/V SPECTRAL RATIO TECHNIQUE

Widely used in microzonation studies and site effect evaluation (Edwards et al., 2013; Atkinson & Boore, 2006; Bonnefoy-Claudet et al., 2006), the H/V spectral ratio technique (horizontal versus vertical noise, HVSR), introduced by Nogoshi and Igarashi (1971) and improved by Nakamura (1989), is capable of mapping soft-sediment thicknesses (e.g. Scherbaum et al., 2003; Ibs-von Seht & Wohlenberg, 1999). The method uses

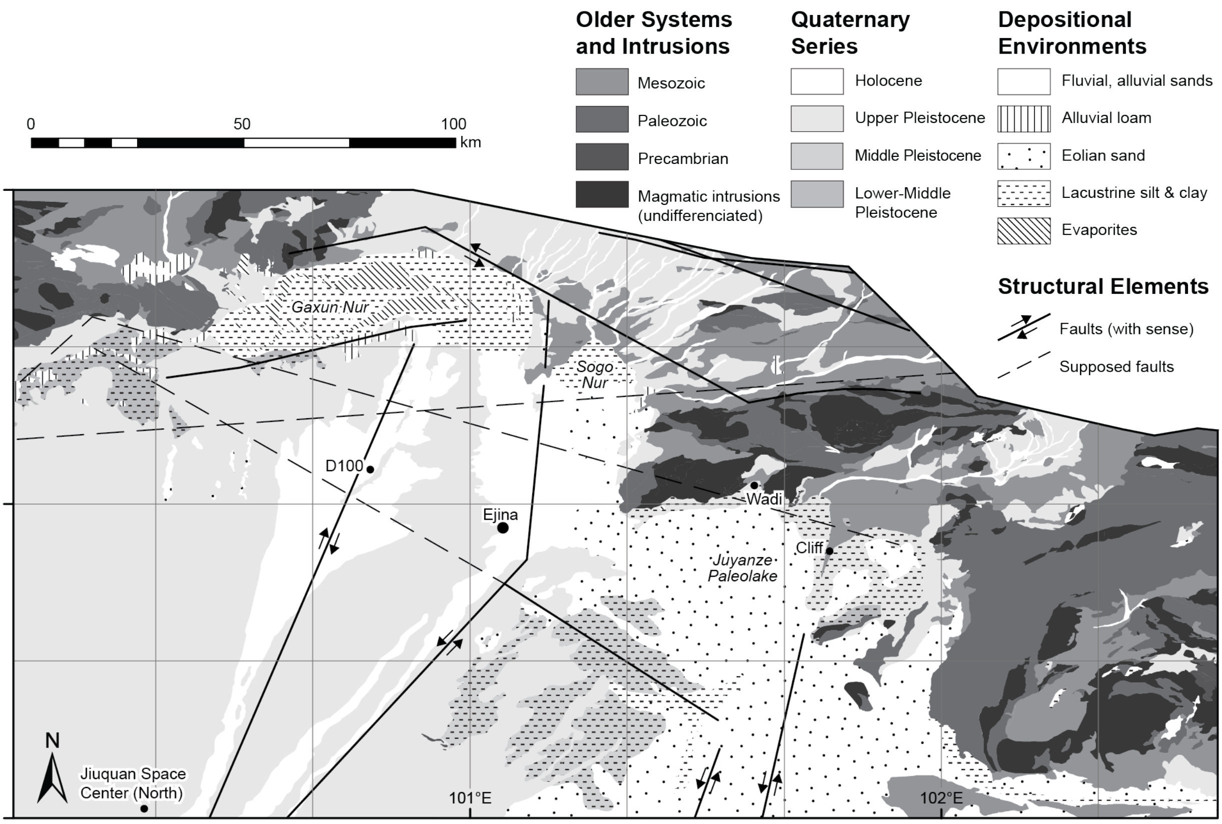


*Fig. 2: Geological map of the northern Ejina Basin, based on Chinese geological maps, digitized and compiled after Gansu Provincial Geological Bureau (1980). Fault lines after Lü et al. (2010) and Cunningham (2013). Study areas Cliff, D100 and Wadi are marked. Note the terminal (paleo) lakes Juyanze, Gaxun Nur (dried during 20th century due to intensive water withdrawal) and Sogo Nur in the northernmost depressions of the Ejina Basin.*

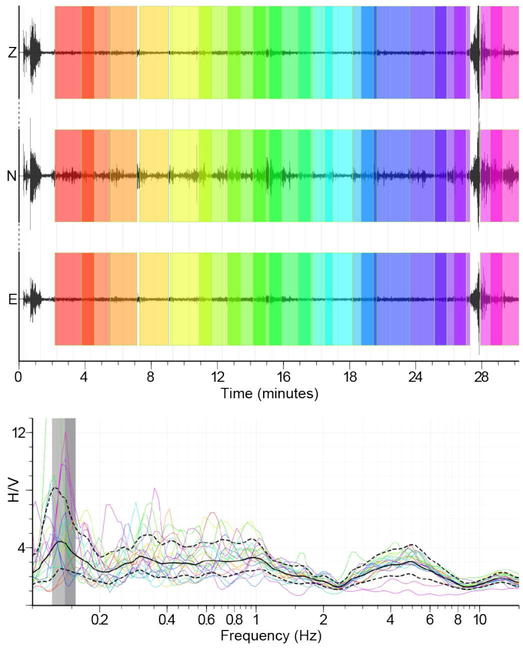


*Fig. 3: Seismogram 201 analysis using GEOPSY 2.9 (http://www.geopsy.org) 300 m south of the D100 study site (Fig. 2). Top: Analyzed windows ($l_w \geq 50$ s) of the horizontal components N, E (north and east) and the vertical component Z. Bottom: computed H/V spectrum with peaks at 0.14, 0.27, 0.43, 1.0, 4.91 Hz; colors indicate the time windows above.*

ambient noise recordings to calculate the Fourier amplitude spectra of the horizontal and vertical noise components and points after analyzing appropriate time windows to resonance frequencies $f_0$, characterizing the subsurface (Bonnefoy-Claudet et al., 2006). However, the method depends either on a piori assumptions of subsurface properties (shear wave velocity $v_s$) or strongly depends on otherwise determined subsurface information and is therefore fragile to unexpected heterogeneities (Scherbaum et al., 2003; Fäh et al., 2001).

We used a Lennartz seismometer and a LEAS CityShark II station for single-station recordings and evaluated the data using GEOPSY 2.9 (open-source software, http://www.geopsy.org). To sustain the stability criteria for reliable results (SESAME group, 2004), we analyzed window lengths $l_w \geq 50$ s (Fig. 3) to reach the deeper subsurface, i.e. the base of Quaternary sediments in depths of up to 300 m. A sufficient number of windows ($n_w \geq 20$) and a standard peak frequency deviation $\sigma_A(f) < 3$) are required (SESAME group, 2004) to identify characteristic peaks.

Since shear wave velocities are not known, we used the D100 core log (Figs. 2 & 4, Wünnemann et al., 2007) to better constrain and relate peak frequencies to certain lithological boundaries (Fig. 4). The interpretation process therefore bases on the adequate correlation of HVSR peak and known subsurface data. We mainly interpret major peaks but also consider smaller peaks, especially when laterally traceable. Possible error sources

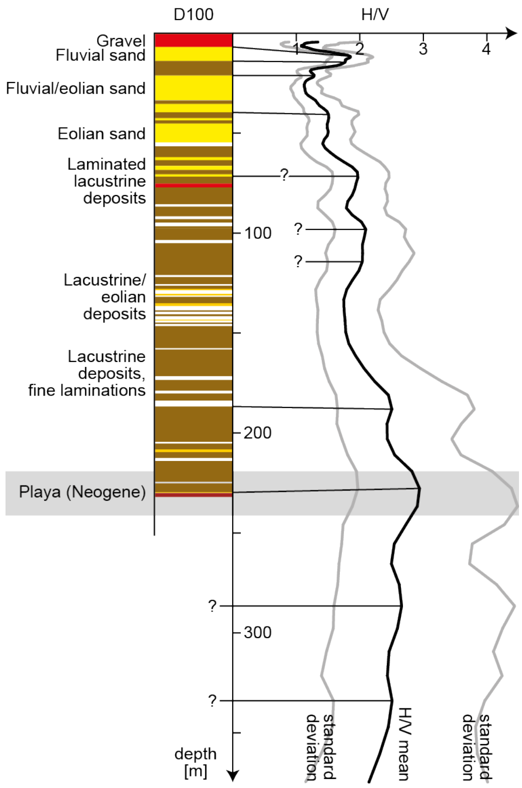


*Fig. 4: Simplified D100 core log data (after Wünnemann et al., 2007) in correlation to a single-station H/V curve (No. 200) taken at the same site; the main peak (grey) sufficiently coincides with the Quaternary-Neogene lithological contact.*

during the measurement process (wind, steadiness, coupling) were omitted by partial burying.

After the calibration we were able to apply similar processing parameters to adjacent survey points to create 2-dimensional profiles (Rudersdorf et al., 2013), which laterally show shifting peaks and therefore changes in the soft-sediment thickness d after: $d = v_s/4f_0$. H/V peaks at survey points 201 (Fig. 3) and 200 (Fig. 4) reveal depth differences of several meters being 300 m apart.

Our calibrated measurements were capable of predicting the base of the Quaternary with an accuracy of > 90% in a pre-drill study 9 km east of D100 (in prep.). Interpretation of a denser survey grid will give evidence for the morphology of the Quaternary base and therefore evidence for paleotopography or Quaternary active faulting (in prep.).

## DISCUSSION

In this study, we introduced the Ejina Basin, Inner Mongolia, China for a closer neotectonic and paleo-seismologic investigation to better understand the basin structure and potential fault behavior in the stress field between the Tibetan Plateau and the Gobi Altai ranges. The active tectonics of the “Gobi corridor of left-lateral transpression” is only extensively studied, i.e. the publications on (active) faults in the Ejina Basin are sparse and often lack ground-truthing.

We showed the applicability of the H/V method as a fast and easy-to-apply method, which is important for areas that lack accessibility and are military sensitive. The results are sufficiently accurate and help to better map the subsurface of the Ejina Basin.

However, the present data base is insufficient to assess fault properties solely, which will be improved in the future by addressing the anisotropy of the H/V signals and inferring predominant wave propagation directions and by the cross-validation with other geological and geophysical data from ground-penetrating radar and transient electromagnetics.

**Acknowledgements:** Our work in Inner Mongolia is funded by the German Federal Ministry for Education and Research (BMBF, FKZ 03G0814A).

## References

Atkinson, G. M. & D.M. Boore (2006). Earthquake ground-motion prediction equations for eastern North America. *Bulletin of the Seismological Society of America* 96, 2181–2205.

Badarch, G., W.D. Cunningham & B.F. Windley (2002). A new terrane subdivision for Mongolia: implications for the Phanerozoic crustal growth of Central Asia. *Journal of Asian Earth Sciences* 21, 87-110.

Becken, M., S. Hölz, R. Fieder-Volmer, K. Hartmann, B. Wünnemann & H. Burkhardt (2007). Electrical resistivity image of the Jingsutu Graben at the NE margin of the Ejina Basin (NW China) and implications for the basin development. *Geophysical Research Letters* 34 (9), L09315.

Bonnefoy-Claudet, S., C. Cornou, P.Y. Bard, F. Cotton, P. Moczo, J. Kristek, & D. Fäh (2006). H/V ratio: A tool for site effects evaluation. Results from 1-D noise simulations. *Geophysical Journal International* 167, 827–837.

Cunningham, D. (2013). Mountain building processes in intracontinental oblique deformation belts: Lessons from the Gobi Corridor, Central Asia. *Journal of Structural Geology* 46, 255-282.

Cunningham, W.D., B.F. Windley, D. Dorjnamjaa, J. Badamgarov & M. Saander (1996). Late Cenozoic transpression in southwestern Mongolia and the Gobi Altai-Tien Shan connection. *Earth and Planetary Science Letters* 140, 67-81.

Edwards, B., M. Clotaire, V. Poggi & D. Fäh (2013): Determination of site amplification from regional seismicity: Application to the Swiss National Seismic Networks. *Seismological Research Letters* 84 (4), July/August 2013, 611-621.

Fäh, D., F. Kind & D. Giardini (2001). A theoretical investigation of average H/V ratios. *Geophysical Journal International* 145, 535-549.

Hartmann, K. (2003). *Spätpleistozäne und holozäne Morphodynamik im nördlichen Gaxun Nur Becken, Innere Mongolei, NW China – unter besonderer Berücksichtigung des Juyanze-Paläosees.* Dissertation, Freie Universität Berlin. Berlin. 134 p.

Hartmann, K., B. Wünnemann, S. Hölz, A. Kraetschell, H. Zhang (2011): Neotectonic constraints on the Gaxun Nur inland basin in north-central China, derived from remote sensing, geomorphology and geophysical analyses. In: *Growth and Collapse of the Tibetan Plateau* (Gloauguen, R. & L. Ratschbacher (eds.). Geological Society, London, Special Publications 353, 221-233.

Hetzel, R. (2013). Active faulting, mountain growth, and erosion at the margins of the Tibetan Plateau constrained by in situ-produced cosmogenic nuclides. *Tectonophysics* 582, 1-24.

Hetzel, R., M. Tao, S. Stokes, S. Niedermann, S. Ivy-Ochs, B. Gao, M.R. Strecker & P.W. Kubik (2004): Late Pleistocene/Holocene slip rate of the Zhangye thrust (Qilian Shan, China) and implications for the active growth of the northeastern Tibetan Plateau. *Tectonics* 23 (6), TC6006.

Hölz, S., D. Polag, M. Becken, R. Fieder-Volmer, H.C. Zhang, K. Hartmann & H. Burkhardt (2007). Electromagnetic and geoelectric investigation of the Gurinai Structure, Inner Mongolia, NW China. *Tectonophysics* 445 (1-2), 26-48.

Ibs-von Seht, M. & J. Wohlenberg (1999). Microtremor measurements used to map thickness of soft sediments. *Bulletin of the Seismological Society of America* 89 (1), 250-259.

Lü, Y.W., Z.Y. Gu, A. Aldahan, H.C. Zhang, G. Possnert & G.L. Lei (2010): 10Be in quartz gravel from the Gobi Desert and evolutionary history of alluvial sedimentation in the Ejina Basin, Inner Mongolia, China. *Chinese Science Bulletin* 55(33), 3802-3809.

Nakamura, Y. (1989). A method for dynamic characteristics estimation of subsurface using microtremor on the ground surface. *Railway Technical Research Institute, Quarterly Reports* 30, 25-33.

Nogoshi, M. & T. Igarashi (1971). On the amplitude characteristics of microtremor (part 2). *Journal of the Seismological Society of Japan* 24, 26-40.

Meade, B.J. (2007). Present-day kinematics at the India-Asia collision zone. *Geology* 35 (1), 81-84.

Meng, Q.R., J.M. Hu, J.Q. Jin, Y. Zhang & D.F. Xu (2003). Tectonics of the late Mesozoic wide extensional basin system in the China-Mongolia border region. *Basin Research* 15, 397-415.

Qi, S.Z. & F. Luo (2005). Water environmental degradation of the Heihe River basin in arid northwestern China. *Environmental Monitoring and Assessment* 108, 205-215.

Royden, L.H., B.C. Burchfiel & R.D. van der Hilst (2008). The Geological Evolution of the Tibetan Plateau. *Science* 321(5892), 1054-1058.

Rudersdorf, A., S. Hölz, A. Torgoev, H.-B. Havenith & K. Reicherter (2013): Hidden faults in the Gobi Desert (Inner Mongolia, China) revealed by microtremor analysis, ground-penetrating radar and SQUID-supported transient electromagnetics. *Geophysical Research Abstracts* 15, EGU2013-9543-1.

Scherbaum, F., K.G. Hinzen, M. Ohrnberger, R.B. Herrmann (2003). Determination of shallow shear wave velocity profiles in the Cologne, Germany area using ambient vibrations. *Geophysical Journal International* 152, 597-612.

SESAME group (2004): Guidelines for the implementation of the H/V spectral ratio technique on ambient vibrations - measurements, processing and interpretation. *European Commission Research Project report*.

Stampfli, G.M., J.F. von Raumer & G.D. Borel (2002). Paleozoic evolution of pre-Variscan terranes: From Gondwana to the Variscan collision. *Geological Society of America Special Papers* 364, 263-280.

Vergnolle, M., E. Calais & L. Dong (2007): Dynamics of continental deformation in Asia. *Journal of Geophysical Research* 112, B11403.

Wünnemann, B., K. Hartmann, N. Altmann, U. Hambach, H.-J. Pachur & H. Zhang (2007). Interglacial and glacial fingerprints from lake deposits in the Gobi Desert, NW China. *Developments in Quaternary Sciences* 7, 313-347.

Zhang H.C., Q.Z. Ming, G.L. Lei, W.X. Zhang, H.F. Fang, F.Q. Chang, B. Wünnemann & K. Hartmann (2006). Dilemma of dating on lacustrine deposits in a hyperarid inland basin of NW China. *Radiocarbon* 48 (2), 219–226.

Zhang, P.Z., Z. Shen, M. Wang, W. Gan, R. Bürgmann, P. Molnar, Q. Wang, Z. Niu, J. Sun, J. Wu, S. Hanrong & Y. Xinzhao (2004). Continuous deformation of the Tibetan Plateau from global positioning system data. Geology 32 (9), 809-812.

INQUA Focus Group on Paleoseismology and Active Tectonics

paleoseismicity.org

# Repeated folding during late Holocene earthquakes on the La Cal thrust fault near Mendoza city (Argentina)

*Salomon, Eric (1,2), Silke Mechernich (1, 3), Ralf Hetzel (1), Francisco Mingorance (4), Andrea Hampel (5)*

(1) Institut für Geologie und Paläontologie, Westfälische Wilhelms-Universität Münster, Correnstraße 24, 48149 Münster, Germany. Email: rahetzel@uni-muenster.de
(2) Institut für Geowissenschaften, Johannes Gutenberg-Universität Mainz, Johann-Joachim-Becher Weg 21, 55128 Mainz, Germany. Email: salomon@uni-mainz.de
(3) Institut für Geologie und Mineralogie, Universität zu Köln, Greinstraße 4, 50939 Köln, Germany. Email: mechernich.s@gmail.com
(4) Instituto de Mecánica Estructural y Riesgo Sísmico, Universidad Nacional de Cuyo, Casilla de Correo 405 – Correo Central, 5500 Mendoza, Argentina. Email: fmingorance@uncu.edu.ar
(5) Institut für Geologie, Leibniz Universität Hannover, Callinstraße 30, 30167 Hannover, Germany. Email: hampel@geowi.uni-hannover.de

***Abstract***: *In 1861, a $M_S$~7.0 earthquake devastated the city of Mendoza (currently 1 million inhabitants). This event occurred on the 31-km-long La Cal thrust fault that extends from Mendoza to the north. An excavated trench on a terrace that is vertically offset by ~2.5 m exposes two stratigraphic units separated by an erosional unconformity. The upper unit is ~800 years old and deformed by three east-vergent folds ($F_1$–$F_3$) whose amount of total displacement is retrodeformed to ~2.0 m, ~2.4 m, and ~0.5 m, respectively. Presumably, the folds were coseismically formed during the 1861 ($F_1$) and a penultimate M ~7 earthquake ($F_2$ and $F_3$). The ~12 ka old sediments below the erosional unconformity contain evidence for at least one older earthquake. These results confirm the continuous release of elastic strain energy at the La Cal thrust which thus poses a serious threat to Mendoza city.*

***Key words***: *palaeoseismology, active thrust fault, retrodeformation, coseismic folding, finite element modelling*

## INTRODUCTION

One of the historically most active zones of thrust faulting in the world is located at the eastern margin of the Andean mountain belt at 30°-33°S, in the southern part of the flat-slab segment of the subducting Nazca plate (Fig. 1a) (e.g. Smalley and Isacks, 1990; Gutscher et al., 2000; Siame et al., 2002). Seismicity in this region is confined to the eastern mountain front of the Precordillera – the easternmost mountain range of the Andes at this latitude – and the basement uplifts of the Sierras Pampeanas farther east.

In the surrounding region of the city of Mendoza the historical record of seismic activity lasts back 230 years and comprises a number of significant earthquakes (Fig. 1a). One of the most devastating seismic events occurred in 1861, which almost completely destroyed the city of Mendoza. This earthquake had an estimated magnitude of $M_S$~7.0 and caused about 6,000 fatalities which at that time was about half of the city's population (The New York Times, 1861; INPRES 2013). The earthquake, which has been related to slip on the La Cal thrust fault (Bastías et al., 1993; Mingorance, 2006) (Fig. 1), emphasizes the threat posed by this fault to the

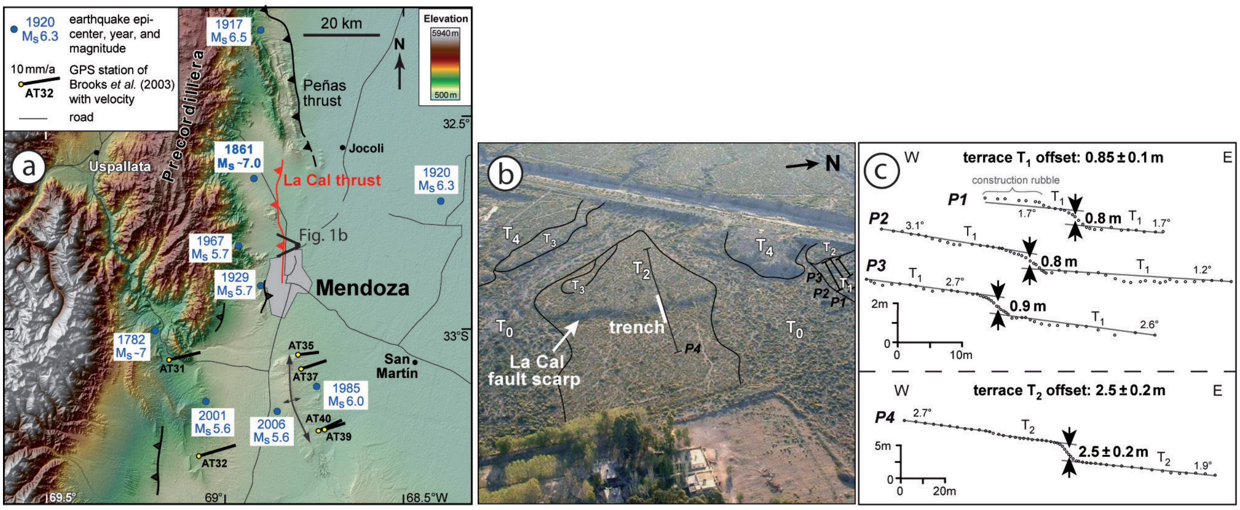


*Fig. 1: (a) Location of the study area. (b) Trench site, Low-angle sunlight photograph of the trench site showing the La Cal fault scarp and the spatial distribution of the four terraces $T_1$-$T_4$. $T_0$ indicates active sediment transport. (c) Topographic profiles across the fault scarp on terraces $T_1$ and $T_2$. The profiles have a vertical exaggeration of 3. (modified after Salomon et al., 2013).*

city of Mendoza and its current population of one million inhabitants. The hypocentre of the 1861 event is inferred to be located in the northern part of the La Cal fault at a depth of 7–12 km (Mingorance, 2006). Here, we present the results of a palaeoseismologic study that we undertook to evaluate the seismic hazard posed by the La Cal thrust fault (Salomon et al., 2013).

The trace of the 31-km-long La Cal thrust fault is characterized by a continuous and easily visible fault scarp that trends north-south (Fig. 1b). In the downtown of Mendoza, the fault scarp is 2–3 m high. In the entire central and northern part of the fault, the incision of ephemeral streams across the fault scarp has formed four well preserved terrace levels, $T_1$–$T_4$, with the highest one ($T_4$) corresponding to the surface of the alluvial fan (Fig. 1c; Schmidt et al., 2011). The absence of lateral displacements affecting the east-west oriented channels suggests that the La Cal fault is a pure thrust fault without a recognizable strike-slip component.

## TRENCH DESCRIPTION AND INTERPRETATION

At the trench site, the La Cal thrust fault offsets terrace $T_2$ by 2.5 ± 0.2 m as determined by a fault scarp profile measured with a total station (Fig. 1c). About 150 m north of the trench, three other scarp profiles show that the younger terrace $T_1$ is vertically offset by 0.85 ± 0.1 m (Fig. 1c). This offset has been inferred to be the result of the earthquake that destroyed Mendoza in 1861 (Schmidt et al., 2011).

The sediments exposed in the trench consist of three markedly different units. In the western part of the trench a prominent erosional unconformity separates the units (a) and (b) (Fig. 2). The upper unit (a) is characterized by coarse-grained gravel deposits, whereas the lower unit (b) consists of thinly bedded, fine-grained sedimentary strata (Fig. 2). The continuous succession of unit (a) strata across the fault indicates that both hanging and footwall represent the same surface $T_2$. In the center of the trench, a coarse-grained unit, subdivided into (c1) and (c2), is exposed which incorporates a block and pieces derived from unit (b). Two colluvial wedges are identified at the base of the scarp, where wedge (II) is cut off and eroded by wedge (I).

The age of the sedimentary units (a) and (b) was constrained previously by optically stimulated luminescence (OSL) dating (Schmidt et al., 2012). Three OSL samples from different horizons in the lower unit (b) yield ages of 12.3 ± 1.2, 12.3 ± 1.2, and 11.8 ± 1.1 kyr (1σ error), whereas one sample from the uppermost layer of unit (a) has an age of 770 ± 76 years (1σ error), which is interpreted to date the formation of terrace $T_2$.

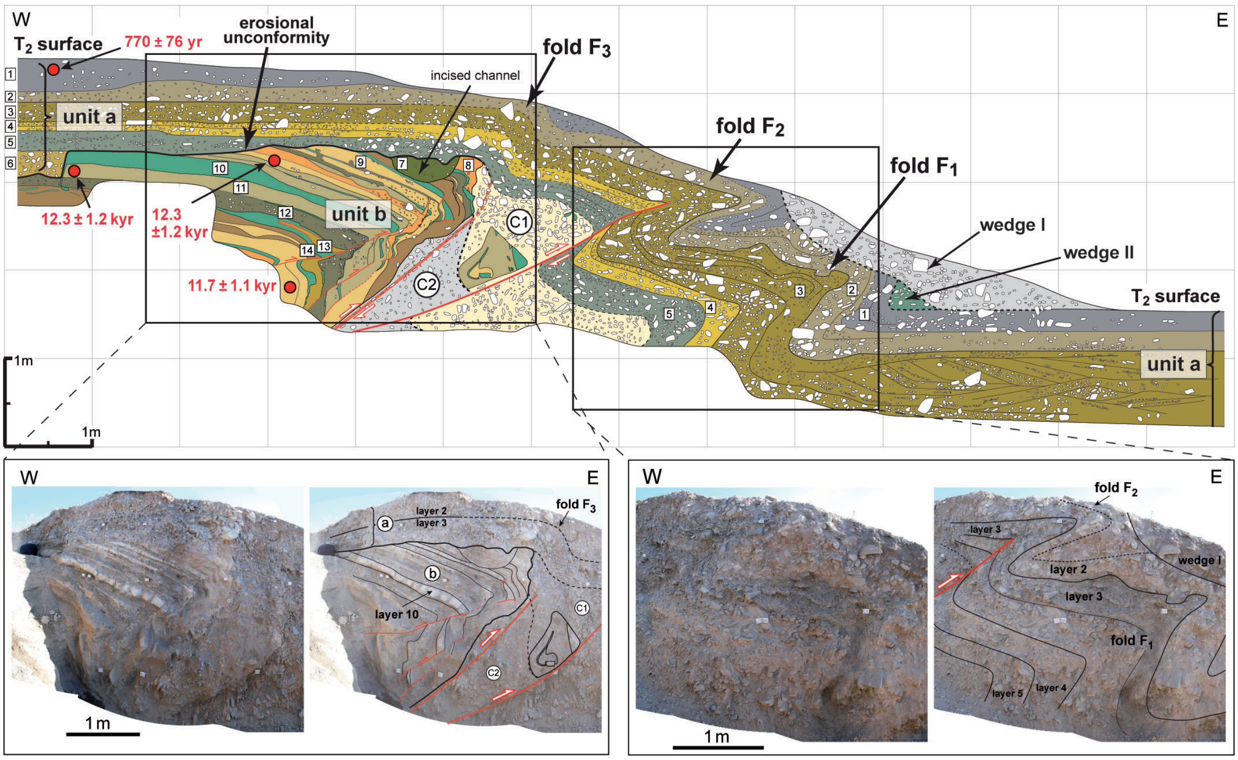


*Fig. 2: Geological interpretation of the northern wall of the trench (Salomon et al., 2013). The deposits exposed in the trench consist of three different units (a) to (c). Upper unit (a) and lower unit (b) are separated by an erosional unconformity. The optically stimulated luminescence (OSL) ages (red numbers) of four samples from units (a) and (b) are interpreted as depositional ages (Schmidt et al., 2012). Three folds, $F_1$–$F_3$, affect the entire stratigraphic unit (a). Two colluvial wedges are indicated with Roman numbers.*

The upper unit (a) is deformed by three major east-vergent folds, $F_1$–$F_3$ (Fig. 2). The easternmost fold, $F_1$, affects all layers of unit (a) and is overlain by colluvial wedge (I). The central fold, $F_2$, lies at the tip of a blind reverse fault, which offsets the coarse-grained unit (c), and the lower layers of unit (a) (Fig. 2). The westernmost fold, $F_3$, is situated above a westward-dipping thrust fault that runs close to the boundary between the fine-grained unit (b) and the coarse-grained unit (c). The two closely spaced thrust faults beneath the anticlinal hinges of $F_2$ and $F_3$ merge at the base of the trench. The fine-grained strata of unit (b) exhibit an east-vergent fold structure that is locally cut by small reverse faults with displacements of several centimeters to a few decimeters (Fig. 2).

## RETRODEFORMATION OF UNIT (A) DEPOSITS

In order to quantify the vertical and horizontal displacements that led to the formation of the three major folds in the trench section, each fold was retrodeformed using the area-balancing technique, which assumes that the cross-sectional area has remained constant (Lee et al., 2004; McCalpin, 2009). The total displacements of folds $F_{1-3}$ are 2.02 m, 2.35 m, and 0.51 m, respectively. The retrodeformation of the folds are used to restore the entire trench section from the formation of terrace $T_2$ to the present-day (Fig. 3).

## DISCUSSION AND CONCLUSION

We interpret the folds to result from ruptures of the La Cal fault at depth that propagated upwards and reached the splay faults which underlie the three folds present in the trench. To explore the mechanism of coseismic folding in more detail, we performed two-dimensional finite-element modeling using the commercial software ABAQUS. Finite-element modelling shows that coseismic folding above the tip of a blind thrust fault is a physically plausible mechanism to generate these folds (Salomon et al., 2013). Their seismogenic origin is also supported by the presence of two colluvial wedges and the

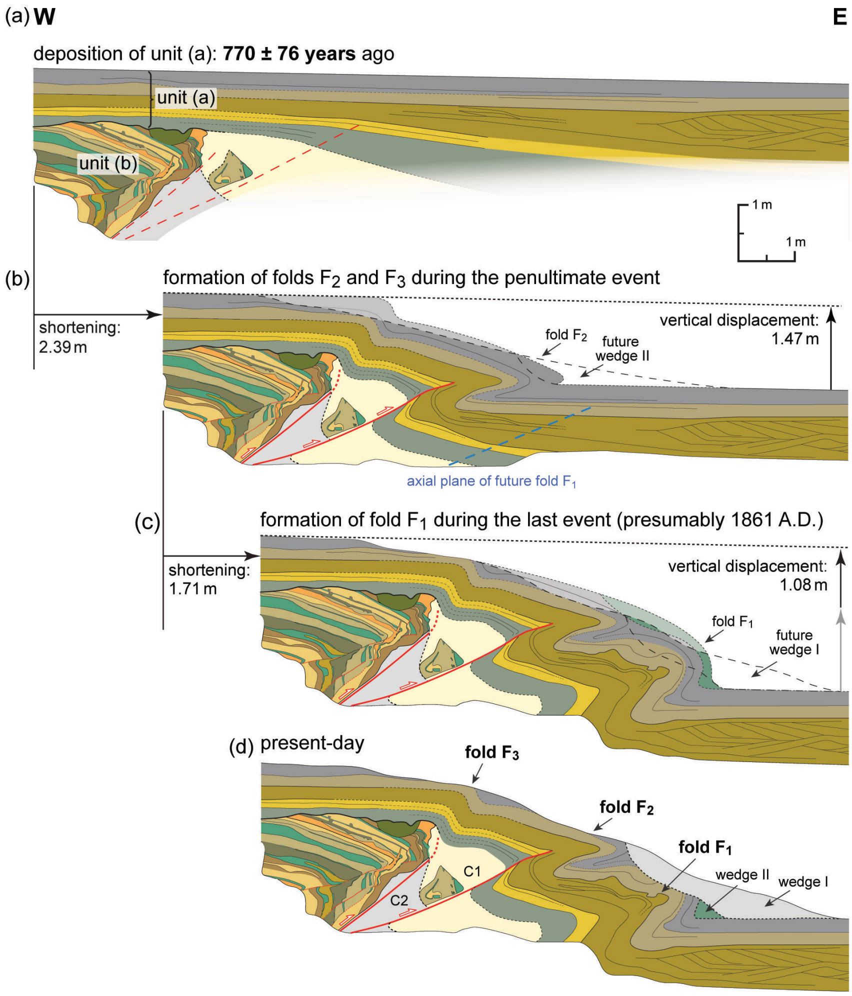


*Fig. 3: Model for the successive deformation of the unit (a) deposits of the trench that led to the generation of the three folds ($F_1$ to $F_3$) and the thrust fault scarp during two earthquakes (Salomon et al., 2013). The initial stage (Fig. 3a) shows the inferred geometry after deposition of unit (a) 770 ± 76 years ago, as deduced from an OSL age of the uppermost layer (Schmidt et al., 2012). The horizontal shortening and vertical displacements given for the two seismic events (Fig. 3b,c) are based on the restoration of the three folds. The eastern fold $F_1$ is interpreted as the result of the 1861 earthquake that destroyed Mendoza city, whereas the folds $F_2$ and $F_3$ are interpreted to have formed during the penultimate event. Alternatively, $F_2$ and $F_3$ may have formed during two separate events.*

similarity between the vertical displacement derived from the youngest fold $F_1$ (~1.08 m; Fig. 3) and the offset of 0.85 ± 0.1 m recorded by the three scarp profiles on the youngest terrace $T_1$ (Fig. 1b,c), which is located only 150-m north of the trench.

The OSL age of 770 ± 76 years (1σ error) for the upper unit (a) dates the formation of terrace $T_2$ (Schmidt et al., 2012) and indicates that two (or three) major earthquakes were produced by ruptures of the La Cal fault during the past ~800 years (Fig. 3). The scarp-forming event that generated fold $F_1$ was most likely the $M_S$ ~7.0 Mendoza earthquake from 1861, because two more recent events in 1929 and 1967 with a magnitude $M_S$ of 5.7 (Fig. 1a) did not produce surface offsets (Mingorance, 2006).

Assuming that these slip values represent the maximum surface displacement (MD) associated with the respective seismic event and applying the relationship $M_w = 6.69 + 0.74 \times \log(MD)$ (Wells and Coppersmith, 1994), we calculate moment magnitudes of $M_w$ ~6.9 (fold $F_1$), and $M_w$ ~7.0 (folds $F_2$ and $F_3$) for the last two earthquakes.

The observation that active crustal shortening is concentrated in a narrow zone along the eastern margin of the Andes is not only supported by the high level of seismicity but also by the modelling of GPS data (Brooks et al., 2003; Kendrick et al., 2006). If the rate of elastic strain accumulation of 2.8 ± 1.3 mm/a, which we estimated from GPS data south of Mendoza (Fig. 1a), is representative for the La Cal thrust fault farther north, active shortening on the La Cal fault continues at a significant rate. By assuming a time-averaged horizontal shortening rate of 2 to 4 mm/a and using a fault dip of 32°, we calculate that elastic deformation representing a total slip of 0.35 to 0.7 m has accrued on the La Cal fault since the last earthquake in 1861. If released today, this would be equivalent to an earthquake with a magnitude of $M_W$ 6.4 to 6.6.

**Acknowledgements:** We are indebted to the management and staff of Cementos Minetti, not only for the permission to work on their property but also for the excavation of the trench at no cost. This work was funded by the German Research Foundation (DFG; grant no. HE 1704/6-1).

## References

Bastías, H., G. E. Tello, L. P. Perucca & J. D. Paredes (1993). Peligro Sísmico y Neotectónica, *Geología y Recursos Naturales de Mendoza* 6, 645–658.

Brooks, B.A., M. Bevis, R. Smalley, E. Kendrick, R. Manceda, E. Lauria, R. Maturana & M. Araujo (2003). Crustal motion in the Southern Andes (26°-36°S): Do the Andes behave like a microplate?, *Geochemistry, Geophysics, Geosystems 4*, 1085, doi:10.1029/2003GC000505.

Costa, C. H., C. E. Gardini, H. Diederix & J. M. Cortés (2000). The Andean orogenic front at Sierra de Las Peñas-Las Higueras, Mendoza, Argentina, *Journal of South American Earth Sciences* 13, 287–292.

Gutscher, M. A., W. Spakman, H. Bijwaard & E. R. Engdahl (2000). Geodynamics of flat subduction: Seismicity and tomographic constraints from the Andean margin, *Tectonics* 19, 814–833.

Instituto Nacional de Prevención Sísmica (INPRES) (2013), http://www.inpres.gov.ar/seismology/historicos1.php, last accessed July 2013.

Kendrick, E., B.A. Brooks, M. Bevis, R.J. Smalley, E. Lauria, M. Araujo & H. Parra (2006). Active orogeny of the south-central Andes studied with GPS geodesy, *Revista de la Asociación Geológica Argentina 61*, 555-566.

Lee, J.-C., C. Rubin, K. Mueller, Y.-G. Chen, Y.-C. Chan, K. Sieh, H.-T. Chu & W.-S. Chen (2004). Quantitative analysis of movement along an earthquake thrust scarp: A case study of a vertical exposure of the 1999 surface rupture of the Chelungpu fault at Wufeng, Western Taiwan, *Journal of Asian Earth Sciences* 23, 263–273.

McCalpin, J. P. (2009). Paleoseismology, *International Geophysics Series* 95, Academic Press, Amsterdam, 613 pp.

Mingorance, F. (2006). Morfometría de la escarpa de falla histórica identificada al norte del cerro La Cal, zona de falla La Cal, Mendoza, *Revista de la Asociación Geológica Argentina* 61, 620–638.

Salomon, E., Schmidt, S., Hetzel, R., Mingorance, F. & A. Hampel (2013). Repeated folding during late Holocene earthquakes on the La Cal thrust fault near Mendoza city (Argentina). *Bulletin of the Seismological Society of America*, 103, 936-949.

Schmidt, S., R. Hetzel, F. Mingorance & V. A. Ramos (2011). Coseismic displacements and Holocene slip rates for two active thrust faults at the mountain front of the Andean Precordillera (~33°S), *Tectonics 30*, TC5011, doi:10.1029/2011TC002932.

Schmidt, S., S. Tsukamoto, E. Salomon, M. Frechen & R. Hetzel (2012). Optical dating of alluvial deposits at the orogenic front of the Andean Precordillera (Mendoza, Argentina), *Geochronometria 39*, 62-75.

Siame, L. L., O. Bellier,M. Sébrier, D. L. Bourlès, P. Leturmy,M. Perez & M. Araujo (2002). Seismic hazard reappraisal from combined structural geology, geomorphology and cosmic ray exposure dating analyses: The Eastern Precordillera thrust system (NWArgentina), *Geophysical Journal International* 150, 241–260.

Smalley, R., Isacks B. L. (1990). Seismotectonics of thin-skinned and thick-skinned deformation in the Andean foreland from local-network data—evidence for a seismogenic lower crust, *Journal of Geophysical Research* 95, 12,487–12,498.

The New York Times. (1861). From Buenos Ayres. The Great Earthquake and Subsequent Conflagration at Mendoza—Horrors of the Occasion —Political Intelligence July 29 1861.

Wells, D. L., Coppersmith, K. J. (1994). New empirical relationships among magnitude, rupture length, rupture width, rupture area, and surface displacement, *Bulletin of the Seismological Society of America* 84, 974–1002.

INQUA Focus Group on Paleoseismology and Active Tectonics

paleoseismicity.org

# Tectonic geomorphology of the eastern extent of the Kashmir Basin Fault (KBF) zone

*Shah A. A.*

Curtin University, Sarawak, Miri, Malaysia, 98009; Email:afroz.shah@curtin.edu.my

***Abstract:*** *The Kashmir Basin Fault (KBF) is exposed as a train of discontinuous active fault traces for a strike length of ~120 km (Shah, 2013), in Kashmir, Himalayas. However, its eastern extent was not mapped previously and therefore, this study demonstrates that the active fault trace extends further east, where the geomorphic expression of active faulting is clear for a distance of ~43 km. The fault shows a very prominent dextral strike-slip motion with little to no dip-slip component associated with it, particularly, on the easternmost portion. Further west it mainly shows dip-slip motion with a slight indication of dextral strike-slip. This new active fault trace extends the total strike length of the KBF zone to ~163 km, which has implications for seismic hazard and the distribution of deformation along the NW portion of the Himalayas.*

***Key words***: *Kashmir Basin Fault, Distributed deformation, NW Himalayas, Active faults*

## INTRODUCTION

A number of previous studies have mapped traces of active thrust faults in the Kashmir Basin, Himalayas (e.g. Madden et al., 2010, 2011; Shabir and Bhat, 2012; Shah, 2013). These faults are formed in response to the active continent–continent collision of the Indian and Eurasian plate. These two tectonic plates collide at geologic and geodetic convergence rates of 30–50 mm/yr (Ader et al., 2012). The presence of active deformation in Kashmir basin suggests that the ongoing collision deformation along the ~2,000-km long Himalayan orogenic belt is distributed differently along the central and western portions of the belt (e.g. Madden et al., 2010, 2011; Shah, 2013).). Thus the bulk shortening along the central part is mainly accommodated along the Himalayan Frontal Thrust (HFT) system (e.g. Ader et al., 2012 as a latest reference) and along the NW Himalayas, the convergent deformation is not concentrated on the front but is distributed across the width of the belt (e.g. Kaneda et al., 2008; Meigs et al., 2010; Shah, 2013). The present study further demonstrates the active nature of the eastern extent of the KBF (Shah, 2013) and its tectonic significance.

## KASHMIR BASIN

The strike length of the Kashmir Basin is ~150 km and is ~50 km across (Fig. 1). It is located on the north-western

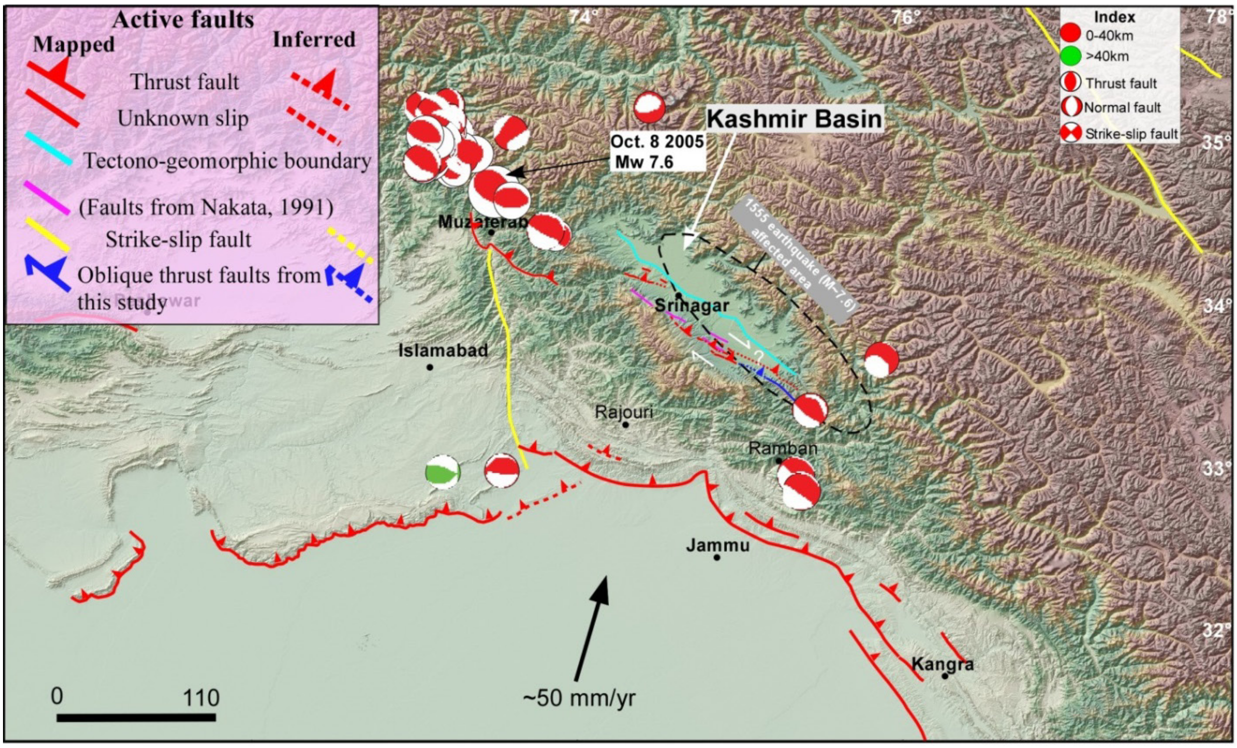


*Fig. 1: Regional tectonic setting of the Kashmir Basin and CMT catalogue data (1976–2012), modified after Shah, 2013.*

portion of the Himalayan orogenic system, about ~100 km away from the actively growing frontal part of the Himalaya. It is classified as one of the Neogene–Quaternary intermontane basins (Burbank & Johnson, 1983) of the Himalayas and contains strata, which are equivalent in age and similar in lithology to the Upper Siwalik Group (Burbank & Johnson, 1982). The basal part of the sequence is slightly older ~5 Ma, but much of the succession is of late Pliocene-Pleistocene age, with deposition continuing locally into the Holocene age (Burbank & Johnson, 1983).

## TECTONIC GEOMORPHOLOGY

The oval-shaped KB, which stretches ~NW–SE,is surrounded by fold and thrust mountainous (Fig. 1). A quick look at the regional topography suggests that the regions on the NE of the valley are drowned, while those on the SW are uplifted. The geomorphic expression of the active faults vary along the strike, where it mostly crops out as discontinues traces and pierces through some of the young deposits(Shah, 2013; Fig. 1), which are ~50–100 ka old (e.g. Jaiswal et al., 2009; Meigs et al., 2010; Madden et al., 2011).The eastern extent of this fault shows a clear right-lateral strike-slip motion for a distance of ~1km and is demonstrated by young stream channels, some of which have captured the lateral motion. For example the Figure 2 shows that offset along some of the streams varies from ~20 to ~40 m. The fault has caused characteristic stream captures along the

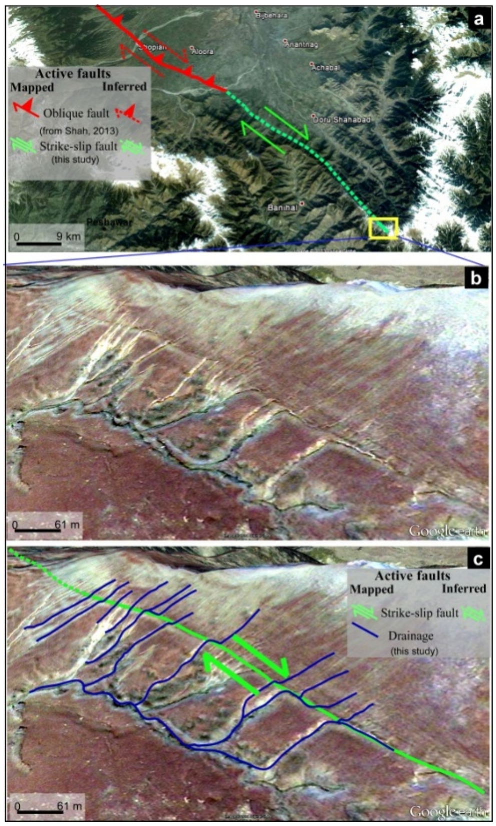


*Fig. 2: 3D Google images show the eastern extent of the newly identified trace of the KBF.(a) Shows the total extent of the fault. (b) Shows an un-interpreted image and in (c) the active dextral strike-slip faults are interpreted.*

strike. Some portion of the fault is not very clear from the available resolution of the Google images, thus, that portion of the trace is inferred (Fig. 1). If we assume the displaced deposits are of ~50 ka year old, then the estimated strike-slip rate will be around 0.08cm/year. However, this could be higher or lower, depending on the exact ages of deposits.

## RESULTS AND INTERPRETATIONS

The KBF traces trend ~ NW–SE and preserve geomorphic evidences of recent activity, wherein they cut across the ~ 50–100 ka old deposits (e.g. Jaiswal et al., 2009; Meigs et al., 2010; Madden et al., 2011).

Some of these fault traces show an indication of an oblique motion, however, the dip-slip component is more prominent on the west and the evidences presented here suggest that dextral strike-slip motion is more prominent on further east. The KBF faults dip towards NE and uplift the young deposits on the SW of the basin thereby drowning everything to the NE portion of the basin, as suggested previously, the geomorphic expression of the Kashmir Valley is modified due to these faults and has therefore roughly divide the valley into two major tectono-geomorphic terranes. These are: (1) north-eastern terrane (NET) and (2) south-western terrane (SWT). The former is a low-relief area, with sediment-filled sluggish streams. The latter is an uplifted region, with actively flowing streams (Shah, 2013). This suggests that the south- west side of the valley is climbing a ramp on the Main Himalayan Thrust (MHT), uplifting the SW side and drowning everything to the NE (e.g. Madden et al., 2011; Shah, 2013). However, the evidences presented here suggest that the deformation on the KBF partitions along two more splays of the major fault. Also, the fault is clearly an oblique fault with a dextral strike-slip component associated with thrusting. The dip-slip component is more towards the west, because of an oblique dextral slip motion. This could be because of the regional stress distribution, wherein the flow of the bulk of the GPS vectors show a more prominent clockwise rotation (dextral slip) on the east than west (Figs. 1 and 2), which is because of the extrusion along the strike-slip faults on the east (Yin, 2000, 2006; Ader et al., 2012).

*Table 1. modified after Bilham et al., 2010.*

| Historical earthquakes of Kashmir (primarily reported in Srinagar) | | | |
|---|---|---|---|
| | Date | Maximum estimated intensities | |
| | | Lyengar and Sharma (1998); Lyenger et al. (1999) | Bashir et al. (2009) |
| 1. | 1123 | VII | VII |
| 2. | 24 September 1501 | XII | VIII |
| 3. | 1 September 1555 | - | VII |
| 4. | ca. 1560/1561 | - | VII |
| 5. | 1569-1577 | IV | |
| 6. | 23 June 1669 | VII | |
| 7. | ca. 1678/1979 | VIII | |
| 8. | 1683 | VII | |
| 9. | 24 March 1736 | VIII | |
| 10. | 1779 | | |
| 11. | ca. 1784/1785 | | |
| 12. | 1803 | | |
| 13. | 26 June 1828 | | |
| 14. | 1863 | | |
| 15. | 30 May 1885 | | |
| 16. | 8-Oct-05 | | |

## DISCUSSION AND CONCLUSION

The ongoing collision deformation along the ~2,000-km-long Himalayan orogenic belt is distributed differently along the central and western portions of the belt. For example, the bulk shortening along the central part is mainly accommodated along the Himalayan Frontal Thrust (HFT) system (e.g. Wesnousky et al., 1999; Lave & Avouac 2000; Ader et al. 2012). In contrast, along the NW Himalayas, the convergent deformation is not concentrated on the front and is distributed across the width of the belt (e.g. Meigs et al., 2010; Kaneda et al., 2008). Distributed deformation is also supported by the active geomorphic observations within the Kashmir Basin (e.g. Madden et al., 2010, 2011; Shabir & Bhat, 2012; Shah, 2013 and this study). The ~N130°E strike of the mapped thrust faults is consistent with the regional ~NE–SW convergence along the collision zone (Fig. 1). Therefore, it is more likely that the Kashmir Basin fault is an independent thrust, a possible ramp on the MHT, which has uplifting the SW portion of the KB and drowning everything to the NE (e.g. Madden et al., 2011; Shah, 2013). The evidences presented here further suggest that the deformation on the KBF shows an oblique motion, where the total deformation partitions along two more splays from the major fault and these faults clearly show an oblique faulting with a dextral strike-slip component associated with thrusting. This, thus, suggests that KBF is a broad zone of an oblique faulting pattern, where deformation is mainly concentrated along the major trend of the fault, which is around 163 km long (Fig. 1).

Further, since the dip-slip component is more towards the west, it suggests that the regional stress distribution is responsible for this deformation pattern. This is primarily, because the flow of the bulk of the GPS vectors show a more prominent clockwise rotation (dextral slip) on the east than west, which is because of the extrusion takes place along the major strike-slip faults on the east (Yin 2006; Ader et al., 2012) and thus, deformation is primarily consumed by motion along the strike-slip faults.

## SIZE OF EARTHQUAKE ON KBF

The future earthquake potential of a fault is commonly evaluated from the estimates of fault rupture parameters that are in turn related to earthquake magnitude (e.g. Wells & Coppersmith, 1994). Therefore, using the strike length of the mapped fault, which is ~81 km, plus the length from the inferred portion, which is ~82 km, the total strike length of the fault would be ~163 km. Further, by assuming a dip of 29 (Avouac et al., 2006) and a down-dip limit of 20 km, a Mw of 7.7 is possible on this fault. Further, a historical record of 13 earthquakes in the valley over the last millennium, which includes the damaging earthquakes of 1555 and 1885, indicates that the Kashmir Valley is a locus of active deformation (e.g. Madden et al., 2011; Table 1). Therefore, the active geomorphic evidences presented here suggest that these historical events must have ruptured the surface, which are now preserved as active fault scarps (Figs. 1 and 2). Therefore, the on-going paleoseismic work (e.g. Madden et al. 2011) and the proposed investigations will further unravel the earthquake chronology of the KB. This will be an extremely useful step towards the hazard mitigation of the region.

## FUTURE WORK

Further, I think that the past events on the KBF were not blind and must have ruptured the surface, therefore, our proposed investigations will answer this question and it will be a very significant quest, primarily, because, none of the historical earthquakes is reported to have produced primary surface rupture and it has generally been assumed on the basis of isoseismals and location, that the earthquakes are the result of slip on the Himalayan Frontal Thrust (Wesnousky et al., 1999). However, since this long-standing consensus was finally challenged by Sapkota et al. (2013) by providing strong evidences that the *M*w 8.2 Bihar–Nepal earthquake on 15 January1934 did break the surface. Therefore, in Kashmir, since the geomorphic expression of the surface rupture is well expressed, it thus, potentially suggests that the rupture has reached surface. Hence, it will be a key location to investigate the timing of the fault activity and will provide data about the supposedly blind great earthquakes in the Himalayan history.

Further, earthquake researchers have learnt from the past experience that most of the faults behave differently and in a unique pattern, which is often characteristic of a particular fault, thus, each fault needs to be investigated in much more details. Kashmir Basin is very unique in its shape and the deformation pattern is also uniquely different from the frontal Himalayas, thus, serious efforts are required to investigate the active faults in the valley, which could be achieved through this a comprehensive study.

## SIGNIFICANCE OF THE PROPOSED WORK

The significance of my proposed work lies in the fact that the surface rupture of earthquakes in the Kashmir, which are reportedly said to have occurred on the blind great Himalayan events, might exist and thus, evidences need to be recollected. This will be useful to understandthe historical earthquakes and to re-evaluate the seismic risk along the NW Himalayas and the frontal portions. Thus, it will suggest reassessing the earthquake potential of the Himalayan faults, which might have ruptured in the past historical events.

**Acknowledgements:** I am very thankful to Prof. Paul Tapponier, Prof. Kerry Sieh and Dr. Javid N Malik for inspiring me to work on active tectonics. Travel grant from Curtin University, Sarawak is highly appreciated.

## References

Ader T, Avouac J-P, Liu-Zeng Jing et al (2012) Convergence rate across the Nepal Himalaya and interseismic coupling on the Main Himalayan Thrust: implications for seismic hazard. *Journal of Geophysical Research* 117:B04403.

Avouac JP, Ayoub F, Leprince S et al (2006) The 2005, Mw 7.6 Kashmir earthquake: sub-pixel correlation of ASTER images and seismic waveforms analysis. *Earth and Planetary Science Letters* 249:514–528.

Burbank DW, Johnson GD (1982) Intermontane-basin development in the past 4 Myr in the north-west Himalaya. *Nature* 298:432–436.

Bilham R, Singh B, Bhat I, Hough S (2010) Historical earthquakes in Srinagar, Kashmir: Clues from the Shiva Temple at Pandrethan, *Geological Society of America Special Paper* 471 on Ancient earthquakes.

Bashir A, Bhat MI, Bali BS (2009) Historical record of earthquakes in the Kashmir Valley: *Journal of Himalayan Geology* 30:75-84.

Burbank DW, Johnson GD (1983) The Late Cenozoic chronologic and stratigraphic development of the Kashmir intermontane basin, northwestern Himalaya. Palaeogeography Palaeoclimatology Palaeoecology 43:205–235 spatial extent of great earthquakes. *Journal of Geophysical Research* 115: B12422.

Jaiswal MK, Bhat MI, Bali BS et al (2009) Luminescence characteristics of quartz and Feldspar from tectonically uplifted terraces in Kashmir Basin, Jammu & Kashmir, India. *Radiation Measurements* 44:523–528.

Kaneda H, Nakata T, Tsutsumi H et al (2008) Surface rupture of the 2005 Kashmir, Pakistan, earthquake, and its active tectonic implications. *Bulletin of Seismological Society of America* 98:521–557.

Kumar S, Wesnousky SG, Jayangondaperumal R (2010) Paleoseismological evidence of surface faulting along the northeastern Himalayan front, India: Timing, size, and extent of great earthquakes, *Journal of Geophysical Research* 115:B12422.

Larson KM, Burgmann R, Bilham R et al (1999) Kinematics of the India–Eurasia collision zone from GPS measurements. *Journal of Geophysical Research* 104:1077–1093.

Lave J, Avouac JP (2000) Active folding of fluvial terraces across the Siwaliks Hills, Himalayas of central Nepal. *Journal of Geophysical Research* 105:5735–5770.

Iyengar RN, Sharma D (1998) Earthquake History of India in Medieval Times: Roorkee, Central Building Research Institute, 124 p.

Iyengar RN, Sharma D, Siddiqui JM (1999) Earthquake history of India in medieval times: *Indian Journal of History of Science* 34:181–237.

Madden C, Trench D, Meigs A (2010) Late quaternary shortening and earthquake chronology of an active fault in the Kashmir Basin, Northwest Himalaya. *Seismological Research Letters* 81(2):346.

Madden C, Ahmad S, Meigs A (2011) Geomorphic and paleoseismic evidence for late quaternary deformation in the southwest Kashmir Valley, India: out-of-sequence thrusting, or deformation above a structural ramp? *American Geophysical Union abstracts* T54B-07.

Meigs A, Madden C, Yule JD et al (2010) Distributed Deformation, Distributed Earthquakes in the Northwest Himalaya. Proceedings of the 25th Himalaya-Karakoram-Tibet Workshop: *U.S. Geological Survey Open-File Report* 20101099. http://pubs.usgs.gov/of/2010/1099/meigs/of2010 1099_meigs.pdf

Shabir A, Bhat MI (2012) Tectonic geomorphology of the Rambiara basin, SW Kashmir Valley reveals emergent = out-of-sequence active fault system. *Himalayan Geology* 33:162–172.

Shah A. A (2013) Earthquake geology of the Kashmir Basin and its implication for large earthquakes. *International Journal of Earth Sciences (in press).*

Sapkota SN, Bollinger L, Klinger Y, Tapponnier P, Gaudemer Y, and Tiwari D, (2013) Primary surface ruptures of the great Himalayan earthquakes in 1934 and 1255, *Nature Geoscience* 6:71-76.

Wells DL, Coppersmith KJ (1994) New empirical relationships among magnitude, rupture length, rupture width, rupture area, and surface displacement. *Bulletin Seismological Society of America* 84:974–1002.

Wesnousky SG, Kumar S, Mohindra R, Thakur VC (1999) Uplift and convergence along the Himalayan Frontal Thrust. *Tectonics* 18:967–976.

Yin A (2006) Cenozoic tectonic evolution of the Himalayan orogen as constrained by along-strike variation of structural geometry, exhumation history, and foreland sedimentation. *Earth Science Review* 76:1–131.

Yin A, Harrison TM (2000) Geologic evolution of the Himalayan-Tibetan orogen. *Annual Reviews of Earth and Planetary Sciences* 28:211–280.

# Earthquake Environmental Effects (EEEs) triggered by the 2011 Lorca earthquake (Mw 5.2, Betic Cordillera, SE Spain): Application of the ESI-07 Macroseismic Scale

*P.G. Silva (1), R. Pérez-López (2) M.A. Rodríguez-Pascua (2), J. L. Giner (3), P. Huerta (1), T. Bardají (4); F. Martín-González (5)*

(1) Dpto. Geología, Escuela Politécnica Superior de Ávila, Universidad de Salamanca. Hornos Caleros, 50. 05003-Ávila. (Spain). Email: pgsilva@usal.es , phuerta@usal.es
(2) Instituto Geológico y Minero de España, IGME. Madrid, Spain. Email: ma.rodriguez@igme.es, r.perez@igme.es
(3) Dpto. Geología y Geoquímica. Fac Ciencias. Universidad Autónoma de Madrid. Madrid, Spain. Email: jorge.giner@uam.es
(4) Dpto. Geología. Fac. Ciencias, Universidad de Alcalá de Henares. Madrid, Spain. Email: teresa.bardaji@uah.es
(5) Area de Geología. ESCET. Universidad Rey Juan Carlos I. Madrid, Spain. Email: fidel.martin@urjc.es

***Abstract:*** *236 slope movements were triggered during the 2011 Lorca earthquake (Mw 5.1). They mainly are disrupted landslides fitting in broad categories (a) Large rock falls and rock avalanches (100-1000 m$^3$; 31 cases); (b) Rock falls (10-100 m$^3$; 89 cases) on cuesta-type structural reliefs; (c) Small rock and debris falls (< 10 m$^3$; 72 cases) on steep slopes of canyon-like valleys; and (d) soil slides and debris falls (<3 m$^3$; 44 cases) in marly slopes or low cohesive materials. Box counting by means of 1 km$^2$ cell-network centred in the epicentral area indicate that the total area affected by slope movements is of 135 km$^2$, but only 82 km$^2$ contain recorded events of which 22 km$^2$ attain the largest rock avalanches (c. 1000 m$^3$). These larger EEE occurred along the main structural reliefs and deep rambla-valleys of the zone. Box counting indicates that the total mobilized volume of material is on the order of 20,000 m$^3$. These values agree with an ESI Intensity VII for most of the affected zone, and ESI mapping allow to delineate and refine the VII isoseismal line in the zone empty of EMS intensity data.*

***Key words**: Earthquake environmental effects, Slope movements, Lorca, Betic Cordillera, SE Spain.*

## INTODUCTION

The 11th May Lorca earthquake (Mw 5.2) has been the focus of seismological and fault-activity research and modelling during the last two years in Spain, resulting in official field reports of different governmental agencies (IGME, 2011; IGN, 2012). The seismic source has been clearly identified with the left-lateral strike-slip Lorca-Alhama de Murcia fault (LAF) and the seismic focus was located at depth of 2 km about 4.5 km to the north of the locality of Lorca (Fig. 1) within the upthrown block of the fault (López-Comino et al., 2012). These preliminary reports and the first published papers (e.g. Alfaro et al., 2012) analyzed the earthquake effects according to the preliminary epicentral location provided by the IGN, about 2 km SE of the updated one. Therefore some of the conclusions of these papers need to be re-checked in relation to the relocation of the event.

The earthquake was felt in the locality of Lorca with a maximum intensity of VII EMS-98 (Martinez-Solares et al., 2012), linked to a peak ground horizontal acceleration of 0.37g unusual for this intensity level (Benito et al., 2012). Ground shaking triggered the collapse of a multi-story building, serious damage to 899 buildings, 9 fatalities, hundred injuries and significant economic loos on the order of 450 M€ (IGN, 2012). Coseismic deformation at surface was on the order of 3-4 cm as evidenced by DinSar and GPS analyses (Frontera, 2012), concordant with a oblique-reverse fault rupture 4 km long and 2 km wide with 13-14 cm slip and an azimuth of 245° at 2 km depth, following the trace of the central segment (Lorca-Totana) of the LAF (Bufforn et al., 2012; Martínez-Díaz et al., 2012).

For the first time in Spain several teams of different institutions and universities proceed to a field survey of the earthquake effects during the two weeks following the event. The first preliminary reports were published few weeks after the earthquake (IGME, 2011). In spite of the checked coseismic deformation on the upthrown block of the fault, no surface rupture was observed in the epicentral area, but numerous slope movements in a broad area of about 100 km$^2$ (Alfaro et al., 2012). The present paper reviews and analyzes the numerous set of earthquake environmental effects (EEE) in relation to the ESI-07 macroseismic scale (Guerrieri and Vittori Eds., 2007) and compares the results with the EMS intensity values reported for the affected zone (IGN, 2012;

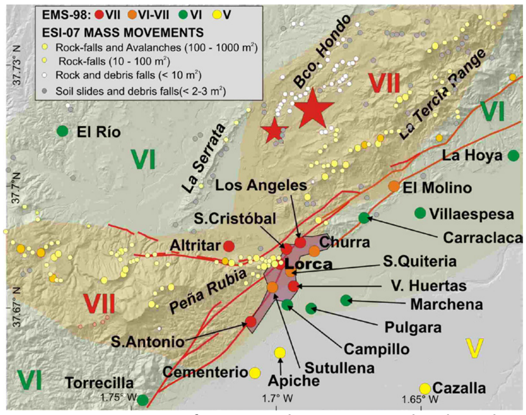

*Fig. 1: ESI mapping of isoseismal zones VII and VI based on slope movements triggered by the Lorca event and EMS data (IGN, 2012).*

Martínez-Solares, 2012) in order to offer a more realistic seismic scenario on the seismic hazard of the zone.

## SLOPE MOVEMENTS

Slope movements triggered by the earthquake occurred in three different geomorphological contexts (Alfaro et al., 2012) and can be subdivided in three main types:

**Type 1)** Rock falls and rock avalanches on the steep cliffs of tabular reliefs and in the steep frontal and lateral cliff zones of cuesta-type reliefs carved on variably weathered Miocene calcarenites, but also in a minor extent on sandstones and conglomerates. Most of them occurred in the structural reliefs culminating the Late Neogene antiform of La Tercia Range north of Lorca, in the Peña Rubia structural relief around the Lorca medieval Castle and in the series of cuesta-type reliefs (e.g. Cejo de Los Enamorados) flanking the Guadalentin valley upstream Lorca. This kind of slope movements were the most prominent ones with individual mobilized material on the order of several cubic decametres to about 1000 $m^3$ and maximum run-outs of about 200 m (Delgado et al., 2012). Only 31 cases reached dimensions up to 100 $m^3$, 11 of those close to 1000 $m^3$. In the rest of the cases (89) total mobilized volumes were between 10-100 $m^3$, but normally less than 50 $m^3$. Individual blocks can reach considerable sizes between 10-30 $m^3$. In the vicinity of the Lorca Castle and Peña Rubia, rock-falls left impact marks of metric scale on asphalt roads and non-asphalted tracks. In other affected zones, heavily damaged tree trunks by block impacts were observed. Lichenometric-age analyses indicate that seven surveyed sites were also subject to similar mass movements during the 1674 AD event (EMS intensity VIII), but engaging a larger volume of mobilized material for each individual case of about two to twenty times (c. 2000 $m^3$) those of the mobilized one during the 2011 event (100 – 200 $m^3$), suggesting a stronger earthquake size in the range of 6.4 Mw for the 1674 event (Pérez-López et al., 2012).

**Type 2)** Rock falls and soil slides in near-vertical slopes of canyon-like valleys, where rock and soil blocks detached from the upper half of the steep valley margins. Most of them occurred in two N-S oriented deep valleys adjacent to La Serrata relief carved in Miocene marly and silty materials north of Lorca (Barranco Hondo). In many cases, Quaternary fluvial terraces and colluvial formations resting on top of these marly materials where subject to mobilization generating small debris falls. This category only concerned the mobilization of volumes between 1 and 10 $m^3$, and attains the 18 % (44 cases) of the mass movements triggered by the earthquake. However in small rambla valleys (e.g. El Dorado) complete slope-valley sections (4x10m) fully collapsed with mobilized values around 1500 -2000 $m^3$. The widespread occurrence of this kind of rock and soil falls in the zone north of La Serrata was confusing from the first reports (Alfaro et al., 2012), since similar canyon-like valleys occurred in the zone, but did not record similar number and frequency of slope movements. Now, after the relocation of the earthquake epicentre (López-Comino et al., 2012), it is patent that this zone is in the epicentral area, above the Mw 5.2 hypocentre.

**Type 3)** Disrupted soil slides involving low cohesive soils and deeply weathered marly slopes irrespective of their orientation or position in the slope, but mainly affecting the slope toes. This category involved the mobilization of material of the order of few cubic meters (<3 $m^3$), but some of them in the epicentral area, especially on unstable slopes can reach 10 $m^3$. This type has 77 cases, around the 38 % of the slope movements occurred in the surveyed zone.

Not catalogued by previous surveys is the rock fall that occurred in the vicinity of the archaeological site of La Bastida, near the Rambla de Lebor (Totana) at about 14 km of the epicentre. The event was witnessed by the archaeologists working in the area, who noticed a strong tremor-like noise and subsequent dust-clouds on the affected slope. Field survey of this site indicates that minor rock-falls occurred, but main slope effects were linked to the remobilization of large blocks (c. 100-200 $m^3$) resting in unstable position on the slope. Similar cases occurred during the Mw 4.8 La Paca (2005) earthquake, where locally large sized blocks (c. 200 $m^3$) detached from steep slopes during the previous Mw 5.0 Bullas (2002) event were re-mobilized several tens of meters (Rodríguez-Peces et al., 2011). In La Paca case secondary mass movements were located in the EMS intensity VII zone less than 5 km away from the epicentre, but in La Bastida case, block motions took place about 14 km away from the 2011 epicentre, within the EMS intensity V zone.

## ESI ANALYSIS AND MAPPING

Preliminary reports indicated that the area affected by mass movements was of c. 50 $km^2$ (IGME, 2011), but further published field surveys (Alfaro et al., 2012; Pérez-López, 2012) estimated a total affected area of c. 100 $km^2$. We have developed a box counting analysis in 1x1 km cells (1 $km^2$) in order to represent the frequency, density and areal extent of slope movements occurred during the 2011 Lorca event, following the ESI-07 mapping developed by Ota et al. (2009). Counting boxes are centred in the earthquake epicentre and consider increasing areas of 10, 100 and 500 $km^2$ (Fig. 2) including 236 data-points.

Box counting indicates that the **100 $km^2$ box contains 170 slope movements** displaying a media of 1.8 cases/$km^2$ and maximum values of 9 cases/$km^2$, all them located within the 10 $km^2$ box. The southern strip of the 100 $km^2$ box include the Lorca city and the eastern half of the structural reliefs flanking the Guadalentín valley upstream Lorca. The complete reliefs constitute a narrow strip 10 km long and 1 km wide (10 $km^2$) in which the frequency of slope movements was of 5 cases/$km^2$, displaying the maximum values in the cell corresponding to the Lorca mediaeval castle (14 cases/$km^2$), were topographic amplification and artificial cut-slopes multiplied the expected values. Also in this strip are recorded the other 6 cases of large rock avalanches, but mainly in the structural reliefs of Cejo de Los Enamorados and Rambla de los 7 Arcos (Alfaro et al., 2012).

The 500 km² box contains the total 240 cases, but with most of the counting cells empties displaying a frequency of c. 0.5 cases/km2. 66 cases occurred out of the 100 km² box. In the epicentral area (10 km² box) most of the triggered events correspond to type 2 and type 3 slope movements mainly occurred along the steep-slopes of canyon-like valleys. However, this epicentral area also reaches the crest of La Tercia Range, where other five cases of large rock-avalanches are recorded.

Intensity VII events, whilst the Lorca case only affected a maximum perimeter area of 135 km², which will correspond to an intensity V event. Following these empirical relationships the Lorca event will be undersized, however in most of the intensity VII cases the affected areas are between 100 and 500 km² (Delgado et al., 2011). Regarding the maximum epicentral distance at which disrupted landslides (e.g. rock-falls) occur, empirical relationships for world wide data-sets indicate maximum distances of 100 km for Mw 5.0/Intensity VII events. The existing relationships for the Betic Cordillera (Delgado et al., 2011) match very well with maximum distances recorded in the Lorca event of c. 14 km.

The only data supporting intensity VII over an area of 80

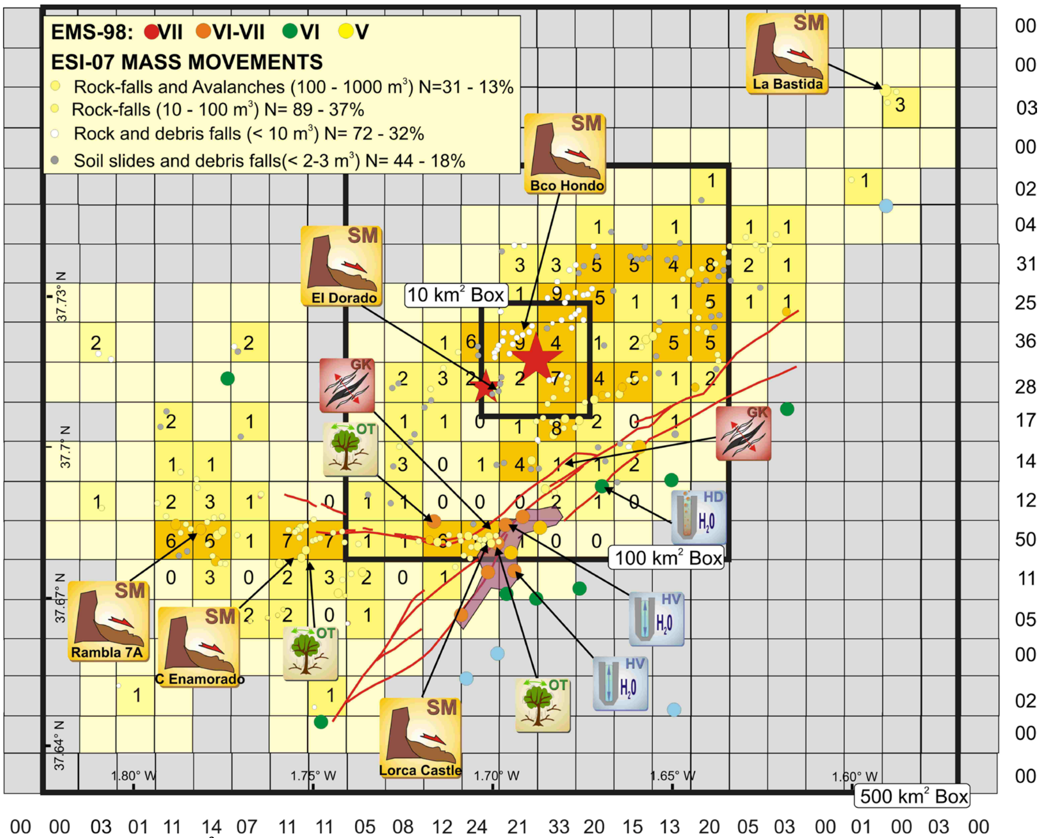


*Figure 2. EEE Box counting (1km² cells) of slope movements triggered by the Lorca 2011 earthquake. Orange cells indicate a frequency of more than 5 cases/ km². Yellow cells surround the perimeter area in which natural effects were recorded. The location of other EEE and EMS data are also illustrated.*

The perimeter of the zone, in which slope movements occurred, cover an area of 135 km², but only 82 km² were subject of these secondary earthquake ground effects as revealed by box counting. In the same way, box counting reveal that the area affected by large rock-avalanches was of only 22 km². In both cases these areas are composed by disperse cells aligned along the existing structural reliefs or rambla valleys. The affected area agrees with the existing empirical relationships for area/magnitude in which a Mw 5.2 event correspond to an affected area of 100 km² for worldwide data sets and of 80 km² for the Betic Cordillera (e.g. Delgado et al., 2011 and references herein). In contrast these empirical relationships predict maximum areas of 10,000 km² for

km² is the application of the ESI-07 Scale, since EMS values confine intensity VII to the vicinity of Lorca only covering c. 5 km². Considering the mean values of mobilized volumes indicated in the previous section, box counting compute a total mean mobilized volume in the range of 20,000 m³. Therefore, the total volume of mobilized material, maximum volumes per case (c. 1000 m3) and the anomalous high number (240) and peak frequencies of triggered landslides (9 to 14 cases/km²) match with a ESI VII intensity. The number and frequency of triggered landslides is very high when compared with inventories of previous events of similar magnitude in the zone (Mw 4.7 to 5.0) and with the results of previous models for predicting slope behaviour during earthquakes (e.g. Alfaro et al., 2012; Rodríguez-Peces et al., 2011). The recorded events are in the range of the relatively high PGA values recorded in the epicentral area (0.37g), which rapidly decreased to 0.02g about 20 km away. Similar behaviour on PGA distribution has been also observed during the Mw 6.3 events of L'Aquila (Italy, 2009 and Christchurch (New Zealand, 2011) (Benito et al., 2012). PGA values recorded during the Lorca earthquake agree with the size and extensive environmental damage occurred within our 10 km$^2$ box, which records the 70% of the triggered slope movements (170 cases). Finally cells used for box-counting clearly delineate and elliptical figure on the upthrown block of the Lorca-Alhama de Murcia Fault following its orientation and covering the area of ESI intensity VII in which the absence of populations make difficult to delineate intensity zones by means of existing EMS data.

Other recorded EEEs are linked to few hydrological anomalies (very small changes on temperature of hot springs; Carraclaca), small changes in the discharge of natural springs (Lorca vicinity), tree shaking triggering the fall of many small tree branches and fruits (El Rio and Lorca), ground cracks of few centimetres width and several tens of meters long in asphalt roads occurring west of Lorca (lateral spreading). Most of these EEE occurred within the EMS intensity VII zone (Figures 1 and 2).

## CONCLUSIONS

Data of secondary earthquake effects induced by the Mw 5.2 Lorca event lead to identifying zones subject to ground motion of intensity VI and VII. Secondary effects were rock falls and rock-soil avalanches of different typology and dimensions. This survey computes a total amount of 240 slope movements and a total mobilized volume in the range of 20,000 m$^3$, maximum volumes per case of c. 1000 m$^3$ and peak frequencies of induced landslides of 9-14 cases/km$^2$. The present survey include new cases of slope movements no reported in previous reports, such as La Bastida within the V EMS Intensity zone 14 km away from the earthquake epicentre. All these data match with ESI intensity VII affecting to 80 km$^2$, but over a total area of 135 km$^2$. EEE Box counting performed in this study completes and expands the existing EMS data (IGN, 2012), which only record intensity VII around the Lorca urban area (c. 5 km$^2$). The observed environmental damage match with the relatively large PGA values (0.37g) probably caused by directivity effects, but not with the moderate magnitude (Mw 5.2) of the event. It is clear that in most of the catalogued cases the steep topography and weathering conditions favoured the occurrence of rock falls and avalanches. This kind of moderate events, without associated surface faulting (invisible in fault-trenching studies), are placed in the lower bound of the ESI-07 scale, but for historical and paleoseismic cases the analysis of secondary effects is the unique tool in order to detect them and evaluate the associated seismic hazard.

**Acknowledgements:** This work is supported by the Spanish research project CGL2012-37281-C02.01 (USAL). This is a contribution of the INQUA TERPRO Project 1299 (EEE Metrics) and the Working group QTECT-AEQUA.

## References

Alfaro P., J. Delgado, F.J. García-Tortosa, L. Lenti, J.A. López, C. López-Casado & S. Martino, (2012). Widespread landslides induced by the Mw 5.1 earthquake of 11 May 2011 in Lorca, SE Spain. *Engineering Geology* 137-138, 40-52.

Alfaro, P., J. Delgado, F.J. García-Tortosa, J. Giner, L. Lenti, C. López-Casado & S. Martino, (2012). The role of near-field interaction between seismic waves and slope on the triggering of a rockslide at Lorca (SE Spain). *Natural Hazards in Earth System Sciences* 12, 3631-43.

Benito, B., A. Rivas, J.M. Gaspar-Escribano & P. Murphy, (2012). El terremoto de Lorca (2011) en el contexto de la peligrosidad y el riesgo sísmico en Murcia. *Física de la Tierra* 24, 255-287.

Buforn, E., C. Pro, S. Cesca, C. Sanz de Galdeano & A. Udías, (2012). Proceso de ruptura del sismo de Lorca de 11 mayo 2011. *Física de la Tierra* 24, 71-82.

Delgado, J., J.A. Pelaez, R. Tomas, F.J. Garcıa-Tortosa, P.C. Alfaro & C. Lopez Casado, (2011). Seismically-induced landslides in the Betic Cordillera (S Spain). *Soil Dynamics and Earthquake Engineering* 31, 1203–121.

Frontera, T., P. Blanco, A. Concha, X. Goula & F. Pérez Aragüés, (2012). Medidas de deformaciones cosísmicas con DInSAR para el terremoto de Lorca del 11 de mayo de 2011. *Física de la Tierra* 24, 151-169.

Guerrieri, L. & E. Vittori, eds. (2007). *Intensity Scale ESI-07*. Mem. Descr. Carta Geologica d'Italia, 74. APAT, Rome (Italy). 41 p.

IGME (2011). *Informe geológico peliminar del Terremoto de Lorca del 11 de mayo de 2011 Mw 5.1*. IGME, Madrid (Spain). 47 p.

IGN (2012). *Informe del sismo de Lorca del 11 de mayo de 2011*. IGN, Madrid (Spain). 129 p.

López-Comino, J.A., F. Mancilla, J. Morales & D. Stich, (2012). Rupture Directivity of the 2011, Mw 5.2 Lorca Earthquake (Spain). *Geophysical Research Letters* 39, L03301.

Martínez-Díaz, J.J., M. Bejar, J.A. Álvarez-Gómez, F. Mancilla, D. Stich, G. Herrera & J. Morales, (2012). Tectonic and seismic implications of an intersegment rupture. The damaging May 11th 2011 Mw 5.2 Lorca, Spain, earthquake. *Tectonophysics* 546-547, 28-37.

Martínez Solares, J.M., J.V. Cantavella Nadal, L. Cabañas Rodriguez & J.F. Valero Zornosa, (2012). El terremoto de Lorca de 11 de mayo de 2011 y la sismicidad de la región. *Física de la Tierra* 24, 17-40.

Mendoza, L., A. Kehm, A. Koppert, J. Martín Dávila, J. Gárate & M. Becker, (2012). The Lorca Earthquake observed by GPS: a Test Case for GPS Seismology. *Física de la Tierra* 24, 129-150.

Pérez-López, R., F. Martín-González, J.J. Martínez-Díaz & M.A. Rodríguez-Pascua, (2012). Rock-falls related to the 1674 historic earthquake in Lorca (spain): lichenometric ages. *Proceedings 3rd INQUA-IGCP 567 Workshop, Morelia, Mexico*. 141-144

Rodríguez-Peces, M.J., J.L. Pérez-García, J. García-Mayordomo, J.M. Azañón, J.M. Insua & J. Delgado, (2011). Applicability of Newmark method at regional, sub-regional and site scales: seismically induced Bullas and La Paca rock-slide cases (Murcia, SE Spain). *Natural Hazards* 59, 1109-1124.

INQUA Focus Group on Paleoseismology and Active Tectonics

paleoseismicity.org

# Development of a numerical system and field-survey charts for earthquake environmental effects based on the Munsell Soil Color Charts

P. G. Silva (1), E. Roquero (2), M.A. Rodríguez-Pascua (3), T. Bardají (4), P. Huerta (1), J. L. Giner (5), R. Pérez-López (3)

(1) Dpto. Geología, Escuela Politécnica Superior de Ávila, Universidad de Salamanca. Hornos Caleros, 50. 05003-Ávila. (Spain). Email: pgsilva@usal.es , phuerta@usal.es
(2) Dpto. Edafología, E.T.S.I Agrónomos. Universidad Politécnica de Madrid, Madrid (Spain). Email: elvira.roquero@upm.es
(3) Instituto Geológico y Minero de España, IGME. Madrid, Spain. Email: ma.rodriguez@igme.es, r.perez@igme.es
(4) Dpto. Geología. Fac. Ciencias, Universidad de Alcalá de Henares. Madrid, Spain. Email: teresa.bardaji@uah.es
(5) Dpto Geología y Geoquímica, Fac Ciencias. Universidad Autónoma de Madrid. Campus Madrid, Spain. Email: jorge.giner@uam.es

***Abstract:*** *This contribution presents the development of a numerical system for cataloguing and classification of the earthquake environmental effects (EEE) considered in the ESI-07 Intensity Scale. The system follows the overall structure of the decimal numerical system for colors developed by Munsell (1905) based in three dimensional parameters (HUE value/chroma; e.g. 10YR 6/4), otherwise commonly used in soil survey in Quaternary research. The EEE system considers nine different EEE classes, one for primary effects, seven for secondary effects and one for other environmental effects. EEE Classes work as the running hue-like headers for the designed EEE charts for earthquake field-survey. Two dimensional parameters are size and intensity combined with a third parameter for characterization of type-effect. Each EEE chart display different type/intensity values identified by color chips resembling the Munsell color charts. So each effect can be easily labelled attending to its Dimension_EEE Class and type/intensity value following this nomenclature e.g. 10GK 2/6.*

***Key words**: ESI-07 Scale, Earthquake effects, Numerical system, Field-charts, Munsell soil color system.*

## INTRODUCTION

The development of the ESI-07 Macroseismic Scale (Guerrieri and Vittori, Eds, 2007) created a first rational framework for the quantification of the environmental effects of the earthquakes (EEE) considered in the classical macroseismic scales of Mercalli, MM, MSK and others. The use of the ESI-07 Scale and cataloguing of the earthquake environmental effects is crucial for the further parameterization of natural effects at different intensity levels. The INQUA International Focus Area on Paleoseismology, Active Tectonics and Archaeoseismology (PATA; TERPRO Commission) launched successive projects on these topics since 2007. Presently after the INQUA EEE Catalogue Project, the Focus area is running the project on EEE parameterization (INQUA Project 1299, 2012-2015). This initiative wants to extend the widespread use of the ESI-07 scale among the paleoseismological community in order to generate a wide data-base on historical and instrumental EEE quantified data to be used for comparison with the geological and geomorphological records of paleoearthquakes.

In this sense, the 1299 INQUA Project launched in May 2013 an android-based application for its use in the geological survey of EEE after an earthquake (Papathanassiou et al., 2013), to facilitate the collection of data to be exported to the EEE Catalogue (www.eeecatalog.sinanet.apat.it/terremoti). Following this initiative this work presents a simple portable chart for EEE cataloguing and quantification based on the

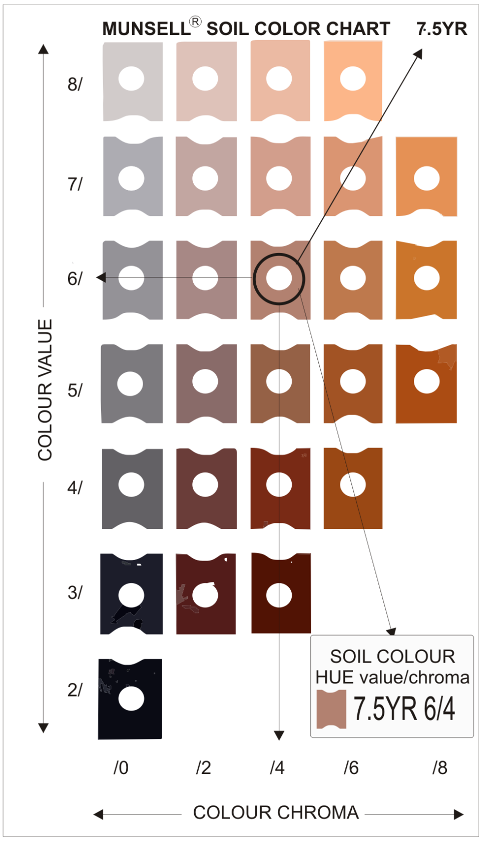


*Fig. 1: Structure and soil numerical nomenclature of the Munsell soil color charts used for soil survey (Munsell Color, 1975).*

Munsell Soil Colour Chart system used for soil survey, furthermore of widespread use in Quaternary research.

**THE MUNSELL COLOR SOIL SYSTEM**

The Munsell Soil Chart is structured in the colour system designed by Albert H. Munsell (1905), former professor of the Massachusetts College of Art and Design, and adopted by the USDA as the official color system for soil research in 1930. The work on Color Notation (Munsell, 1905) established a rational way to describe the colors using a decimal notation instead of colour names. This rational system label the colours based on three colour dimensions: hue, value, and chroma.

The Munsell system establish five principal colour hues (Red, Yellow, Green, Blue and Purple), along with five more intermediate ones (e.g. YR, BP) subdivided in different colour-steps increasing in 2.5 units (e.g. 10YR to 2.5 YR). The value dimension is related with the colour intensity (lightness) and varies vertically along the colour hue from dark (value 0) to light colors (value 10). The chroma dimension is related with the colour saturation (purity) and varies along the colour value from lower chromas being less pure (less saturated colours) and higher chromas more pure (more saturated colours). The chroma subdivision is commonly given in steps from 1 for the lower chroma to 12 for the more pure one. In the practice, the Munsell soil color charts consider hues between 10R and 7.5Y (pages), codified in unitary colour values between 2 and 8 (2, 3, 4, 5, 6, 7, 8) in the vertical axis and colour chromas between 0 and 8, in two units steps (0, 2, 4, 6, 8) in the horizontal axis. This make possible offer color notations defined by these three dimensional parameters following a decimal nomenclature such as 10 YR 5/4 (yellowish brown), 2.5Y 7/2 (light grey), etc, identified by individual value/chroma colored chips. Summarizing, the Munsell color system clearly identify soil colors by their hue and chroma/value numerical codes. In this way the proposed EEE chart system intends to identify EEE by their dimension and type/intensity numerical codes proposed here.

**EEE NUMERICAL SYSTEM: PARAMETERS AND STRUCTURE**

The proposed numerical system for codification of Earthquake Environmental Effects (EEE) follows a similar structure than the Munsell soil color charts. In our case we consider four parameters, two dimensional parameters for quantification and other two descriptive ones for characterization. The Dimensional parameters are those related with the Intensity (ESI-07) and the size or dimension of the considered environmental effect. The descriptive parameters are the EEE classes considered in the ESI-07 Scale, subdivided in five different EEE types. Types are numbered from 1 to 5 for each class attending to their occurrence for increasing intensity levels and their decreasing potential to be preserved in the geological record.

The proposed structure for codification considers the EEE divided in nine different classes, extracted from the descriptions of the different EEE ESI categories and codified alphabetically in relation to primary and secondary effects. Therefore there are one primary class **(PR)** gathering surface faulting and ground uplift/subsidence and seven secondary ones related to Hydrological anomalies **(HA)**, Hydrological Disturbances **(HD)**, Ground cracks and fractures **(GK)**, Liquefaction and land subsidence **(LQ)**, Slope movements **(SM)**; Anomalous waves and variations in inland water bodies **(WA)**; anomalous littoral waves and Tsunamis **(WT)**. A last EEE class groups the ESI-07 categories related to other difficult to quantify environmental effects, such as tree shacking, jumping stones and dust clouds and is labelled as "other effects" **(OT)**. Anomalies on water

*Table 1: Decimal (quantitative) and binary (qualitative) numerical codes used to describe the dimensions or size of the observed earthquake environmental effects in the proposed EEE Numerical System.*

QUANTITATIVE DIMENSION (DECIMAL CODES)

| Code | Observable effect scale | Metric system range |
|---|---|---|
| 00 | millimetres (mm) | 0.001-0.009 m |
| 01 | centimetres (cm) | 0.01-0.05 m |
| 02 | several centimetres (cms) | 0.01-0.05 m |
| 03 | decimetres(dm) | 0.1-0.9 m |
| 1 | meters (m) | 1-5 m |
| 2 | several meters (ms) | 5-9 m |
| 10 | decametres (dc) | 10-50 m |
| 11 | several decametres (dcs) | 50-90 m |
| 100 | hectometres (hm) | 100-500 m |
| 101 | several hectometres (hms) | 500-900 m |
| 111 | kilometres (km) | 1000-5000 m |
| 121 | several kilometres (kms) | 3000-9000 m |
| 122 | tens of kilometres (tkm) | 10-90 km |
| 202 | hundred of kilometres (hkm) | 100-500 km |
| 222 | several hundred of kilometres (hks) | 500-900 km |
| 303 | thousand of kilometres (Mkm) | 1000-5000 km |
| 333 | several thousand of kilometres (Mks) | >5000 km |

QUALIITATIVE DIMENSION (BINARY CODES)

| Observable effect feature | Code |
|---|---|
| **Frequency** | |
| Few | 00 |
| Some | 01 |
| Several | 10 |
| Many | 11 |
| **Amount** | |
| Very small | 00 |
| Small | 01 |
| Moderate | 10 |
| Large | 11 |
| **Range** | |
| Feasible | 00 |
| Weak | 01 |
| Moderate | 10 |
| Strong | 11 |

bodies (WA and WT) are subdivided from the wider ESI category of “Anomalous waves and Tsunamis”. In a similar way hydrological classes HA and HD does it the same from the boarder ESI-07 category of “Hydrological Anomalies”. These nine EEE classes constitute the heading “EEE hues” for the proposed EEE numerical system ordered in nine different charts for field survey (Fig. 2).

Each EEE Class chart display a vertical axis subdivided in the nine ESI intensity levels from /4 to /12 in which the EEE are observables, and also a horizontal axis subdivided in five different EEE types for each class, numbered from 1/ to 5/ attending to their occurrence for increasing intensity levels and therefore to their potential to be preserved in the geological record. Each chart could have a maximum of forty five different type/intensity values from 1/4 to 5/12. Consequently the type/intensity values of 2/4 or 3/5 are dimensionless and have less potential to be preserved, whilst type values 4/8 or 5/10 have moderate or considerable sizes and a greater potential of preservation in the geological record. As in the Munsell soil color charts each type/intensity value is identified by color chips, in which color gradation are only related with the vertical axis increasing the color saturation for increasing intensity levels. Each EEE class is identified by a particular color: SF (red); GK (brown); SM (orange); LQ (Green); HA (pale blue); HD (dark blue); WA (bright blue); WT (deep blue); and TH (lime). The idea to use different colors is to provide the basic framework to identify easily the different effects for future mapping purposes, such as geological maps (colur id age) or geomorphological maps (color id processes) do.

The dimensional parameter of size appear labelled in the type/intensity value colored chips following a decimal code from 00 to 03 for sub-metric effects, from 1 to 101 for metric-hectometric effects and from 111 to 333 for effects up to the kilometric scale (Table 1). The numerical increment of this parameter attends to the increasing dimension-scale or extent of each particular EEE as displayed in Table 1. Therefore 0N sizes are submetric, N sizes are metric, 1N sizes decametric; 10N hectometric and 111 kilometric scales. To identify supra-kilometric dimensions 1N1 identify effects of tens of kilometres, 2N2 hundreds of kilometres and 3N3 thousands of kilometres, being 333 the maximum dimensional value. In each EEE Class the measure parameter in length/width (m), areal extent (m2) or volume (m3) is also specified (Fig. 2). For some special EEE classes or particular type-effects the ESI-07 scale only provides qualitative or semi-quantitative descriptions, so particular labels in binary code between 00 and 11 are used to specify semi-quantitative evaluations on the frequency, amount and/or range of the EEE, such as few (00), some (01), several (10) and many (11) as illustrated in Table 1. These binary codes have been also used to specify other

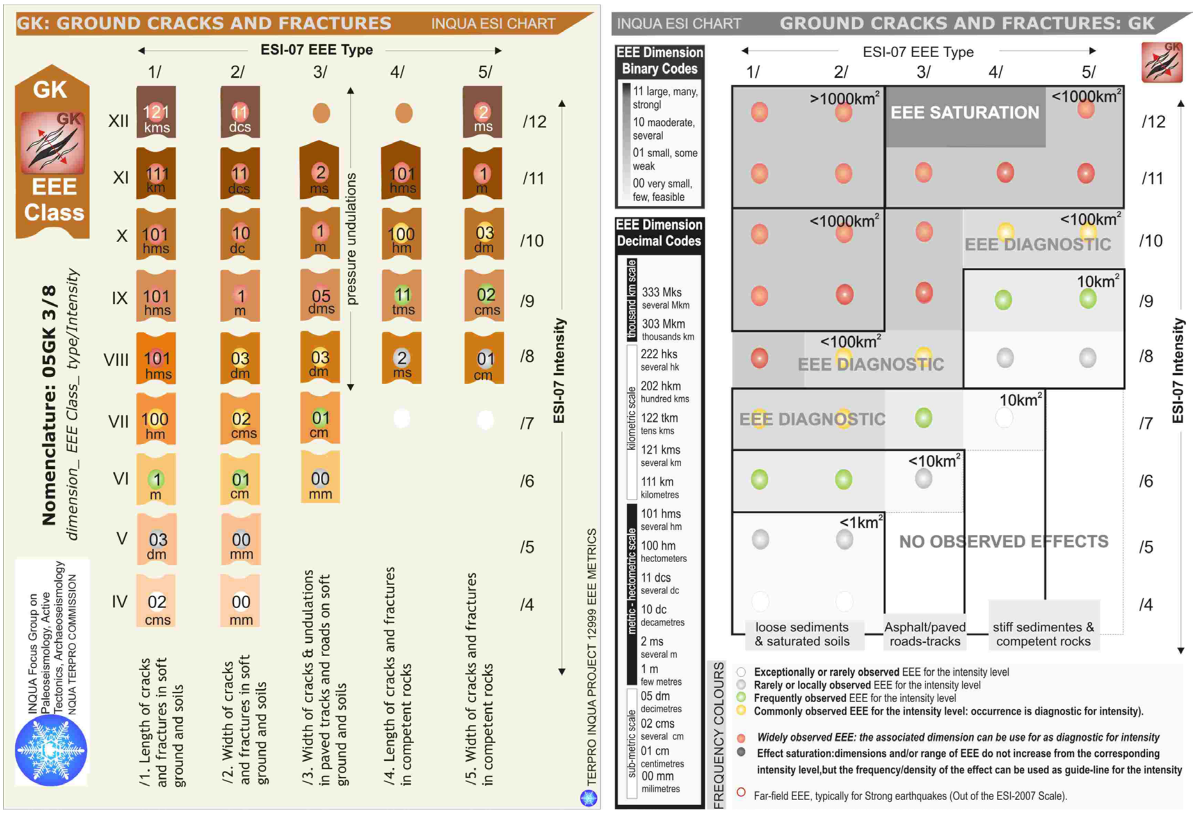


*Fig. 2: Example of EEE ESI-07 CHART for Ground Cracks and fractures (left)) displaying the corresponding back-page illustrating occurrence frequency zones and accompanying explanations of dimensional parameters for dimensional parameters.*

parameters related with the temporal occurrence of a particular effect (time; e.g. hydrological disturbations) or intensity of the vibration in vegetation.

## EEE NUMERICAL SYSTEM: DECIMAL NOMENCLATURE, STYLE AND GUIDELINES

According to the Munsell system the nomenclature of earthquake effects in the EEE numerical system give the size_EEE Class_type/intensity following this example for decimal quantitative dimensions: 00GK 4/8, indicates a milimetric-scale(00) ground crack (GK) width developed on stiff ground (4/) in the intensity VIII zone (/8). In the same way, a 06PR 2/10 will indicate a several meters scale (06) primary fault rupture (PR) width (2/) in the intensity X zone (/10). For binary semi-quantitative effect dimensions e.g. 01HD 2/6 will indicate small variations (01) on water turbidity (HD 2/) in intensity VI zone (/6).

In addition, each EEE chart provide a guide on the frequency of the observed type effect for each intensity level preserving the vocabulary of the ESI-07 scale. Frequency guides follow a traffic light-like color code in order to facilitate field surveys (Fig. 2). These frequency codes appear as central colored circles inset in each type/intensity chip. White circles indicate exceptionally or very rarely observed features for a particular intensity level. Grey circles illustrate rarely or locally observed features. Green circles indicate frequently observed features. Orange circles indicate commonly observed features diagnostic for a particular intensity level. Finally, red circles designate widespread occurrence of a particular type-effect from a particular intensity level. Also in the charts are marked with empty circles without colored chips those effects characteristic of the far-field of strong earthquake-tsunami events out of in the ESI-07 Scale for intensity levels down to IV (4). The surveyor is therefore free to label these effects following the numerical system below intensity 4 as for instance 2/3 or 5/2 if occur.

The EEE charts follow the style of the Munsell soil charts and the colored chips run from light colors for low intensity levels (/4) and more dark ones for the high intensity levels (/12). Consequently colours are vertically graded with a different colour for each EEE chart (Fig. 2). Geometry of the color chips defining type/intensity values can be straight, notched, or arrow shaped. Chips with straight lower boundaries indicate that a particular type/intensity value starts to be recorded in the environment. Chips with notched boundaries indicate that the type/intensity runs commonly for different intensity levels, if a notched chip appear in the first intensity level indicates that the effect can be exceptionally observed in the immediately lower intensity level.

Final chips for strong intensity levels can have a straight upper boundary indicating that at this particular intensity level the effect stops, but final arrow shaped chips signify that the dimension /occurrence of a particular type-effect saturates from this particular intensity level. Therefore their dimension doesn't increase significantly from that intensity, as stated in the ESI-07 Scale. However, the surveyor may decide to label a particular uncommon type/intensity value (e.g. 3/11) giving the observed size (00 to 333) and class in the zone of saturation (e.g. 10LQ 3/11). The reverse of each chart is subdivided in spaces delineating the intensity zones of no observation, common occurrence, diagnostic occurrence and saturation for each particular EEE class. This provides a simplified visual guide to the surveyors of the intensity levels in which each EEE class commonly occurs. These intensity zones are identified by grey scales. In these spaces are also highlighted the common extent of the observed earthquake effects specified in the ESI-07 scale (Fig. 2).

Following the guidelines of the ESI-07 Scales (Guerrieri and Vittori Eds., 2007) the proposed EEE numerical system has to be used for EEE description and quantification at "locality level". If there are sufficient quantified EEE sites in a locality we can proceed to assign the ESI Intensity to the selected locality. Isolated effects can be classified at "site level" but normally this is insufficient to assign a particular intensity. Taking into account all the collected data at different localities we can asses the epicentral intensity (I0) considering the EEE distribution parameters at "earthquake level" (e.g. surface faulting parameters and total area distribution of classified EEEs).

## FINAL REMARKS

The EEE numerical system and its summarization in easy to use portable charts follow different purposes: a) provide a numerical system of classification for EEE in order to facilitate its further identification and cataloguing; b) offer a graphic rational translation and systematization of the ESI-07 scale; c) facilitate field-data collection for instrumental, historical and paleoseismic events by means a friendly chart-system similar to the Munsell soil color charts commonly used in Quaternary research; and d) give basic numerical guidelines to no expertise researchers on EEE data collection. The structure and nomenclature of both, the proposed numerical system and the portable EEE charts preserve the significancy and the vocabulary of the ESI-07 scale in order to provide a graphic tool for earthquake research and cataloguing. This system can be additionally implemented in portable electronic devices and applications, such as that developed by Papathanassiou and Kopsachilis (2013).

**Acknowledgements:** This work is supported by the INQUA TERPRO Project 1299: EEE Parameterization (2012 – 2015) and by the Spanish research project CGL2012-37281-C02.01 (QTECBETICA-USAL).

## References

Guerrieri, L. & E. Vittori, (eds.), (2007). Intensity Scale ESI-07, *Memorie descrittive della Carta geologica d'Italia*, APAT, Rome. 41 pp.

Munsell, A. H. (1905). *A Color Notation*. G. H. Ellis Co. Boston, USA. 89 pp.

Munsell Color (1975). *Munsell Soil Color Charts*. Macbeth Division, Kollmorgen Corporation, Baltimore.

Papathanassiou, G. & V. Kopsachilis, (2013). Development of an android-based application for earthquake research: Earthquake Geo Survey 1.1. In: *Proceedings of the 4th INQUA workshop on Paleoseismology, Active Tectonics & Archeoseismology* (Grützner, C., A. Rudersdorf, R. Pérez-López & K. Reicherter, eds., this volume), Aachen, Germany.

# Tfc Ssk_rp_l Aargtc F_sjr_lb grq n_jcmqcgqkgagrw

*Asdani Soehaimi (1) Marjiyono(1), Kamawan(1) and Dicky Muslim(2)*

(1) Geological Agency, Ministry of Energy and Mineral Resources Indonesia, 57 Diponegoro Street, Bandung. Email: s.asdani@yahoo.com.

(2) Padjadjaran State University, Km.21 Raya Sumedang Street, Sumedang, Indonesia

***Abstract:*** *The Sumatra fault zone (SFZ) is one of the most active faults in the Indonesian archipelago. The Sumatra fault is highly segmented and divided into 20 major segments based on their geomorphic features, mechanism of expression and activity, and range in length from 35 km to 200 km. The Sumatran fault has generated many historical destructive earthquakes with magnitudes M > 7; since 1890 there have been about 21 major earthquakes rupturing different segments of this fault with magnitudes ranging from 6.5 to 7.7 $M_w$. On average, the repetition of major earthquakes along the SFZ is about one or two every decade . Two historical destructive earthquakes occurred in Lampung Province along the Semangko Segment (Ranau – Suoh), Hamkatir and Sukabumi subsegment in 1933 and 1994 (Mw 7.0). A trenching study was carried out on the Hamkatir sub segment. Through studying the stratigraphy in the excavation, 3 Quaternary sedimentation sequences can be determined. The first sedimentation sequence occurred 5370 ± 120 yr BP and the second sedimentation process occurred at 2980 ± 120 BP. The fault fracture exposed in the trench, therefore, occurred after 5370 ± 120 yr BP and experienced a reactivation after 2980 ± 120 BP. The youngest sedimentation sequence shows no evidence of faulting.*

***Keywords:*** *Sumatra Active Fault and Present Reactivation*

## TECTONIC ACTIVITY OF SUNDALAND

The Sumatran fault zone (SFZ) runs along the axis of the Sumatra Island Arc located on the western margin of the Sunda Shelf, also known as Sundaland. It has an orientation of N 330°E and a total length of approximately 1650 km. This fault zone lies above the oblique subduction zone between the Indo-Australian oceanic plate and the Eurasian continental plate.

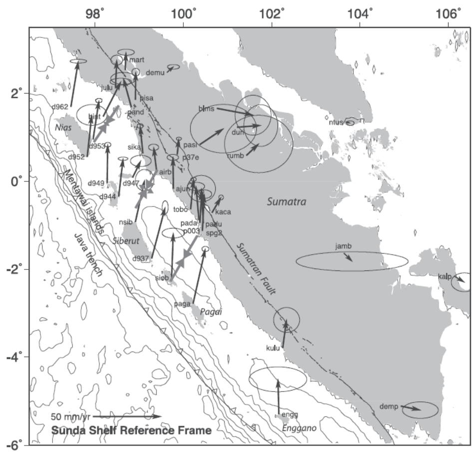


*Fig. 1: GPS velocity field of Sumatra and adjacent areas relative to the estimated Sunda Shelf reference frame (Bock et al., 2003).*

Tectonic activity within this region is shown by the GPS velocity field of Sumatra and adjacent areas relative to the estimated Sunda Shelf reference frame (Figure 1). The velocity of the Sunda Shelf, relative to Indo-Australian oceanic plate, increases southwards across Sumatra from ~56 mm/yr to ~62 mm/yr (Chlieh *et al.*, 2008). Other plate models for the Sumatran plate boundary yield about the same relative motion (Michel *et al.*, 2001); at a longitude of 107°E at the Sunda trench the relative velocity vector is approximately 71 mm/yr in a N20°E direction (Bock *et al.*, 2003).

The dynamics of the northeast-dipping subducting slab along the eastern margin of Sundaland plays an important role in the resulting tectonic activity of the region. The Sumatran fault accommodates the strike-slip (dextral) component of active deformation along the Sunda trench, which is derived from oblique slab motion with respect to the Sunda margin, shown in figure 1. GPS data from Indonesia indicates that Sumatra (on the Sunda side of the Sumatran fault) is moving approximately 6 mm/yr north-eastwards relative to "stable" Sunda, consistent with the NE–SW maximum horizontal stress orientations observed from fault plane solutions and borehole breakouts (Mount and Suppe, 1992).

## QUATERNARY HISTORY OF SUNDALAND

The Quaternary history of Sundaland encompasses the larger region, including the South China Sea, part of the West Java Sea, coastal eastern Java and islands nearby, a great portion of the Malaysia peninsula and western Borneo. During Quartenary the Sunda Shelf has been one of the worlds largest shelf area.

An explanation of the Sunda Shelf's evolution throughout the Neogene can be found in Molengraaff and Weber (1921) and Molengraaff (1922). These authors interpret the present day biogeography and morphology of the region caused by the Pleistocene glaciations. They also attempt the first river drainage reconstruction in the Sunda shelf at the time of the last glacial maximum (20-22 ka) and sea level lowstand, as shown in Figure 2.

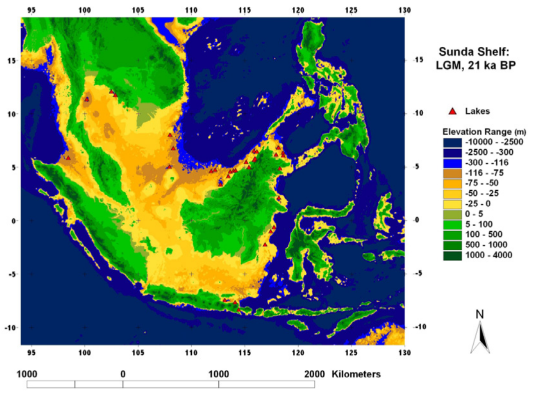


*Fig. 2: Exposed land (Sundaland) during the Last Glacial Maximum (20-22 ka), corresponding here to isobath -116 m (brown to yellow), compared to present day coastline (green) (Sathiamurthi and Voris, 2006).*

## THE SUMATRAN ACTIVE FAULT

Geotectonic activity of the Sumatran Island Arc during the Quaternary is shown by the high activity of both the Sumatran fault and the volcanoes along the Barisan Range. The Sumatran fault has generated many historical earthquakes with magnitudes M > 7; since 1890 about 21 major earthquakes ruptured the segments of the SFZ with magnitudes ranges from 6.5 to 7.7 (Figure 3). Recent earthquakes occurred in south Sumatra (Liwa area) in 1933 and 1994 ($M_w$ 7.0) and around Mount Kerinci in central Sumatra in 1995 ($M_w$ 7.1). On average, the repetition of major earthquakes along the SFZ is about one or two every decade. This fault zone poses a major hazard as most large earthquakes have occurred in highly populated regions; many human casualties as well as great economic losses have occurred.

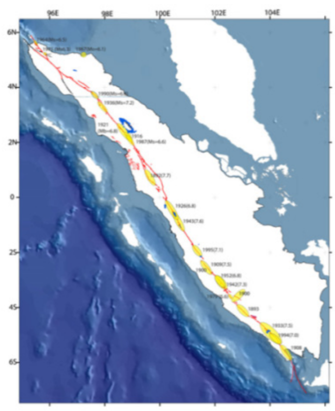

*Fig. 3: Historical and modern earthquakes associated to the Sumatran fault (Sieh and Natawidjaja, 2000).*

The Sumatran fault is highly segmented. Sieh and Natawidjaja (2000) divide it into 20 major segments ranging in length from 35 km to 200 km (Figure 4) based on their geomorphic expression. Each segment bears the name of the major river or bay located along the segment, and includes: Banda Aceh Anu, Lam Teuba Baro, Reuengeuet Blangkejeren, Kla-Alas, Ulu-Aer, Batang-Gadis, Kepahiang-Makakau, Ketahun, Muara Labuh, and Semangko (Katili and Hehuwat, 1967; Cameron *et al*., 1983; Durham, 1940).

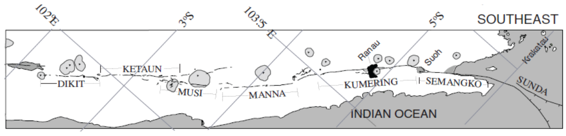


*Fig. 4: Fault segments of the Sumatran fault, from northwest to southeast (Sieh and Natawidjaja, 2000).*

A paleoseismic study on the Sumatran fault in Liwa City (southeast Sumatra) and surrounding areas was undertaken in 2012 by the Geological Agency, Ministry of Energy and Mineral Resources of Indonesia.

The Sumatra fault in this region based on the current research is divided into two major segments namely Ranau – Suoh and Suoh - Semangko Bay. The Ranau – Suoh segment has 7 (seven) sub-segments. These are:

1. Sub-segment Hamkatir (east), length = 19 Kilometres, maximum displacement is 0.18 cm, Mmax = 6.0 $M_w$.
2. Sub-segment Sukabumi (east), length = 31.5 Kilometres, maximum displacement is 0.25 cm, Mmax = 6.4 $M_w$.
3. Sub-segment Limau Kunci (west), length = 17.4 Kilometres, maximum displacement is 0.17 cm, Mmax = 6.0 $M_w$.
4. Sub-segment Sermau (west), length = 30.4 Kilometres, maximum displacement is 0.24 cm , Mmax = 6.4 $M_w$.
5. Sub-segment Liwa City 1 (middle), length = 21 Kilometres, maximum displacement is 0.19 cm , Mmax = 6.1 $M_w$.
6. Sub-segment Liwa City 2 (middle), length = 20.1 Kilometres, maximum displacement is 0.19 cm , Mmax = 6.1 $M_w$.
7. Sub-segment Liwa City 3 (middle), length = 14.4 Kilometres, maximum displacement is 0.14 cm , Mmax = 5.9$M_w$.

*Paleoseismology*

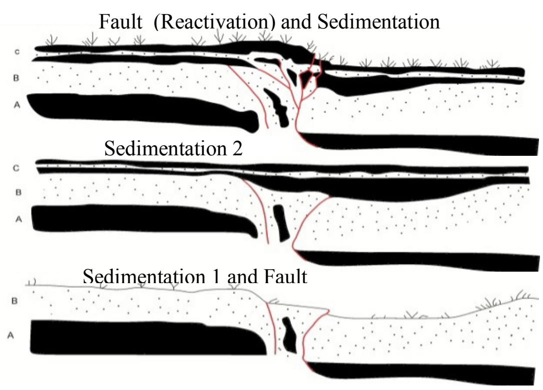


*Fig: 5: Cycles of Sumatra active fault, segment Semangko (Ranau – Suoh). Sub segment Hamkatir (Soehaimi, 1995).*

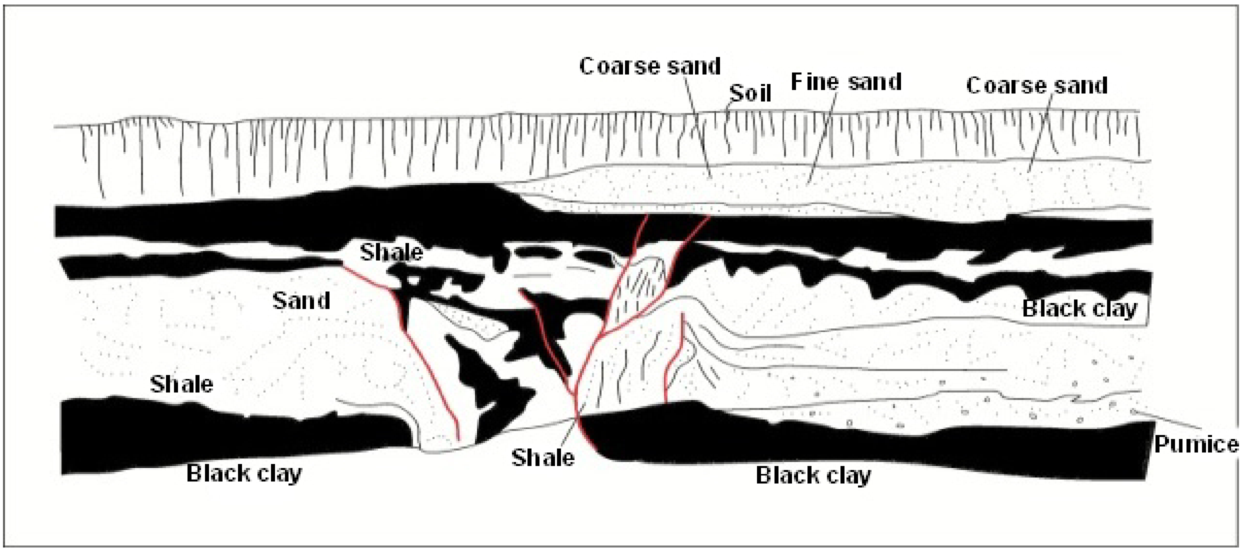


*Fig. 6: Vertical cross section of Sumatera Fault (Semangko segment Ranau – Suoh). Sub segment Hamkatir (Soehaimi, 1995).*

The Sumatran fault was trenched at sub-segment Hamkatir. The trench had a length of 15 meters and was 2.5 meters deep. The orientation of the trench was N230°E and the strike of sub-segment Hamkatir is N110°E at this location. The oldest layer within the trench is as tuffaceous sand (coarse – fine grained) and conglomerate with fragments of pumice gravel. Overlying this is a black clay marshland layer rich with organic material with a thickness of 20-30 cm. Based on radiocarbon analyses, this black clay has an age of 5370 ± 120 yr BP. Above this black clay is a tuffaceous sand layer containing pumice gravel with a thickness of 110 cm. This tuffaceous sand is covered by brownish - black clay containing a lot of organic material and a thickness varying between 50 and 120 cm. Radiocarbon analyses on this organic material provide an age of 2980 ± 120 BP. This brownish - black clay layer in the trench is cut by a fault with a strike of N110°E. The fault is characterized by separated lenses of brownish - black clay against a sharp boundary. Covering this brownish - black clay layer is a layer of clay intercalated with coarse - fine sand, showing a fining-up sequence, and a thickness of 90 cm. Covering this layer is a 10 cm thick blackish brown soil containing roots. The topmost layer consisted of sandy clay with a thickness of 90 cm.

Through studying the stratigraphy in the excavation, 3 Quaternary sedimentation sequences can be determined. The first sedimentation sequence occurred at 5370 ± 120 yr BP and the second sedimentation process occurred at 2980 ± 120 BP. The fault fracture exposed in the trench, therefore, occurred after 5370 ± 120 yr BP and experienced a reactivation after 2980 ± 120 BP. The youngest sedimentation sequence shows no evidence of faulting. Sketches of the trench wall showing the tectonic cycles are shown in figures 5 and 6.

**REFERENCES**


Bock Y., Prawirodirdjo L., Genrich J. F., Stevens C. W., McCaffrey R., Subarya C., Puntodewo S. S. O., Calais E., 2003. Crustal motion in Indonesia from Global Positioning System measurements. *J. Geophys. Res*. 108, B8, 2367, 17p.

Cameron, N., et al, (1983). Geology of the Takengon quadrangle, Sumatra, *report Geol. Res. and Dev. Cent., Bandung, Indonesia*, 1983.

Chlieh M, Avouac J P, Sieh K, Natawidjaja D H and Galetzka J., 2008. Heterogeneous coupling of the Sumatran megathrust constrained by geodetic and paleogeodetic measurements; *J. Geophys. Res*. 113 B05305, doi:10.1029/2007JB004981.

Durham, J., (1940). Oeloe Aer fault zone, Sumatra, *Bull. Am. Assoc. Pet Geol*., 24, 359-362.

Hanebuth T.J.J., Stattegger K., 2004. Depositional sequences on a late Pleistocene–Holocene tropical siliciclastic shelf (Sunda Shelf, southeast Asia). *Journal of Asian Earth Sciences*, 23(1), 113–126.

Katili, J., and F. Hehuwat, (1967). On the occurrence of large transcurrent faults in Sumatra, Indonesia, *J. Geoscœ, Osaka City Univ., 10*, 5- 17.

Michel, G. W., 2001. Crustal motion and block behaviour in SE-Asia from GPS measurements, *Earth Planet. Sci. Lett*., 187, 239–244.

Molengraaff, G.A.F, (1922). De Geologie der zeen van de Nederlandsch Oost-Indie Archipel. *De Zeen van Nederlandsch Oost-Indie, Ch g, pp. 1–566. K. Nederlandsch Aardrijkokundig Genootschap, Amsterdam.*

Molengraaff, G.A.F., Weber, M, (1921). On the relation between the Pleistocene glacial period and the origin of the Sunda Sea (Java and South China Sea) and its influence on the distribution of coral reefs and on the land and freshwater fauna. *Proceedings of the Section of Sciences. Koninklijke (Nederlandse) Akademie van Wetenschappen te Amsterdam, 23*, 395–439.

Mount, V. S. and Suppe, J, 1992. Present-day stress orientations adjacent to active strike-slip faults: California and Sumatra: *Journal of Geophysical Research*, 97, 11,995-12,031.

Sathiamurthy, E., Voris, H. K, (2006). Maps of Holocene Sea Level Transgression and Submerged Lakes on the Sunda Shelf. *The Natural History Journal of Chulalongkorn University. Supplement 2*, 1-43.

Soehaimi, A, 1995. Joint Technical Cooperation between Geological Research and Development Centre of Indonesia and Geological Survey of Japan, JICA

Sieh, K. and Natawidjaja, D, (2000). Neotectonics of the Sumatran fault, Indonesia. *Journal of Geophysical Research, 105, 28*,295–28,326.

# Seismic hazard assessment for the Ada Tepe site (Bulgaria) – case study

*Solakov,Dimcho, Stela Simeonova, Petya Trifonova, Metody Metodiev*

(1) National Institute of Geophysics, Geodesy and Geography, Bulgarian Academy of Sciences, Acad. G. Bonchev Str., Bl. 3, Sofia, Bulgaria.

***Abstract:*** *Among the many kinds of natural and man-made disasters, earthquakes dominate with regard to their social and economic impact on the urban environment. Seismic hazard assessment is of a substantial importance, because it provides valuable information for seismic safety and disaster mitigation and support decision making for the benefit of society. The main objective of this study is hazard assessment based on integrated basic geo-datasets in thematic mapping products. Probabilistic techniques that are applied utilize all the details and parameters of the seismotectonic model. The so-called "deductive methods" is used – it deduces what are the causative sources, characteristics, and ground motion for future earthquakes (McGuire, 1993).*

***Key words****: Seismic hazard assessment, Data integration, Seismotectonic model, Seismicity, Bulgaria.*

## INTRODUCTION

Earthquakes are the most important natural disaster that is concerned in risk assessment for individual critical infrastructure facilities. Seismic hazard is beyond human control, but a good knowledge of its spatial-temporal distribution is essential for risk mitigation. The assessment of seismic hazard is the first link in the disaster prevention chain and the first step in the evaluation of the seismic risk.

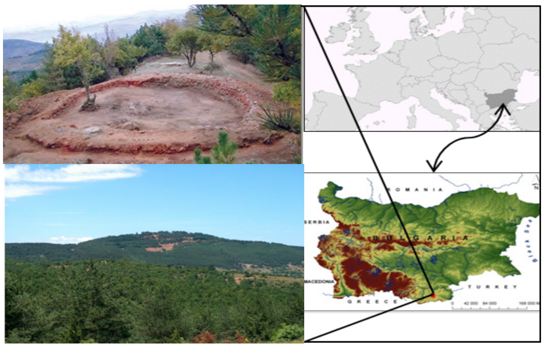

*Fig. 1: The study area of Ada Tepe site , Bulgaria. Life at Ada Tepe has existed since 3500, with some interruptions. The villages were inhabited by the ancient miners, pulls gold from the XVto the VIII century BC. On the flat hilltop a sanctuary is raised.*

The main objective of the present study is to integrate basic spatial geo-datasets in thematic mapping products used to assess the seismic hazard thus providing a basis for disaster management of the Ada Tepe region in Bulgaria (Fig. 1).

According to the current archeological investigations, Ada Tepe (called "Golden Island") is the oldest gold mine in Europe with Late Bronze and Early Iron age (Popov et al., 2011). It is a typical low-sulfidation epithermal gold deposit and is hosted in Maastrichtian-Paleocene sedimentary rocks above a detachment fault contact with underlying Paleozoic metamorphic rocks. Recently, archeological field data indicate some effects that can be caused by hard ground shaking, i. e. a strong earthquake occurred in the Ada Tepe surroundings. Archeological evidence dates destructions of a village (situated on Ada Tepe) to sometime between XV and X century BC. Concerning the fact that no seismicity is reported in the historical catalogues (e.g. Ambraseys, 2009) for the Eastern Balkan region during that time period the useful archeological information needs further studies.

Ada Tepe (25°.39'E; 41°.25'N) is located in the Eastern Rhodope unit. The region is highly segmented despite the low altitude (470-750 m) due to widespread volcanic and sediment rocks susceptible to torrential erosion during the cold season. Besides the thorough geological exploration focused on identifying cost-effective stocks of mineral resources, a detailed geophysical analysis concerning different stages of the gold extraction project was accomplished. Here we present the main results from the geophysical investigation aimed to clarify the complex seismotectonic setting of the Ada Tepe site region. The overall study methodology consists of collecting, reviewing and estimating geo-physical and seismological information to constrain the model used for seismic hazard assessment of the area.

## MATERIALS AND METHODS

Spatial pattern of seismogenic structures in the Ada Tepe region (within a radius of 200 km) is identified by integration of geological and geophysical data with the seismological information (historical and instrumental seismicity).

From plate-tectonic point of view the territory of Bulgaria and the Balkans belongs to the southern edge of the Eurasian plate. The geodynamics of the region is determined mainly by the subduction of the African plate in the Aegean subduction zone and the collision of the Arabe plate in Eastern Anatolia. The area belongs almost entirely to a region of low rates of recent horizontal displacements and deformations, not exceeding 4-5 mm/y and vertical deformations of the range 0-1 mm/y. Based on GPS data the strain field has also very low values. All these low values are the reason for the low rate of deformation and the low frequency of strong earthquakes – over a 1000 years period. The contemporary active faults in the considered region (Report NIGGG, 2012a) are presented in Fig. 2.

Geophysical data consist of grids with a cell of 1 km for gravity and 3 km for magnetics. Fifteen profiles having NE – SW orientation are also used to constrain gravity and magnetic interpretation results. The Total Horizontal Gradient (Stavrev et al., 2009) is calculated from gravity data (Bouguer reduction).

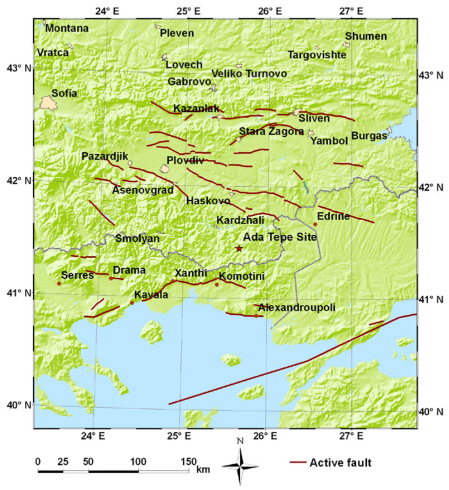


*Fig. 2 Active faults in the Ada tepe region (modified from Report NIGGG, 2012a).*

The map in Fig. 3 indicates the axes of steep gravity transitions by the lines of maximum gradient values, given in dark colours. The most intensive among them are marked by white lines as potential axes of faults, flexures and other structures of dislocation (Trifonova et al., 2013).

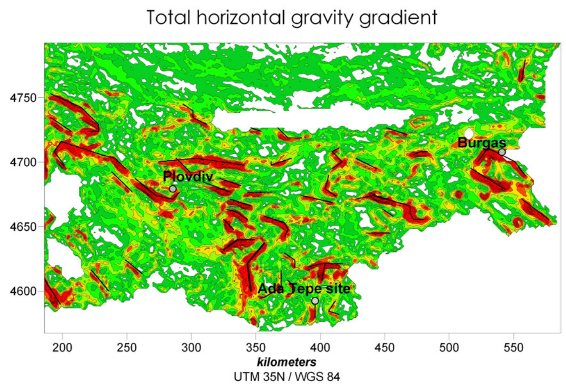


*Fig. 3 Axes of faults, flexures and other structures of dislocation obtained from the modulus of the total horizontal gravity gradient (THG).*

Euler deconvolution (Reid et al., 1990) and Werner deconvolution (Telford et al., 1991), are applied to gridded and profile data. These inverse methods yield valuable information for investigation concerning multiple source anomalies interpretation and need of averaged depth/position results. Observed magnetic anomalies in Ada Tepe region are related mainly to magnetic products from volcanic activity with different age and less commonly to varieties of metamorphic rocks. Some of them are connected to the post collisional faulting (Trifonova et al., 2009).

Regional seismicity pattern is illustrated in Fig. 4. The map suggests that seismicity in the region (within a radius of 200 km) is not uniformly distributed in space. Therefore, the seismicity is described in distributed geographical zones. Each zone is characterised by its own specific tectonic, seismic, and geological features. The proposed seismic zonation corresponds to the seismotectonic model of Bulgaria and Northern Greece as one seismotectonic unit and can be considered to influence the seismic hazard for Ada Tepe site (e.g. Solakov et al., 2009).

A homogenized catalogue for the region is compiled based on available historical and instrumental seismological information (Simeonova et al., 2008).

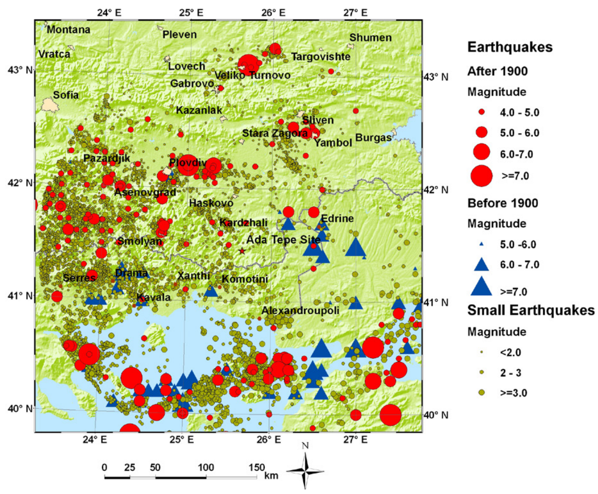


*Fig. 4 Regional seismicity (historical and instrumental earthquakes) pattern (modified from Report NIGGG, 2012a)*

## RESULTS AND DISCUSSION

A geo-database is developed for seismic hazard assessment. The geo-database design includes an identification of data themes, specification of the contents and representation of each thematic layer, additional spatial and database elements, such as spatial and attribute relationships. A key component of seismic hazard assessment is the creation of seismic source model, which demands translating seismotectonic information in to a spatial approximation of earthquake location and recurrence. The connection between the collected database and seismic source model is a regional seismotectonic map (model). A seismic source model is a simplification of regional seismotectonic model into a form that can readily be employed for hazard computation.

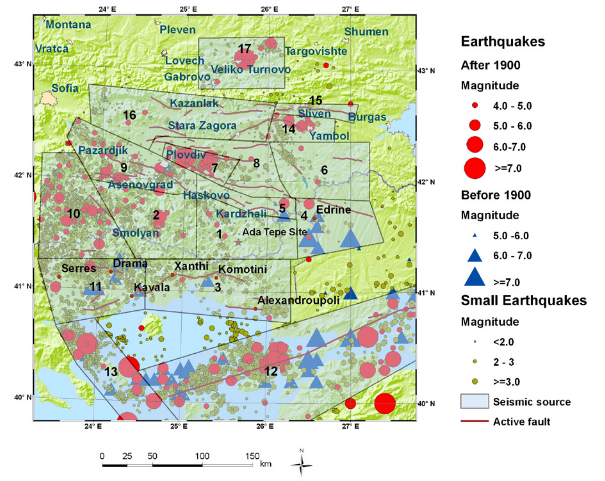


*Fig. 5 Seismic source model (modified from Report NIGGG, 2012b)*

The created model (Fig. 5) consists of 17 seismic sources: For each seismic source are defined: geometry, earthquake distribution in the source, earthquake recurrence frequency and the maximum potential earthquake magnitude.

The probabilistic seismic hazard analysis (PSHA) carries out integration over the total expected seismicity during a given exposure period to provide the estimate of a strong-motion parameter of interest with a specified confidence level. Modern PSHA considers multiple hypotheses on input assumptions and thereby reflect the relative credibility of competing scientific hypotheses. Thus, the PSHA allow the ground motion hazard to be expressed at multiple sites consistently in terms of earthquake sizes, frequency of occurrence, attenuation and associated ground motion. Seismic hazard analysis for the Ada Tepe site is performed using the model of seismic sources in the region presented in Fig. 5 and specified in Table 1.

*Table 1. Parameters of the seismic sources*

| N | Source | *a* normalized to N(Ms>=4.5), for a period of 110 years | | | | *a* normalized to N(Ms>=6.0), for a periog of 300 years | | | | $M_{max}$ |
|---|---|---|---|---|---|---|---|---|---|---|
| | | *b*=0.7 (Ms) | *b*=0.8 (Ms) | *b*=0.85 (Mw) | *b*=1.0 (Mw) | *b*=0.7 (Ms) | *b*=0.8 (Ms) | *b*=0.85 (Mw) | *b*=1.0 (Mw) | |
| 1 | Eastern Rhodope | 1.71 | 2.15 | 2.93 | 3.66 | - | - | - | - | 6 |
| 2 | Central Rhodope | 2.19 | 2.62 | 3.4 | 4.14 | - | - | - | - | 6 |
| 3 | Ksanti | 1.09 | 1.53 | 2.28 | 3.02 | 1.76 | 2.35 | 2.65 | 3.54 | 7.5 |
| 4 | Edrine | 1.38 | 1.82 | 2.91 | 3.33 | 2.24 | 2.83 | 3.25 | 4 | 7.5 |
| 5 | Haskovo | 1.38 | 1.82 | 2.57 | 3.31 | 1.78 | 2.35 | 2.64 | 3.51 | 7 |
| 6 | Elhovo | 1.09 | 1.53 | 2.29 | 3.04 | - | - | - | - | 6.8 |
| 7 | Marica_75 | 2.12 | 2.56 | 3 | 3.7 | 2.03 | 2.61 | 2.9 | 3.79 | 7.5 |
| 8 | Marica | 1.09 | 1.53 | 2.28 | 3.02 | - | - | - | - | 7.5 |
| 9 | Plovdiv | 2.12 | 2.56 | 3.3 | 4.05 | 2.37 | 2.95 | 2.64 | 3.51 | 7 |
| 10 | Western Rhodope | 2.32 | 2.76 | 3.52 | 4.27 | - | - | - | - | 6.5 |
| 11 | Drama | 1.56 | 2.03 | 2.91 | 3.55 | 2.37 | 2.95 | 3.25 | 4.14 | 7 |
| 12 | Aegean sea | 2.72 | 3.16 | 3.91 | 4.67 | 2.99 | 3.59 | 3.89 | 4.78 | 8 |
| 13 | Thessaloniki | 2.09 | 2.48 | 3.23 | 3.99 | 2.61 | 3.19 | 3.49 | 4.38 | 7.5 |
| 14 | Jambol | 1.56 | 2.01 | 2.76 | 3.52 | 2.03 | 2.61 | 2.9 | 3.79 | 7 |
| 15 | Sliven | 1.09 | 1.53 | 2.28 | 3.02 | - | - | - | - | 7.5 |
| 16 | Balkans | 1.21 | 1.61 | 2.44 | 3.15 | - | - | - | - | 7.5 |
| 17 | Gorna Orjahovitca | 2.08 | 2.52 | 3.28 | 4.03 | - | - | - | - | 7 |

The attenuation relationship proposed by Ambraseys et al. (2005) and Next Generation Attenuation (NGA) model developed by Campbell, Bozorgnia (2007) are used in the computation. For propagating the epistemic uncertainties through the probabilistic seismic hazard analysis logic tree is developed that consists of 5 nodes and 192 branches. In the present study a version of machine code EQRISK (McGuire, 1976) is used for probabilistic hazard assessment (the code was developed for practical application in Bulgaria).

A set of 192000 hazard curves is the result from the seismic hazard analysis performed for Ada Tepe site. The mean, median 15th and 85th percentile hazard curves are computed on the bases of calculated 192 000 hazard curves. The mean and 85th percentile values of peak ground acceleration for annual probability of exceedance $10^{-3}$ are 0.15 g and 0.17 g respectively.

The family of hazard curves and their associated weights contain the information about the seismic hazard at the site and its uncertainties.

The hazard results shows that the maximal on-site effects for Ada Tepe are exerted from earthquakes occurred in Ksanti, Edrine and Marica seismic sources.

The results produced for the Ada Tepe will constitute an important tool for the local authorities responsible with disaster management. The hazard estimates are to be considered as a substantial phase of the risk management cycle associated with hazards (mitigation and preparedness, early warning, response, and recovery).

**Acknowledgements:** The study was supported by the Balkan Mineral and Mining EAD.

## References

Ambraseys N., J. Douglas, S. Sarma & P. Smit, (2005). Equations for the Estimation of Strong Ground Motions from Shallow Crustal Earthquakes Using Data from Europe and the Middle East: Horizontal Peak Ground Acceleration and Spectral Acceleration. *Bulletin of Earthquake Engineering* 3, 1–53.

Ambraseys N., (2009). *Earthquakes in the Mediterranean and Midldle East*. Printed in UK at the University Press, Cambridge. 947.

Campbel K. & Y. Bozorgnia, (2007). *NGA Ground Motion Relations for the Geometric Mean Horizontal Component of Peak and Spectral Ground Motion Parameters*. Technical report, PEER 2007/02.

McGuire, R., (1978). Computer Program for Seismic Risk Analysis using faults as earthquake sources, USGS. *Open-File Report* 76-67, 78-1007.

McGuire, R., (1993). Computations of seismic hazard, *Annali di Geofisica* XXXVI (3-4), 181-200.

Popov H., A. Jockenhövel, Z. Tsintsov & S. Iliev, (2011): Montanarchäologische Forschungen in den Ostrhodopen. In: Nikolov V., K. Bachvarov, H. Popov (eds.): *Interdisziplinäre Forschungen zum Kulturerbe auf der Balkanhalbinsel*, Sofia.

Reid A., J. Allsop, H. Granser, A. Millett & I. Somerton, (1990). Magnetic interpretation in three dimensions using Euler deconvolution. *Geophysics* 55, 80–91.

Report NIGGG (2012a): *Activities I, II, III: Analysis of the geological, geophysical and seismological settings in the locality of "Ada Tepe" deposit*. Fund material.

Report NIGGG (2012b): *Activity IV: Seismic hazard assessment for "Ada Tepe" site.* Fund material.

Simeonova S., D. Solakov, G. Leydecker, H. Busche, T. Schmitt & D. Kaiser, (2006). Probabilistic seismic hazard map for Bulgaria as a basis for a new building code. *Natural Hazards Earth System Sciences* 6, 881–887.

Solakov D., S. Simeonova & L. Christoskov, (2009). Seismic hazard maps for the new national build-ing code of Bulgaria. *Comptes Rendus de L'Academie Bulgare des Sciences* 62 (11), 1431-1438.

Stavrev P., D. Solakov, S. Simeonova & P. Trifonova, (2009). Regional set of dislocations in the Earth's crust of Bulgaria according to gravity data, *Proceedings of the 5th Congress of Balkan Geophysical Society*, Belgrade, Ref.# 6507.

Telford W., L. Geldart & R. Sheriff, (1991). *Applied Geophysics*. Cambridge University Press, Cambridge.

Trifonova P., Zh. Zhelev, T. Petrova, K. Bojadgieva, (2009). Curie point depths of Bulgarian territory inferred from geomagnetic observations and its correlation with regional thermal structure and seismicity. *Tectonophysics* 473, 362-374.

Trifonova P., D. Solakov, S. Simeonova, M. Metodiev, & P. Stavrev, (2013). Regional pattern of the earth's crust dislocations on the territory of Bulgaria inferred from gravity data and its recognition in the spatial distribution of seismicity, *Pattern Recognition in Physics* 1, 25-36.

INQUA Focus Group on Paleoseismology and Active Tectonics

paleoseismicity.org

# Active tectonics in the West Carpathian Foreland: Nysa-Morava Zone and Upper Morava Basin System (Czech Republic)

*Špaček, Petr (1)*

(1) Institute of Earth Physics, Masaryk University, Tvrdého 12, 60200 Brno, Czech Republic. E-mail: spacek@ipe.muni.cz

***Abstract:*** *Main features are described of an active tectonic domain in the West Carpathian Foreland, the Nysa-Morava Zone. Plio-Quaternary volcanic eruptions and subsidence in a system of graben-shaped basins document a Late Cenozoic increase in strain of the region, which is still going on as indicated by increased microseismicity and post-volcanic $CO_2$ flux. A simple tectonic model is given to explain and link the deformation process in Plio-Quaternary and Recent. A trench-based research of slip history at selected faults is currently carried out.*

***Key words**: active tectonics, Carpathian foreland, Bohemian Massif*

## INTRODUCTION

Active tectonics in the extra-Alpine central Europe is mostly restricted to the European Cenozoic rift system (ECRIS; Fig. 1a), whose development started in Eocene, culminated in Oligocene and Miocene and has been continuing throughout Quaternary.
However, Late Cenozoic far field stresses have activated also regions outside ECRIS. One such example is a rather neglected active tectonic domain in the West Carpathian Foreland - the Nysa-Morava Zone (NMZ; Fig. 1a, b) - which hosts the system of graben-shaped basins with sediment fill of largely Plio-Quaternary age. The onset of major subsidence in Pliocene (after post-Langhian uplift and erosion) suggests that the tectonic history in NMZ differs significantly from that of ECRIS. The present-day microseismicity as well as post-volcanic $CO_2$ flux indicate an ongoing activity. Morphological features of many fault scarps raise questions about the fault slip history in Late Quaternary and their capability to produce larger earthquakes.
This short paper gives a brief description of main features of NMZ and associated basins whose major faults are currently under trench-based study.

## THE NYSA-MORAVA ZONE AND THE UPPER MORAVA BASIN SYSTEM

A domain with anomalous seismic activity is observed in the NE part of the Bohemian Massif, extending over an area of >8000 km$^2$. This region sharply contrasts with adjacent parts of the Bohemian Massif and Carpathians which are generally aseismic. Since our earlier paper we call this seismogenic domain the Nysa-Morava Zone (NMZ).
Based on historic records since 15$^{th}$ century, NMZ is characterized by weak (M<4) seismic activity with only few events reaching magnitude of $4<M<5$. Nearly 1000 events located in the period of detailed instrumental monitoring (1998-2012) exhibit magnitude range of $-0.6<M_L<2.5$ and typical hypocentral depths 9-18 km. Since 2008 (after major upgrade of the local MONET network) we register within NMZ approximately 200-300 microearthquakes per year, of which 100-180 are located by conventional routines.
Nearly two decades of instrumental monitoring show that the main activity concentrates in a remarkably well defined rhomb-shaped region which continues beneath the fold-and-thrust belt of the Outer Carpathians at the southeast (Fig. 1b; Špaček et al., 2011). The northeastern and the southwestern margins of NMZ are clearly linear, both having NW-SE strike. The latter clearly co-incides with a regionally important fault zone, while for the former such correlation is poor.
The seismicity concentrates spatially in several more or less well defined clusters of epicentres with mostly NNW-SSE to NW-SE orientation (Fig. 1b), near-parallel to the known tectonic structures in their close neighbourhood. Few M≥2 events produced well constrained focal mechanisms. The nodal planes with N-S to WNW-ESE strikes correspond to known local structures expressed in relief or in surface geology and, at larger scale, to epicentre clusters and faults in whole NMZ. These nodal planes indicate dip-slips on steep to moderately inclined, mostly normal faults, and a dextral strike slip (Fig. 1b).
Local, low-volume eruptions of alkali basalts took place in NMZ during Late Oligocene/Early Miocene and later in Pliocene and Pleistocene. Today, NMZ hosts approximately 80 known carbonated mineral springs which are likely to reflect declining magmatic activity in a deeper lithosphere. Some of these springs have very high flux with an annual release of up to 500 tons of $CO_2$. It is interesting to note that the spatial extent of carbonated mineral springs is very close to that of earthquake epicentres (Fig. 1b). In spite of the increased magmatic activity, the crustal and lithospheric thicknesses are normal in a central European perspective (28-35 km and ~100 km, respectively; Geissler et al., 2012).

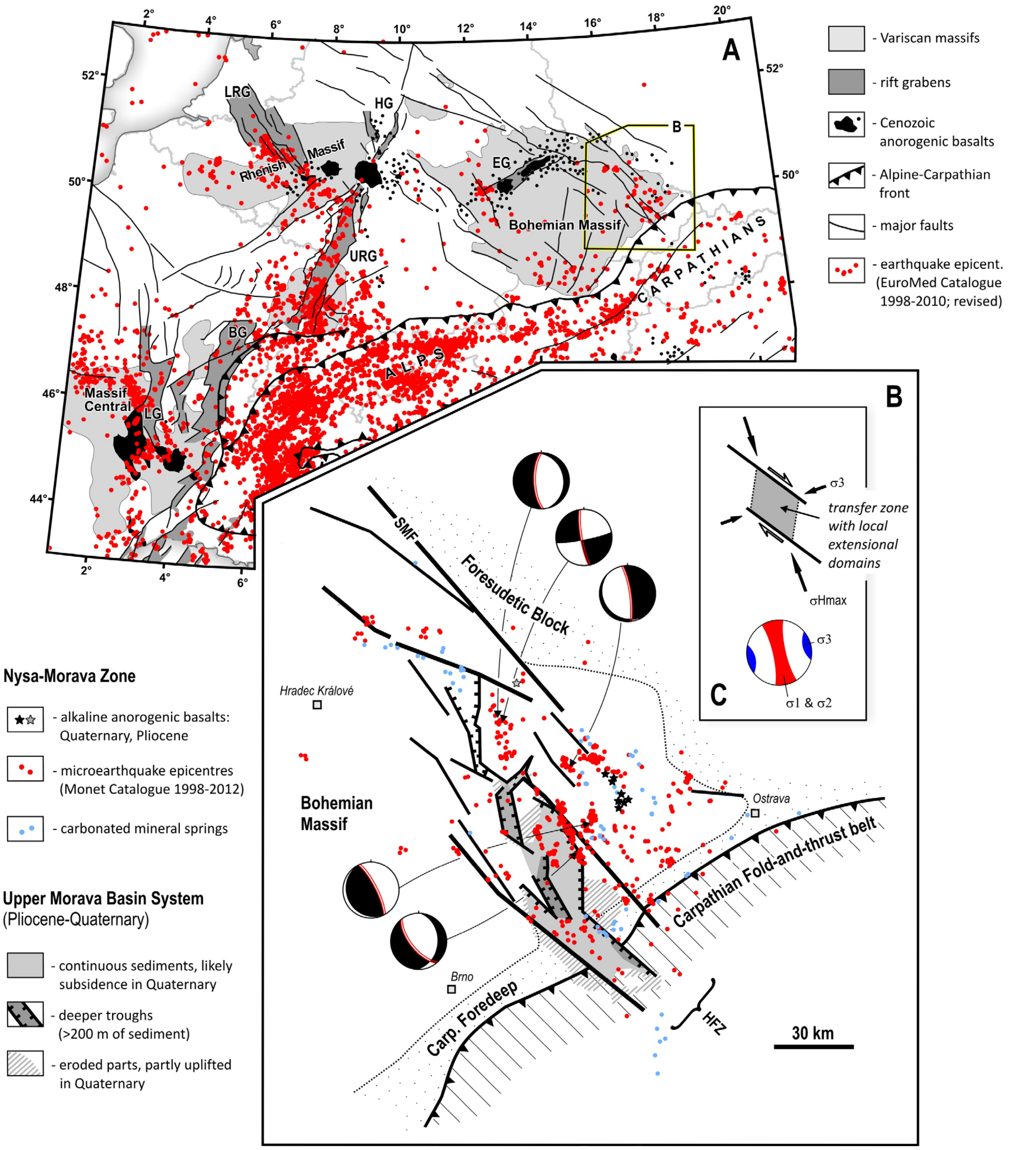


*Fig. 1. a - Position of the studied region in Central European scale. Map shows Varsican Massifs, sedimentary grabens of ECRIS, volcanic rocks of Central European Volcanic Province and present-day seismicity in a foreland of Alpine-Carpathian front. Epicentres are from EuroMed Catalogue for period 1998-2010, partly revised. BG - Bresse Graben, E - Eifel, EG - Eger Graben, HG - Hesse Graben, LG - Limagne Graben, LRG - Lower Rhine Graben, URG - Upper Rhine Graben. b - Simplified tectonic scheme showing the main features of the Nysa-Morava Zone and Upper Morava Basin System and focal mechanisms with preferred nodal planes highlighted. SMF - Sudetic Marginal Fault, HFZ - Haná Fault Zone. c - Top: simplistic model explaining the NMZ as a transfer zone with local extensional domains developed in transpressional setting between the non-coalesced NW-SE striking faults. Bottom: model orientation of principal stresses within NMZ suggested by preliminary statistical analysis of first motion - backazimuth/incidence angle relations performed on large dataset for weak events.*

NMZ exhibits high elevation range between 180-1490 m asl. The low topography is associated with the basins of the Upper Morava Basin System (UMBS) which are located in a diagonal position within the rhomb-shaped NMZ (Fig. 1b). Their formation and development have been apparently controlled by the 25-35 km wide Haná Fault Zone formed by steeply dipping, NW-SE striking master faults and associated NNW-SSE to N-S striking faults. The basins exhibit flat morphology with broad floodplain up to 8 km wide. The height difference between basin bottom and adjacent parts of uplands is 200-300 m and the basin margins are mostly formed by steep scarps. The thickness of Pliocene and Quaternary fluvial and lacustrine sediments is largely variable and reaches maximum of approx. 300m in two narrow, NNW-SSE oriented troughs.

## TECTONIC MODEL

The formation and development of UMBS can be viewed as a result of extension in pull-apart domains between NW-SE trending southern and northern boundary faults of the Haná fault zone in dextral slip regime. We suggest that similar mechanism can explain the present-day tectonic activity in the whole NMZ which may be understood as an inhomogeneous transfer zone developed between the non-coalesced NW-SE striking faults in generally transpressional setting (Fig. 1c). The observed focal mechanisms indicating dextral shearing and normal faulting, are consistent with such model. The extension seems to be more or less persistent since Pliocene in UMBS, while the existence of local, intermittent, extensional domains in the NMZ are indicated by Late Oligocene to Quaternary volcanic eruptions and present-day increased $CO_2$ flux.

The fact that the NMZ as a whole does not exhibit negative topography, implies generally small displacements associated with the extensional domains possibly resulting from their temporal character and/or spatial migration throughout the region due to the variation of mechanical coupling between individual fault-bounded blocks. The small-magnitude multiplet earthquake sequences, which are characteristic for NMZ may reflect some specific local conditions of deformation related to the increased flux of fluids.

Although we have still no reliable data on stress in NMZ, the steep dip-slips indicated by focal solutions suggest local rotation of maximum compressional stress from sub-horizontal direction, characteristic for large part of central and western Europe, to a steeper orientation. Preliminary statistical analyses of the first motion-backazimuth/incidence angle relations performed on large dataset for weak events indicates well constrained subhorizontal $\sigma_3$ in E-W to ENE-WSW orientation and poorly constrained $\sigma_1$ and $\sigma_2$ in a subvertical girdle of NW-SE to N-S orientation (Fig. 1c). This can be explained by heterogeneous stress and small scale permutations of $\sigma_1$ and $\sigma_2$.

## TRENCHING IS UNDERWAY

Paleoisesmic research on the Sudetic Marginal Fault (Štěpančíková et al., 2010, pers. communication and this volume) shows that this major fault located just at the northern margin of NMZ (Fig. 1b), was active in Late Pleistocene but seems to be inactive in Holocene. In spite of its proximity, the relation of this fault to NMZ is not clear and at present there is no direct evidence for fault slip in NMZ in Late Quaternary. The up to 300 m high scarps at UMBS margin mostly contrast with small sediment thickness and their origin is apparently dominated by strong differential erosion. We are currently trenching selected faults in Haná Fault Zone to learn about their late slip history and to support regional tectonic model.

**Acknowledgements:** Research is funded from Czech Science Foundation project No. P210/12/0573 and CzechGeo/EPOS program No. LM2010008.

## References

Geissler, W.H., H. Kämpf, Z. Skácelová, J. Plomerová, V. Babuška, & R. Kind, (2012). Lithosphere structure of the NE Bohemian Massif (Sudetes) - A teleseismic receiver function study. *Tectonophysics* 564-565, 12-37.

Špaček P., P. Zacherle, Z. Sýkorová, & J. Pazdírková, (2011). Microseismic multiplets in the northeastern Bohemian Massif. *Zeitschrift für Geologische Wissenschaften* 39, 5/6, 367-386.

Štěpančíková, P., J. Hók, D. Nývlt, J. Dohnal, I. Sýkorová & J. Stemberk, (2010). Active tectonics research using trenching technique on the south-eastern section of the Sudetic Marginal Fault (NE Bohemian Massif, central Europe). *Tectonophysics* 485, 269-282.

INQUA Focus Group on Paleoseismology and Active Tectonics

paleoseismicity.org

# Late Quaternary Activity of the Sudetic Marginal Fault in the Czech Republic: A signal of Ice Loading?

*Petra Štěpančíková (1), Thomas Rockwell (2,) Filip Hartvich (1), Petr Tábořík (1,3) ,Jakub Stemberk (1, 3), María Ortuño (4), Neta Wechsler (2)*

(1) Institute of Rock Structure and Mechanics, Czech Academy of Sciences, V Holešovičkách 41, 18209, Prague 8
Email: petra.stepancikova@gmail.com
(2) Dpt. of Geological Sciences, San Diego State University, 5500 Campanile Drive, San Diego, California, CA 92182-1020
(3) Faculty of science, Charles University, in Prague, Albertov 6, Prague 2, 12843, Czech Republic
(4) Dpt.of Geodynamics and Physics, Faculty of Geology, University of Barcelona, Martí i Franquès, s/n 08028 Barcelona

***Abstract:*** *The study area is situated in the north-eastern part of the Bohemian Massif in central Europe and comprises the SE part of the NW-SE trending Sudetic Marginal Fault (SMF) with pronounced mountain front. Fourteen new trenches were excavated at the locality Bila Voda combined with geoelectric profiles (ERT) to study 3D distribution of the truncated alluvial fan on the NE block and to find the "feeder channel" as the source of the deposits. We consider a small drainage of about 30-45 m to the southeast of the fan apex as the feeder channel. It gives us left-lateral slip for the ~25 ka alluvial fan, corresponding to a long-term slip rate of ~1.5 mm/yr. As the Holocene deposits do not show significant displacement, most of the recorded slip took place during late Pleistocene with slip rate 1.8 to 2.8 mm/yr. The acceleration of slip rate was probably due to ice-loading/deglaciation of the Weichselian ice-sheet, which had its margin about 150 km from the locality at ~20 ka.*

***Key words****: Sudetic Marginal Fault, paleoseismicity, ice loading, Late Glacial, Bohemian Massif*

The Sudetic Marginal fault is a major structural element defining the northeastern limit of the Bohemian Massif (Figure 1), which has been active at least since Late Cretaceous time (Danišík et al. 2012). It is a part of regional-scale Elbe Fault system with alternating kinematics since late Carboniferous (Variscan orogeny) (Scheck et al., 2002). Likely initiating as a predominantly dextral fault (Oberc, 1991), it acted as a normal fault during early Late Cretaceous basin formation and the sense of slip was reversed in the late Cretaceous/early Paleogene (Danišík et al. 2012), resulting in basin inversion, which affected much of central Europe (Kley and Voigt, 2008). The fault was reactivated in the Miocene again with a normal component of motion resulting in the accumulation of Miocene sediments in several sub-basins in northeastern Czech Republic and southwestern Poland (Oberc and Dyjor, 1969). Evidence for Quaternary reactivation of the fault is found in the geomorphology of the landscape along the fault, with relatively linear mountain fronts, deflected drainages, and deep incision of the Sudetic Mountains, with consequent deposition of alluvial fans along the range

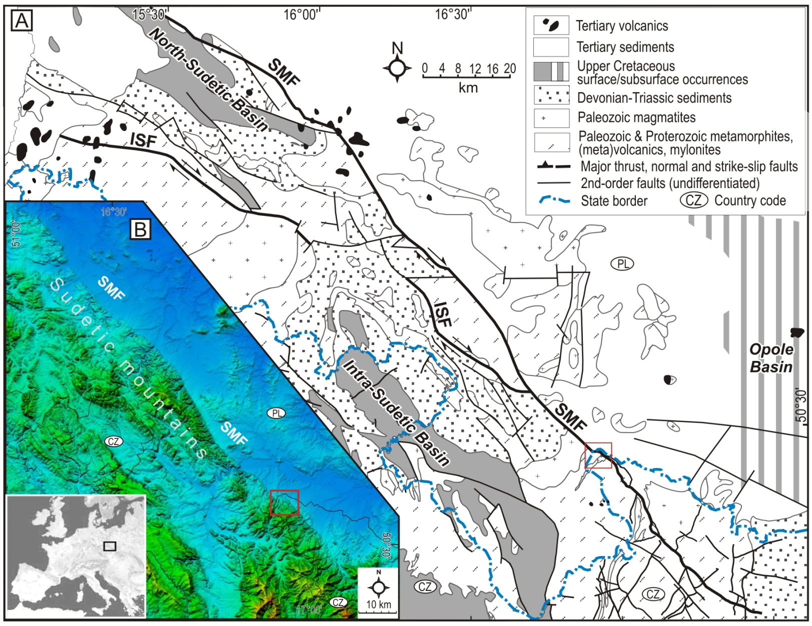


*Fig.1. A) Simplified geological map of the Sudetes (modified after Badura et al. 2007, and Danišík et al. 2012). B) Morphology of the Sudetic Marginal fault that borders the Sudetic Mountains. Country code CZ-Czech Republic, PL – Poland.*
*Red square – study area*

margin (Figure 1B). Middle and Upper Pleistocene fluvial terraces that are truncated by the SMF show 5 - 20 m high scarp in their longitudinal profiles in the Polish portion of the fault (e.g. Krzyszkowski et al., 1995). There is also sparse microseismicity and rare historical moderate earthquakes (I=7 MSK) that suggest that this fault is still a potential seismic threat to the region (Guterch and Lewandowska-Marciniak, 2002).

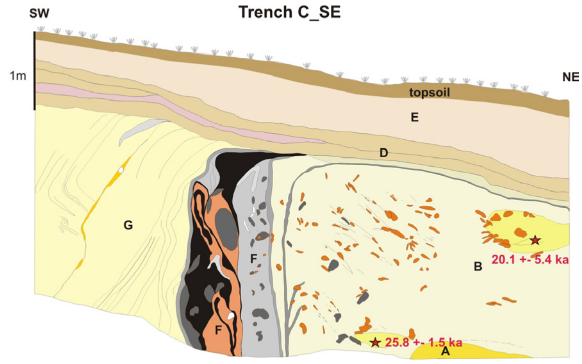


*Fig. 2. Log of the trench C. See text for explanation of units A to E. Unit A – mid-Miocene lacustrine deposits, B – late Pleistocene alluvial fan deposits, D – geliflucted crystalline rocks, E – youngest Holocene colluvium, F – fault zone with tectonic breccia, G - Paleozoic schists – phyllonites, Red star – OSL dating.*

To study the late Quaternary activity of this fault, we first excavated a trench across the fault at Bila Voda that exposed Paleozoic schist juxtaposed against Quaternary alluvium (Figure 2), with the alluvium folded down into the fault zone (Štěpančíková et al., 2009). Classic features indicative of significant motion included rotation of clasts into the fault and the complete mismatch of units across the fault. The Quaternary alluvium displayed some bedding and channeling with an otherwise relatively massive matrix, indicating an alluvial fan origin. The alluvial fan deposits are overlain by distinct layers of geliflucted material, each of which could be traced back to the bedrock stratum from which it originated. Geliflution in this region of the Czech Republic was limited to the periglacial climate of the late Pleistocene, indicating that the alluvial fan as well as the overlying gelifluction layers is late Pleistocene in age. The Late Glacial age of gelifluction was also demonstrated in the previous trenches by radiocarbon dating of overlying layers (Štěpančíková et al. 2010). Direct dating of the alluvial fan deposits close to the eastern limit of the fan using optically stimulated luminescence (OSL) method yielded ages of 25.8 ± 1.6 ka to 9.5 ± 0.9 ka for the alluvial fan deposits in the Trench C (Štěpančíková et al. 2011) and 40.9 ± 2.5 ka for fault-related colluvial wedge overlying the base of the alluvial fan deposits and interfingering with it further to the NW (Trench J) obtained by radiocarbon dating. Overlying, locally preserved strata that do not exhibit evidence of gelifluction yielded radiocarbon ages as old as 8.2 – 9.7 ± 0.02 ka, confirming the late Pleistocene inference on the age of the gelifluction process.

We explored the 3-dimensional distribution of the alluvial fan deposits with additional trenches (Figure 3). The thickness of the fan deposits varies systematically throughout the site, with the alluvial thickness the greatest at the inferred apex of the paleo-fan. The fan appears to have spread out parallel to the fault against a paleo-scarp to the northwest, which is downslope from the apex, and to have cut a channel to the northeast. The apex thickness is between 2 and 3 m, with the majority of the deposit less than 1.5 m near the fault, as exposed in the trenches. Altogether, the well-defined apex, along with the distribution of fan deposits, can be used to assess the sense and rate of slip of this fault.

Trenches excavated southwest of the fault (Trench T and Trench X, Figure 3A) exposed only Paleozoic schist across the entire site. The top of the schist is remarkably smooth and is capped by the gelifluction layers that originated a few meters upslope (see figure 2 and 4 for an example), so any paleo-channel cut into the schist would be readily apparent.

We searched for a possible “feeder channel” as the source of the alluvial fan deposits to the northwest to test for right-lateral slip, but no such channel exists on the southwest of the fault northwest of the fan apex for at least 40 m, as exposed in the fault-parallel trench, nor for at least 100 m based on geoelectric profiles (electrical resistivity tomography – ERT). Furthermore, there is no indication in the surface morphology for a relict paleo-channel for at least 250 m, beyond which the fault crosses into a major drainage, which is much too large to have generated the relatively small fan deposits exposed in our trenches. In contrast, a small drainage of the appropriate size for the fan deposit is present about 45-50 m to the southeast of the fan apex. Based on these observations, the simplest interpretation is that the alluvial fan is displaced by a few tens of meters in a left lateral sense.

To better estimate the amount of late Quaternary left-lateral motion, we reconstruct the apex to the small channel to the southeast. Along a straight-line projection of the average channel trend, this results in about 45 m of reconstruction. Taking the apex to the position of the currently incised drainage adds another 10-15 m, although it is likely that this is an over-estimate as the drainage veers to the right whereas the alluvial fan appears to have spilled along the same trend as the upslope portion of the channel.

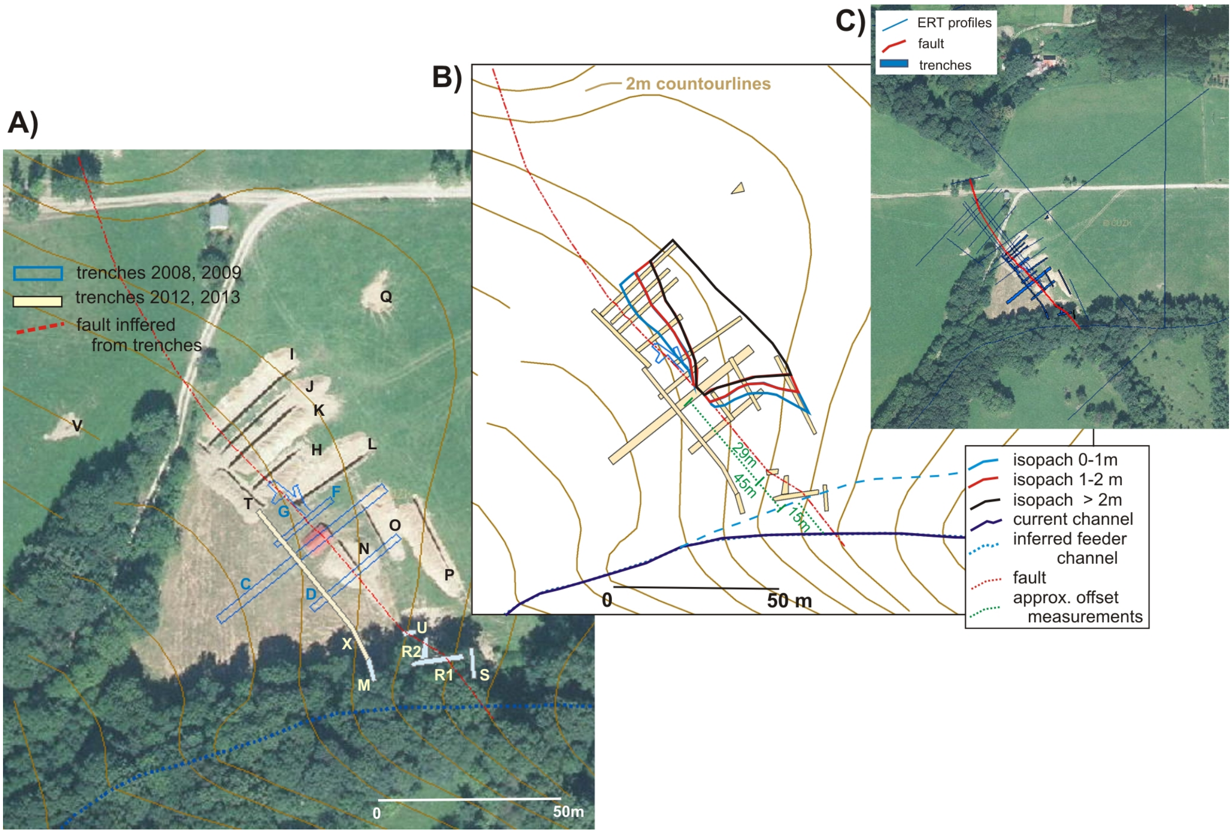


*Fig. 3. A) Position of trenches at the locality Bila Voda, B) Isopach map of the truncated alluvial fan deposits, C) Position of geoelectric profiles.*

An alternative minimum estimate is to assume that the feeder channel did exist on the southwest side of the fault to the southeast of the apex but that it has been eroded away during incision of the modern drainage. To account for this and make an estimate of the minimum displacement, we take the elevation of the base of the alluvium at the apex and reconstruct it horizontally to the same elevation contour in the modern topography. This yields a reconstruction of about 29 m, and this value may decrease a small amount if this has been significant component of dip-slip motion along with the strike-slip. However, significant dip-slip should be reflected by deposition of colluvium above the channel deposits on the down-thrown side, and no such evidence is present in any of the trenches. At most, we estimate something on the order of a half meter of dip slip could have been missed, which does not affect our estimate for the horizontal slip reconstruction.

Based on the reconstructions, we estimate that the fan apex is left-laterally offset by 29 to 45 m, with a maximum displacement of about 60 m if taken all of the distance to the modern drainage. As the actual value could fall anywhere between, and because we consider the maximum value to be an overestimate, we use a best estimate of 37$\pm$8 m of left slip for the ~25 ka alluvial fan.

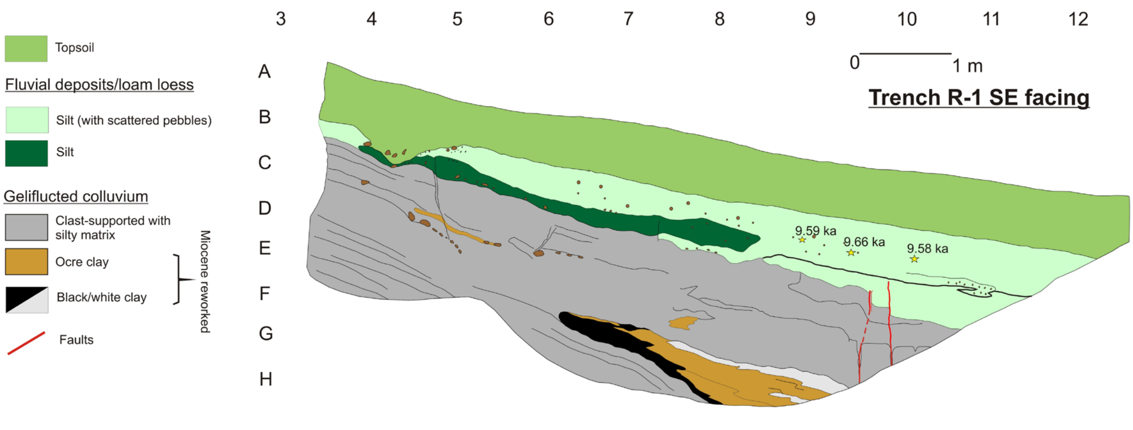


*Fig. 4. Trench log of TR1, SE wall. Yellow stars – radiocarbon dating.*

Thus, at face value, the average long-term rate is about 1.5 mm/yr.

We excavated several trenches on the northern side of the modern drainage, in part to search for remnants of the alluvial fan, and in part to search for younger faulted deposits. Trench R1 (Figure 4) exposed faulted alluvium capped/sealed by unfaulted fine sandy silt strata. Charcoal from the unfaulted layers yielded radiocarbon ages of 8-10 ka, indicating that the last period of motion was greater than 10,000 years ago. This is surprising when the amount of late Pleistocene displacement is considered. In fact, if all observations are correct, this implies that the 37$\pm$8 m of left lateral displacement occurred in the period between about 25 and 10 ka BP. If correct, this indicates that the slip rate was between 1.8 and 2.8 mm/yr during the late Pleistocene, and has been essentially zero during the Holocene.

Bila Voda lies about 150-170 km south from the late Pleistocene Weichselian culmination (~20 ka) ice front (Lokrantz and Sohlenius, 2006). At face value, it appears that most or all of the activity on the Sudetic Marginal fault occurred during the time when ice was locked up on the European continent or was receding, with the margin not too far from the fault. After the close of the Pleistocene, surface movement on the fault ceased, at least until the present. These observations suggest a cause and effect between ice loading and fault movement. The modern maximum principal stress ( ▯)s oriented nearly parallel to the Sudetic Marginal fault (NNW-SSE; Havíř, 2004), which is currently unfavorable for fault motion. We hypothesize that the forebulge may have caused a change in the local stress field, rotating ▯ and forcing left lateral motion of the Sudetic Marginal fault, or at least an acceleration of the rate of motion, which has been reported also from other regions due to deglaciation (Arvidsson 1996, Houtgast et al. 2005, etc.). If that is the case, then removal of the ice may have caused relaxation of the stress field, locking the fault in the Holocene and explaining the lack of Holocene motion.

We plan additional studies to further explore the timing of late Quaternary motion on this fault near Bila Voda, with specific interest in testing the lack of Holocene motion. With this in mind, consider this a progress report to be continued.

**Acknowledgements:** The research was supported by the Czech Science Foundation project No. P210/12/0573 and Czech Ministry of Education, Youth and Sports project No. LH12078.

**References**

Arvidsson, R., (1996). Fennoscandian earthquakes: Whole crustal rupturing related to postglacial rebound. *Science* 274, 1, 744–746.

Badura, J., Zuchiewicz, W., Štěpančíková, P., Przybylski, B. Kontny, B., Cacoń S. (2007). The Sudetic Marginal Fault: A young morphotectonic feature at the NE margin of the Bohemian Massif, central Europe, *Acta Geodyn. Geomater.* 4(4), 7–29.

Danišík, M., Štěpančíková P., and Evans N. (2012). Constraining long-term denudation and faulting history in intraplate regions by multi-system thermochronology - an example of the Sudetic Marginal Fault (Bohemian Massif, Central Europe), *Tectonics* 31, Tc2003, 19pp.

Guterch, B., Lewandowska-Marciniak, H., (2002). Seismicity and seismic hazard in Poland. *Folia Quaternaria* 73, 85–99.

Havíř J. (2004). Orientations of recent principal stress axes in the Jeseníky region. *Acta Geodynamica et Geomaterialia* 1, 3(135), 49-57.

Houtgast, R.F., Van Balen, R.T. , C. Kasse C. (2005). Late Quaternary evolution of the Feldbiss Fault (Roer Valley Rift System, the Netherlands) based on trenching, and its potential relation to glacial unloading. *Quaternary Science Reviews* 24, 491–510.

Kley, J., T. Voigt (2008). Late Cretaceous intraplate thrusting in central Europe: Effect of Africa-Iberia-Europe convergence, not Alpine collision, *Geology*, 36(11), 839–842.

Krzyszkowski, D., Migoń, P., Sroka, W., (1995). Neotectonic Quaternary history of the Sudetic Marginal fault, SW Poland. *Folia Quaternaria* 66, 73–98.

Lokrantz, H., Sohlenius G. (2006). Ice marginal fluctuations during the Weichselian glaciation in Fennoscandia, a literature review. Technical report TR-O6-36, 55p.

Oberc, J. (1991). Systems of main longitudinal strike-slip faults in the vicinity of the Gory Sowie Block (Sudetes), *Kwart. Geol.* 35, 403–420.

Oberc, J., Dyjor S. (1969). Uskok sudecki brzeżny, *Biul. Inst. Geol*, 236, 41–142.

Scheck, M., U. Bayer, V. Otto, J. Lamarche, D. Banka, and T. Pharaoh (2002), The Elbe Fault System in north central Europe — A basement controlled zone of crustal weakness, *Tectonophysics* 360, 281–299.

Štěpančíková, P., Hók, J., Nývlt, D., (2009). Trenching survey on the south-eastern section of the Sudetic Marginal Fault (NE Bohemian Massif, intraplate region of central Europe). In: *Archaeoseismology and Palaeoseismology in the Alpine-Himalayan Collisional Zone* (Pérez-López, R., Grützner, C., Lario, J., Reicherter, K., Silva, P.G. eds). Baelo Claudia, Spain, 149–151.

Štěpančíková, P., Hók, J., Nývlt, D., Dohnal, J., Sýkorová, I., Stemberk, J., (2010). Active tectonics research using trenching technique on the south-eastern section of the Sudetic Marginal Fault (NE Bohemian Massif, central Europe). *Tectonophysics* 485, 269–282.

margin (Figure 1B). Middle and Upper Pleistocene fluvial terraces that are truncated by the SMF show 5 - 20 m high scarp in their longitudinal profiles in the Polish portion of the fault (e.g. Krzyszkowski et al., 1995). There is also sparse microseismicity and rare historical moderate earthquakes (I=7 MSK) that suggest that this fault is still a potential seismic threat to the region (Guterch and Lewandowska-Marciniak, 2002).

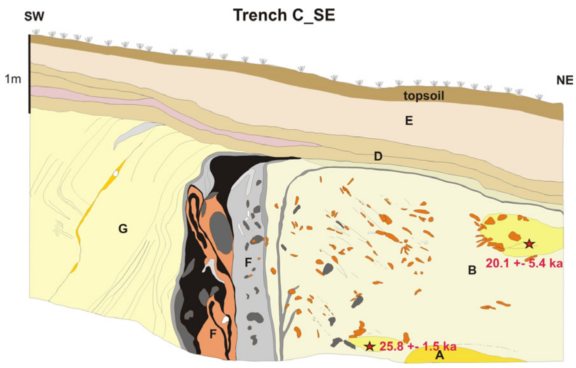


*Fig. 2. Log of the trench C. See text for explanation of units A to E. Unit A – mid-Miocene lacustrine deposits, B – late Pleistocene alluvial fan deposits, D – gelifluncted crystalline rocks, E – youngest Holocene colluvium, F – fault zone with tectonic breccia, G - Paleozoic schists – phyllonites, Red star – OSL dating.*

To study the late Quaternary activity of this fault, we first excavated a trench across the fault at Bila Voda that exposed Paleozoic schist juxtaposed against Quaternary alluvium (Figure 2), with the alluvium folded down into the fault zone (Štěpančíková et al., 2009). Classic features indicative of significant motion included rotation of clasts into the fault and the complete mismatch of units across the fault. The Quaternary alluvium displayed some bedding and channeling with an otherwise relatively massive matrix, indicating an alluvial fan origin. The alluvial fan deposits are overlain by distinct layers of geliflucted material, each of which could be traced back to the bedrock stratum from which it originated. Gelifluction in this region of the Czech Republic was limited to the periglacial climate of the late Pleistocene, indicating that the alluvial fan as well as the overlying gelifluction layers is late Pleistocene in age. The Late Glacial age of gelifluction was also demonstrated in the previous trenches by radiocarbon dating of overlying layers (Štěpančíková et al. 2010). Direct dating of the alluvial fan deposits close to the eastern limit of the fan using optically stimulated luminescence (OSL) method yielded ages of 25.8 ± 1.6 ka to 9.5 ± 0.9 ka for the alluvial fan deposits in the Trench C (Štěpančíková et al. 2011) and 40.9 ± 2.5 ka for fault-related colluvial wedge overlying the base of the alluvial fan deposits and interfingering with it further to the NW (Trench J) obtained by radiocarbon dating. Overlying, locally preserved strata that do not exhibit evidence of gelifluction yielded radiocarbon ages as old as 8.2 – 9.7 ± 0.02 ka, confirming the late Pleistocene inference on the age of the gelifluction process.

We explored the 3-dimensional distribution of the alluvial fan deposits with additional trenches (Figure 3). The thickness of the fan deposits varies systematically throughout the site, with the alluvial thickness the greatest at the inferred apex of the paleo-fan. The fan appears to have spread out parallel to the fault against a paleo-scarp to the northwest, which is downslope from the apex, and to have cut a channel to the northeast. The apex thickness is between 2 and 3 m, with the majority of the deposit less than 1.5 m near the fault, as exposed in the trenches. Altogether, the well-defined apex, along with the distribution of fan deposits, can be used to assess the sense and rate of slip of this fault.

Trenches excavated southwest of the fault (Trench T and Trench X, Figure 3A) exposed only Paleozoic schist across the entire site. The top of the schist is remarkably smooth and is capped by the gelifluction layers that originated a few meters upslope (see figure 2 and 4 for an example), so any paleo-channel cut into the schist would be readily apparent.

We searched for a possible "feeder channel" as the source of the alluvial fan deposits to the northwest to test for right-lateral slip, but no such channel exists on the southwest of the fault northwest of the fan apex for at least 40 m, as exposed in the fault-parallel trench, nor for at least 100 m based on geoelectric profiles (electrical resistivity tomography – ERT). Furthermore, there is no indication in the surface morphology for a relict paleo-channel for at least 250 m, beyond which the fault crosses into a major drainage, which is much too large to have generated the relatively small fan deposits exposed in our trenches. In contrast, a small drainage of the appropriate size for the fan deposit is present about 45-50 m to the southeast of the fan apex. Based on these observations, the simplest interpretation is that the alluvial fan is displaced by a few tens of meters in a left lateral sense.

To better estimate the amount of late Quaternary left-lateral motion, we reconstruct the apex to the small channel to the southeast. Along a straight-line projection of the average channel trend, this results in about 45 m of reconstruction. Taking the apex to the position of the currently incised drainage adds another 10-15 m, although it is likely that this is an over-estimate as the drainage veers to the right whereas the alluvial fan appears to have spilled along the same trend as the upslope portion of the channel.

# Lake sediments as natural seismographs: A compiled record of Late Quaternary earthquakes in Central Switzerland

*Strasser, Michael (1), Katrin Monecke (2), Michael Schnellmann (3), Flavio S. Anselmetti (4)*

(1) Geological Institute, ETH Zurich, 8092 Zürich, Switzerlan. Email: strasser@erdw.ethz.ch
(2) Wellesley College, Department of Geosciences, Wellesley, MA, 02481, USA. Email: kmonecke@wellesley.edu
(3) Nagra, Nat. Genossenschaft für die Lagerung radioaktive Abfälle, 5430 Wettingen, Switzerland. Email Michael.Schnellmann@nagra.ch
(4) Institute of Geological Sciences and Oeschger Centre for Climate Change Research, University of Bern, 3012 Bern, Switzerland. Email: flavio.anselmetti@geo.unibe.ch

***Abstract:*** *Central Switzerland lies tectonically in an intraplate area and recurrence rates of strong earthquakes exceed the time span covered by historic chronicles. Consequently, they are not sufficient to document the full range of neotectonic processes. However, many lakes are present in the area that act as natural seismographs: their continuous, datable and high-resolution sediment succession allows to extend the earthquake catalogue from instrumental and historic periods to prehistoric times, all the way to the end of the last glaciation (i.e. back to ~16'000 years BP), when the modern lakes formed after glacier retreat.*

*In this presentation we review recently compiled data sets and results from more than 10 years of lacustrine paleoseismologic research in lakes of northern and Central Switzerland (Strasser et al., 2013). The concept of using lacustrine mass-movement event stratigraphy to identify paleo-earthquakes is showcased by presenting data and results from Lake Zurich. The Late Glacial-to-Holocene mass-movement units in this lake document a complex history of varying tectonic and environmental impacts. Results include sedimentary evidence of three major (2200, 11530, 13840 cal yr. B.P.) and three minor (640, 3300 and 7270 cal yr. B.P), simultaneously-triggered basin-wide lateral slope failure events interpreted as the fingerprints of paleoseismic activity. In all lakes, historic calibrations were used to identify these "seismic fingerprints" in the sedimentary archives. These calibrations indicate that the macroseismic intensity (I) threshold to trigger subaquatic slope failures is VII (Intensity on the European Macroseismic Scale EMS-98).*

*A refined earthquake catalogue, which includes results from previous lake studies, reveals a non-uniform temporal distribution of earthquakes in northern and Central Switzerland. Higher frequency of earthquakes in the Late Glacial and Late Holocene period documents two different phases of neotectonic activity. They are interpreted to be related to isostatic post-glacial rebound and relatively recent (re-)activation of seismogenic zones, respectively. Magnitudes (M) and epicenter reconstructions for the largest identified earthquakes give evidence for two possible earthquake sources: (1) source area in the region of the Alpine or Subalpine Front due to release of accumulated NW-SE compressional stress related to an active basal thrust beneath the Aar massif and (2) source area beneath the alpine foreland due to reactivation of deep-seated strike-slip faults. Such activity has been repeatedly observed instrumentally, e.g. during the most recent M 4.2 and M 3.5 earthquakes of February 2012, near Zug. The combined lacustrine record from northern and Central Switzerland indicates that at least one of these potential sources has been capable of producing M=6.2-6.7 events in the past.*

***Key words****: lacurstrine paleoseismology, limnogeology, Alpine neotectonics, subaqueous mass movements, earthquake trigger.*

## References

Strasser, M., K. Monecke, M. Schnellmann, F. S. Anselmetti (2013). Lake sediments as natural seismographs: A compiled record of Late Quaternary earthquakes in Central Switzerland and its implication for Alpine deformation. *Sedimentology* 60, 319–341

# Constraints and promises of earthquake-triggered landslides discrimination

*Alexander Strom*

Geodynamics Research Center – branch of JSC "Hydroproject Institute", Moscow, Russia. Email: strom.alexandr@yandex.ru

***Abstract:*** *Confident and well-grounded discrimination of those prehistoric landslides that had been triggered by earthquakes from those of different origin is one of the most controversial paleoseimological issues. Neither volume of failure, nor shape of rockslide deposits, nor its mobility can prove seismic origin due to prevailing role of gravity force in the landslides' formation, i.e. the potential energy of rock massif resting on slope is several orders larger than the kinetic energy that could be supplied to this massif by seismic shaking. Most widely applied discrimination methods based on landslides simultaneity and on numerical back analysis of the collapsed slope stability have some constraints that could make univocal solution questionable, if not impossible. Additional promising way to justify seismic origin of large rockslides could be based on identification of spatially distributed sedimentary features indicating seismic shaking. The best conditions for such analysis are in the lacustrine environment associated with river-damming landslides, which allows close timing of spatially distributed minor features with main river-damming event.*

***Key words***: *Landslide, rockslide, rock avalanche, liquefaction, paleoseismicity.*

## INTRODUCTION

Confident and well-grounded discrimination of those prehistoric landslides that had been triggered by earthquakes from those of different origin is one of the most controversial paleoseimological issues (McCalpin, 2009). Presence of large and/or long runout prehistoric rockslides is often equalized with an evidence of strong past earthquakes without providing any additional reasons in favour of such assumption – just due to their enormous size and expressiveness. However, method based on comparison of the morphology, internal structure and stratigraphic and geomorphic position of past features and of those originated during large historical earthquakes, that works well for surface ruptures or liquefaction phenomena, is quite controversial for prehistoric landslides. It is predetermined by prevailing role of gravity in the formation of any landslide regardless of its origin. Earthquakes, as well as precipitation or river erosion, just trigger slope failure, while further motion is driven by gravity. It results in similarity of volumes, runouts, fahrböschung (H/L ratio) and morphological peculiarities of seismically and non-seismically triggered landslides. Since neither volume of failure, nor its mobility, nor shape of rockslide deposits themselves can prove their seismic origin, interpretation of any large-scale prehistoric slope failure as a seismically induced feature should be justified by some additional evidence, otherwise it would remain emotional rather than scientific.

I want to point out that in most publications on prehistoric Alpine rockslides like Flims, Tamins or Köfels (e.g. Abele, 1974, Brückl & Heuberger, 2001, Poschinger et al., 2006, Poschinger, 2011) or on Deep-Seated Gravitational Slope Deformations (DSGSD) in this region (Agliardi et al., 2013) they are considered to be associated with the Holocene deglaciation or with long-term deformational processes. An alternative – seismic triggering is rarely discussed. In contrast, the majority of papers about quite similar features in the presently more seismically active Central Asia (Korjenkov, 2006), Baikal region (Solonenko, 1977) or New Zealand (Bull, 1996 Barth, 2013) threat earthquakes as the top-priority candidate for large rockslides or DSGSD trigger.

Promising approaches to seismically induced landslides identification and, on the other hand, constraints that could make univocal solution contradictable, if not impossible, at least at the present stage of our knowledge, are discussed hereafter briefly.

## TEMPORAL AND SPATIAL CLUSTERING

One of the reliable and most often used arguments in favour of the prehistoric large-scale bedrock slope failures' seismic origin is the simultaneity of their occurrence within some area, treated as past earthquake strong shaking zone. It is quite logical that large earthquake would trigger several voluminous slope failures in the most affected zone as it happened, for example, during 2008 Wenchuan earthquake that triggered several dozens landslides exceeding 1 million cubic meters (Huang et al., 2009, Yin et al. 2009, Chigira et al., 2010, Dai et al., 2011).

However, this event is an exception. Many large earthquakes with M>7.0 had been accompanied with only one, or just very few large bedrock landslides, that would remain recognisable for a very long time even being eroded significantly – just what had happened with presumed paleoseismic features, and with numerous minor slope failures, which, most likely, will disappear soon. It is exemplified by the 1887 Verniy (Mushketov, 1890), the 1911 Sarez (Ambraseys & Bilham, 2012), the 1949 Khait (Evans et al., 2009); the 1992 Suusamyr (Korjenkov et al., 2004), the 1957 Gobi Altai (Florensov & Solonenko, 1965), the 1959 Hebgen Lake (Hadley, 1964), the 2005 Kashmir (Dunning et al., 2007, Owen et al., 2008, Schneider, 2009) and many other earthquakes. This regularity, typical also for other extreme events like typhoons and forest fires, was described by D. Turcotte, B. Malamud and their co-authors (Turcotte, Malamud, 2004, Malamud et al., 2004). Thus, there is high probability that the assumed past earthquake could be accompanied by a single large slope failure that could be recognized centuries and millennia after its occurrence. Additional uncertainty is introduced by accuracy of dating methods. Therefore, absence of coeval features does not exclude seismic origin of any single bedrock landslide.

Of course, statistically representative spatial and temporal clustering of landslides is a strong argument in favour of their seismic origin, especially if such cluster coincides with well-known causative fault zone, as it was described by W.B. Bull (1996) for Southern Island of New Zealand. Another example is an extreme concentration of landslides in the Neogene – Quaternaty sediments of the Naryn intermountain depression in Central Tien Shan bounded to the Kalmak-Ashu surface rupture (Abdrakhmatov & Lemzin, 1989). Nothing similar was found in the adjacent part of the depression despite similar topography and geology of the area.

Concentration of large gravitational mass movements, either catastrophic landslides and rockslides or Deep seated gravitational slope deformations (DSGSD), within limited areas is typical of many mountainous regions. However, slope failure density could be quite unequal even along large fault zones where landslide-rich clusters are divided by large gaps. In many cases there are no visible structural, lithological or geomorphic differences that can explain such 'dashed' pattern (Strom & Abdrakhmatov, 2004). Landslide clusters could be composed of features of either the same age (e.g. the above New Zealand case described by Bull, 1996), or of distinct multi-age features indicating recurrence of triggering phenomena. Such repetitive slope failures at a rather limited area, where more recent landslides have affected previously undisturbed slopes could be considered as an indirect evidence of seismic triggering: it is likely that climatic triggering factor such as rainstorms, would be distributed within the region more regularly rather than affect same small area every time. Contrary, earthquake strong motion are exhibited over tens kilometre-long zones quite often.

Additional evidence that can be indicative for earthquake-induced landslides within such clusters is the similarity of the affected slopes' aspect (Fig. 1). It allows assumption on directivity of forces that had triggered large-scale failure on the adjacent slopes.

## SLOPE STABILITY NUMERICAL MODELLING

One of the most promising ways to prove or disprove seismic origin of past slope deformation is the numerical back analysis of slope stability. This rapidly developing methodology is, however, not omnipotent. Well justified results can be provided if pre-rockslide slope morphology and geological conditions can be reconstructed with confidence, like, for example, at the Seimareh landslide in Iran (Roberts et al., in press), numerous landslides in North-Eastern Caucasus, or in Appenines (Scarascia Mugnozza et al, 2006) that occur on large box folds limbs armoured by thick carbonate layers involved in slope failure (Fig. 2) which sliding surfaces had developed within weaker marl or claystone interbeds. Uniform thickness of the affected layers and almost the same geological conditions along fold limbs provide optimal chances for precise pre-slide slope reconstruction and, thus, for reliable back analysis.

*Fig. 1: Aerial photograph of 2 nearby Holocene rock avalanches in Central Tien Shan (Kyrgyzstan) with nearly same directions of the initial slope failure marked by white arrows*

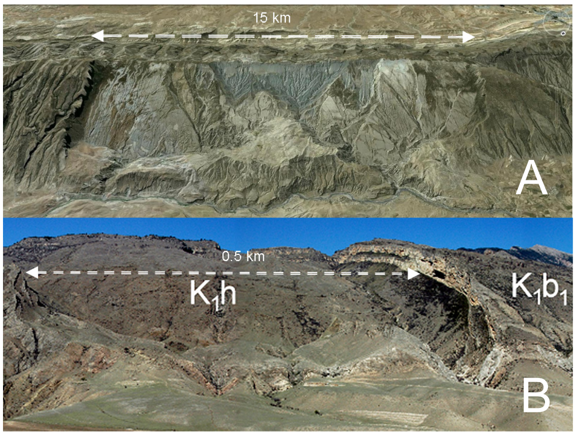


*Fig. 2: Prehistoric rockslides headscarps on the limbs of large box folds allowing precise reconstruction of the pre-failure conditions. A – the Seimareh rockslide (Iran), B – the Gergebil Airport Rockslide (Dagestan, Russia), which represents a natural model of giant Seimareh at about 1:25 scale*

In contrast, confident reconstruction of the original relief and geological/geotechnical conditions of large bedrock landslides where failure had occurred on slopes composed of igneous or metamorphic rocks or of sedimentary rocks with complex structure is rarely possible. In such cases numerical modelling could turn easily just into exercise on parameters fitting.

## SEDIMENTARY INDICATORS OF SEISMIC SHAKING

If definition of seismic origin of large prehistoric bedrock landsides based on their simultaneity is impossible, a promising way to justify such origin of a single large rockslide is the analysis of spatially distributed minor sedimentary features that reflect intensive seismic shaking within the area adjacent to the landslide in question. Such features are deposits of spatially distributed rockfalls and debris flows or liquefaction evidence, typical of epicentral zones of large earthquakes. In such cases the critical point is to prove that these features and the 'main' landslide had the same age. Same problem arises if there is a surface rupture nearby the landslide in question that could be considered as possible causative fault.

Ages of surface rupture and of the single large-scale landslide can be derived by the traditional dating methods widely used in paleoseismological studies (McCalpin, 2009, Walker, 2005). When we have to date minor spatially distributed sedimentary features, the first and critically important step is to define their ages relative to that of a large landslide. The most favourable conditions for such relative dating exist where the past landslide had dammed the river forming the lake that have been breached leaving lacustrine sedimentary successions closely timed to river damming event. Indeed, damming of deep and narrow river valley cause accumulation of fine-graded lake sediments which basal units have almost the same age as the damming feature itself. Thus, if multiple rockfall or debris flow deposits, which could be triggered by strong motion, directly underlay basal units of lake sediments or interbed with them it would be logical to assume that same seismic shaking had triggered river-damming landslide. Such evidence were found about 5 km upstream from the Late Pleistocene Kokomeren rockslide (Strom & Stepanchikova, 2008, Strom, 2013). Considering present-day sediment yield of the Kokomeren River, it could be assumed that rockfalls overplayed by lake sediments, had occurred not later than within few days after river damming. Such evidence, along with surface rupture that stretches towards the headscarp area and with the fact that rockslide caved on the high terrace, which exclude slope undercutting by erosion, allow assumption that Kokomeren rockslide was really triggered by a Late Pleistocene earthquake.

Another example of indirect evidencing of seismic origin of river-damming landslide, also from the Kokomeren River valley, deals with liquefaction features in the Holocene lake sediments about 7 km upstream from the presently breached Lower-Aral rockslide dam (Strom, 2013). Here the lowermost layers of laminated silt sank into the underlying basal coarse sandy unit being overlaid by undisturbed silt laminae (Fig. 3). Liquefaction should occur soon after deposition while massive poorly sorted basal sandy layer and lowermost silt unit were in nonlithified state. It was hypothesized that intensive liquefaction could be caused by strong aftershock few months after the main shock that triggered river-damming rock avalanche from the top of the ridge about 1 km above the riverbed, which formed the 70-m high dam. Such position of the source area is in line with the assumption of its seismic triggering (Huang, 2013). Months-long time span between river-damming events and silt deposition was derived by division of the dammed lake volume at a level where outcrop with liquefaction is located by mean river discharge.

*Fig. 3: Liquefaction features in the lacustrine sediments of the Lower-Aral rockslide-dammed lake. Silt unit above the event horizon marked by ejected sand have not been affected.*

The important advantage of timing determination based on the analysis of basal units of dammed lakes sediments is that accuracy of relative age definition (from days to months) is much higher than that provided by any physical dating method. Of course, it can not provide absolute age of the event, but we can say with confidence that both main rockslide and minor features in the adjacent area had occurred within very short time interval, likely simultaneously.

## DISCUSSION AND CONCLUSIONS

Any estimates of past earthquake magnitude and/or intensity, based on statistical relationships between parameters of seismically induced landslides and earthquakes (Keefer, 1984, Nikonov & Sergeev, 1998) could be valid if seismic origin of slope disturbances was proved independently. Otherwise we can get into vicious circle and earthquake parameters estimates based on size of landslides or on their spatial distribution can lead to erroneous conclusions.

The erroneous assumption on seismic origin of a particular landslide or group of landslides would cause not only an overestimation of seismic hazard, but, also, underestimation of an overall landslide hazard. If one relates large-scale slope failures to large earthquakes exclusively, their recurrence interval should be similar to that of such earthquakes, which, generally, is much longer than of most of other triggering phenomena like rainstorms.
Consistent combination of various indirect indicators of seismic origin of landslides, which do not contradict each-other, provides additional opportunity for reliable seismic and landslide hazard assessment, based on correct discrimination of prehistoric seismically triggered slope failures.

### References

Abdrakhmatov, K.E., I.N. Lemzin, (1989). Active faults of the Alabuga-Naryn depression. In: *The Newest stage of the Tien Shan geological evolution*, Frunze, Ilim Publishers, 78-90.

Abele, G. (1974). *Bergstürze in den Alpen*, Wissenschaftliche Alpenvereinshefte 25, 1-230.

Agliardi, F., G.B. Crosta, P. Frattini & M.G. Malus, (2013). Giant non-catastrophic landslides and the long-term exhumation of the European Alps. *Earth and Planetary Science Letters* 365, 263–274.

Ambraseys, N & R. Bilham, (2012). The Sarez-Pamir earthquake and landslide of 18 February 1911. *Seismological Research Letter* 83 (2), 294–314.

Barth, N.C. (2013). The Cascade Rock Avalanche: A very large Alpine Fault-triggered failure, South Westland, New Zealand. *Landslides*, in press.

Brückl, J. & H. Heuberger, (2001). Present structure and prefailure topography of the giant rockslide of Köfels, *Zeitschrift für Gletscherkunde und Glazialgeologie* 37, 49–79.

Chigira, M., X.Y. Wu, T. Inokuchi & G.H. Wang, (2010). Landslides induced by the 2008 Wenchuan earthquake, Sichuan, China. *Geomorphology* 118, 225-238.

Dai, F.C., Q. Xu, X. Yao, L. Xu, X.B. Tu & Q.M. Gong, (2011). Spatial distribution of landslides triggered by the 2008 Ms 8.0 Wenchuan earthquake,Chia. *Journal of Asian Earth Sciences* 40, 833-895.

Dunning, S.A., W.A. Mitchell, N.J. Rosser & D.N. Petley, (2007). The Hattian Bala rock avalanche and associated landslides triggered by the Kashmir Earthquake of 8 October 2005, *Engineering Geology* 93, 130–144.

Evans, S.G., N.J. Roberts, A. Ischuck, K.B. Delaney, G.S. Morozova & O. Tutubalina, (2009). Landslides triggered by the 1949 Khait earthquake, Tajikistan, and associated loss of life. *Engineering Geology* 109 (3-4), 195-212.

Florensov, N.A. & V.P. Solonenko, (1965). *The Gobi-Altai Earthquake,* Israel Program for Scientific Translations (in English) U.S. Department of Commerce, Washington, DC. 424 pp.

Hadley, J.B. (1964). Landslides and related phenomena accompanying the Hebgen Lake earthquake of August 17, 1959. In: *The Hebgen Lake, Montana, Earthquake of August 17, 1959, U.S. Geological Survey Professional Paper* 435, 107–138.

Huang, R.Q. (2013). Strong motion response and failure under strong earthquakes recording, monitoring and modeling. In: Ugai, K., et al. (eds.) *Earthquake-induced landslides*, Springer-Verlag, Berlin Heidelberg, 59-73.

Huang, R.Q. & W.L. Li, (2009). Analysis of the geo-hazards triggered by the 12 May 2008 Wenchuan earthquake, China. *Bulletin of Engineering Geology and the Environment* 68, 363-371.

Keefer, D.K. (1984). Landslies caused by earthquakes. *Geological Society of America Bull*. 95, 404-421.

Korjenkov, A.M. (2006). *Seismogeology of the Tien Shan (within the limits of the Kyrgyztan and ajacent regions)*. Bishkek, Ilim Publishers, 289 pp. (in Russian).

Korjenkov, A.M., E. Mamyrov, M. Omuraliev, V.A. Kovalenko & S.F. Usmanov, (2004). Rock avalanches and landslides formed in result of strong Suusamyr (1992, M=7,4) earthquake in the Northern Tien Shan - test structures for mapping of paleoseismic deformations by satellite images. In: Buchroithner MF (ed) *High Mountain Remote Sensing Cartography* VII (HMRSC VII). Kartographische Bausteine, Band 23, Dresden, 117–136.

Mushketov I.V. (1890). The Vernyi earthquake of 28/05 (9/06) 1887. *Proceedings of Geological Committee*, 10(1), St. Petersburg, 154 pp (in Russian).

Malamud, B.D., D.L. Turcotte, F. Guzzetti & P. Reichenbach, (2004). Landslides, earthquakes and erosion. *Earth Planet Scientific Letters* 229, 45–59.

McCalpin, J.P. (ed.) (2009). *Paleoseismology. 2nd Edition. International Geophysics Series,* 95, Elsevier, 613 pp.

Nikonov A.A. & A.P. Sergeev, (1998). Identification and quantification of seismogravitational mass movements: the Caucasian mountain area as an example. *Landslide News*, 12, 20-24.

Owen, L.A., U. Kamp, G.A. Khattack, E.L. Harp, D.K. Keefer& M. Bauer, (2008). Landslides triggered by the 8 October 2005 Kashmir earthquake, *Geomorphology* 94, 1–9.

Poschinger, A.v. (2011). The Flims Rockslide Dam, in S.G. Evans, G. Scarascia-Mugnozza, A. Strom and R.L. Hermanns (eds.), *Natural and Artificial Rockslide Dams, Lecture Notes in Earth Sciences* 133, 407-421.

Poschinger, A.v., P. Wassmer, & M. Maisch, (2006). The Flims Rockslide: history of interpretation and new insights. In S.G. Evans, G. Scarascia-Mugnozza, A. Strom and R.L. Hermanns (eds.), *Landslides from Massive Rock Slope Failure, NATO Science Series* IV, 49, 329–356.

Roberts N.J., S.G. Evans, M. Ghahramani, (in press). Causes and possible triggers of the gigantic Seymareh rock avalanche, Iran. *Abstract submitted to XII International IAEG Congress, Torino, 2014.*

Scarascia Mugnozza, G., G. Bianchi Fasani, C. Esposito, S. Martino, M. Saroli, E. Di Luzio & S.G. Evans, (2006). Rock avalanche and mountain slope deformation in a convex, dip-slope: the case of the Majella Massif (central Italy). In: Evans, S.G., Scarascia Mugnozza, G., Strom, A.L., Hermanns, R.L. (eds). *Landslides from Massive Rock Slope Failure, NATO Science Series Book, IV. Earth and Environmental Sciences*, Springer Publisher, Dordrecht, The Netherlands, 49, 357-376.

Schneider, J.F. (2009) Seismically reactivated Hattian slide in Kashmir, Northern Pakistan, *Journal of Seismology* 13, 387–398.

Solonenko, V.P. (1977). Landslides and collapses in seismic zones and their prediction. *Bull. Int. Assoc. Eng. Geol*. 15, 4–8.

Strom, A. (2013). Use of indirect evidence for prehistoric earthquake-induced landslides identification. In: Ugai, K., et al. (eds.) *Earthquake-induced landslides*, Springer-Verlag, Berlin Heidelberg, 21-30.

Strom, A.L. 6 K.E. Abdrakhmatov, (2004). Clustering of large rockslides: the phenomenon and its possible causes. In: Lacerda WA, Ehrlich M, Fontoura AB, Sayao A (eds) *Landslides: evaluation and stabilization*. Taylor & Francis Group, London, 317–320.

Strom, A.L., P. Stepanchikova, (2008). Seismic triggering of large prehistoric rockslides: Pro and Con case studies. *Proceedings of the International Conference on Management of Landslide Hazard in the Asia-Pacific Region (Satellite symposium of the First World Landslide Forum, Tokyo), Sendai, 11th – 12th November 2008*, 202-211.

Turcotte, D.L. & B.D. Malamud, (2004). Landslides, forest fires, and earthquakes: examples of self-organized critical behaviour. *Physica A* 340, 580 – 589.

Walker, M. (2005). *Quaternary dating Methods*. John Willey & Sons, Ltd, 286 pp.

Yin, Y.P., F.W. Wang & P. Sun, (2009). Landslide hazards triggered by the 2008 Wenchuan earthquake, Sichuan, China. *Landslides* 6, 139-151.

INQUA Focus Group on Paleoseismology and Active Tectonics

paleoseismicity.org

# Paleoseismological study of the San Mateo fault, Acambay Graben (México)

Suñé-Puchol, Ivan (1), Lacan, Pierre (1), Villamor, Pilar (2), Ortuño, María (3), Aguirre-Díaz, Gerardo (1), Audin, Laurence (4), Lawton, Timothy (1), Langridge, Robert (2), and Zúñiga, Ramón (1)

(1) Centro de Geociencias, Universidad Nacional Autónoma de México, Blvd. Juriquilla, 3001, 76230, Juriquilla, Querétaro, México
Email: ivanbatea@gmail.com
(2) GNS Science, PO Box 30-368, Lower Hutt 5010, New Zealand
(3) Dept. de Geodinàmica i Geofísica, Universitat de Barcelona, C/ Martí i Franquès s/n, 08028, Barcelona, Spain
(4) Institut des Sciences de la Terre, ISTerre, IRD, Université Joseph Fourier, Grenoble I, INSU, OSUG, France

**Abstract:** In 1912 a mb = 6.9 earthquake occurred in Acambay, Central Mexico, 150 km northeast of the Mexico City. The earthquake produced more than 150 casualties and caused extensive damage to the townships located in the Acambay Graben. As part of our on-going neotectonic and paleoseismological studies throughout the graben, we present here preliminary results from a paleoseismological trenching campaign on the San Mateo fault. We identified at least two paleoearthquakes with vertical displacements between 0.6-1.8 m in the central part of a ~20 km fault, which suggest a potential magnitude of ~7. We are currently dating the sedimentary and volcanic deposits to be able to estimate the recurrence period for strong earthquakes along this fault. Dating results and further interpretations of the data from San Mateo, in conjunction with other paleoearthquakes in the region, is crucial to understanding the seismic hazard in a region with rapid population growth.

**Key words**: San Mateo fault, Acambay Graben, paleoseismological studies, paleoearthquakes and recurrence period

## INTRODUCTION

We present here a paleoseismic study on the San Mateo Fault, located in the central part of the Trans-Mexican Volcanic Belt (TMVB). The TMVB is a volcanic arc associated with the subduction of the Cocos and Rivera plates under the Northamerican plate (Verma, 1996). The TMVB has general E-W trend and crosses the central part of Mexico from the Pacific Coast to the Gulf of Mexico (Ferrari et al., 2011). The tectonic activity within the TMVB has led to a series of grabens and semigrabens with E-W and N-S trends. One of them, the W-E trending Acambay graben, is the focus of this study.

The currently active Acambay graben is associated with trans-arc related extension since the Pliocene. The extension rate of the Acambay graben is estimated to 0.2mm/y by Suter et al., (2001). The eastern part of the graben is bounded by the Pastores fault to the south and by the Acambay–Tixmadeje fault to the north. The Temascalcingo-San Mateo fault system is located along the graben axis. Volcanic edifices, such as Temascalcingo volcano, Santa Lucia dome and Altamirano Volcano were emplaced along this central fault zone (Fig.1).

The only historical records of fault surface rupture in central Mexico are associated with the 1912 mb=6.9 earthquake (red star in Fig 1). The 1912 seismic event generated a 41 km long surface rupture along the Acambay-Tixmadeje fault and around 20 km long surface rupture for the Temascalcingo and San Mateo faults (Urbina and Camacho., 1913; Suter et al., 1995). Urbina and Camacho (1913) reported a 30 cm vertical displacement along the Temascalcingo fault.

Previous studies undertaken along various active faults of the Acambay graben (Fig 1), identified several paleoearthquakes. In the Acambay-Tixmadeje fault, Langridge et al. (2000) identified four Holocene ruptures with average vertical displacement up to 60 cm, recurrence interval of 3600 years and vertical displacement rate of 0.17 mm/y. Persaud et al. (2006) showed that at least one seismic event occurred on the Pastores fault since 21-28 ka with a minimum displacement of 45 cm, which corresponds to a minimum vertical displacement rate of 0.02 mm/a. Ortuño et al. (2011) found at least four paleoseismological events in the last 12.000 years on the Temascalcingo fault and estimate a vertical displacement rate of 0.13 mm/yr.

In this study we aim to identify and characterize paleoseismic events along the San Mateo fault. We chose to excavate paleoseismological trenches across this fault for the following reasons: (1) it was active during the 1912 earthquake but no paleoseismological trenches have been excavated there to date to confirm a 1912 rupture; (2) it has a clear geomorphologic expression for at least 15-20 km that suggests the fault can produce destructive earthquakes; and (3) the potential correlation or lack correlation with others paleoseismic events within the graben, will allow for understanding the potential connection of these faults in depth.

One of the objectives of the project is to integrate as much information as possible on active faults of the Acambay graben to propose a seismic hazard map.

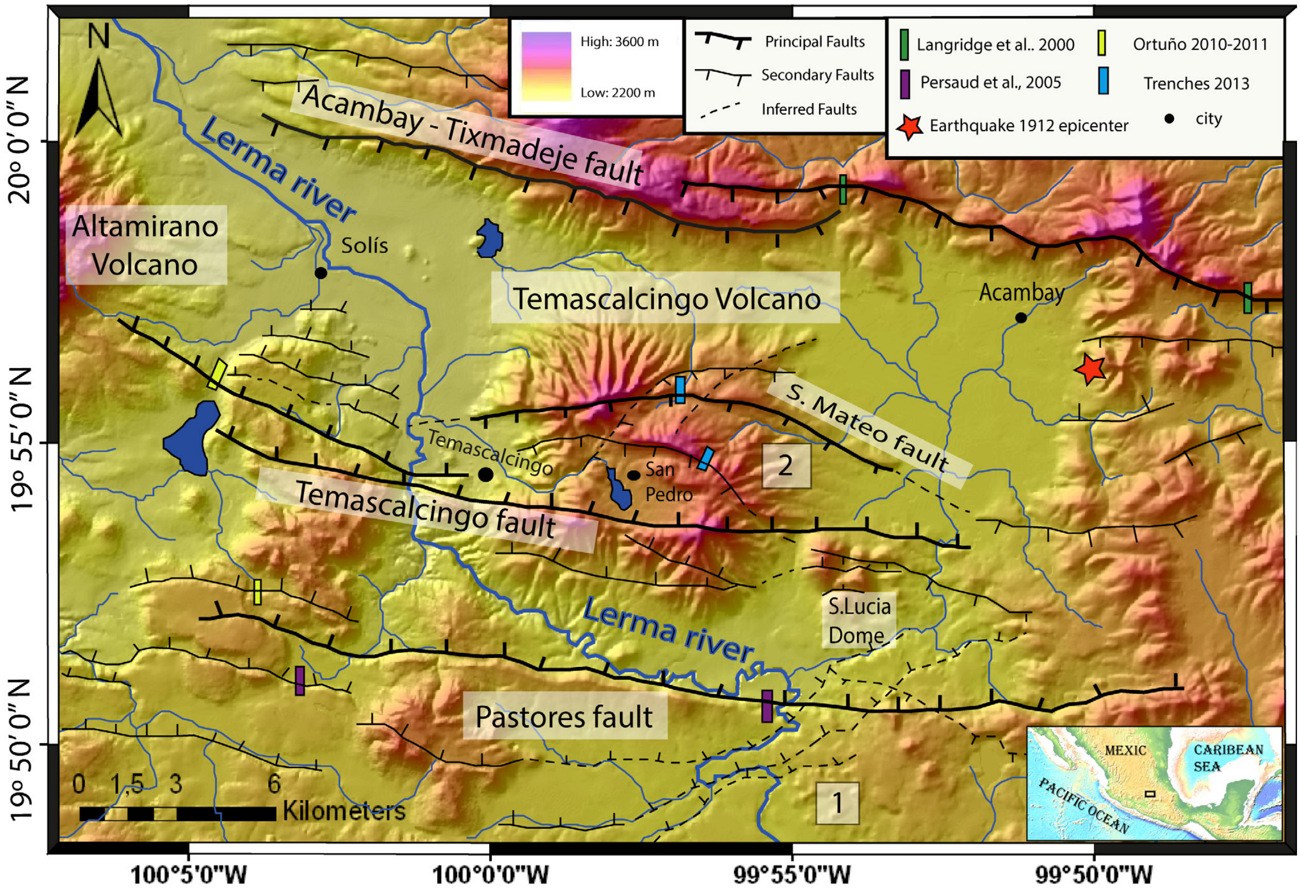


*Fig. 1: Digital Elevation Model of the Acambay graben (highest areas are shown in purple and reach to 3600 meters above sea level, and the lowest in yellow, 2200 m). The Lerma River crosses the basin in NW direction (we can see how the neotectonic affects the drainage system, number 1). The number 2 indicates the area of interaction between the Temascalcingo volcano and the central system faults. The paleoseismological studies performed are also represented.*

## VOLCANIC SETTING

The Temascalcingo volcano (also known as San Pedro volcano) is a Pliocene andesitic-dacitic stratovolcano with a morphology highly controlled by the summit volcanic caldera and several normal faults (Aguirre-Diaz and McDowell, 2000). These faults have a semicircular trace due to the conical geometry and mass of the volcano (Suñé-Puchol et al., 2012). The volcano is composed mainly by dacitic lavas, pumice fall deposits, ignimbrites, andesitic-basaltic domes, parasites cinder cones, etc. The city of Temascalcingo that was destroyed during the Acambay 1912 earthquake is built on top of a deposit of avalanche debris flow produced by a regional collapse of the western flank of the volcano (Roldan-Quintana et al. 2011).

From a volcanic perspective, the dating of C14 samples from the trench could allow to date the last volcanic phases, unknown until now and discuss if it is an active volcano or not.

## PALEOSEISMOLOGICAL TRENCHES

*Location*

The geomorphological study and fieldworks led us to perform a paleoseismological trench on the northern flank of the Temascalcingo volcano, where the geomorphic expression of the San Mateo fault is very well preserved. This fault extends more than 20 km in length and has 100 m high scarps at some locations. From west to east, the San Mateo fault extends from the avalanche deposits (near Temascalcingo city), it crosses the lavas of the northern flank of the volcano and according to Urbina and Camacho, (1913), continues through the sediments of the Acambay basin. However, this last segment does not have any geomorphic expression (Fig.1).

The trench was excavated over lacustrine deposits from "La Lechuguilla" field, a paleolake where the uplifted block of the fault had blocked the drainage and created a small endorheic basin. Figure 2 shows "La Lechuguilla" site, situated along the San Mateo fault.

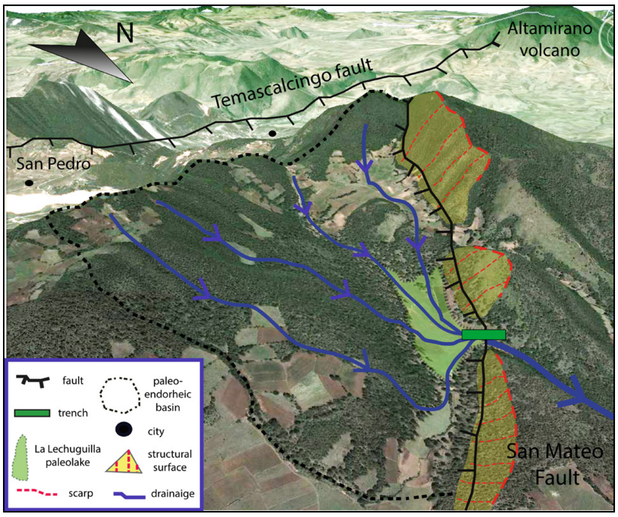


*Fig.2: 3D view of the northern flank of the Temascalcingo volcano. Green polygon is "La Lechuguilla" site, and the green rectangle is the trench across over the San Mateo fault, excavated between two structural surfaces.*

## *Results*

The excavation of a 24 m long paleoseismological trench with a depth ranging from 2 to 4 meters on "La Lechuguilla" site, permitted to identify at least two historical earthquakes generated by San Mateo fault. Fig. 3 shows trench log of this site with an horizontally distribution of the stratigraphic units, mostly formed by volcanic materials and displaced by the fault. The basement, only exposed on the foot-wall, is formed by dacitic lava. Pyroclastic flows and fluvio-lacustrine deposits overlay the basement. A coseismic coluvial wedge formed by dacitic clasts from the basement indicates the oldest event recorded at this site.

Above the wedge, a pyroclastic flow with its corresponding paleosol filled a small local depression that formed on the hanging-wall as a consequence of the first earthquake (U7; green in Fig.3). Deformation of units U5 and U3 was caused by a second seismic event. U5 is a pyroclastic flow of homogeneous thickness with a lithic-rich base (orange layer in Fig. 3) and the U3 is an rich-ash ignimbrite. The fluvio-lacustrine deposits of units U2 and U1 are not displaced by the fault, suggesting that, the last event occurred before the deposition of U2.

A second paleoseismological trench was excavated during this campaign in another fault of the northern flank of Temascalcingo volcano (Fig. 1). On the walls of that trench, situated along the San Pedro fault, was identified another paleoseismic event.

## DISCUSION AND CONCLUSION

The thickness of the coseismic colluvial wedge can be used as a measure of the minimum scarp height created during the first event. According to Mc Calpin (1996) the protoscarp could be two times higher than the coseismic coluvial wedge. So, if the coluvial wedge is ~0.9 m, we estimate a vertical displacement that ranges between 0.9 an 1.8m. The vertical displacement of the second event ~0.5 is estimated from the displacement of unit U5.

We can estimate the earthquake magnitude from fault displacement and/or for fault length. If we use a displacement per event of 0.5 m to 1.8 m and a ~20 km fault length, we obtain a range of magnitudes of 6.5 to 7 (Wells and Coopersmith ,1994).

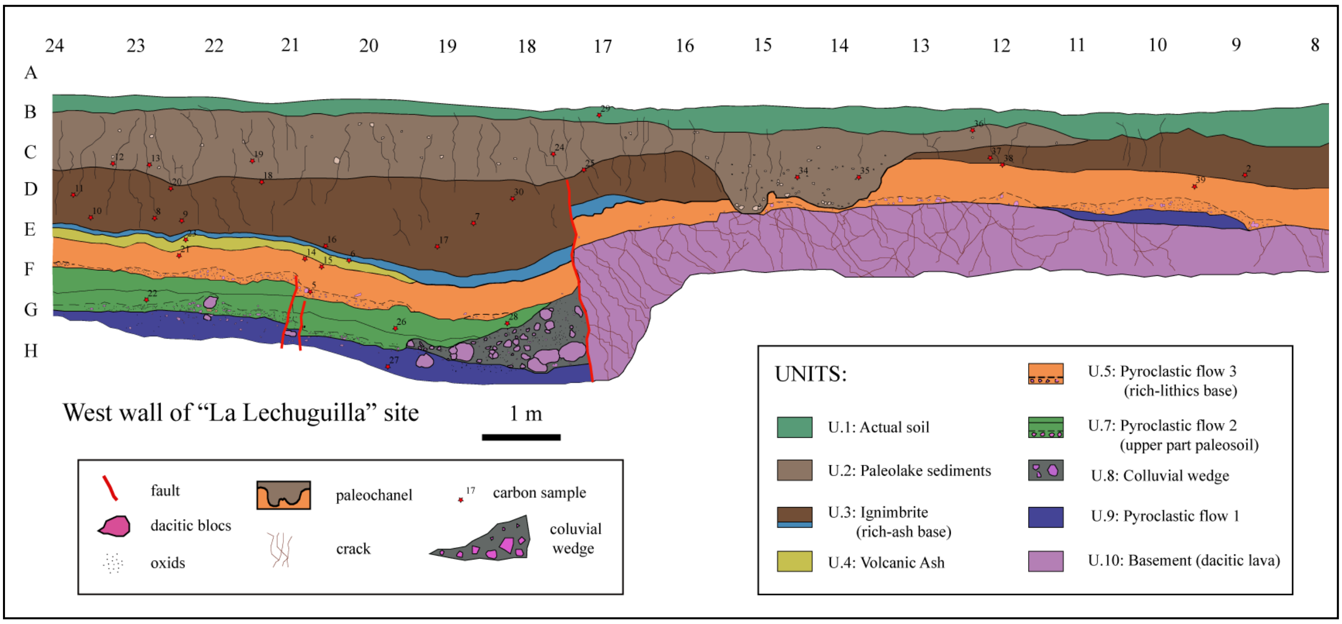


*Fig. 3: Log of the west wall of the "La Lechuguilla" paleoseismological trench.*

The results from C14 dating analysis will determine the ages of these two paleoearthquakes and will allow for assessment of the recurrence period of strong earthquake along the San Mateo fault. The C14 dating analysis will also determine the age of the unit U3 ignimbrite, which could be related to the last magmatic phases of the Temascalcingo volcano, which will improve our knowledge on the volcano history.

If we find a chronological correlation between seismic events along the faults of the graben, we will support our interpretation of the data from Urbina and Camacho (which indicate the simultaneous formation of cracks in different faults of the Acambay graben during the 1912 earthquake), and we will continue to analyse the possibility of a fault connection in depth.

**Acknowledgements:** This research was founded by the Mexican Government through CONACYT (Ciencia Básica- 2009) and by the Universidad Nacional Autónoma de México-UNAM (PAPIIT- 2009). I am very grateful to my girlfriend, my fellow students of the CGEO and the Temascalcingo municipal Presidency for their help during the fieldwork

### References

Aguirre-Díaz, G.J. and McDowell, F.W.(2000). The volcanic evolution of the Amealco caldera, central Mexico. In: *Delgado-Granados, H., Stocks, J., Aguirre-Díaz, G.J., eds., Cenozoic Tectonics and Volcanism of Mexico, Geol. Soc. Amer. Spec. Paper 334, p. 167-178.*

Ferrari, L., Orozco-Esquivel, T., Manea, V., Manea, M. (2011). The dynamic history of the Trans-Mexican Volcanic Belt and the Mexico subduction zone.Tectonophysics.

Landgridge R.M., Weldon R. I., Moya J.C., and Suaréz G. (2000). Paleoseismology of the 1912 Acambay earthquake and the Acambay-Tixmadejé fault. Trans-Mexican Volcanic Belt. *Journal of Geophysical Research vol. 105, NO. B2, PAGES 3019-3037.*

Mc Calpin, J.P. (2006). Paleoseismology, 2nd Edition , Academic Press Inc., 848 p., California.

Ortuño M., Zúñiga R., Corominas O., Perea H., Ramirez-Herrera M.T., Štěpančikova P., Villamor P., Aguirre-Diaz G., Norini G. (2011). Caracterización de fallas sismogenéticas en el centro del Cinturón Volcánico Trans-mexicano: resultados preliminares. *Congreso Latinoamericano de Geología, 2011.*

Ortuño, M., Zúñiga, F. R., Aguirre, G., Carreón, D., Cerca, M, Roverato, M (2012). Holocene earthquakes recorded at the tip of the Pastores fault system (central Mexico). *Abstract volume of the 3rd INQUA-IGCP -567* International Workshop on Earthquake Archaeology and Palaeoseismology.

Persaud, M., Zúñiga, F. R., Aguirre- Díaz, G., Villamor, P., Langridge, R. (2006). First Steps Towards the Paleoseismological History of the Pastores and Venta de Bravo Faults, Acambay Graben, Trans-Mexican Volcanic Belt, Central Mexico. *American Geophysical Union, Fall Meeting, abstract #T13B-0501*

Roldan-Quintana, J., Aguirre-Diaz, G. and Rodriguez-Castañeda J.L.(2011). Depósito de avalancha de escombros del volcán Temascalcingo en el graben de Acambay, Estado de México. *Revista Mexicana de Ciencias Geológicas, v. 28, núm. p. 118-131*

Suñé-Puchol I., Lacan P., Zúñiga R., Cerca M., Aguirre-Diaz G. and Ortuño M. (2012). Analogue Model of the San Pedro volcano in the Acambay Graben, México" *3rd INQUA-IGCP-567 International Workshop on Active Tectonics, Paleoseismology and Archaeoseismology, Morelia, Mexico.*

Suter M., López-Martinez M., Quintero-Legorreta O. and Carrillo-Martinez M. (2001). Quaternary intra-arc extension in the central Trans-Mexican volcanic belt. *Geological Society of America, GSA Bulletin; v. 113; no 6; p. 693-703.*

Suter, M., Quintero, O., López, M., Aguirre, G., Farrar, E. (1995). The Acambay graben: Active intraarc extension in the trans-Mexican volcanic belt, Mexico. *Tectonics, v. 14, p. 1245-1262.*

Urbina F. y Camacho H. (1913) Zona Megaseismica Acambay-Tixmadeje, estado de México. *Instituto Geológico de México, Secretaria de Fomento.*

Verma, S. P. (1996) Mexican Volcanic belt: Present state of knowledge and unsolved problems. *Geof´ıs. Int., special volume on Mexican Volcanic Belt, 1987* ***26****(3B), 309–340.*

Wells, D.L. and Coopersmith, KJ. (1994). New empirical relationships among magnitude, Rupture Length, Rupture Width, Rupture area and surface displacement. *Bulletin Seismological Society of America 84: 974-1.002.*

# Limitations of tsunami deposits identification - problem of sediment sources, sedimentary environments and processes, and post-depositional changes

*Szczuciński, Witold (1)*

(1) Institute of Geology, Adam Mickiewicz University in Poznań, Maków Polnych 16, 61-606 Poznań, Poland. Email: witek@amu.edu.pl

***Abstract:*** *Identification of tsunami deposits is the key to improve tsunami hazard assessment. However, recent studies of modern tsunami deposits using a large set of characteristics ("proxies") have revealed that the deposit's identification is far from being an easy task. This paper reviews some outcomes from studies of 2004 Indian Ocean tsunami (Thailand), 2011 Tohoku-oki tsunami (Japan) and 2000 Paatuut landslide-generated tsunami (Greenland), and provides modern-case based limitations of tsunami deposits identification. They include aspects of sediment sources, environments and processes of deposition, and post-depositional changes in variable climatic and topographic conditions. It is shown that even large tsunamis may leave onshore deposits without marine indicators due to sediment source being on land or due to post-depositional changes. The depositional processes in many cases may be the same as during storms or floods. Finally the sedimentary record of tsunamis in various settings may be very variable, in particular in marine environment.*

***Key words***: *tsunami deposits, sediment sources, depositional processes, post-depositional changes, sedimentary environments*

## INTRODUCTION

Tsunami waves often leave fingerprints in coastal zones in the form of sedimentary event deposits. During the last 15 years, much effort has been devoted to documenting the various recent tsunami deposits. This has been done in order to provide good diagnostic criteria to help identify paleotsunami deposits, as they are necessary to improve the regional tsunami hazard assessment. These deposits may be used in estimations of the long-term tsunami recurrence intervals, as well as of the paleotsunami inundation area and flow height.

The explicit identification of paleotsunami deposits is often difficult mainly because the tsunami deposits may be represented by various sediment types and may be similar to storm deposits. There is probably no simple universal diagnostic set of criteria that can be applied to interpret tsunami deposits with certainty (Goff et al., 2012). However, in many studies a set of "typical" tsunami deposits characteristics is used. Following classical works (e.g. Dawson & Shi, 2000), it is very common to interpret sand sheets which thins and fines landward, reveal fining upward and contain marine components (sediments, diatoms, nannoliths, foraminifera) as tsunami deposits.

The objective of the present contribution is to show modern examples of tsunami deposits, where those "typical" characteristics are absent and to discuss the limiting factors with particular focus on the importance of sediment sources, sedimentary processes and environments, and post-depositional changes in various climatic zones.

## CASE STUDIES

This paper reviews some outcomes from studies of two largest recent tsunamis 2004 Indian Ocean tsunami and 2011 Tohoku-oki tsunami and a major local landslide-generated tsunami at Paatuut (west Greenland).

The deposits from 2004 Indian Ocean tsunami were studied along circa 100 km of the coast of Thailand, both onshore (Szczuciński et al. 2012b) and offshore (Sakuna et al., 2012). Moreover, over 100 of sites were documented shortly after the tsunami and monitored annually for 5 years to assess post-depositional changes (Szczuciński, 2012).

The studies on tsunami deposits resulting from 11 March 2011 Tohoku-oki tsunami were investigated in detail along an circa 5 km long shore perpendicular transect nearby Sendai (Goto et al., 2011; Szczuciński et al., 2012a). The post-depositional changes of tsunami deposits were assessed during several visits during the following two and a half years (Szczuciński et al., submitted).

The effects of the AD 2000 large rock avalanche and tsunami with runup height up to 50 m a.s.l. in Vaigat Strait (Greenland) were studied 12 years after the event, along several tens of km of the coastline (Szczuciński et al., 2012c).

## DISCUSSION

The most commonly reported characteristic of tsunami deposits is their marine origin. For instance, in Indian Ocean tsunami deposits it was common to find marine microfossils (diatoms, foraminifera). However, it is strongly related to their sediment sources. If there are no marine sediments and associated microfossils available for erosion then also tsunami deposits will be composed mainly of terrigenous material. Alternatively, it may happen that sediment laden marine waters are reflected from the offshore slope and only waters poor in suspended sediments flood the coastal zone. Such a case was documented for large Tohoku-oki tsunami along the Sendai plain, where a tsunami more than 11 m high, inundated up to 5 km inland and left tsunami deposits composed of beach, coastal dune and soil sediments with microfossils typical for freshwater and brackish environments (Szczuciński et al., 2012a; confirmed also by other studies). Very few marine microfossils were found also in onshore tsunami deposits in Vaigat Strait (Greenland), where tsunami in AD 2000 eroded mainly beach and beach ridge sediments (Szczuciński et al., 2012c).

The depositional processes during the tsunami may be quite complex. The "typical" tsunami deposits are believed to result mainly from suspension settling (fining upward sediments). Although, such deposits are indeed common (Szczuciński et al., 2012b), the deposits composed of laminated sands deposited from bedload transport - considered as typical feature of storm deposits, are very common in tsunami deposits left on Sendai Plain in Japan (Szczuciński et al., 2012a).

The spatial distribution of onshore tsunami deposits is also far from "typical" thinning landward trend. In all the studied cases a strong relation to local topography was found (Szczuciński et al., 2012a,b,c) with thicker deposits in front of ground elevations. Moreover, it is typical to find maximum thickness not at the coastline, where erosion or transport dominate, but at some distance landward. Analysis of a dozen of transects in Thailand, with similar topography, revealed that the higher the tsunami wave the more inland is located the maximum of tsunami deposits thickness (Szczuciński et al., 2012b). Moreover, as documented in detail along Sendai Plain transect, the deposits layer may be not continuous and composed partly of mud instead of sand (Goto et al., 2011; Szczuciński et al., 2012a). The effect of sedimentary environment is even more obvious in case of marine setting. The so far documented examples of recent tsunami deposits left in inner shelf water are quite variable and it is difficult to find common features for them (see Sakuna et al., 2012 and discussion therein).

The significance of post-depositional processes was addressed before but no systematic studies had been undertaken. The monitoring of the recent tsunami deposits (Szczuciński, 2012; Szczuciński et al., submitted) allowed to assess the associated processes and the rate of changes. The most of physical changes take place within first months after the tsunami, before vegetation may develop and stabilise the ground. To the most important processes belong wind reworking (as in Japan) and washing out of finer sediments and formation of residual layer of coarser sediments (as observed in Thailand). In the following months/years, changes related to soil formation, mixing by roots and chemical changes (salt removal, dissolution of carbonates and silica microfossils) are the most important and are related to climate (faster in tropical zone) and topography (flat areas and depressions are of higher preservation potential). It was also discovered that thinner deposits left in areas of lower tsunami wave runup height have smaller preservation potential (Szczuciński, 2012) and may be missing in geological record. In the polar climate (Greenland), the post-depositional changes were found to be the slowest. After 12 years "salt burn" vegetation was still observed until the inundation limit and the only major change was local sediment redeposition by seasonal snowmelt streams (Szczuciński et al., 2012c).

The paleotsunami deposits are often known only to some extent and their local context at the time of deposition is not always well constrained. However, the recent findings of modern tsunami deposits and their post-depositional changes suggest that the older event deposits should be analysed with even greater scrutiny and consideration of potential sediment sources, offshore and onshore topography (if possible), and climate governed post-depositional changes.

**Acknowledgements:** The contribution results from review of several co-authored works (listed in references) and fruitful discussions with co-authors to whom I express my sincere thanks. The study was partly funded by Polish National Science Centre grant No. 2011/01/B/ST10/01553.

## References

Dawson, A. & S. Shi, (2000). Tsunami deposits. *Pure and Applied Geophysics* 157, 875-897.

Goff, J., C. Chagué-Goff, S. Nichol, B. Jaffe & D. Dominey-Howes, (2012). Progress in palaeotsunami research. *Sedimentary Geology* 243–244, 70–88.

Goto, K., C. Chagué-Goff, S. Fujino, J. Goff, B. Jaffe, Y. Nishimura, B. Richmond, D. Sugawara, W. Szczuciński, D. R. Tappin, R. C. Witter & E. Yulianto, (2011). New insights of tsunami hazard from the 2011 Tohoku-oki event. *Marine Geology* 290, 46–50.

Sakuna, D., W. Szczuciński, P. Feldens, K. Schwarzer & S. Khokiattiwong, (2012). Sedimentary deposits left by the 2004 Indian Ocean tsunami on the inner continental shelf offshore of Khao Lak, Andaman Sea (Thailand). *Earth, Planets and Space* 64, 931-943.

Szczuciński, W., (2012). The post-depositional changes of the onshore 2004 tsunami deposits on the Andaman Sea coast of Thailand. *Natural Hazards* 60 (1), 115-133.

Szczuciński, W., K. Goto, D. Sugawara, C. Chagué-Goff, J.R. Goff, B. Jaffe, Y. Nishimura & B. Richmond, (submitted). The early stage post-depositional changes of the tsunami deposits left by 2011 Tohoku-oki tsunami, Sendai plain, Japan. *Marine Geology*.

Szczuciński, W., M. Kokociński, M. Rzeszewski, C. Chagué-Goff, M. Cachao, K. Goto & D. Sugawara, (2012a). Sediment sources and sedimentation processes of 2011 Tohoku-oki tsunami deposits on the Sendai Plain, Japan - insights from diatoms, nannoliths and grain size distribution. *Sedimentary Geology* 282, 40-56.

Szczuciński, W., G. Rachlewicz, N. Chaimanee, D. Saisuttichai, T. Tepsuwan & S. Lorenc, (2012b). 26 December 2004 tsunami deposits left in areas of various tsunami runup in coastal zone of Thailand. *Earth, Planets and Space* 64, 843-858.

Szczuciński, W., N.J. Rosser, M.C. Strzelecki, A.J. Long, T. Lawrence, A. Buchwal, C. Chague-Goff & S. Woodroffe (2012c). Sedimentary Record and Morphological Effects of a Landslide-Generated Tsunami in a Polar Region: The 2000 AD Tsunami in Vaigat Strait, West Greenland. *American Geophysical Union (AGU) Fall Meeting, San Francisco* ID: 1479941.

INQUA Focus Group on Paleoseismology and Active Tectonics

paleoseismicity.org

# Paleoseismology of the Geleen fault, Lower Rhine Graben

*Kris Vanneste (1), Koen Verbeeck (1), Thierry Camelbeeck (1)*

(1) Royal Observatory of Belgium, Ringlaan 3, B-1180 Brussels, Belgium. Email: kris.vanneste@oma.be

***Abstract:*** *We present a synthesis of the paleoseismic research conducted by the Royal Observatory of Belgium on the Geleen fault in the Lower Rhine Graben (LRG) over more than a decade. Our investigations along the Bree fault scarp section of this fault in Belgium were the first in stable continental Europe to provide evidence that large surface-rupturing earthquakes with magnitudes greater than 6.3 have occurred during the Holocene and the late Pleistocene. Since 2000, we investigated also the region southeast of the Bree fault scarp where the Geleen fault intersects much younger (Saalian and Late Weichselian) terraces of the Meuse River. The analysis of two paleoseismic trenches excavated on this fault section raised the question whether or not the entire Geleen fault defines a single rupture segment.*

***Key words****: intraplate, normal fault, paleoearthquake, late Pleistocene.*

## INTRODUCTION

In most intraplate regions such as northwest Europe, tectonic deformation related to earthquake activity is slow and not well expressed in the landscape, as a result of which very few geological studies have been carried out up to recently to evidence a relationship between geology and earthquake activity. In stable continental Europe, our investigations (Camelbeeck & Meghraoui, 1996, 1998; Meghraoui et al., 2000; Vanneste et al., 1999, 2001) along the Bree fault scarp section of the Geleen fault in Belgium were the first to provide evidence that large surface-rupturing earthquakes occurred during the Holocene and late Pleistocene. The purpose of this contribution is to provide a summary of the paleoseismic research carried out on this fault.

## SEISMICITY AND QUATERNARY FAULTS IN THE LOWER RHINE GRABEN

The LRG is situated in the border area between Belgium, The Netherlands, and Germany, and is bounded by two NNW-SSE trending Quaternary normal fault systems (Fig. 1). The eastern boundary is defined by the Peelrand fault, bifurcating SE-ward into the Rurrand and Erft faults. The western border is defined by the Feldbiss fault zone, which consists of a bundle of en échelon faults, among which the Geleen fault. We addressed the question of the capability of these faults to produce large earthquakes by undertaking paleoseismic investigations along the western border of the graben since 1996.

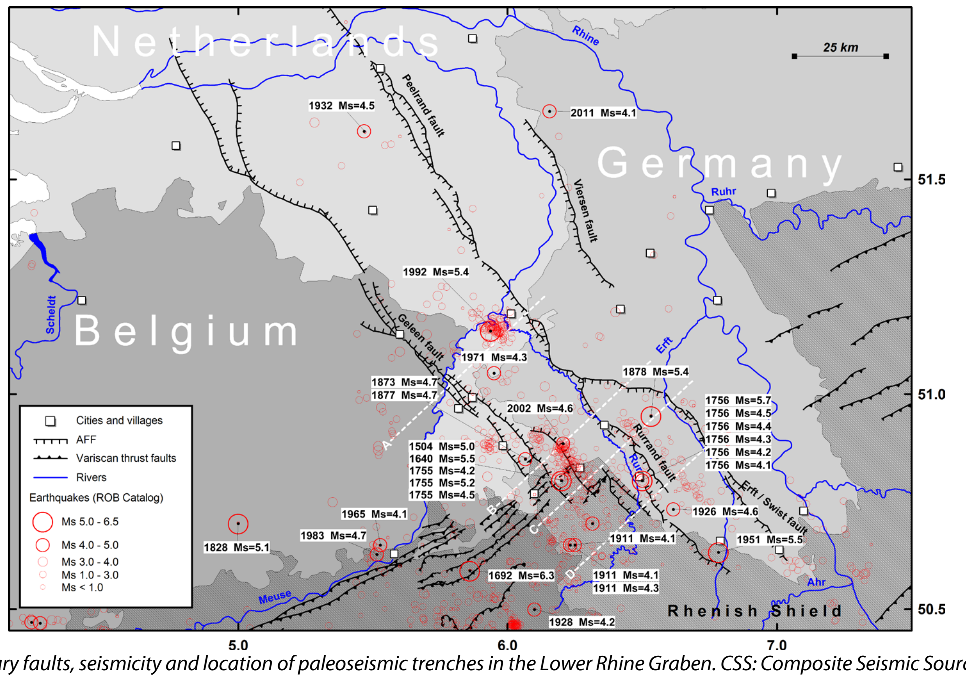


*Fig. 1: Quaternary faults, seismicity and location of paleoseismic trenches in the Lower Rhine Graben. CSS: Composite Seismic Sources, AFF: Active Faults, ROB: Royal Observatory of Belgium*

Re-evaluated historical earthquake and present-day seismological data (Camelbeeck et al., 2007) indicate that much of the known seismic activity in northwest Europe is concentrated in the LRG. The LRG experienced 7 earthquakes with $M_S$ between 5.0 and 6.0 since 1350 (Fig. 1). The largest instrumentally recorded earthquake was the $M_S$ 5.4 Roermond earthquake in 1992, and the largest historical earthquake was the 1756 Düren earthquake, with estimated $M_S$ ~5 ¾. Focal mechanisms show mainly normal faulting. However, it is worth noting that the three strongest known earthquakes with estimated magnitude ≥ 6.0 occurred outside of the LRG, in the northern Ardennes (1692, M ~6 ¼), the southern North Sea (1382, M ~6.0) and the Strait of Dover (1580, M ~6.0).

Many faults have been mapped in the LRG, but so far a model of fault hierarchy or fault segmentation was lacking. In the frame of a European database of seismogenic sources, we have devised a seismic-source model for the LRG, consisting of so-called composite seismic sources (Vanneste et al., 2013). Each composite seismic source may encompass one or more fault segments, but it is considered unlikely that a rupture segment would extend across more than one source. We distinguished 15 seismic sources based on major stepovers, bifurcations, gaps, and important changes in strike, dip direction or slip rate (Fig. 2). The sources are further subdivided into one or more informal fault sections, each with an associated surface trace. We compiled all relevant data concerning the seismic-source parameters required for the database, putting lower and upper bounds on strike, dip, rake, slip rate, and depth, and an upper bound on earthquake magnitude. We also compiled vertical displacement observations (cumulative offset and age of marker horizons), allowing us to assign minimum and maximum vertical deformation rates to each source. These vertical displacement rates range mostly between 0.01 and 0.07 mm/yr, and corresponding slip rates between 0.01 and 0.09 mm/yr. The Peelrand and Erft/Swist faults appear to be the fastest slipping faults, followed by the Geleen fault, which has a slip rate of ~0.055 mm/yr.

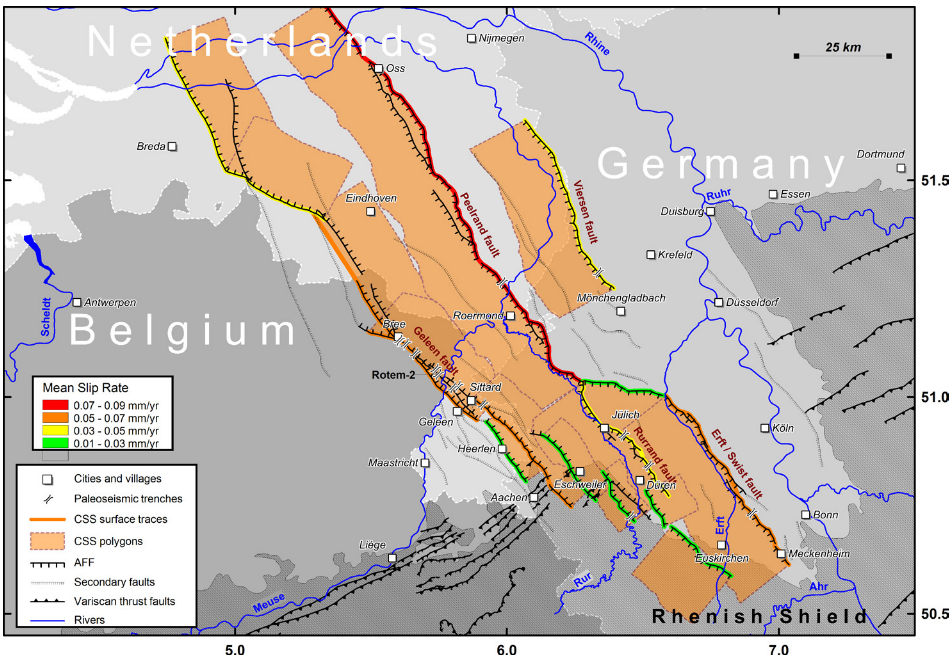


*Fig. 2: Hierarchical fault model for the Lower Rhine Graben. Surface traces are colored according to the slip rate. CSS: Composite Seismic Sources, AFF: Active Faults*

## PALEOSEISMIC INVESTIGATION OF THE GELEEN FAULT

The Geleen Fault runs NW-SE over a distance of ~27 km between the cities of Bree (Belgium) and Geleen (The Netherlands). The northern and southern sections of this fault are well expressed in the topography, in contrast to the central section, which traverses the Meuse River valley. The first paleoseismic trenches were excavated across the northern section of the fault (the "Bree fault scarp"). Later studies focused on the central section.

### *Bree fault scarp*

The Bree fault scarp is a linear, 10-km-long and 15-to-20-m-high scarp, juxtaposing gravel of the middle Pleistocene (> 300 kyr) main terrace of the Meuse River on the Campine Plateau, against Late Weichselian (ca. 27-12 kyr) sands in the graben. Five palaeoseismic trenches have been studied here between 1996 and 2000 (Camelbeeck & Meghraoui, 1998; Meghraoui et al., 2000; Vanneste et al., 2001). These trenches provided evidence for the occurrence of large, surface-rupturing earthquakes on this fault in the recent geological past. In one trench, six paleoearthquakes were identified, five of which occurred in the past 101.4 ± 9.6 kyr. The last three paleoearthquakes could be correlated along the entire Bree fault scarp, and caused vertical displacements of 0.5–1.0 m. The most recent event (MRE) was shown to have a Holocene, most likely even late Holocene, age. The return period was found to range between ca. 14 and 23 kyr. Strong indications for the coseismic nature of faulting were found in the form of colluvial wedges, and the association with various types of soft-sediment deformation. However, the paleoseismic studies were also faced with some problems that are directly or indirectly related to the slow rate of deformation: evidence for the MRE is situated at shallow depth and obscured by soil development, as a result of which the MRE remained poorly dated; the tectonic signal is overprinted by a strong climatic signal (transition from periglacial to temperate conditions); dating resolution rapidly decreases for older events, etc.

*Meuse River Valley*

In more recent years, we extended the investigation to the adjacent section of the Geleen fault in the Belgian Meuse River valley. The surface sediments in this area are much younger (predominantly late Weichselian to Late Glacial), and thus record less cumulative vertical offset. Consequently, the geomorphic expression of the fault is strongly reduced, and generally does not exceed that of other landforms. Using electric-resistivity tomography and ground-penetrating radar, we were able to identify the fault in the shallow subsurface (Vanneste et al., 2008), and we found evidence for a left stepover a few hundreds of meters wide. Two paleoseismic trenches were excavated, one close to this stepover, and another one 2 km SE. We found evidence for a late Holocene paleoearthquake in both trenches (Fig. 3). Radiocarbon and OSL dating (Vandenberghe et al., 2007) constrain the event between 2.5 ± 0.3 and 3.1 ± 0.3 kyr BP, and between 2790 ± 20 and 3770 ± 50 calibrated years before AD 2005, respectively. Thin-section analysis (Vanneste et al., 2008) confirmed our identification of the pre-faulting soil and the overlying scarp-derived colluvium, which are primary coseismic evidence. In both trenches, this event is associated with liquefaction, including various sand blows and a gravel dike. These features are unmistakable evidence for strong co-seismic shaking. In one trench, we identified a second paleoearthquake which was OSL-dated between 15.9 ± 1.1 and 18.2 ± 1.3 kyr BP. The interval between both events has a two-sigma range of 11,600 – 17,200 yr.

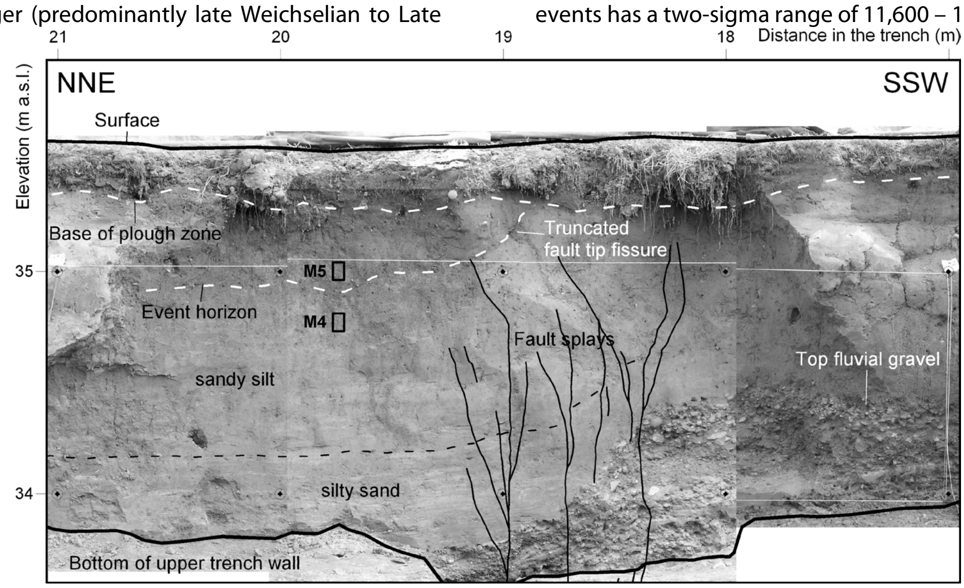


*Fig. 3: Paleoseismic evidence for the most recent surface-rupturing earthquake in a trench across the Geleen fault near Rotem. Location shown in Fig. 2*

*Southeastern part of the Geleen fault*

Our findings contradict the earlier general consensus that faulting in the LRG occurs largely aseismic. In a paleoseismic study on the southeastern portion of the Geleen fault near Born (The Netherlands), Houtgast et al. (2003) concluded that there is no evidence for large, surface-rupturing earthquakes. Their main argument concerns the observation, at some distance from the fault, of a liquefaction feature which is attributed to a moderate earthquake around 15 kyr BP, but does not seem to be directly linked with displacement on the fault itself. The offset they observe follows a short period (max. 2700 years) of erosion, separating both events in time. From this, it is inferred that this offset was created by post-seismic relaxation creep as a delayed response at the surface to the earthquake that triggered the liquefaction. However, the authors appear to have overlooked features such as fault terminations and a fault-zone unconformity. Reinterpreting their trench log, we can demonstrate that the stratigraphic boundary truncating the liquefaction feature in the hanging wall does correspond with an event horizon in the fault zone, and that it is associated with a small, but significant amount of fault offset. We also show that the later offset interpreted by Houtgast et al. (2003) as post-seismic creep resulting from the earthquake that caused the liquefaction, is in fact much younger (post-dating post-depositional soil development), and thus unrelated to the liquefaction event. The event horizon for the event associated with liquefaction corresponds to a well-known and widespread gravel pavement, known as the Beuningen horizon, which is the same stratigraphic horizon as the event horizon for the second event in one of our trenches in the Meuse River valley.

*Possible linkage of fault segments*

The ages obtained for the two paleoearthquakes on the Geleen Fault in the Meuse River valley are in relatively good agreement with those obtained in the trenches along the Bree fault scarp. This raises the possibility that the Geleen fault defines a single, 27-km-long rupture segment, which would be capable of producing M 6.7 earthquakes. The stepover between both parts of the fault is less than 500 m wide, which is probably not sufficient to stop propagation of a large M6+ earthquake (Wesnousky, 2006). However, the data also demonstrate that the stratigraphic and dating resolution are not sufficient to distinguish between this hypothesis and the possible occurrence of two different large earthquakes closely spaced in time, on the two segments separately. It is not likely that additional trenches will provide the definitive answer to this question.

## DISCUSSION

Our investigations along the Geleen fault provide information on the recurrence of large earthquakes along a single seismogenic source in the LRG. The synthesis of data collected in the four trenches excavated on the Bree fault scarp allows us to calculate the fault slip rate and return period for large earthquakes. If we consider the two most recent complete earthquake cycles (between event 3 and event 1), which are best constrained in time and can be correlated across the entire fault scarp, we obtain an average return period of 13.7 ± 7.8 kyr. The average fault slip rate for the same interval, averaging the displacements of events 1 and 3, is 0.050 ± 0.036 mm/yr. Using the longer faulting record from Bree trench 4 (Vanneste et al., 2001), we can make the same calculations for the last 100 kyr. Considering that 5 paleoearthquakes are recorded in trench 4 since 101.4 ± 9.6 kyr BP, corresponding to 4 or 5 complete earthquake cycles, we calculate an average return period of 22.7 ± 4.3 kyr. The corresponding average fault slip rate is 0.031 ± 0.012 mm/yr, which is in good agreement with the values obtained for the two last earthquake cycles. The trenches in the Meuse River valley allowed better constraining the timing of the MRE, between 2.5 ± 0.3 and 3.1 ± 0.3 kyr BP. However, even in this case, the information is not sufficient to define the rupture length with certainty. Investigating the other Quaternary faults of the LRG is therefore a necessity if we want to understand their mechanical behavior and the variation of strain in space and time.

**Acknowledgements:** The authors thank all people who assisted with the field and trenching work over the years.

## References

Camelbeeck, T. (1993). *Mécanisme au foyer des tremblements de terre et contraintes tectoniques: le cas de la zone intraplaque belge*. Ph.D. thesis, Université Catholique de Louvain, 295 p.

Camelbeeck, T. & M. Meghraoui (1996). Large earthquakes in northern Europe more likely than once thought. *EOS, Transactions, American Geophysical Union* 77, 405-409.

Camelbeeck, T. & M. Meghraoui (1998). Geological and geophysical evidence for large palaeoearthquakes with surface faulting in the Roer Graben (northwestern Europe). *Geophysical Journal International* 132, 347-362.

Camelbeeck, T., K. Vanneste, P. Alexandre, K. Verbeeck, T. Petermans, P. Rosset, M. Everaerts, R. Warnant & M. Van Camp (2007). Relevance of active faulting and seismicity studies to assess long term earthquake activity in Northwest Europe In: Stein S. and Mazzotti S. (eds.), *Continental Intraplate Earthquakes: Science, Hazard, and Policy Issues*. Geological Society of America Special Paper 425, 193-224.

Houtgast, R.F., R.T. Van Balen, C. Kasse & J. Vandenberghe (2003). Late Quaternary tectonic evolution and postseismic near surface fault displacements along the Geleen Fault (Feldbiss Fault Zone - Roer Valley Rift System, the Netherlands), based on trenching, *Netherlands Journal of Geosciences* 82, 177-196.

Meghraoui, M., T. Camelbeeck, K. Vanneste, M. Brondeel & D. Jongmans (2000). Active faulting and paleoseismology along the Bree fault zone, Lower Rhine graben (Belgium). *J. Geophys. Res.* 105, 13,809-13,841.

Vandenberghe, D., K. Vanneste, K. Verbeeck, E. Paulissen, J.-P. Buylaert, F. De Corte & P. Van den haute (2007). Late Weichselian and Holocene earthquake events along the Geleen fault in NE Belgium: OSL age constraints. *Quaternary International*, doi: 10.1016/j.quaint.2007.11.017.

Vanneste, K., Camelbeeck, T. & Verbeeck, K. (2013). A Model of Composite Seismic Sources for the Lower Rhine Graben, Northwest Europe: Bulletin of the Seismological Society of America, v. 103, no. 2A, p. 984–1007, doi: 10.1785/0120120037.

Vanneste, K., F. Mees & K. Verbeeck (2008). Thin-section analysis as a tool to aid identification of palaeoearthquakes on the “slow”, active Geleen Fault, Roer Valley Graben. *Tectonophysics* 453, 94-109.

Vanneste, K., M. Meghraoui & T. Camelbeeck (1999). Late Quaternary earthquake-related soft-sediment deformation along the Belgian portion of the Feldbiss fault, Lower Rhine Graben system. *Tectonophysics* 309, 57-79.

Vanneste, K., K. Verbeeck, T. Camelbeeck, F. Renardy, M. Meghraoui, D. Jongmans, E. Paulissen & M. Frechen (2001). Surface rupturing history of the Bree fault escarpment, Roer Valley Graben : new trench evidence for at least six successive events during the last 150 to 185 kyr. *Journal of Seismology* 5, 329-359.

Vanneste, K., K. Verbeeck & T. Petermans (2008). Pseudo-3D imaging of a low-slip-rate, active normal fault using shallow geophysical methods: The Geleen fault in the Belgian Maas River valley: *Geophysics*, v. 73, no. 1, p. B1–B9, doi: 10.1190/1.2816428.

Wesnousky, S.G. (2006). Predicting the endpoints of earthquake ruptures: *Nature*, v. 444, p. 358–360, doi: 10.1038/nature05275.

INQUA Focus Group on Paleoseismology and Active Tectonics

paleoseismicity.org

# North-western Himalayan active front: what paleoseismology tells us about very large thrusts

*Vassallo, Riccardo (1), Jean-Louis Mugnier (1), Hervé Jomard (2), Manzoor Malik (3), François Jouanne (1), Jean-François Buoncristiani (4), Ramperu Jayangondaperumal (5)*

(1) Institut des Sciences de la Terre, Université de Savoie, France. Email: riccardo.vassallo@univ-savoie.fr
(2) Institut de Radioprotection et de Sûreté Nucléaire, Fontenay-aux-Roses, France
(3) Jammu University, Jammu, India
(4) Laboratoire Biogéosciences, Université de Bourgogne, Dijon, France
(5) Wadia Institute of Himalayan Geology, Dehradun, India

***Abstract:*** *Along the North-western Himalayan front, in the Riasi town area (India), the Medlikot-Wadia thrust (MWT) splays into 3 segments that put in contact Precambrian limestones with Quaternary fluvial deposits of the Chenab river and its tributaries. While the internal-most segments are sealed by late quaternary deposits of the Nodda river, the two external-most segments affect these deposits, dated at 14 +/-2 ka. These two segments forms two sub-parallel scarps of 20 $\pm$ 2 m and 23 $\pm$ 2 m at a distance of a few hundred meters. Two trenches were excavated on these segments, showing each the occurrence of at least 2-3 main events with co-seismic displacements of several meters. First radiocarbon ages obtained on these trenches tend to show an in-sequence rupture behavior at the local scale, with the last event that would correspond to the major 1555 Kashmir historical earthquake.*

***Key words**: India, Himalaya, paleoseismology, thrusts, scarps.*

## INTRODUCTION

This study is focused on the seismic behavior and timing of the main thrust faults of the North-western Himalayan front, in the Jammu and Kashmir state, India. This region is characterized by one of the largest seismic gap of all Himalaya, around 100-km-long, with a last strong event that presumably dates to 1555 AD (Ambraseys and Douglas, 2004). The zone is bordered to the East by the 1905 Kangra Mw 7.8 earthquake and to the West by the recent 2005 Muzzaffarabad Mw 7.6 earthquake (Fig. 1).

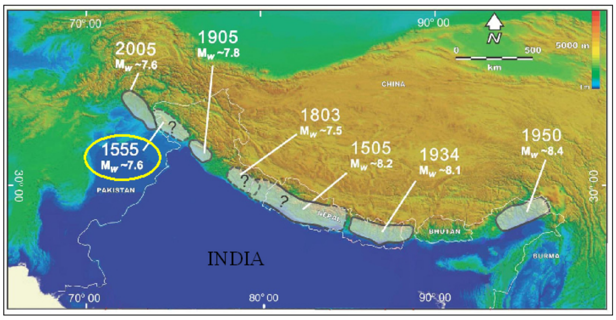


*Fig. 1: Main historical co-seismic ruptures along the Himalayan front (modified from Kumar et al., 2010).*

These events are triggered on a main décollement plane, gently dipping northward (Main Himalayan Thrust) at 10-15 km depth (Fig. 2). Ruptures propagate on ramps that reach the surface producing a cumulative topography at the regional and at the local scale. In particular, where these faults affect Quaternary surfaces, typical active scarps of several tens of meters are built. In the Riasi region, at the toes of the main Himalayan relief, the so called Medlikot-Wadia Thrust (MWT) forms two sub-parallel scarps of 20 $\pm$ 2 m and 23 $\pm$ 2 m within an alluvial fan, at a distance of few hundred meters. These scarps correspond to two splays of the main fault at surface, and their quite steep morphology suggests that they have both been active in the Holocene (Fig. 3). The high activity of these splays is confirmed by the fact that the Precambrian bedrock clearly overthrusts the Quaternary alluvia, and by a morphotectonic study that estimated at around 1 cm/yr for the India-Eurasia convergence accommodated across this fault zone (Vignon, 2011).

However, two questions concerning the faulting behavior and the seismic hazard arise from our morpho-structural analysis: 1) did the fault break during the last 1555 Kashmir event? 2) do the two splays break co-seismically together or do they alternate their activity?

To answer these questions we trenched across the two scarps, where their respective heights are maximum, in order to identify, measure and date seismo-sedimentary horizons.

The two trenches are around 25-m-long, 5-m-wide, and up to 8-m-deep. The deposit of the fan is mainly constituted by pluridecimetric units of angular carbonate gravels alternating with fewer sand units. Some coarser, less continuous units are also present. Undeformed units gently dip towards the South-West.

The two trenches show colluvial wedges (sometimes folded or faulted), buried free scarps, tilted and folded units as well as liquefaction features. Both show complex histories with several co-seismic ruptures, with in-sequence and out-of-sequence patterns at the scale of one scarp. Sedimentary units could be dated by 14C analysis of charcoals and bulk soils. This allows proposing a relative chronology among the different ruptures and an absolute dating of the co-seismic events.

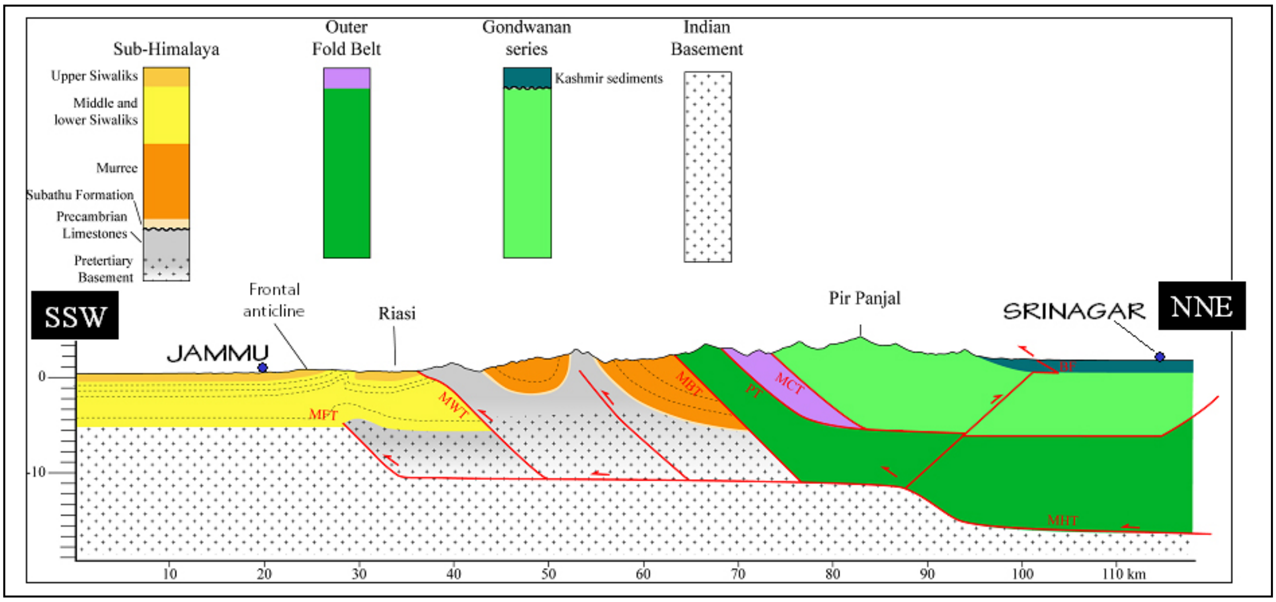


*Fig. 2: Crustal cross-section of the actively deforming front in the North-western Himalayan region, characterized by a main flat décollement and a series of ramps (modified from Vignon, 2011).*

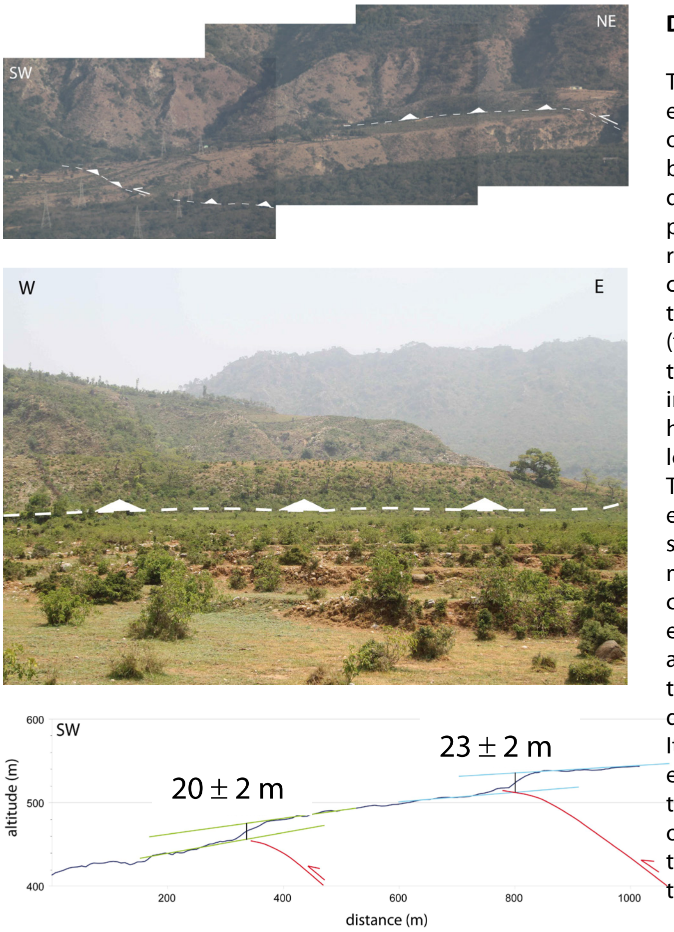


*Fig. 3: a) Tectonic scarps built by the two active splays of the MWT in the Riasi region. b) Close up on the upper scarp. c) Topographic profile across the two splays.*

**DISCUSSION**

The trench dug on the most external scarp provides evidence for 3 main events (Fig. 4). The dating of the organic material contained in the colluvial wedge that buries the last rupture is consistent with a co-seismic displacement in 1555. Therefore, this splay of the fault probably experienced and recorded the last strong regional earthquake. A previous event produced a colluvial wedge dated between 410 and 780 AD, while a third event occurred some time after 1120-810 BC (faulted paleosoil). Co-seismic displacements are difficult to estimate because they are likely to be very large, implying systematical collapse of a great part of the hanging block. However, we can say that since ~3 ka, at least 12 m of cumulative displacement occurred.

The 2nd trench was dug in late 2012 onto the 2nd external-most fault splay. Within the trench, the fault splays into two branches. A first one situated in the middle part of the main scarp, showing strong cumulative offsets (several meters) of at least 2 main events that led to the formation of two colluvial wedges, and faulting of the older one. A second one, toward the toes of the main scarp, displaying a single rupture with a displacement of ~1 m (Fig. 5).

It is not clear whether this rupture corresponds to a third event, or if it is related to one of the event observed on the first branch. However, first results obtained on organic materials show that this scarp should be older than the external-most one, with events occurring in a time span of 14000 to 3000 BC.

Therefore these two paleoseismological trenches tell us:

1) At least 2-3 main Holocene events with co-seismic displacements of several meters occurred on both splays;

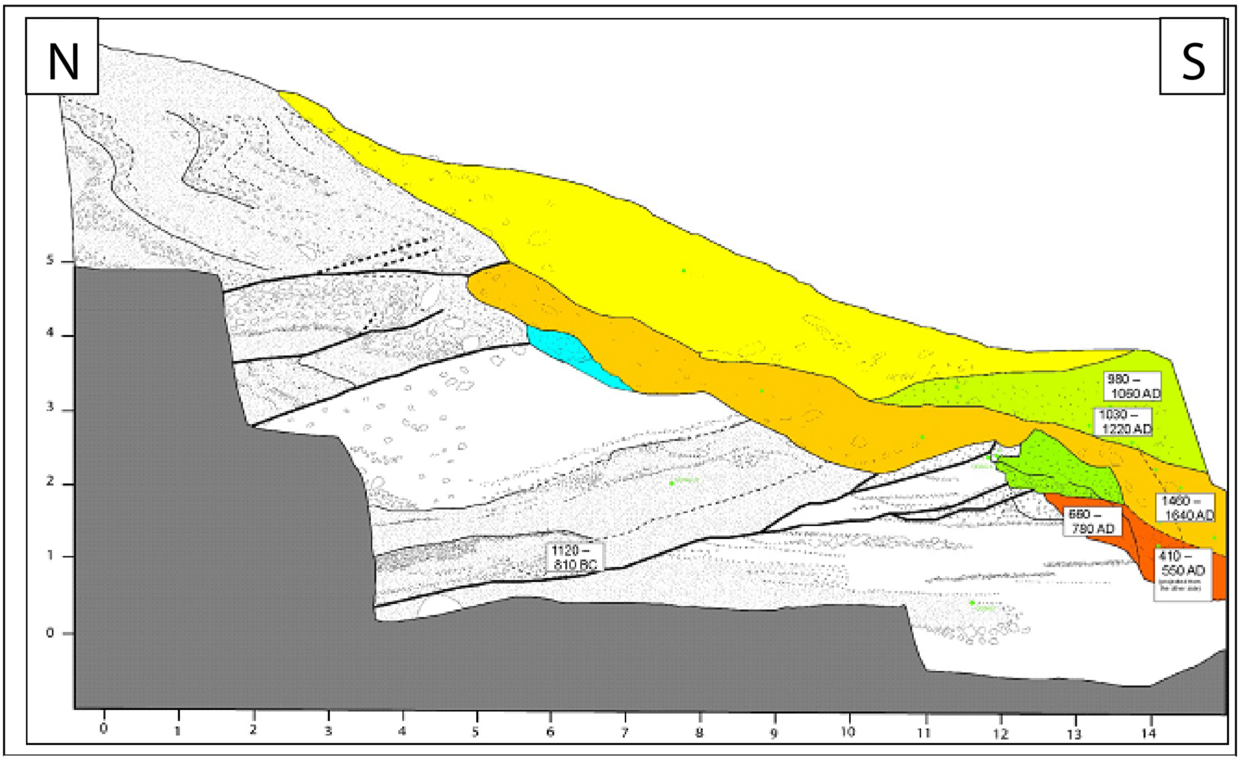


*Fig. 4: tectono-stratigraphic log of the eastern wall of the trench dug into the external-most scarp.*

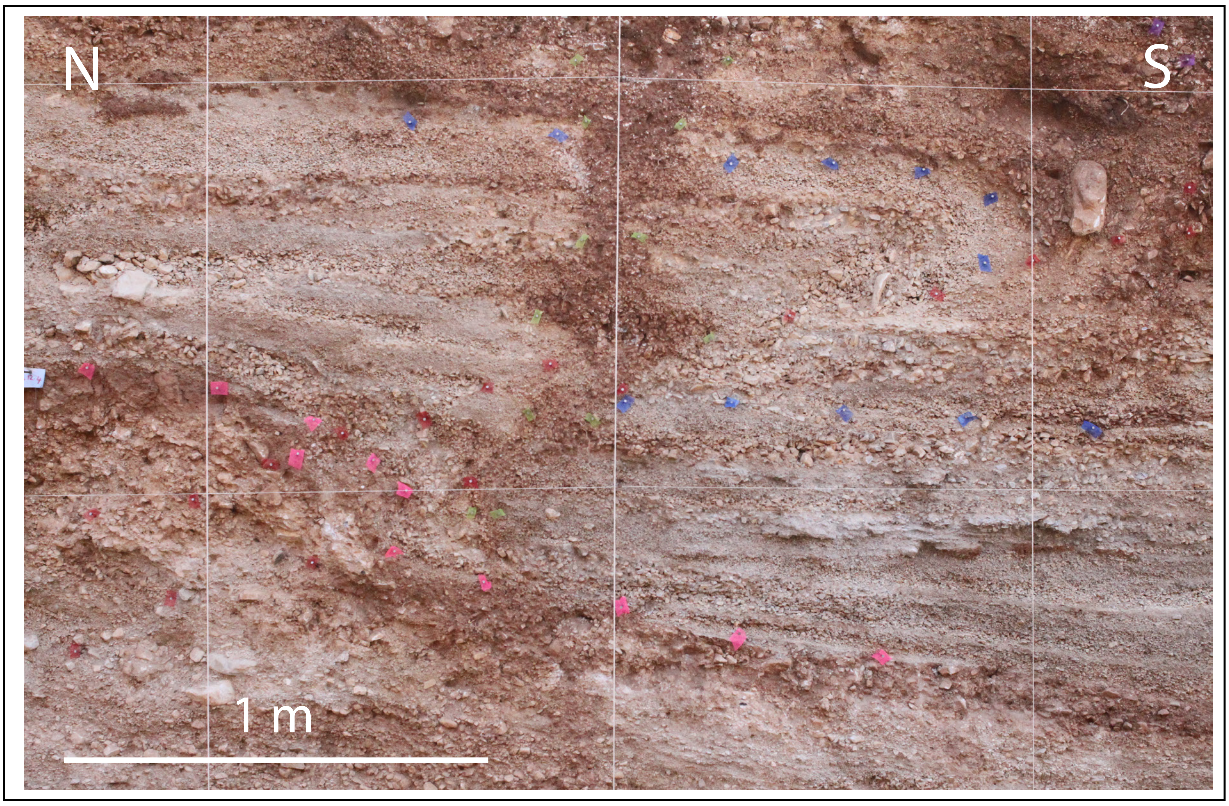


*Fig. 5: Detail of the eastern wall of the trench dug into the 2nd external-most scarp. Layers (blue and pink flags) and a sand dyke (green flags) are displaced of around 1 m by a rupture (red flags).*

2) The rupture of the last strong regional event (1555 Kashmir earthquake) deformed the surface deposits at this site, but was limited to the external-most splay;
3) An in sequence activity (pre and post ~3 ka) is observed at the scale of the two scarps. This implies very large displacements for each event in order to have a cumulative seismic deformation consistent with the high long-term slip rate (around 1 cm/yr) deduced by morphotectonic studies.

**Acknowledgements:** This project has been supported by grants from ANR catel Paksis, LabEx Osug@2020 and AAP Université de Savoie. We thank all the Indian people that helped us in digging the trenches and the laboratories of Poznan (Poland) and Gif-sur-Yvette (France) for radiocarbon dating.

**References**

Ambraseys, N.N., and J. Douglas, (2004). Magnitude calibration of north Indian earthquakes: *Geophysical Journal International*, v. 159, p. 165-206.

Kumar S., S. G. Wesnousky, R. Jayangondaperumal, T. Nakata, Y. Kumahara, V. Singh, (2010). Paleoseismological evidence of surface faulting along the northeastern Himalayan front, India: Timing, size, and spatial extent of great earthquakes, *JGR*, vol. 15 B12422.

Vignon V., (2011). Activité hors séquence des chevauchements dans la syntaxe nord- ouest himalayenne : apports de la modélisation analogique et quantification quaternaire par analyse morphotectonique, *PhD thesis*, Université de Grenoble, France, 278 p.

INQUA Focus Group on Paleoseismology and Active Tectonics

paleoseismicity.org

# ESI2007 assessment of paleoseismic features in the Acambay and Ixtlahuaca graben, Mexico: evidence for capability along the Perales Fault

*Velázquez-Bucio, M. Magdalena (1), Alessandro Maria Michetti (2), Luigi Benente (3), Gianluca Groppelli (3), Victor Hugo Garduño-Monroy (4), Sara Filonzi (3), Miguel Angel Rodríguez-Pascua (5), Raul Pérez-López (5), Kervin Chunga (6)*

(1) CIGA, Universidad Nacional Autónoma de México. Antigua Carretera a Pátzcuaro No. 8701, Col. Ex-Hacienda de San José de la Huerta. 58190 Morelia, Michoacán, Mexico. Email: magda_vb@yahoo.com.mx
(2) Dipartimento di Scienza e Alta Tecnologia, Università dell'Insubria, Via Valleggio 11, 22100 Como, Italy.
(3) C.N.R. - Istituto per la Dinamica dei Processi Ambientali, sez. di Milano, Via Mangiagalli 34, 20133 Milano, Italy.
(4) Departamento de Geología y Mineralogía, Instituto de Investigaciones Metalúrgicas, Edificio U. Ciudad Universitaria. Universidad Michoacana de San Nicolás de Hidalgo. 58060, Mexico.
(5) IGME, Instituto Geológico y Minero de España, C/Ríos Rosas 23, 28003 Madrid, Spain.
(6) Centro de Investigaciones de Geociencias CIGEO. Facultad de Ciencias de la Ingeniería. Universidad Estatal Península de Santa Elena UPSE, La Libertad, Ecuador.

***Abstract:*** *We compare published macroseismic data from the Nov. 19$^{th}$, 1912, Ms 6.9 Acambay earthquake with new analyses of paleoseismic evidence preserved in the stratigraphy and geomorphology of three Mid-Pleistocene to Holocene lacustrine subbasins (San Pedro El Alto and San Bartolo Lanzados, in the epicentral area of the 1912 event; and Ixtlahuaca de Rayón, along the Perales Fault, ca. 40 km S of the 1912 epicenter) using the ESI 2007 scale. In the Ixtlahuaca paleobasin (Mid Pleistocene?), liquefaction, megaslumping features, and synsedimentary surface faulting are genetically associated, suggesting A) a seismically induced origin, and B) a local earthquake source, at least for some of the observed deformational paleoevents. In the studied sub-basins, the preliminary intensity assessment from the paleoseismic environmental effects is comparable, and consistent with the epicentral intensity of the 1912 event ($I_0$ = X in the Cancani scale). The three sub-basins are controlled by the growth of the same system of extensional structures during the Quaternary, showing very similar tectonic and geomorphic features. This includes the Pastores, Temascalcingo and Acambay-Tixmadejé faults, which ruptured during the 1912 earthquake, and the Perales Fault. We argue that within such a coherent seismic landscape the ESI 2007 intensity assessed from paleoseismic features in the Ixtlahuaca paleobasin indicates a seismic potential in the order of Mw 7 for the Perales Fault, equivalent to the one demonstrated by the master faults of the Acambay graben.*

***Key words****: Acambay Graben, Ixtlahuaca de Rayón, macroseismic intensity, paleoseismicity, ESI2007 scale, Perales fault*

## INTRODUCTION

Mexico is divided into five main tectonic blocks whose relative movement causes strong to large earthquakes (M > 6), commonly deeper than 50 km, which place the country as one of those with highest seismic risk in the World. Our study area is located in the central sector of Mexico, characterized by numerous and large lacustrine depressions, which have stored Pleistocene to Holocene sedimentary series recording the most important geological and paleoenvironmental events (Israde-Alcantara, 1995). These natural archives have been principally exploited for understanding the Quaternary climatic evolution of the region, however the extensive deformations induced by faults and earthquakes in these recent lake sediments have been relatively overlooked until now.
The central region of Mexico is characterized by large, E-W trending, tectonic basins, controlled by a belt of Quaternary normal faults. The Acambay and Ixtlahuaca graben are among the biggest intra-arc basins of the Trans-Mexican Volcanic Belt (TMVB), an active volcanic arc related to the subduction along the Middle America trench.
The 40 km long and 15 km wide Acambay structure, one of the best known shallow crustal seismic source in Mexico (Suter et al., 1995), is located approximately 100 km NW of Mexico City. The Acambay graben has been the site of Quaternary and historical surface ruptures, and recent lake sediments (Pleistocene to Present) are highly deformed because of faults and/or deformation structures (Garduño and Israde, 2006; Langridge et al., 2000; Suter et al, 2001; Rodriguez-Pascua et al. 2010). The November 19$^{th}$, 1912, Ms 6.9 event is representative of ground-rupturing earthquakes on the Acambay-Tixmadejé fault and demonstrates that important seismic events (in the order of Mw 7) can be generated by TMVB normal faults (Norini et al., 2006).

The present work aims to apply the ESI 2007 scale to

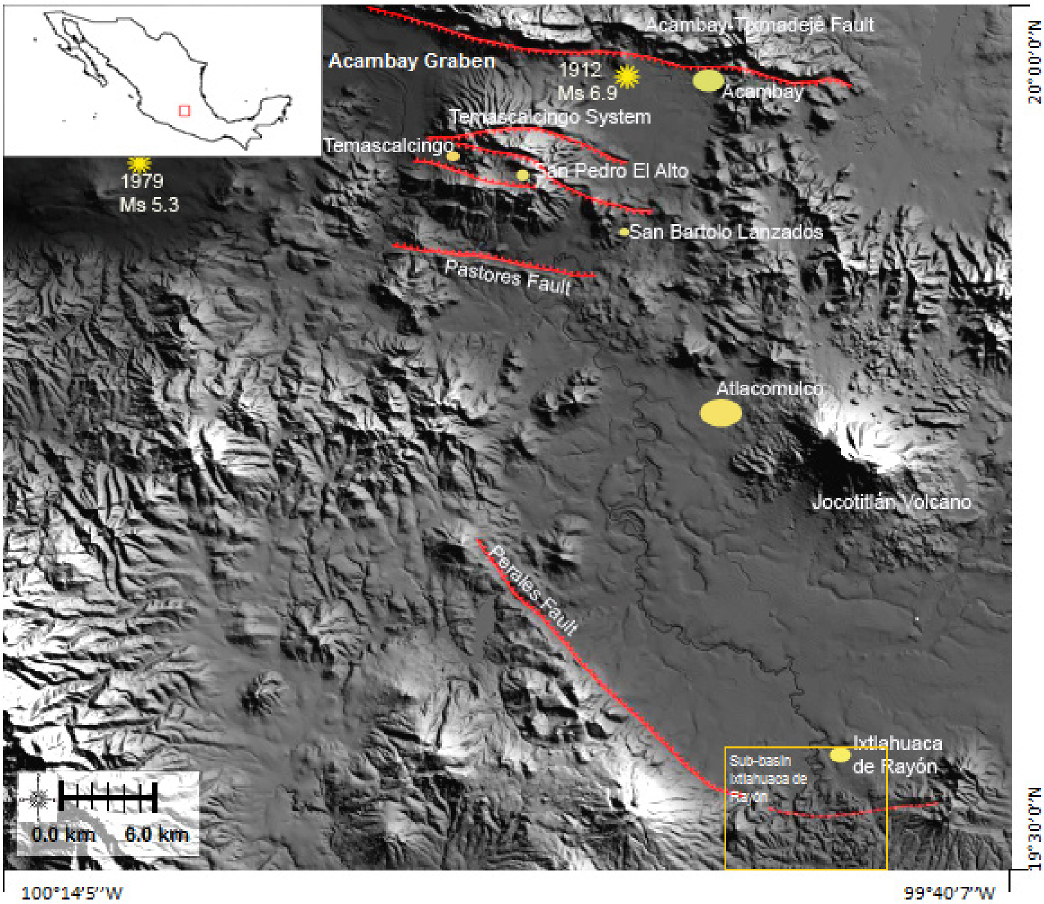


*Fig. 1: Study area, including the location of lacustrine subbasins (San Pedro El Alto, San Bartolo Lanzados and Ixtlahuaca de Rayón; yellow box locates Fig. 7) linked to the Acambay graben and nearby Perales Fault; epicenters of instrumental strong earthquakes are also shown.*

the effects on physical environment produced by paleoseismic events identified in three subbasins linked to the Acambay graben (San Pedro El Alto, San Bartolo Lanzados and Ixtlahuaca de Rayón; Fig. 1). We compare published ESI 2007 scale assessment for the 1912 event with paleoseismic evidence (liquefaction, soft-sediment deformations, surface faulting) observed during detailed field mapping in the study area (Benente, 2005; Filonzi, 2005, Rodriguez-Pascua et al. 2010; 2012; Velázquez, in prep.). Particularly remarkable for the purpose of this note, the Ixtlahuaca de Rayón subbasin, located at the S boundary of the graben and controlled by the Quaternary growth of the Perales Fault (Fig. 1), does not show any historical record of significant local earthquake, and is therefore commonly regarded as non-seismic. The three basins are formed by a volcanoclastic lacustrine sequence, alternating with ash levels typical of TMVB, and preserve similar coseismic deformation structures.

## DESCRIPTION OF COSEISMIC DEFORMATION STRUCTURES

### San Bartolo Lanzados

This basin is located in the S sector of the Acambay graben, bounded by the Pastores Fault (Fig. 1). In the exposed stratigraphic sequence, structures related to soft sediment deformation and liquefaction (Fig. 2) are widespread. Such structures are linked to liquefaction processes, which have led to the formation of dikes, small sand volcanoes and pseudonodules. Detailed logs of several stratigraphic sections allowed to identify a total of seven events of deformation,

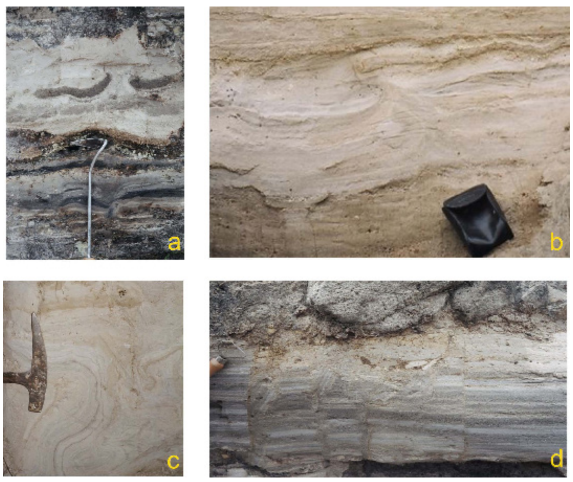


*Fig. 2: Structures identified in San Bartolo Lanzados. a) pseudonodules (VII-ESI2007); b) dike and sills in the clear ash (VII-ESI2007); c) plastic deformation, "box fold" (VII-ESI2007); d) "rigid" seismites (VIII-ESI2007).*

interpreted as paleoearthquakes. The maximum epicentral intensity assessed for this area is VIII in the ESI 2007 scale.

**San Pedro El Alto**

The San Pedro El Alto sub-basin is sited in the center of the Acambay graben (Fig. 1), at an average altitude of 2640 m a.s.l. within the dacitic caldera of the Temascalcingo volcano. The intervening E-trending faults belong to the Central System of the graben, with steep fault planes dipping up to 80° to the N and S. The presence of secondary structures interpreted as seismites was recognized by detailed stratigraphic analyses, also through exploratory trenching (Fig. 3). Some of the structures identified in this area include: numerous open cracks, more than 3.5 m deep, with intrusion of recent surficial material; unconformity and displacement of sediment; thickness variation of certain stratigraphic units affected by faulting, small slumps and pseudonodules.

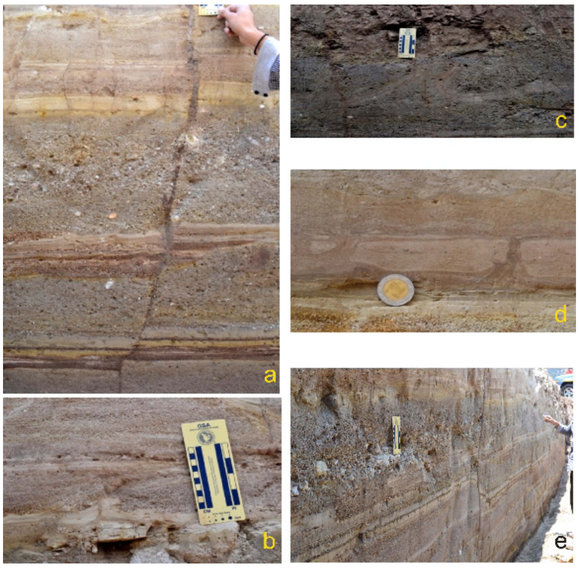


*Fig. 3. Structures identified in the San Pedro El Alto basin: a) thickening of displaced sediment along the fault plane, and crevice filling with recent material (VII-ESI2007); b) small sand volcano into fine volcanic ash (VII-ESI2007); c) small slump (VII-ESI2007); d) pillow structures (VII-ESI2007); e) faulting in the trench wall (VII-ESI2007)*

**Ixtlahuaca de Rayón**

The Ixtlahuaca basin is a tectonic depression ca. 40 km$^2$ wide (Fig. 1), structurally related to the Acambay graben. The master fault that controls the kinematic evolution of the Ixtlahuaca basin is the Perales fault, which presents an orientation NW - SE in the western part, whereas in the oriental sector its trend is E - W. The local lacustrine and fluvial sequence has settled during the Middle Pleistocene, and is constituted by terrigenous and biogenic sediments intercalated with pyroclastic and epiclastic deposits that indicate an intense synchronous volcanic activity. This sequence is presently faulted and uplifted in the footwall of the Perales Fault, which during the Late Quaternary therefore migrated basinward.

The deformational structures identified near Ixtlahuaca (Figs. 4-6) occur at precise stratigraphic levels between undeformed depositional horizons. The areal diffusion of these structures is basinwide, and is similar to the seismically-induced structures described in the literature. Most critical for the purpose of this study, soft sediment deformations and paleoliquefaction features are clearly genetically related with synsedimentary faulting of the lake basin floor (Fig. 6). For these reasons, it has been suggested that their origin is due to ancient earthquakes; the observation of surface faulting within the lake basin also indicates that at least some of these paleoearthquakes have been generated by a local seismic source.


*Fig. 4: Structures identified in the Ixtlahuaca basin: a-a') flame structure in silt-sandy sediment, (ESI2007-VII); b) post-liquefaction collapse structure in sandy-silty sediment, (ESI2007-VII). EEE 2 and 3 in table 1, fig.7.*

The seismites described in Figure 4 and 5 have been observed at specific locations. The megaslump features in Figure 5, however, affect the whole studied area. Using the megaslump layer as a marker horizon, Benente (2005) concluded that there have been at least two earthquakes preceding the event creating the slump and two later events (Table 1). The ESI 2007 scale value for the observed environmental effects are mapped in Figure 7.

*Fig. 5: Seismically-induced megaslump, consisting of sand and silt; a similar feature is found throughout the basin at the same stratigraphic level (ESI2007-VIII). EEE 8 in table 1, fig. 7.*

*Table1. Summary of deformational structures found in the Ixtlahuaca de Rayón basin; see location in Figure 7.*

| Event | Unit (Member) | EEE | Distribution | Intensity (ESI2007) |
|---|---|---|---|---|
| T4 | El Salto | 1) Dykes cross | local | VII |
| T2 | Rio Lerma | 2) Flame | local | VII |
| T1-2 | El Salto<br>Rio Lerma | 3) Post-liquefaction collapse structure | local | VII |
| T5 | El Salto | 4) Pseudonodules | local | VII |
| T1 | El Junco | 5) Centimeter faults | local | VII |
| T1 | El Salto | 6) Tilted blocks | local | VIII |
| T3 (?) | Rio Lerma | 7) Fold and surface faulting | local | IX |
| T3 | All members | 8) Slump | All area | VIII |
| T3 | Rio Lerma | 9) Lateral spread | local | VII |
| T? | All members | 10) Surface faulting | All area | IX |

## PRELIMINARY INTERPRETATION AND DISCUSSION

The November 19th, 1912, Acambay earthquake produced relevant environmental effects, including liquefaction and surface faulting. Rodriguez-Pascua et al. (2012) published new macroseismic intensity maps for this event, also using the ESI 2007 scale. Comparison of historical and paleoseismic ESI 2007 intensities in the San Pedro el Alto and San Bartolo Lanzados sub-basins, located in the epicentral area near two of the surface faulting segments of the Acambay earthquake, shows that the size of ancient earthquakes was similar to that of the 1912 event. In fact, the same is true also for the ESI 2007 values mapped from the Ixtlahuaca de Rayón lacustrine paleoseismites, located 40 km S of the 1912 epicenter, in an area that according to the seismic catalogue was never affected by strong local earthquakes.

Obviously, soft-sediment deformations, liquefaction and slumping in lake floor might be triggered also by large, far away, subduction events, as dramatically illustrated by the effects generated during the September 19, 1985, Mw 8.1 earthquake in Mexico City. However, at Ixtlahuaca the association of seismites and synsedimentary surface faulting indicates that at least some of the observed paleoeffects have been induced by a local source.

Also, it is well known that in volcanic environments tectonic faulting may occur as aseismic slip, as already shown for other TMVB structures (e.g., Norini et al., 2006). However, at Ixtlahuaca the coexistence of surface faulting and liquefaction suggests that at least some of the slip along the Perales Fault took place during strong surface faulting earthquakes.

Therefore, paleoseismic ESI 2007 intensity data, interpreted in the framework of the same seismic landscape, strongly suggest that the Perales Fault is capable of generating strong earthquakes, with magnitude of the same order as the one produced by the faults in the Acambay graben in 1912.

The epicentral intensity from paleoseismic features at Ixtlahuaca is in the order of IX ESI2007; however, we have no direct data yet on the coseismic rupture length and surface displacement of the capable Perales Fault. Rupture of its whole length (ca. 45 km; Fig. 1) might result in $I_0$ = X ESI2007, as during the 1912 Acambay event. Of course, this hypothesis must be confirmed by specific trenching and dating across the fault trace. In any case, our data emphasize that the Perales Fault should be regarded as a major seismic source, to be considered for the assessment of seismic hazards in the Ixtlahuaca basin and nearby region, including the Mexico City metropolitan area which is located only 80 km to the East.

*Fig. 6: Isoclinal fold within a diatomite horizon, affected by synsedimentary faulting (ESI2007-IX). EEE 7 and 10 in table 1, fig. 7.*

### References

Benente L. 2005. Carta Geologica di Ixtlahuaca de Rayón – México. Inquadramento e assetto tettonico. Laurea in Science Geologiche. Università degli Studi di Milano. Facoltà di Scienze MM.FF.NN. Italia.

Filonzi S. 2005. Analisi paleosismologica del bacino lacustre di San Bartolo Lanzados – Arco Vulcanico Messicano. Università degli Studi di Milano. Facoltà di Scienze MM.FF.NN. Italia.

Garduño M.V.H., Israde-Alcántara I., 2006. Field guide for the excursion of Central Mexico basins from Acambay to Patzcuaro Basins. Depto de Geologia y Mineralogía– IIM–UMSNH. Mexico: 1- 10.

Israde-Alcántara I., 1995, Bacini Lacustri dal Settore Centrale dall'arco vulcanico messicano. Stratigrafia ed evoluzione vulcanotettonica basata sulle diatomme: Università degli Studi di Milano, Tesis doctoral, Italia: 254

Langridge R.M., Weldon II R. J., Moya J.C., Suárez G. 2000. Paleoseismology of the 1912 Acambay earthquake and the Acambay-Tixmadejé fault, Trans-Mexican Volcanic Belt. Journal of Geophysical Research, Vol. 105. No. B2: 3019-3037.

Michetti A.M., E. Esposito, L. Guerrieri, S. Porfido, L. Serva, R. Tatevossian, E. Vittori, F. Audemard, T. Azuma, J. Clague, V. Comerci, A. Gürpinar, J. McCalpin, B. Mohammadioun, N.A. Mörner, Y. Ota, E. Roghozin, 2007. Environmental Seismic Intensity Scale 2007 - ESI 2007. Memorie Descrittive della Carta Geologica d'Italia, 74, 7-54, Servizio Geologico d'Italia – Dipartimento Difesa del Suolo, APAT, Roma, Italy.

Norini G., Groppelli G., Lagmay A.M.F., Capra L. 2006. Recent left-oblique slip faulting in the central eastern trans-Mexican volcanic belt: Seismic hazard and geodynamic implications. Tectonics 25: 1–21.

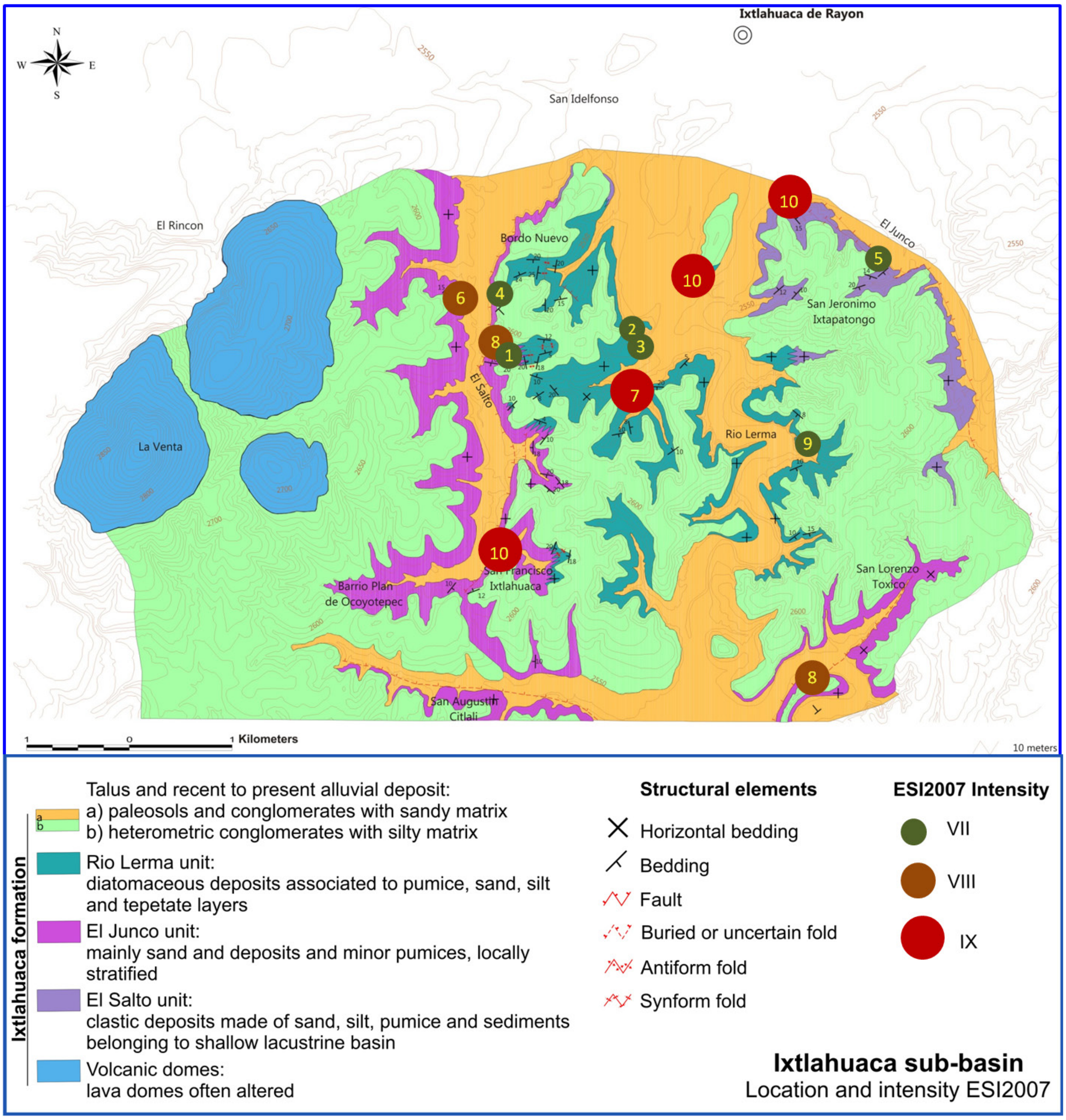


*Fig. 7: Location and intensity ESI2007 of sediment deformation structures and surface faulting identified in the subbasin Ixtlahuaca de Rayón (modified after the Geological Map of Ixtlahuaca de Rayón; Benente, 2005); numbers refers to the type of earthquake environmental effect, as described in Table 1.*

Rodríguez-Pascua, M.A., Garduño-Monroy, V.H., Israde-Alcántara, I., Pérez-Lopéz, R. 2010. Estimation of the paleoepicentral area from the spatial gradient of deformation in lacustrine seismites (Tierras Blancas Basin, Mexico). Quaternary International 219 (1): 66-78.

Rodríguez-Pascua, M.A., V.H. Garduño-Monroy, R. Pérez-Lopéz, Perucha-Atienza, M.A., Israde-Alcantara, I. 2012. The Acambay Earthquake of 1912, revisited 100 Years After. 3rd INQUA-IGCP-567 International Workshop on Active Tectonics, Paleoseismology and Archaeoseismology, Morelia, Mexico (2012), Abstract Volume: 157-159.

Suter, M., Quintero-Legorreta, O., López-Martínez, M., Aguirre-Díaz, G., Farrar, E. 1995. The Acambay graben: Active intra-arc extensión in the trans-Mexican Volcanic Belt, Mexico. Tectonics. 14 (5): 1245-1262.

Suter, M., López Martínez, M., Quintero Legorreta, O., Carrillo Martínez, M., 2001. Quaternary intra-arc in the central Trans-Mexican volcanic belt. Bulletin, Geological Society of America 113, 693–703.

Velázquez B.M.M. Estratigrafía cosísmica en secuencias lacustres del Holoceno en el graben de Acambay, Estado de México y evaluación del peligro sísmico. Tesis de doctorado en Geografía. CIGA, UNAM. México. In prep.

INQUA Focus Group on Paleoseismology and Active Tectonics

paleoseismicity.org

# Possible Quaternary activity of the Rauw Fault in the Belgian Campine basin?

*Verbeeck, Koen (1), Kris Vanneste (1), Thierry Camelbeeck (1), Laurent Wouters (2), Pim Demecheleer (3), Noël Vandenberghe (4)*

(1) Royal Observatory of Belgium, Ringlaan 3, 1180 Brussels. Email: koen.verbeeck@oma.be
(2) NIRAS/ONDRAF
(3) Scr. Sibelco
(4) KULeuven, Earth and Environmental Sciences

***Abstract:*** *Due to the closeness of the Rauw fault to sensitive installations (nuclear site of Mol-Dessel and SEVESO industries) it is important to study the potential for large earthquakes on this low slip-rate fault on the western shoulder of the Roer Valley Graben (figure 1). To address this need, we performed geophysical and paleoseismologic research to try to determine the plausibility and recurrence rate of large earthquakes on the Rauw Fault. In literature, there are only vague indications for Quaternary movement of the Rauw Fault. Our first targeted geophysical/geomorphological research for Quaternary activity of the Poppel and Rauw Faults identified the Rauw Fault as the best candidate for a paleoseismic trench investigation in 2003. This, unpublished, trench improved our understanding of the sediments and their deep cryoturbation but did not reveal the expected Quaternary fault displacement. Since 2010 we did much more geophysical research in a wide zone around the trench, which revealed that the Rauw Fault consists of several branches and that we missed the main fault with our trench. Due to the limited Quaternary thickness at the 2003 trench site it is better to shift our present efforts further northward along the fault where the Quaternary is thicker and has better stratigraphic resolution. There, we have recently measured several long H/V ambient noise profiles across the Poppel, Rauw, Reusel, Veldhoven and some minor faults to better locate them. In the near future we plan to acquire a new geophysical image from the upper 100m (above existing seismic profiles and our H/V profiles), locate the fault at the surface and find a good candidate site for a new trench investigation.*

***Key words***: *Rauw Fault, Campine Basin, Active Fault*

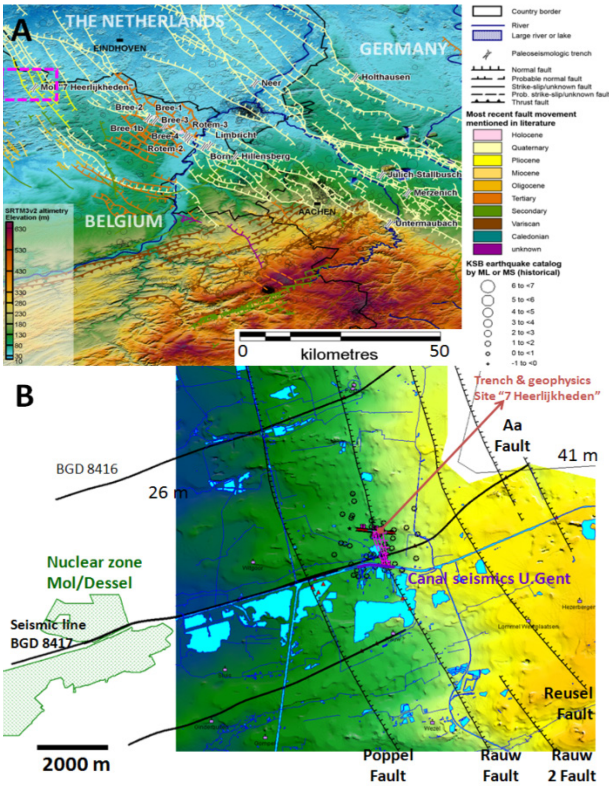


*Figure 1: Location map and DEM of A: The Roer Valley Graben Area with faults activity and seismicity, the magenta rectangle is the investigated area shown in B: with indication of faults and seismic lines by Belgian Geological Survey and Ghent University*

**Acknowledgements:** This specific study of the Rauw Fault is performed within the framework of a seismic hazard assessment for the Mol-Dessel nuclear zone, financed by NIRAS/ONDRAF and is also part of the first author's PhD project at KULeuven.

## References

De Batist, M., J. Van Lint, W. Versteeg & P. Van Rensbergen, (1992). *Structureel ondiepwater seismisch onderzoek. R.C.M.G. Gent*, Ministerie van de Vlaamse Gemeenschap, Brussel.

Gullentops, F., Huyghebaert, Wittewrongel & Dricot, (1974). *Verslag van de buitengewone vergadering op 21 tot 23 juni.* Belgische Vereniging voor Geologie en Société Géologique de Belgique.

Gullentops, F. & N. Vandenberghe, (1995). *Toelichtingen bij de Geologische kaart van België: Kaartblad 17 Mol*. Belgische Geologische Dienst & Anre, 64p.

Pannekoek, A.J., (1924). Einigen Notizien über die Terrassen in Mittel- und Nord-Limburg. *Natuurhistorisch Maandblad* 13, 305-336.

Vandenberghe, J., (1982). Geoelectric investigation of a fault system in Quaternary deposits. *Geophysical Prospecting* 30, 879-897.

Vandenberghe, J., (1990). Morphological effects of Pleistocene faulting in unconsolidated sediments (Central Graben, Netherlands). *Zeitschrift für Geomorphologie N.F.* 34 (1), 113-124.

Verbeeck, K., T. Camelbeeck, K. Vanneste, L. Wouters & M. Dusar, (2001). *Studie van de tektonische activiteit van de breuken van Rauw en Poppel.* Report for convention CCHO 2000-508/00/00 between the Royal Observatory of Belgium and NIRAS, 138p.

INQUA Focus Group on Paleoseismology and Active Tectonics

paleoseismicity.org

# Pull-apart Basins as Fault Segment Boundaries – the case of the Sea of Galilee, Israel

*Wechsler, Neta (1), Sagea Tahan (1), Moshe Reshef (1), Shmulik Marco (1)*

(1) Department of Geophysics, Atmospheric and Planetary Sciences. Tel-Aviv University, Israel. Email: netawe@post.tau.ac.il

***Abstract:*** *The Sea of Galilee (SoG) pull-apart basin is an important link in the chain of structures along the Dead Sea Transform (DST), a major plate boundary fault in the Middle-East. Similar basins are prevalent along transform faults all over the world, yet their behavior and kinematics are not fully understood. The prominent difference between structures to the south and north of the SoG basin hints at the basin's complex tectonic history. We present first results from a multidisciplinary study of the recent tectonic activity in the basin, using shallow seismic methods combined with paleoseismic trenching investigations in the south-eastern side of the SoG. We find young faulting evidence mostly west of the Tel-Katzir uplifted block, which lead us to suggest a change in the basin structure south of the SoG during the Quaternary due to the migration of the main strike-slip bearing fault westward into the basin.*

***Key words***: *Pull-apart basins, active faults, transform plate boundary, Paleoseismology, reflection seismics.*

## INTRODUCTION

Pull-apart basins (PAB) are tectonic structures associated with transform plate boundaries and strike-slip faults, and are thought to represent a discontinuity in the fault at seismogenic depths, though their surface geometry does not necessarily represent their structure at depth (Rodgers, 1980). Our current understanding of PAB kinematics is based mostly on numerical modeling and laboratory experiments, where geometry and rheology are necessarily simplified, while there are only few field studies that examine the deformation within active PAB. By studying their recent deformation history we can investigate the roles of PAB as large asperities which control earthquake propagation and arrest, fault interaction and slip partitioning. Moreover, by comparing and contrasting structures at depth (which represent development history) and at the surface (which represent current activity on the fault), the evolution history of PAB in the large context of fault behaviour can be better understood.

The chosen case study, the Sea of Galilee (SoG), is a pull-apart structure along the Dead-Sea Transform (DST), a sinistral plate boundary fault which separates the Arabian plate and Sinai sub-plate and is capable of generating large magnitude earthquakes (at least up to M7.5). Left-lateral movement on the DST since the mid-Miocene offsets numerous pre-Miocene geologic features by 105 km (Freund et al. 1968). PAB were first recognized along the DST, and there have been numerous studies about the deep structure of the SoG. Yet, despite its importance, the detailed geological structure and physical evolution of the basin are inadequately characterized and there are still many unknowns, including the location of the active fault strands, the location and timing of large earthquakes in and around the basin, and the relation between plate-motion and faulting geometry. The surface expressions of active faults in the SoG basin have been masked by fast sedimentation in the lake, intense agricultural activity on land and by repeated basin flooding events,

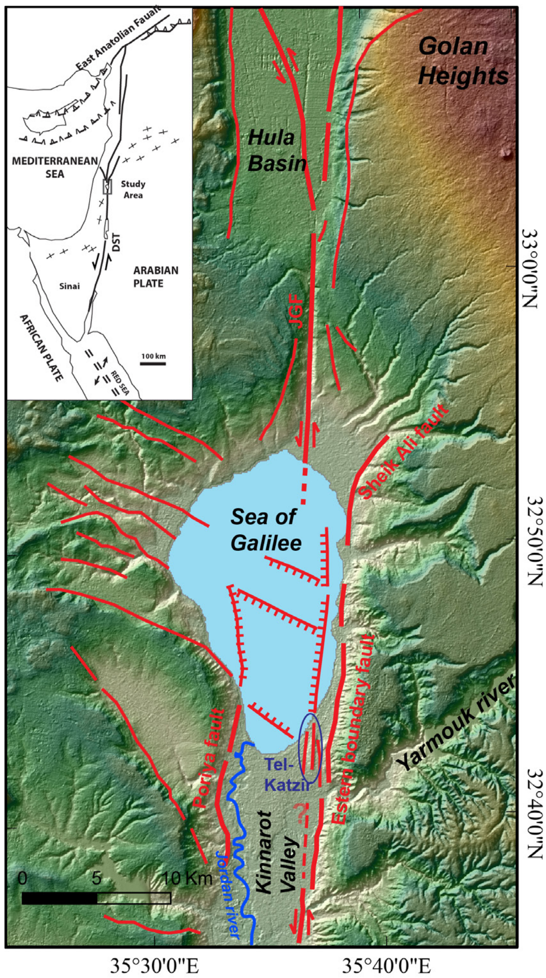


*Fig. 1: Location map of the study area with major faults after Sagi et al. (2013). Faults in the lake after Reznikov (2004). Inset – general location map with major tectonic features after Garfunkel (1981). JGF – Jordan Gorge fault.*

so there is critical need of finding, mapping and characterizing fault activity using adequate methods.

Here we present first results from an effort to characterize young deformation in the south-eastern SoG basin, where the DST arrives from the south and continues underwater in the lake (Figure 1). We use both shallow reflection-refraction surveys and paleoseismic trenching to locate active faults and study recent fault movements south of the SoG.

## LOCAL SETTINGS

*The southern part of the SoG basin, also called the Kinnarot Valley, is a deep depression, 6-7 km wide and 20 km long, with elevations measuring 170 to 220 m bmsl. It is bounded to the east and west by two major normal fault systems which are part of the Dead Sea Transform system (Figure 1). In the southeast corner of the SoG basin is a north-south elongated hill called Tel-Katzir hill. This hill protrudes out of the flat topography surrounding it, and it is bounded by two normal faults to the east and west. This down-faulted block is considered, structurally and lithologically, a part of the Golan Heights because similar strata are exposed on its flanks. There are several hypotheses regarding the origin of this hill; (1) It is a part of a series of rim blocks down-faulted by normal step faults along the margins of the Golan Heights (Marcus and Slager, 1983). (2) It is an uplifted block which formed due to a right jog of the main strike-slip fault (Zurieli, 2002). (3) Strong magnetic anomalies and the existence of pyroclasts at the Tel-Katzir hill led to a suggestion that it was a part of an ancient volcano, and that an 8 km of lateral slip occurred along its eastern boundary fault during a period of 2.5-1.5 Ma (Agnon et al., 2002).*

## RESULTS

*Reflection/refraction surveys*

Previous explorations in the southern SoG Basin, including in the region around Tel Katzir hill, were conducted with the purpose of describing sub-surface structures and characterizing internal deformation, fault geometry and fault evolution. However, the interpreted data is inadequate for locating and characterizing young faulting in the upper layers (10-50 meters below the surface). The young sediments in the southern part of the SoG are mostly fluvial/alluvial and lacustrine, representing lake level changes throughout the Holocene. The Holocene and late Pleistocene sediments are mostly horizontal and lie unconformably above older Pleistocene sediments, which are highly tilted. It is thought that the unconformity represents a period of change in the local geometry of the DST (Heimman and Braun, 2000). Therefore we consider faulted sediments above this unconformity as evidence for active faulting. Previous seismic lines in the area placed the unconformity at ~ 50 m depth below the surface and therefore in our seismic survey we focused on shallow depths (less than 50 m).

We conducted several reflective/refractive (high definition) seismic surveys on the south-eastern side of the basin, with the goal of locating the main young faults in that area. We focused on sites where faults were interpreted in previous, lower resolution seismic surveys, in order to determine which of those faults can be considered active, i.e. offset Holocene sediments. The experiment consisted of 3 seismic lines, all with an east-west orientation, strategically placed to intersect the previously mapped faults which have a north-south orientation. Each line consists of 2 overlapping, 96-channel lines with offset shots. Receiver distance (geophone spacing) was 1 meter and shot spacing was 0.5 meters.

The results from our seismic survey reveal evidence of active faults cutting through young sediments on the south-western side of the Tel-Katzir hill. The sense of movement on one of the observed faults appears to be reversed with respect to the topography (Figure 2). Faults that accommodate oblique slip have locally changing geometries along their surface traces, which is expressed as localized uplift or subsidence, occasionally contrary to the overall sense of movement. We therefore consider the sense of movement on the fault as an indicator for oblique slip movement.

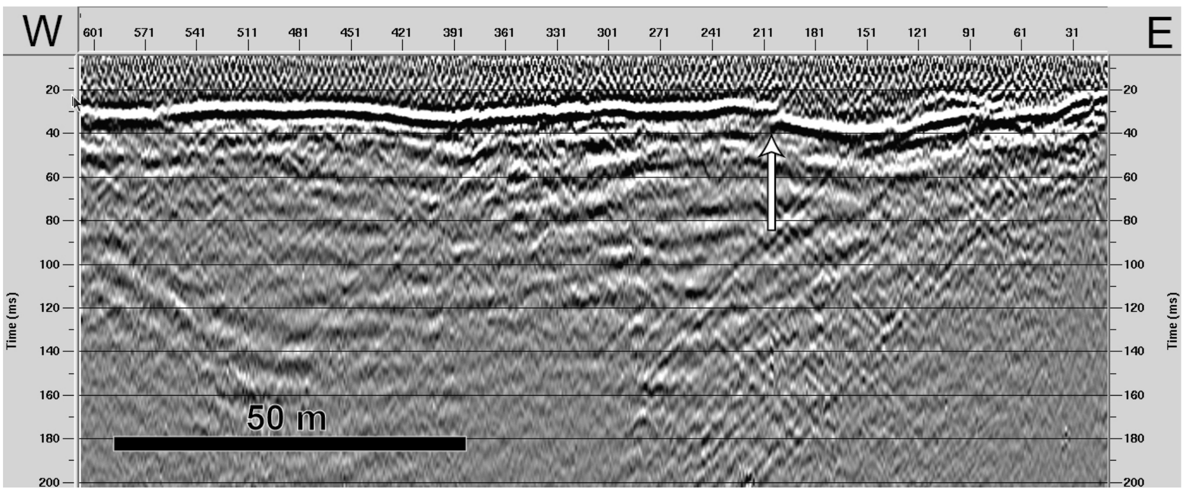


*Fig. 2: Stacked cross section of one line with evidence of young faulting (marked with an arrow).*

*Paleoseismic and outcrop fault mapping*

Wechsler (2005) opened several paleoseismic trenches on suspected active faults in several locations around Tel-Katzir hill. While the main transform, the fault that bears most of the strike-slip movement was not located in the trenches, she did find evidence of secondary faults that had been active during the Holocene, as well as during the late Pleistocene, based on bulk carbon dates.

The first site was located to the southeast of Tel-Katzir hill, where a possible young fault was detected in previous seismic lines. Even though there was faulting evidence in the trenches, it was clear that no significant dip-slip occurred on the faults. The sediments dated to late-Pleistocene - early Holocene. The horizontal movement on this fault was determined to be quite small based on a gravel lens that crossed the fault. Other sites along the continuation of the same fault were devoid of useful stratigraphy.

The second site was located northwest of Tel-Katzir, where a projected continuation of the western Tel-Katzir fault was connected with an underwater bathymetric feature that is interpreted as a possible fault scarp. The trenches exposed Holocene lacustrine sediments that were faulted, though the geometry of the faulting did not fit the expected main fault geometry. This is most likely because the main fault was not exposed in the trenches and is possibly located more to the east.

## DISCUSSION AND CONCLUSIONS

Preliminary results from seismic surveys and paleoseismic trenches show evidence of active, oblique-slip faulting west of the Tel-Katzir hill. There is scant evidence of faulting with no discernible horizontal movement east of the hill. We conclude that the main strike-slip fault in the south-east part of the SoG PAB may be located on the west side of the Tel-Katzir hill. If true, then the hill is not a recent push-up structure, but rather an older fault block, possibly related to the normal faults of the Golan Heights or to Quaternary volcanic activity in the valley. Previous studies mapped the main transform fault to coincide with the base of the Golan Heights topographic slope, which is also the eastern boundary fault for the PAB, based on deep seismic sections that targeted older strata. We consider the possibility that the evolution of the PAB included a migration of the main strike-slip fault westward into the basin, a phenomenon that was observed in other basins along the DST (Marco, 2007), as there is no evidence of strike-slip movement on the current expression of the eastern boundary fault. Fault evolution and offset accumulation through time demonstrably corresponds with the geometrical simplification of its surface expression (Wechsler et al., 2010), and faults can overcome asperities such as PAB and form a simpler, through-going structure, as is the case in the Hula basin to the north of the Sea of Galilee (Schattner and Weinberger, 2009).

The Jordan Valley segment of the DST which extends from the north shore of the Dead Sea to the south shore of the Sea of Galilee, in our study area, has been known to rupture historically in large earthquakes (for example in 749/747 and 1033CE). Paleoseismic investigations to the south demonstrated surface rupture evidence for those events (Ferry et al. 2011) and archaeoseismic evidence support estimated magnitudes of ~M7.5. The rupture most likely extended all the way north to the southern shore of the SoG and may have even crossed the basin entirely to produce rupture on the Jordan Gorge fault (Wechsler et al. 2012). Therefore we expect to find evidence of Holocene deformation along this fault. Further mapping efforts will hopefully shed light on the timing and location of large historical earthquakes in the basin.

**Acknowledgements:** We would like to thank Adi Yurman and Matan Shustack for assistance in data collection and processing.

## REFERENCES

Agnon, A., McWilliams, M.O. and Ram, E. (2002). Tel-Katzir - En-Gev magnetic anomalies: a 5 ma volcano offset 8 km on the Dead Sea Transform. In: A. Beck, Y. Katz and R. Ken-Tor (Editors), *Isr. Geol. Soc. Ann. Meeting*, Ma'agan, pp. 2.

Ferry, M., M. Meghraoui, N. Abou Karaki, M. Al-Taj, and L. Khalil. (2011). Episodic Behavior of the Jordan Valley Section of the Dead Sea Fault Inferred from a 14-ka-Long Integrated Catalog of Large Earthquakes. *Bulletin of the Seismological Society of America* 101(2), 926-927.

Heimann, A. and Braun, D. (2000). Quaternary stratigraphy of the Kinnarot Basin, Dead Sea Transform, northeastern Israel. *Israel Journal of Earth Science* 49, 31-44.

Marco, S., (2007) Temporal variation in the geometry of a strike-slip fault zone: Examples from the Dead Sea Transform, *Tectonophysics*, v. 445, p. 186 – 199

Marcus, E. and Slager, J. (1983). *Geological evaluation of the Tel-Katzir block*. Report 83/78, Oil Exploration Ltd.

Rodgers, D. A. (1980). Analysis of pull-apart basin development produced by en-echelon strike-slip faults, *Spec. Publ. int. Ass. Sediment* 4, 27-41.

Schattner, U., & Weinberger, R. (2009). A mid-Pleistocene deformation transition in the Hula basin: Implications for the tectonic evolution of the Dead Sea Fault plate boundary. In *EGU General Assembly Conference Abstracts*, 11, 10023.

Wechsler, N. (2005). *Paleoseismology in the Eastern Kinnarot Basin, Dead Sea Transform*. Unpublished M.Sc. Thesis, Tel Aviv University.

Wechsler, N., Ben-Zion, Y., & Christofferson, S. (2010). Evolving geometrical heterogeneities of fault trace data. *Geophysical Journal International*, 182(2), 551-567.

Wechsler, N., Klinger, Y., Rockwell, T. K., Agnon, A. and Marco, S. (2012). How Long Is Long Enough? Estimation of Slip-Rate and Earthquake Recurrence Interval on a Simple Plate-Boundary Fault Using 3D Paleoseismic Trenching, Abstract T13D-2647, *AGU 2012 Fall Meeting*, San Francisco, Calif., 3-7 Dec.

Zurieli, A. (2002). *The structure and neotectonics of the Kinarot Valley based on seismic surveys*. Unpublished M.Sc. Thesis, Tel Aviv University.

# Long range t-LiDAR and close range photogrammetry in an active tectonic environment

*Thomas Wiatr (1), Aggelos Pallikarakis (2)*

(1) Neotectonics and Natural Hazards, RWTH Aachen University, Lochnerstraße 4-20, 52064 Aachen, Germany. Email: t.wiatr@nug.rwth-aachen.de

(2) Mineralogy-Geology Laboratory, Department of Earth and Atmospheric Sciences, Agricultural University of Athens, Iera Odos 75, 118-55, Athens, Greece. Email: agpall@aua.gr

***Abstract:*** We have studied the fault plane of an active structure in Crete with two different terrestrial non-penetrating systems. With the usage of photogrammetry, and the active remote sensing technique of light detection and ranging (LiDAR), we were able to take measurements of Lastros fault scarp with high accuracy. With these data we have analyzed the paleostress regime on the fault. We suggest that the fault's long-term slip rate is approximately 0.54 mm/yr for the last 13 ka by a mean scarp height of 4.7 m and we have estimated an earthquake recurrence of an 6.3 to 6.6 M earthquake in every 688 years.

**Key words**: *long range t-LiDAR, close range photogrammetry, active bedrock fault, Lastros, Crete*

## INTRODUCTION

Greece is the most seismically active country in Europe due to its location close to the Hellenic Arc and Trench System. The exposed part of the Hellenic fore-arc is the island of Crete and since the Oligocene - lower Miocene Crete has been advancing towards the African plate (e.g. Angelier et al., 1982; Seyitoglu & Scott, 1992; Ganas & Parsons, 2009). As a result, since at least the late Pliocene (Pirazzoli et al., 1982; Meulenkamp et. al., 1994), Crete has undergone uplift at a rate of over 6 mm/yr according to Ganas & Parsons (2009).

The geometry of the subduction zone though is not the same everywhere. Pliny, Ptolemy and Strabo trenches, which form part of the Hellenic trench southern than the eastern part of Crete, show a significant sinistral motion (Kreemer and Chamot-Rooke, 2004). As a result researchers suggest that in Crete there is an east-west extension (Lyon Caen et al., 1988, Armijo et al., 1992). Onshore active faults have N-S (western Crete) to NNE-SSW (eastern Crete) orientation. In this study we present research on the Lastros fault at the eastern part of Crete (Fig. 1) with two different terrestrial non-penetrating systems.

Our study area is situated in eastern Crete at the immediate footwall of the Ierapetra-Kavousi fault system (Fig. 1). The Ierapetra-Kavousi fault zone is considered to be the most significant structure at eastern Crete. Its onshore length is approximately 20 km and has a NNE-SSW orientation and dips towards NW. The whole structure consists of three main segments (Karotsieris et al., 2000; Gaki-Papanastasiou et al., 2009). The northern segment comprises the Kavousi fault, the second segment is Monastiraki fault and the southern segment is buried under alluvial formations close to Ierapetra. Due to the presence of the onshore segments, there can also be an offshore segment propagating to the north. Armijo et al. (1992) indicate the presence of an offshore fault with a length of at least 10 km, which has the same orientation as the IKFS (NNE). This increases the total length of the fault system to approximately 30 km. The center of the IKFS must be the Kavousi segment where the highest throw can be observed.

The studied structure is Lastros fault system, which consists of fault segments which are hard-linked with each other (Fig. 2). This structure is parallel to the IKFS, but the dip of the fault surface is $60^{0}$ towards the SE. The IKFS and the Lastros faults comprise a tectonic horst (Kapsas mountain). The Lastros fault with the antithetic Sfaka fault, which is located eastwards, forms the boundary of a graben (Mochlos graben). The total length of the Lastros fault is approximately 6 km according to Karotsieris et al. (2000). A clear fault scarp up to 7.1 m in height can be traced. Striations were also present on the fault plane. However, other authors suggest that the Lastros fault is 11 km long and had a maximum throw of 15 m (Caputo et al., 2006, 2010; Jusseret & Sintubin, 2012). Caputo et al. (2006), have traced a 40 cm light-coloured ribbon at the base of the fault scarp, indicating previous earthquake events (the penultimate?).

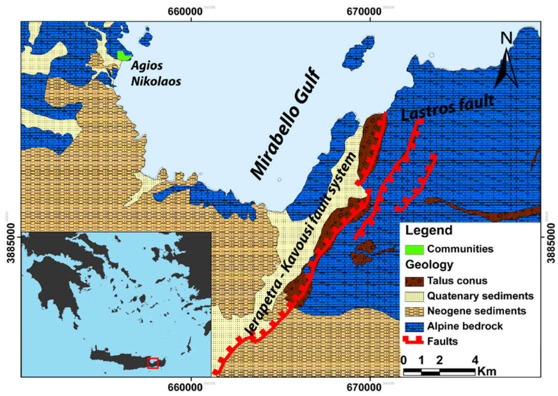


*Fig. 1: Simplified geological map of the study area as was modified by Karotsieris et al., (2000), Caputo et al.,(2006) showing the most significant onshore faults including the Lastros fault.*

## METHODS

For the remote data collection, two different terrestrial methods were used to characterize the fault segments. These are passive remote sensing techniques of photogrammetry and the active remote sensing technique of light detection and ranging (LiDAR). Both methods are established systems in geosciences and have also been applied in investigations on faults (Sagy et al., 2007; Candela et al., 2009, 2011; Bistacchi et al., 2011; Brodsky et al., 2011; Renard et al., 2012).

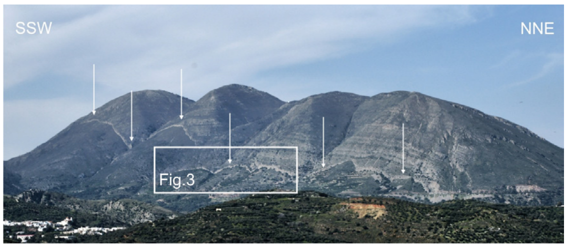


*Fig. 2: Panoramic view of Lastros fault zone. The scanned area is highlighted (box).*

One reason for using these two different techniques is the additional information gained from comparing the monochromatic (near infrared) and panchromatic (visible light) data at different scales, ranges and resolutions in the same study area. This is, therefore, an experimental study to quantify relevant information to determine the faulting history of individual fault scarp segments. The study is based on static t-LiDAR data (hundred metre scale investigation; long range and low resolution) and terrestrial photogrammetry data (several centimetre scale investigation; close range and high resolution) in an active tectonic environment.

For data collection the t-LiDAR system ILRIS 3D by Optech (1500 nm) and a Sony alpha digital camera with 14 Megapixel resolution and a 50 mm objective (lens) were employed. The t-LiDAR system was used to analyse the in-situ environmental conditions of the investigated area and also the geometry of hanging wall, footwall and fault scarp conditions, which are the primarily fields of research. The data obtained are useful for paleoseismological studies and paleostress analysis; the present environmental conditions can be studied to estimate the long-term slip rate and to reconstruct the slip vector and sense of motion using kinematic indicators on the fault surface (Papanikolaou & Roberts, 2007). Moreover, we used the spatial dataset of the scanned segments (600 m of the Lastros fault) for morphological indices to obtain the characteristics of the fault system. The selected point cloud resolution during the data collection in the field was between 4 and 6 cm at the Lastros segment for two scan windows. This implies around 2.4 million points by the Lastros fault study area. The processing of the point clouds comprised data cleaning (remove of vegetation manually), northing, data transformation and pitch angle correction. GIS analysis was undertaken using a cell size resolution of 50 x 50 cm for both fault segments. This indicates that a spatial calculation of every 50 cm is possible. Analyses included the production of digital elevation models (DEM) using the topography, slope, hillshade and aspect. Morphological analyses were then used to determine the fault properties, such as the topographic ruggedness index (TRI) (Riley et al., 1999) and the slope variation. These methods are used to determine the spatial differences between the footwall and hanging wall blocks, and to quantify any characteristics or changes between the colluvial wedge(s) and the bedrock (limestone). Furthermore, we extracted profiles for scarp height variation analysis to determine the disparity between long-term slip rates along the strike of the studied fault segments.

Terrestrial close range photogrammetry was used on the Lastros fault to identify scarp surface changes along the scarp height in defined 0.3 m high strips. The scarp height at the studied area is around 4.2 m; our photogrammetric investigation, however, only covered the lower 2.1 m. Seven continuous DEMs for morphological analysis were, therefore, produced with a spatial resolution (cell size) of around 0.25 mm. For each individual study area 5 to 10 photos were taken from different directions (range between camera and fault plane amounts around 0.5 m to1 m) to minimize shadow effects and maximize data quality. The individual photos from one study area were computed in the open source software *VisualSFM version 0.5* to create a point cloud. Point clouds were imported into the open source software *MeshLab V1.3.2* to scale and to orientate the data to the correct dimensions and in the same position. The point clouds were exported in an *ASCII* data (x-, y-, z-values; the values of the coordinate system are relative and individual for each analyzed scene; no superordinate coordinate system) format and imported into a GIS. In GIS the points were transformed to a raster format with the *topo to raster* interpolation method, and for orientation each photo was georeferenced within the generated DEM. Subsequently, the TRI was calculated; only the central part of the sequence (20 x 5 cm) was used for the interpretation of the results. Finally, the minimum, maximum, mean and standard deviation were calculated and plotted in a box-plot diagram for each study area.

## RESULTS AND DISCUSSION

First of all, the results of t-LiDAR and photogrammetry are not yet combined into one project. Therefore, the results of both analyses should be considered separately. The next step for this project is to combine these remote sensing investigations. We have scanned the northern segment of Lastros fault system by using long range t-LiDAR investigation. Footwall, hanging wall, fault scarp and other morphological features are shown in Fig. 3. The fault scarp that was measured perpendicular to the fault plane without considering the direction of motion has a 7.1 m and 4.7 m mean height (Fig. 3, profile A-A', profile B-B'). Caputo et al. (2004, 2010), (based on Benedetti et al., 2002) and Palumbo et al. (2004), suggest that the age of postglacial faults scarp in Greece is 13 ka. Therefore, we imply a long-term slip rate approximately 0.54 mm/yr (7.1 m) the last 13 ka (Fig. 3, profile A-A'). Scarp height is shorter in profile B-B' (mean 4.7 m height and a long term slip rate of around 0.31 mm/yr) than in profile A-A'. Profile B-B' is closer to the tip of this fault segment while A-A' is towards its center, but there are also deeply cut valleys perpendicular to the fault scarp. The investigation of the close-range photogrammetry was carried out at the Lastros fault up to a height of 2.1 m. The changes of TRI values are plotted along the fault scarp height. Fluctuations are evident between 0.05 and 0.2 cm at each of the investigation areas (every 30 cm). The profile indicates a repetition of higher and lower ruggedness values.

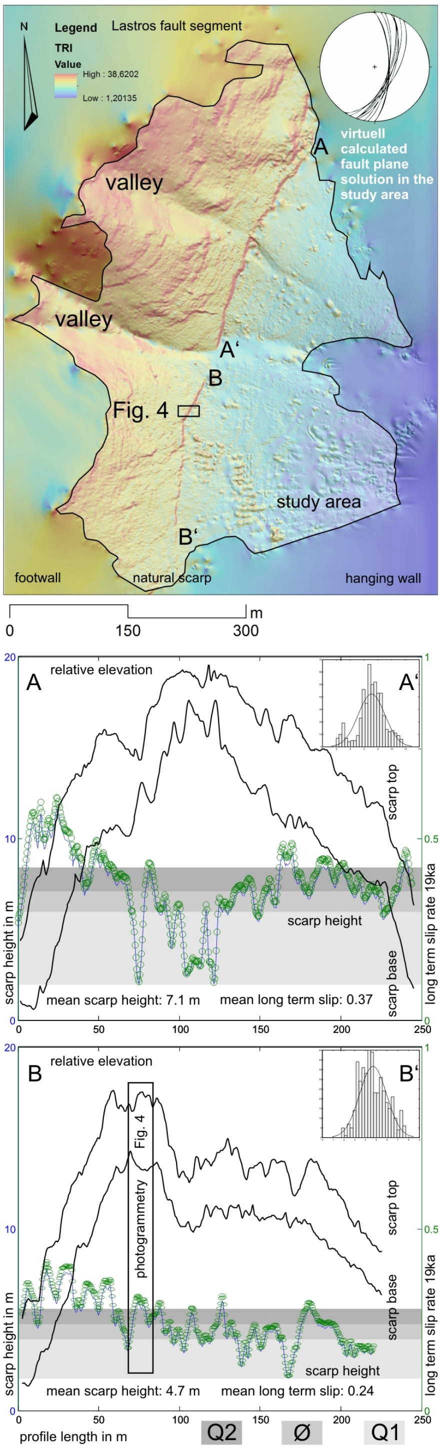


*Fig. 3: Scanned fault plane where morphological features on the fault plane are shown (footwall, hanging wall, scarp). In profiles A-A' and B-B', with the fault scarp height we estimate the long term slip rate for the last 19 ka (green circle). The around 500 calculated values of each fault segment are normal distributed (Q1, 25% quartile; Ø, mean; Q2, 75% quartile). For this reason we chose the mean values for further analysis.*

A repetition rate of mean maximal and minimal values at a metre scale is evident at this resolution. The top of the fault scarp was not studied using this method. The study of close range photogrammetry has shown that the ruggedness of the free face is not continuous throughout the scarp height. The ruggedness values vary between low and high in the shape of a wave (Fig. 4). We interpret the areas with high ruggedness as low active interstate of the fault, and are as a result of the exhumed fault scarp and its longer exposure to weathering (Fig. 4). One explanation could be that, in relatively quiet periods, erosion has more time to act on the same area on the fault surface, which will in turn produce more ruggedness. Similarly, when the ruggedness has lower values, the motion of the fault should be faster. This implies that with successive faulting events, the area undergoing erosion becomes larger and the time span for erosion processes becomes shorter. In other words, the ruggedness is decreasing with increasing slip (Candela et al., 2009, 2011; Bistacchi et al., 2011; Renard et al., 2012).

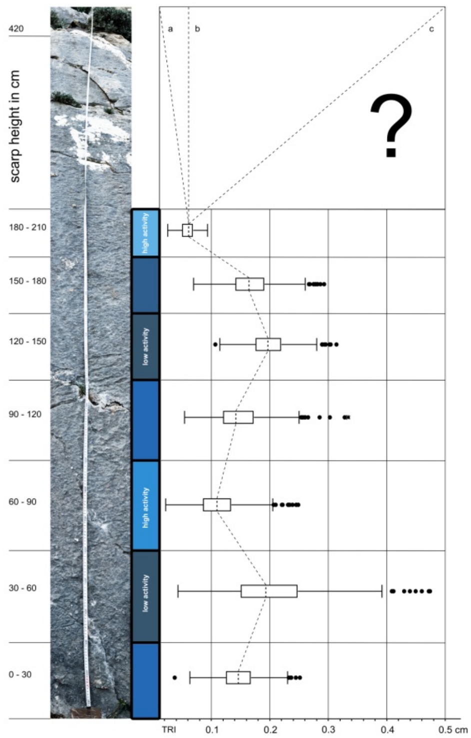


*Fig. 4 TRI results along the scarp height up to 210 cm of the photogrammetric investigation on the Lastros fault segment. The colour code shows the areas with more or less the same mean TRI index and includes an interpretation*

Within the first 150 cm above the colluvium, the fault appears to have undergone two extended time periods of tectonic rest shown by high ruggedness values (30-60 cm to 120-150 cm). Between these distinct features (max. 120 cm, mean 90 cm, min. 60 cm) the fault scarps appears to have undergone a period of high slip activity. To produce this offset indicated by low ruggedness values it is, unfortunately, not possible to estimate the number of earthquake events or magnitudes using the ruggedness information alone; however, we can provide an estimation based on the empirical relationship provided by Wells and Coppersmith (1994) and Pavlides & Caputo (2004). The length of this fault is around 11 km and could produce earthquakes with a maximum magnitude of around 6.3-6.6 M. Therefore, there may be 20 to 30 cm average displacement and up to 40-56 cm of vertical offset (max.) occurring for every maximum magnitude event. To produce an offset of 120 cm using this average offset, the fault must have undergone a minimum of at least 4 to 6 earthquakes. Therefore for a mean 4.7 m height fault scarp we can imply that at least 16 to 23 earthquake events the last 13 ka should have occurred with a repetition rate of 688 years. We use the average displacement instead of maximum, because the change of TRI values indicate fluctuations every 30 cm.

Open questions and further investigations include the combining of close range photogrammetry with close range t-LiDAR to cross-validate the different datasets to find threshold values for quality assurance. Moreover, the top of the scarp needs investigation. Thus, there are various theoretical scenarios (Fig. 4, dot lines a, b, c) for the upper fault surface: (1) the changes in ruggedness are decreasing with height (Fig. 4a); (2) the changes have the same ruggedness signature like the lower part (0 - 210 cm) of the free face (Fig. 4b); and (3) the ruggedness is increasing with height (Fig. 4c). Additionally, the fault surface within the colluvial wedges needs investigation in order to determine if it is having an influence on the fault surface before exhumation. Furthermore, an error analysis between the individual methods and the calculated long term results must be performed.

**Acknowledgment:** This study was financially supported by the German Research Foundation (DFG project RE 1361/12-1) and by the RWTH Aachen University. We would like to thank Jack Mason, Ioannis Papanikolaou, and Klaus Reicherter for the fruitful discussion and Benjamin Koster for support during field work.

## References

Angelier, J., (1979). Neotectonique de l'arc egéen. *Annales de la Société géologique du Nord* 3, 417 pp.

Angelier, J., N. Lyberis, X. Le Pichon, E. Barrier & P. Huchon, (1982). The tectonic development of the Hellenic arc and Sea of Crete: a synthesis. *Tectonophysics* 8, 159-196.

Armijo, R., H. Lyon-Caen & D. Papanastassiou, (1992). East-west extension and Holocene normal-fault scarps in the Hellenic arc. *Geology* 20, 491-494.

Benedetti, L., R. Finkel, D. Papanastassiou, G. King, R. Armijo, F. Ryerson, D. Farber & F. Flerit, (2002). Postglacial slip history of the Sparta Fault (Greece) determined by 36Cl cosmogenic dating: evidence for non-periodic earthquakes. *Geophysical Research Letters* 29, 87-1–87- 4.

Bistacchi, A., W.A. Griffith, S.A.F. Smith, G.D. Toro, R. Jones & S. Nielsen, (2011). Fault roughness at seismogenic depths from LIDAR and photogrammetric analysis. *Pure and Applied Geophysics* 168 (12), 2345-2363.

Brodsky, E.E., J.J. Gilchrist, A. Sagy & C. Collettini, (2011). Faults smooth gradually as a function of slip. *Earth and Planetary Science Letters* 302, 185-193.

Candela, T., F. Renard, M. Bouchon, A. Brouste, D. Marsan, J. Schmittbuhl & C. Voisin, (2009). Characterization of fault roughness at various scales: implications of three-dimensional high resolution topography measurements. *Pure and Applied Geophysics* 166 (10-11), 1817-1851.

Candela, T., F. Renard, J. Schmittbuhl, M. Bouchon & E.E. Brodsky, (2011). Fault slip distribution and fault roughness. *Geophysical Journal International* 187, 959-968.

Caputo, R., C. Monaco & L. Tortorici, (2006). Multiseismic cycle deformation rates from Holocene normal fault scarps on Crete (Greece), *Terra Nova* 18, 181-190.

Caputo, R., S. Catalano, C. Monaco, G. Romagnoli, G. Tortorici & L. Tortorici, (2010). Active faulting on the island of Crete (Greece). *Geophysical Journal International* 183, 111-126.

Gaki-Papanastasiou, K., E. Karymbalis, D. Papanastasiou & H. Maroukian, (2009). Quaternary marine terraces as indicators of neotectonic activity of the Ierapetra normal fault SE Crete (Greece). *Geomorphology* 104, 38-46.

Ganas, A. & T. Parsons, (2006). Three-dimensional model of Hellenic Arc deformation and origin of the Cretan uplift. *Journal of Geophysical Research* 114 (B06), 1-14.

Jusseret, S. & M. Sintubin, (2012). All that rubble leads to trouble: Reassessing the seismological value of archaeological destruction layers in Minoan Crete and beyond. *Seismological Research Letters* 83(4), 736-742.

Karotsieris, Z., S. Lozios & M. Dermizakis, (2000). The neotectonic structure of the broader area of Ierapetra region — Ag. Nikolaos (Lasithi-Crete). *Annales Géologiques des Pays Helleniques* 38, 77-115.

Lyon-Caen, H., R. Armijo, J. Drakopoulos, J. Baskoutass, N. Delibassis, R. Gaulon, V. Kouskouna, J. Latoussakis, K. Makropoulos, D. Papadimitriou & G. Pedotto, (1988). The 1986 Kalamata (south Peloponnesus) earthquake: detailed study of a normal fault, evidences for east-west extension in the Hellenic Arc. *Journal of Geophysical Research* 93 (B12), 14967-15000.

Meulenkamp, J.E., G.J. van der Zwaan & W.A. van Wamel, (1994). On Late Miocene to recent vertical motions in the Cretan segment of the Hellenic arc. *Tectonophysics* 234, 53-72.

Palumbo, L., L. Benedetti, D. Bourlès, A. Cinque & R. Finkel, (2004). Slip history of the Magnola Fault (Apennines, Central Italy) from 36Cl surface exposure dating: evidence for strong earthquakes over the Holocene. *Earth and Planetary Science Letters* 225, 163-176.

Papanikolaou, I.D. & G.P. Roberts, (2007). Geometry, kinematics and deformation rates along the active normal fault system in the southern Apennines: Implications for fault growth. *Journal of Structural Geology* 29, 166-188.

Pavlides, S.B. & R. Caputo, (2004). Magnitude versus faults' surface parameters: Quantitative relationships from the Aegean, *Tectonophysics,* 380, 159-188.

Pirazzoli, P.A., J. Thommeret, Y. Thommeret, J. Laborel & L.F. Montaggioni, (1982). Crustal block movements from Holocene shorelines: Crete and Antikythira (Greece). *Tectonophysics* 86, 27-43.

Renard, F., K. Mair & O. Gundersen, (2012). Surface roughness evolution on experimentally simulated faults. *Journal of Structural Geology* 45, 101-112.

Riley, S.J., S.D. DeGloria & R. Elliot, (1999). A Terrain ruggedness index that quantifies topographic heterogeneity. *Intermountain Journal of Sciences* 5, 23-27.

Sagy, A., E.E. Brodsky & G.J. Axen, (2007). Evolution of fault-surface roughness with slip. *Geology* 35, 283-286.

Seyitoglu, G. & B.C. Scott, (1992). Late Cenozoic volcanic evolution of the northeastern Aegean region, *Journal of Volcanology and Geothermal Research* 54(1-2), 157-176.

Wells, D. L. & K J. Coppersmith, (1994). New empirical relationships among magnitude, rupture length, rupture width, rupture area, and surface displacement. *Bulletin of the Seismological Society of America* 84, 974-1002.

INQUA Focus Group on Paleoseismology and Active Tectonics

paleoseismicity.org

# Active bedrock fault scarps and terrestrial laser scanning: Insights into active tectonics and seismic hazards

*Wiatr, Thomas (1), Ioannis Papanikolaou (2), Tomás Fernandez-Steeger (3), Klaus Reicherter (1)*

(1) Neotectonics and Natural Hazards, RWTH Aachen University, Lochnerstraße 4-20, 52056 Aachen, Germany. Email: t.wiatr@nug.rwth-aachen.de
(2) Mineralogy-Geology Laboratory, Department of Earth and Atmospheric Sciences, Agricultural University of Athens, Iera Odos 75, 118-55, Athens, Greece
(3) Department of Engineering Geology and Hydrogeology, RWTH Aachen University, Lochnerstraße 4-20, 52056 Aachen, Germany.

***Abstract:*** *In this paper we explain how the static terrestrial remote sensing method (t-LiDAR) has the potential to support the knowledge of active limestone bedrock fault scarps in defined areas. The focus is on fundamental approaches to analyze fault segments based on 3D data sets. The development of various modular approaches is, therefore, created to determine the relevant information in a neotectonic/paleoseismic context.*

***Key words****: t-LiDAR, active bedrock scarps, limestone formation, Greece*

## INTRODUCTION

Advantages of using terrestrial remote sensing methods are that it is non-destructive and can be used in hazardous or inaccessible investigation sites. By using these methods, fast and precise data with a high spatial resolution are generated from the remotely investigated object and the present situation is captured during the data recording. For this, active and passive systems can be employed for the exploration of study areas. Depending on the environmental conditions and the objectives of the study, an appropriate system should be chosen. In our study, we used the laser ranging system ILRIS 3D from OPTECH Inc., Ontario, Canada. The active remote sensing method known as terrestrial laser scanning (TLS) produces data on the object's geometry (three dimension; x-, y-, z-coordinates), information of the reflection properties of the detected object (monochromatic information), and photos of the scanned area can be merged on the 3D data (panchromatic information). The high spatial resolution of a scanned object's surface allows this method to be combined with other data (e.g. shallow subsurface information) or attributes (e.g. absolute dating values).
This method was established in geosciences in the last 20 years. The use of the t-LiDAR technique on active faults and neotectonic/paleoseismic studies is, however, not yet well established. Only a small number of projects have been carried out on the detection and characterization of active bedrock faults with t-LiDAR (e.g. Fardin et al., 2001; Renard et al., 2004; Rahman et al., 2006; Renard et al., 2006; Kokkalas et al., 2007; Sagy et al., 2007; Kondo et al., 2008; Candela et al., 2009; Candela et al., 2011; Candela & Renard, 2012; Renard et al. 2012). Descriptive approaches are, however, more common and they are a supporting method to quantify, design, develop and establish the terrestrial remote sensing technique in the neotectonic studies.

The decoding of paleoearthquakes in a defined environment on bedrock fault scarps is important for the estimation of seismic hazard potential in active fault zones. The segments of fault scarps, which are now exposed, have resulted from shallow earthquakes (about 10 - 15 km) with magnitudes greater than 6 $M_S$ (Stewart & Hancock, 1990). Fault plane surfaces contain preserved information regarding the displacement, stress field and slip rates of past earthquakes. These bedrock scarps therefore, remain preserved in the landscape as indicators of past earthquakes (Fig.1).


Fig. 1: Segment of an active bedrock fault scarp (Sfaka fault, west Crete) showing the impressive natural free face.

The point cloud dataset gained from observation of active bedrock fault scarps using the TLS method can be used to analyze the motion of an active bedrock fault scarp segment (*stress solution*), to calculate the long-term slip rate (*neotectonics*) and to detect structural changes on the fault scarp surface (*finding individual events to quantify strong earthquakes and fault history*). Furthermore, the method makes use of monitoring postseismic deformation to detect changes between the hanging-wall and foot-wall (Wilkinson et al., 2010).

Data recording using TLS on faults in limestone formations was carried out from 2009 to 2012. A total of 15 different fault systems on mainland Greece (eight fault zones) and on the island of Crete (seven fault zones) have been scanned. All investigated faults have large segment lengths which have a potential for earthquakes with magnitudes greater than 6 $M_S$.

## METHODS

The primary objectives of this research approach are to use the terrestrial remote sensing method on active bedrock fault scarps to study neotectonics, the present stress field and relative age determination of individual earthquake events. For this purpose, different data recording methods (long/close range investigation) and different spatial resolutions were used. Close-range and long-range ground based LiDAR was used for the different modular approaches (Tab. 1).

Tab. 1: Different investigations on fault scarps used during the t-LiDAR study

| *LiDAR operation* | *Question and modular approach* | *Fault segments* | *resolution* |
|---|---|---|---|
| Long range | Neotectonics | Delphi; Kaparelli; Loutraki; Sfakia; Asterousia; Kastelli; Lastros; Irapetra/Kavoussi; Spili; Perachora | Decimetre and centimetre |
| Long and close range | Paleostress | Delphi; Kaparelli; Pisia; Loutraki; Perachora; Spili; Irapetra/Kavoussi; Dionysos | Centimetre and millimetre |
| Close range | Relative dating of past coseismic events | Kaparelli; Delphi; Erythres; Dionysos; Pisia; Perachora; Loutraki; Sparta; Spili; Archanes | Millimetre |

Separate modular approaches and new strategies had to be created for the evaluation and processing of the static t-LiDAR data sets in order to analyze the virtual 3D information in a semi-automated workflow (Fig. 2). For this, various software packages and data formats are needed. The results of all individual modular approaches in this study demonstrate a useful method when evaluating the hazard potential in tectonic environments.

The following factors and goals were the focus of our research:

- Acquisition and processing of static t-LiDAR data.
- Image analysis and processing: Image information from the backscattered signal of the monochromatic, coherent laser beam is analyzed in order to identify and classify the different surface conditions, especially the presence of vegetation, lichen, slickensides, breccias and influence of paleosols on the fault plane. Furthermore, the changes of roughness on the fault plane can be identified by the scattering behaviour. Geostatistical methods, supervised classification and clustering, such as the like maximum likelihood method, are applied to quantify and investigate the spatial distribution of relevant phenomena on the fault plane.
- Creating high resolution digital elevation models (HRDEM), high resolution digital backscattered signal models (HRDBSM) and scarps profiles.

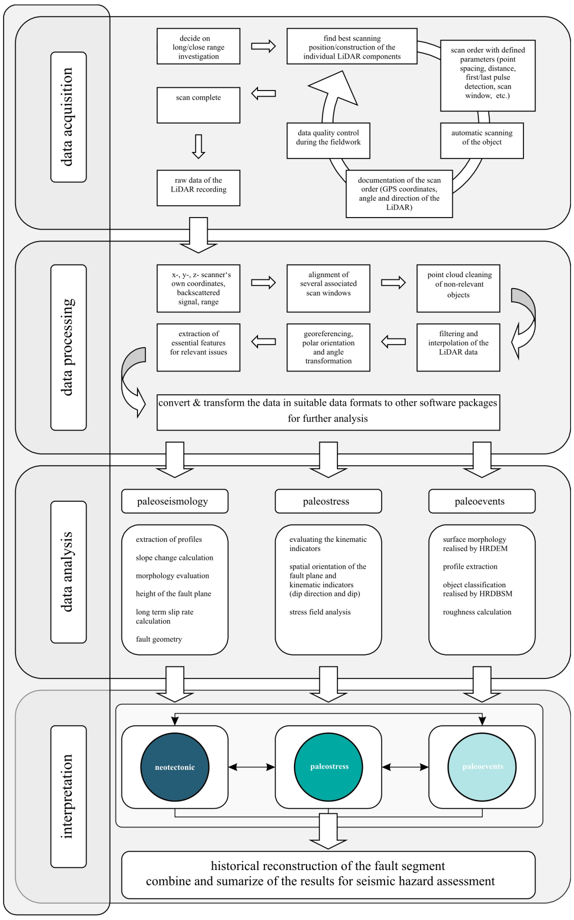


Fig. 2: Workflow for fault scarps analyses using static t-LiDAR.

- Studying the characteristics of fault planes for relative age dating of co-seismic slip events. The HRDEM datasets are analyzed in terms of morphological parameter values through the application of appropriate models. For the roughness characterization internationally standard methods are common. The topographic ruggedness index (TRI) was calculated in defined windows (10x20cm) of line-up transition along the scarp height (Riley et al., 1999). Thus, the results are compared with the results of other author's (e.g. Candela et al., 2009, 2011; Renard et al., 2012)
- Quantitative measurements of faults scarp geomorphic indices (e.g. slope gradient) are used as a reconnaissance tool to identify areas experiencing tectonic deformation (the length of the fault segments; minimum, maximum and average of scarp heights; minimum, maximum and average long-term slip rates; fault geometry and fault morphology; maximum magnitudes) (Papanikolaou & Roberts, 2007).
- Analysis of stress and the investigation of faults and fault systems and their relation to regional tectonic

structures: Fault-slip data obtained from the normal fault scarps are used to unravel the paleostress history of the area. Fault-slip data include dip variations of striae along strike; dip and strike of the fault plane; kinematic indicators; and sense of motion (Hancock & Barka, 1987; Doblas et al., 1997; Doblas, 1998, Gold et al., 2012).

*Neotectonics based on long range t-LiDAR investigations*

For paleoseismological issues, data from the long range t-LiDAR investigation are used. The selected spatial resolution of these data ranges from decimetre to centimetre. After the alignment of the associated scan sequences the irregularly distributed point cloud is georeferenced, orientated to the north and an angle transformation is made. Therefore, the spatial reference and the natural spatial location of the data are recorded. After the data is cleaned of irrelevant elements (vegetation, artefacts, etc.), the point clouds are converted into a grid format with the respective resolution. A spatially regular distribution of the point data is, therefore, possible, which is important for the analysis of the extracted profile (particularly for the modular approaches of paleoseismology and paleoevents). Then morphological analyses (slope, aspect, elevation contours, curvature, hillshade, TRI, etc.) are performed on the obtained HRDEM. This allows the fault plane to be defined as well as for the definition of issue-relevant areas of work. Profiles perpendicular to the fault surface are extracted from the HRDEM to calculate the scarp height and the throw rate of the normal fault. These profiles consist of segments which correspond to the spatial resolution of the long range t-LiDAR investigation. From the HRDEM, any number of profiles can be generated from the scanned fault segment to capture the variation of the scarp height (Fig. 3).

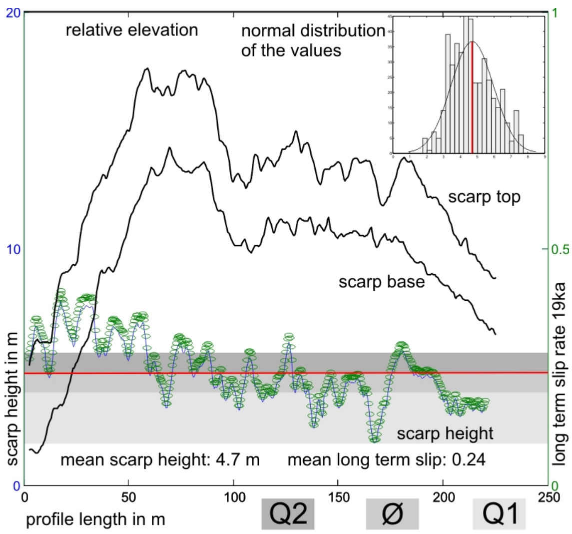


Fig. 3: Distribution of the fault scarp height, extracted from more than 500 values (Lastros fault, Crete).

*Present stress field based on close and long range t-LiDAR investigation*

In order to determine the sense of motion of the normal fault scarp segment, paleostress analysis needs to be undertaken. In this process, the combination of the data from the long and close range t-LiDAR investigations are used. Therefore, the fault plane orientation, the orientation of slickenside lineation and the shear sense of motion, i.e. the movement of the hanging wall, were determined by using static t-LiDAR data. The combination of both t-LiDAR investigations with the corresponding spatial resolution of the data sets allows the stress field reconstruction along the strike of the fault and of the height of the fault scarp. In a remote sensing context, the challenges of a sensitive detection of the kinematic indicators are necessary and needed to determine the direction of the fault movement (Fig. 4). A related investigation in this modular approach will be studying reactivated fault scarps with multiple kinematic indicators to characterise the stress field history with static t-LiDAR (Wiatr et al. (in press)).

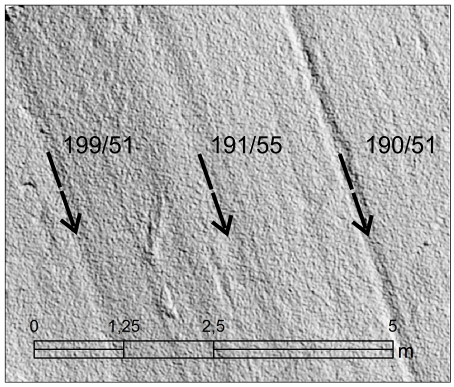


Fig. 4: Slickenside orientation on a fault plane.

*Individual events based on close range t-LiDAR investigation*

In order to understand and reconstruct a fault scarps' slip history, the structural changes and backscatter behaviour must be correlated. For this approach the static t-LiDAR data from the close range investigation was used on various natural and anthropogenically exhumed bedrock fault scarps. The research focused on the changes in roughness, backscattered signal and surface conditions from the bottom up to the top of the scarp. In the analysis of the HRDBSM, a supervised and unsupervised classification are performed by defining training areas or generating signature files which are subsequently transferred with the maximum likelihood method in different classes. After that the link-up of HRDEM and HRDBSM makes it possible to analyze the different surface structures virtually in scale preservation and is used for the interpretation of the roughness changes.

A fundamental assumption we use is that the ruggedness of a fault plane is increasing during quite phases between shallow earthquakes events. In this intra-active period, the external processes have the potential to increase the roughness on the fault plane. This means that the processes for producing roughness (weathering, erosion) affect the surface during the inactive phases significantly more than during the displacement. This imprint on the fault plane should be noticeable and could be used for relative dating between two long inactive intervals on an active bedrock fault system (Fig. 5). When the amount between these two stages is known, and the length of the fault system, the maximum magnitude can be calculated after Wells & Coppersmith (1994) and verified with this offset.

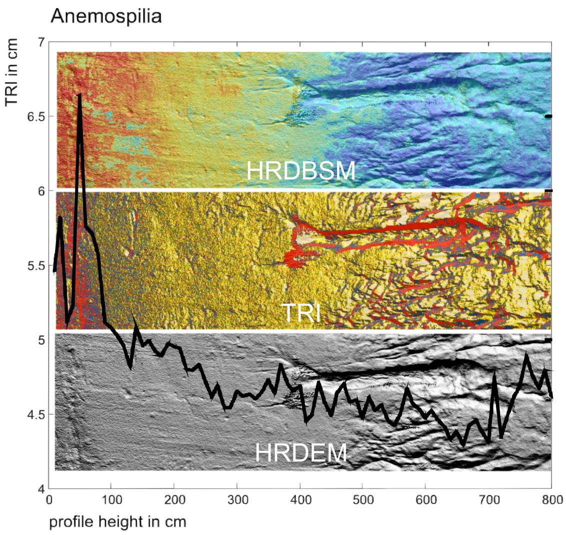


Fig. 5: TRI ruggedness profile along the scarp plane height including the HRDBSM, TRI and HRDEM (Anemospilia fault plane, Crete).

All of these various approaches and their results in the different modular methods are interconnected and all have to be considered during the analyses.

**Acknowledgments:** This study was financially supported by the German Research Foundation (DFG project RE 1361/12-1) and by the RWTH Aachen University. We would like to thank Jack Mason for the fruitful discussion.

## References

Candela, T., F. Renard, M. Bouchon, A. Brouste, D. Marsan, J. Schmittbuhl & C. Voisin, (2009). Characterization of fault roughness at various scales: Implications of three-dimensional high resolution topography measurements. *Pure and Applied Geophysics* 166 (10-11), 1817-1851.

Candela, T., F. Renard, J. Schmittbuhl, M. Bouchon & E.E. Brodsky, (2011). Fault slip distribution and fault roughness. *Geophysical Journal International* 187, 959-968.

Candela, T. & F. Renard, (2012). Segment linkage process at the origin of slip surface roughness: Evidence from the Dixie Valley fault. *Journal of Structural Geology* 45, 87-100.

Doblas, M., V. Mahecha, M. Hoyos & J. López-Ruiz, (1997). Slickenside and fault surface kinematic indicators on active normal faults of the Alpine Betic Cordilleras, Granada, southern Spain. *Journal of Structural Geology* 19 (2), 159-170.

Doblas, M., (1998). Slickenside kinematic indicators. *Tectonophysics* 295, 187-197.

Fardin, N., O. Stephansson & J. Jing, (2001). The scale dependence of rock joint surface roughness. *International Journal of Rock Mechanics & Mining Science* 38, 659-669.

Gold, P.O., E. Cowgill, O. Kreylos & R.D. Gold, (2012). A terrestrial lidar-based workflow for determining three-dimensional slip vectors and associated uncertainties. *Geosphere* 8 (2), 431-442.

Hancock, P.L. & A.A. Barka, (1987). Kinematic indicators on active normal faults in western Turkey. *Journal of Structural Geology* 9 (5/6), 573-584.

Kokkalas, S., R.R. Jones, K.J.W. McVaffrey & P. Clegg, (2007). Quantitative fault analysis at Arkitsa, Central Greece, using terrestrial laser-scanning (LiDAR). *Bulletin of the Geological Society of Greece* XXXX,1959-1972.

Kondo, H., S. Toda, K. Okumura, K. Takada & T. Chiba, (2008). A fault scarp in an urban area identified by LIDAR survey: A Case study on the Itoigawa-Shizuoka Tectonic Line, central Japan. *Geomorphology* 101, 731-739.

Papanikolaou, I.D. & G.P. Roberts, (2007). Geometry, kinematics and deformation rates along the active normal fault system in the southern Apennines: Implications for fault growth. *Journal of Structural Geology* 29, 166-188.

Rahman, Z., S. Slob & R. Hack, (2006). Deriving roughness characteristics of rock mass discontinuities from terrestrial laser scan data. Proceedings of the 10th IAEG Congress: *Engineering geology for tomorrow's cities*, Nottingham, United Kingdom.

Renard, F., J. Schmittbuhl, J.P. Gratier, P. Meakin & E. Merino, (2004). Three-dimensional roughness of stylolites in limestone. *Journal of Geophysical Research* 109, B03209.

Renard, F., C. Voisin, D. Marsan & J. Schmittbuhl, (2006). High resolution 3D laser scanner measurements of a strike-slipe fault quantify its morphological anisotropy at all scales. *Geophysical Reserach Letters* 33, L04305.

Renard, F., K. Mair & O. Gundersen, (2012). Surface roughness evolution on experimentally simulated faults. *Journal of Structural Geology* 45, 101-112.

Riley, S.J., S.D. DeGloria & R. Elliot, (1999). A Terrain ruggedness index that quantifies topographic heterogeneity. *Intermountain Journal of Sciences* 5, 23-27.

Sagy, A., E.E. Brodsky & G.J. Axen, (2007). Evolution of fault-surface roughness with slip. *Geology* 35, 283-286.

Stewart, I.S. & P.L. Hancock, (1990). Brecciation and fracturing within neotectonic normal fault zones in the Aegean region. In: *Deformation Mechanisms, Rheology and Tectonics* (Knipe, R.J. & Rutter, E.H., eds.), Geological Society of London Special Publication 54, 105-112.

Wells, D.L. & J.K. Coppersmith, (1994). New empirical relationships among magnitude, rupture length, rupture width, rupture area, and surface displacement. *Bulletin of the Seismological Society of America* 84, 974-1002.

Wiatr, T., K. Reicherter, I.D. Papanikolaou, T. Fernández-Steeger & J. Mason, (in press): Slip vector analysis with high resolution t-LiDAR scanning. *Tectonophysics*, doi:10.1016/j.tecto.2013.07.024

Wilkinson, M., K.J.W. McCaffrey, G. Roberts, P.A. Cowie, R.J. Phillips, A.M. Michetti, E. Vittori, L. Guerrieri, A.M. Blumetti, A. Bubeck, A. Yates & G. Sileo, (2010). Partitioned postseismic deformation associated with the 2009 Mw 6.3 L'Aquila earthquake surface rupture measured using a terrestrial laser scanner. *Geophysical Research Letters* 37, L10309.

# Field evidence for paleoliquefaction features in western Algeria: A step toward paleoseismic investigation

*Youcef, Bouhadad(1)*

(1) Earthquake Engineering Center (CGS), Rue Kadour, H. Dey, Algiers, B.P.252, Algeria. Email: bouhadad_y@yahoo.com

***Abstract:*** *Earthquakes are associated to a various secondary induced effects that may be preserved in geological records and thus constitute a useful material for paleoseismic studies. Field investigations allowed us to identify past liquefaction traces in the quaternary deposits in western part of Algeria, characterized by the shortness of the historical seismicity catalogue. The morphology and the geometry of the observed features as well as the observed deformation of the hosted layers are among characteristics of the seismically induced-features. Our observations represent a step towards paleoseismological investigation in the region, knowing that the December 22nd 1999 ($M_s$=5.6) Ain Temouchent earthquake has been produced by a blind reverse fault-related fold, where a direct study of the fault is inaccessible.*

***Key words****: earthquake, active fault, paleo-liquefaction, Algeria.*

## INTRODUCTION

Strong and even, in some cases, moderate-sized earthquakes are associated to a various kind of ground deformation represented by: (i) primary effects such as fault ruptures usually preserved as geomorphic scarps in the landscape and/or (ii) secondary effects, that may occur far from the fault trace such as, landslides, liquefaction, earthquake related inundation deposits (tsunamis deposits known as tsunamites, damming deposits due to faulting or landslides obtruding rivers), damage in caverns affecting stalactites and stalagmites, alluvial and marine terraces uplifts, trees growth perturbation as well as soft sediment deformations known as seismites (Philip and Meghraoui, 1983; Meghraoui and Crone, 2001; Mghraoui et al., 2004; Bouhadad et al., 2009; Maouche et al., 2010; Maouche et al., 2011;Peters et al., 2007; Melnick et al.2012).The above mentioned features can be used as materials for paleoseismic studies aiming to identify and assess the size of past earthquakes (De Martini, 2001, Gerard, 2005; Mc Calpin, 2009). On the other hand, effects of earthquakes shaking may be recorded in manmade structures, mainly of ancient civilization, and serves also to retrieve and assess past earthquake through archeoseismological studies. The use of paleoliquefaction features in studying inaccessible fault has been used in the case of New Madrid buried/bind fault (Obermeier, 1996) and in south Carolina coastal plain (Talwani & Schaffer, 2001). In general, earthquakes of magnitude Ms ≥ 5.5 may trigger liquefaction (Ambraseys, 1988). Seismic waves shaking may be the source of sedimentary deformations affecting soft sediments and generates structures widely known as “seismite” (Seilacher, 1966; Plaziat et al., 1990). The most known features of seismic origin are those associated to the liquefaction phenomena such as fluid escape structures and sand intrusions represented by sand dikes, sills and sand vents (Estevez et al., 1994; Munson et al., 1995; Obermeier, 1996; Alfaro et al., 2001; Bezzera et al., 2005). The interest of such induced features is highlighted during the last decade since it can be used in seismic hazard assessment through paleoseismic studies (Serva et Slemmons,1995; Talwani & Schaffer, 2001; Tuttles et al., 2003). Evaluation of paleoearthquake parameters such as acceleration and magnitude using paleoliquefaction features is now possible through analytical geotechnics procedures (Green et al., 2005; Obermeier et al., 2005; Olson et al., 2005). In Northern Algeria only earthquake of magnitude ≥ 6.0 are associated to liquefaction. Indeed widespread liquefaction has been described during the El-Asnam 1980 (Ms = 7.3) and Zemmouri (Mw = 6.8) earthquakes (Philip and Meghraoui, 1983; Bouhadad et al., 2004). While liquefaction has not been reported during moderate-sized earthquakes of Constantine (Ms=5.7), Chenoua (Ms=6.0), and Mascara (Ms= 5.6).We aim in this work to present the paleoliquefaction features identified in Western Algeria and to highlight their Interest for paleoseismic studies in the area.

## SESIMOTECTONIC SETTING

The studied area is situated in the Tellean Atlas chain of Algeria, a segment of the peri - Mediterranean plate boundary belt, where the African and the Eurasian tectonic plates are converging 4 to 6 mm/yr in the NW-SE direction (Argus et al., 1989; De Mets et al., 1990, Nocquet and Calais, 2004). Several active faults, mainly of reverse mechanism have been mapped in the area (Meghraoui et al., 1996; Bouhadad, 2001; Meghraoui et al., 2004; Maouche et al., 2011). Consequently, during the last two centuries many moderate-sized to strong earthquakes have been recorded (Mokrane et al., 1994; Ambraseys et Vogt, 1988; Benouar, 1994). Such earthquakes have been produced by blind and/or offshore located active faults which are inaccessible for direct paleoseismic study. The available seismicity catalogues in northern Algeria are characterized by only three hundreds years of records. Therefore, the need of plaeoseismic data is required in order to understand the long term behaviour of active geological structures.

## PALEOLIQUEFACTION FEATURES

Paleoliquefaction features have been already described in northern Algeria (Bouhadad et al., 2009). Field search undertaken along waterways in the epicentral area of the December 22nd, 1999 (Ms= 5.6) AinTemouchent earthquake (Belabbes et al., 2009) allowed us to identify several sedimentary features interpreted herein as paleoliquefaction induced by past strong earthquakes. The features include sand and silt dikes, vented sand, and sand sills in quaternary alluvial terraces (figure 1). The hosted layer exhibits also fractures and centimeter-sized fold. Such deformation is due to ground settlement that is associated to soil liquefaction as observed in present day earthquakes.

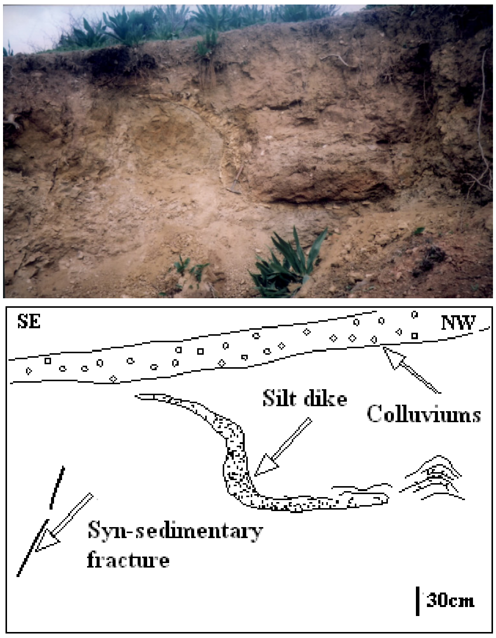


*Fig. 1: Photography and it's depiction showing a paleo-liquefaction feature represented by silt dyke in the epicentral area of the 1999, $M_s$=5.6 Ain Temouchent earthquake.*

## CONCLUSION AND DISCUSSION

A first step of any paleoseismic study is the identification of earthquake records in the geology (primary or secondary trace) and the availability of datable materials. Trench technique is the usually used throughout the world. Ideally, paleoseismic studies are conducted through cutting by trenching through the fault trace. In some cases this is not available such as the case of blind faults in compressive seismotectonic context and the case of offshore located faults. Thus in such case secondary induced effects by earthquakes may serves as precious tools. In the Ain Temouchent area the only known fault has been identified by InSar following the 1999 Moderate sized earthquake (Ms=5.6) and is a blind fault related fold. Nevertheless, field work allowed us to identify paleoliquefaction Features that may serves for a paleoseismic study in the area in order to understand the long term behavior of this 20 km-long active fault.

## References

Alfaro, P., J. Delgano, A. Estevez, C. Lopez-Casado, (2001). Paleoliquefaction in the Bajo Segura basin (Eastern Betic Cordillera). *Acta Geologica Hispanica* 36 (3-4), 233-244.

Ambraseys, N.N., (1988). Engineering Seismology. *Earthquake Engineering and Structural Dynamics* 17, 1-105.

Ambraseys, N.N. & J. Vogt, (1988). Materials for the investigation of the seismicity of the region of Algiers, *European Earthquake Engineering* 3, 16-29.

Argus, D.F., R.G. Gordon, C. De Mets & S. Stein, (1989), Closure of the Africa-Eurasia-North America plate motion circuit and tectonics of the Glauria fault, *Journal of Geophysical Research* 94, 5585-5602.

Belabbes, S., M. Meghraoui, Z. Cakir & Y. Bouhadad, (2009). InSAR analysis of the moderate size Ain Témouchent (Algeria) blind thrust earthquake (22/12/1999, Mw = 5.7. *Journal of Seismology* 13, 421-432.

Benouar, D., (1994). Material for the investigation of the seismicity of Algeria and adjacent region during the twentieth century, *Annali di Geofisica* XXXVII (4), 860.

Bezzera, F.H.R., V.P. Da Fonseca, C. Vita-Finzi, F.P. Lima-Filho & A. Saadi, (2005). Liquefcation- induced structures in Quaternary alluvial gravels and gravely sediments, NE Brazil, *Engineering Geology* 76, 191-208.

Bouhadad, Y., (2001). The Murdjadjo, western Algeria, fault-related fold: implication for seismic hazard, *Journal of Seismology* 5, 541-558.

Bouhadad, Y., A. Nour, A. Slimani, N. Laouami & D. Belhai, (2004). The Boumerdes (Algeria) earthquake of May 21, 2003 MW=6.8): Ground deformation and intensity. *Journal of Seismology* 8, 497-506.

Bouhadad Y., A. Benhammouche, S. Maouche & D. Belhai, (2009). Evidence for quaternary liquefaction-induced features in the epicentral area of the 21 May 2003 Zemmouri earthquake (Algeria, MW =6.8), *Journal of Seismology* 13, 161-172.

Bouhadad Y., A. Benhammouche, H. Bourenane, A. Aitouali, M. Chik & N. Guessoum, (2009). The Laalam (Algeria) damaging landslide triggered by a moderate earthquake (Mw=5.2). *Natural Hazards* 54, 261-272.

De Mets, C., R.C. Gordon, D.F. Argus & S. Stein, (1990). Curent plate Motion. *Geophysical Journal International* 101, 425-478.

Estevez, A., J.M. Soria & P. Alfaro, (1994). Un nouveau type de seismites dans le Miocène supérieure d'alicante (Cordière bétique orientale, Espagne): les coins détritiques. *C.R.Acad.Sci. Paris* 318 (II), 507-512.

Gerald G.K., (2005). Paleoseismic features as indicators of earthquake hazards in North Coastal, San Diego County, California, USA, *Engineering Geology* 80 (2005), 115–150.

Green, R.A., F.S. Obermeier & S.M. Olso, (2005). Engineering geologic and geotecnical analysis of paleoseismic shaking using liquefaction effects: Field examples. *Engineering Geology* 76, 263-293.

Maouche, S., C. Morhange & M. Meghraoui, (2009). Large boulders accumulation on the Algerian coast evidence tsunami events in the western Mediterranean, *Marine Geology* 262, 96-104.

Maouche S., M. Meghraoui, C. Morhange, S. Belabbes Y. Bouhadad & H. Haddoum, (2011). Active coastal thrusting and folding, and uplift rate of the Sahel Anticline and Zemmouri earthquake area (Tell Atlas, Algeria), *Tectonophysics* 509, 69-80.

McCalpin, J.P. (ed.), 2009, *Paleoseismology*, 2nd Edition: International Geophysics Series, Vol. 95, Elsevier Publishing, 647 p.

Meghraoui, M. & F. Doumaz, (1996). Earthquake-induced flooding and paleoseismicity of the El Asnam (Algeria) fault-related fold, *Journal of Geophysical Research* 101, 17617-17644.

Meghraoui, M., J.L. Morel, J. Andrieux & M. Dahmani, (1996). Tectonique plio-quaternaire de la chaine tello-rifaine et de la mer d'Alboran. Une zone complexe de convergence continent –continent, *Bulletin de la Société Géologique de France* 1,141-157.

Meghraoui, M & A.J. Crone, (2001). Earthquakes and their preservation in the geological records, *Journal of Seismology* 5, 281-285.

Melnick, D., M. Cisternas & R. Norambuena, (2012). Estimating coseismic coastal uplift within an intertidal mussel: Calibration for the Maule Chile earthquake (Mw=8.8), *Quaternary Science Reviews* 2, 29-42.

Munson, P.J., C.A. Munson & E.C. Pond, (1995). Paleoliquefaction evidence for a strong Holocene earthquake in south-central Indiana, *Geology* 23(4), 325-328.

Munson, P.J., S.F. Obermeier, C.A. Munson & E.R. Hajic, (1997). Liquefaction Evidence for Holocene and Late Pleistocene Seismicity in the Southern Halves of Indiana and Illinois: A Preliminary Overview. *Seismological Research Letters* 68 (4), 521-536.

Mokrane, A., A. Ait Messaoud, A. Sebai, N. Menia, A. Ayadi, M. Bezzeghoud & H. Benhallou, (1994). *Les séismes en Algérie de 1365 à 1992*. Publication du CRAAG, Alger, 227 p.

Nocquet, J.M. & E. Calais, (2004). Geodetic measurements of crustal deformation in the western Mediterranean and Europe, *Pure and Applied Geophysics* 161, 661-681.

Obermeier, S.F., (1996). Use of paleoliquefaction-induced features for paleoseismic analysis. An overview of how seismic liquefaction features can be distinguished from other features and how their regional distribution and properties of source sediment can be used to infer the location and strength of Holocene paleoearthquakes. *Engineering Geology* 44, 1-76.

Obermeier, S.F., S.M. Olson & R.A. Green, (2005). Field occurrence of liquefaction induced features: a primer for engineering geologic analysis of paleoseismic shaking. *Engineering Geology* 76, 204-234.

Olson, S.M., R.A. Green & S.F. Obermeier, (2005). Geotechnical analysis of paleoseismic shaking using liquefaction features: a major updating, *Engineering Geology* 76, 235-261.

Peters, R., B. Jaffe & G. Gelfenbaum, (2007). Distribution and sedimentary characteristics of tsunami deposits along the Cascadia margin of western North America, *Sedimentary Geology* 200, 372-386.

Philip, H. & M. Meghraoui, (1983). Structural analysis and interpretation of the surface deformation of the El-Asnam earthquake of October 1980, *Tectonics* 2, 17-49.

Plaziat, J.C., B.H. Purser & E.R. Philobbos, (1990). Seismic deformation structures (seismites) in the syn-rift sediments of the NW Red Sea (Egypte). *Bulletin de la Société Géologique de France* 4 (8), 419-434.

Seilacher, A., (1969). Fault-graded beds interpreted as seismites, *Sedimentology* 13, 155-159.

Serva, L. & D.B. Slemmons, eds., (1995). Perspectives in Paleoseismology, *Association of Engineering Geologists Special Publication* 6, 139 p.

Talwani, P. & W.T. Schaeffer, (2001). Recurrence rates of large earthquakes in the South Carolina Coastal Plain based on paleoliquefaction data, *Journal of Geophysical Research* 106, B4, 6621-6642.

Tuttles, M.P., C.S. Prentice, K.D. Williams, L.R. Rena & G. Burr, (2003). Late Holocene Liquefaction features in the Dominican Republic: A powerful Tool for Earthquake Hazard Assessment in Northeastern Caribbean. *Bulletin of the Seismological Society of America* 93 (1), 27-46.

.